Exolysin, a novel virulence factor of Pseudomonas aeruginosa clonal outliers

Pauline Basso

Communauté
UNIVERSITÉ Grenoble Alpes

THÈSE

Pour obtenir le grade de

DOCTEUR DE LA COMMUNAUTE UNIVERSITE GRENOBLE ALPES

Spécialité : **Virologie-Microbiologie-Immunologie**

Arrêté ministériel : 25 mai 2016

Présentée par

Pauline BASSO

Thèse dirigée par **Ina ATTREE**
et
codirigée par **Eric FAUDRY**

préparée au sein du **Laboratoire Biologie du Cancer et de l'Infection**
dans **l'École Doctorale Chimie et Sciences du Vivant**

Exolysine, un facteur de virulence majeur de *Pseudomonas aeruginosa*

Thèse soutenue publiquement le **24 Octobre 2017**,
devant le jury composé de :

Madame Patricia RENESTO
Directeur de Recherche, TIMC (GRENOBLE), Présidente du Jury
Madame Olivera FRANCETIC
Directeur de Recherche, Institut Pasteur (PARIS), Rapportrice
Monsieur Alain FILLOUX
Professeur, Imperial College of London (LONDRES), Rapporteur
Madame Andrea DESSEN
Directeur de Recherche, IBS (GRENOBLE), Membre
Monsieur Stephen LORY
Professeur, Harvard Medical School (BOSTON), Membre
Madame Ina ATTREE
Directeur de Recherche, BIG (GRENOBLE), Directrice de Thèse

Acknowledgments

First of all, I would like to thank all the members of my jury. Especially Olivera Francetic and Alain Filloux to be my reporters, and Andrea Dessen, Patricia Renesto and Stephen Lory to be my examiners. I really appreciate that you have taken the time to read and evaluate my work. I address many thanks to Francoise Jacob-Dubuisson and Jean-Michel Jault, the members of my thesis advisory committee for their discussions and scientific ideas.

I thank the Doctoral School of Chemistry and Life Sciences of Grenoble and the French Ministry of Research for my thesis funding. Also, Jean-Jacques Feige, the director of the laboratory to welcoming me into the lab.

Je voudrais remercier du fond du coeur Ina, ma directrice de thèse, pour la transmission de ta passion pour la recherche, ton determinisme: "quand on veut, on peut!". Merci pour ta patience, tes corrections et ton exigence. Ainsi que pour toutes nos sorties extraprofessionnelles, les entraînements EKIDEN, les verres de Ubi chez Olivier... Un grand merci à Eric, mon co-directeur de thèse, pour ta patience, tes corrections, "ton remonte moral", ton enthousiame pour tout et les longues heures passées à l'Arrayscan. Merci à tous les deux pour cet équilibre durant ces trois ans.

Un grand merci à Sylvie et Mylène, pour vos précieux conseils aussi bien scientifiques que personnels. Merci à Michel pour ta persévérance pour les multiples "purif" d'ExlA, pour toutes ces discussions. Merci à toute l'équipe PBRC, pour les discussions, le soutien, les p'tis dej et les sorties.

I would like to thank Stephen Lory for welcoming me, three months in his lab and for his implication in this project. I would like to thank all his lab for the discussion and the beer parties. I would like to thank Fikadu Tafesse, for his confidence in the CRSIPR/Cas project, all the discussions, his availability and his support.

Je voudrais remercier aussi tous nos collaborateurs, Emmanuelle, pour ses conseils et sa disponibilité lors de ma formation Arrayscan. Odile et Déborah pour leurs précieux conseils en matière de CRISPR/cas !

Une thèse c'est long et ça ne se fait pas seule, alors un grand merci à mes deux complices Emeline et Alice, pour ces moments de soutien, ces moments potins, ces photos mythiques, et toutes ces sorties... Ce n'est que le début d'une belle amitié.

Merci à ma nouvelle famille adoptive, Paule et Jean, pour votre soutien et votre gentillesse. Merci à Coline et Lou pour ces soirées films "fétiches".

Un immense merci à toute ma famille, plus particulièrment à ma Maman, qui m'a toujours soutenue et sans qui je ne serai pas l à aujourd'hui. Merci à ma petite soeur, Laurène, pour ton soutien dans certains moments difficiles ainsi qu'à Jeremy. Merci à tous d'avoir cru en moi sans forcément comprendre ce que je cherchais. Mille

Merci.

Une thèse c'est aussi du stress et heureusement que vous avez tous été là pour me faire décompresser. Merci à Julie, ma binome depuis la L1, pour tes encouragements et ton soutien. Merci pour ton amitié. Merci à toi Erika, pour ta joie de vivre, tes encouragements et ton soutien sous plusieurs formes (sport et mojitos!). Merci Alex, pour ces soirées dejantées et tes precieux conseils...

Merci à tous les amis et copains plus au moins loin, Eric, Christophe, Matthieu, Jérémy, Alexandre et Manon, Karim et ceux que j'aurais pu oublier.

The last but not the least, Mon cher Quentin. Je te remercie d'avoir été présent dans tous les moments de cette aventure plus ou moins faciles, de m'avoir soutenue et aidé pendant ces années plus ou moins loin. With or without you... Mais on a réussi à deux. Une nouvelle vie à s'offre à nous à l'autre bout du monde.

Contents

List of Figures

List of Tables

List of Abbreviations

ADPRT Adenosine diphosphatase ribosyl transferase

AT Autotransporter

ATP Adenosine triphosphate

c-di-GMP Cyclic diguanylate monophosphate

C-ter C-terminal

CDC Centers for Disease Control and Prevention

CDI Contact-dependent growth inhibition

CDS Coding DNA sequences

CF Cystic fibrosis

GAP GTPase activating protein

GTP Guanosine triphosphate

IM Inner membrane

MDR Multi-drugs resistant

N-ter N-terminal

NETs Neutrophil extracellular traps

NLR Nod-like receptors

OM Outer membrane

ORFs Open reading frames

PAMP Pathogen-associated molecular Pattern

PFT Pore-forming toxin

PI Propidium iodide

PMNs Polymorphonuclear neutrophils

QS Quorum sensing

RBC Red blood cell

RGP Regions of genomic plasticity

SNPs Single nucleotides polymorphisms

SP Signal peptide

T2SS Type II secretion system

T3SS Type III secretion system

T4P Type IV pili

T5SS Type V secretion system

T6SS Type VI secretion system

TAAs Trimeric autotransporter adhesins

TLR Toll-like receptor

TPS Two-partner Secretion

Foreword

Pseudomonas aeruginosa is a human opportunistic pathogen responsible for severe acute and chronic infections. Different secretions systems and surface proteins are involved in the virulence of *P. aeruginosa*. Among them, *P. aeruginosa* possesses several Type V secretion systems (T5SS), responsible for the secretion of toxins or adhesins. Here we stidied, a group of strains defined as clonal outliers, that don't possess the Type III secretion system (T3SS) considered as the major virulence factor but employ a novel T5SS toxin for their virulence. This toxin is named Exolysin (ExlA).

The major objective of this work was to decipher the molecular mechanisms of the Exolysin action, in particular, the mechanism of pore formation and its action towards eukaryotic cells. Moreover, I attempted to identify bacterial and eukaryotic host factors that could participate in the Exolysin function.

The first part of the Results section concerns the characterization of the pore-forming activity of the Exolysin determined by biochemical approaches. In addition, I demonstrated, by a genetic screen of a transposon library, that the type IV pili are required for the Exolysin-dependent cytotoxicity. A part of this work was done in collaboration with the laboratory of Prof. Stephen Lory (Harvard Medical School (HMS, Boston)) and the screening facility of HMS (Article 1).

The second axis of my thesis was to understand the mechanism cell death and the host response after an infection with Exolysin-positive strains. Using bone marrow primary macrophage mutants and several *Pseudomonas* species, I demonstrated by live microscopy that ExlA induces pyroptosis cell death dependent of the NLRP3 inflamasomme. This work was performed in collaboration of the team of Thomas Henry from the International Center of Research in Infectiology (CIRI) (Lyon) and with the Chemogenomic facility of our Institute (CMBA, Grenoble) (Article 2).

Furthermore, I started identifying the host factors involved in the Exolysin-dependent cytotoxicity, by a genetic screen of a CRISPR/Cas9 RAW library. The CRISPR RAW library was obtained from the Prof. Fikadu Tafesse (Broad Institute, Boston). This work is undergoing and will be presented in a separate chapter.

Finally, I participated in different projects of the team. To characterize the first hypervirulent strain, CLJ, of the PA7-like group, we employed a multi-omics approach. I contributed to this work by preparing the samples for the proteomic analysis, analyzing CLJ genomes and participating in analyzing multi-omics data. The manuscript is in preparation.

I also performed the phylogeny tree analysis based on MLST and the genomic characterization of all the PA7-like stains studied by our team. These studies were published in Environmental Microbiology [1] and in Environmental Microbiology Report [2].

During my PhD, I developed competences in liposomes studies that allowed me to participate in two projects. The first concerns the characterization the activity of the phospholipase PlpD, a protein secreted through the type Vd secretion system of *P. aeruginosa*. This work, done in collaboration with Dr. Andrea Dessen's Laboratory was published in Journal of Molecular Biology [3]. The second project was done in collaboration with Dr. Charlotte Lombardi IBS, the aim was to study the activity of the T3SS translocon proteins PopB and PopD obtained by cell free methods against liposomes, compared to purified PopB and PopD proteins.

Moreover, my competences in high-content microscopy allowed me to work with Pierre Wallet on the Guanylate Binding Proteins (GBP) action in the *Francisella novocida* immune response [4].

Part I

Introduction

1

Virulence of the opportunistic pathogen *Pseudomonas aeruginosa*

Contents

Pseudomonas aeruginosa was described for the first time by Carle Gessard in 1882 [5].

Performing an experiment under the ultra-violet light, he described blue-green bacteria due to its pigments. The name *Pseudomonas aeruginosa* comes from the Greek composed of *"pseudo"* meaning imitation and *"monas"* meaning unity and the word of Latin origin *"aeruginosa"* meaning "vert-de-gris" (the color obtained from the copper oxidation). *P. aeruginosa* is a Gram-negative bacterium of the *Pseudomonadae* family and belongs to γ-proteobacteria. It is an aerobic bacterium and its optimal growth temperature is between 30°C and 42°C [6, 7].

P. aeruginosa is an opportunistic human pathogen causing serious, sometimes life-threatening infections. It colonizes diverse ecological niches including human tissues, causing a wide range of infections including pneumonia, bacteremia, keratitis, urinary tract infection, burns and surgical wound infections [8, 9]. In France, *P. aeruginosa* is the third pathogen causing hospital-acquired infections (9%) after *Escherichia coli* (26%) and *Staphylococcus aureus* (16%) [10]. The major sites of infections acquired in hospitals are the urinary and respiratory tracts; *P. aeruginosa* represents more than 50 % of those infections. This can be explained by its capacity to adapt easily to different environments and to invade different organs. Approximately 13% of *P. aeruginosa* infections are caused by multidrug resistant strains (Centers for Disease Control and Prevention (CDC) 2013[1]) and nosocomial *P. aeruginosa* infections have been identified as a worldwide healthcare issue[11]. The World Health Organization has recently pointed out to *P. aeruginosa* as a target of the highest priority for the development of new antibiotics[2].

The adaptability of *P. aeruginosa* to different environments or stress conditions encountered in the host can be attributed to its genomic diversity, its large arsenal of virulence factors and its important number of regulatory genes [9, 12–14].

1.1 Evolutionary dynamics of the *P. aeruginosa* genome

The genome of *P. aeruginosa* PAO1 strain, isolated from wound infection, was the first to be sequenced and its complete genome was published in 2000 [15]. The PAO1 genome size is 6.3 Mbp with 5570 predicted open reading frames (ORFs). Since

[1]https://www.cdc.gov

[2]http://www.who.int/mediacentre/news/releases/2017/bacteria-antibiotics-needed/en/

2000, several hundred clinical and environmental strains have been sequenced, listed and analysed on a website dedicated to *P. aeruginosa*[3]. Their genomes vary in size between 5.5 and 7 Mbp.

Whole genome comparison of *P. aeruginosa* strains shows that 90 % of the genome is composed of a set of conserved genes, coding for functions necessary for survival and metabolism, corresponding to the core genome. Across the core genome are integrated dispersed polymorphic strain-specific segments called regions of genomic plasticity (RGP) [16] also referred as the accessory genome. The genetic sequences occupying many contiguous RGPs are often referred to as genomic islands (>10 kb) or islets (<10 kb). The average size of the accessory genome of a *P. aeruginosa* strain was 727 kbp, representing 11.1% (with range of 6.9-18%) of the total genome. The accessory genome can be identified by an aberrant GC content, lower than in the core genome of *P. aeruginosa*, and by an insertion targeted to the tRNA of the core genome [16–18], suggesting that the accessory genome have been acquired by horizontal genetic transfer from other bacteria or phages [16].

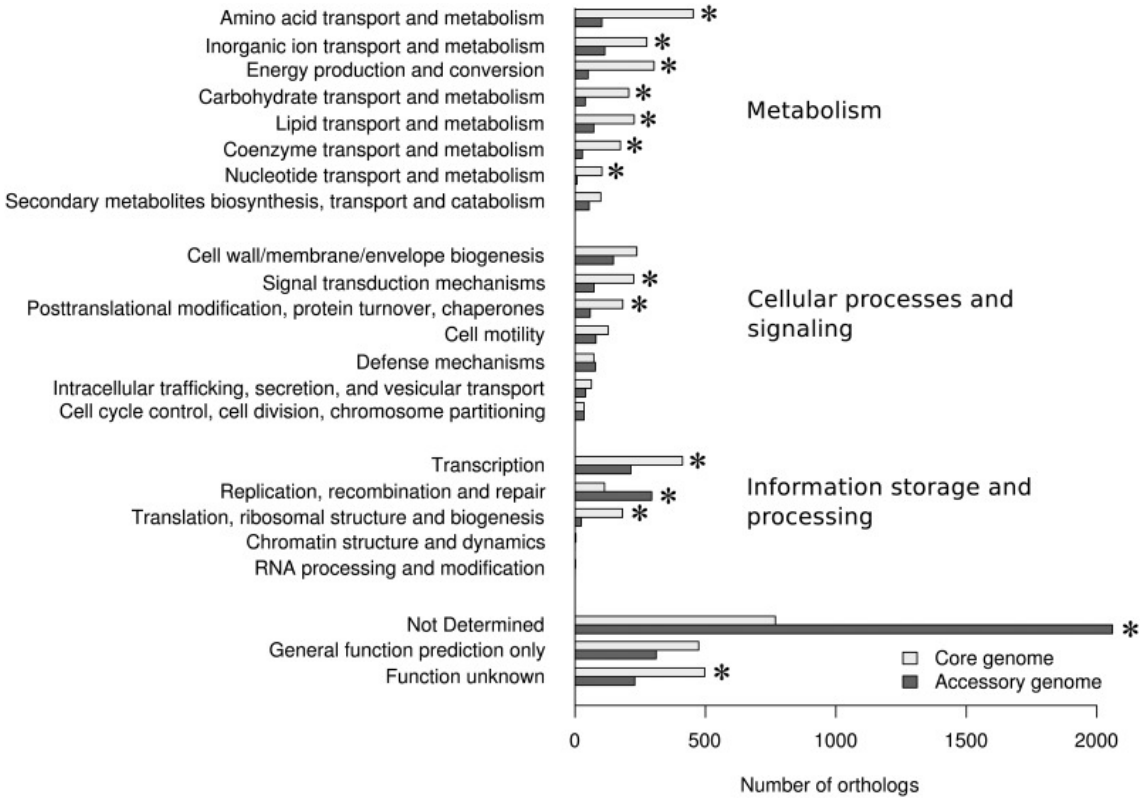

Figure 1.1. **Distribution of the core and accessory genes in *P. aeruginosa* strains.** (from [17])

[3]www.pseudomonas.com

The Figure 1.1 shows that the genes encoding proteins of central metabolism, cellular processes and signalling are found principally in the core genome. More precisely, 1,840 out of the 2,304 metabolic genes were found in the core genome (79.9%). In contrast, genes involved in replication, recombination and DNA repair are found in the accessory genome. Moreover, many genes (more than 2,000) found in the accessory genome have no determined function yet [17]. Of importance, the accessory genome carries genes coding for virulence factors, proteins related to antibiotic resistance, survival and persistence of *P. aeruginosa*, during host infection [19].

PA7 is a non-respiratory clinical isolate collected in Argentina showing a highly divergent genome from the well-characterized strains as PAO1, LESB58 and PA14 classical strains [20]. Its 6.5 Mpb genome includes 6286 open reading frames (ORFs) representing 90 % of the total genomic DNA. The G+C content of the genome (66.5 %) is similar to those from PAO1, LESB58 and PA14. PA7 presents more coding DNA sequences (CDS) for the functions of the DNA replication, recombination and repair than the classical strains. This is predominantly due to the large number of additional transposase and integrase genes present in the genomic islands [20].

The genome of PA7 shares 93 % of identity on gene level with that of classical strains and is considered as a taxonomic outlier. The major genomic feature of the PA7 strain is the absence of the entire 36-genes locus encoding the Type III secretion system (T3SS) (PA1690-PA1725), considered as the major virulence factor. In addition, genes encoding effectors exported by T3SS ExoS, ExoT, ExoY and ExoU are also absent from the PA7 genome [20]. Several other strains have been sequenced and referenced in the Pseudomonas database as being PA7-like. The phenotypic and genomic characterization of these PA7-like strains has been done by our team, and will be developed in Section 1.6.

1.2 *P. aeruginosa* causes acute and chronic infections

P. aeruginosa causes acute and chronic infections involving a balance between two lifestyles: "mobile" versus "sessile" (Figure 1.2) [21–23] .

Usually in acute infection, *P. aeruginosa* displays swimming and swarming motility using extracellular appendages, the flagellum and the type IV pili [24–26]. The motile bacteria are associated with a highly virulent phenotype [27]. *P. aeruginosa* employs several toxins including the effectors of the T3SS [28] and proteases, such as ToxA [29], AprA [30] and LasB [31] to target host cells. The

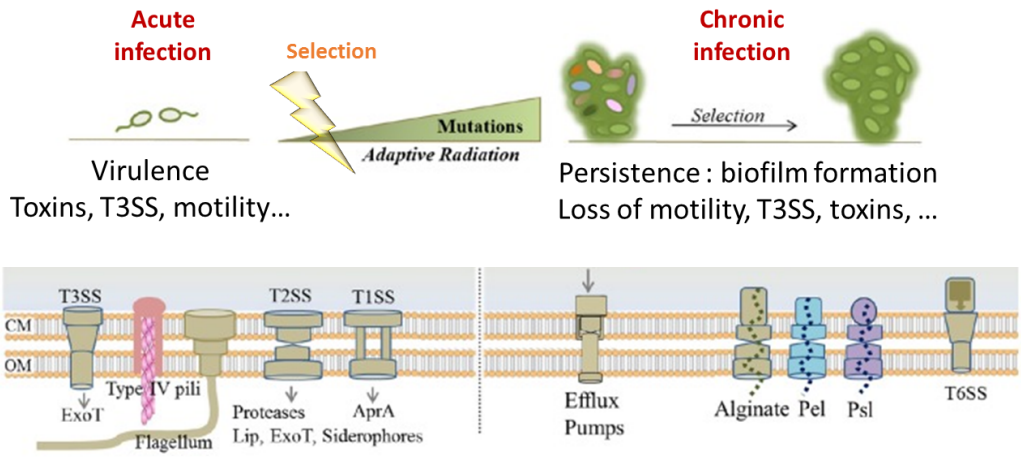

Figure 1.2. Acute vs chronic infections by *P. aeruginosa*. Factors needed for acute and chronic infections and the phenotype evolution of the strains shown (adapted from [9]). The acute infection is synonym with virulence and motility of the bacteria. In contrast, during chronic infections, bacteria become sessile and loose their aggressive virulence determinants.

expression of these so-called "acute virulence factors" is reduced when shifting to a chronic infection stage, which is characterized by biofilm formation due to the overexpression of extracellular polysaccharides.

Biofilms confer resistance to phagocytosis, oxidative stress, nutrient restrictions, interspecies competitions and antibiotic treatment. *P. aeruginosa* produces three exopolysaccharides, alginate, PsI (stand for Polysaccharides Synthesis Locus) and Pel (for Pellicule) [32, 33]. Alginate is the major component of so-called "mucoid" biofilms, which is the hallmark of chronic infection in (CF) patients, associated with a poor prognosis[34, 35]. This mucoid phenotype is due to the overexpression of alginates due to mutations in *mucA*. MucA is a transmembrane protein with a cytoplasmic portion sequestering the alternative RNA polymerase AlgU [36]. Mutations in *mucA* lead to constitutive expression of *algU* and its large regulon including alginate biosynthesis genes [37–39]. In addition, AlgU responds to general cell envelope stress and plays a role in maintenance of envelope homeostasis, and regulation of metabolism, motility and virulence [37–39].

One of the best characterized regulators of this transition between acute and chronic infection is the two-component system GacS-GacA. The phosphorylated GacA activates the transcription of two sRNAs RsmY and RsmZ, leading to the inhibition of RsmA, which is a RNA-binding protein acting on post-transcriptional

regulation [40, 41]. RsmA binds to mRNAs of different genes (*psl*, *pel*, (T6SS) and degrades them; when RsmZ and RsmY are overproduced, they "titrate" RsmA and releave this repression, so there is more mRNAs of those operons and more products.

Recent studies showed the variation in clonally related isolates in chronically infected CF patient lungs. The *P. aeruginosa* isolates occupying different regions of the lung had evolved independently, and they differ in phenotypic characteristics such as nutritional requirements, antibiotic resistance, and virulence [42]. Thus divergent sublineages co-exist within individual patients with CF [43].

The virulence of *P. aeruginosa* is multifactorial and the bacteria possess an arsenal of virulence factors that facilitate successful infection and colonization in a wide range of environments. In a mouse model, it was shown that the T3SS, with elastase, is one of the main virulence factors associated with pneumonia [44]. Moreover, the prevalence of the T3SS-positive strains is significantly higher in acutely infected patients than in chronically infected CF patients [45].

1.3 The Type III Secretion system is the major virulence factor of classical strains of *P. aeruginosa*.

1.3.1 Structure and regulation of the T3SS

The T3SS machinery (also called injectisome) is a needle-like apparatus, capable of crossing three membranes and dedicated to injection of exotoxins directly in the cytoplasm of host cells [46].

The T3SS machinery is composed of more than 20 proteins, many of them form oligomers and are membrane-embedded. There are four principal components: the sorting platform, the basal body inserted in IM and OM of the bacteria, an extracellular needle and the translocon, inserted in the host cell membrane (Figure 1.3). In *P. aeruginosa*, 36 genes encoded in five operons are involved in the biogenesis and regulation of the T3SS whereas genes encoding the effectors proteins (*exoT*, *exoY*, *exoS* and *exoU*) are scattered over the chromosome [46].

The sorting platform is the cytoplasmic base of the T3SS. PscN is the ATPase (ATP) of the T3SS and is localized in the cytoplasm. It has been proposed that PscN is involved in the production of energy needed for the secretion of the proteins. PscN interacts with PscK and the regulator PscL inhibiting its activity.

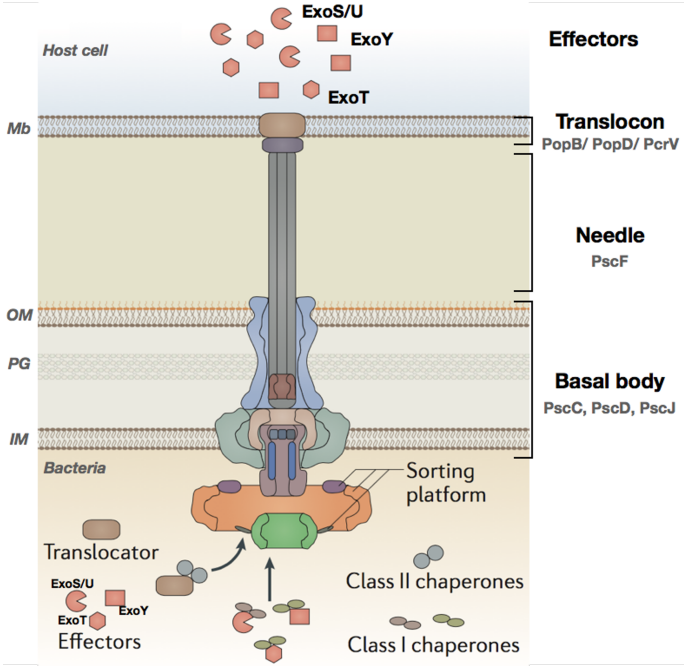

Figure 1.3. **Structure of the T3SS.** The T3SS consists of a needle complex, translocating apparatus, and effector toxins that are translocated directly from the bacterium to the host cell cytosol [47].

This complex is linked to a cytoplasmic ring constituted of PscQ [48, 49]. The basal body is mainly composed of three proteins, named PscC, PscD and PscJ. The needle is a filament that forms an 80 nm long channel with an outer diameter of 8 nm and an inner diameter of 2 nm. The needle is composed of multiple copies of PscF [50]. The translocon is composed of three proteins PopD, PopB and PcrV [46, 51–53]. PopB and PopD are inserted in the host cell membrane and form a pore around 3 nm that provokes a cell death called "oncosis" due to swollen appearance of infected cells [54]. PcrV links the needle complex to the PopB/PopD translocation pore, forming part of a continuous conduit through which effector proteins move from the bacterial cytosol to the host cell cytosol.

The regulation of the T3SS takes place at two different levels, at the transcriptional level of T3SS genes and at the level of secretion itself. These two regulations are linked: the transcription is induced upon the activation of the secretion process [55, 56], allowing the transcription of the T3SS genes when they are the most needed, following contact with host cells. The regulation involves a mechanism of "catch and release" of four majors regulators ExsA, ExsC, ExsD and ExsE. Under conditions that prevent the secretion, ExsA is bound to ExsD, an "anti-activator", which inhibits

the ExsA-dependent transcription. ExsC is an "anti-anti-activator" which inhibits the ExsA-ExsD interaction by sequestrating ExsD and the released ExsA can bind to the target promoters. The coupling of transcription with secretion is achieved by the export of ExsE through the T3S-needle into the host cell cytoplasm and the subsequent release of ExsC [56–58]. *In vitro*, the T3SS can be activated by a calcium depletion.

1.3.2 Effectors of the T3SS

Different strains of *P. aeruginosa* have different combinations of genes encoding the effectors, and can be divided into two groups: those expressing either *exoS* or *exoU*, generally *exoS* and *exoU* are mutually exclusive. The first group represented by PAO1, LESB58 or PAK express ExoS, ExoT and ExoY, and in the second group, PA14, PA103 and PP34 express ExoT, sometimes ExoY, and ExoU. The clinical isolates possessing *exoS* are the majority and represent 80% of the strains compared to 20% for the ones that are *exoU* positive [59].

ExoS is a bifunctional toxin that possesses two domains with distinct activities, a GTPase activating protein (GAP) domain and an adenosin diphosphatase ribosyl transferase domain (ADPRT) (Figure 1.4).

The GAP (GAP) domain of ExoS (96-233 residues) targets the small GTPase ((GTP) proteins Rho, Rac, Cdc42 in epithelial cells required for the stability of actin cytoskeleton. The inactivation of these GTPase proteins by the GAP domain of ExoS leads to the disruption of the host cell actin cytoskeleton, cell rounding and cell death [46].

The ADPRT (ADPRT) domain located from residues 233 to 453 catalyzes the transfer of ADP-ribose to other proteins in the host cell. Its main targets are the GTPase proteins Ras, Rac, Cdc42. Ras is linked to the cellular proliferation and to actin cytoskeleton structure. In addition, ADPRT blocks the reactive oxygen species burst in neutrophils by ADP-ribosylation of Ras, thereby preventing the activation of phosphoinositide-3-kinase (PI3K), which is required to stimulate the phagocytic NADPH-oxidase [60]. This domain is essential for the persistence of *P. aeruginosa* through escaping the immune system. The ADPRT domain contributes to disruption of the pulmonary-vascular barrier during pneumonia and leads to the rapid expansion of cell-injected region [61].

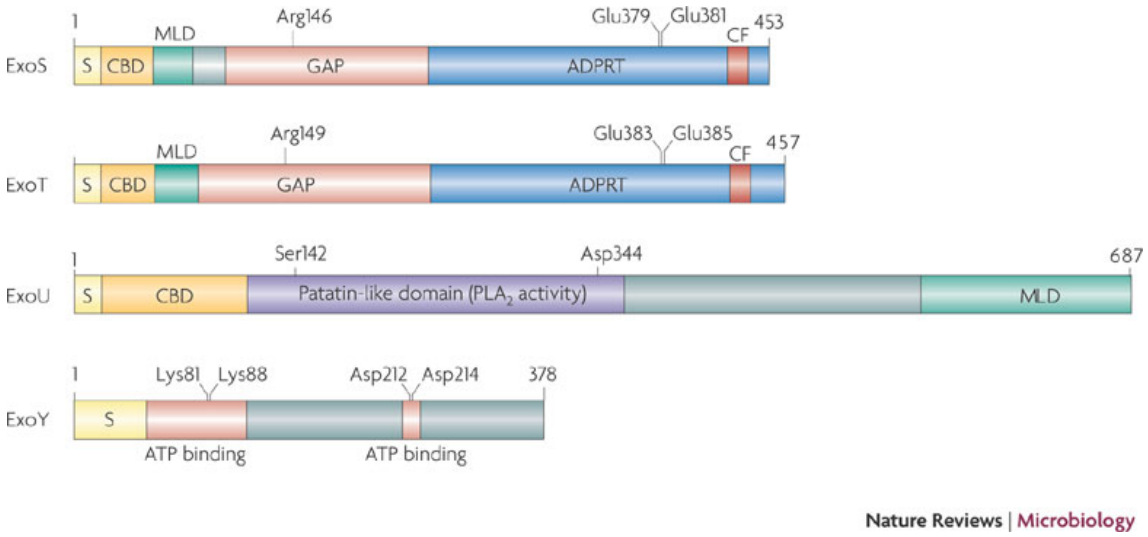

Figure 1.4. **Modular domains of ExoS, ExoT, ExoU, and ExoY.** ExoS is a bi-functional toxin that has both GAP and ADPRT activity. Arg146 is required for GAP activity and both Glu379 and Glu381 are required for efficient catalytic addition of the ADP-ribose moiety of NAD+ to substrate. ExoT is closely related to ExoS. Arg149 is required for the GAP activity of ExoT 76 and residues Glu383 and Glu385 are crucial for its ADPRT activity. ExoU contains a patatin-like domain necessary for PLA2 activity. Residues Ser142 and Asp344 are required for this activity. ExoY is an adenylate cyclase. Residues Lys81, Lys88, Asp212, and Asp214 are required for its activity and are thought to be necessary for interactions between ExoY and ATP. S, secretion signal; CBD, chaperone binding site; MLD, membrane localization domain; GAP, GTPase activating protein activity; ADPRT, ADP-ribosyl transferase activity; PLA2, phospholipase A2; CF, cofactor binding site, from [46].

ExoT shares 76% of identity with ExoS and is composed of two domains, GAP and ADPRT (Figure 1.4). The GAP domain targets the same GTPases as ExoS protein and triggers the mitochondrial intrinsic pathway leading to apoptosis [62].

ADPRT domain activity transforms the focal adhesion adaptor protein Crk of the host cell into a cytotoxin that induces a form of programmed cell death known as anoikis, which occurs in cells when they detach from the surrounding extracellular matrix. The effect of ExoT on endothelial cells is similar to that of ExoS [63]. In acute pneumonia model, ExoT does not play a major role, but in the keratitis model, it can promote neutrophil apoptosis [64].

ExoU is encoded together with its chaperone, SpcU, in the PAPI-2 in PA14. PAPI-2 is an 11-kb-integrative region conjugative element (ICE) probably acquired via horizontal gene transfer, inserted close to the tRNA-Lys gene (PA0976.1). Its acquisition was shown to increase the virulence of the PA14 *P. aeruginosa* strain [65,

66]. ExoU is a 74 kDa protein containing a patatin-like domain with phospholipase A2 (PLA2) activity (Figure 1.3) [67]. ExoU, after its injection, is rapidly associated to the host cell membrane and leads to the plasma membrane disintegration. The toxicity of ExoU has been demonstrated *in vitro* on many cell types including epithelial and endothelial cells [68], neutrophils, and macrophages.

In vivo, ExoU is the most toxic of the T3SS-effectors. ExoU could also contribute to the pathogenesis of lung injury as it induces a tissue factor-dependent procoagulant activity in airway epithelial cells [69], vascular hyperpermeability, platelet activation, and thrombus formation during *P. aeruginosa* pneumonia and sepsis. In a model of acute pneumonia, the alveolar macrophages are the first targets of ExoU [70].

ExoY is a toxin with nucleotidyl cyclase activity involved in the production of cGMP and cUMP (Figure 1.4) [71, 72]. Its effect on cells is still a matter of debate. Some authors showed that ExoY has no important impact on epithelial cells [63, 73], whereas others showed an increase of the Tau protein phosphorylation, leading to microtubule disassembly [74]. Moreover, a recent study showed that ExoY is an F-actin binding protein and that F-actin is a potent activator of ExoY, able to stimulate its adenylate and guanylate cyclase activity more than 10,000 fold [75].

The role of ExoY during infection still needs to be elucidated. ExoY synthesizes numerous cyclic nucleotides (cCMPs and cUMP). cUMP is the most prominent cNMP generated in the lungs of mice infected with ExoY-overexpressing *P. aeruginosa*. cUMP was detectable in body fluids, suggesting that cUMP is not rapidly degraded and thus may interfere with the second messenger signalling of the host [76].

Recently, some T3SS-positive strains highly resistant to antibiotics have emerged. The prevalence of *exoU+* strains among the multi-drugs resistant (MDR) strains (40.2 %) is higher than in non-MDR (25 %) [77]. The *exoU+* strains were shown to be more resistant to fluoroquinolone, carbapenems and gentamicin than *exoS+* strains. These isolates have a mutation in the *gyrA* gene and exhibit an efflux pump overexpression phenotype. Although, there is no clear genetic explanation for this phenotype, clinical *exoU+* MDR isolates are more dangerous especially for immunocompromised patients.

The role of the translocation apparatus may not be limited to transport of effector proteins; the translocation pore by itself may be sufficient to cause the death of host cells either directly through pore-mediated increase in membrane permeability or indirectly through the activation of cellular defense responses. The T3SS has

been shown to activate NLRC4 inflammasome [78]; in particular, the inner rod PscI and the needle subunit PscF of the toxin-injection machinery T3SS [79]. Activation of the inflammasome and caspase-1 results in IL-1β and IL-18 production and cell death by pyroptosis [79–84]. *P. aeruginosa*-triggered inflammasome activation induces autophagy, which seems to be associated with defective killing of the bacteria. Moreover, in an acidic environment, as is typically the case within bacterial infection foci, *P. aeruginosa* T3SS triggers enhanced inflammasome activation of immune cells. Of note, the pH of the CF lung is more acidic than in healthy individuals [77]. These findings can explain why CF patients are more vulnerable to *P. aeruginosa* lung infection, the lower pH being associated with more important inflammasome activation and decreased bacterial clearance.

The virulence factors employed by *P. aeruginosa* during infection are multiple, and exert different roles to successfully colonize host tissue, disseminate and avoid the host defense mechanisms. Tools and strategies of bacterial genetics have been extensively exploited for precise determination of the requirement for particular gene products during the different steps of infection process. Several studies based on DNA microarrays such as signature-tagged mutagenesis [85] or transposon site hybridization [86] have demonstrated the importance of individual genes in the infection process and showed that genes involved in motility are key virulence determinants. Moreover, a genome-wide identification of genes important for PA14 fitness was performed employing high-throughput sequencing of transposon libraries (Tn-seq). In this work, Skurnik et al., developed a mouse model to study the gastrointestinal (GI) tract colonization and the systemic dissemination. Three functional classes of genes were found to be important: "Transport of small molecules", "Motility and Attachment" and "Chemotaxis". The examination of specific genes with transposon insertions revealed that many are involved in the formation of the type IVa pili [87].

1.4 Role of the Type IV pili in *P. aeruginosa* virulence

The Type IV pili (T4P) are long, polar and thin appendages found at the surface of bacteria, playing a role in the adherence, cell-cell aggregation, biofilm formation and motility. They play a role in the initiation of the immune response. In *P. aeruginosa*, there are two types of T4P, a and b characterized by differences in the major and minor pilin subunits. Type IVb pili are conjugative pili allowing the transfer of DNA

between bacteria. Their role in *P. aeruginosa* virulence remains still unknown and will not be described in this Chapter.

1.4.1 Type IV pili assembly machinery

Pili are flexible filaments with a diameter estimated between 5 and 8 nm [88]. Figure 1.5 presents the organization of the type IV pili.

There are over 40 genes, distributed among the genome, involved in the assembly and the regulation of the T4P. Type IV pilus apparatus assembly can be divided in four interdependent sub-complexes, with most components located in the inner membrane (IM) [89].

The outer membrane (OM) subcomplex consists of the secretin, a massive and highly stable dodecamer of PilQ subunits, and its lipoprotein pilotin PilF. PilF is responsible for the correct localization and oligomerization of PilQ in the OM. PilQ, provides an OM channel for the pilus fiber to exit the cell [89–92] .

The motor subcomplex comprises PilB, PilC, PilT and PilU proteins and plays a role in the assembly of the pilus. PilB is an hexameric ATPase required for the pilus assembly. PilT and PilU are PilB-like ATPases required for the pilin depolymerization and the adhesion to eukaryotic cells [93, 94].

The "alignment" subcomplex mediates the connection between the IM motor and the OM subcomplexes to ensure the correct position of the pilus to the bacterial surface. It is composed of four proteins PilM, PilN, PilO, PilP. PilM is cytoplasmic, actin-like protein bound to PilN. PilP is an IM lipoprotein that forms a heterodimer with PilN and PilO and interacts with PilQ secretin [89, 95].

The pilus is the most dynamic subcomplex of the four because it is repeatedly assembled and disassembled. It is composed of the major pilin PilA and minor pilins FimU, PilV, PilW, and PilX. Both major and minor pilins are highly conserved. A large non-pilin protein PilY1 is the tip of the pilus and plays an important role for the pilus function, including the adherence [91, 96, 97].

The major pilin PilA is O-glycosylated. In *P. aeruginosa*, two distinct O-glycosylation systems have been reported. The first is mediated by TfpO (PilO) that adds an O-antigen unit synthesized by the LPS pathway of the C-ter Ser148 of the PilA (Figure 1.6) [98].

The second pilin glycosylation system was identified in PA7, which lacks *tfpO* gene. However, it presents an unusual glycosylation at multiple Thr and Ser residues and are potentially α-1,5-linked arabinofuranose (Figure 1.6). This glycosylation is

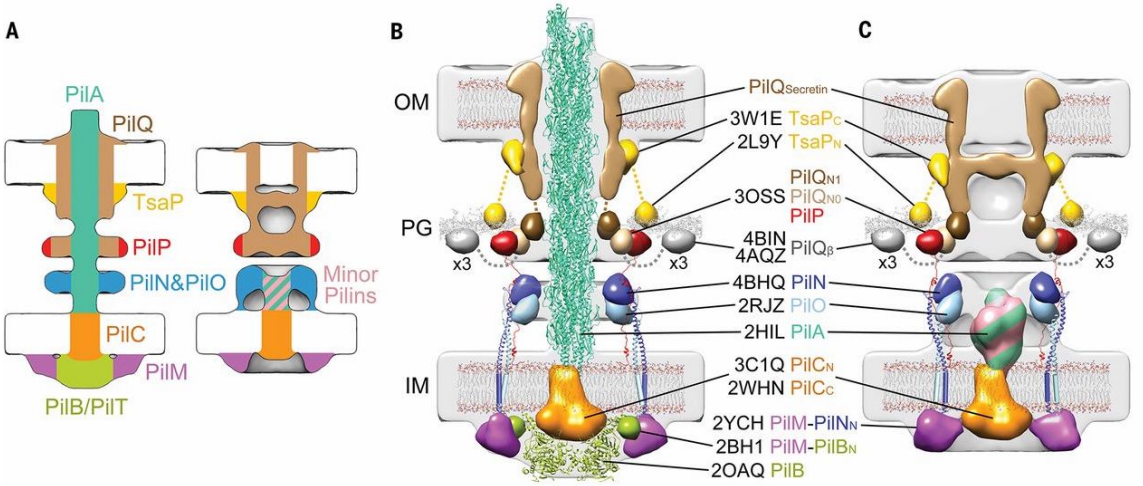

Figure 1.5. **Type IV pili.** (A) Summary schematics showing the component locations identified in the piliated and empty T4PM basal body structures. (B and C) Central slices of the architectural models of piliated and empty T4PM basal bodies, respectively, in which atomic models of T4PM components are placed in the *in vivo* envelopes according to the component maps in (A) and previously reported constraints and filtered to 3-nm resolution. Models of each component are colored as in (A), with the transmembrane segments of PilN and PilO shown as cylinders; "x3" indicates three AMIN domains per PilQ monomer, only one of which is shown. Note that the empty T4PM basal body is shown with five PilA major pilin subunits in the short stem; however, the short stem likely also contains minor pilins [91]

mediated by TfpW. The lack of TfpW leads to fewer surface pili and reduced motility, suggesting that the glycosylation is involved in pilus assembly and dynamics [99].

1.4.2 Regulation of the IV pili

In *P. aeruginosa*, the transcription of the *pilA* gene is controlled by an alternate sigma factor RpoN (σ54) and a two-component system PilR-PilS in an autoregulatory model [100, 101]. When levels of intracellular PilA are low, *pilA* transcription is significantly increased [89]. Depletion of PilA in the IM leads to fewer PilA-PilS interactions. In the absence of such interactions, PilS adopts a kinase conformation and phosphorylates PilR, activating *pilA* transcription until intracellular PilA inventory increases. Conversely, when PilA levels are high, *pilA* transcription is dramatically reduced. It is also possible that PilS-PilR could impact PilA levels by regulating the expression of additional factors that indirectly impact *pilA* expression, contributing to the difference in magnitude between transcription and protein levels[89].

The expression of the Type IV pili is controlled in part by the cyclic AMP (cAMP)-binding protein called Vfr (Virulence factor regulator). Vfr regulates the expression

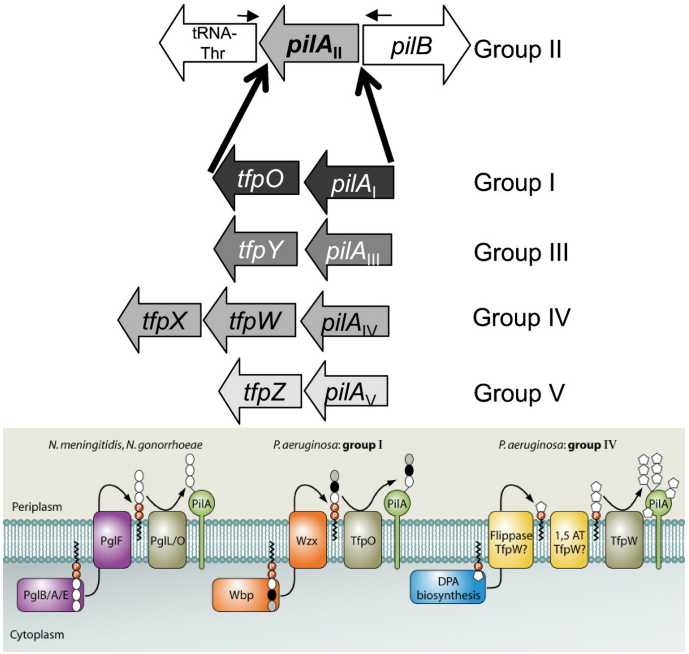

Figure 1.6. **Type IV pili glycosylation systems.** In *P. aeruginosa* , group I pilins are modified at the C-terminal Ser148 by TfpO (PilO) with an undecaprenol-linked O-antigen subunit generated by the Wbp enzymes of the lipopolysaccharide pathway (orange) and are flipped to the periplasmic face of the membrane by the O-unit flippase, Wzx (orange). Group IV pilins are modified at multiple Ser and Thr residues by monomers, dimers, and longer polymers of D-arabinofuranose synthesized by cytoplasmic enzymes on a lipid carrier to form decaprenol-arabinofuranose (DPA) (blue), polymerized into 1,5-linked homopolymers, translocated to the periplasm by an unknown enzyme(s), and attached to the pilin by TfpW. TfpW is significantly larger than TfpO (694 versus 461 amino acids) and may be responsible for both the flippase and 1,5-arabinosyltransferase (AT) functions (yellow) in the group IV system [98].

of genes encoding subcomplex (*pilMONPQ*) and minor pilins (*fimU-pilVWXY1*). cAMP is synthesized by two adenylate cyclases CyaA and CyaB. Mutants lacking both *cyaA* and *cyaB* exhibit reduced virulence factor expression and are severely attenuated in a mouse model of acute pneumonia [102]. *P. aeruginosa* mutants defective in cAMP synthesis or lacking *vfr* are nearly identical, suggesting that Vfr activity is dependent on cAMP availability [103].

1.4.3 Role of the Type IV pili in virulence

The injection of purified pili proteins lead to a local inflammation. Indeed, mutants defective for the Type IV pili present an enhanced GI colonization, suggesting that during this stage of infection the pilus structure is a potential target of early

recognition by host defense mechanisms, promoting clearance of bacteria. It was shown that type IV pilin is a novel activator of the inflammasome acting as pattern recognition receptor of the innate immune system.

Type IV pili are involved in the virulence by exerting different functions such as the adherence to cell surface or motility.

The most frequently reported function of the Type IV pili is adherence to a diverse range of surfaces, from glass, plastics to various host tissues. The major pilin subunits can act as the adhesive component [104]. Pilin was shown to bind to its receptors, the glycosphingolipid asialo-GM1, at the apical surface of the respiratory epithelial cells promoting the initial attachment of bacteria. At the basal surface of the cells, Type IV pili interact with integrins, mediated by the PilY1 that harbors an "RGD" motif [105]. Adherence plays a crucial role in the first step of colonization, biofilm formation and microcolony formation. Type IV pili are also necessary for the injection of T3SS toxins, promoting a contact between the bacteria and the cells [106–108]. The adhesin function of the pili, mediated by PilY1 is essential for the T3SS-toxin injection. It has been demonstrated that the injection of the T3SS was still possible after a substitution of the Type IV pili adhesin PilY1, by the nonfimbrial adhesin pH 6 antigen of *Yersinia pestis*.

Many Type IV pili-expressing strains exhibit pilus-mediated twitching motility, which is the best characterized type of movement associated with the T4P and is due to the retractile properties of pili. Twitching occurs on moist surfaces of moderate viscosity. Mutants lacking PilT or PilU, which are two ATPases of the system, are unable to twitch [109]. The second motility is the swarming, involving cooperation between the flagellum and the Type IV pili. The Type IV pili might be required for the coordinate movement of the bacteria by enhancing the bacterial interaction. The primary functions of these two type of motility are the exploration of surfaces and the dispersion of bacteria. Finally, it has been proposed that Type IV pili act as "mechanical sensors" during the infection, detecting the surfaces and enhancing the expression of virulence factors [110].

Pili can further contribute to the virulence and *P. aeruginosa* adaptation by mediating of pilus-dependent phage infection [111]. Indeed there is evidence that temperate phages strengthen selection for mutations in type IV pilus associated genes, accelerating the evolutionary loss of type IV-pilus dependent motility presumably to avoid superinfection and subsequent lysis by phages which infect *via* the type IV pilus. A recent Tn-Seq of *P. aeruginosa* PA14 shows that mutations in type IV pilus genes increase bacterial fitness in the murine lung [112]. Moreover, loss of

both motility and quorum sensing (QS) functions are known to frequently evolve in *P. aeruginosa* chronic infections of the CF lung.

In *P. aeruginosa* the second factor mediating motility and attachment is the flagellum. Surprisingly, in the model of GI tract colonization and systemic dissemination, strains with Tn insertion in gene encoding components of the flagellum was also positively selected.

1.5 Role of the flagellum in virulence

P. aeruginosa has a single polar flagellum of 15-20 μm long that provides the ability to swim in a liquid environment and to swarm in a semi-solid surface. The flagella play a critical role in the pathogenesis through motility and adhesion to cells.

The flagellum is constituted of three parts (Figure 1.7): (i) the rotor embedded in the membrane and playing a role in the rotation of the flagella (ii) the hook, and (iii) the filament which is principally composed of flagellin (FliC) subunits.

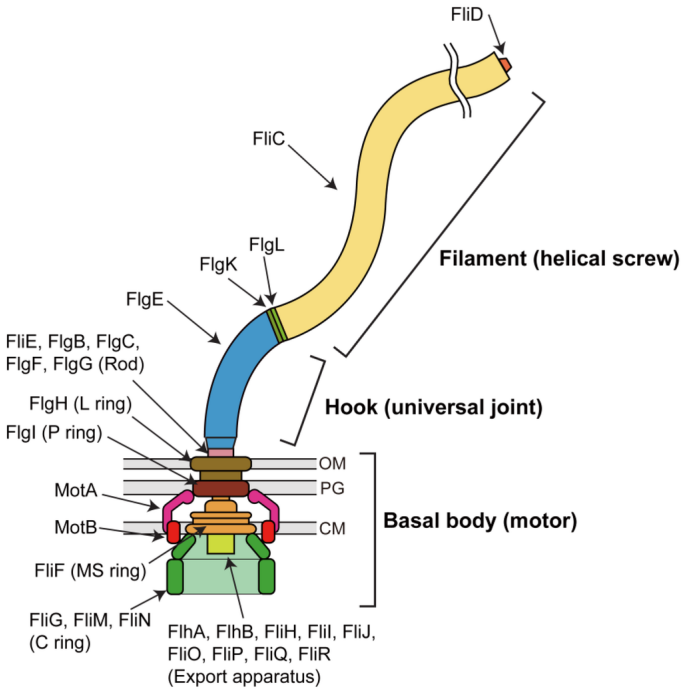

Figure 1.7. **Flagellum.** The flagellum consists of the basal body, which acts as a reversible rotary motor, the hook, which functions as a universal joint and the filament, which works as a helical screw. OM, outer membrane; PG, peptidoglycan layer; CM, cytoplasmic membrane.

Flagellum is typically expressed in environmental isolates of *P. aeruginosa* and in early clinical isolates of CF patients [24]. Loss of the flagellum is one of the charac-

teristic changes accompanying the adaptation of *P. aeruginosa* in CF airways[25, 26]. Biofilms are dynamic structures, and motile, flagellated bacteria likely break free from biofilms and are possibly detected by polymorphonuclear neutrophils (PMNs).

Flagellum is involved in two types of motility, the swimming and the swarming, in function of the viscosity of the media. The swimming motility happens in a low viscosity medium. The rotation of the hook triggers propulsion of the bacteria, forward (clockwise rotation) or backward (anti-clockwise rotation) in function of the orientation of the rotation. This type of motility is the most rapid, the velocity can reach several micrometres per seconds. The swarming motility occurs in semi-solid medium. The swarming also depends on others factors such as the quorum sensing or biosurfactant production, and Type IV pili as described before [113–115]

Swimming motility triggers the formation of neutrophil extracellular traps (NETs) [116] and phagocytosis by neutrophils, the first line of defense in human infections. The flagellum is powered by a complex motor containing dual stator units, MotAB and MotCD, generating the torque used to turn the flagellar rotor. Both *motAB* and *motCD* mutants are severely impaired for NET release by human PMNs. These data highlight the importance of swimming motility in *P. aeruginosa* virulence [116] and imply that flagellum also contributes to bacterial virulence. *P. aeruginosa*-induced NET release is independent of the Toll-like receptor 5 (TLR5) (TLR) in both human and murine PMNs [25, 33].

TLR5 is expressed in airway epithelial cells and in several innate immune cell types including PMNs [117]. TLR5 is the main receptor mediating activation of airway epithelial cells by *P. aeruginosa* via flagellin (FliC) recognition [118], which is detected as a Pathogen-Associated Molecular Pattern (PAMP). The TLR5-flagellin interaction is a major mediator of airway inflammation in CF by the production of pro-inflammatory cytokines and mucin, the major componemt of respiratory mucus [119] that enhances the clearance of the pathogen [120].

The flagellum also plays an important role in the adhesion of the bacteria in the early steps of infection [121]. Flagellum mediates bacterial binding to N-glycan at the apical surface of polarized epithelium. At the basolateral pole, flagellum binds heparan sulfate leading to the activation of EGFR and the PI3K/Akt pathways [122].

In addition to T3SS, Type IV pili and flagella, other molecules are important for *P. aeruginosa* virulence. For example, the LPS is recognized by the host *via* TLR4. It has been reported that the LPS-TLR4 binding stimulates the production of pro-inflammatory cytokines [123]. In a chronic murine pulmonary infection model, IL-17 cytokine signalling was found to be essential for mouse survival and the

prevention of chronic infection with *P. aeruginosa*. These examples demonstrate the context-dependent, balance of harm and benefit of host defense mechanisms against *P. aeruginosa* [124, 125].

1.6 *P. aeruginosa* renews its virulence factors

As mentioned in the first section, a new clade of strains lacking the T3SS has been characterized. However, this does not imply that these strains are innocuous. These strains harbor the recently discovered two-partner secretion system ExlAB, a new Type II secretion system and PumA.

Exolysin

Exolysin (ExlA) has been first identified by comparative proteomics in the supernatant of a clinical isolate CLJ1, collected from a patient suffering from a hemorrhagic pneumonia [126]. ExlA shares 35% of identity with ShlA, the hemolysin of *S. marcescens*. Moreover, ExlA is encoded by *exlA* in operon with *exlB*, encoding an OM porin, suggesting that ExlBA form a novel Two Partner Secretion (TPS) System. CLJ1 exerts its virulence through the activity of ExlA. *In vitro*, ExlA provokes a rapid plasma membrane rupture on epithelial, endothelial cells and macrophages, leading to their death. The mechanism of action of ExlA, constitutes the main part of my work and will be developed in the Results section of this manuscript.

Up to date, 30 *exlA*-positive strains have been sequenced. The phenotypic and genomic characterizations of *exlA*-positive strains were done by Emeline Reboud, a PhD student in our team and were presented in the review paper presented here. For these two manuscripts [1, 2], I performed the phylogenetic analysis of all the strains, constructed the tree based on the MLST analysis (Figure 1) and performed analysis of major virulence gene content by genome comparison (Table1).

A phylogenic analysis based on the single nucleotides polymorphisms (SNPs) from the core genome of *P. aeruginosa* strains (*exlA*-positive strains and 97 classical PAO1 and PA14 strains) showed the high genomic diversity of the *P. aeruginosa* strains (Figure1.8). *exlA*-positive strains are probably more divergent between them, than the group of the PAO1- or PA14-like strains. Indeed, although most of the strains group together with PA7 in the group of taxonomic outliers, some other strains (for example CF_PA39) are closer to groups populated by strains possessing T3SS, such as PA14.

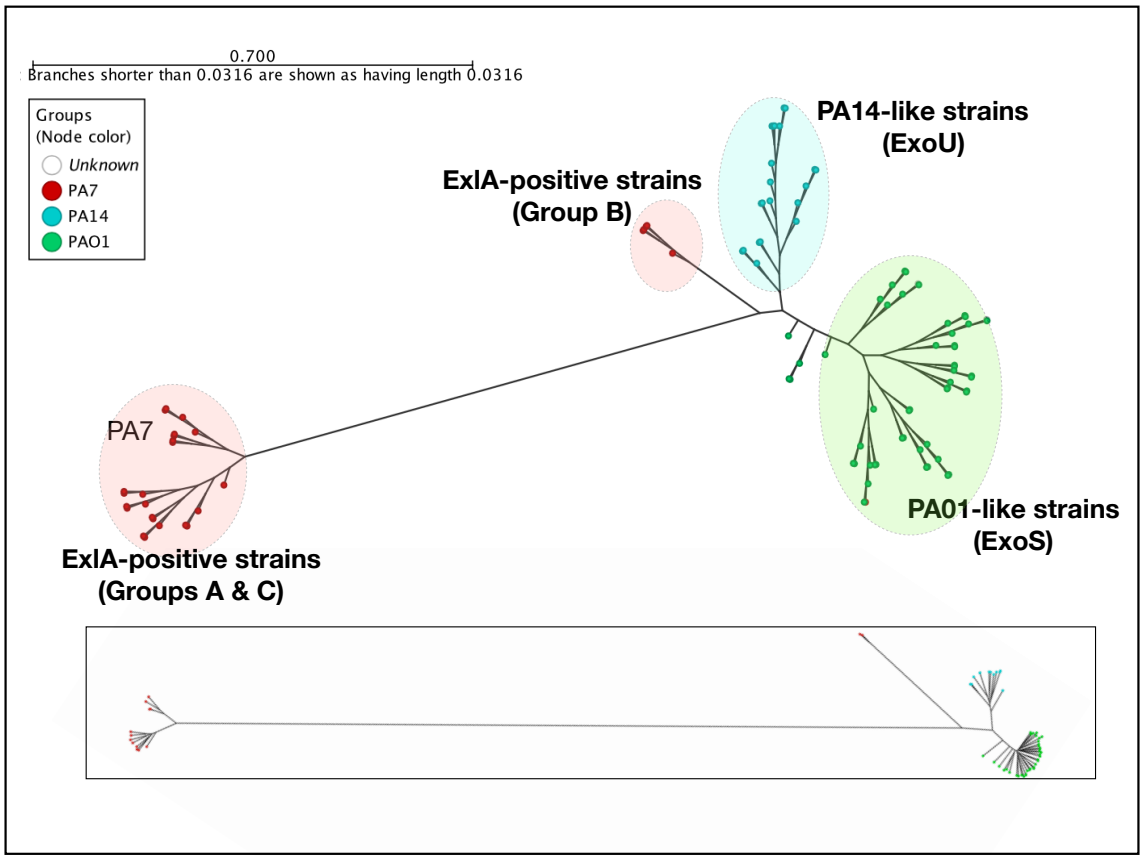

Figure 1.8. Phylogenetic tree based on the core genome single nucleotides polymorphisms (SNPs). Unrooted maximum likelihood tree of 97 *Pseudomonas aeruginosa* genomes based on SNPs within the core genome as defined by Harvest (100 bootstraps). The tree representation was done using CLC workbench software. Strains are divided into three major groups (group 1: PAO1 (green circles), group 2: PA14 (blue circles) and group 3: PA7 (red circles)). Basso P, unpublished data

PumA is a PA7 protein modulating TLR signalling

PumA is encoded by PSPA7_2375 on RGP56 carries a TIR domain (Toll/interleukin-1 receptor) that interacts with the TIRAP domain of MyD88 or TLR4. PumA also recognizes the UBAP1 (Ubiquitin-associated protein 1) domain of the ESCRT-I (endosomal-sorting complex required for transport I) protein. These proteins are involved in the TNFR1 dependent pathway, leading to the transcription of genes involved in the pro-inflammatory response by NF-κB [127]. Therefore, the secretion of PumA by PA7 during infection leads to the inhibition of this gene transcription and inhibits the pro-inflammatory cytokines production. *In fine*, PumA allows PA7 to escape the innate immune response, disseminate and grow within the host (Figure 1.9) [128].

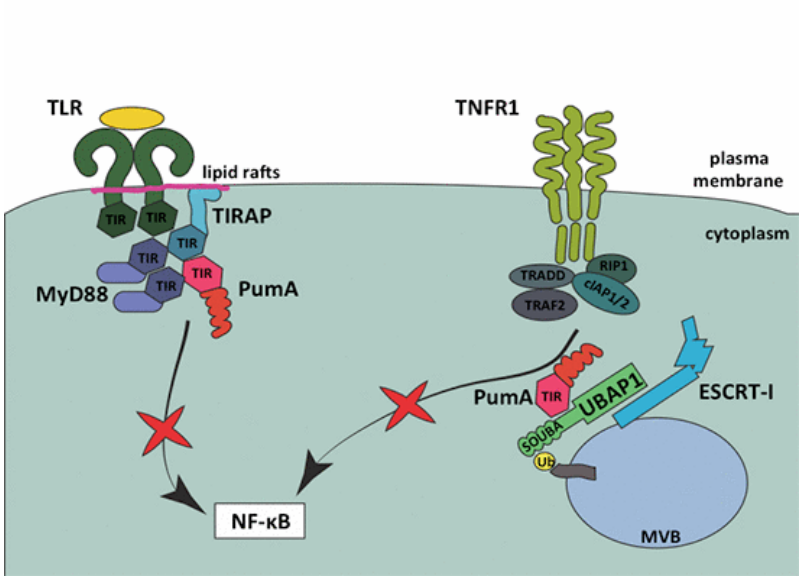

Figure 1.9. **PumA is a virulence factor of PA7.** PumA is a TIR domain-containing protein. PumA interacts with TLR adaptors but also UBAP1, targeting ESCRT-I to simultaneously inhibit TLR and TNFR1 signalling [128].

Txc is a novel Type II secretion system of PA7

The Type II secretion system (T2SS) is found in different *Pseudomonas* species. T2SS transports folded proteins from the cytoplasm to the extracellular environment. T2SS allows the secretion of a diverse array of proteins that contribute to the virulence of *P. aeruginosa*. These secreted proteins possess a large panel of biological functions, mainly enzymes, including proteases, lipases or phosphatases [53].

The T2SS is composed of (i) a platform at the basis in the IM, (ii) a large channel, called secretin anchored in the OM and (iii) a fimbrillar structure, called pseudopilus which can expel exoproteins through the channel out of the cell.

The classical strains like PAO1 or PA14 have two complete T2SSs [53]: the Xcp system and the Hcx sytem, whereas, PA7 strain possesses an additional system called Txc [20, 129]. The proteins of the Xcp system are encoded by 11 genes *xcpP-X*, organized in two operons, one encodes *xcpP-Q* genes and the other *xcpR-Z* genes. The *xcpA/pilD* gene is encoded in the same operon as *pilC*. The Xcp system is constitutively expressed. The exoproteins secreted by the Xcp system are diverse and cover a large diversity of functions, including the elastase LasB [130], the Staphylolysin LasA [130], the protease PrpL [131] and ToxA (Exotoxin-A) which is the only one to have an intracellular target [132] and plays a major role in the virulence of *P. aeruginosa* acute infections. LasA cleaves peptide bonds Gly-Gly, and

plays an important role in the defense against *Staphyloccoccus aureus* by cleaving its peptidogylycan. The other protease, PrpL cleaves host proteins such as the fibrinogen, plasminogen, immunoglobulin G and the proteins of the complement C3 and C1q [133]. This protease plays an important role in the acute lung injuries, by the cleavage of the surfactant proteins A, B and D [134]. LasB is a zinc metalloprotease capable of disrupting the tight junctions of epithelial cells through the degradation of elastin, the cadherin and collagen [31, 135]. It was shown to be a pro-inflammatory factor since it can contribute to an inflammatory response (production of IL-8 and neutrophil recruitment) after 4 hours of infection in a mouse model. It can also alter lung permeability and modify innate immune response by degrading surfactant proteins A and D. More recently, LasB was shown to degrade exogenous flagellin, under calcium-replete conditions and ensure effective immune evasion. By degrading free flagellin, the ligand of immune receptors, the pathogen retains its motility phenotype but escapes flagellin-dependent immune recognition [136]. The Hcx system (homologous to Xcp) is functional only in phosphate limitation conditions. It is also encoded by 11 genes *hxcP-Z*. This system secretes the alkaline phosphatase LapA [137], which is encoded in the same cluster as the *hxcP-Z* genes.

The Txc system of PA7 is encoded within RGP69, composed of a cluster of 14 genes encoding the complete T2SS machinery, secreted and the regulatory proteins (Figure 1.10) [129].

cbpE (PSPA7_1419) gene encodes a putative substrate for the Txc system. CbpE is a chitin-binding protein belonging to the family of proteins binding N-acetyl-glucosamin. CbpE shares 28 % of residue identity with CbpD (chitin-binding protein D) that is secreted by the Xcp-T2SS. CbpE secretion is regulated by the two-component system TtsR/TtsS, in which TtsR is the transcriptional regulator and TtsS is the sensor [21, 129]. The Txc system can also be found in other *Pseudomonas* species including *P. fluorescens* and *P. putida*. Genetic evidence suggests that RGP69 was not acquired by horizontal gene transfer but was lost in classical strains of *P. aeruginosa*. Indeed, marks of the RGP69 extremities were found in PAO1. Furthermore the GC content of RGP69 and the rest of the PA7 genome are similar and finally the absence of prepilin petidase gene encoded in the RGP69 suggest that the Txc pseudopilins use the general prepilin peptidase XcpA/PilD for their maturation [21, 129].

environmental microbiology reports

Environmental Microbiology Reports (2016) **00**(00), 00–00 doi:10.1111/1758-2229.12443

Minireview

Pseudomonas aeruginosa renews its virulence factors

Philippe Huber,[1,2,3,4]* Pauline Basso,[1,2,3,4] Emeline Reboud[1,2,3,4] and Ina Attrée[1,2,3,4]

[1]*University of Grenoble Alpes, Grenoble 38000, France.*
[2]*CNRS, ERL5261, Grenoble 38000, France.*
[3]*CEA, BIG-BCI, Grenoble, 38000, France.*
[4]*INSERM, U1036, Grenoble 38000, France*

Summary

Highly divergent strains of the major human opportunistic pathogen *Pseudomonas aeruginosa* have been isolated around the world by different research laboratories. They came from patients with various types of infectious diseases or from the environment. These strains are devoid of the major virulence factor used by classical strains, the Type III secretion system, but possess additional putative virulence factors, including a novel two-partner secretion system, ExlBA, responsible for the hypervirulent behavior of some clinical isolates. Here, we review the genetic and phenotypic characteristics of these recently-discovered *P. aeruginosa* outliers.

Introduction

The Gram-negative bacillus *Pseudomonas aeruginosa* is a wide-spread bacterium that inhabits soil and aquatic environments. Its metabolic versatility, adaptive regulatory systems and high intrinsic antibiotic resistance favor its persistence in different habitats, notably in hospital settings. *P. aeruginosa* is recognized as a major human opportunistic pathogen responsible for acute life-threatening infections in individuals with diverse underlying affection, such as burns, cancer, HIV infections, or patients with surgical wounds, carrying catheters or submitted to bone marrow and organ transplantations which results in bacteremia, urinary tract infections and pneumonia. *P. aeruginosa* is also capable to provoke persistent, chronic infections, notably in patients with cystic fibrosis and chronic obstructive pulmonary disease (Williams *et al.*, 2010; Gellatly and Hancock, 2013).

Received 6 June, 2016; accepted 13 July, 2016. *For correspondence. E-mail phuber@cea.fr; Tel. 33 438 78 58 47; Fax 33 438 78 50 58.

Access to genome sequences of several hundreds of *P. aeruginosa* isolates, together with several reports on the phenotypic characteristics of individual clones, suggested a highly diverse population structure. Indeed, detailed phylogenic analysis based on single nucleotide polymorphisms of the core genomes allowed to divide *P. aeruginosa* population in four major clades, with the most divergent clade populated by clonal outliers related to the PA7 strain (Thrane *et al.*, 2015).

Genomics of P. aeruginosa *outliers*

In 2010, the teams of Roy and Paulsen (Roy *et al.*, 2010), reported the whole-genome sequence of a *P. aeruginosa* wound isolate from Argentina, PA7, showing a highly divergent genome from all other classical strains, represented by two in-laboratory used strains: PAO1 and PA14. With on average 93.5% of pairwise identity, the PA7 strain is characterized by two major differences comparing to classical strains (i) the absence of the whole type III secretion system (*T3SS*) loci comprising five operons and 36 genes and (ii) the absence of all genes encoding the T3SS toxins (*exoS*, *exoT*, *exoY* and *exoU*). In addition, the PA7 genome possesses 18 genomic islands inserted in regions of genomic plasticity (RGP) that are absent in PAO1 and PA14. Since this first publication in 2010 and the advances in next-generation sequencing technology, the genomes of 14 'PA7-like strains' (Dingemans *et al.*, 2014; Boukerb *et al.*, 2015; Kos *et al.*, 2015; Mai-Prochnow *et al.*, 2015; van Belkum *et al.*, 2015) and of five related strains (Dingemans *et al.*, 2014; Boukerb *et al.*, 2015; van Belkum *et al.*, 2015) have been fully sequenced, deposited in NCBI and made available at Pseudomonas genome project website (www.pseudomonas.com) (Table 1).

Isolation of a hypervirulent PA7-like strain, named CLJ1, from a patient with hemorrhagic pneumonia in Grenoble University Hospital, France, allowed the identification and characterization of a novel two partner secretion (TPS) system exporting a 172-kDa protein, called Exolysin, belonging to the hemaglutinin/hemolysin family (Elsen *et al.*, 2014). The identified TPS, encoded by a two-gene operon *PSPA_4641 – PSPA_4642*, dubbed *exlB-exlA*, was found directly related to the hyper-virulence of strains secreting ExlA in various

Table 1. Genomic characteristics of *exlA*+ strains.

Strains	Synonyms	Sequence types	Countries	References	Biosamples	*toxA*	*txc* system operon	Mutated *mvfR*	*cbpE*	*tfpW*	*pyocin S6*	*oprA*
Group A												
PA7		1195	Argentina	(Roy *et al*., 2010)	SAMN02603435	−	+	+	+	+	+	+
JT87		1978	USA	(Toska *et al*., 2014)		−	+	−	+	+	−	+
CPHL11451		2214	USA	(Pirnay *et al*., 2009)		−	+	−	+	+	−	+
CLJ1		2028	France	(Elsen *et al*., 2014)		−	+	−	+	+	−	+
IHMA567230	AZPAE14941	2213	China	(Kos *et al*., 2015)	SAMN03105639	−	+	−	+	+	−	+
IHMA879472	AZPAE15042	2211	Germany	(Kos *et al*., 2015)	SAMN03105739	−	+	−	+	+	+	+
IHMA434930	AZPAE14901	2212	India	(Kos *et al*., 2015)	SAMN03105599	−	+	−	+	+	+	+
ATCC 33359	IMG 243	2228		(King *et al*., 2008)	SAMN04028048	−	+	−	+	+	+	+
BL043		1195	USA			na	na	−	na	na	na	na
EML548		191		(Boukerb *et al*., 2015)	SAMN03840672	−	+	−	+	+	−	+
DSM1128	ATCC 9027	191	USA	(Mai-Prochnow *et al*., 2015)	SAMN04045728	−	+	−	+	+	−	+
Zw26		2165	Germany			na	na		na	na	na	na
LMG5031	WH-SGI-V-07287	2039	Puerto Rico	(Pirnay *et al*., 2009)	SAMN04128729	+	+	−	+	+	+	+
WH-SGI-V-07261	Br680	2031	Belgium	(van Belkum *et al*., 2015)	SAMN04128711	−	+	−	+	+	+	+
WH-SGI-V-07370		2047	France	(van Belkum *et al*., 2015)	SAMN04128555	−	+	−	+	+	+	+
WH-SGI-V-07618		2023	USA	(van Belkum *et al*., 2015)	SAMN04128628	−	+	−	+	+	+	+
WH-SGI-V-07055		2023	USA	(van Belkum *et al*., 2015)	SAMN04128482	−	+	−	+	+	+	+
WH-SGI-V-07050		2020	France	(van Belkum *et al*., 2015)	SAMN04128502	+	+	+	+	−	+	+
WH-SGI-V-07064		1195	USA	(van Belkum *et al*., 2015)	SAMN04128496	−	+	−	+	+	+	+
WH-SGI-V-07234		2028	USA	(van Belkum *et al*., 2015)	SAMN04128540	−	+	−	+	+	−	+
Group B												
CF_PA39		2229	Belgium	(Dingemans *et al*., 2014)	SAMN02602860	+	+	−	+	−	+	+
PA213		1328	UK	(De Soyza *et al*., 2014)		na	na	na	na	na	na	na
PA70		1328	UK	(De Soyza *et al*., 2014)		na	na	na	na	na	na	na
DVL1758		2215	Belgium	(Pirnay *et al*., 2009)		na	na	na	na	na	na	na
TA19		2227	Australia	(Pirnay *et al*., 2009)		na	na	na	na	na	na	na
Can5		1716	UK	(Pirnay *et al*., 2009)		na	na	na	na	na	na	na
Group C												
EML545		2228	Germany	(Boukerb *et al*., 2015)	SAMN03840665	−	+	+	+	+	+	+
EML528		nd	Germany	(Boukerb *et al*., 2015)	SAMN03840633	−	+	+	+	+	−	+
WH-SGI-V-07072		1195	USA	(van Belkum *et al*., 2015)	SAMN04128498	−	+	+	+	+	+	+
WH-SGI-V-07165		1006	France	(van Belkum *et al*., 2015)	SAMN04128503	−	+	+	+	+	−	+

na, genome sequence not available; nd, not determined.

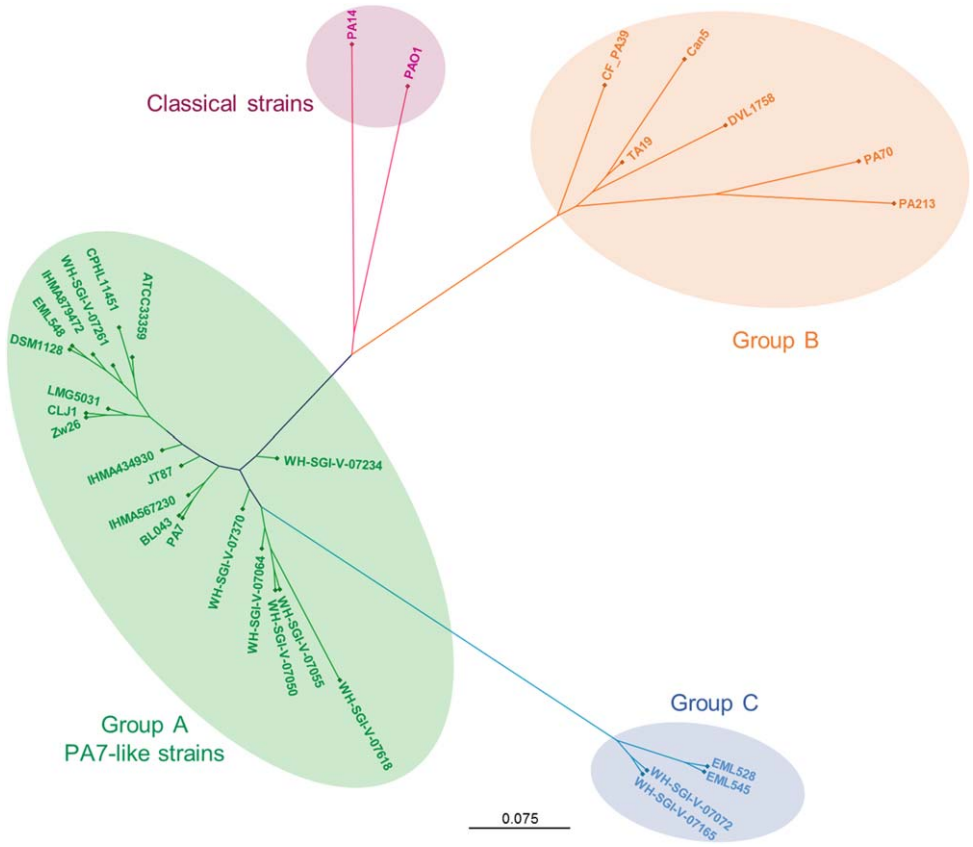

Fig. 1. Phylogenetic tree of *exlA*+ *P. aeruginosa* strains. Maximal-likelihood tree based on single nucleotide polymorphisms of seven housekeeping genes (*ascA, aroE, guaA, mutL, nuoD, ppsA and trpE)*. The gene sequences were concatenated and aligned using CLC bio software. The classical strains are represented by PAO1 and PA14 strains. See Table 1 for the references of the genome sequences.

models of infection (see below). When comparing with the PAO1 genome organization, *exlB-exlA* locus is present between genes corresponding to *PA0874* and *PA0873*, and this organization is conserved in all PA7-like strains sequenced to date ((Reboud *et al.*, 2016) and Basso, unpublished results). Therefore, *exlB-exlA* could be considered as a novel RGP, potentially specific to PA7-like strains. Interestingly, a recent systematic search for strains lacking the T3SS genes, but possessing *exlA*, revealed that, in addition to the PA7-like clonal outliers, *exlB-exlA* could be found in strains that are closer phylogenetically (using the divergence of seven housekeeping genes) to PAO1/PA14 than to PA7 (Fig. 1 and Table 1). We named those strains 'Group B', in comparison to the 'Group A' formed by the PA7-like strains (Reboud *et al.*, 2016). Notably, Group A and Group B strains, while all lacking T3SS toxins, differ by the extent of the deletion occurring at the T3SS loci, suggesting that *exlB-exlA* locus has been acquired before exclusion of the T3SS. Finally, a phylogenetic analysis of recently published *T3SS*-negative, *exlB-exlA*-positive strains (Boukerb *et al.*, 2015; van Belkum *et al.*, 2015) revealed the existence of a third group of strains that we propose to call Group C (Fig. 1 and Table 1). Strains from Group C possess the same type of T3SS deletion as in Group A and the *exlB-exlA* locus is inserted in the same genetic environment. Until now, no *P. aeruginosa* strain with both *exlB-exlA* and *T3SS* genes has been identified.

The novel hypervirulent ExlA-ExlB system

Exolysin (ExlA) was identified in the secretomes of various Group A and Group B strains and displays 35% identity with ShlA hemolysin from *Serratia marcescens* (Elsen *et al.*, 2014). ExlB, encoding an outer membrane porin which is required for ExlA secretion, has 34% identity with ShlB from *S. marcescens* and belongs to the TPS family of OM transporters. Although not found in other *P. aeruginosa* classical clades, highly homologous *exlB-exlA* loci are present in *P. putida*, *P. fluorescens* and *P. entomophila*, strongly suggesting that this locus was acquired by horizontal transfer from other *Pseudomonas* species (Basso *et al.*, unpublished).

ExlA rapidly induces the formation of a pore in eukaryotic host plasma membranes, eventually leading to plasma membrane rupture and cell death (Basso *et al.* unpublished). The secreted ExlA protein has no toxic

Table 2. Phenotypes of group A and B strains.

			Virulence factors			Motility	Biological activity		
Name	Origin	Serotype	ExlA Secretion	HCN	LasB activity	Swarming	Cytotoxicity[a]	Mice[b]	Chicory leaves[b]
Group A									
PA7	Burn	O12	+/−	++	−	−	55	nd	6
JT87	Urinary	O12	+/−	++	+/−	+	96	6	16
CPHL11451	Unknown	O12	+/−	−	−	−	83	2	9
CLJ1	Expec. (COPD)	O12	+++	++	++	−	108	7	10
IHMA567230	Peritoneal	O12	+	−	−	−	55	nd	11
IHMA879472	Urinary	O11_O12	+	++	++	−	103	3	17
IHMA434930	Abscess/Pus	O11_O17	+	++	++	−	100	nd	19
ATCC 33359	Burn	O12	+	−	−	−	86	nd	2
BL043	Bacteremia	O12	+	−	−	−	45	nd	1
EML548	Otitis	O1	+/−	+	−	−	71	nd	15
DSM1128	Otitis	O1	+	+	−	−	69	nd	19
Zw26	Expec. (CF)	O11	+/−	−	−	−	40	nd	8
LMG5031	*Aglaonema commutatum*	nt	+	−	−	−	74	5	4
Group B									
CF_PA39	Expec. (CF)	O3	−	−	+	+/−	11	nd	3
PA213	Expec. (Non-CF Bronchiectasis)	PA	−	+	+	−	15	nd	5
PA70	Expec. (Non-CF Bronchiectasis)	PA	−	+	+	−	12	nd	7
DVL1758	Pond water	nt	−	++	++	++	43	4	13
TA19	Urinary	nt	+/−	+/−	−	+	23	nd	12
Can5	Unknown (canine)	O6	−	++	−	−	51	1	14

a. Sum of rank number of the cytotoxicity in six cell types (epithelial, endothelial, fibroblastic, myeloid and lymphoid), from less to most toxic (min: 6, max: 114).

b. Toxicity range from less to most toxic in acute pneumonia (out of 7) and chicory leave (out of 19) models.

CF, cystic fibrosis; Expec., Expectoration; COPD, Chronic obstructive pulmonary disease; nt, not typable; nd, not determined. Derived from Reboud and colleagues (2016).

activity on nucleated cells, either because the protein is unstable in the medium or more likely (but not exclusively) because the bacterium has to be in the vicinity of the host, as shown in experiments where host cells and bacteria are filter-separated. This latter hypothesis is further supported by the requirement of Type IV pili proteins for toxicity, suggesting an involvement of pili in the toxic behavior of ExlA (Basso *et al*., unpublished). ExlA is present in purified host membranes after infection, yet the mechanisms of toxin insertion into host membranes are totally unknown. In particular, the putative receptor for ExlA on host cells is unidentified.

ExlA+ strains secrete variable amounts of ExlA (Table 2), although their *exlBA* locus sequences are highly homologous (> 85% identity)(Reboud *et al*., 2016), suggesting the existence of differential regulatory pathways for ExlA and ExlB expressions. The more detailed pangenomic analysis of *exlA*+ strains together with genome-wide mutagenesis on selected strains for loss or gain of ExlA secretion could give a hint in the regulation of ExlA-dependent virulence. Interestingly, the majority of the Group B strains neither express nor secrete the Exolysin, and in consequence are poorly cytotoxic.

Among the Group A strains, a direct correlation was observed between the secreted ExlA levels and cell lysis activity (Table 2)(Reboud *et al*., 2016). Target cells can be epithelial, endothelial, myeloid and fibroblastic cells from human, dog or mouse origins. Human erythrocytes are weakly lysed by *exlA*+ strains, unless ExlA is over-expressed, suggesting that high affinity receptors for ExlA are lacking at the surface of erythrocytes. Similar observations were made on mouse erythrocytes *in vivo*. Therefore, ExlA has to be considered as a cytolysin rather than an hemolysin.

ExlA-secreting strains displayed virulence in the mouse pneumonia model, but their toxicity were not completely correlated with their cytolytic properties (Reboud *et al*., 2016). Data on strain toxicity towards neutrophils and macrophages, as well as the capability of the inflammatory cells to phagocyte *exlA*+ strains are missing to better understand the behavior of these strains *in vivo*.

As for the classical strains, the capacity of *exlA*+ strains to infect plants is heterogeneous and there is a correlation neither with ExlA secretion levels, nor with their lytic activity on mammalian cells (Table 2) (Reboud *et al*., 2016). Therefore, it is likely that these bacteria use different virulence mechanisms to infect mammals and plants, and that ExlA is not required for bacterial toxicity on plants. It seems thus that *exlA*+ strains behave much like *T3SS*+ strains concerning global

pathogenicity profiles (Hilker *et al*., 2015), meaning they show unequal level of virulence that could not be attributed only to one toxin, ExlA.

A third type II secretion system

Type II secretion is a two-stage process: effectors are first translocated into the periplasm through the Sec or Tat translocons, and then excreted in the extracellular milieu using macromolecular complexes called secretons. Two types of T2SS secretons have been identified in classical *P. aeruginosa* strains: the Xcp complex, which secretes a broad range of proteins, and the Hxc complex, which is only active under phosphate-limiting conditions and specialized in alkaline phosphatase secretion. These systems have been reviewed previously (Bleves *et al*., 2010; Filloux, 2011).

Xcp and Hxc complexes are present and functional in PA7 (Cadoret *et al*., 2014). The main effector of Xcp is exotoxin A (ToxA), a potent inhibitor of protein translation in the host. The gene encoding ToxA is lacking in PA7 genome (Roy *et al*., 2010), as well as in most genomes of Group A and Group C strains, except for LMG5031 and WH-SGI-V-07050, while *toxA* is present in the only reported Group B genome, CF_PA39 (Table 1). Other major Xcp substrates are proteases, including LasB that targets several extracellular proteins and host cell receptors (Hong and Ghebrehiwet, 1992; Mariencheck *et al*., 2003; Schmidtchen *et al*., 2003; Dulon *et al*., 2005; Leduc *et al*., 2007; Beaufort *et al*., 2011; Kuang *et al*., 2011; Golovkine *et al*., 2014). Most *exlA*+ strains display caseinolytic activity, demonstrating a general proteolytic activity, but only a few of them exhibit a prototypical LasB activity (Table 2), while this activity is present in most classical strain secretomes (Coin *et al*., 1997; Schaber *et al*., 2004). The *lasB* gene was found in all strains at same position and with sequence identity ranging 91–98% from the *lasB* PAO1 sequence. LasB expression is under the control of the quorum sensing (QS), and lack of the QS genes might affect *lasB* expression. The *QS* genes: *vqsM vqsR*, *lasR, lasI*, *rhlR, rhlI* are all present at identical locations in the genomes of all strains, and their sequences display 98% identity, except for strain PA39 (92%). However, an internal frameshift mutation in the *mvfR* gene, coding for an important regulator of the QS, was noted in PA7 genome (Roy *et al*., 2010). This mutation is also present in *mvfR* genes of WH-SGI-V-07050 and Group C strains (Table 1), but is absent in most Group A strains lacking LasB activity (Table 2). Thus, reported *QS* and *lasB* sequences cannot simply explain the absence of LasB activity in most of these strains.

The lack of these two major virulence factors, ToxA and LasB, in most Group A and C strains, in addition to the absence of T3SS, indicate that the toxic behavior of the *exlA*+ strains *in vivo* is likely totally different from that of classical strains.

A third T2SS has been identified in PA7, called Txc for third homolog for Xcp (Cadoret *et al*., 2014). A cluster of 14 genes, including 11 'core' genes (*txcP* to *txcZ* or *PSPA7_1417* to *PSPA7_1407*), a secreted substrate (*cbpE* or *PA7_1419*) and a regulatory protein (*ttsS* or *PSPA7_1420*) have been identified in a region of genome plasticity (RGP69). CbpE is a chitin-binding protein that can only be secreted by the Txc system, and whose secretion is regulated by the two-component system TtsR/TtsS, in which TtsR is the regulator and TtsS the sensor. The Txc locus is a hallmark of strains from Group A, B and C, for which genomic data are available (Table 1), suggesting that these strains are adapted to grow on insect carapaces. Interestingly, Txc systems are also found in two other *Pseudomonas* species: *P. fluorescens* and *P. putida*, as well as in *Yersinia enterocolitica*. However, multiple genetic evidences are in favor of a loss of Txc locus in classical strains, rather than an acquisition in PA7-like strains (Cadoret *et al*., 2014).

Serotype O12 is prevalent in exlA+ strains

Detailed phenotypic analysis of *exlA*+ strains established in our laboratory also revealed that the majority of strains are of O12 serotype (Table 2), as already reported for PA7 (Reboud *et al*., 2016). In recent years, O12 serotype isolates have attracted a lot of attention due to several related outbreaks and high antibiotic resistance (Maatallah *et al*., 2011; Witney *et al*., 2014). Wide comparative genomic approach performed on 83 isolates pointed out the horizontal transfer of the so called 'serotype island' between PA7 and non-PA7 strains that confers to the majority of isolates both O12 serotype and resistance to fluoroquinolone, notably due to mutation in *gyrA* gene located in the island (*PSPA7_1944* to *PSPA7_2005*). Intriguingly, 'serotype islands' in different O12 isolates may vary in size from 62 to 185 kbp (Thrane *et al*., 2015) possibly carrying other strain-specific genes of unknown function. The link between *exlA* and 'O12 serotype islands' still needs to be investigated.

Motility is nearly normal

Pseudomonas aeruginosa uses a polar flagellum for swimming in liquid medium and Type IV pili for surface motility, a motility type generally referred to as 'twitching'. A third motility behavior, called 'swarming', has been identified, which may use the flagellum, Type IV pili and bacterium-produced surfactants in different possible associations (Josenhans and Suerbaum, 2002; Burrows, 2012). Swarming allows bacterial motion on soft substrates. As for classical strains, all possible combinations exist for *exlA*+ strains, and the proportions of

swimming or twitching strains are similar in classical and *exlA*+ strains (Table 2) (Murray *et al*., 2010; Reboud *et al*., 2016). However, it was noticed that the proportion of strains able to engage swarming motility is lower in *exlA*+ strains compared to classical strains (21% and 63% respectively) (Murray *et al*., 2010; Reboud *et al*., 2016). Swarming may be considered as a transition step between attachment and biofilm formation, a process involved in tissue or material colonization, and promoting chronic infections. However, two *exlA*+ strains isolated from patients with chronic infections were unable to swarm (Reboud *et al*., 2016), suggesting that swarming deficiency does not preclude colonization.

Type IV pili are composed of monomeric subunits of pilin encoded by the *pilA* gene. In the majority of strains studied so far, the pilins are glycosylated at Ser148 (Comer *et al*., 2002). An oligosaccharide transferase (TfpO) attaches an O-antigen subunit of membrane lipopolysaccharide to this single amino-acid. Therefore, pilins of classical strains have a glycan moiety that matches the serotype of the strain. In *P. aeruginosa* as well as in other bacteria, roles for pilin glycosylation have been demonstrated in adhesion, protection from proteolytic cleavage, solubility, antigenic variation and protective immunity (Doig *et al*., 1988; Kuo *et al*., 1996; Marceau and Nassif, 1999; Szymanski *et al*., 2002). However, in some strains, including PA7, the pilin is glycosylated at multiple sites with unusual α1,5-linked D-arabino-furanose (α1,5-D-Ara*f*) glycans, identical to those found in the cell wall of *Mycobacterium spp* (Voisin *et al*., 2007). In PA7, D-Ara*f* biosynthetic pathway requires three genes: *PSPA_6246, 6248* and *6249* that are sufficient for D-Ara*f* synthesis in heterologous system (Harvey *et al*., 2011). The transfer on pili is operated by an arabinosyltransferase, TfpW, specific of these strains (Kus *et al*., 2008). TfpW deficiency leads to fewer surface pili and reduced motility, indicating that arabinosylation modifies pili assembly or dynamics. The various genes encoding the D-Ara*f* pathway were identified in all *exlA*+ strains, except WH-SGI-07050 and CF_PA39 (Table 1), indicating that this feature can be used as a general marker of these strains.

Hydrogen cyanide and pyocins

Hydrogen cyanide (HCN) is released as a volatile compound by most *P. aeruginosa* strains, and is relatively specific to *P. aeruginosa* species (Gilchrist *et al*., 2011; Smith *et al*., 2013). HCN is a poison inhibiting mitochondrial cytochrome c oxidase, hence halting cellular respiration of eukaryotic cells. HCN belongs to the arsenal of *P. aeruginosa* factors participating to its pathogenicity. Interestingly, *exlA*+ strains are much more heterogeneous regarding HCN production than classical strains, again suggesting that the entire repertoire of toxins, independent of the T3SS, is different in these strains (Table 2) (Reboud *et al*., 2016).

Another example is a specific bacteriocin, pyocin S6, released by the *exlA*+ strain CF_PA39 (Dingemans *et al*., 2014). Bacteriocins, called pyocins when secreted by *P. aeruginosa*, are produced as antagonistic molecules, usually in stress conditions, to compete with closely related bacteria (Michel-Briand and Baysse, 2002; Ghequire and De Mot, 2014).

Pyocin S6 is a soluble pyocin (S-type), endowed with 16S RNA cleavage activity, that kills bacteria lacking the immunity protein Imm6. The pyocin S6 gene is shared by other *exlA* strains (61% of reported genomes, Table 1). Thus, *exlA*+ strains developed (or retained) the ability to compete with other bacteria using a specific weapon.

Antibiotic resistance

In general, treatment of *P. aeruginosa* infections has become extremely difficult due to inefficiency of available antibiotics. The PA7 strain has been reported as multiresistant (Roy *et al*., 2010). Typical mutations in genes responsible for fluoroquinolone resistance, *gyrA* and *parC*, and to tobramycin, *aacA4*, have been identified in PA7 genome (Roy *et al*., 2010). In addition, the resistance to aminoglycosides (including, amikacin, gentamicin and tobramycin) can be attributed to the presence of an additional outer-membrane protein of the Opr family, OprA, encoded by a gene located in the operon of the major *P. aeruginosa* efflux pump, MexXY. While the deletion of the whole operon makes the strain sensitive to aminoglycosides, the deletion of *oprA* alone is not sufficient to modify resistant phenotype, suggesting that OprA could be replaced by other OMPs (Morita *et al*., 2012). Based on available genomes, the presence of *oprA* gene is a general feature of *exlA*+ strains, regardless of the phylogenetic group (Table 1). Moreover, Morita and colleagues 2015 identified in PA7 a novel variant of a regulatory gene, *mexS*, responsible for upregulation of another multidrug efflux pump, MexEF-OprN, contributing further to multi-antibiotic resistance of this strain. Although the integrated data of antibiograms are lacking for the majority of the *exlA*+ strains, we noted that the strain CLJ3, isolated from the same patient as CLJ1 but after the antibiotic treatment, has increased resistance to numerous hospital-used antibiotics (Elsen *et al*., 2014). Genetic determinants that are responsible for this adaptation and multiresistance are under investigation.

Conclusion

The discovery of these atypical strains demonstrates that *P. aeruginosa* species is not restricted to PAO1- and PA14-like strains, but encompasses a much larger and diverse bacterial family than previously thought.

Accession to bacterial whole genomes together with the characterization of virulence strategies of clinical strains allowed to re-classify *P. aeruginosa* members. Several strains lacking *T3SS*, but employing a novel virulence strategy to intoxicate host cells have been collected and analysed. Their presence in hospital units, together with reports on multi-drug resistance, calls for more research on their distribution, as well as their diversity and pathogenicity in order to foresee anti-infective interventions. In particular, as *exlA*+ strains use virulence modes highly different from classical *P. aeruginosa* strains, it will be important to diagnose these strains in hospital units, which is easy to perform using PCR or mass spectrometry approaches. Clearly, accumulation of genomic data and raising collections of phenotypically characterized *exlA*+ strains should give in the future a more global picture of evolution and occurrence of those strains in hospital settings.

Acknowledgements

This study was performed thanks to institutional grants from CEA, Inserm, University Grenoble-Alpes and CNRS, and from ANR grants (ANR-10-LABX-49-01 and ANR-15-CE11-0018).

References

Beaufort, N., Corvazier, E., Hervieu, A., Choqueux, C., Dussiot, M., Louedec, L., *et al*. (2011) The thermolysin-like metalloproteinase and virulence factor LasB from pathogenic pseudomonas aeruginosa induces anoikis of human vascular cells. *Cell Microbiol* **13**: 1149–1167.

van Belkum, A., Soriaga, L.B., LaFave, M.C., Akella, S., Veyrieras, J.B., Barbu, E.M., *et al*. (2015) Phylogenetic distribution of CRISPR-Cas systems in antibiotic-resistant pseudomonas aeruginosa. *MBio* **6**: e01796–e01715.

Bleves, S., Viarre, V., Salacha, R., Michel, G.P., Filloux, A., and Voulhoux, R. (2010) Protein secretion systems in Pseudomonas aeruginosa: a wealth of pathogenic weapons. *Int J Med Microbiol* **300**: 534–543.

Boukerb, A.M., Marti, R., and Cournoyer, B. (2015) Genome sequences of three strains of the Pseudomonas aeruginosa PA7 Clade. *Genome Announc* **3**: e01366–15.

Burrows, L.L. (2012) Pseudomonas aeruginosa twitching motility: type IV pili in action. *Annu Rev Microbiol* **66**: 493–520.

Cadoret, F., Ball, G., Douzi, B., and Voulhoux, R. (2014) Txc, a new type II secretion system of pseudomonas aeruginosa strain PA7, is regulated by the TtsS/TtsR two-component system and directs specific secretion of the CbpE chitin-binding protein. *J Bacteriol* **196**: 2376–2386.

Coin, D., Louis, D., Bernillon, J., Guinand, M., and Wallach, J. (1997) LasA, alkaline protease and elastase in clinical strains of Pseudomonas aeruginosa: quantification by immunochemical methods. *FEMS Immunol Med Microbiol* **18**: 175–184.

Comer, J.E., Marshall, M.A., Blanch, V.J., Deal, C.D., and Castric, P. (2002) Identification of the Pseudomonas aeruginosa 1244 pilin glycosylation site. *Infect Immun* **70**: 2837–2845.

De Soyza, A., Perry, A., Hall, A.J., Sunny, S.S., Walton, K.E., Mustafa, N., *et al*. (2014) Molecular epidemiological analysis suggests cross-infection with Pseudomonas aeruginosa is rare in non-cystic fibrosis bronchiectasis. *Eur Respir J* **43**: 900–903.

Dingemans, J., Ye, L., Hildebrand, F., Tontodonati, F., Craggs, M., Bilocq, F., *et al*. (2014) The deletion of TonB-dependent receptor genes is part of the genome reduction process that occurs during adaptation of Pseudomonas aeruginosa to the cystic fibrosis lung. *Pathog Dis* **71**: 26–38.

Doig, P., Todd, T., Sastry, P.A., Lee, K.K., Hodges, R.S., Paranchych, W., and Irvin, R.T. (1988) Role of pili in adhesion of Pseudomonas aeruginosa to human respiratory epithelial cells. *Infect Immun* **56**: 1641–1646.

Dulon, S., Leduc, D., Cottrell, G.S., D'alayer, J., Hansen, K.K., Bunnett, N.W., *et al*. (2005) Pseudomonas aeruginosa elastase disables proteinase-activated receptor 2 in respiratory epithelial cells. *Am J Respir Cell Mol Biol* **32**: 411–419.

Elsen, S., Huber, P., Bouillot, S., Coute, Y., Fournier, P., Dubois, Y., *et al*. (2014) A type III secretion negative clinical strain of Pseudomonas aeruginosa employs a two-partner secreted exolysin to induce hemorrhagic pneumonia. *Cell Host Microbe* **15**: 164–176.

Filloux, A. (2011) Protein secretion systems in Pseudomonas aeruginosa: an essay on diversity, evolution, and Function. *Front Microbiol* **2**: 155.

Gellatly, S.L., and Hancock, R.E. (2013) Pseudomonas aeruginosa: new insights into pathogenesis and host defenses. *Pathog Dis* **67**: 159–173.

Ghequire, M.G., and De Mot, R. (2014) Ribosomally encoded antibacterial proteins and peptides from Pseudomonas. *FEMS Microbiol Rev* **38**: 523–568.

Gilchrist, F.J., Alcock, A., Belcher, J., Brady, M., Jones, A., Smith, D., *et al*. (2011) Variation in hydrogen cyanide production between different strains of Pseudomonas aeruginosa. *Eur Respir J* **38**: 409–414.

Golovkine, G., Faudry, E., Bouillot, S., Voulhoux, R., Attree, I., and Huber, P. (2014) VE-cadherin cleavage by LasB protease from Pseudomonas aeruginosa facilitates type III secretion system toxicity in endothelial cells. *PLoS Pathog* **10**: e1003939.

Harvey, H., Kus, J.V., Tessier, L., Kelly, J., and Burrows, L.L. (2011) Pseudomonas aeruginosa D-arabinofuranose biosynthetic pathway and its role in type IV pilus assembly. *J Biol Chem* **286**: 28128–28137.

Hilker, R., Munder, A., Klockgether, J., Losada, P.M., Chouvarine, P., Cramer, N., *et al*. (2015) Interclonal gradient of virulence in the pseudomonas aeruginosa pangenome from disease and environment. *Environ Microbiol* **17**: 29–46.

Hong, Y.Q., and Ghebrehiwet, B. (1992) Effect of Pseudomonas aeruginosa elastase and alkaline protease on serum complement and isolated components C1q and C3. *Clin Immunol Immunopathol* **62**: 133–138.

Josenhans, C., and Suerbaum, S. (2002) The role of motility as a virulence factor in bacteria. *Int J Med Microbiol* **291**: 605–614.

King, J.D., Mulrooney, E.F., Vinogradov, E., Kneidinger, B., Mead, K., and Lam, J.S. (2008) IfnA from Pseudomonas aeruginosa O12 and wbuX from Escherichia coli O145 encode membrane-associated proteins and are required for expression of 2,6-dideoxy-2-acetamidino-L-galactose in lipopolysaccharide O antigen. *J Bacteriol* **190**: 1671–1679.

Kos, V.N., Deraspe, M., McLaughlin, R.E., Whiteaker, J.D., Roy, P.H., Alm, R.A., *et al*. (2015) The resistome of Pseudomonas aeruginosa in relationship to phenotypic susceptibility. *Antimicrob Agents Chemother* **59**: 427–436.

Kuang, Z., Hao, Y., Walling, B.E., Jeffries, J.L., Ohman, D.E., and Lau, G.W. (2011) Pseudomonas aeruginosa elastase provides an escape from phagocytosis by degrading the pulmonary surfactant protein-A. *PLoS One* **6**: e27091.

Kuo, C., Takahashi, N., Swanson, A.F., Ozeki, Y., and Hakomori, S. (1996) An N-linked high-mannose type oligosaccharide, expressed at the major outer membrane protein of Chlamydia trachomatis, mediates attachment and infectivity of the microorganism to HeLa cells. *J Clin Invest* **98**: 2813–2818.

Kus, J.V., Kelly, J., Tessier, L., Harvey, H., Cvitkovitch, D.G., and Burrows, L.L. (2008) Modification of Pseudomonas aeruginosa Pa5196 type IV Pilins at multiple sites with D-Araf by a novel GT-C family Arabinosyltransferase, TfpW. *J Bacteriol* **190**: 7464–7478.

Leduc, D., Beaufort, N., de Bentzmann, S., Rousselle, J.C., Namane, A., Chignard, M., and Pidard, D. (2007) The Pseudomonas aeruginosa LasB metalloproteinase regulates the human urokinase-type plasminogen activator receptor through domain-specific endoproteolysis. *Infect Immun* **75**: 3848–3858.

Maatallah, M., Cheriaa, J., Backhrouf, A., Iversen, A., Grundmann, H., Do, T., *et al*. (2011) Population structure of Pseudomonas aeruginosa from five Mediterranean countries: evidence for frequent recombination and epidemic occurrence of CC235. *PLoS One* **6**: e25617.

Mai-Prochnow, A., Bradbury, M., and Murphy, A.B. (2015) Draft genome sequence of Pseudomonas aeruginosa ATCC 9027 (DSM 1128), an important rhamnolipid surfactant producer and sterility testing strain. *Genome Announc* **3**: e01259–15.

Marceau, M., and Nassif, X. (1999) Role of glycosylation at Ser63 in production of soluble pilin in pathogenic Neisseria. *J Bacteriol* **181**: 656–661.

Mariencheck, W.I., Alcorn, J.F., Palmer, S.M., and Wright, J.R. (2003) Pseudomonas aeruginosa elastase degrades surfactant proteins a and D. *Am J Respir Cell Mol Biol* **28**: 528–537.

Michel-Briand, Y., and Baysse, C. (2002) The pyocins of Pseudomonas aeruginosa. *Biochimie* **84**: 499–510.

Morita, Y., Tomida, J., and Kawamura, Y. (2012) Primary mechanisms mediating aminoglycoside resistance in the multidrug-resistant pseudomonas aeruginosa clinical isolate PA7. *Microbiology* **158**: 1071–1083.

Morita, Y., Tomida, J., and Kawamura, Y. (2015) Efflux-mediated fluoroquinolone resistance in the multidrug-resistant Pseudomonas aeruginosa clinical isolate PA7: identification of a novel MexS variant involved in upregulation of the mexEF-oprN multidrug efflux operon. *Front Microbiol* **6**: 8.

Murray, T.S., Ledizet, M., and Kazmierczak, B.I. (2010) Swarming motility, secretion of type 3 effectors and biofilm formation phenotypes exhibited within a large cohort of Pseudomonas aeruginosa clinical isolates. *J Med Microbiol* **59**: 511–520.

Pirnay, J.P., Bilocq, F., Pot, B., Cornelis, P., Zizi, M., Van Eldere, J., *et al*. (2009) Pseudomonas aeruginosa population structure revisited. *PLoS One* **4**: e7740.

Reboud, E., Elsen, S., Bouillot, S., Golovkine, G., Basso, P., Jeannot, K., *et al*. (2016) Phenotype and toxicity of the recently discovered exlA-positive Pseudomonas aeruginosa strains collected worldwide. *Environ Microbiol* doi: 10.1111/1462-2920.13262.

Roy, P.H., Tetu, S.G., Larouche, A., Elbourne, L., Tremblay, S., Ren, Q., *et al*. (2010) Complete genome sequence of the multiresistant taxonomic outlier Pseudomonas aeruginosa PA7. *PLoS One* **5**: e8842.

Schaber, J.A., Carty, N.L., McDonald, N.A., Graham, E.D., Cheluvappa, R., Griswold, J.A., and Hamood, A.N. (2004) Analysis of quorum sensing-deficient clinical isolates of Pseudomonas aeruginosa. *J Med Microbiol* **53**: 841–853.

Schmidtchen, A., Holst, E., Tapper, H., and Bjorck, L. (2003) Elastase-producing Pseudomonas aeruginosa degrade plasma proteins and extracellular products of human skin and fibroblasts, and inhibit fibroblast growth. *Microb Pathog* **34**: 47–55.

Smith, D., Spanel, P., Gilchrist, F.J., and Lenney, W. (2013) Hydrogen cyanide, a volatile biomarker of Pseudomonas aeruginosa infection. *J Breath Res* **7**: 044001.

Szymanski, C.M., Burr, D.H., and Guerry, P. (2002) Campylobacter protein glycosylation affects host cell interactions. *Infect Immun* **70**: 2242–2244.

Thrane, S.W., Taylor, V.L., Freschi, L., Kukavica-Ibrulj, I., Boyle, B., Laroche, J., *et al*. (2015) The widespread multidrug-resistant serotype O12 Pseudomonas aeruginosa clone emerged through concomitant horizontal transfer of serotype antigen and antibiotic resistance gene clusters. *MBio* **6**: e01396–e01315.

Toska, J., Sun, Y., Carbonell, D.A., Foster, A.N., Jacobs, M.R., Pearlman, E., and Rietsch, A. (2014) Diversity of virulence phenotypes among type III secretion negative Pseudomonas aeruginosa clinical isolates. *PLoS One* **9**: e86829.

Voisin, S., Kus, J.V., Houliston, S., St-Michael, F., Watson, D., Cvitkovitch, D.G., *et al*. (2007) Glycosylation of Pseudomonas aeruginosa strain Pa5196 type IV pilins with mycobacterium-like alpha-1,5-linked d-Araf oligosaccharides. *J Bacteriol* **189**: 151–159.

Williams, B.J., Dehnbostel, J., and Blackwell, T.S. (2010) Pseudomonas aeruginosa: host defence in lung diseases. *Respirology* **15**: 1037–1056.

Witney, A.A., Gould, K.A., Pope, C.F., Bolt, F., Stoker, N.G., Cubbon, M.D., *et al*. (2014) Genome sequencing and characterization of an extensively drug-resistant sequence type 111 serotype O12 hospital outbreak strain of Pseudomonas aeruginosa. *Clin Microbiol Infect* **20**: O609–O618.

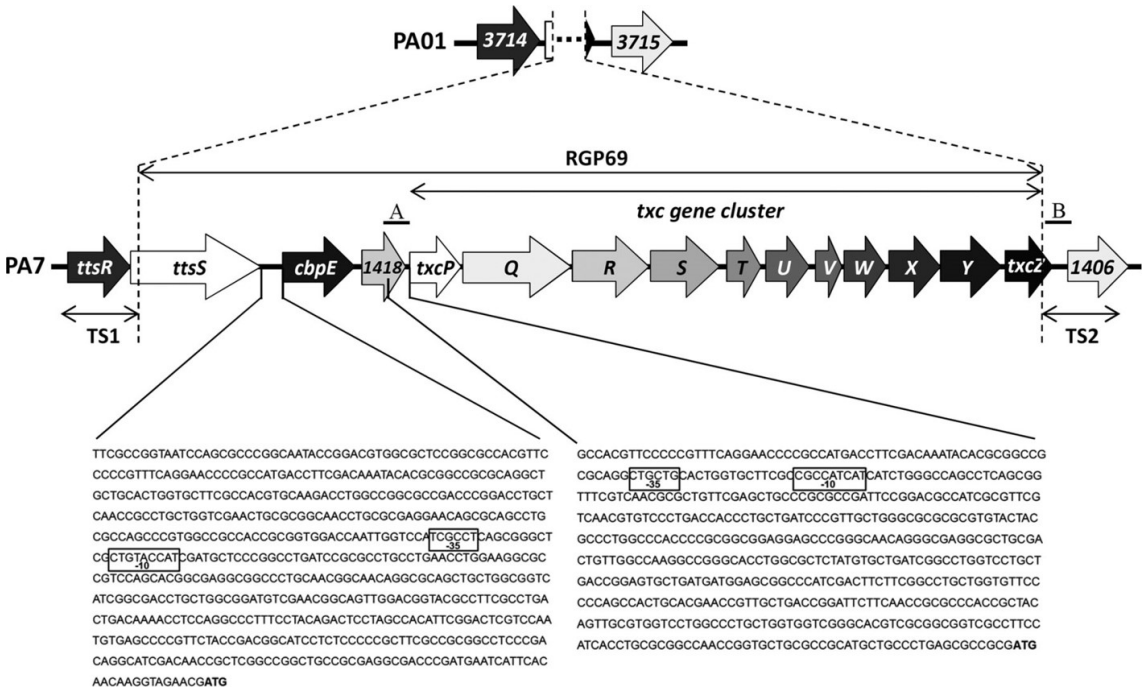

Figure 1.10. **Genomic organization of the RGP69 of PA7.** The genomic island RGP69 possesses 14 predicted ORFs encoding the 11 putative T2SS Txc components (TxcP to TxcZ) and 3 genes, a gene encoding a predicted chitin-binding protein (CbpE), a gene encoding an unorthodox sensor protein (TtsS), and PSPA7_1418, which is predicted to encode a protein belonging to the cytochrome b superfamily. RGP69 is externally flanked by the ttsR and PSPA7_1406 (1406) genes, which are homologous to the two contiguous genes PA3714 (3714) and PA3715 (3715), respectively, in strain PAO1, from [129].

2

Type V Secretion Systems

Contents

The Type V secretion systems (T5SS) are exclusively found in Gram-negative bacteria and are widespread among them. The T5SS are involved in diverse bacterial functions through the secretion of virulence factors directed against eukaryotic or bacteria cells. These functions are related for example to contact-dependent growth inhibition (CDI) systems , cell-to-cell adhesion and biofilm formation [138].

Recent bioinformatics analysis showed different subtypes of T5SSs based on the functions of the substrates (Table 2.1). In general, secreted proteins are adhesins, proteases, cytolysins/haemolysins and toxins of CDI system [139, 140].

T5SSs are composed of a so-called "passenger domain" polypeptide (T5SS-substrates or secreted domain) and a transporter domain that forms a β-barrel pore. The passenger proteins are generally high-molecular proteins ranging from 70 kDa (McaP of *M. catarrhalis*) to 230 kDa (FHA of *B. pertussis*) and form fibrous structures, often β-helices. Two major classes comprise the T5SS: autotransporters (AT) and the Two-partner Secretion (TPS) systems. Among AT, four subtypes are defined (Va, Vc, Vd and Ve). The major difference between AT and TPS system resids in the localization of the passenger domain: in the AT system the passenger domain remains bound to the the membrane, whereas in TPSs (subtype Vb) the substrate is secreted in their environment.

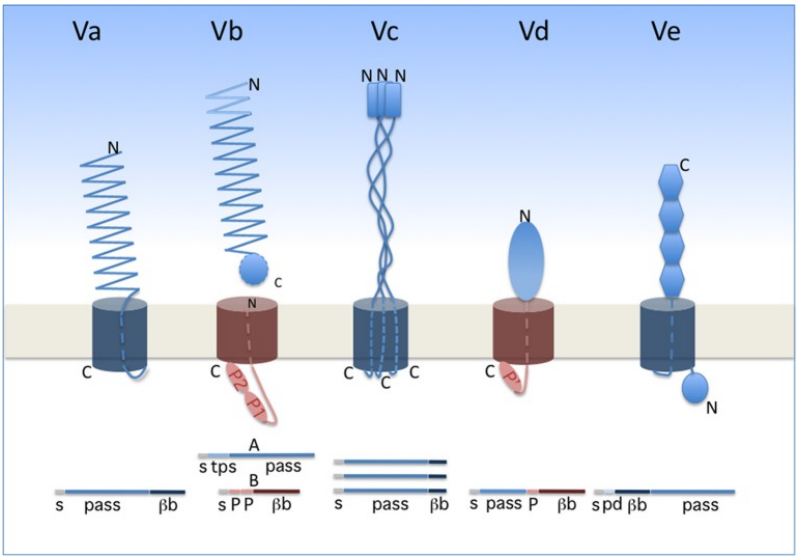

Figure 2.1. **Type V secretion subtypes.** A linear representation is shown underneath the schematics. The orientation of each protein is indicated by its N and C termini (denoted N and C). The POTRA domains (small ovals) are denoted P1, P2, and P' (POTRA-like domain in PlpD). s, signal peptide; pass, passenger domain; β-barrel domain; tps, TPS domain of TpsA proteins; pd, periplasmic domain of type Ve proteins [141].

Proteins	Organisms	Mol WT	Classe	T5SS types	Motifs	Characteristics
Ag43	*E. coli*	106,842	Adhesin	classical AT	RGD cell attachement sequence, aspartyl protease active site, leucine zipper pattern	autoagglutinination/biofilm formation
AIDA-I	*E. coli*	132,272	Adhesin	classical AT	none	adherence
AlpA	*H. Pylori*	56,124		classical AT	leucine zipper pattern	Lipoprotein, binds epithelial cell and human laminin
Apr58 (EnfA)	*E. coli*		Adhesin	TPS		adhesion and hemagglutination activities
BadA	*B. henselae*	328 kDa/ monomer	Adhesin	TAA		Cat scratch disease, bacillary angiomatosis, peliosis hepatis
BcpA	*Burholderia* species		CDI system	TPS		contact grotwth inhibition, biofilm formation
BrkA	*B. pertussis*	103,377	other	classical AT	RGD cell attachment sequence	resistance serum
BrpA	*B. vinsonii*		Adhesin	TAA		Not known
CdiA	*E. coli*		CDI system	TPS		contact grotwth inhibition,
CdrA	*P. aeruginosa*		Adhesin	TPS		Biofilm, binding to PSl exopysaccharides
EatA	*E. coli*	147,696	Protease	classical AT	peptidase S6 IgA endopeptidase/ peptidase S1 chymotrypsin	none
EpeA	*E. coli*	147,34	Protease	classical AT	peptidase S6 IgA endopeptidase/ P-loop ATP/GTP binding site motif	mucinolytic activity
EspC	*E. coli*	140,861	Protease	classical AT	peptidase S6 IgA endopeptidase	Enterotoxic activity
EspI	*E. coli*	146,131	Protease	classical AT	peptidase S6 IgA endopeptidase/ P-loop ATP/GTP binding site motif	degradation of plasma proteins
EspP	*E. coli*	141,758	Protease	classical AT	peptidase S6 IgA endopeptidase/ P-loop ATP/GTP binding site motif	cytotoxic activity
EstA	*P. aeruginosa*	69,609	other	classical AT	Lipolytic GDSL active-site enzyme	Lipolytic activity/ esterase
EthA	*E. tarda*		Cytolysin/hemolysin	TPS		Cytolysin, mediates cellular invasion fish
EtpA	*E. coli*		Adhesin	TPS		Adhesin, mediating binding of flagella to host cells
ExlA	*P. aeruginosa*	172	Cytolysin/hemolysin	TPS		Pore forming toxin
FHA	*B. pertussis*	230	Adhesin	TPS		Adhesin, binds epithelial ells, biofilm formation, immunomodulation
Hap	*H. influenzae*	155,44	Protease	classical AT	Peptidase S6 IgA endopeptidase, peptidase S1 chymotrypsin	Adhrence, microcolony formation
HecA	*E. chrysanthemi*		CDI system	TPS		Adhesion to plant tissues, auto aggregation
HhdA	*H. ducreyi*		Cytolysin/hemolysin	TPS		
Hia	*H. influenzae*	114	Adhesin	TAA		humans RTIs, meningitis
HlpA	*P. putida*		Cytolysin?	TPS		Seed and root colonization
HMW1	*H. influenzae*		Adhesin	TPS		Adhesion to epithelial cells
HMW2	*H. influenzae*		Adhesin	TPS		Adhesion to epithelial cells
HpmA	*P. mirabilis*		Cytolysin/hemolysin	TPS		Ca2+ -dependent cytotlysin
HrpA	*N. meningitidis*		CDI system	TPS		Adhesin, intracellulaire survival, biofilm formation
Hsf	*H. influenzae*		Adhesin	TAA		humans RTIs, meningitis

(Continued)

(Continuation)

Proteins	Organisms	Mol WT	Classe	T5SS types	Motifs	Characteristics
HxuA1	*H. influenzae*		Iron acquisition	TPS		Binding of heme and heme hemopexin
IcsA/VirG	*S. flexneri*	116,244	other	classical AT	none	Intracellular spread/motility/Actin-based mobility
IgA protease	*N. gonorrheae*	196,351	Protease	classical AT	Peptidase S6 IgA endopeptidase	Immunoglobulin protease: degradation of IgA1 LAMP-1 and synaptobrevin
Intimin	*E. coli*		Adhesin	Inverse AT		attachement to host cells
invasin	*Ysersinia* species		Adhesin	Inverse AT	Ig domain	bind directly the b1 integrin
LepA	*P. aeruginosa*		Protease	TPS		Secreted protease cleaves human protease-activated receptors
LspA1/ A2	*H. ducreyi*		unknown/ Adhesin?	TPS		Inhibition of phagocytosis
McaP	*M.catarrhalis*	71,484	other	classical AT	Lipolytic GDSL active-site enzyme	esterase/phospholipase B activity, adherence to human epithelial cells
MhaA	*M. catarrhalis*		Adhesin	TPS		binding to epithelial cells
MisL	*S. typhimurium*	101,216	other	classical AT	none	Adhesion bonds fibronectin
NadA	*N. meningitidis*		Adhesin	TAA		human meningitis sepsis
NalP	*N. meningitidis*	113,64		classical AT	peptidase S8A subtilisin-like serine protease, prokaryotic membrane lipoprotein lipid attachement site	proteolytic processing of secreted proteins
PdtA	*P. aeruginosa*		unknown	TPS		virulence of nematode model
Pertactin	*B. pertussis*	93,453	Adhesin	classical AT	adherence RGD cell attachement sequence	Adhesin
Pet	*E. coli*	139,769	Protease	classical AT	peptidase S6 IgA endopeptidase/ P-loop ATP/GTP binding site motif	enterotoxic and cytopathic toxin effects, cleavage of spectrin
PhlA	*P. luminescens*		Cytolysin/hemolysin	TPS		
Pic	*E. coli*	146,45	Protease	classical AT	Peptidase S6 igA endopeptidase	Mucinase-activity, colonization
PlpD	*P. aeruginosa*	80,899	other	Type Vd		Lipolytic activity/phospholipase A2
pmpD	*C. trachomatis*	160,748		classical AT	none	Adherence/ Cysteines proteinase involved in virulence
rOmpB	*Rickettsia sp.*	168,184	other	classical AT	none	adherence/ S-layer
RscA	*Y. enterocolitica*		Adhesin	TPS		limitation of splenic dissemination
Sat	*E. coli*	140,043	Protease	classical AT	peptidase S6 IgA endopeptidase/ P-loop ATP/GTP binding site motif	vacuolating cytotoxin
SepA	*S. flexneri*	145,938	Protease	classical AT	peptidase S6 IgA endopeptidase/ peptidase S1 chymotrypsin	tissue invasion/ inflammation
ShdA	*S. enterica*	207,033	Adhesin	classical AT	Heamaglutinin repeat, P-loop, ATP/GTP binding site motif	adherence, prolonged fecal shedding of bacteria
ShlA	*S. marcescens*		Cytolysin/hemolysin	TPS		cytolysin, hemolysin, pore forming toxin
SigA	*S. flexneri*	139,676	Protease	classical AT	Peptidase S6 igA endopeptidase	Cythopathic effect on host cells by cleaving intracellular targets
SphB1	*B. pertussis*	109,801	Protease	classical AT	peptidase S8A subtilisin-like serine protease	proteolytic processing of secreted proteins
SSP	*S. marcescens*	112,345	Protease	classical AT	peptidase S8A subtilisin-like serine protease RGD cell attachement sequence	
TibA	*E. coli*	101,112	Adhesin	classical AT	none	Adhesin, invasions, bacterial aggregation, biofilm formation
Tsh/Hbp	*E. coli*	148,227	Protease	classical AT	peptidase S6 IgA endopeptidase/ P-loop ATP/GTP binding site motif	heme binding protein
UspA1 and 2	*M. catarrhalis*		Adhesin	TAA		human RTIs/ serum resistance
VacA	*H. pylori*	139,761	toxin/other	classical AT	none	vacuolating toxin/ PFT
XadA	*X. campestris*		Adhesin	TAA		Black rot
XadA	*X. oryzae*		Adhesin	TAA		Bacterial leaf blight
YadA	*Y. enterocolitica*	43 kDa	Adhesin	TAA	Oligomeric coiled-coil	enteritis, mesenterc lymphadenitis, reactive arthritis/ serum resistance

Table 2.1. **Type V secretion system substrates** adapted from [141]

2.1 Autotransporters

2.1.1 Architecture and biogenesis of AT

ATs are single polypeptide containing components that allow them to secrete themselves. ATs carry (i) a signal peptide (SP) in N-terminal region (N-ter) that targets the protein to the Sec translocon for the transport across the IM, (ii) a passenger domain which is the actual secreted and functional protein, (iii) a linker and (iv) in C-terminal region (C-ter) a 12-stranded transmembrane β-barrel of 30 kDa (the β-domain), that facilitates, with the linker domain, the translocation of the passenger domain across the OM constituting a translocation pore to transfer the passenger (Figure 2.2) [142].

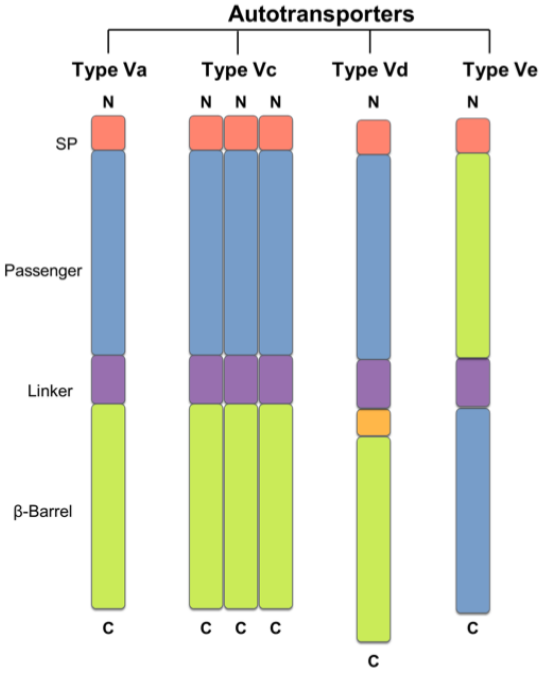

Figure 2.2. **Schematic representation of domain organization among ATs.** SP: signal peptide; Passenger domain; Linker; β-barrel (from)

Signal peptide

The Sec machinery is composed of a membrane embedded protein conducting channel that consists of three integral membrane proteins, SecY, SecE and SecG, and a peripheral associated ATPase, SecA, that functions as a molecular motor to drive the translocation of secretory proteins across the membrane. This system is involved in the secretion of unfolded proteins across the IM and the insertion of membrane proteins into the OM [143]. The signal peptide is a short sequence recognized by the Sec machinery and allows the export. It is defined by 20 amino-acid residues with a tripartite structure: *i.e.* a positively charged amino-terminal (n-region), a hydrophobic core (h-region) and a polar carboxyl-terminal (c-region) region. This

sequence is highly conserved and is required to direct transport of the AT proteins across the IM. It is typically cleaved after the translocation at the consensus motif (AxA) (Figure 2.3).

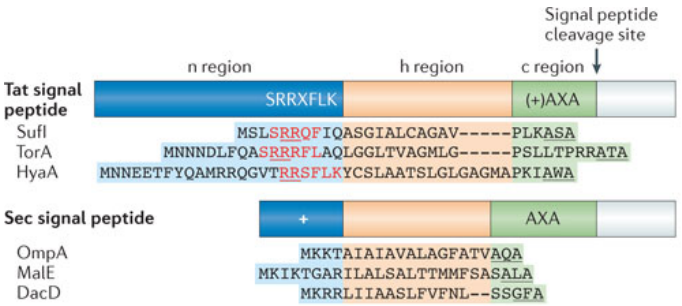

Figure 2.3. **Signal peptide.** The tripartite structure of Sec-dependent non-lipoprotein signal peptides, where the N-terminus is characterized by the presence of positively-charged residues (blue), the core of the peptide is comprised of hydrophobic residues (orange), and the C-terminus is typically neutral, but polar and contains the cleavage site (green) [144].

Around 10% of identified ATs contain an unusual N-ter extension of 50 to 60-residues signal peptide beginning by the motif MN(R/K). These long signal peptides maintain the passenger domain in a conformation compatible with its translocation across the OM. Long signal peptides are especially common in TAAs family [143].

Passenger domain

The passenger domains of the type V-proteins displays common features. Especially they adopt a stable and defined structure containing repeated structural units. This domain varies widely in size (from 20 kDa to 400 kDa) and in sequence and this variability reflects their functional diversity[142, 145].

The primary structure of the passenger domain does not carry a specific motif. However, *in silico* and structural prediction analyses show that they possess a common tertiary structure. The passenger domain generally folds into elongated β-helical structure and these fibers appeared to be rigid rods. In many cases, the passenger is cleaved in an auto-catalytic process after translocation is completed, releasing the passenger into the extracellular medium. In some cases, the passenger domain remain anchored to the membrane. Generally, the difference of process results in the difference of "functions"; the passengers of cleavable proteins have enzymatic functions such as protease or lipases, while noncleavable ones, act as

adhesins proteins [145].

The *B. pertussis* protein pertactin forms a sticking 16-turn parallel β helix with a hydrophobic core [146]. Recently the crystal structure of 1048-residues of Hbp, a member of serine protease ATs was solved and found similar to the pertactin except that it is longer (24 turns), less regular and twisted in the center. These two examples suggest a general design in which autotransporter use β-helix as scaffolding on which are appended various loops and domains that mediate the effector function of the protein. This structure was predicted in more than 95% of the passenger domains [147, 148].

Linker domain

All the AT proteins possess a linker, defined as the region connecting the C-terminus domain of the passenger to the N-terminus of the transmembrane β-barrel domain [149, 150]. The linker is an α-helix within the center of the transmembrane β-barrel. In many ATs, the linker included a disordered region in N-ter to the α-helix. If the passenger is cleaved from the β-barrel after the OM translocation, this cleavage site can be located within the linker and after OM translocation will be positioned either on the cell surface or within the folded β-barrel structure.The linker is required for the secretion in all characterized ATs [149, 151].

β-barrel domain

The last domain of the ATs is the β-barrel. The first structure solved was the β-domain of *Neisseria meningitidis* NalP, a 12-stranded structure inserted in the OM. The β-barrel is a hydrophilic pore of 1 nm in diameter [152] blocked by the α-helix of the linker. EspP of *E. coli* shows the same features as NalP [153]. EstA also possesses a 12-stranded β-barrel linked to the passenger domain. Apparently, there is a common structure for the β-barrel, whether or not the passenger domain is cleaved.

The β-barrel is annotated in PFAM databases and corresponds to PFAM03797. It is relatively easy to identify this region in protein sequences. The β-domains, unlike the passenger domains are very similar in size consisting of the last 300 amino acids.

Outer membrane β-barrel (OMBBs) proteins form a major group of OM proteins in Gram-negative bacteria, chloroplasts and mitochondria. Remmert *et al.*, found evidence that β-barrel domain from T5SS are homologous and evolved from an ancestral β-β hairpin sequence [154].

2.1.2 Classification

Classical ATs (type Va)

The type Va systems are the prototype of the AT systems and were first described in 1987, with the example of IgA1 protease of *Neisseria gonorrhoeae* [155].

It has been proposed that classical ATs are composed of a C-terminal 12-stranded-β-barrel domain forming a pore in the OM though which the passenger domain is transported toward bacterial surface (Figure 2.1). For example, IgA1 is further cleaved by auto-proteolyis and is found in the extracellular medium. Since, the discovery of IgA1, many other ATs have been described [155] (Table 2.1).

In silico analyses identified three putative ATs in *P. aeruginosa* genome: PA0328, PA3535, PA5112 [156, 157]. PA0328 (AaaA) is an arginine-specific aminopetidase. Absence of AaaA led to attenuation of virulence in a mouse chronic wound infection which correlated with lower levels of the cytokines TNF, IL-1α, KC and COX-2. The exact molecular mechanism of its action on the immune system remains still unclear.

EstA (PA3535) exhibits an esterase activity (PFAM00657) (Table 2.1) [158, 159] and is composed of two distinct domains, of which the N-terminal domain harbors the enzymatic activity whereas the C-terminal transporter domain represents a β-barrel pore in the OM. EstA remains anchored to the OM [158, 160]. EstA was the first AT for which the crystal structure of the entire protein has been solved. The EstA passenger domain displays the characteristic alpha-beta-alpha globular fold of the Serine-Glycine-Asparagine-histidine (SGNH) hydrolase family [161], with a small central four-stranded parallel β-sheet sandwiched on both sides by α-helices (Figure 2.4) .

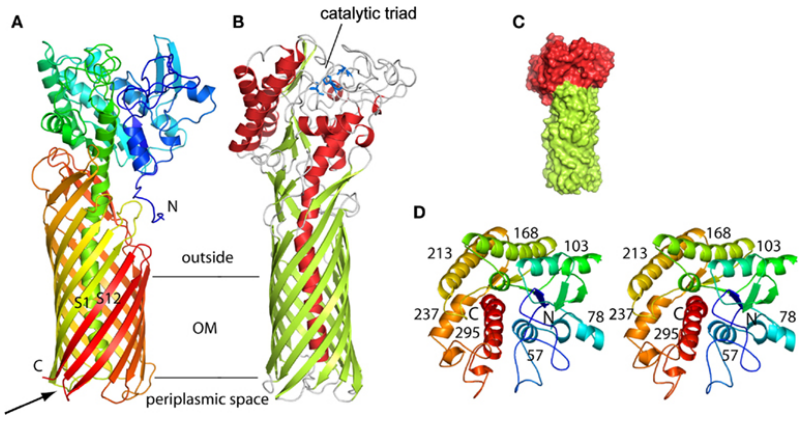

Figure 2.4. ***P. aeruginosa* EstA autotransporter (T5aSS).** Structure of the *P. aeruginosa* EstA autotransporter (T5aSS), reproduced from [148]. (A) Backbone representation viewed from the side, with the protein colored by a gradient from blue at the N-terminus to red at the C-terminus. (B) Backbone view 90°C rotated within the plane of the membrane relative to (A), with helices colored red β-strands colored green, and loops colored gray. The catalytic triad residues are shown as blue stick models. Horizontal lines indicate the approximate location of the OM core. (C) Surface view of EstA from the side with the β-barrel domain colored green and the passenger domain colored red. (D) Stereo view of the EstA passenger from the extracellular side, colored as a rainbow from dark blue at the N-terminus to dark red at the C-terminus. The numbers are those for the central residue of the α-helix.

EstA was first identified by signature-tagged mutagenesis (STM) performed in a rat model of chronic respiratory infection [162]. Furthermore, EstA is required for swimming, swarming, and twitching of *P. aeruginosa*. These effects were found to

depend on the catalytic activity of EstA and it has been proposed that EstA may modify rhamnolipid biosynthesis [159].

Trimeric AT (type Vc)

The type Vc systems are the most complex of the AT systems and are called trimeric autotransporter adhesins (TAAs) [163]. The best characterized TAA is YadA from enteropathogenic *Yersinia* species, which cause a variety of diseases in humans such as diarrhoea, septicaemia, reactive arthritis and plague [163, 164]. YadA is essential for the infection [163], because its provides to bacteria serum resistance thought its adhesin function. The passenger domains of TAA are highly diverse and modular while the translocation domains are highly conserved. Electron microscopy of several TAAs revealed a similar architecture that resembles a lollipop and consists of a head, stalk and anchor domains (Figure 2.5) [165].

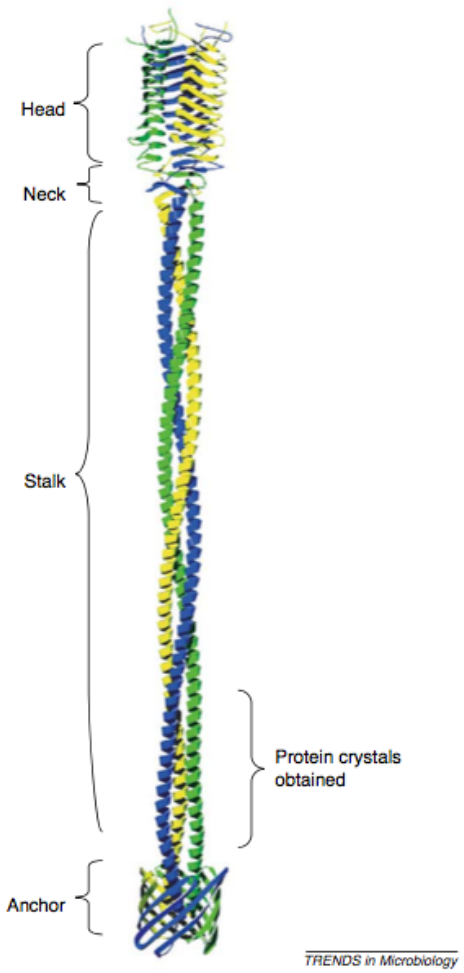

Figure 2.5. **Structure of YadA.** The head and neck domains are known in molecular detail and crystals have been obtained for parts of the stalk and for the anchor domain [163].

The anchor is a 70-residues long domain, essential and sufficient for the transport

of the passenger domain through the OM [164, 166]. The membrane anchor domain contains four heptads of a left-handed coiled coil followed by four transmembrane β-strands, which presumably assemble into 12-stranded β-barrel in the trimer.The stalk domain is fibrous, highly repetitive structure and extremely variable in length. It is composed of α-helices [163]. The "neck" is a small part connecting the stalk and the head. It does not possess a defined secondary structure [167]. Moreover, the neck creates a hydrophobic core thanks to several hydrogen liaisons. The head at the N-terminal extremity of the protein, after the signal peptide, is responsible for TAAs adherence capacity. This domain is a trimer of single-stranded left-handed β-helices. Up to date, no TAAs has been described in *P. aeruginosa*.

Patatin-like proteins (type Vd)

The Type Vd is very similar to the type Va systems with a C-terminal translocation domain and an N-terminal "passenger domain". The major difference between them is the presence of an additional periplasmic domain homologous to the periplasmic domain (POTRA) of the Type Vb translocation proteins. This new family of bacterial lipolytic enzymes is composed of patatin-like proteins (PLPs). The first PLP-protein that has been characterized in *P. aeruginosa* was ExoU which is a toxin secreted through the T3SS [168, 169]. *In silico* analyses revealed that around 200 proteins harbor a PLP domains, both in Gram-negative or Gram-positive-bacteria. One of them was characterized from *P. aeruginosa* [170]. PlpD is a 728-residue protein that harbors an N-terminal signal peptide, a central functional domain and a C-terminal region that is predicted to fold into a 16-stranded transporter β-barrel. The crystal structure of its passenger domain (amino-acids from 20 to 233) shows an extremely compact fold (Figure 2.6), characterized by an α/β-hydrolase fold with a twisted 6-stranded central β-sheet surrounded by 8 major helices, which is common to a number of esterases and hydrolytic enzymes, including human cPLA2, VipD and ExoU, PLPs from *Legionella pneumophila* and *P. aeruginosa*, respectively [3].

PlpD has a phospholipase A1 activity [3] and is the first example of an active phospholipase secreted by T5SS. In collaboration with the team of Dr. Andrea Dessen (IBS, Grenoble), I participated to demonstrate the functionality of PlpD. My work showed that PlpD destabilizes liposomes composed of Phosphatidyl-Choline and Phosphatidyl-Serine at pH8. Moreover, a mutation at Ser60 in the catalytic site provoked the loss of enzymatic activity of PlpD but not of its liposome disruption activity (Figure 2.7), suggesting that PlpD could employ both its catalytic activity and its membrane-interacting C-terminal region to bind to and disrupt membranes, possibly in a cooperative fashion [3].

The function of the POTRA domain of PlpD remains unclear as it is more comparable to Omp85/BamA family than to the TpsB one, suggesting a different function.

Inverted AT (type Ve)

The type Ve are called inverse autotransporters based on the fact that the domain order is reversed. The C-terminal part comprises the passenger domains, while the N-ter part forms the translocation pore [171]. Intimin and invasin are the prototypical

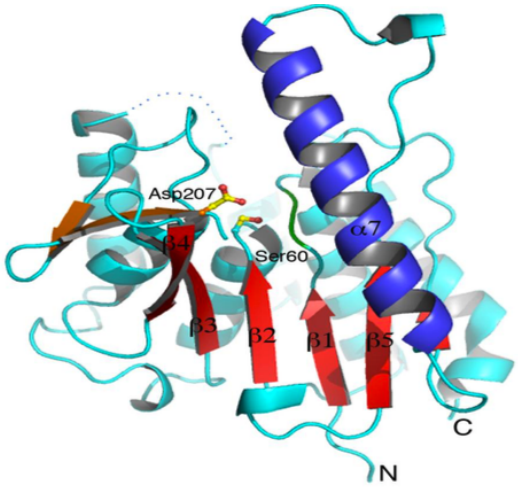

Figure 2.6. **Tertiary fold of PlpD 20-333.** PlpD 20-333 presents a compact α/β-hydrolase fold and an unusual 23-residue helix (α-7) towering over the active site [3].

members of inverted ATs composing a large family of virulence-related bacterial adhesins. Their modular passenger domains are composed of IgG-like and lectin-like domains. Intimins are found in enteropathogenic and enterohaemorrhagic *E. coli* (EPEC and EHEC), pathogens that adhere "intimately" to the colonic epithelium and cause the formation of actin pedestals and the disruption of the microvilli on the enterocyte surface. Intimin plays a central role in this attachment. Invasin is found in the two enteropathogenic *Yersinia* species, *Y. enterocolitica* and *Y. pseudotuberculosis* and binds directly to host β-1 integrins [172].

Polar localization of autotransporters

The polar localization of ATs has been established for some of ATs and is required for their function, as is the case for IcsA from *Shigella flexeneri* [173]. AIDA-I, BrkA and SepA exhibit a unipolar localization, suggesting a secretion at the pole of the bacteria. While the Sec machinery is distributed uniformly in the IM, the peptidoglycan and the OM are relatively inert at the pole compared to along the length of the cell (Figure 2.8) [173].

Since many ATs are widespread among gram-negative pathogens and have important roles in the virulence, their localization at the pole suggests an importance of orientation of the bacterial body in pathogen-host interactions.

2.2 Two-partner secretion system

The Type Vb or TPS systems are a split version of the classical AT systems (Type Va) (Figure 2.9). The passenger domain and the translocator domain (β-barrel) are two separate proteins, called TpsA and TpsB respectively. The TpsA is responsible for the toxic or adhesive activities and the TpsB allows the secretion of the TpsA.

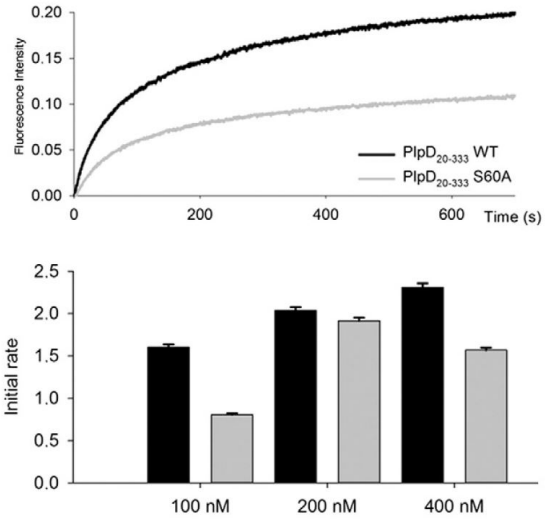

Figure 2.7. **PlpD displays phospholipase activity.** (Top) Liposome disruption assay showing that PlpD20-333 is active against lipid bilayers. Large unilamellar vesicles containing the encapsulated sulforhodamine B dye were incubated with 100 nM PlpD20-333Ser60Ala (gray) and fluorescence increase was monitored, reflecting dye release upon vesicle disruption. (Bottom) Initial rates were calculated during the first 50 s of liposome disruption at three protein concentrations [3].

The term TPS was first used to define the ShlBA of *S. marcescens* [174], FhaBC of *B. pertussis* [175], HmpAB of *P. mirabilis* [176], HMW1ABC and HMWABC of non-typeable *H. influenzae*.

More than hundred genes encoding TpsA and TpsB are found in the genomes of both pathogenic and environmental bacterial species [139]. The hallmarks of the TPS systems are the POTRA domains of the TpsB proteins and the TPS domain of the TpsA proteins. By BLAST, it is easy to identify new TPS system by searching these specific sequences. Genome analyses and in particular the GC% content of these genes suggest that some of them may have been acquired by horizontal transfer [177].

2.2.1 Anatomy of TpsA and TpsB proteins

2.2.1.1 TpsA

Functions associated to TpsA proteins are highly diverse and can be involved in cytolysis, adherence, CDI and iron acquisition (reviewed in [141]). The TpsA proteins are proteins of more than 100 kDa that possess very divergent sequences. However, they carry some conserved domains, including the signal peptides allowing their export via the Sec machinery and the TPS domain for their secretion through the TpsB.

TPS domain All TpsA proteins share a conserved, 250-residue-long TPS domain corresponding to the minimal region needed for its secretion, as demonstrated for

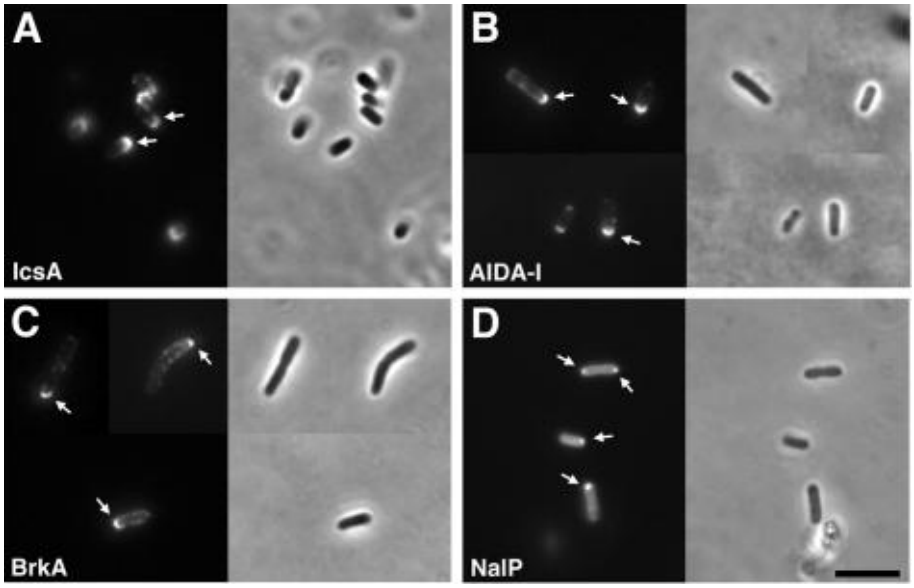

Figure 2.8. **Distribution of autotransporter proteins as detected by labeling live bacteria prior to fixation.** (A) *S. flexneri* autotransporter IcsA on the surface of intact *S. flexneri*. (B) Diffusely adherent *E. coli* autotransporter AIDA-I on the surface of intact *E. coli* cells, which express a complete LPS. (C) *Bordetella* autotransporter BrkA on the surface of intact *E. coli* cells . (D) *N. meningitidis* autotransporter NalP on the surface of intact *E. coli* BL21(DE3) cells, which expresses a complete LPS. Arrows, polarly localized autotransporter protein. Left panel, fluorescence image; right panel, phase-contrast image. Size bar, 5 μm [173].

FHA, HMW1A and ShlA. Located at the N-terminus of the mature TpsA protein, this essential domain mediates molecular recognition of TpsB-POTRA domains in the periplasm. The direct interaction between TPS and POTRA domains has been observed by co-immunoprecipitation and surface plasmon resonance (SPR). This interaction allows the coupling of the secretion and the TpsA folding at the surface of the bacteria [178–183].

Sequence alignment of the TPS domains shows that few residues are highly conserved. Two motifs ILNEV (109-114 residues) and ANPNGI (136-141) are essential in the secretion of the TpsA proteins (Figure 2.10). Moreover, theses motifs play a role in the stabilization of the protein structure. The mutation of the first asparagin residue in "ANPNGI" region leads to the loss of the secretion of FHA and ShlA [178, 183]. However this same mutation has no impact on the secretion of HMW1A.

The phylogenetic tree based on TPS domains allows to distinguish subfamilies of TPS domains (Figure 2.10)[141], with cytolysins/hemolysins (in red), the adhesins (in green), the CDI systems (in yellow) and the proteins involved in iron acquisition and proteases (black). The different TPS sub-families are in agreement with the functions exerting by the TpsA proteins.

The structures of TPS domains of FHA30 of *B. pertussis* [182], HpmA of *P. mirabilis* [184], HMW of *H. influenza* [185] and HxuA of *H. influenzae* [186, 187] are

Figure 2.9. **Two Partner Secretion system (TPS).** SP: signal peptide (red), TPS domain (purple); passenger domain (blue); POTRA domains (orange); β-barrel (green)

available (Figure 2.11). They show a similar β-helical structure with 3 extra-helical motifs displaying a triangular shape. The crystal structure itself does not explain the "secretion signal", because interactions between the cargo and the transporter only occur with an unfolded TPS domain [183].

Transported domain This part of the protein is responsible for the function of the TpsA. The different functions of the TpsA protein are detailed in the section 2.2.3.

Due to the large size of the TpsA proteins, the entire organization of the protein is still unknown. However, the structure of FHA was investigated using electron microscopy and the global shape was described as an elongated β-helix 50 nm long formed from regions of tandem repeats.

2.2.1.2 TpsB proteins

The second partner of the TPS system is the TpsB protein belonging to the superfamily of Omp85 from which BamA transporter, that assemble proteins in the OM, is the best known. The TpsB are composed from 500 to 800 residues. The structure of FhaC, the only one available, serves as a model for TpsB proteins [188]. They are composed of POTRA domains, located in the periplasm and the β-barrel in the OM. The resolution of the FhaC structure followed by biochemical approaches helped to understand the role of these domains.

The N-ter of FhaC is located on the extracellular side of the membrane domain and is followed by 20-residues organized in α-helix, called the H1. H1 passes through the β-barrel pore and is connected by a 30-residue proline-rich linker to two successive POTRA domains in the periplasm. It is constituted of a small sheet of 3 β-antiparallel strands lined by two α-helices (Figure 2.12) [188, 191]. These structures are organized as β-α-α-β-β motifs and create a hydrophobic cavity necessary for the secretion of the TpsA proteins. The deletion of POTRA domain does not destabilize the global conformation of the FhaC protein, but totally abolished the secretion of FHA [188, 192]. As previously described, the interaction of POTRA domains and TPS domains allows the secretion of the TpsA protein.

The C-ter domain of FhaC forms the β-barrel composed of 16 anti-parallel β-strands (B1 to B16) in the OM [193]. The external diameter of the pore is around 3.5 nm and the internal diameter is around 0.3 nm. This difference of size is explained

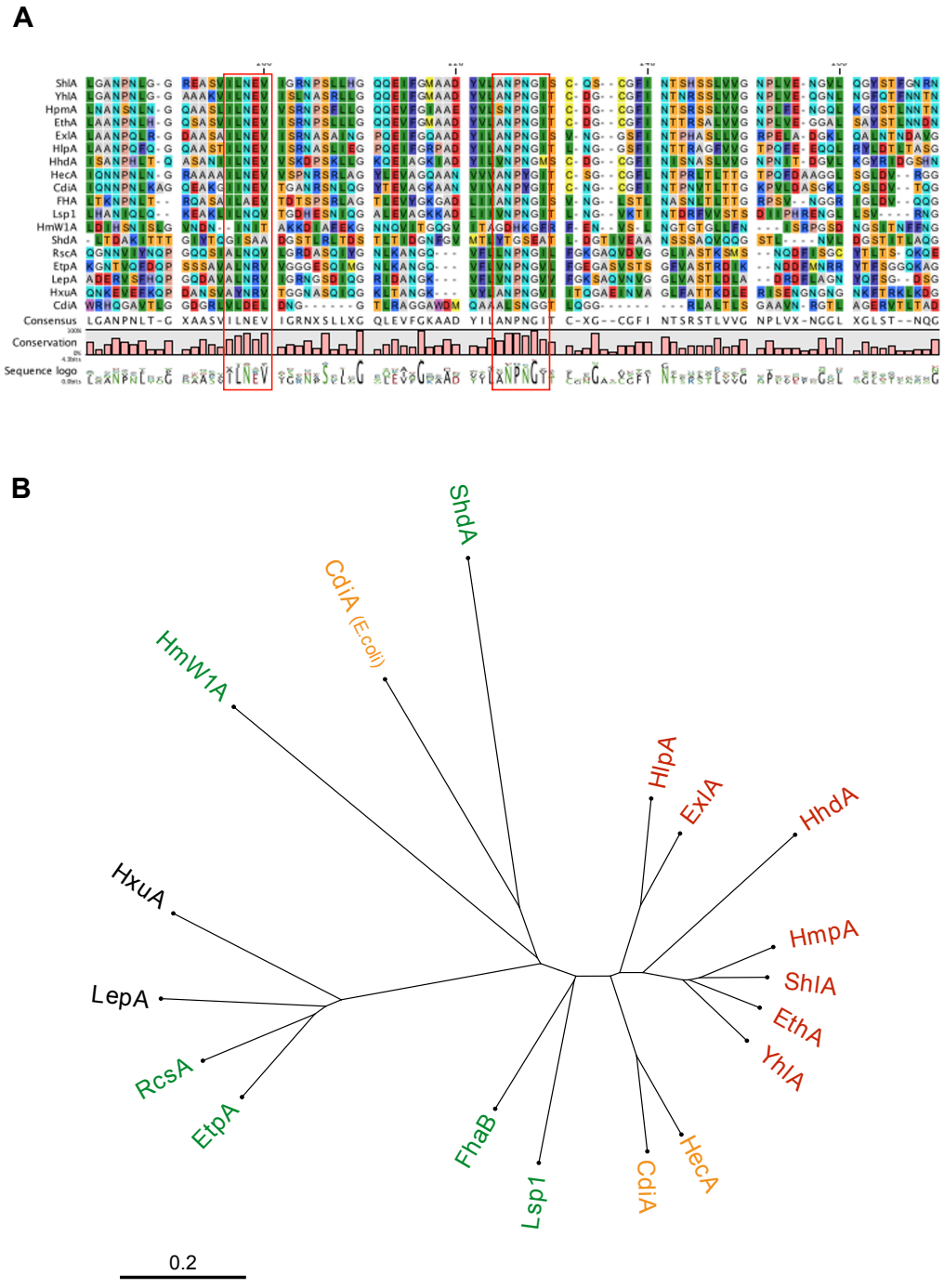

Figure 2.10. Phylogenetic tree based on TPS domains. (A-B) TPS domain sequences of TpsA proteins were aligned and the unrooted phylogenetic tree was constructed using Neighbor joining method with CLC software. Red for cytolysins/hemolysins, green for adhesins, orange for CDI systems, black for proteases and iron acquisition, adapted from [141]

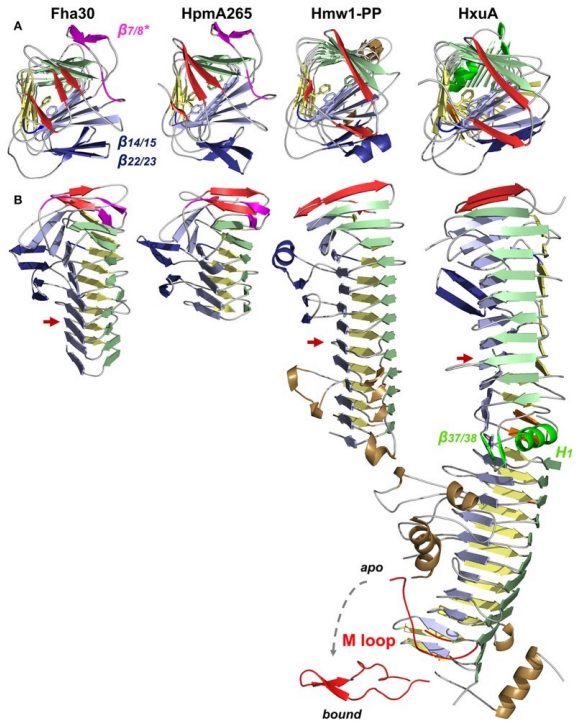

Figure 2.11. **X-ray structures of TpsA proteins.** (A) Views from the N-terminal top of the β-helix axis. Residues of the aromatic cluster are shown in stick representation. (B) Side view of TpsA structures. Red arrows indicate the end of the TPS domain.

by the presence of the α-helix H1 and the long extracellular loop L6 occluding partially the pore. The loop L6 is a hallmark of the Omp85 transporters with the VRGY/F motif. L6 is essential for the activity of Omp85 proteins [194–196].

2.2.2 Pathway of TpsA proteins across the cell envelope

Inner membrane and periplasm. TpsA proteins are synthesized as preproteins and their N-terminal signal peptide determines the Sec-dependent export across the cytoplasmic membrane. The signal peptide has been already described in section 2.1.1. The TpsA proteins reach the periplasm, where they remain in extended conformations for their interactions with their TpsB transporters.

Some periplasmic intermediates were detectable for TpsA proteins such as ShlA and OtpA. In the periplasm, ShlA was shown to be inactive (ShlA*) [197–199]. It was shown for OtpA of *E. coli*, that the export of OtpA in the periplasm can be done before the expression of *otpB* (TpsB), meaning that OtpA can remain stable in the periplasm until its export by OtpB [199]. In other TPS systems they appear to be quickly degraded, as it is the case for HMW1A and HMW2A. The passage in the periplasm was also described in the case of FHA. DegP, a protein-chaperonne associated with the cytoplasmic membrane, was shown to facilitate the secretion of FHA [200, 201]. The role of DegP has been shown in type Va, Vc, and Ve systems, suggesting that it might play a common role in the type V pathway [171, 202, 203].

Figure 2.12. **Omp85 transporters: X-ray structures to mechanistic models.** (A) Cartoon representations of FhaC from *B. pertussis* (PDB entry 4ql0) [189] and BamA from *N. gonorrhoeae* (4k3b) [190]. The common structural features include the 16-strand barrel in gold, the L6 loop in blue and the last two POTRA domains in wheat and brown (POTRA1 and POTRA2 for FhaC). The β-1 and β-16 strands are shown in red. Specific elements include the N-terminal α-helix of FhaC in purple, and the POTRA3-2-1 domains of BamA in yellow, pink, and cyan, respectively.

Outer membrane The first step of secretion is the binding of the TPS domain to the POTRA domains is followed by the transport of the TpsA protein to the cell surface. The path of translocation of FHA across the OM has been partially investigated and up to date two models have been proposed for the translocation across the TpsB (Figure 2.13).

In the first one, the TpsA protein forms a hairpin in the pore. The TPS domain remains bound to the POTRA domains of the TpsB protein throughout the entire process and the rest of the TpsA is progressively translocated and folds at the cell surface. The TPS domain is then released at the late stage of the translocation [205].

According to the second model, the TPS domain reaches the surface first and nucleates the folding of the rest of the protein [206]. The second mechanism seems to be confirmed for the secretion of FHA [139, 207]. In addition, the stable TPS fold and the observation that a TPS domain can initiate TpsA folding *in vitro* [208, 209] indicate that the TPS domain may have a similar role in initiating folding in two-partner secretion as that suggested for autotransporter secretion [210–212].

The translocation by FhaC and the dynamic of FhaC have been extensively investigated by Jacob-Dubuisson and colleagues, using electron paramagnetic resonance (EPR). This model provides information on the mobility of specific regions of the protein as well as the distances between them, suggesting the existence of an equilibrium of several conformations of FhaC. In the first conformation, the N-terminal α-helix of H1 spontaneously moves to the periplasm [207]. The movement of H1 breaks linker-POTRA interactions, thus allowing the TPS domain of the

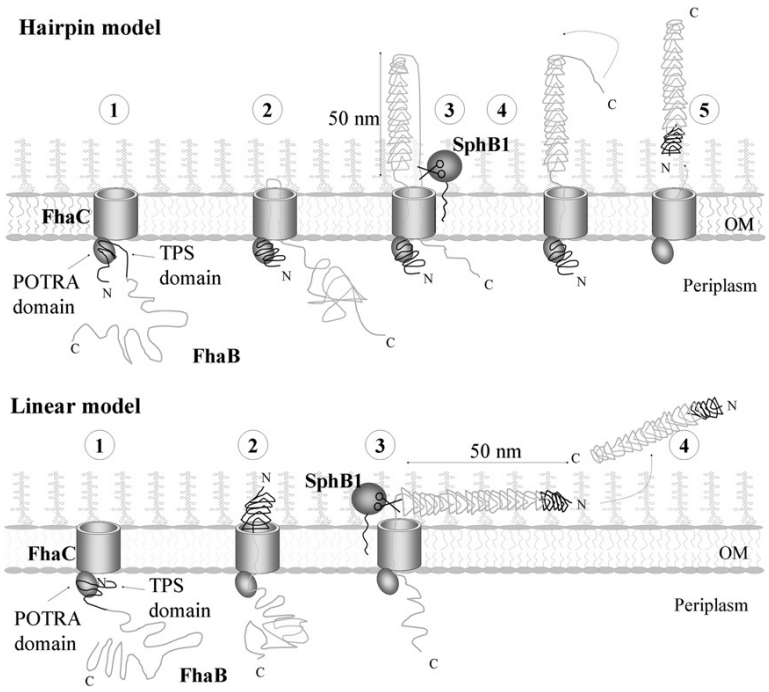

Figure 2.13. **The TPS secretion models** [204].

substrate protein to bind to the POTRA domains. The equilibrium between the resting, closed conformation of FhaC and the open conformation of FhaC with H1 in the periplasm might thus be displaced by the binding of FHA [189, 207]. Similarly in the LepB transporter of LepA in *P. aeruginosa*, the linker may transiently interact with POTRA2 and be displaced by the substrate. The second equilibrium concerns the conserved loop L6 that is folded back inside the pore from the cell surface and interacts with the inner wall of the barrel [189, 213]. The position of L6 appears to change in the pore and to modulate channel opening [213].

2.2.3 Functions of the TpsA proteins

TpsA acting as adhesins The HMW adhesin from *H. influenzae* is one of the best characterized adhesins. HMW adhesins are widespread among the strains and were isolated from human respiratory tract infections [214]. HMW is encoded by *hmw1A* gene in the *hmw1ABC* operon. In this case HMW is glycosylated in the cytoplasm by a glycosyltransferase encoded by *hmwC* and then it is anchored to the cell surface through an interaction between its C-ter and HMWB [215].

Another example is the filamentous haemagglutinin FHA from *B. pertussis*. The mature FHA adhesin of *B. pertussis* results from several proteolytic maturation steps [216, 217]. The protease involved in the release of the mature FHA protein from the cell surface is a subtilisin autotransporter called SphB1 [216]. Although no other substrates are known for SphB1, its gene does not belong to the locus encompassing *fhaB* and *fhaC*. Nevertheless, all three are regulated in a coordinated fashion, being part of the virulence regulon of *B. pertussis* [218]. FHA binds several components

exposed at the cell surface such as carbohydrates, heparan sulfates and integrins. This binding leads to bacterial aggregation and the formation of microcolonies and biofilm [219]. Finally, FHA modulates the innate immune response of the hosts by suppression of the inflammation pathway mediated by IL-17 [220].

In *P. aeruginosa*, the adhesin CdrA is encoded by *cdrA* in operon with *cdrB*. CdrA is produced in biofilm condition and the intracellular level of cyclic diguanylate monophosphate (c-di-GMP) controls the *cdrAB* operon [221] through the transcriptional regulator FleQ [222]. CdrA is a substrate for the periplasmic protease LapG whose activity is also controlled by the intracellular level of c-di-GMP [223, 224]. At low c-di-GMP level, LapG cleaves the periplasmic C-terminal tail of CdrA and releases this adhesin from the cell surface to prevent CdrA-dependent biofilm formation.

In few cases, TpsB transporters have more than one TpsA substrates. This is the case for the TPS system found in *Haemophilus ducreyi*, where LspB transporter secretes LspA1 and LspA2. The TpsA proteins LspA1 and LspA2 of *H. ducreyi* are required for full virulence of this pathogen by inhibiting phagocytosis through the phosphorylation of the eukaryotic Src tyrosine kinase [225, 226].

In the case of enterotoxigenic *E. coli* (ETEC), the TpsA protein EtpA is necessary for intestinal colonization. By binding to the tips of flagella, EtpA mediates bacterial adherence to intestinal cells showing the cooperation between two extracellular appendices [227].

Growth contact inhibition (the CDI system) A new group of TPS named "contact-dependent growth inhibitions" (CDI) have been found in *E. coli*, *Burkholderia pseudomallei* and *Yersinia pestis* [228] and were shown to mediate inter-bacterial interactions involving molecular recognition of closely related bacteria leading to collective-cooperative or competitive behaviors. Operons of CDI system contain also additional genes. For example, the *cdiAB* genes are followed by *cdiI* gene encoding for an immunity protein that protects the producing CDI+ cells from auto-inhibition.

The growth inhibition requires direct cell-to cell contact with the targets. The CdiB is a predicted OM β-barrel protein and CdiA protein is an exoprotein that adopts a β helical structure. The activation of growth inhibition is localized in the C-ter of CdiA (CdiA-CT), and the CdiI protein neutralizes the activity of CdiA-CT from auto-inhibition. The genetic organization differ between species [228].

TpsA acting as toxins The TpsA cytolysin/hemolysin group is probably the most common in bacteria and more particularly, TpsA proteins acting as pore-forming toxins. The pore forming toxins characterization is detailed in the next Chapter. The hemolysin ShlA from *S. marcescens* and HmpA from *P. mirabilis* are the prototypes for this pore formation activity.

ShlA represents a new type of hemolysin in terms of structure, activation and secretion. It has nothing in common with the RTX hemolysin of *E. coli*. ShlA forms pores in eukaryotic membranes but not in prokaryotic membranes. The pore formation of ShlA has been observed using liposomes and RBC models. Using liposomes it has been shown that phosphaditylethanolamide is essential for the activation of the protein and the pore formation. Moreover, RBC model revealed that the ShlA pore is around 3 nm in diameter. ShlA provokes a rapid vacuolation of

epithelial cells [174, 229, 230] leading to cell lysis. In macrophages, it was shown that ShlA induced a necroptosis, dependent of RIPK pathway [231]. In *S. marcescens*, the regulator RcsB controls the transcriptional level of *shlBA* expression by direct interaction with a specific recognition motif within the *shlBA* promoter region [232]. Up to date, no structure of ShlA is available.

3

Pore forming toxins

Contents

Pore-forming toxins (PFT) are the most common bacterial cytotoxic proteins required for virulence in a large number of important pathogens, including *Streptococcus pneumoniae*, *Staphylococcus aureus* and *Escherichia coli*. 25% to 30% of cytotoxic bacterial proteins are PFTs, making them the largest category of virulence factors. PFTs generally disrupt host cell membranes, but they can have additional effects independent of pore formation. PFTs are classified into two groups α-PFTs and β-PFTs, based on whether the secondary structure of their membrane-spanning elements is composed of α-helices or β-barrels, respectively.

3.1 Mechanism of pore formation

PFTs initially fold generally into a water soluble, monomers. In many reported cases, PFTs recognize their target cell by binding to specific receptors, which can be sugars, proteins or lipids. The increased local concentration of PFTs in the proximity of the cell membrane allows their oligomerization. Proteins then change their conformation exposing hydrophobic domains and leading to the membrane insertion. The stoichiometry of the assembly of the PFTs varies, as well as the size of the pore from 1 to 30 nm [233].

3.1.1 α-PFT

α-PFTs are composed of α-helices when inserted in the membranes. α-PFTs regrouped Colicins, ClyA , Cry and Cyt toxins from *Bacillus thuringiensis* and RTX families. Cry and Cyt protein families are a diverse group of proteins with activity against insects, and will not be described in this Chapter.

Colicins are produced by *E. coli* to kill related bacterial species by forming pores in their IM [234]. They have a crucial role in shaping the microbial population, by killing the competitors and invading the occupied niches [235]. There are four types of Colicins E1, Ia, A and N. These colicins contain at least three domains: an N-terminal translocation domain responsible for transport across the OM and periplasmic space, central domain responsible for receptor recognition; and a C-terminal cytotoxic domain responsible for the channel formation in the cytoplasmic membrane[236, 237].

The pore formation by colicins requires the insertion of the hydrophobic helical hairpin into the IM, producing a nonspecific voltage gated channel, that leads to a membrane depolarization, ATP depletion and target bacteria death (Figure 3.1). The structure of the colicins and their exact stoichiometry are not completely known due to incapacity to form stable oligomers in laboratory conditions. Upon interaction with the target membrane, the amphipathic helices move away from the hydrophobic helical hairpin, enabling its insertion into the membrane. This arrangement lead to the formation of the so-called "umbrella" structure. This structure was confirmed for the colicin by electron paramagnetic resonance (EPR). However, the formation of this "umbrella" structure seems to be insufficient for the channel formation. It is expected that other mechanisms operate in concert with the umbrella formation.

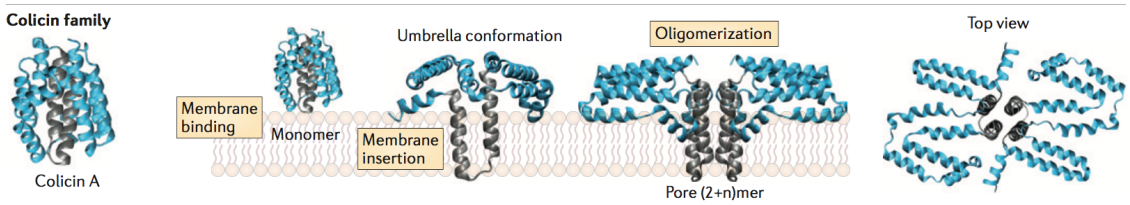

Figure 3.1. Structural architectures and pore formation mechanism of the Colicins family. For PFTs from this family, the extraction of the hydrophobic hairpin and its insertion into the membrane results in an "umbrella" conformation that is thought to drive pore formation by inducing oligomerization into dimers or higher-order assemblies of varied stochiometries (RCSB Protein Data Bank (PDB) entry 1COL) [238].

Indeed, the electrostatic complementary and negatively charged bacterial membranes may promote the insertion of amphipathic helices into the membranes [239, 240].

The ClyA family includes the Cytolysin A, also known as hemolysin E (HlyE) produced by *E.coli*, *S. enterica*, *S. flexneri*, NhE (non-heamolytic tripartite enterotoxin) and Hbl B-component of hemolysin BL enterotoxin [241, 242]. The structure of ClyA has been solved, in both soluble [243] and transmembrane form [244], revealing the unique pore-formation process of this family, which involves several conformational changes.

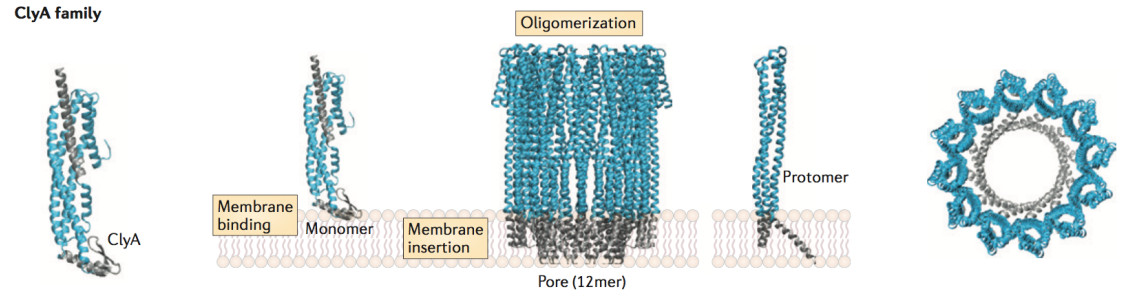

Figure 3.2. Structural architectures and pore formation mechanism of the ClyA family. The structure of ClyA has been solved in its soluble monomers form (PDB entry 1QOY) [243] and mature dodecameric pore conformation (PDB entry 2WCD) [244].

In solution, ClyA is an α-helices elongated protein with a short hydrophobic β-hairpin, called β-tongue (Figure 3.2). The cholesterol-containing membrane is required for the detachment of the β-tongue from the core of the protein its insertion into the membrane. This insertion triggers a massive rearrangement of the α-helices which swing around to reach the membrane and form a ring structure [243–246].

An alternative process for the pore formation of ClyA has been also proposed, in which ClyA would oligomerize into soluble pre-pores encapsulated with bacterial OM vesicles (OMVs) of *E. coli* [247]. Pre-pore containing OMVs would be protected

from pore formation as the conformational changes leading to membrane insertion require cholesterol. A similar OMV-mediated delivery mechanism of PFTs has been proposed for *V. cholerae* cytolysin (VCC) and will be described in the next part [247].

The RTX family includes more than 1000 known toxins that exhibit various specific activities. These toxins possess a typical domain in the C-terminal half that contains a variable number of glycine-rich and aspartate-containing nonapeptide repeats of the consensus sequence G-G-X-G(N/D)-X-(L/I/F)-X, where X can be any amino acid. Alpha Hemolysin of *E. coli* (HlyA) is one of the best-studied RTX-toxin. The N-terminal hydrophobic domain is predicted to contain nine amphipathic α-helices [248] where the region comprised between residues 177-411 is the one that becomes inserted into membranes. The C-terminal calcium-binding domain contains 11-17 of the glycine- and aspartate-rich nonapeptide β-strand repeats. Although the membrane interaction of HlyA is assumed to occur mainly through the amphipathic α-helical domain, both major domains of HlyA are directly involved in the membrane interaction of HlyA, with the calcium-binding domain in particular being responsible for the early stages of the HlyA's docking to the target membrane [249].

In summary, in α-PFTs monomers bind to the membrane in a step that precedes pore formation. Once bound to the membrane, pore formation relies on the extraction of α-helical domains from the monomer and subsequent insertion of the domain into the membrane.

3.1.2 β-PFT

The haemolysin family. This family is composed of the cytolysin VCC of *V. cholerae*, NetB, γ-toxin of *C. perfringens* and the several PFTs of *S. aureus*. This pathogen possesses an arsenal of PFTs such as the α-hemolysin (Hla), the two components γ-hemolysin AB (HlgAB), HlgCB, leukocidin ED (LukED), Panton-valentine leukocidin (PVL) and leukocidin AB (LukAB). These are not redundant toxins and target different cell types, such as epithelial, endothelial cells and monocytes for Hla, monocyte and neutrophils for PVL, monocytes and erythrocytes for HlgAB, and T-lymphocyte for LukED [250–255]. The most studied one is HlA, which is a 33.2 kDa water soluble monomer. The structures of the soluble and transmembrane forms have been solved. In the soluble state, Hla forms a compact structure, rich in β-strands packed in three-stranded β-sheet in the core of the protein. Oligomerization into a heptamer or octamer leads to a ring-like structure of 14-stranded β-barrel (Figure 3.3). This barrel spontaneously inserts into the lipid bilayer [240]. The fully assembled toxin is 10 nm wide and 10 nm in height, with a minimum pore inner diameter of 1.4 nm. After binding to the membrane, the pre-stem loop starts extracting to form a partial β-barrel, leading to a pre-pore state, the structure of which has been solved for γ-hemolysin (Hlg). The pre-pore evolves into a mature pore by the insertion of the complete β-barrel into the membrane.

This family of PFTs also includes the VCC toxin of *V. cholerae*, VVH of *Vibrio vulnificus* or γ-toxin of *Clostridium perfringens* [240].

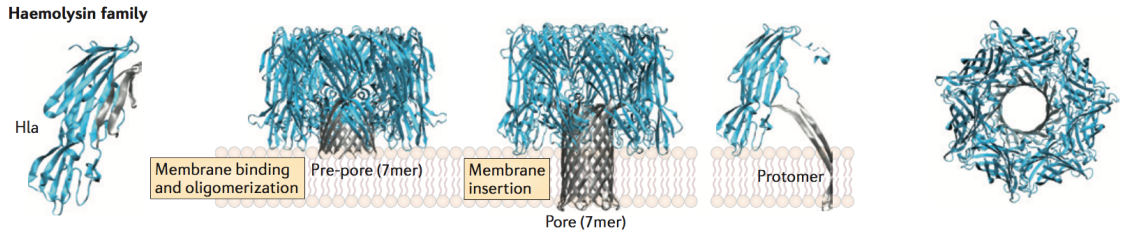

Figure 3.3. Structural architectures and pore formation mechanism of the heamolysin family. The structure of α-haemolysin (Hla) from *Staphylococcus aureus* has been solved in monomer conformation (PDB entry 4IDJ) and single-component heptameric conformation (PDB entry 7AHL) [254].

The aerolysin family. The first member which has been described is the toxin from *Aeromonas spp.* Others have also been described such as the monalysin produced by *P. entomophila* [256] and several parasporins produced by *B. thuringiensis*. The soluble form of aerolysin is a highly elongated, multidomain protein. At high protein concentration, used for crystallography, aerolysin is dimeric. In this dimeric form, the pre-stem region forms a β-strand-containing loop in the middle region of the elongated domain. An uncommon feature of the aerolysin is that it is synthesized as a pro-toxin with a carboxyl-terminal extension that prevents premature oligomerization. Following cleavage of the C-terminal peptide, the toxin oligomerizes into heptameric ring-like structures (Figure 3.4) [257].

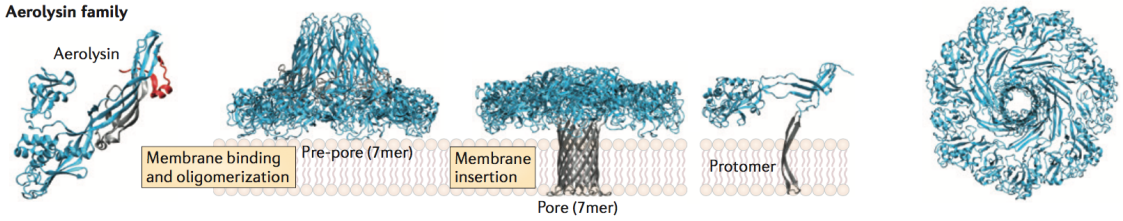

Figure 3.4. Structural architectures and pore formation mechanism of the aerolysin family. Aerolysin first assembles in a pre-pore state and, after extraction of the pre-stem loop (in grey), it eventually reaches the heptameric pore conformation, as determined by integrative modelling. [257].

New techniques combining X-ray crystallography and cryo-electron microscopy (cryo-EM) revealed that the pore of aerolysins has a large, flat, disk-like extracellular structure [240].

The cholesterol-dependent cytolysin family (CDC). This is a large family of proteins (more than 20 members) mostly produced by the Gram-positive bacteria such as *C. perfringens* and *L. monocytogenes*. The most characterized CDCs toxins with the role in virulence are the Streptolysin O (SLO), the Pneumolysin (Ply) from *S. pneumoniae*, the listeriolysin O (LLO) and perfringolysin O (PFO)[258]. Ply is required for tissue invasion, and contributes to inflammation and activation

of the complement cascade and PFO has an important role in the development of gangrene [259, 260].

CDCs share a high degree of sequence similarities (40-80 %) suggesting that they have similar structures and activities. Several CDCs have been crystallized in their soluble forms, including PFO, SLO and LLO. However, no CDC have been crystallized in the pore configuration due to the stoichiometry of the complexes, in which up to 50 monomers could be assembled into a very large ring-link structures. Such structures can be visualized by electron microscopy (EM) [261] and atomic force microscopy (AFM) [262] providing information on the pore formation. Monomers of CDCs are elongated β-sheet rich multidomain proteins. Oligomerization leads to the formation of a giant β-barrel composed of 80 to 200 β-strands, depending on the protein. Oligomerization seems to occur by the sequential addition of monomers or multimers (Figure 3.5).

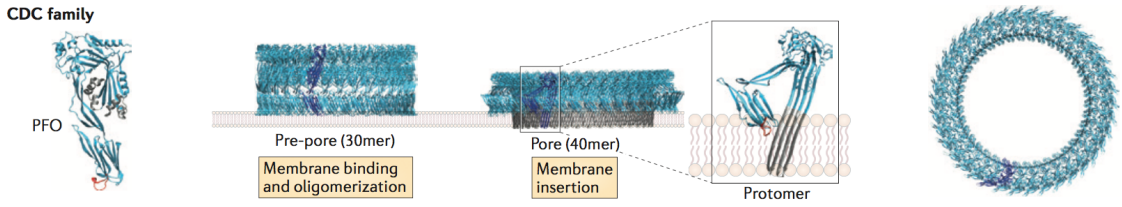

Figure 3.5. Structural architectures and pore formation mechanism of the CDC family. The structure of the CDC family PFT perfringolysin (PFO) has been solved in its monomer form (PDB entry 1PFO95 [258]; the undecapeptide that binds to cholesterol is shown in red). PFOs oligomerize to form large pre-pores, which, after an extended conformational change, form a membrane-inserted β-barrel. The models of the high-order assemblies of CDCs that form the pre-pore and pore; the stochiometries of these structures can be highly variable according to the conditions.

The most interesting structural aspect of CDCs is that they form very large pore around 30 nm in diameter. The correct alignment of the β-strands is essential for pore assembly, especially for such a large complex. It was shown that in the pore state, the β-barrel conformation is locked, producing a 20° tilt in the orientation of the β-strands with respect to the membrane [263].

In summary, for β-PFTs the pore formation relies on the extraction of a pre-stem loop that inserts into the membrane where it ultimately combines with the extracted pre-stem loops of other protomers to form a β-barrel.

PFTs are generally defined as toxins for which pore formation represents the primary toxic activity. However, many other proteins have pore-forming domains or subunits, which are used as translocons to deliver a catalytic subunits with a toxic activity into a target cell. As opposed to the effectors of bacterial secretion systems, bacterial toxins with pore-forming domains are autonomous, as a secretion system apparatus is not required for target cell entry. For example, the translocation subunit (protective antigen PA) of the anthrax toxin was shown to form heptameric or octameric pores. The lumen of the pore translocates the catalytic subunits, but remain impermeable to most ions. The T3SS is another example of the translocon

formation in the host cell allowing the injection of toxins. Membrane insertion is associated with conformational changes, leading to oligomerization occurring through coiled-coil domain interactions, required for the pore formation. Interestingly, coiled-coil domain of translocator proteins shares homology with PFT, suggesting common origins and oligomerization mechanisms.

3.1.3 Specificity of PFTs towards eukaryotic cells membrane

PFTs evolved to target membranes by binding to exposed molecular components of the host cell surface, such as proteins, sugars or lipids, and thus using them as specific receptors.

Sugars

Many PFTs bind to sugar molecules. PFTs targeting eukaryotic plasma membranes usually bind glycans that are convalently attached to membrane-associated proteins or sugars that are present in the glycophosphatidylinositol (GPI) proteins with a GPI anchor [264]. Aerolysin binds to the target membrane through its first N-terminal domain, which protrudes from the elongated core of the protein. Aerolysin requires N-glycan on GPI-anchored proteins for efficient host cell binding [265, 266]. Moreover, Colicin N which is secreted and active against *E. coli*, binds to bacterial inner core of LPS which serves as high affinity receptor before translocating through OM porins to the IM [258].

Lipids

The major structural lipids in eukaryotic membranes are the glycerophospholipids (GSL): phophatidylcholine (PC), phosphatidylserine (PS), phosphatidylethenolamine (PE), phosphatidylinositol (PI). Their hydrophobic portion is a diacylglycerol (DAG), which contains saturated or cis-unsaturated fatty acyl chains of varying lengths. PC represents almost 50 % of the phospholipids in most eukaryotic membranes [267]. Sphingolipids constitute another class of structural lipids. Their hydrophobic backbone is ceramide (Cer). The major sphingolipids in cells are sphingomyelin (SM) and glycerophospholipids (GSLs), which contain mono- di- or oligo-saccharides (glucose or galactose) [267].

Many PFTs have an affinity for specific lipids or lipid domains. Lipid rafts are specific membrane regions enriched in cholesterol and sphingolipids and their role in the pore formation process was proposed for CDCs toxins that require cholesterol to oligomerize and form pore [268].

For example, the PFO *C. perfringens* oligomerization is dependent on the concentration of cholesterol in the target membrane. The membrane composition is asymmetric between the two-bilayer leaflets and it is crucial to maintain the optimal concentration in cholesterol for the stabilization of the intermediate state of the membrane-inserted toxin during the CDC pore formation. The cholesterol interaction is mediated by the highly conserved peptide composed of amino acids ECTGLAWR-WWR which is one of the most conserved among CDCs [269]. Headgroups of lipid

molecules are the primary target of PFTs and are generally more exposed in more fluid bilayers, promoting the binding.

Anthrax toxin PA binds to either CMG2 or TEM8 at the cell surface clustered in the lipid rafts. By using β-methyl-cyclodextrin, a reagent that removes cholesterol from the plasma membrane and thus disaggregates rafts, it has been demonstrated that anthrax toxin uses rafts for internalization [270].

Lipids specificity has also been reported for lipids not directly associated with rafts. In the hemolysin family, Hla from *S. aureus* and NetB from *C. perfringens* have a PC binding pocket.

Finally, lipid specificity has also been reported in PFTs that target bacterial membranes. For colicins, the presence of anionic lipids species, such as cardiolipin, in the bacterial IM seems to promote the formation of the "umbrella" conformation and conductive pores [271].

Protein receptors

In addition to sugars and lipids, some PFTs require interaction with host membrane proteins to target the host cell membrane. These PFTs recognize the polypetides chains themselves.

For example, Hla oligomerizes and forms pores in the host cell plasma membranes in a wide range of eukaryotic cells. In 2010, Wilke and Bubeck Wardenburg used a biochemical approach to identify the cell surface metalloprotease, A Disintegrin and Metalloprotease 10 (ADAM10), as the specific proteinaceous receptor of Hla [272, 273]. Loss of ADAM10 expression through shRNA knockdown reduced Hla binding and cytotoxicity, and ADAM10 surface expression levels on various cell lines correlated with Hla binding levels. The binding of Hla to ADAM10 increases the protease activity, which disrupts the epithelial barrier and leads to lung injuries. More recently, Winter *et al.* [274] used a genome-wide CRISPR/cas screen in U937 cells to identify additional host factors that are involved in the Hla activity. They identified three proteins participating in ADAM10 regulation (SYS, ARFRP1 and TSPAN14) and thus Hla activity. Disruption of ADAM10 in the lung tissues turns mice resistant to lethal pneumonia. Moreover, when mice were treated with a metalloprotease inhibitor, they survived an otherwise lethal *S. aureus* dose and showed increased resistance to an intravenous challenge.

3.2 Consequences of pore formation

The primary consequence of pore formation by PFTs is membrane permeabilization, but there are generally additional effects. Bacteria that replicate in the host cytoplasm produce PFPs to trigger rupture of the vacuole in which the bacterium resides following cell entry. For example, Listeriolysin O (LLO) is required for the release of *L. monocytogenes* into the cytosol [275], an event that is potentiated by the cystic fibrosis transmembrane conductance regulator (CFTR) [276].

PFTs induce two major effects during *in vivo* infections. First, many PFT effects result in compromised integrity of epithelial and endothelial layers. PFTs can induce

barrier dysfunction through (i) direct attack of epithelial and endothelial cells, (ii) damage caused by PFT-driven inflammation, (iii) local vascular effects (mediated either by affecting endothelial cells directly or via the modulation of the nervous system) and (iv) the hijacking of host cell molecular pathways that regulate the extracellular matrix.

Second, PFTs interfere with immune responses. PFTs can contribute to the disruption of the host immune response by (i) preventing the attraction of immune cells, (ii) destroying immune cells (by direct lysis or by inducing programmed cell death), (iii) aiding bacterial invasion of host cells and intracellular survival, and (iv) hijacking host molecular defense pathways.

3.2.1 Changes in cellular ion composition

The primary effects of PFTs are changes in the concentration of ions in the target cell cytosol. These changes trigger secondary effects, many of them are probably still unknown. Calcium, potassium and ATP have been identified as the major players in the cellular response to plasma membrane damage. The effects depend on the concentration of PFTs, the pore diameter, the number of pores per cell/membrane domain, and the stability of the pore.

For example, high concentrations of any CDC will lead to the formation of stable, nonselective pores of >30 nm in diameter that allow a rapid and massive calcium entry as well as potassium efflux [260]. In contrast, PFTs of the RTX family make very transient pores (a few seconds life time) [277], that can adopt two conformations, one that allows the passage of potassium and the other that allows the passage of calcium [278, 279]. The calcium entry does not lead to a sustained calcium rise but to calcium oscillations [280]. The efflux of cellular potassium was found in many PFTs to induce the activation of Nod-like receptor pyrin domain-containing 3 (NLRP3) inflammasome.

Changes in cellular ion composition following exposure to PFTs may also be the result of a secondary effect due to the activation of host channels. For example, if ATP is released into the extracellular milieu upon pore formation, it may trigger the activation of P2X receptors-ligand-gated cation channels activated by extracellular ATP [281] as it has been shown for the pore formed by *E. coli* HlyA [282] and *S. aureus* HlA [283] in erythrocytes.

3.2.2 Cell death

It has been thought for a long time that the main purpose of PFTs is to kill cells, either to liberate materials necessary for bacterial growth and colonization or to protect the bacterium from cells of the immune system, such as phagocytes. Excessive pore formation indeed leads to target cell death. At high PFT concentrations, nucleated cells will generally undergo necrosis [284], in particular due to deregulation of mitochondrial activity resulting from dramatically reduced levels of ATP and potassium. At lower concentrations, death may occur via programmed necrosis (also

known as pyronecrosis, oncosis, or necroptosis), apoptosis or pyroptosis (caspase-1 mediated cell death) [285].

Necroptosis is characterized by swelling, vacuolation of the cytoplasm, ATP depletion, early plasma membrane rupture and the release of pro-inflammatory proteins. *S. aureus* Hla [286], *C. septicum* α-toxin [284] and *H. pylori* vacuolating toxin VacA [287] are the toxins that provoke necroptosis. However, these same toxins have also been shown, in some conditions, to trigger apoptosis towards epithelial cells.

VacA permeabilises the IM of the mitochondria leading to a change of membrane potential and decreased ATP production, consequently provoking an apoptosis cell death [288]. Moreover, VacA induces a necroptosis cell death of intestinal epithelial cells [287]. In the same way, Hla induces an apoptosis cell death of diverse cell types, such as epithelial, endothelial, keratinocytes, macrophages and lymphocytes. However, it induces pyroptosis of monocytes [286].

It is currently unclear what determines the pathway activated upon exposure of cells to PFTs, although toxin concentration and cell type are no doubt important.

ShlA is the pore forming toxin of *S. marcescens*. Although no structural features have been characterized for ShlA, the consequences of the pore formation have been widely studied in several cell types. It has been demonstrated that ShlA provoked necroptosis of primary macrophages [231].

Moreover, certain *S. aureus* toxins have also been described to have effects on necroptosis in a manner that may link to their activation of the inflammasome. For example, it was found that the virulent methicillin-resistant (MRSA) strain USA300 induces receptor-interacting serine-threonine kinase (RIP)1/RIP3/mixed lineage kinase domain-like (MLKL)-dependent necroptosis, thereby contributing to inflammatory lung pathology. Interestingly, Hla-induced inflammasome activation has been shown to be dependent on MLKL pore formation, supporting the link between the NLRP3 inflammasome and necrosome components RIP1, RIP3, and MLKL [289–293]. Necroptosis contributes to lung pathology and reduced bacterial clearance *in vivo* by depleting immunoregulatory resident alveolar macrophages that are essential for bacterial clearance [293].

3.2.3 Inflammasome activation

Pyroptosis is a programmed cell death involving inflammosome complex leading to the release of mature IL-1β and IL-18. Pyroptosis is mediated by a Nod-like receptors (NLRs). NLR proteins are composed by a sensor domain, a NACHT nucleotide-binding domain (NBD) and a signaling/effector domain: a Pyrin domain, a baculoviral inhibitory repeat (BIR)-like domain or a CARD (Caspase Recruitment Domain) domain (reviewed in [294]).

There are three different types of NLRs: NLRP1, NLRP3 and NLRC4. NLRC4 contains a CARD domain that directly interacts with the Pro-Caspase-1, in contrary to NLRP1 and NLRP3 that contain a pyrin domain [295, 296]. NLRs oligomers bind to pro-Caspase-1 and constitute the inflammasome (Figure3.6).

Many bacterial proteins have also been described activating inflammasome. For

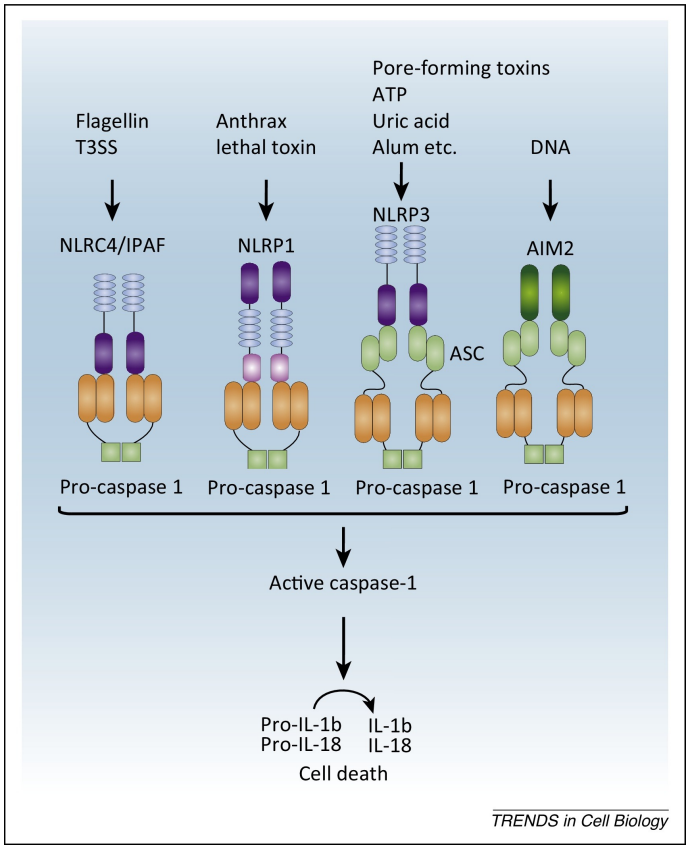

Figure 3.6. **Infammasome.** Canonical inflammasomes contain sensors belonging to the NLR or ALR family. NLRC4 is activated by bacterial flagellin and T3SS components, NLRP1b is activated by the anthrax lethal toxin, and AIM2 is activated by cytosolic dsDNA. NLRP3 is activated by a wide variety of signals including pore-forming cytotoxins, ATP, uric acid, and alum. Once activated the receptors form an inflammasome complex with or without the adaptor, ASC, and recruit procaspase-1, which is subsequently cleaved into active caspase-1. Caspase-1 cleaves pro-forms of IL-1β and IL-18 into their active forms as well as induces cell death from [297].

example, NLRC4 is able to recognize the flagellin and T3SS components including PscI and PscF. The response of the macrophages to *P. aeruginosa* infection includes the activation of Caspase-1 and IL-1β secretion (Figure 3.7). IL-1β, an inflammatory cytokine, mostly secreted by macrophages, but also by other cells (epithelial cells and neutrophils) induces a rapid recruitment of neutrophils to the site of infection [298] leading to the bacterial clearance.

PFTs also activate the inflammasome. They are the best example of an indirect activation of NLRP3. Indeed, the pore in the membrane leads to potassium (K+) efflux, decreasing the K+ intracellular concentration that triggers the activation of NLRP3.

The first demonstration of NLRP3-dependent inflammasome activation in response to a pore-forming toxin was reported with studies using aerolysin purified

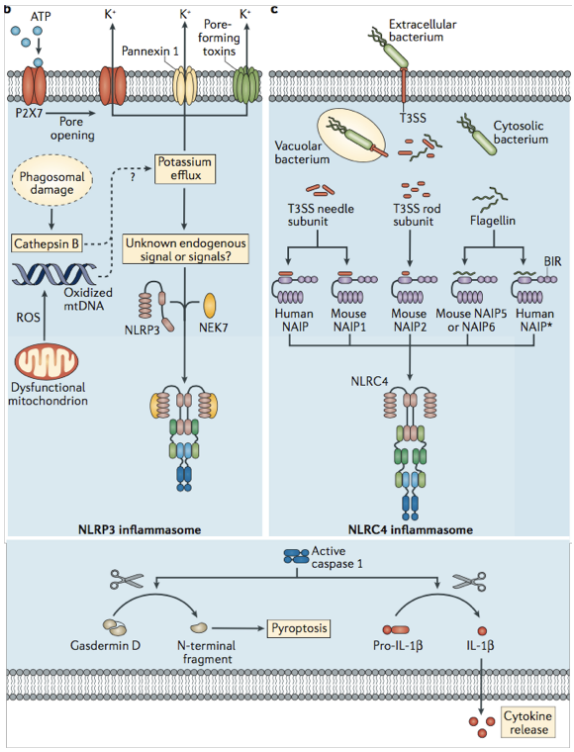

Figure 3.7. **NLR Infammasome.** NLR family, apoptosis inhibitory proteins (NAIPs) are direct receptors for flagellin and T3SS needle and rod subunits. Activated receptors recruit adaptor protein ASC, which consists of a pyrin domain (PYD) and a caspase recruitment domain (CARD), through PYD-PYD (NLRP3) or CARD-CARD interactions (NLRP1B and NLRC4). The CARD of ASC is necessary to recruit pro-caspase 1. Following its proximity-induced autoproteolytic activation within the complex, caspase 1 processes pro-IL-1β and pro-IL-18 to their mature forms and cleaves gasdermin D. The N-terminal fragment of gasdermin D drives pyroptosis, which is a lytic type of cell death and allows the release of mature IL-1β and IL-18 from the cell. mtDNA, mitochondrial DNA; NOD, nucleotide-binding oligomerization domain; P2RX7, P2X purinoceptor; ROS, reactive oxygen species (adapted from [294]).

from *Aeromonas hydrophila* [299]. Interestingly, this study identified a novel caspase-1-dependent protective response in cells treated with either aerolysin or *S. aureus* Hla. In contrast to the pyroptosis usually observed following caspase-1 activation, NLRP3-mediated activation of caspase-1 by sublytic doses of the pore-forming toxins resulted in induction of sterol regulatory element-binding proteins that altered membrane biogenesis and promoted cell survival [300]. Other cholesterol-dependent pore-forming toxins similar to aerolysin were also previously linked to IL-1β production [301, 302]. For example, Tetanolysin O from *Clostridium tetani* induces maturation and release of IL-1β from bone marrow-derived macrophages (BMDMs) at low, non-lytic doses in an NLRP3- and caspase-1-dependent manner [303]. Listeriolysin, originally suggested to play a role in IL-1β responses during *Listeria* infection via pore formation [304], directly activates the inflammasome by K+ efflux induction [305].

The host cytokine response to pneumolysin (PLY) (*S. pneumoniae*) has also been shown to increase protection against pneumonia in a mouse model [306]. In a murine model of pneumococcal meningitis, the extent of caspase-1 activation via the NLRP3 inflammasome has been linked to clinical disease severity [307]. In this model, inflammasome activation was associated with pathology rather than bacterial clearance. Pneumolysin was the key inducer of the IL-1β response associated with disease, and inhibitors of IL-1β and IL-18 signaling-altered pathological responses. Pneumolysin activation of the inflammasome was suggested to require ATP release and lysosomal destabilization associated with cathepsin B cytosolic activity [307].

Gram-negative bacteria also produce a variety of heamolysins that have been implicated in activation of the NLRP3 inflammasome. Enterohemorrhagic *E. coli* (EHEC) O157:H7 produces hemolysin that induces IL-1β from the THP-1 macrophage/monocyte cell line in NLRP3-caspase-1 dependent manner [308, 309]. *Vibrio fluvialis* produces hemolysin that can activate the inflammasome in mouse and human macrophages. Importantly, in a mouse model, this toxin was associated with IL-1β production and toxin-containing cell-free culture supernatants induced higher levels of cytokine production. Hemolysin-deficient bacteria and their supernatants had lower levels of response *in vivo* [310].

3.2.4 Barrier dysfunction and dissemination

Another major consequence of the PFT activity is the loss of the epithelial and endothelial layer integrity.

Damage to epithelial and endothelial barriers is especially obvious in pneumonia where PFTs by themselves can cause the clinical manifestations of the disease, as observed with *S. pneumoniae* PLY and *S.aureus* PVL. PFTs cause damages directly or indirectly by the PFTs-induced inflammatory effects. These two mechanisms are not mutually exclusive and the available data cannot allow separation of these two mechanisms.

Examples of PFTs that directly damage epithelial cells are *S. aureus* Hla [311], *C. perfringens* β-toxin [309] and *V. cholerae* VCC [312, 313].

PFTs can also kill epithelial cells by inducing programmed cell death, as observed

in vivo for *S. pneumoniae* PLY [314] and *V. cholerae* VCC [313]. Another factor that induces barrier dysfunction is the disruption of cell-cell junctions, as seen with *S. aureus* Hla, and the CDCs SLO from *S. pyogenes* that provoke a rupture of aleolar-capillary barrier by the E-cadherin cleavage mediated by ADAM10 [315].

Also, in many cases, the PFT-induced damage to epithelia is secondary, caused by the actions of neutrophils that are recruited to the site of infection (described for *S. pneumoniae* PLY, *S. aureus* PVL, and *V. cholerae* VCC) or by ischemic effects due to PFT-induced damages. PVL triggers the increase of local levels of IL-8 and monocyte chemotactic protein 1 (MCP-1) resulting in a more extensive infiltration of neutrophils which is responsible for the necrosis, alveolar hemorrhage and pulmonary edema [316]. Moreover, PLY (*S. pneumoniae*) at sublytic doses is capable of triggering the lethal effects of pneumonia, the destruction of lung tissues mediated by induction of apoptosis and recruitment of neutrophils to the site of infection. Purified PLY also caused increased alveolar epithelial permeability in mice after intracheal administration. Thus, it appears that PLY may cause barrier dysfunction via both direct and indirect mechanisms [314].

The barrier dysfunction and the innate immune response caused by the PFTs promote pathogen dissemination. For example, after infection via intracisternal injection in rat meningitis model, PLY did not affect bacterial growth in the cerebrospinal fluids, but it appears to be involved in breaching the blood-brain barrier. After intracerebral infection, PLY was dispensable for subsequent spreading to the spleen. Moreover, during intratracheal infection of rabbits with *S. aureus*, PVL was found dispensable for initial colonization and bacterial growth rates. However, in a rabbit bacteria model caused by intravenous injection of bacteria, PVL was found to contribute to early bacterial spreading to the kidney. Thus, PFTs are found to contribute, in some cases to colonization or early stages of bacterial growth, while in other studies no effects are found. Many experimental factors could influence these findings, such as the host model, host immune status and route of infection.

3.3 Membrane repair mechanism

The mechanism of the pore formation, the concentration of PFTs and the number of pores per cells play an essential role for the fate of the cells. The ability of cells to restore plasma membrane integrity following damage caused by PFTs, and the speed with which this occurs, varies between cell types and depends on the toxin and its concentration.

Furthermore, membrane repair following damage by cholesterol-dependent cytolysins (CDCs) is highly dependent on the entry of calcium. Three main mechanisms of membrane repair have been proposed.

The first is the disassembly of the pore-forming complex, although there is currently no real evidence for this and it is unlikely for pores such as those formed by aerolysin, the stability of which is remarkable [317].

The second is the uptake of the pores by endocytosis, with the aim of degrading the pores in lysosomes or secreting them into the extracellular space via exosomes. Repair by endocytosis has been proposed for Streptolysin O (SLO) and may involve the uptake of caveolae [318] (Figure 3.8).

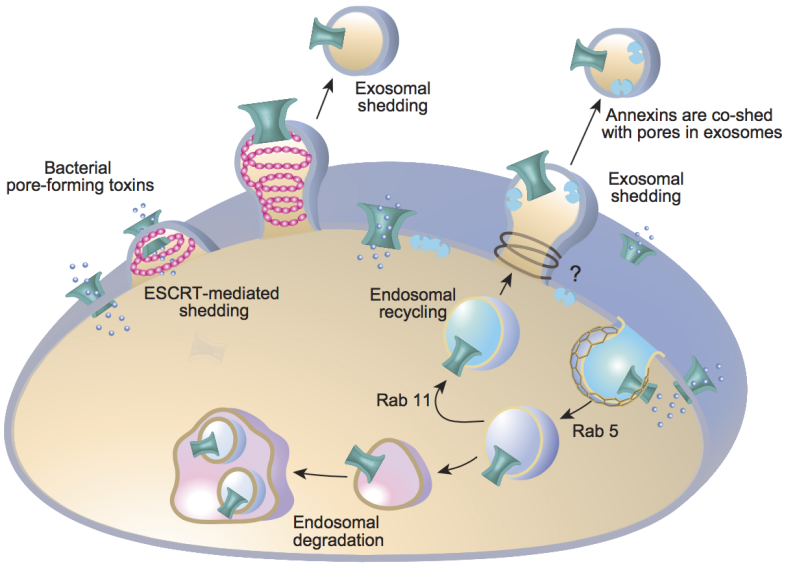

Figure 3.8. **Membrane repair mechanism.**. Endocytosis and Exocytosis mechanisms [317].

The third proposed mechanism is shedding of PFT-containing membrane patches through the formation of extracellular vesicles, which has also been proposed for SLO. It was recently shown that the endosomal sorting complex required for transport (ESCRT) machinery was required for membrane repairs following mechanical damage or damage caused by PFTs. This machinery is classically involved in the biogenesis of intraluminal vesicles or multivesicular bodies, but has also been shown to be involved in viral budding, consistent with the fact that both events require budding of the membrane away from the cytosol. This finding would be consistent with membrane repair through the budding of extracellular vesicles [318] (Figure 3.8).

Finally, a recent work reveals that different small β-pore-forming toxins may either trigger calcium influx-dependent repair. For example repair of PhylP (Phobalysin P from *V. cholerae*) pores involves calcium, lysosomal exocytosis and calveolin. In contrast, its orthologue VCC, subverts calcium influx-dependent repairs [319].

In summary, PFTs are sophisticated and widespread virulence factors produced by pathogenic bacteria. They disrupt barriers and modulate cellular pathways and kill cells of the host immune system, contributing to the bacterial dissemination. All PFTs are inactive, soluble and monomeric proteins undergoing changes to assemble into conductive transmembrane pores within plasma to target cell membranes. Identification of lipids, sugars and protein receptors of PFTs not only allows the global understanding of their action, but may lead to developing strategies that inhibit their function.

Part II

Results

4

Phenotype and toxicity of the recently discovered *exlA*-positive *P. aeruginosa* strains collected worldwide

Emeline Reboud, Sylvie Elsen, Stephanie Bouillot, Guillaume Golovkine, Pauline Basso, Katy Jeannot, Ina Attree, and Philippe Huber (Environmental Microbiology (2016))

We recently identified a hypervirulent strain of *Pseudomonas aeruginosa*, differing significantly from the classical strains in that it lacks the type 3 secretion system (T3SS), a major determinant of *P. aeruginosa* virulence. This new strain secretes a novel toxin, called ExlA, which induces plasma membrane rupture in host cells. For this study, we collected 18 other *exlA*-positive T3SS-negative strains, analyzed their main virulence factors and tested their toxicity in various models. Phylogenetic analysis revealed two groups. The strains were isolated on five continents from patients with various pathologies or in the environment. Their proteolytic activity and their motion abilities were highly different, as well as their capacity to infect epithelial, endothelial, fibroblastic and immune cells, which correlated directly with ExlA secretion levels. In contrast, their toxicity towards human erythrocytes was limited. Some strains were hypervirulent in a mouse pneumonia model and others on chicory leaves. We conclude that (i) *exlA*-positive strains can colonize different habitats and may induce various infection types, (ii) the strains secreting significant amounts of ExlA are cytotoxic for most cell types but are poorly hemolytic, (iii) toxicity in plants does not correlate with ExlA secretion.

My contribution in this work was to perform the phylogenetic analysis of all the *exlA*-positive strains, to construct the tree based on the MLST analysis (Figure 1C) and to determine the general content of putative virulence determinants by whole genome analysis.

environmental microbiology

Environmental Microbiology (2016) **18**(10), 3425–3439 doi:10.1111/1462-2920.13262

Phenotype and toxicity of the recently discovered *exlA*-positive *Pseudomonas aeruginosa* strains collected worldwide

Emeline Reboud,[1,2,3,4] Sylvie Elsen,[1,2,3,4] Stéphanie Bouillot,[1,2,3,4] Guillaume Golovkine,[1,2,3,4] Pauline Basso,[1,2,3,4] Katy Jeannot,[5] Ina Attrée[1,2,3,4†] and Philippe Huber[1,2,3,4*†]

[1]*Univ. Grenoble Alpes, 38000 Grenoble, France.*

[2]*CNRS, ERL5261, 38000 Grenoble, France.*

[3]*CEA, iRTSV-BCI, 38000 Grenoble, France.*

[4]*INSERM, U1036, 38000 Grenoble, France.*

[5]*Hôpital Universitaire de Besançon, 25030 Besançon, France.*

Summary

We recently identified a hypervirulent strain of *Pseudomonas aeruginosa*, differing significantly from the classical strains in that it lacks the type 3 secretion system (T3SS), a major determinant of *P. aeruginosa* virulence. This new strain secretes a novel toxin, called ExlA, which induces plasma membrane rupture in host cells. For this study, we collected 18 other *exlA*-positive T3SS-negative strains, analyzed their main virulence factors and tested their toxicity in various models. Phylogenetic analysis revealed two groups. The strains were isolated on five continents from patients with various pathologies or in the environment. Their proteolytic activity and their motion abilities were highly different, as well as their capacity to infect epithelial, endothelial, fibroblastic and immune cells, which correlated directly with ExlA secretion levels. In contrast, their toxicity towards human erythrocytes was limited. Some strains were hypervirulent in a mouse pneumonia model and others on chicory leaves. We conclude that (i) *exlA*-positive strains can colonize different habitats and may induce various infection types, (ii) the strains secreting significant amounts of ExlA are cytotoxic for most cell types but are poorly hemolytic, (iii) toxicity *in planta* does not correlate with ExlA secretion.

Received 16 December, 2015; revised: 9 February, 2016; accepted 11 February, 2016. *For correspondence. E-mail phuber@cea.fr; Tel. 33 438 78 58 47; Fax 33 438 78 50 58. †These authors contributed equally.

Introduction

Pseudomonas aeruginosa is a Gram-negative bacterium capable of surviving and thriving in various habitats. It can colonize a number of hosts ranging from plants to animals. In humans, *P. aeruginosa* behaves like an opportunistic pathogen and is frequently involved in nosocomial infections. In particular, it can induce acute infections in patients using internal medical devices, such as ventilators, blood and urinary catheters. It is also the main pathogen causing chronic infections in cystic fibrosis patients. *P. aeruginosa* produces numerous secreted or cell-surface-attached macromolecules affecting the host organisms in many different ways (reviewed by Hauser, 2009; Bleves *et al.*, 2010; Filloux, 2011; Gellatly and Hancock, 2013). The most potent virulence factor of classical clinical strains is the type 3 secretion system (T3SS), a syringe-like apparatus injecting effectors directly into the cytoplasm of target cells. These effectors, namely ExoU, ExoS, ExoT and ExoY, alter eukaryotic signaling pathways causing plasma membrane rupture, disorganization of the cytoskeleton or apoptosis, depending on which ones are injected (Hauser, 2009). Two other secretion systems, T1SS and T2SS, secrete proteases and other effector molecules into the extracellular milieu (Bleves *et al.*, 2010; Filloux, 2011). *P. aeruginosa* strains release several other virulence factors, including hydrogen cyanide (HCN), which inhibits many cellular processes, including aerobic respiration (Smith *et al.*, 2013).

In addition to these virulence factors, *P. aeruginosa* possesses motility factors: type 4 pili (hereafter called pili) and a flagellum. These structures are located at bacterial poles and both contribute to its virulence (Josenhans and Suerbaum, 2002; Burrows, 2012). Pili promote twitching motility on solid surfaces, while the flagellum allows bacteria to swim in liquid media. A third means of locomotion, known as swarming, allows motility across semi-solid surfaces. This motion is powered by the flagellum, the pili and bacterial surfactants (mainly rhamnolipids), but the precise contribution of each of these factors has so far remained elusive (Murray *et al.*, 2010). Finally, *P. aeruginosa* can also move passively on soft surfaces, by a process known as sliding, occurring in absence of pili and flagellum, but

requiring surfactants (Murray and Kazmierczak, 2008). In addition to their role in motility, both pili and the flagellum mediate attachment to host cells and trigger inflammatory processes by activating pro-inflammatory receptor signaling (Kazmierczak *et al*., 2015).

The individual role of each *P. aeruginosa's* virulence factors has been examined using mutant strains and various cellular models of infection, as well as animal and plant models (Tamura *et al*., 1992; Azghani, 1996; Feldman *et al*., 1998; Josenhans and Suerbaum, 2002; Vance *et al*., 2005; Hauser, 2009; Heiniger *et al*., 2010; Jyot *et al*., 2011). In addition, several studies have examined clinical isolates to investigate the presence/absence of some virulence factors, mostly the T3SS (Hauser *et al*., 2002; Le Berre *et al*., 2011; El-Solh *et al*., 2012). Taken together, these studies revealed that all the mentioned virulence/motility factors contribute at various levels to host colonization, infection, dissemination and bacterial survival in the host, and confirmed that most hypertoxic isolates expressed the T3SS.

However, a few strains devoid of the whole T3SS-encoding locus and lacking all T3SS effector-encoded genes were recently described (Roy *et al*., 2010; Dingemans *et al*., 2014; Elsen *et al*., 2014; Toska *et al*., 2014; Kos *et al*., 2015). These strains constitute a group considered to be taxonomic outliers and are represented by the PA7 strain. Whole-genome sequences are available for six of these strains (www.pseudomonas.com; Roy *et al*., 2010; Dingemans *et al*., 2014; Boukerb *et al*., 2015; Kos *et al*., 2015; Mai-Prochnow *et al*., 2015). The sequences revealed that the PA7-like strains are phylogenetically highly divergent from the classical strains, as represented by the laboratory strains PAO1 and PA14 (Roy *et al*., 2010; Freschi *et al*., 2015; Kos *et al*., 2015). Although the PA7-like strains were isolated from patients with a range of pathologies, only limited virulence studies have been reported so far (Elsen *et al*., 2014; Toska *et al*., 2014).

Our laboratory recently reported on a PA7-like strain named CLJ1, isolated from a patient with hemorrhagic pneumonia (Elsen *et al*., 2014). Despite the absence of a T3SS, this strain was hypervirulent in a mouse model of acute pneumonia and towards cultured human endothelial cells and macrophages. We identified a novel toxin, called exolysin A (ExlA), secreted by CLJ1, along with its cognate porin (ExlB). ExlA and ExlB form a novel two-partner secretion system (TPS/T5SS), inducing plasma membrane permeability in human cells and linked to hypervirulence in mice. As previously shown, *exlA*/*exlB* genes, constituting the *exlBA* locus, were detected in PA7 and in six other strains collected in Europe and Northern America. However, only four of the strains secreted ExlA and caused plasma membrane damage.

To further describe the virulence potential of PA7-like strains, we extended our original cohort with additional strains obtained from various collections. Strains were first selected based on the absence of the genes coding for two T3SS toxins, *exoS* and *exoU*, and then for the presence of *exlA*. The new cohort consisted of 19 isolates (hereafter, *exlA*+ strains) of various origins, e.g. human infections and environmental samples, which could be classed in two distinct genetic groups. We examined the capacity of the strains to display virulence-associated phenotypes in different models. To this end, we characterized their phenotypic properties by analyzing the presence of major recognized virulence factors and their toxicity toward various cell types, in mice and chicory leaves. This study represents the first comprehensive biological characterization of this group of *P. aeruginosa* isolates.

Results and discussion

Identification of exlA*-positive* P. aeruginosa *strains*

The previously identified *exlA*+ strains all lacked T3SS-associated genes (Elsen *et al*., 2014), therefore in our quest for *exlA*+ strains in different *P. aeruginosa* collections, we searched for strains annotated as lacking two T3SS effector genes: *exoS* and *exoU* (Pirnay *et al*., 2009; Toska *et al*., 2014). A few strains were recovered based on their whole-genome sequence and similarity to PA7 (Dingemans *et al*., 2014; Boukerb *et al*., 2015; Kos *et al*., 2015; Mai-Prochnow *et al*., 2015). All strains were PCR-screened using primers amplifying either *exlA*, one end of the *T3SS* locus ('T3SS') or primers external of the *T3SS* locus ('ΔT3SS') (Fig. 1A). All the genes located outside the T3SS locus in classical strains, which encode T3SS effectors (ExoS, ExoT, ExoY and ExoU), were also absent from the genome of *exlA*+ strains (not shown). The retained strains are listed in Table 1.

This analysis revealed the existence of two amplicon sizes for the *T3SS* locus (Fig. 1A), corresponding to two distinct locus deletion patterns (represented in Fig. 1B). The sequences bordering the deleted loci were identical for the two types of isolates, suggesting two original excision events on the *T3SS* locus. When whole-genome sequence information was available, we searched for the location of the *exlBA* operon. In strains with either amplicon size, its position was identical to that in PA7 (www.pseudomonas.com), suggesting that the *exlBA* insertion occurred before either deletion event on the *T3SS* locus.

Interestingly, the origin of the different strains was not restricted to one country/continent or to a single pathological settings (Table 1). Disease-related strains were isolated in the lungs of cystic fibrosis and non-cystic fibrosis patients, or in outer ear, urinary, blood and peritoneal infections. The fact that some of the *exlA*+ strains were isolated from patients with acute infections indicates that they may cross the epithelial barrier despite the absence of T3SS, which is consistent with the results of our study of

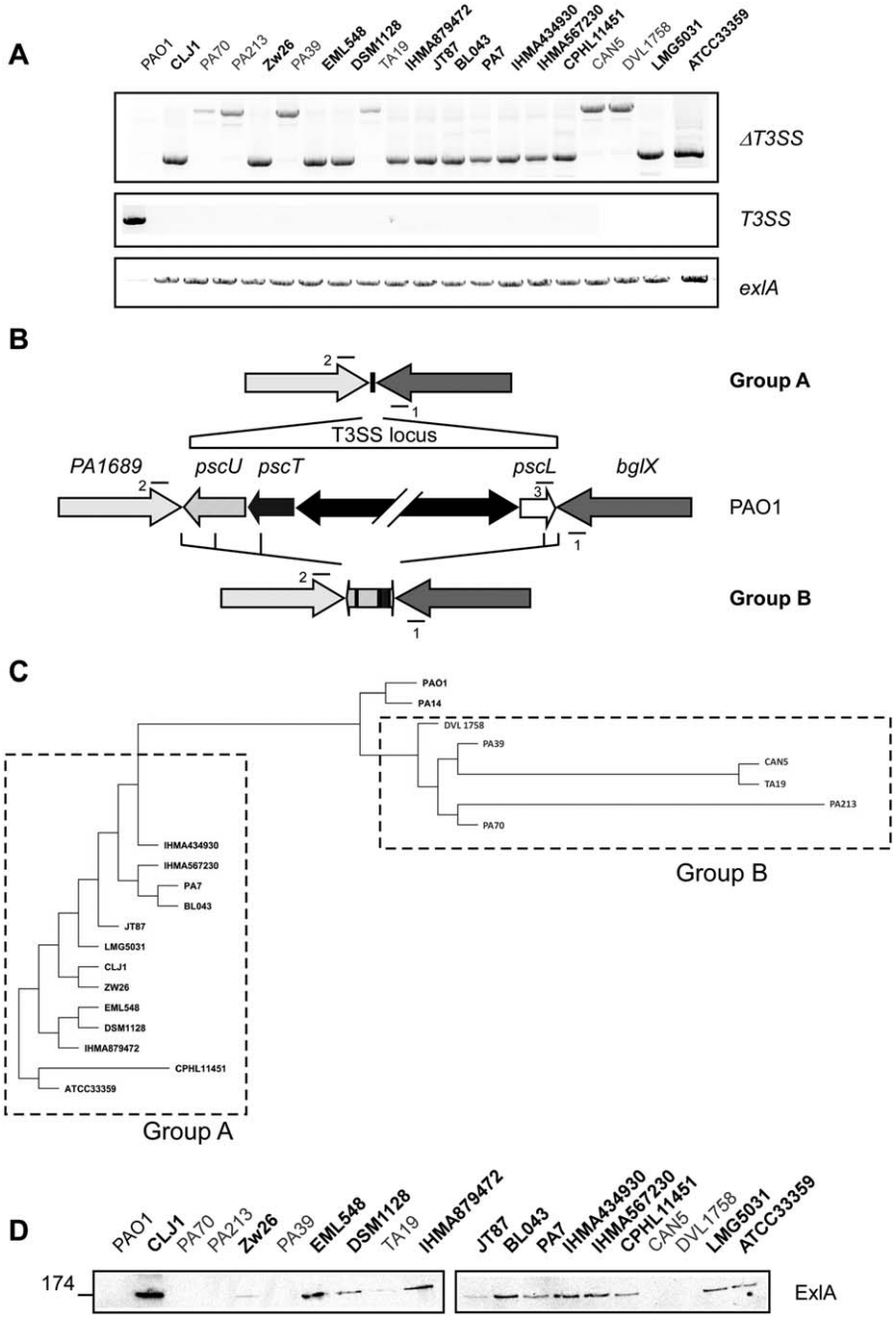

Fig. 1. Genetic analysis of T3SS and exlA loci, and ExlA secretion.
A. Amplicons generated with primers annealing to the external boundaries of the deleted T3SS locus (ΔT3SS, primers 1 + 2 in B), to one end of the T3SS locus and one bordering gene (T3SS, primers 1 + 3 in B) and to an internal exlA sequence (exlA). Primers are listed in Table S1.
B. Diagram showing the two possible genomic sequences found in place of the T3SS locus.
C. Phylogenetic tree of maximal likelihood based on single nucleotide polymorphisms of seven housekeeping genes. The two distinct groups (A and B) of exlA+ strains match with the two excision patterns at the T3SS locus.
D. Bacterial secretomes were TCA-precipitated and analyzed by Western blot using anti-ExlA antibodies. Molecular weight is indicated on the left. Group A strains are indicated in bold and Group B strains in grey. Data are representative of three independent experiments.

CLJ1 infection in mice (Elsen *et al.*, 2014). One strain was isolated from a dog, one from a pond and another from a plant. Altogether, these features suggest that the *exlA*-positive T3SS-negative strains appear able to colonize different habitats and to induce infections in diverse organs, like the classical strains.

To further assess the genetic relationship between strains in our collection, we performed multilocus sequence typing (MLST) analysis using seven housekeeping genes, as recommended at http://pubmlst.org/paeruginosa/. Based on this analysis, a sequence type (ST) was assigned to each strain. Among the 19 *exlA*+ strains, 16 different STs were identified, 7 of which had not previously been assigned. Two isolates from Newcastle, PA70 and PA213, shared the same ST number and thus probably derived from the same clone. Similarly, EML548 and DSM1128 shared the same ST number and serotype, and are also probably linked. Surprisingly, BL043, isolated in the United States, and PA7, isolated in Argentina, were in the same case, suggesting that the clone was dispersed across the two continents.

A phylogenetic tree was constructed based on the MLST analysis (Fig. 1C). This phylogenetic tree showed that

Table 1. List of *exlA*-positive *P. aeruginosa* strains.

Name[a]	Other names	Origin	Country (City)	Serotype	References	sequence type	Sequence accession number
CLJ1		Expec. (COPD)	France (Grenoble)	O12	(Elsen *et al.*, 2014)	2028	
PA70		Expec. (Non-CF Bronchiectasis)	UK (Newcastle)	PA[b]		1328	
PA213		Expec. (Non-CF Bronchiectasis)	UK (Newcastle)	PA[b]		1328	
Zw26		Expec. (CF)	Germany (Karlsruhe)	O11[b]		2165	
PA39	CF-PA39	Expec. (CF)	Belgium	O3	(Dingemans *et al.*, 2014)	1744	NZ_JDVE00000000
EML548		Otitis	Unknown	O1[b]	(Boukerb *et al.*, 2015)	191	LFXR00000000.1
DSM1128	ATCC9027	Otitis	USA	O1[b]	(Mai-Prochnow *et al.*, 2015)	191	LJGL00000000
TA19	LMG25202	Urinary	Australia	nt	(Pirnay *et al.*, 2009)	2227	
IHMA879472	AZPA15042 SAMN03105739	Urinary	Germany	O11_O12	(Kos *et al.*, 2015)	2211	NZ_JTNE00000000
JT87		Urinary	USA (Cleveland)	O12[b]	(Toska *et al.*, 2014)	1978	
BL043		Bacteremia	USA (Chicago)	O12[b]		1195	
PA7		Burn	Argentina	O12	(Roy *et al.*, 2010)	1195	NC_009656
IHMA434930	AZPAE14901 SAMN03105599	Abscess/Pus	India	O11_O17	(Kos *et al.*, 2015)	2212	NZ_JTSO00000000
IHMA567230	AZPAE14941 SAMN03105639	Peritoneal	China (Hong Kong)	O12	(Kos *et al.*, 2015)	2213	NZ_JTRA00000000
CPHL11451		Unknown	USA (Kentucky)	O12	(Pirnay *et al.*, 2009)	2214	
CAN5	IDEXX CANINE 5	Unknown (canine)	UK	O6	(Pirnay *et al.*, 2009)	1716	
DVL1758		Pond water	Belgium	nt	(Pirnay *et al.*, 2009)	2215	
LMG5031		*Aglaonema commutatum*	Puerto Rico	nt	(Pirnay *et al.*, 2009)	2039	
ATCC33359	IMG 243	Unknown	Unknown	O12	(King *et al.*, 2008)	2228	

a. Group B strains are highlighted in grey.
b. Serotype determined in this study.
CF, cystic fibrosis; Expec., expectoration; COPD, chronic obstructive pulmonary disease; PA, polyagglutinable; nt, not typable.

exlA+ strains can be subdivided into two different groups, hereafter called Groups A and B. Group A includes PA7, and thus can be designated as PA7-like strains. Group B strains are much phylogenetically closer to PAO1/PA14 strains and constitute an independent clade. Group B isolates corresponded to the strains producing a long PCR fragment at the ΔT3SS locus, while strains from Group A produced a short fragment, similar to PA7 (Fig. 1A). Based on the sequences of the two recombination patterns and the phylogenetic tree, we hypothesized that *exlA*+ strains have evolved from at least two different ancestors.

It was not possible at this stage to determine the original location of Group A strains, as they were identified from samples collected in a number of locations worldwide. However, all Group B strains except TA19 were isolated in Europe, hinting that they derive from a European clone.

After genetic screening, all the strains were tested for *in vitro* secretion of ExlA in LB medium (Fig. 1D). ExlA secretion levels were highly variable across the strains, from high for CLJ1 to undetectable levels for PA70, PA213, PA39, CAN5 and DVL1758. This suggests that ExlA synthesis and/or secretion is differentially regulated among these strains, which remains to be studied further. Importantly, no ExlA could be detected in Group B strain secretomes, except for TA19 for which a faint band was detected (Fig. 1D), indicating that this virulence factor is attenuated in these strains.

Serotyping revealed eight of fourteen typable strains (57%) to display an O12 serotype (Table 1), which is much higher than previously reported percentages for this type, ranging from 2 to 22% (Allemeersch *et al.*, 1988; Pitt *et al.*, 1989; Bert and Lambert-Zechovsky, 1996; Pirnay *et al.*, 2009; Maatallah *et al.*, 2011). In line with these findings, a recent study suggests that the gene cluster linked to serotype O12 originated from a PA7-like strain (Thrane *et al.*, 2015). The predominance of the O12 serotype is thus a characteristic of most *exlA*+ strains and could be used as an inclusion criterion when attempting to discover strains in this clade in the future.

Infection of various cell types by exlA+ *strains*

We previously characterized the toxicity of a limited number of strains on human primary endothelial cells

(HUVECs) and on a human macrophage cell line (J774) (Elsen *et al.*, 2014). Here, we extended this study to all 19 isolates and tested their cytotoxicity on six different cell types. Two epithelial cell lines, A549 cells derived from human lung alveoli and MDCK from dog kidney, THP-1, a human monocytic cell line, Jurkat cells, derived from T lymphocytes, L929, a mouse fibroblastic cell line and HUVECs were used in this study. Damage to plasma membranes was assessed by measuring lactate dehydrogenase (LDH) activity in cell supernatants (Fig. 2A). A549, THP-1 and Jurkat cells were highly sensitive to most *exlA*+ strains, while MDCK, L929 cells and HUVECs were only sensitive to some strains and to a lesser extent, indicating that cell lines were differentially permissive to infection. Toxicity was also significantly different between strains ($P < 0.0001$ by Friedman's aligned rank test). The relative toxicity of the different strains was ranked for every cell line and the overall cytotoxicity was determined by adding the rank numbers for each strain (Table 2). This ranking revealed CLJ1, IHMA879472 and IHMA434930 to be the most toxic strains (sum of rank >100), whereas PA70, PA213, PA39 and TA19 were the least cytotoxic ones (sum of rank <25). The other strains had an intermediate phenotype. The differential responses of the six cell types to the 19 strains were assessed by calculating rank number differences (Table 2). Most strains had comparable relative toxicity for all the cellular models used. The main exception was LMG5031, which was toxic in most cell lines except in L929. The sum of the toxicity rank number was correlated to ExlA secretion ($P = 0.03$, using Spearman's correlation test), suggesting that ExlA is one of the major factors used by these strains to cause damage to cell membrane. It is noteworthy that Group B strains were significantly less toxic than Group A strains (Table 2), possibly due to their lack of secretion of ExlA.

The hemolytic activity of the different strains was assessed using human blood (Fig. 2B). PP34, an ExoU-secreting strain, was used as positive control in this assay, while PAO1, which induces hemoglobin release much less effectively, was used as a low-activity control. The e*xlA*+ strains had a hemolytic activity in the same range as or below PAO1 activity in this assay (Fig. 2B). The differential responses of *exlA*+ strains were not correlated with ExlA secretion levels. Thus, ExlA does not seem to be a major contributor of erythrocyte lysis.

Altogether, these results indicate that toxicity is generally strain-dependent, but the extent of toxicity depends on the target cell line. Importantly, the limited hemolysis induced by *exlA*+ strain corroborated previous reports in mice (Elsen *et al.*, 2014), where the broncho-alveolar lavages of CLJ1-infected lungs contained erythrocytes, but not free hemoglobin, indicating that CLJ1 is hemorrhagic, but not hemolytic in this model.

Proteolytic activity of exlA *strains*

Secreted proteases have a significant impact on bacterial virulence both *in vitro* and *in vivo* (Hong and Ghebrehiwet, 1992; Tamura *et al.*, 1992; Azghani, 1996; Bleves *et al.*, 2010; Beaufort *et al.*, 2011; Golovkine *et al.*, 2014). The secreted proteolytic activity of the 19 isolates was first assessed for casein, using milk-agar plates. This functional test monitors both LasB, the main protease secreted by a T2SS of classical strains (PAO1- and PA14-like), and AprA, which is released by a T1SS (Caballero *et al.*, 2001). PAO1 was used as the positive control for T1SS- and T2SS-dependent proteolytic activities and showed a proteolytic halo on plates (Fig. 3A). PAO1Δ*xcpR*, which cannot secrete T2SS proteases and PAO1Δ*lasB*, which lacks LasB, also presented some proteolytic activity, probably due to AprA secretion. Most *exlA*+ strains displayed a proteolytic halo of varying size, indicating that exoproteases form part of their arsenal of virulence factors. The only two protease-negative strains were BL043 and Zw26.

LasB was previously shown to be an important contributor to *P. aeruginosa* virulence (Bleves *et al.*, 2010). This protease degrades various extracellular proteins, including fibronectin, plasma proteins and pulmonary surfactants, as well as membrane proteins, such as upaR and VE-cadherin (Alcorn and Wright, 2004; Leduc *et al.*, 2007; Beaufort *et al.*, 2011; Kuang *et al.*, 2011; Golovkine *et al.*, 2014). Degradation of these proteins is known to facilitate bacteria-epithelium interactions and transmigration across the vascular barrier, and promote breach of the basal lamina.

To precisely examine the LasB activity secreted by the strains, VE-cadherin and fibronectin were incubated with strain secretomes. CLJ1, IHMA 879472, IHMA 434930 and DVL 1758 secretomes, cleaved VE-cadherin to a similar extent to PAO1 secretome (Fig. 3B). PA70, PA213, PA39 and JT87 secretomes induced partial cleavages, but those of the other strains did not degrade VE-cadherin. Identical results were obtained using fibronectin as substrate (Fig. 3C). Thus, only 37% of *exlA*+ strains exhibited a LasB-dependent activity, which is much lower than the percentages previously reported for clinical strains of various origins (90–97.5%) (Coin *et al.*, 1997; Schaber *et al.*, 2004). However, the methodology was different and their results may not be comparable to ours. Nevertheless, we can conclude that LasB prototypical activity is not a common feature of *exlA*+ strains, as opposed to classical strains.

Motility of exlA+ *strains*

P. aeruginosa's motility in various media mainly depends upon pili and the flagellum, while surfactant production contributes to swarming and sliding motions. The

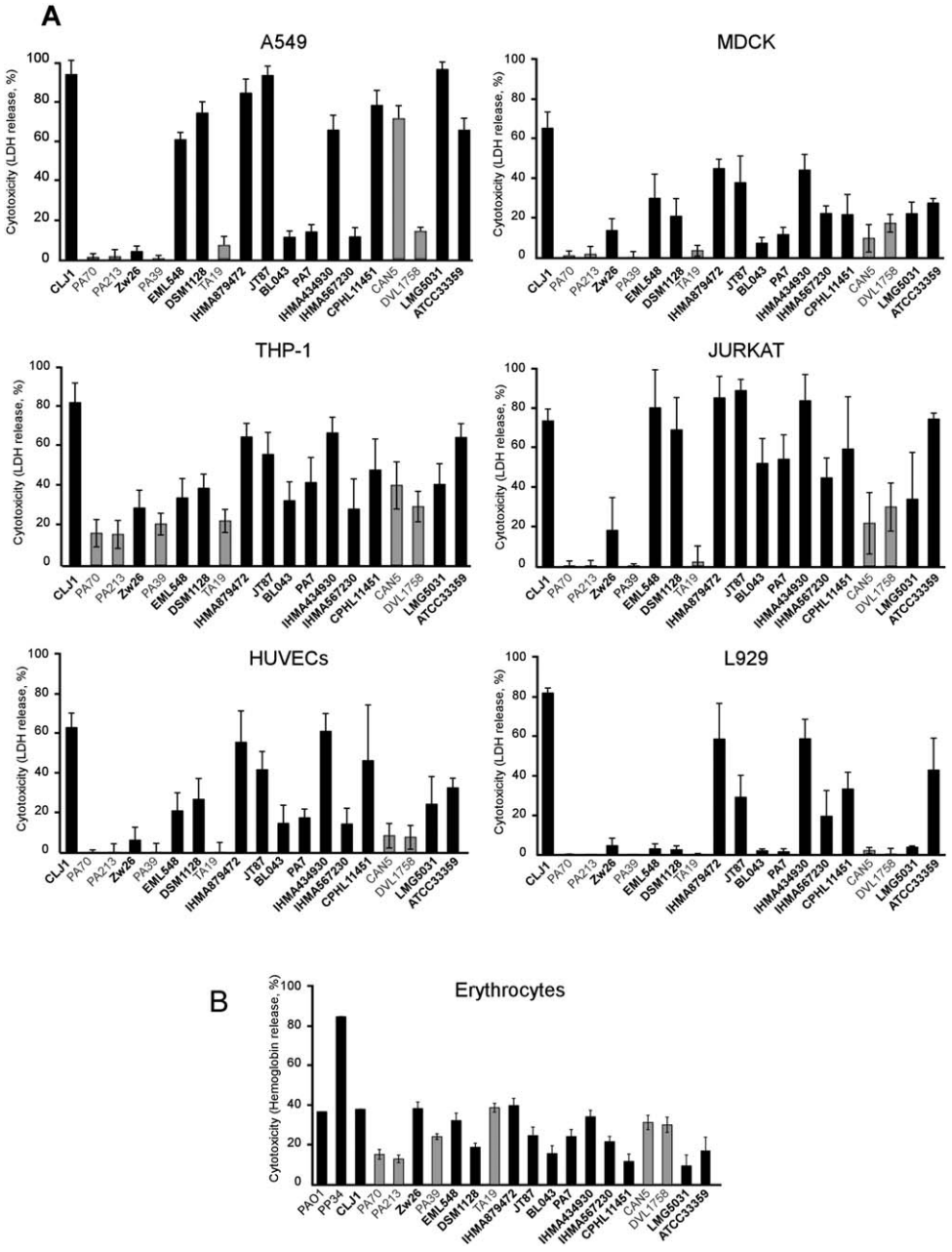

Fig. 2. Cytotoxicity of exlA+ strains on different cell types and erythrocytes.
A. Disruption of plasma membrane was examined by LDH release in the cell supernatant at 4 hpi. Data show the percentages of total cellular LDH and are representative of three independent experiments performed in triplicate. PAO1 was not toxic in this assay, while PP34 (ExoU+) was highly toxic (not shown).
B. Hemolytic activity towards human erythrocytes, measured by hemoglobin release at 3 hpi. Results are shown with black bars for Group A strains and with grey bars for Group B strains. Data are representative of three independent experiments. The results are summarized in Table 2.

swimming, twitching and swarming/sliding capacities of the *exlA*+ strains were investigated on agar plates of variable rigidity, using established procedures (Figs. S1–S3; data summarized in Table 3). The production of wetting material (surfactant) on the surface of swarming plates was also measured (Fig. S4; data are summarized in Table 3).

Most strains swarm and twitched, however CLJ1, IHMA879472, IHMA434930 and DVL1758 displayed atypical morphologies in the swimming assay (Fig. S1), similar to those generally observed in the swarming assay. To further examine the swimming abilities of these strains, we analyzed the bacterial behavior in a liquid medium by high-

Table 2. Rank presentation of the virulence of the 19 strains towards six cell types.

Name[a]	Rank number in A549 infection[b]	Rank number in MDCK infection[b]	Rank number in THP-1 infection[b]	Rank number in Jurkat infection[b]	Rank number in HUVEC infection[b]	Rank number in L929 infection[b]	Rank number differences	Sum of rank number[c]	Hemolytic activity[c]
CLJ1	18	19	19	14	19	19	5	108	+/−
PA70	2	2	2	2	1	3	2	12	−
PA213	3	3	1	3	4	1	3	15	−
Zw26	4	8	6	5	5	12	8	40	+/−
PA39	1	1	3	1	3	2	2	11	+/−
EML548	10	15	9	16	11	10	7	71	+/−
DSM1128	14	10	10	13	13	9	5	69	+/−
TA19	5	4	4	4	2	4	3	23	+/−
IHMA879472	16	18	17	18	17	17	2	103	+/−
JT87	17	16	15	19	15	14	5	96	+/−
BL043	6	5	8	10	9	7	5	45	+/−
PA7	8	7	13	11	10	6	7	55	+/−
IHMA434930	12	17	18	17	18	18	6	100	+/−
IHMA567230	7	13	5	9	8	13	8	55	+/−
CPHL11451	15	11	14	12	16	15	5	83	−
CAN5	13	6	11	6	7	8	7	51	+/−
DVL1758	9	9	7	7	6	5	4	43	+/−
LMG5031	19	12	12	8	12	11	11	74	−
ATCC33359	11	14	16	15	14	16	5	86	+/−
Statistical differences Groups A/B[d]	0.02	0.001	0.005	0.001	0.001	0.001		0.002	n.d.

a. Group B strains are highlighted in grey.
b. Statistical differences of strain toxicity between cell lines: $P < 0.0001$ by Friedman's aligned rank test.
c. No correlation between toxicity on cell lines and on erythrocytes: $P = 0.7$ by Spearman's correlation test.
d. *P*-value of statistical differences between Groups A and B using Mann-Whitney's test.
n.d., not determined.

speed dark-field videomicroscopy (data summarized in Table 3). This microscopy analysis confirmed the swimming results obtained on agar plates, for all strains but CLJ1, which did not swim under the microscope, thus demonstrating the usefulness of microscopic examination of bacteria in assessing this type of motion. Interestingly, three strains with atypical morphology in the swimming plate assay (CLJ1, IHMA879472, IHMA434930) displayed no swarming (Fig. S3), suggesting that the atypical swimming behavior is not related to swarming. The few swarming strains exhibited the typical branching morphology of the colonies.

All possible situations were found among these 19 strains for the different types of motility, as for classical strains. The results suggest that the functionality or the presence of pili and flagellum is highly variable between these strains. Several strains (PA70, EML548, IHMA879472, IHMA434930, CAN5), displaying swimming and twitching abilities and producing surfactant, did not swarm, which indicates that the mechanisms promoting swarming motility remain elusive. Interestingly, TA19 did not twitch nor swim, but produced surfactant and exhibited a swarming phenotype that may be related to sliding (Murray and Kazmierczak, 2008).

Altogether, the proportions of swimming and the twitching strains (79% and 74% respectively) were similar to those reported previously for classical strains (88% and 76% respectively) (Murray *et al.*, 2010). The percentage of swarming strains (21%, taking the poorly swarming clones into account) was very low compared to classical isolates (63%). This concurs with previous linkage analyses showing that swarming is correlated with T3SS expression (Murray *et al.*, 2010). In our hands, a correlation between swimming and twitching properties was noted ($P = 0.0009$), suggesting that flagellum-positive isolates also harbor pili. Swarming was also correlated with surfactant production ($P = 0.04$), as previously reported for classical strains (Murray *et al.*, 2010).

All these results suggest that the functionality or the presence of pili and a flagellum is highly variable between strains. Swarming is the motility type most affected among *exlA*+ strains. Swarming could be considered to be part of the transition step between surface colonization and the development of biofilms (Shrout *et al.*, 2006; Caiazza *et al.*, 2007) usually associated with chronic infections. It will therefore be important to test *exlA*+ strains in chronic models of infection and to examine their behavior in this context.

HCN production

All *P. aeruginosa* strains tested so far release HCN in the gas phase (Gilchrist *et al.*, 2011; Smith *et al.*, 2013). This

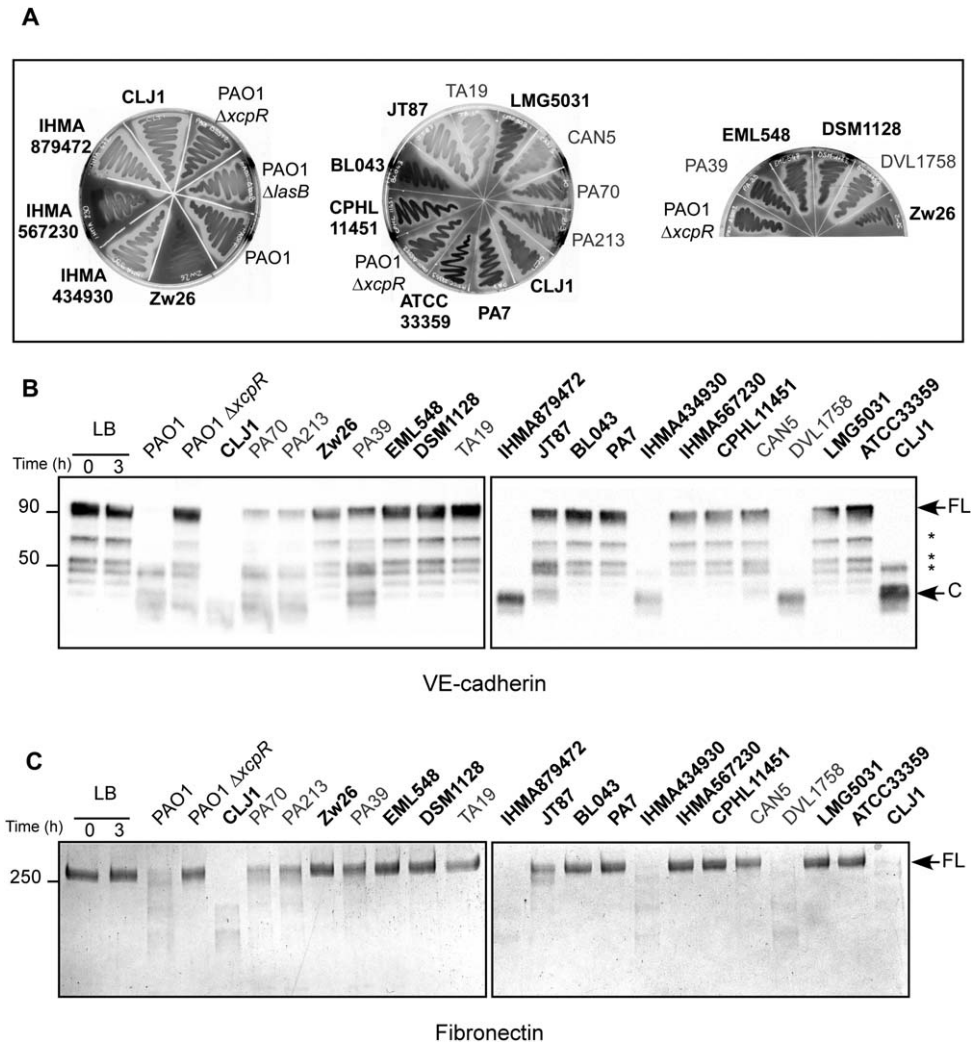

Fig. 3. Proteolytic activity of exlA+ strains.
A. LasB and AprA activities were determined by growing bacteria onto milk-agar plates. The white halo around the colonies results from casein degradation. Strains PAO1F as well as PAO1ΔxcpR and PAO1ΔlasB were used as controls for full and reduced proteolytic activities respectively.
B. The purified extracellular domain of VE-cadherin was incubated for 3 h at 37°C with filtered bacterial secretomes. The reaction products were analyzed by Western blot using anti-VE-cadherin antibodies. The full-length (FL) extracellular domain and the cleaved product (C) are indicated by arrows. (*) designates degradation products already present in the starting VE-cadherin preparation.
C. Fibronectin was incubated with filtered bacterial secretomes at 37°C for 2 h, and was analyzed by electrophoresis and Coomassie staining. Group A strains are indicated in bold and Group B strains in grey. Data are representative of three independent experiments. The results are summarized in Table 4.

virulence factor is relatively specific to *P. aeruginosa*. A paper impregnated with a reaction mixture containing Cu^{2+} was used to detect HCN production – revealed by a white-to-blue color transition. The detection paper was placed above bacteria seeded onto agar plates. As shown in Fig. S5, a gradient of decreasing HCN production was obtained for the different strains: CLJ1, IHMA879472, JT87 > PA7, IHMA434930, CAN5, DVL1758 > 70, 213 > EML548, DSM1128, TA19. No HCN production was detected for Zw26, PA39, BL043, IHMA567230, CPHL 11451, LMG5031 and ATCC3359 (data summarized in Table 4). Thus, 37% of *exlA*+ strains produced no HCN (or undetectable levels), suggesting that this clade is much more heterogeneous than the classical *P. aeruginosa* strains, with regard to this factor.

Toxicity in a mouse model of acute pneumonia

Pneumonia is the main infectious disease induced by *P. aeruginosa*. To evaluate strain toxicity *in vivo*, we used a mouse model of pneumonia induced by inhalation of bacteria. In this model, infection is mainly located in the lower

Table 3. Motile capacities of *exlA* strains (summary of Figs. S1–S4).

Name[a]	Swimming (agar plates)	Swimming[c] (microscopy)	Swarming[c]	Twitching[c]	Surfactant[c]
CLJ1	+[b]	−	−	−	++
PA70	+	+	−	+	++
PA213	+	+	−	+	−
Zw26	−	−	−	−	−
PA39	+	+	+/−	+/−	−
EML548	+	+	−	+	+
DSM1128	+	+	−	+	−
TA19	−	−	+	−	++
IHMA879472	+[b]	+	−	+	+
JT87	+	+	+	+	++
BL043	+	+	−	−	−
PA7	+	+	−	+/−	+
IHMA434930	+[b]	+	−	+	++
IHMA567230	−	−	−	+/−	−
CPHL11451	+	+	−	+/−	−
CAN5	+	+	−	++	+
DVL1758	+[b]	+	++	+++	+++
LMG5031	+	+	−	+	−
ATCC33359	+	+	−	+/−	−
Positive strains (%)	84	79	21	74	53

a. Group B strains are highlighted in grey. No significant differences between Groups A and B were found for any mobility factors using Mann-Whitney's test.
b. Atypical phenotypes.
c. Spearman's correlation test: swimming/twitching $P = 0.0009$; swarming/surfactant $P = 0.04$; $P > 0.5$ for other comparisons.

Table 4. Summary of exlA strain toxicity in different models.

	ExlA	Other virulence factors			Biological activity		
Name	ExlA Secretion	HCN Production	Proteases *Casein*	Proteases *VE-cadherin/ Fibronectin*	Sum of cytotoxicity[a]	Mice[b]	Chicory leaves[b]
CLJ1	+++	++	++	++	108	7	10
PA70	−	+	++	+	12	nd	7
PA213	−	+	++	+	15	nd	5
Zw26	+/−	−	+/−	−	40	nd	8
PA39	−	−	+	+	11	nd	3
EML548	+/−	+	+	−	71	nd	15
DSM1128	+	+	+	−	69	nd	19
TA19	+/−	+/−	++	−	23	nd	12
IHMA879472	+	++	++	++	103	3	17
JT87	+/−	++	++	+/−	96	6	16
BL043	+	−	−	−	45	nd	1
PA7	+/−	++	++	−	55	nd	6
IHMA434930	+	++	++	++	100	nd	19
IHMA567230	+	−	+	−	55	nd	11
CPHL114516	+/−	−	+	−	83	2	9
CAN5	−	++	++	−	51	1	14
DVL1758	−	++	++	++	43	4	13
LMG5031	+	−	+	−	74	5	4
ATCC33359	+	−	+	−	86	nd	2
Statistical differences Groups A/B[c]	0.01	0.6	0.7	0.5	0.002	nd	0.6

a. Sum of rank number of the cytotoxicity in 6 cell types, from less to most toxic.
b. Toxicity range from less to most toxic.
c. *P*-values of statistical differences between Groups A and B using Mann-Whitney's test. Spearman's correlation test: ExlA secretion/Sum of cytotoxicity $P = 0.03$; Sum of cytotoxicity/Chicory leave infection $P = 0.073$; $P > 0.5$ for comparisons between other datasets.
nd, not determined.

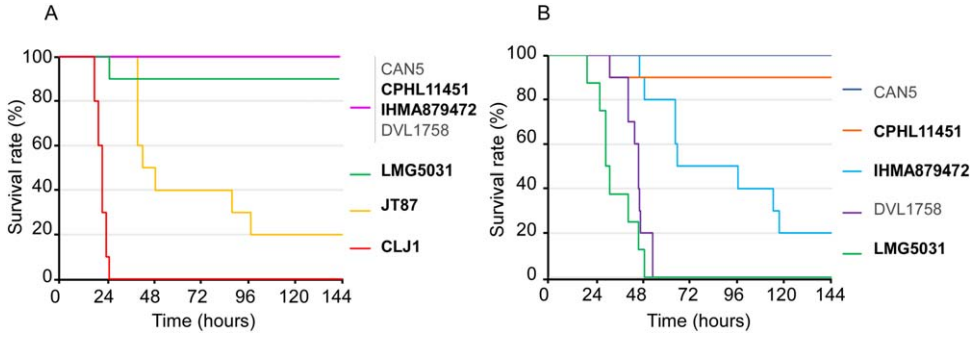

Fig. 4. Strain virulence in mouse model of acute pneumonia.
A. Bacterial suspensions (5×10^6) were instilled in mouse airways to induce acute pneumonia. Kaplan-Meyer survival curves are presented for CLJ1, IHMA879472, JT87, CPHL11451, CAN5, DVL1758, and LMG5031 (8–10 mice per condition).
B. Similar experiment with 15×10^6 bacteria per mouse. Group A strains are indicated in bold and Group B strains in grey. Data are summarized in Table 4.

airways. Based on the above results, seven strains were selected from the 19 studied here, representing several functional characteristics. In a first set of experiments, the mice (10 per lot) were infected with 5×10^6 bacteria, a dose calibrated in previous studies using classical strains (PAO1, CHA, PP34) and also CLJ1 (Elsen *et al.*, 2014; Perdu *et al.*, 2015). Under these conditions, all mice infected with CLJ1 died within 24 h (Fig. 5A). Most (80%) JT87-infected mice died within 96 h, while the other infected mice recovered from the febrile state after 48 h (Fig. 4A).

In a second set of experiments, the bacterial burden was increased to 15×10^6 bacteria (Fig. 4B). In these conditions, most or all mice infected with LMG5031, DVL1758 and IHMA879472 died within 7 days.

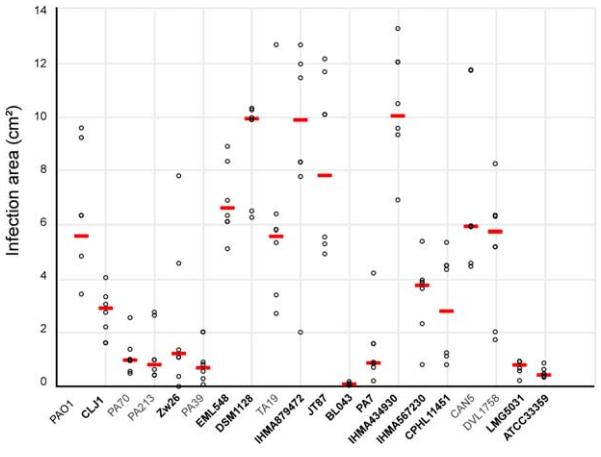

Fig. 5. Chicory leaf infection.
The center part of the leaf was injected with 10^4 bacteria ($n = 6$ leaves per strain). Infected leaves were incubated for 72 h at 37°C and the infection areas were measured (images are shown in Fig. S6). Individual data are presented as circles and medians by red lines. Group A strains are indicated in bold and Group B strains in grey. Data are representative of three independent experiments. Results are summarized in Table 4.

Taken together, the mouse survival experiments showed a gradient of toxicity among the strains that would not have been predictable from the *in vitro* data, as no direct correlation was found with any other datasets. For example, IHMA879472 and CAN5 were among the most toxic strains on cellular models but showed minimal toxicity in mice. More work will be needed to understand the behavior of these strains in vivo, notably their interactions with the immune system.

Chicory leaf infection

In addition to animals, *P. aeruginosa* is known to infect plants, and one of the *exlA*+ strain (LMG5031) was isolated from a plant. We therefore investigated the capacity of the 19 strains to infect chicory leaves (Fig. 5), a model of *P. aeruginosa* infection which has been used previously (Fito-Boncompte *et al.*, 2011). Surprisingly, LMG5031 was not toxic in this assay, whereas it was highly virulent on cells and in mice. In contrast, some clinical isolates (DSM1128, IHMA879472, JT87 and IHMA434930) produced large necrotic areas on chicory leaves. Furthermore, CLJ1, the most toxic strain in all other assays, was avirulent on chicory leaves. No significant correlation was found with the other datasets. Notably, PAO1 induced a larger necrotic area than CLJ1, suggesting that ExlA does not play a major role in plant intoxication.

Taken together, these observations indicate that the virulence modes used by *P. aeruginosa* to infect animals and plants are different.

Conclusion

Genomic information about the PA7 clade is gradually becoming available, with a number of recent publications

and database releases (Roy *et al*., 2010; Dingemans *et al*., 2014; Elsen *et al*., 2014; Toska *et al*., 2014; Boukerb *et al*., 2015; Kos *et al*., 2015; Mai-Prochnow *et al*., 2015) www.pseudomonas.com. Here, we investigated the general phenotypes of *exlA*+ strains that represent two distinct phylogenetic groups, one related to PA7 (Group A) and one much closer phylogenetically to PAO1/PA14 strains (Group B). We showed that the behavior and the virulence traits of *exla*+ strains are highly variable, even inside each group (the main results are summarized in Table 4). Interestingly, classical *P. aeruginosa* strains (i.e. PAO1- and PA14-like strains), although sharing the most recognized virulence mechanisms, namely the T3SS and its effectors, and LasB, displayed highly diverse phenotypes in classical laboratory models when tested for virulence (Hilker *et al*., 2015), similar to what was observed here for *exlA*+ strains. It is well established that *P. aeruginosa* strains possess a mosaic genome structure carrying a variable number of regions of genomic plasticity in addition to a conserved core genome, but the role these regions play in strain-specific phenotypes remains unknown. Our results show that not only the genetic content, but differences in gene expression and regulation may contribute to the infection-related phenotype. This may be a conserved feature of *P. aeruginosa* isolates and will need further functional genomic analysis to link overall virulence to gene regulation. Importantly, phylogenetic information suggested that these strains were likely to have originated from two clones with differential virulence; this hypothesis was supported by the PCR data. As suggested above, *exlBA* insertion likely occurred before *T3SS* locus deletion. It may thus be possible to find strains possessing both virulence factors. The approach used here, screening for T3SS-negative strains, could not have identified any such strains. A more systematic screen of *P. aeruginosa* strains should allow unbiased identification of any new *exlA*+ strains.

The *exlA*+ strains exhibited a gradient of virulence in cell line and in mouse models ranging from high (CLJ1, JT87) to very low (PA70, PA213, Zw26), with some specificities. These strains display some overrepresented traits, such as serotype O12, and some underrepresented like the capacity to engage in swarming behavior, to secrete LasB or produce HCN. However, all possible combinations were observed. Interestingly, Group B strains were less cytotoxic than Group A strains (Table 2) and ExlA was undetectable (or poorly for TA19) in Group B secretomes (Table 4) even though the *exlBA* locus is located in the same location in strains from both groups. This suggests a lack of appropriate transcriptional regulation pathways in Group B strains.

The results presented here demonstrate that *exlA*+ *P. aeruginosa* strains have a similar ability to colonize and infect animals and plants as classical strains. This suggests that the *exlA*+ strains can spread using different supports. In addition, our results show that different repertoires of factors are required for virulence in mouse and plants. Furthermore, the pathogenicity of strains for specific organisms is independent of their origins. Interestingly, one strain, CAN5, displayed some toxicity in cellular models and in chicory leaves even though its secretome contained no detectable amounts of ExlA. Similarly, JT87 produced low levels of ExlA, but it exhibited high virulence in all cells and *in vivo* assays. It is thus possible that another, as yet unidentified, virulence factor is produced by these two strains.

This study is the first step towards the understanding of the general phenotypic properties of the *exlA*+ *P. aeruginosa* strains. Although they lack a major virulence factor, these strains emerged in a range of different habitats, and some of them efficiently infected various hosts. An important issue will now be to understand ExlA toxicity at the molecular level and its interaction with the other virulence determinants identified in these bacteria.

Experimental procedures

Ethical statement

All protocols in this study were conducted in strict accordance with the French guidelines for the care and use of laboratory animals. The protocols for mouse infection were approved by the animal research committee of the institute (CETEA, project number 13-024).

P. aeruginosa *strains and culture*

The strains used in this study are described in Tables 1 and S1. Bacteria were grown in liquid LB medium at 37°C with agitation until the cultures reached an optical density value of 1.0 unless indicated.

Serotyping

Determination of the serotype of the strains was performed using polyvalent and monovalent antisera (BioRad) and interpreted according to the International Antigenic Typing Scheme (Liu and Wang, 1990).

PCR

For each strain, the overnight culture was diluted 100 fold in sterile water and heated at 100°C for 10 min. Then, gene amplification was performed using GC Advantage Polymerase kit (Clontech), with specific primers designed from PAO1 and PA7 genomes (Table S1). The amplification fragments were analyzed by electrophoresis and Gel Red staining.

ExlA *secretion*

For ExlA detection, the secretomes were collected when bacterial cultures were at OD = 1.0 were concentrated by trichloroacetic acid (TCA) precipitation. Briefly, 300 μL of 2% Na deoxycholate were added to 30 mL of bacterial

supernatant and incubated 30 min at 4°C. Then, 3 mL of TCA were added and the mixture was incubated overnight at 4°C. After centrifugation for 15 min, at 15,000*g* and 4°C, the pellet was resuspended in 100 μL of electrophoresis loading buffer. For ExlA antibodies, rabbits were immunized with three synthetic peptides derived from the predicted protein sequence of the *PSPA7_4642* gene (Elsen *et al.*, 2014). The anti-ExlA serum was used at 1:1,000 dilution. The secondary anti-rabbit-HRP antibody (Sigma-Aldrich) was used at 1:10,000 dilution.

Phylogenetic tree and MLST analysis

Phylogenetic analysis was performed on seven housekeeping genes (*ascA, aroE, guaA, mutL, nuoD, ppsA and trpE).* The sequences of these seven genes were already available on Genebank for most strains, but for PA213, Zw26, EML548, DSM1128, TA19, BL043 and ATCC33359 strains, gene sequences were obtained by PCR amplification using specific primers (Table S1) followed by sequencing.

The gene sequences were concatenated and aligned using CLC bio software. A tree was generated by neighbor joining method with 500 bootstrap replicates for all sequences, using CLC bio software.

For each strain, we determined a ST which is the combination of the seven allele numbers. Strain STs were obtained from *P. aeruginosa* MLST website (http://pubmlst.org/paeruginosa/).

Cell culture and infection

A549, THP-1, Jurkat cells were grown in RPMI medium and MDCK, L929 cells in DMEM, both supplemented with 10% fetal calf serum (all from Invitrogen). HUVECs were prepared from human umbilical cords as previously described (Huber *et al.*, 2014) and were grown in supplemented EBM2 (Lonza).

LDH release in the supernatant was measured using the Cytotoxicity Detection Kit by Roche Applied Science, following the recommended protocol. Briefly, cells were seeded at 5×10^4 in 96-well plates the day before, and infected in non-supplemented EBM2 medium at MOI 5 with bacteria at OD = 1.0. At 4 hpi, 30 μL of supernatant were mixed with 100 μL of reaction mix and OD was read at 492 nm. OD values were substracted with that of uninfected cells and Triton-solubilized cells were used to determine the total LDH present in the cell culture.

Human heparinized blood, obtained from the Etablissement Français du Sang, was centrifuged at 2,000*g* for 5 min at 4°C, washed three times with PBS and stored at 4°C for 1 week maximum. Infections were performed as previously described (Dacheux *et al.*, 2001) the following days, to prevent bacteria killing by neutrophils. Briefly, 50×10^6 cells in 100 μL of EBM2 were distributed in microplates, together with 100 μL of bacteria also in EBM2 (MOI = 5). The microplate was centrifuged for 5 min at 1,000 rpm at room temperature, in order to facilitate the contact between bacteria and cells, and incubated at 37°C for 3 h. Then, the pellets were resuspended by gentle shaking, and the microplate was centrifuged (1,000 rpm, 5 min, 4°C). The hemoglobin content of the supernatants was determined on 100 μL, by measuring the OD_{560}.

Proteolytic activity assays

Elastase and alkaline protease activities were observed after plating on 'milk plates' (40 g L^{-1} Tryptic soy agar and 10% skim-milk from Difco).

VE-cadherin extracellular domain was prepared as previously described (Golovkine *et al.*, 2014) and used as substrate for LasB activity in bacterial secretomes. The filtered bacterial secretomes at OD 1.5 were incubated with VE-cadherin extracellular domain (100 ng) at 37°C during 3 h. Then, samples were heated in electrophoresis loading buffer and VE-cadherin was revealed by Western blot using antibodies against VE-cadherin extracellular domain (cad3).

Purified fibronectin (300 ng) was incubated in presence of bacterial secretomes (OD 1.5) at 37°C. After 2 h, samples were electrophoresed and stained with Coomassie dye.

Motility assays and surfactant production

The swarming motility test was performed on 0.5% agar M8 plates supplemented with 1 mM $MgSO_4$, 0.2% glucose, 0.1 mM $CaCl_2$, 0.5% casamino acid. The plates were incubated 24–48 h at 37°C.

For twitching motility, bacteria were inoculated at the plastic-agar interface (10 g L^{-1} tryptone, 5 g L^{-1} yeast extract, 1% agar, 10 g L^{-1} NaCl, 1% agar). After 48 h at 37°C, the agar medium was removed, and the twitching zone was observed after Coomassie blue staining.

Bacterial swimming was observed after 48 h at 30°C in 0.3% agar medium plate (10 g L^{-1} tryptone, 5 g L^{-1} NaCl).

The swimming capacity was also evaluated by dark field microscopy. Bacteria were diluted in LB and observed with a LEICA DMIRE2 inverted microscope at 37°C, using a 40× objective (oil, numerical aperture 0.5). Images were acquired at 25 frames s^{-1} for 100 s. Time projections were done using ImageJ software to obtain bacterial trajectories. Strains could be scored as immobile or swimming, with no intermediary phenotype.

The surfactant production was examined on the swarming plates by measuring the diameter of the visible zone of wetting material around the colonies at 24 h post-plating.

Production of HCN

Hundred microliters of bacterial suspension at 10^8 cells mL^{-1} were dropped at the center of the HCN induction medium plate (40 g L^{-1} tryptic soy agar, 4.4 g L^{-1} glycine) (Wei *et al.*, 2013). Then a Whatman paper impregnated with reaction mix ($CHCL_3$ containing copper (II)-ethylacetoacetate complex (5 mg L^{-1}) and *N,N*-dimethylaniline (5 mg L^{-1}) (Nair *et al.*, 2014) was fixed to the underside of the petri dish covers. Petri dishes were sealed with parafilm and incubated 24 h at 28°C.

P. aeruginosa*-induced lung injury*

Pathogen-free BALB/c female mice (8–10 weeks) were obtained from Harlan Laboratories and housed in the institute animal care facility. Bacteria from exponential growth (OD = 1.0) were centrifuged and resuspended in sterile PBS at 1.7×10^8 or 5.1×10^8 per mL. Mice were anesthetized by

intraperitoneal administration of a mixture of xylazine (10 mg Kg^{-1}) and ketamine (50 mg Kg^{-1}). Then, 30 μL of bacterial suspension (5×10^6 or 15×10^6) were deposited into the mouse nostrils. To study survival rates, mice were inspected six times per day; moribund mice were considered as dead. Experiments were stopped at day 7.

Chicory leaf infection

Chicory leaf infection was adapted from (Fito-Boncompte *et al.*, 2011). Briefly chicory leaves were washed with 0.1% bleach and injected with 10 μL of a suspension of bacterial cells at 10^6 cells mL^{-1} in 10 mM $MgSO_4$. Then chicory leaves were placed in hermetic boxes containing a Whatman filter impregnated with sterilized water. The boxes were incubated at 37°C and the area of infection on the chicory leaves was measured at 72 h using ImageJ software on captured images.

Statistics

All experiments were reproduced at least three times, except for mouse infection, for which only one test was performed for ethical reasons. Spearman's correlation tests were performed between datasets of all experiments using StatXact software. Mann-Whitney's test and Friedman's aligned rank test were performed using StatXact software. Correlation or differences were considered significant when $P < 0.05$.

Acknowledgements

This work was performed thanks to institutional grants from CEA, Inserm, University Grenoble-Alpes and CNRS, and from the Labex-GRAL (ANR-10-LABX-49-01). Strains TA19, CPHL11451, CAN5, DVL1758, and LMG5031 were obtained from Dr. Jean-Paul Pirnay, EML548 from Dr. Benoît Cournoyer, JT87 from Dr. Arne Rietsch, PA39 from Dr. Pierre Cornelis, DSM1128 and Zw26 from Dr. Burkhard Tümmler, PA70 and PA213 from Dr. Craig Winstanley, ATCC33359 from Dr. Lars Jelsbak, BL043 from Dr. Alan Hauser, PAO1Δ*xcpR* and PAO1Δ*lasB* from Dr Romé Voulhoux, IHMA879472, 434930, and 567230 from International Health Management Associates, Inc. (Schaumburg, IL). We thank TWS Editing for proofreading of the manuscript.

References

Alcorn, J.F., and Wright, J.R. (2004) Degradation of pulmonary surfactant protein D by Pseudomonas aeruginosa elastase abrogates innate immune function. *J Biol Chem* **279:** 30871–30879.

Allemeersch, D., Beumer, J., Devleeschouwer, M., De Maeyer, S., Dony, J., Godard, C., *et al.* (1988) Marked increase of Pseudomonas aeruginosa serotype 012 in Belgium since 1982. *Eur J Clin Microbiol Infect Dis* **7:** 265–269.

Azghani, A.O. (1996) Pseudomonas aeruginosa and epithelial permeability: Role of virulence factors elastase and exotoxin A. *Am J Respir Cell Mol Biol* **15:** 132–140.

Beaufort, N., Corvazier, E., Hervieu, A., Choqueux, C., Dussiot, M., Louedec, L., *et al.* (2011) The thermolysin-like metalloproteinase and virulence factor LasB from pathogenic Pseudomonas aeruginosa induces anoikis of human vascular cells. *Cell Microbiol* **13:** 1149–1167.

Bert, F., and Lambert-Zechovsky, N. (1996) Comparative distribution of resistance patterns and serotypes in Pseudomonas aeruginosa isolates from intensive care units and other wards. *J Antimicrob Chemother* **37:** 809–813.

Bleves, S., Viarre, V., Salacha, R., Michel, G.P., Filloux, A., and Voulhoux, R. (2010) Protein secretion systems in Pseudomonas aeruginosa: A wealth of pathogenic weapons. *Int J Med Microbiol* **300:** 534–543.

Boukerb, A.M., Marti, R., and Cournoyer, B. (2015) Genome sequences of three strains of the Pseudomonas aeruginosa PA7 clade. *Genome Announc* **3:** e01366-15, doi: 10.1128

Burrows, L.L. (2012) Pseudomonas aeruginosa twitching motility: Type IV pili in action. *Annu Rev Microbiol* **66:** 493–520.

Caballero, A.R., Moreau, J.M., Engel, L.S., Marquart, M.E., Hill, J.M., and O'Callaghan, R.J. (2001) Pseudomonas aeruginosa protease IV enzyme assays and comparison to other Pseudomonas proteases. *Anal Biochem* **290:** 330–337.

Caiazza, N.C., Merritt, J.H., Brothers, K.M., and O'Toole, G.A. (2007) Inverse regulation of biofilm formation and swarming motility by Pseudomonas aeruginosa PA14. *J Bacteriol* **189:** 3603–3612.

Coin, D., Louis, D., Bernillon, J., Guinand, M., and Wallach, J. (1997) LasA, alkaline protease and elastase in clinical strains of Pseudomonas aeruginosa: Quantification by immunochemical methods. *FEMS Immunol Med Microbiol* **18:** 175–184.

Dacheux, D., Goure, J., Chabert, J., Usson, Y., and Attree, I. (2001) Pore-forming activity of type III system-secreted proteins leads to oncosis of Pseudomonas aeruginosa-infected macrophages. *Mol Microbiol* **40:** 76–85.

Dingemans, J., Ye, L., Hildebrand, F., Tontodonati, F., Craggs, M., Bilocq, F., *et al.* (2014) The deletion of TonB-dependent receptor genes is part of the genome reduction process that occurs during adaptation of Pseudomonas aeruginosa to the cystic fibrosis lung. *Pathog Dis* **71:** 26–38.

El-Solh, A.A., Hattemer, A., Hauser, A.R., Alhajhusain, A., and Vora, H. (2012) Clinical outcomes of type III Pseudomonas aeruginosa bacteremia. *Crit Care Med* **40:** 1157–1163.

Elsen, S., Huber, P., Bouillot, S., Coute, Y., Fournier, P., Dubois, Y., *et al.* (2014) A type III secretion negative clinical strain of Pseudomonas aeruginosa employs a two-partner secreted exolysin to induce hemorrhagic pneumonia. *Cell Host Microbe* **15:** 164–176.

Feldman, M., Bryan, R., Rajan, S., Scheffler, L., Brunnert, S., Tang, H., and Prince, A. (1998) Role of flagella in pathogenesis of Pseudomonas aeruginosa pulmonary infection. *Infect Immun* **66:** 43–51.

Filloux, A. (2011) Protein secretion systems in Pseudomonas aeruginosa: An essay on diversity, evolution, and function. *Front Microbiol* **2:** 155.

Fito-Boncompte, L., Chapalain, A., Bouffartigues, E., Chaker, H., Lesouhaitier, O., Gicquel, G., *et al.* (2011) Full virulence of Pseudomonas aeruginosa requires OprF. *Infect Immun* **79:** 1176–1186.

Freschi, L., Jeukens, J., Kukavica-Ibrulj, I., Boyle, B., Dupont, M.J., Laroche, J., *et al.* (2015) Clinical utilization of genomics data produced by the international Pseudomonas aeruginosa consortium. *Front Microbiol* **6:** 1036.

Gellatly, S.L., and Hancock, R.E. (2013) Pseudomonas aeruginosa: New insights into pathogenesis and host defenses. *Pathog Dis* **67:** 159–173.

Gilchrist, F.J., Alcock, A., Belcher, J., Brady, M., Jones, A., Smith, D., *et al.* (2011) Variation in hydrogen cyanide production between different strains of Pseudomonas aeruginosa. *Eur Respir J* **38:** 409–414.

Golovkine, G., Faudry, E., Bouillot, S., Voulhoux, R., Attree, I., and Huber, P. (2014) VE-cadherin cleavage by LasB protease from Pseudomonas aeruginosa facilitates type III secretion system toxicity in endothelial cells. *PLoS Pathog* **10:** e1003939.

Hauser, A.R. (2009) The type III secretion system of Pseudomonas aeruginosa: Infection by injection. *Nat Rev Microbiol* **7:** 654–665.

Hauser, A.R., Cobb, E., Bodi, M., Mariscal, D., Valles, J., Engel, J.N., and Rello, J. (2002) Type III protein secretion is associated with poor clinical outcomes in patients with ventilator-associated pneumonia caused by Pseudomonas aeruginosa. *Crit Care Med* **30:** 521–528.

Heiniger, R.W., Winther-Larsen, H.C., Pickles, R.J., Koomey, M., and Wolfgang, M.C. (2010) Infection of human mucosal tissue by Pseudomonas aeruginosa requires sequential and mutually dependent virulence factors and a novel pilus-associated adhesin. *Cell Microbiol* **12:** 1158–1173.

Hilker, R., Munder, A., Klockgether, J., Losada, P.M., Chouvarine, P., Cramer, N., *et al.* (2015) Interclonal gradient of virulence in the Pseudomonas aeruginosa pangenome from disease and environment. *Environ Microbiol* **17:** 29–46.

Hong, Y.Q., and Ghebrehiwet, B. (1992) Effect of Pseudomonas aeruginosa elastase and alkaline protease on serum complement and isolated components C1q and C3. *Clin Immunol Immunopathol* **62:** 133–138.

Huber, P., Bouillot, S., Elsen, S., and Attree, I. (2014) Sequential inactivation of Rho GTPases and Lim kinase by Pseudomonas aeruginosa toxins ExoS and ExoT leads to endothelial monolayer breakdown. *Cell Mol Life Sci* **71:** 1927–1941.

Josenhans, C., and Suerbaum, S. (2002) The role of motility as a virulence factor in bacteria. *Int J Med Microbiol* **291:** 605–614.

Jyot, J., Balloy, V., Jouvion, G., Verma, A., Touqui, L., Huerre, M., *et al.* (2011) Type II secretion system of Pseudomonas aeruginosa: In vivo evidence of a significant role in death due to lung infection. *J Infect Dis* **203:** 1369–1377.

Kazmierczak, B.I., Schniederberend, M., and Jain, R. (2015) Cross-regulation of Pseudomonas motility systems: The intimate relationship between flagella, pili and virulence. *Curr Opin Microbiol* **28:** 78–82.

King, J.D., Mulrooney, E.F., Vinogradov, E., Kneidinger, B., Mead, K., and Lam, J.S. (2008) lfnA from Pseudomonas aeruginosa O12 and wbuX from Escherichia coli O145 encode membrane-associated proteins and are required for expression of 2,6-dideoxy-2-acetamidino-L-galactose in lipopolysaccharide O antigen. *J Bacteriol* **190:** 1671–1679.

Kos, V.N., Deraspe, M., McLaughlin, R.E., Whiteaker, J.D., Roy, P.H., Alm, R.A., *et al.* (2015) The resistome of Pseudomonas aeruginosa in relationship to phenotypic susceptibility. *Antimicrob Agents Chemother* **59:** 427–436.

Kuang, Z., Hao, Y., Walling, B.E., Jeffries, J.L., Ohman, D.E., and Lau, G.W. (2011) Pseudomonas aeruginosa elastase provides an escape from phagocytosis by degrading the pulmonary surfactant protein-A. *PLoS One* **6:** e27091.

Le Berre, R., Nguyen, S., Nowak, E., Kipnis, E., Pierre, M., Quenee, L., *et al.* (2011) Relative contribution of three main virulence factors in Pseudomonas aeruginosa pneumonia. *Crit Care Med* **39:** 2113–2120.

Leduc, D., Beaufort, N., de Bentzmann, S., Rousselle, J.C., Namane, A., Chignard, M., and Pidard, D. (2007) The Pseudomonas aeruginosa LasB metalloproteinase regulates the human urokinase-type plasminogen activator receptor through domain-specific endoproteolysis. *Infect Immun* **75:** 3848–3858.

Liu, P.V., and Wang, S. (1990) Three new major somatic antigens of Pseudomonas aeruginosa. *J Clin Microbiol* **28:** 922–925.

Maatallah, M., Cheriaa, J., Backhrouf, A., Iversen, A., Grundmann, H., Do, T., *et al.* (2011) Population structure of Pseudomonas aeruginosa from five Mediterranean countries: Evidence for frequent recombination and epidemic occurrence of CC235. *PLoS One* **6:** e25617.

Mai-Prochnow, A., Bradbury, M., and Murphy, A.B. (2015) Draft genome sequence of Pseudomonas aeruginosa ATCC 9027 (DSM 1128), an important rhamnolipid surfactant producer and sterility testing strain. *Genome Announc* **3:** e01259-15, doi: 10.1128

Murray, T.S., and Kazmierczak, B.I. (2008) Pseudomonas aeruginosa exhibits sliding motility in the absence of type IV pili and flagella. *J Bacteriol* **190:** 2700–2708.

Murray, T.S., Ledizet, M., and Kazmierczak, B.I. (2010) Swarming motility, secretion of type 3 effectors and biofilm formation phenotypes exhibited within a large cohort of Pseudomonas aeruginosa clinical isolates. *J Med Microbiol* **59:** 511–520.

Nair, C.G., Ryall, B., and Williams, H.D. (2014) Cyanide measurements in bacterial culture and sputum. *Methods Mol Biol* **1149:** 325–336.

Perdu, C., Huber, P., Bouillot, S., Blocker, A., Elsen, S., Attree, I., and Faudry, E. (2015) ExsB is required for correct assembly of the Pseudomonas aeruginosa type III secretion apparatus in the bacterial membrane and full virulence in vivo. *Infect Immun* **83:** 1789–1798.

Pirnay, J.P., Bilocq, F., Pot, B., Cornelis, P., Zizi, M., Van Eldere, J., *et al.* (2009) Pseudomonas aeruginosa population structure revisited. *PLoS One* **4:** e7740.

Pitt, T.L., Livermore, D.M., Pitcher, D., Vatopoulos, A.C., and Legakis, N.J. (1989) Multiresistant serotype O 12 Pseudomonas aeruginosa: evidence for a common strain in Europe. *Epidemiol Infect* **103:** 565–576.

Roy, P.H., Tetu, S.G., Larouche, A., Elbourne, L., Tremblay, S., Ren, Q., *et al.* (2010) Complete genome sequence of the multiresistant taxonomic outlier Pseudomonas aeruginosa PA7. *PLoS One* **5:** e8842.

Schaber, J.A., Carty, N.L., McDonald, N.A., Graham, E.D., Cheluvappa, R., Griswold, J.A., and Hamood, A.N. (2004) Analysis of quorum sensing-deficient clinical isolates of Pseudomonas aeruginosa. *J Med Microbiol* **53:** 841–853.

Shrout, J.D., Chopp, D.L., Just, C.L., Hentzer, M., Givskov, M., and Parsek, M.R. (2006) The impact of quorum sensing and swarming motility on Pseudomonas aeruginosa biofilm formation is nutritionally conditional. *Mol Microbiol* **62:** 1264–1277.

Smith, D., Spanel, P., Gilchrist, F.J., and Lenney, W. (2013) Hydrogen cyanide, a volatile biomarker of Pseudomonas aeruginosa infection. *J Breath Res* **7:** 044001.
Tamura, Y., Suzuki, S., and Sawada, T. (1992) Role of elastase as a virulence factor in experimental Pseudomonas aeruginosa infection in mice. *Microb Pathog* **12:** 237–244.
Thrane, S.W., Taylor, V.L., Freschi, L., Kukavica-Ibrulj, I., Boyle, B., Laroche, J., *et al.* (2015) The Widespread multidrug-resistant serotype O12 Pseudomonas aeruginosa clone emerged through concomitant horizontal transfer of serotype antigen and antibiotic resistance gene clusters. *MBio* **6:** e01396–01315.
Toska, J., Sun, Y., Carbonell, D.A., Foster, A.N., Jacobs, M.R., Pearlman, E., and Rietsch, A. (2014) Diversity of virulence phenotypes among Type III secretion negative Pseudomonas aeruginosa clinical isolates. *PLoS One* **9:** e86829.
Vance, R.E., Rietsch, A., and Mekalanos, J.J. (2005) Role of the type III secreted exoenzymes S, T, and Y in systemic spread of Pseudomonas aeruginosa PAO1 in vivo. *Infect Immun* **73:** 1706–1713.
Wei, X., Huang, X., Tang, L., Wu, D., and Xu, Y. (2013) Global control of GacA in secondary metabolism, primary metabolism, secretion systems, and motility in the rhizobacterium Pseudomonas aeruginosa M18. *J Bacteriol* **195:** 3387–3400.

Supporting information

Additional Supporting Information may be found in the online version of this article at the publisher's web-site:

Table S1. Reference strains and oligonucleotides used in this study
Fig. S1. exlA+ strain phenotype on swimming plates. The test was performed on agar plates as indicated in Experimental Procedures. Group A strains are indicated in bold and Group B strains in grey. Data are summarized in Table 3.
Fig. S2. exlA+ strain phenotypes on twitching plates. The test was performed on agar plates as indicated in Experimental Procedures. Group A strains are indicated in bold and Group B strains in grey. Data are summarized in Table 3.
Fig. S3. exlA+ strain phenotype on swarming plates. The test was performed on agar plates as indicated in Experimental Procedures. Group A strains are indicated in bold and Group B strains in grey. Data are summarized in Table 3.
Fig. S4. Surfactant production. The diameter of the visible zone of wetting material around the colonies of swarming plates was measured at 24 h post-plating. Individual data are represented by circles and the medians by a red bar. Group A strains are indicated in bold and Group B strains in grey. Data are summarized in Table 3.
Fig. S5. Hydrogen cyanide production. The volatile HCN produced by the bacteria grown on HCN induction medium plates for 24 h was monitored by membranes impregnated with an HCN-reactive mixture (see Experimental Procedures). HCN induced a white-to-blue color transition. Group A strains are indicated in bold and Group B strains in grey. Data are representative of three independent experiments. The results are summarized in Table 4.
Fig. S6. Images of infected chicory leaves. Chicory leaves were infected by injection of 10^4 bacteria in their center part and were incubated at 37°C for 72 hours in a closed humidity chamber. Images were captured for surface measurement of necrotic areas (brown). Quantifications are shown in Fig. 5. Group A strains are indicated in bold and Group B strains in grey. The results are representative of three independent experiments.

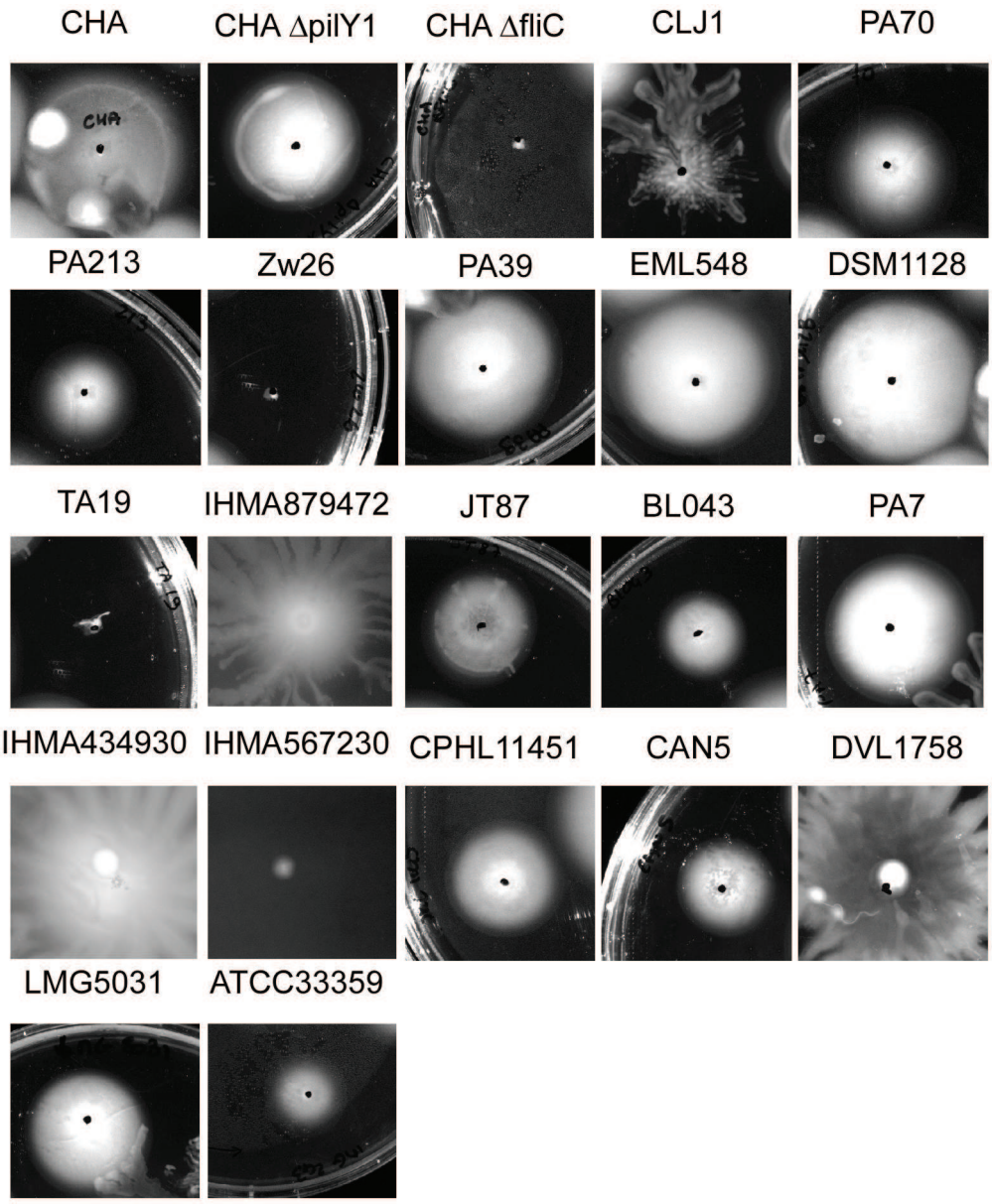
CHA
CHA ΔpilY1
CHA ΔfliC
CLJ1
PA70
PA213
Zw26
PA39
EML548
DSM1128
TA19
IHMA879472
JT87
BL043
PA7
IHMA434930
IHMA567230
CPHL11451
CAN5
DVL1758
LMG5031
ATCC33359

Figure S1

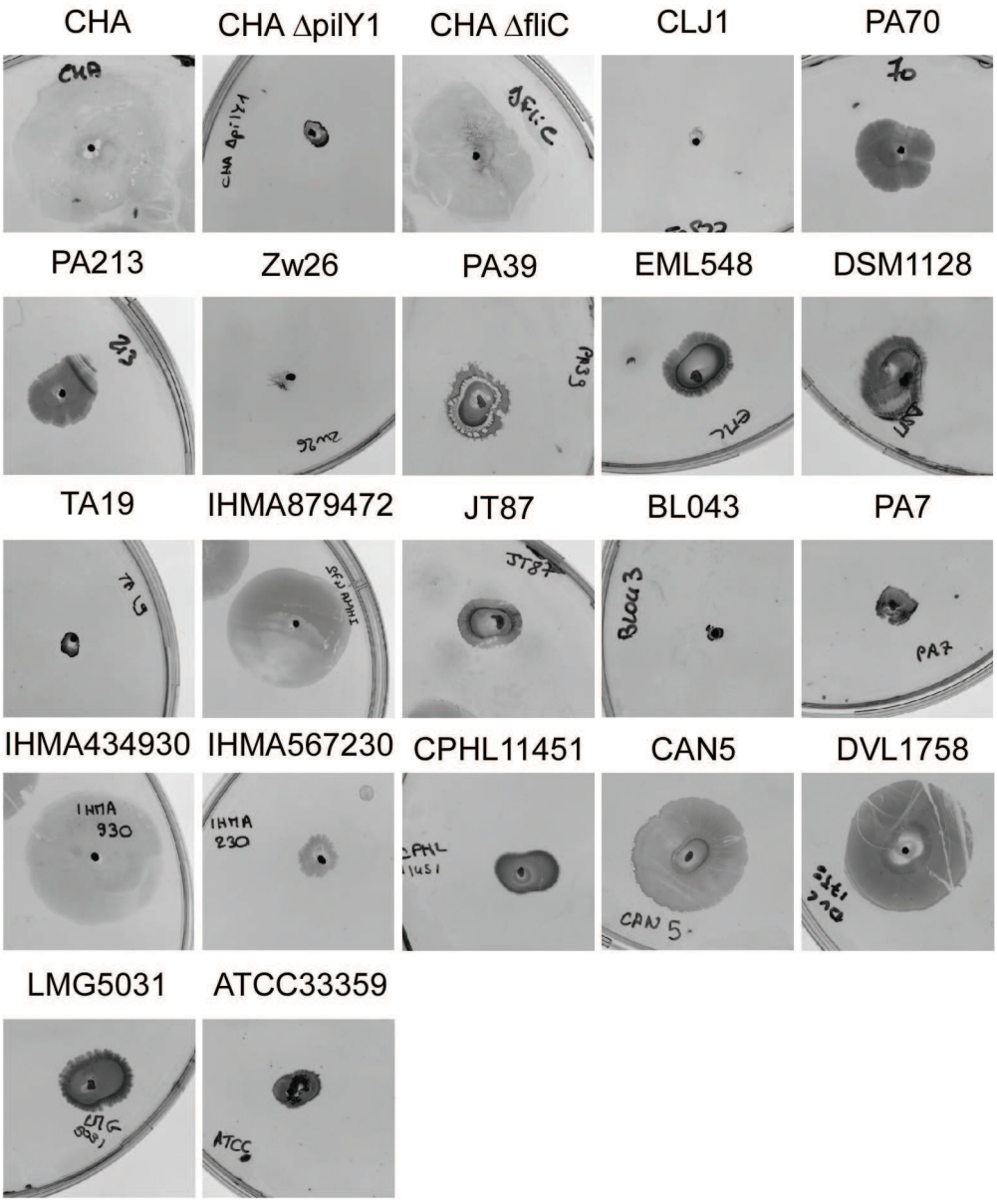
CHA
CHA ΔpilY1
CHA ΔfliC
CLJ1
PA70
PA213
Zw26
PA39
EML548
DSM1128
TA19
IHMA879472
JT87
BL043
PA7
IHMA434930
IHMA567230
CPHL11451
CAN5
DVL1758
LMG5031
ATCC33359

Figure S2

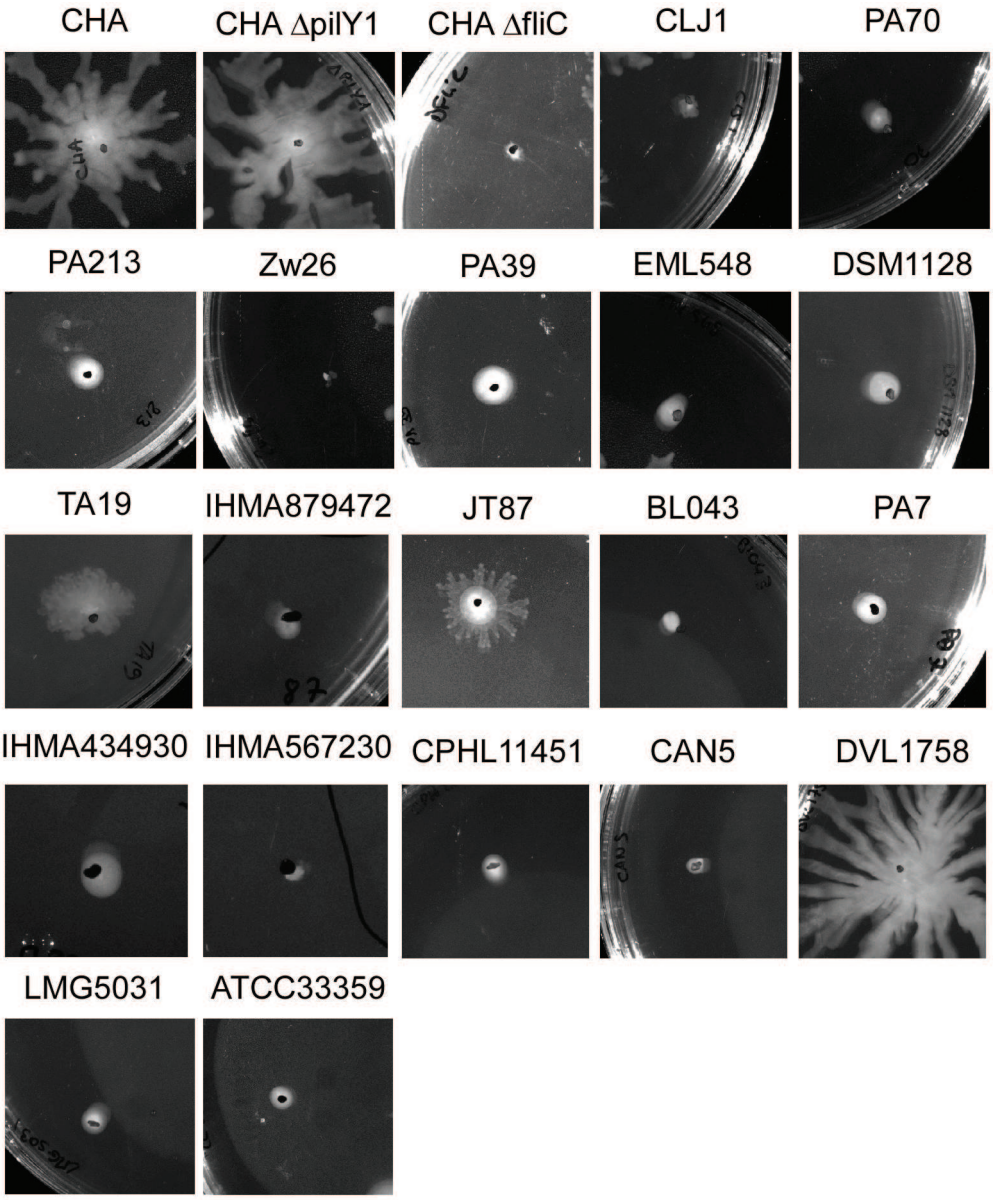
CHA
CHA ΔpilY1
CHA ΔfliC
CLJ1
PA70
PA213
Zw26
PA39
EML548
DSM1128
TA19
IHMA879472
JT87
BL043
PA7
IHMA434930
IHMA567230
CPHL11451
CAN5
DVL1758
LMG5031
ATCC33359

Figure S3

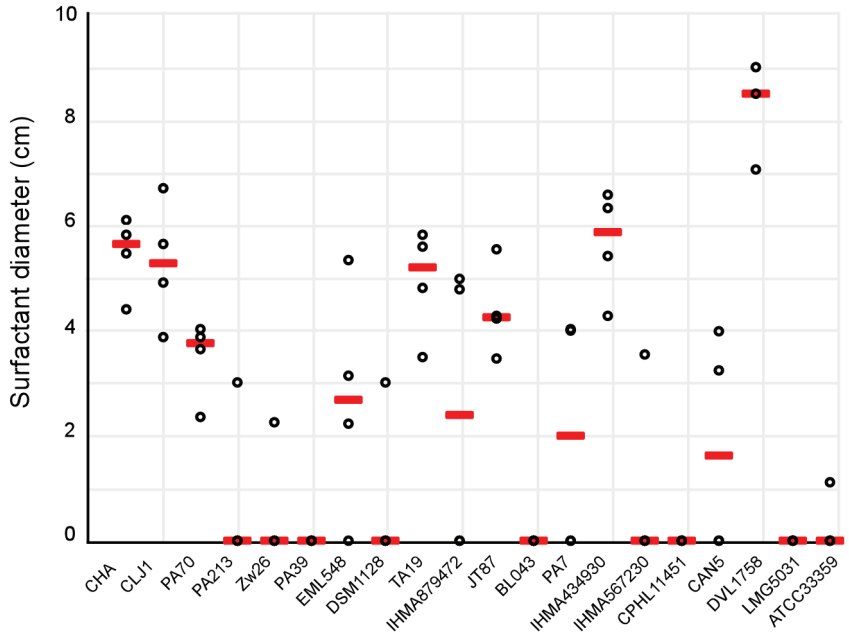
Surfactant diameter (cm)
10
8
6
4
2
0
CHA
CLJ1
PA70
PA213
Zw26
PA39
EML548
DSM1128
TA19
IHMA879472
JT87
BL043
PA7
IHMA434930
IHMA567230
CPHL11451
CAN5
DVL1758
LMG5031
ATCC33359

Figure S4

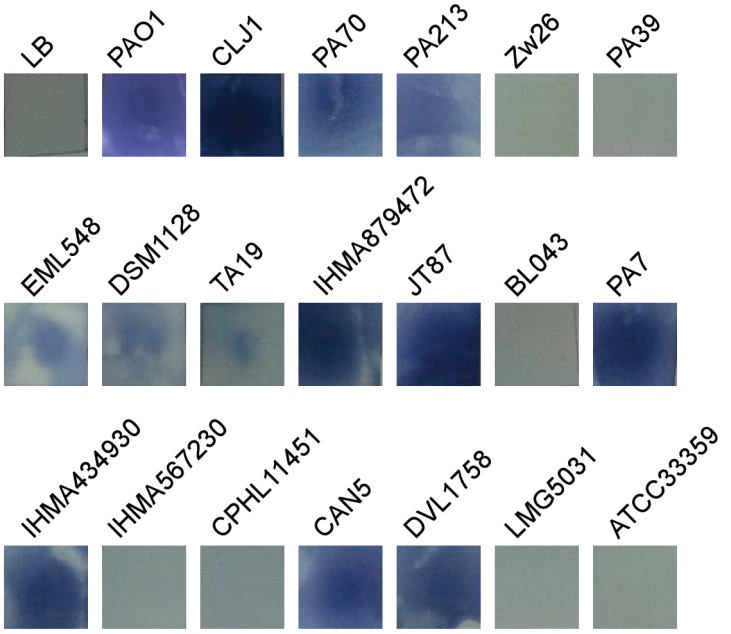
LB
PAO1
CLJ1
PA70
PA213
Zw26
PA39
EML548
DSM1128
TA19
IHMA879472
JT87
BL043
PA7
IHMA434930
IHMA567230
CPHL11451
CAN5
DVL1758
LMG5031
ATCC33359

Figure S5

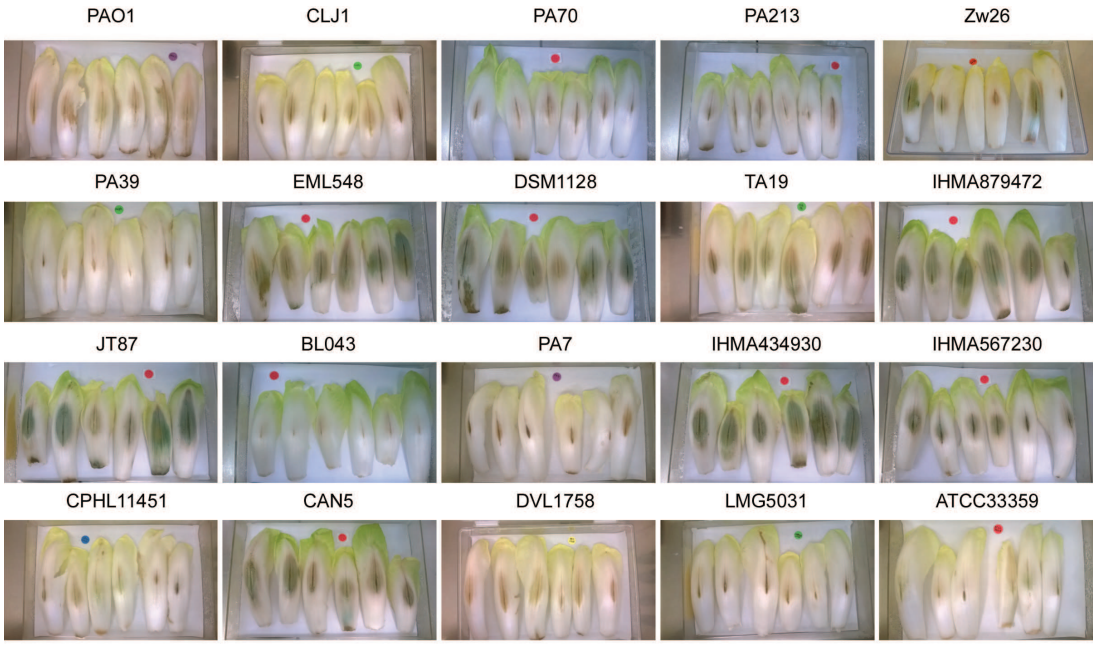
PAO1
CLJ1
PA70
PA213
Zw26
PA39
EML548
DSM1128
TA19
IHMA879472
JT87
BL043
PA7
IHMA434930
IHMA567230
CPHL11451
CAN5
DVL1758
LMG5031
ATCC33359

Figure S6

5

P. aeruginosa Pore-Forming Exolysin and Type IV Pili Cooperate To Induce Host Cell Lysis.

Pauline Basso, Michel Ragno, Sylvie Elsen, Emeline Reboud, Guillaume Golovkine, Stephanie Bouillot, Philippe Huber, Stephen Lory, Eric Faudry, Ina Attree (mBio vol. 8 no. 1 e02250-16 (2017))

Exolysin (ExlA) has been first identified in the clinical isolate of *P. aeruginosa* CLJ1 by comparative proteomic analysis and was found homologous to ShlA, the hemolysin of *Serratia marcescens* [126].

This manuscript describes the results I obtained concerning the characterization of the *in vitro* activity of ExlA on eukaryotic cells. By comparison with the domains found in ShlA, I identified the different domains in the ExlA sequence and their roles. The N-terminal part corresponds to the Two-Partner Secretion (TPS) domain and is predicted to be responsible for the ExlA secretion. The POTRA domains of ExlB, an outer membrane protein, were found required for the ExlA secretion. The C-terminal part of ExlA was not found to be homologous to other proteins in databases. However its deletion abolished the cytotoxicity. Finally, the five RGD (Arginine-Glycine-Acid aspartic) motifs did not play a role in ExlA activity.

We succeeded in the purification of three forms of recombinant proteins, the full-length ExlA lacking the signal peptide ($ExlA_{NoSP}$), $ExlA_{NoSP}$ lacking the C-ter domain, and the C-ter domain exclusively. I demonstrated, using two models currently employed in pore-forming studies (liposomes and red blood cells (RBC)) that ExlA forms 1.6-nm pores in membranes. The liposome model allowed to show that the negative charges brought by phosphatidyl-serine were necessary for pore-forming activity. Moreover, the C-ter domain of ExlA was required for the pore formation in liposomes, confirming results of cytotoxicity assays. Finally, kinetics of entry of Yo-Pro1, a membrane impermanent-dye, into epithelial cells were measured by time-lapse fluorescence microscopy to show the formation of ExlA pores in membranes of nucleated cells.

We showed that the living bacteria were absolutely required for the ExlA-dependent cytotoxicity. Neither the recombinant proteins nor the bacterial supernatant provoked cell damage. We hypothesized that other bacterial factors could be involved. A high-throughput cellular live-dead screening of a transposon library made in an ExlA-secreting clinical strain allowed to show that the type IV pili are involved in ExlA-dependent cytolysis. A part of this work has been done during my 3-months stay in the Laboratory of Prof. Stephen Lory (HMS, Boston) and at the HMS screening facility (Longwood facility, HMS). This cooperation between two virulence factors has already been demonstrated for the T3SS and the Type IV pili. However, this work showed the first example of cooperation between a pore forming toxin and Type IV pili[109].

We proposed a model in which the Type IV pili mediate a close bacterium-cell contact to increase the local concentration of ExlA at the membrane proximity. These results suggest that the ExlA mechanism of the pore formation is different from that of ShlA and of other pore forming toxins. The visualization of the pore formation in the membrane and the oligomerization of ExlA needs to be investigated in more detail.

AMERICAN SOCIETY FOR MICROBIOLOGY | mBio®

RESEARCH ARTICLE

Pseudomonas aeruginosa Pore-Forming Exolysin and Type IV Pili Cooperate To Induce Host Cell Lysis

Pauline Basso,[a,b,c,d] Michel Ragno,[a,b,c,d] Sylvie Elsen,[a,b,c,d] Emeline Reboud,[a,b,c,d] Guillaume Golovkine,[a,b,c,d*] Stephanie Bouillot,[a,b,c,d] Philippe Huber,[a,b,c,d] Stephen Lory,[e] Eric Faudry,[a,b,c,d] Ina Attrée[a,b,c,d]

University of Grenoble Alpes, Grenoble, France[a]; CNRS, ERL5261, Grenoble, France[b]; CEA, BIG-BCI, Grenoble, France[c]; INSERM, U1036, Grenoble, France[d]; Department of Microbiology and Immunobiology, Harvard Medical School, Boston, Massachusetts, USA[e]

ABSTRACT Clinical strains of *Pseudomonas aeruginosa* lacking the type III secretion system genes employ a toxin, exolysin (ExlA), for host cell membrane disruption. Here, we demonstrated that ExlA export requires a predicted outer membrane protein, ExlB, showing that ExlA and ExlB define a new active two-partner secretion (TPS) system of *P. aeruginosa*. In addition to the TPS signals, ExlA harbors several distinct domains, which include one hemagglutinin domain, five arginine-glycine-aspartic acid (RGD) motifs, and a C-terminal region lacking any identifiable sequence motifs. However, this C-terminal region is important for the toxic activity, since its deletion abolishes host cell lysis. Using lipid vesicles and eukaryotic cells, including red blood cells, we demonstrated that ExlA has a pore-forming activity which precedes cell membrane disruption of nucleated cells. Finally, we developed a high-throughput cell-based live-dead assay and used it to screen a transposon mutant library of an ExlA-producing *P. aeruginosa* clinical strain for bacterial factors required for ExlA-mediated toxicity. The screen resulted in the identification of proteins involved in the formation of type IV pili as being required for ExlA to exert its cytotoxic activity by promoting close contact between bacteria and the host cell. These findings represent the first example of cooperation between a pore-forming toxin of the TPS family and surface appendages in host cell intoxication.

IMPORTANCE The course and outcome of acute, toxigenic infections by *Pseudomonas aeruginosa* clinical isolates rely on the deployment of one of two virulence strategies: delivery of effectors by the well-known type III secretion system or the cytolytic activity of the recently identified two-partner secreted toxin, exolysin. Here, we characterize several features of the mammalian cell intoxication process mediated by exolysin. We found that exolysin requires the outer membrane protein ExlB for export into extracellular medium. Using *in vitro* recombinant protein and *ex vivo* assays, we demonstrated a pore-forming activity of exolysin. A cellular cytotoxicity screen of a transposon mutant library, made in an exolysin-producing clinical strain, identified type IV pili as bacterial appendages required for exolysin toxic function. This work deciphers molecular mechanisms underlying the activity of novel virulence factors used by *P. aeruginosa* clinical strains lacking the type III secretion system, including a requirement for the toxin-producing bacteria to be attached to the targeted cell to induce cytolysis, and defines new targets for developing antivirulence strategies.

Received 16 December 2016 **Accepted** 19 December 2016 **Published** 24 January 2017

Citation Basso P, Ragno M, Elsen S, Reboud E, Golovkine G, Bouillot S, Huber P, Lory S, Faudry E, Attrée I. 2017. *Pseudomonas aeruginosa* pore-forming exolysin and type IV pili cooperate to induce host cell lysis. mBio 8:e02250-16. https://doi.org/10.1128/mBio.02250-16.

Editor Samuel I. Miller, University of Washington

Address correspondence to Ina Attrée, ina.attree-delic@cea.fr.

* Present address: Guillaume Golovkine, UC Berkeley, Berkeley, California, USA.

E.F. and I.A. contributed equally to this work.

This article is a direct contribution from a Fellow of the American Academy of Microbiology. External solicited reviewers: Alain Filloux, Imperial College London; Joanna Goldberg, Emory University School of Medicine; Daniel Wozniak, The Ohio State University.

Pseudomonas aeruginosa is a major human opportunistic pathogen, frequently associated with nosocomial infections, notably in intensive care units, where it is responsible for approximately 40% of deaths of patients with ventilator-associated

pneumonia (1). This Gram-negative bacterium also causes life-threatening chronic infections in cystic fibrosis patients and numerous acute infections of eyes, ears, urinary tracts, and injuries such as burns (2). A combination of several factors, including its metabolic adaptability, a panoply of virulence factors, and the development of multiresistance among clinical strains, makes *P. aeruginosa* extremely difficult to eradicate. Facing the rise in bacterial antibiotic resistance, there is an alarming deficiency in therapeutic options for the majority of human and animal bacterial pathogens. *P. aeruginosa* belongs to the family of so-called "ESKAPE" pathogens (*Enterococcus faecium*, *Staphylococcus aureus*, *Klebsiella pneumoniae*, *Acinetobacter baumannii*, *P. aeruginosa*, and *Enterobacter* species), which effectively "escape" the effects of currently available antibiotics and are considered by the Infectious Diseases Society of America (IDSA) as being the priority pathogens for the urgent development of novel antimicrobial agents (3). One of the strategies for novel therapeutics against bacterial pathogens is based on the discovery of molecules capable of interfering with their determinants of pathogenicity. This "antivirulence" approach requires a complete knowledge of factors and molecular mechanisms used by pathogens for successful colonization of humans and avoidance of host defenses.

Several hundred available whole-genome sequences of various *P. aeruginosa* strains (http://www.pseudomonas.com [4]) were used in phylogenetic analyses to define two distant clades. One of these contains strains previously referred to as "clonal outliers" (5–7); the first identified member of this group is strain PA7 (8). Although the virulence of *P. aeruginosa* is multifactorial, the two clades differ mainly in the way that they exert their cytolytic activity on human cells (6, 9, 10). The genomes of the PAO1/PA14 group contain the determinants of a well-studied export nanomachine called the type III secretion system (T3SS) that allows the injection of four main *P. aeruginosa* effectors harboring enzymatic activities (ExoS, ExoT, ExoY, and ExoU) directly into the host cell cytoplasm (reviewed in reference 11). The virulence of clinical strains from this clade in human infections has been clearly correlated with the synthesis of T3SS and the injection of the four exoenzymes (12–15). The second clade not only lacks the entire T3SS-encoding locus composed of five operons but also lacks the genes encoding the type III secreted exoenzymes (6, 9). We recently discovered a completely novel virulence mechanism used by those strains lacking T3SS (i.e., the PA7-like clade), by studying the highly virulent and cytolytic strain CLJ1, isolated from a patient with hemorrhagic pneumonia. Using quantitative comparative proteomic analysis of CLJ1 secreted proteins, we identified a toxin responsible for eukaryotic cell lysis and named it exolysin (ExlA) (6). Bioinformatics analysis of ExlA showed several sequence features found in two-partner secretion (TPS) systems (16), including an N-terminal general Sec (*sec*retion) export signal peptide followed by a sequence with a TPS motif. Moreover, immediately upstream of *exlA* we identified a gene encoding the putative TPS outer membrane protein and designated it ExlB. It is noteworthy that the *exlBA* genes are present not only in strains of the PA7 clade but also in some clinical and environmental isolates phylogenetically closer to PAO1/PA14-like classical strains (reviewed in reference 9), and their localization between genes corresponding to *PA0874* and *PA0873* is conserved. All *exlBA*$^+$ strains characterized until now lack the T3SS locus. Interestingly, the quantity of secreted ExlA differs greatly between the *exlA*-positive strains, determining the degree of their cytotoxic activity and virulence in mice (17).

In this work, we further characterize exolysin secretion and activity *in vivo* and *in vitro*. Using cellular cytotoxicity assays, hemoglobin release, and a liposome leakage assay with purified recombinant proteins, we show that exolysin is a TPS pore-forming toxin (PFT) and that its activity requires its C-terminal domain. A cellular screen of a transposon (Tn) mutant library for the loss of exolysin-dependent cytolysis, created in the ExlA-producing *P. aeruginosa* urinary isolate IHMA879472 (IHMA), resulted in the identification of type IV pili (T4P) as being required for host cell intoxication. This shows that type IV pili are cooperating with ExlA in its cytotoxic activity, probably by mediating bacterial adhesion and establishing adequate ExlA local concentrations.

RESULTS

The POTRA domains of the outer membrane partner ExlB are required for ExlA secretion. We previously showed that neither ExlB nor ExlA alone is able to induce eukaryotic cell lysis (6), suggesting that they form an ExlB-ExlA TPS system. Indeed, only a *P. aeruginosa* strain harboring both *exlB-exlA* genes, expressed from an arabinose-inducible promoter, was cytolytic on epithelial and endothelial cells (6). As with other TPS systems, the TpsB homologue ExlB, in addition to the β-barrel-forming domain, possesses two predicted conserved domains predicted to be oriented toward the bacterial periplasm and is responsible for TpsA (ExlA) export (18, 19). These domains are called the POTRA domains (for *po*lypeptide-associated *tra*nsport) and are located in ExlB between amino acids 85 to 160 and 162 to 230 for POTRA1 and POTRA2, respectively (Fig. 1A). In TPS systems, these domains interact with the secreted proteins. In *Bordetella pertussis* TPS filamentous hemagglutinin (FHA)/FhaC, the deletion of the POTRA domains in FhaC does not affect its stability and outer membrane location but completely abolishes the secretion of FHA (20). In order to further demonstrate the dependence of ExlA secretion on ExlB and to assess the role of the two POTRA domains, we deleted the whole *exlB* gene and created two *exlB* mutants in which each POTRA domain is deleted. The mutations were done in the engineered heterologous PAO1 strain lacking both the essential components of the T2SS (Δ*xcpR*) and T3SS (Δ*pscC*), in order to abolish any cytotoxic activity due to these two systems, and harboring *exlB-exlA* genes on the integrative plasmid described previously (6). All strains synthesized the ExlA protein, but strains lacking ExlB and either POTRA1 or POTRA2 were unable to secrete it into bacterial supernatants, as visualized by immunoblotting using anti-ExlA antibodies (Fig. 1B). Consequently, the strains lacking ExlB or expressing ExlB without both POTRA domains were noncytotoxic (Fig. 1B). Therefore, we concluded that ExlB is indeed the cognate partner of ExlA permitting its secretion, probably through the interaction between the POTRA domains and the N-terminal TPS signal of ExlA, as previously shown for the FHA and FhaC of *B. pertussis* (21–23).

The C-terminal part of ExlA, but not the five RGD motifs, confers on the protein its cytolytic activity. ExlA is a 172-kDa protein belonging to the family of polymorphic toxins (24). In addition to the conserved secretion motifs based on an analysis in the Pfam database (http://pfam.xfam.org), ExlA shares five β-sheet domains (Fil HAEM) and one hemagglutinin domain (HAEMA) (Fig. 1C) with FHA (25). The ExlA protein also carries five arginine-glycine-aspartic acid (RGD) motifs that are often involved in cell-to-cell recognition with proteins of the integrin family (26). As well, in the majority of polymorphic toxins, as well as in the filamentous hemagglutinin adhesion protein FHA (27), the C-terminal portions specify various activity functions and share conserved features (24), However, the ExlA C-terminal part of approximately 300 amino acids shares no homology with any other protein or domain of known function. Therefore, we undertook to determine the roles of the RGD motifs and the C-terminal domain in cytotoxicity. To that aim, in ExlA we replaced the five RGD motifs with RGA, a mutation known to prevent integrin binding, and also engineered a truncated ExlA ($ExlA_{\Delta Cter}$) which lacks the last 296 amino acids. Both mutant proteins were produced and secreted at the same level as the wild-type protein (Fig. 1D). Cytotoxicity assays on epithelial A549 cells showed that while the $ExlA_{RGA}$ pentamutant exhibited high cytotoxicity (90%) similar to that of the wild-type ExlA, $ExlA_{\Delta Cter}$ completely lost the ability to lyse epithelial cells (Fig. 1D), showing that the cytolytic activity of the ExlA protein requires its C-terminal domain but does not depend on the RGD motifs.

ExlA forms pores in RBCs. Strains expressing ExlA induce plasma membrane rupture of cultured eukaryotic cells, leading to rapid cell death (within 3 h postinfection) (6). To further decipher the mechanism of ExlA action, we examined its capacity to form pores within membranes, as is the case for several bacterial membrane-damaging toxins, including ShlA of *Serratia marcescens* (28). The classical model to study the ability of a toxin to form pores in biological membranes utilizes red blood cells (RBCs), where pore formation is evaluated by measuring hemoglobin release (29). RBCs were incubated with *P. aeruginosa* strains expressing different ExlA variants, and

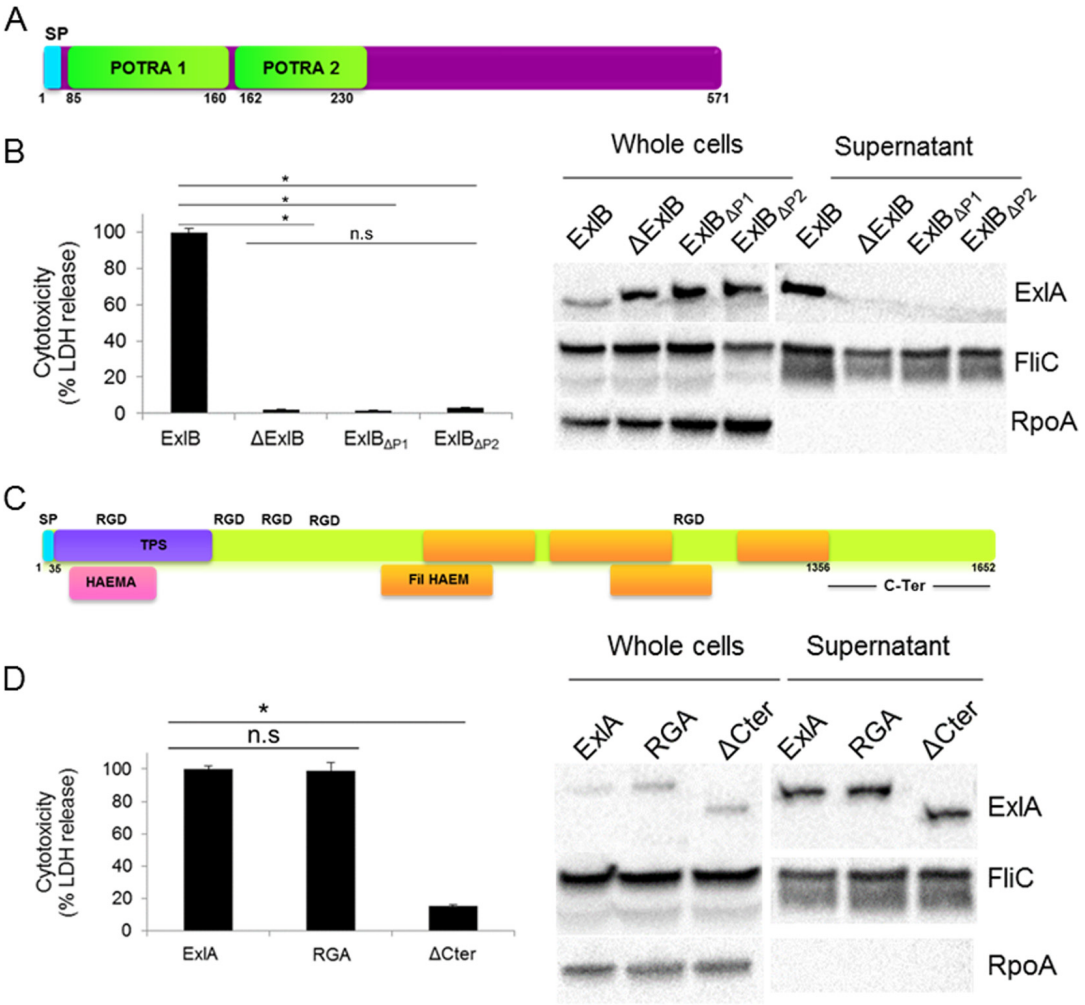

FIG 1 ExlB and ExlA represent a *P. aeruginosa* TPS system, and the ExlA C-terminal region is required for toxicity. (A) ExlB possesses an N-terminal type I secretion signal peptide (SP) and two POTRA domains. (B) (Left) The cytotoxic effect of *P. aeruginosa* PAO1 expressing ExlB mutant proteins on epithelial A549 cells. Analysis of variance was used to compare mutants (*, $P \leq 0.05$; n.s., not significant). Monolayers were infected with PAO1Δ*xcpR*Δ*pscC*::pSW196*exlBA* (ExlB) or PAO1Δ*xcpR*Δ*pscC*::pSW196*exlA* carrying the deletion of *exlB* (ΔExlB) or the deletion of either POTRA domain 1 (PAO1Δ*xcpR*Δ*pscC*::pSW196*exlB*ΔP1-*exlA*) (ΔP1) or POTRA domain 2 (PAO1Δ*xcpR*Δ*pscC*::pSW196*exlB*ΔP2-*exlA*) (ΔP2), and cytotoxicity was measured by the release of lactate dehydrogenase (LDH). (Right) Immunoblot analysis of the corresponding strains. Western blot assays were performed on bacterial lysates (whole cells) and secreted proteins (supernatant), and proteins were revealed by anti-ExlA antibodies. FliC and RpoA were used as loading controls, probed with the corresponding antibodies. (C) ExlA belongs to the family of polymorphic toxins and carries the N-terminal type I secretion signal peptide (SP), the conserved TPS secretion domain, hemagglutinin-like domains, FHA repeats, and a C-terminal domain of unknown function. ExlA also possesses five RGD motifs. (D) Cytotoxicity assays of A549 cells infected with *P. aeruginosa* PAO1 expressing ExlA mutants (left) (analysis of variance was used to compare mutants [*, $P \leq 0.05$; n.s., not significant]) and Western blot analysis (right) of PAO1Δ*xcpR*Δ*pscC*::pSW196*exlBA* (ExlA) and penta-RGA PAO1Δ*xcpR*Δ*pscC*::pSW196$exlBA_{RGA}$ (RGA) and PAO1Δ*xcpR*Δ*pscC*::pSW196$exlBA_{\Delta Cter}$ (ΔCter) mutants, performed as described for panel B.

hemoglobin release was measured after 90 min of coincubation. The well-characterized pore-forming toxin α-hemolysin from *Staphylococcus aureus*, *S. marcescens* expressing ShlA, and *P. aeruginosa* PP34, which produces the T3SS-exported phospholipase ExoU, all induced more than 90% hemolysis within 90 min of incubation (Fig. 2A). Negative controls included *S. marcescens* strain 21c4, unable to secrete ShlA, and *P. aeruginosa* lacking ExoU (PP34Δ*exoU*), which showed weak (ca. 20%) hemolysis (Fig. 2A). The T2SS/T3SS-deficient *P. aeruginosa* PAO1Δ*xcpR*Δ*pscC* ("Parental" in Fig. 2A) was poorly hemolytic with approximately 25% hemolysis, whereas expression of *exlB-exlA* in the same strain resulted in >80% hemolysis. As already observed for the cytolysis of A549 cells, *P. aeruginosa* expressing $ExlA_{\Delta Cter}$ induced reduced hemolysis; however, this was higher (by about 50%) than that of the parental ExlA$^-$ strain (Fig. 2A). For the

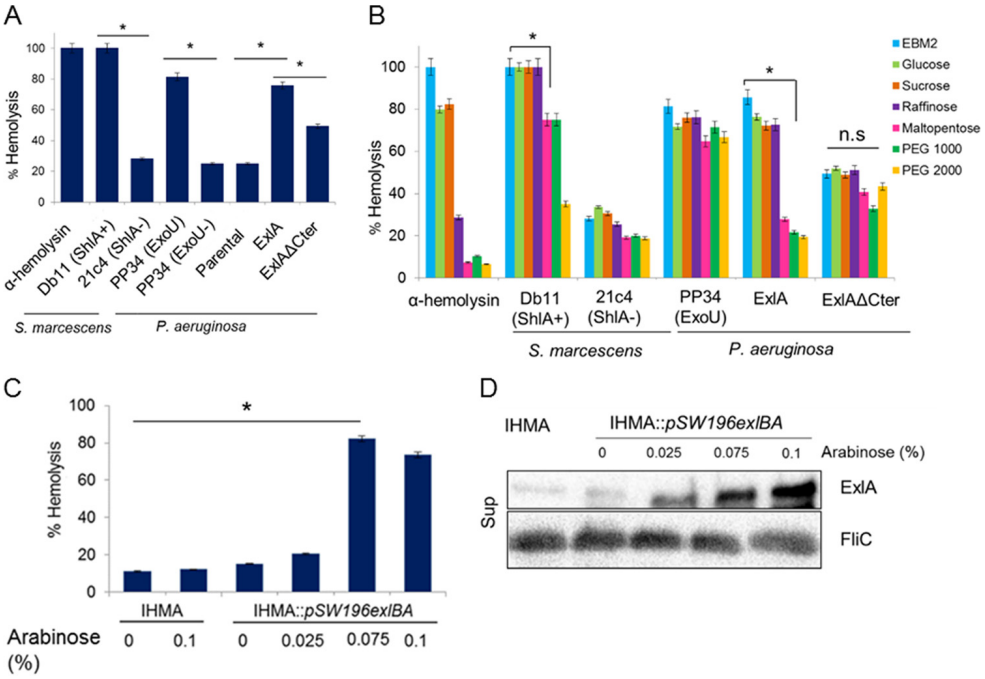

FIG 2 Exolysin is a pore-forming toxin. (A) Lysis of RBCs incubated with α-hemolysin from *S. aureus* or infected (at an MOI of 10) with *S. marcescens* secreting ShlA (Db11), an *S. marcescens* ShlA$^-$ mutant (21c4), *P. aeruginosa* strain PP34 expressing T3S toxin ExoU (ExoU), *P. aeruginosa* PP34ΔExoU, the *P. aeruginosa* PAO1Δ*xcpR*Δ*pscC* strain (Parental), and the *P. aeruginosa* PAO1Δ*xcpR*Δ*pscC*::*pSW196exlBA* strain secreting ExlA (ExlA) or the *P. aeruginosa* PAO1Δ*xcpR*Δ*pscC*::*pSW196exlBA*$_{\Delta Cter}$ strain secreting ExlA$_{\Delta Cter}$ (ExlAΔCter). (B) Hemolysis assays performed with α-hemolysin (100 nM) and the indicated strains as described in the legend to Fig. 3A in the presence of 30 mM sugars and PEG osmoprotectants. (C) Hemolysis following incubation with *P. aeruginosa* IHMA or IHMA::*pSW196exlBA*. For induction of *exlBA*, bacteria were grown in the presence of 0.025%, 0.075%, and 0.1% arabinose for 3 h and used at an MOI of 10. In a control, the hemolysis assay was done with IHMA in the presence of arabinose (0.1%) in EBM-2. In panels A to C, hemolysis was determined by measuring the release of hemoglobin into the supernatants (OD_{549}). Complete (100%) lysis of RBCs was accomplished using 1% SDS. Statistical analysis was performed by analysis of variance (*, $P \leq 0.05$; n.s., not significant). (D) Western blot analysis of ExlA secreted by IHMA or IHMA::*pSW196exlBA* in the presence of arabinose. FliC (Sup) probed with anti-FliC antibody was used as a loading control.

demonstration that ExlA is indeed a pore-forming toxin, we approximated the pore size using a variety of osmoprotectants in the cytolytic assays. In these experiments, osmoprotectants (sugars and polyethylene glycols [PEGs]) of different sizes allowed us to evaluate the diameter of the pore (Fig. 2B). As expected based on a previous report (30), the α-hemolysin forms a pore of about 1 nm and the hemolysis is inhibited by raffinose, while ShlA forms a pore of about 2 nm, with hemolysis being inhibited by PEG 2000 (31). Hemolysis induced by ExoU was not inhibited by any sugars or PEGs, an observation in agreement with the fact that ExoU is not a pore-forming toxin but a potent phospholipase (32). The smallest molecule inhibiting ExlA-induced hemolysis was maltopentaose, which indicated that the diameter of the ExlA pore is approximately 1.6 nm, based on the hydrodynamic radius of the osmoprotectant molecules, as described previously (29). In contrast, the 50% hemolysis generated by ExlA$_{\Delta Cter}$ could not be inhibited by any of the osmoprotectants. This response is similar to that observed with ExoU, suggesting that this hemolysis was not due to pore formation but rather was caused by some other membrane-disruptive activity detectable on RBCs. Initially, we observed that natural clinical isolates synthetizing ExlA are in general poorly hemolytic (9). We hypothesized that the difference between the clinical isolates and the PAO1 strain ectopically overexpressing ExlA, which was used in the hemolytic assays, is due to the difference in the quantities of ExlA secreted by individual strains. Since PA7 is not amenable to genetic manipulation, we selected strain IHMA, a clinical isolate from our laboratory collection that secretes ExlA and is lytic on epithelial cells (see Table S1 in the supplemental material). In this strain, we introduced pBAD-*exlB-exlA* into the

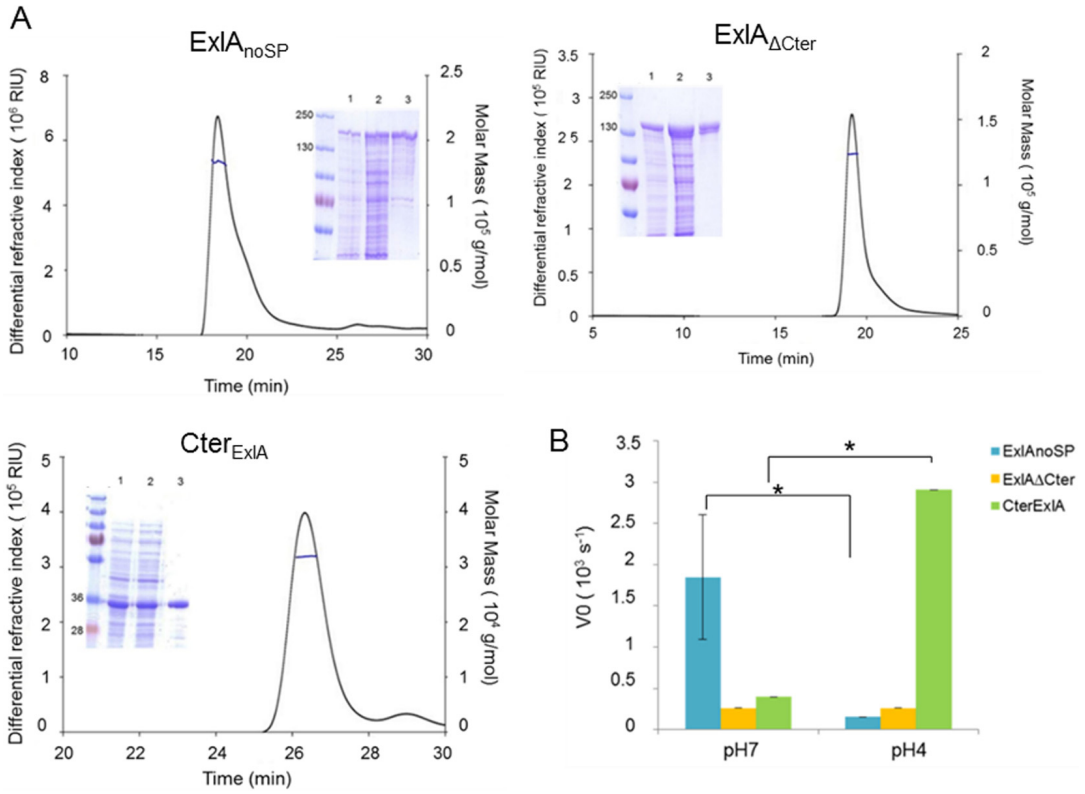

FIG 3 ExlA induces dye leakage from PC/PS liposome. (A) SEC-MALLS analysis of three ExlA variants, ExlA lacking the signal peptide (ExlA$_{noSP}$), ExlA$_{noSP}$ lacking the C-terminal domain (ExlA$_{\Delta Cter}$), and the C-terminal fragment of ExlA (Cter$_{ExlA}$), showing their soluble and monomeric form. The insets show SDS-PAGE analyses of the corresponding proteins at different stages of purification (lane 1, total lysate; lane 2, soluble lysate; lane 3, eluted fraction after the second step of purification). The values to the left are molecular masses in kilodaltons. (B) Permeabilization of PC/PS liposomes by ExlA proteins. Sulforhodamine B-containing liposomes composed of PC and PS were incubated with ExlA proteins, and the release of SRB was measured over 500 s. The initial rate of dye release (*V*0) was plotted for the three ExlA proteins, at pH 4 and pH 7. Statistical analysis was done by analysis of variance (*, $P \leq 0.05$).

chromosome and performed a hemolysis assay using variable arabinose concentrations to induce different levels of *exlA* expression. Indeed, raising the concentrations of arabinose significantly increased the capacity of a clinical strain to lyse RBCs in a dose-dependent manner (Fig. 2C), and this lytic activity correlates with the increased quantity of secreted ExlA (Fig. 2D).

Both the recombinant ExlA and its C-terminal domain induce liposome leakage. The observed phenotypes of ExlA-expressing *P. aeruginosa* strains on nucleated cells and on RBCs strongly suggest that ExlA may directly interact with membranes to induce pore formation. To further gain insight into the mode of action and to evaluate the association of the protein with membranes, we purified recombinant ExlA variants and tested their ability to induce membrane damage on the phospholipid bilayers of lipid vesicles. Three ExlA variants were designed for the experiment: (i) the full-length ExlA protein lacking the N-terminal export signal peptide and starting at Gly^{35} (ExlA$_{noSP}$), (ii) a truncated version of ExlA lacking the last C-terminal 296 amino acids (ExlA$_{\Delta Cter}$), and (iii) a polypeptide comprising the C-terminal 296-amino-acid region (Cter$_{ExlA}$). After optimization of the overexpression conditions and purification steps (see Materials and Methods for further details), the three variants were obtained in soluble forms and in quantities required for biochemical characterization (1, 6, and 28 mg of protein/liter of culture for ExlA$_{noSP}$, ExlA$_{\Delta Cter}$, and Cter$_{ExlA}$, respectively). Proteins were stable except for ExlA$_{noSP}$, which over time showed some degradation (Fig. 3A). Size exclusion chromatography with detection by multiangle laser light scattering analysis (SEC-MALLS) of the three variants showed that all of them are produced as soluble monomers (Fig. 3A). The various proteins were tested in a

liposome leakage assay as described previously (33, 34, 35) (Materials and Methods), where the large unilamellar vesicles (LUVs) incorporating sulforhodamine B (SRB) were prepared by freeze-thaw cycles followed by extrusion and subsequently checked by dynamic light scattering. As a control for vesicle preparation, we used the T3SS translocator PopB, which was previously shown to promote membrane permeabilization at pH 5 (33, 35). We tested the three ExlA variants at various pHs and on LUVs consisting of phosphatidylcholine (PC) alone or a mixture of PC and phosphatidylserine (PS) or other lipids. $ExlA_{noSP}$ was highly efficient in inducing SRB leakage from LUVs composed of PC/PS at neutral pH (Fig. 3B), whereas other types of LUVs were resistant to permeabilization even at higher protein concentration (up to 5 times the initial concentration) (Fig. S1). For comparison, ShlA similarly requires PS and PC for pore formation, and the addition of phosphatidylethanolamine (PE) furthermore increases the susceptibility of LUVs to ShlA (34). $ExlA_{noSP}$ lacking the C-terminal region ($ExlA_{\Delta Cter}$) was unable to induce significant liposome leakage at any tested pH, confirming the experiments on nucleated cells, which showed that the C-terminal domain is required for cytolysis (Fig. 3B). Moreover, the 35-kDa polypeptide comprising only the C-terminal domain ($Cter_{ExlA}$) possesses on its own a significant membrane permeabilization activity, though exclusively at pH 4 (Fig. 3B). This result shows that the $Cter_{ExlA}$ protein's activity requires conformational changes induced by low pH and these are not required for the full-length protein activity, suggesting that the N-terminal domain contributes to conformational changes required for membrane binding and the induction of liposome leakage.

Kinetics of pore formation and membrane disruption on nucleated cells seen by video microscopy. Having established that ExlA displays a pore-forming activity on RBCs and liposomes, we sought to determine the kinetics of the various events leading to the death of eukaryotic cells induced by clinical strains of *P. aeruginosa* expressing ExlA. To that aim, we observed epithelial A549 cells infected with IHMA or its genetic variants by time-lapse microscopy. To follow the plasma membrane permeability, the infection was performed in the presence of YoPro-1, a membrane-impermeant dye (629 Da) that fluoresces upon interaction with RNA in the cytoplasm and DNA in the nucleus and can be used as a marker of small pores occurring during early apoptosis (Invitrogen). In A549 cells infected with ExlA-expressing strains, we observed and measured an increase of YoPro-1 fluorescence at early time points in the cytoplasm and later in the nucleus (as illustrated in Fig. 4A). The data show an initial phase of slow fluorescence increase from 30 to 60 min corresponding to the complete entry of the dye in the cytoplasm. This is followed by a phase of rapid increase of fluorescence until it reaches a plateau corresponding to the entry into the nucleus. Infection with IHMAΔ*exlA* and IHMA$exlA_{\Delta Cter}$ did not show any fluorescence in the cytoplasm or in the nuclei at any time points (Fig. 4A). We quantified the first phase of YoPro-1 incorporation on 100 cells for each condition and found significant differences in calculated slope values for IHMA versus IHMAΔ*exlA* and IHMA versus IHMAΔ*exlA*::pSW196$exlBA_{\Delta Cter}$ (Fig. 4B). We conclude that the ExlA-induced pore formation, as visualized by YoPro-1 incorporation, starts at 30 min postinfection. To further characterize early steps of ExlA-induced morphological changes in epithelial cells, we performed time-lapse microscopy with a confocal microscope to generate three-dimensional (3D) images. A549-EGFP (enhanced green fluorescent protein) cells, with membranes labeled with wheat germ agglutinin (WGA)-Alexa 647, were infected with various strains secreting ExlA. Under these conditions, we observed that IHMA-infected cells initially became round (Fig. 4C; time 140 min), followed by a loss of their internal EGFP content, leaving shells of empty plasma membranes (Fig. 4C; time 220 min). Therefore, ExlA rapidly forms pores in the membranes of A549 cells, allowing the entry of small molecules (such as YoPro-1) into the cytoplasm. At later time points, the cell morphology changes and cells become round. ExlA eventually leads to plasma membrane rupture, an event detected by GFP release and visualized by discontinuous WGA labeling.

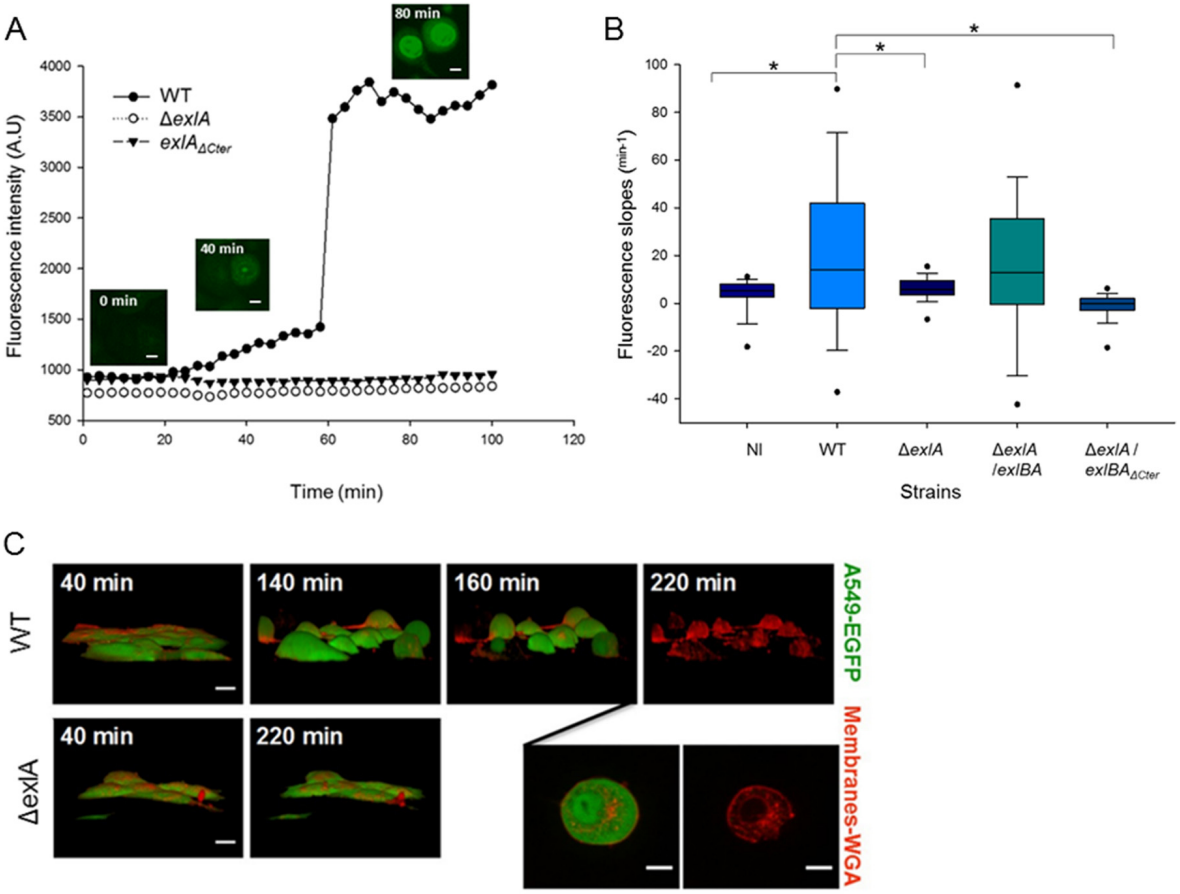

FIG 4 ExlA-induced pore formation precedes plasma membrane disruption. (A) Incorporation of YoPro-1 (green) into infected A549 cells was visualized and measured by time-lapse microscopy. The representative images (inset figures) taken with an ArrayScan wide-field microscope are shown for the wild-type infection. Bars, 10 μm. A549 cells were infected with *P. aeruginosa* IHMA (WT), IHMAΔ*exlA* (Δ*exlA*), and IHMA*exlA*$_{\Delta Cter}$ (*exlA*$_{\Delta Cter}$). (B) YoPro-1 incorporation was analyzed for *P. aeruginosa* IHMA (WT)-, IHMAΔ*exlA* (Δ*exlA*)-, IHMAΔ*exlA*::*pSW196exlBA* (Δ*exlA/exlBA*)-, and IHMAΔ*exlA*::*pSW196exlBA*$_{\Delta Cter}$ (Δ*exlA/exlBA*$_{\Delta Cter}$)-infected A549 cells and compared to a noninfected (NI) control. Fluorescence intensities were measured using HCS studio analysis software. The box plot represents slopes of phase I YoPro-1 intensities (from 30 to 60 min postinfection) (n = 100 cells per condition). Asterisks indicate statistically significant differences (Kruskal-Wallis, $P < 0.05$). (C) A549-EGFP cells, whose plasma membranes were labeled with WGA-Alexa 647, were infected at an MOI of 10 with *P. aeruginosa* IHMA (WT) or IHMAΔ*exlA* (Δ*exlA*) and observed by confocal spinning-disk microscopy. Two inset images represent the same cell infected by the wild-type strain at 200-min and 220-min time points. Note the cell rounding (at 140 min postinfection), absence of EGFP labeling, and rupture of cell membrane (at 220 min postinfection) for infection with the wild-type strain (WT). 3D images were constructed from *z*-planes. Bars, 10 μm. The film with the entire sequence is provided in Movie S1 in the supplemental material.

Type IV pili are required for ExlA-dependent cytolysis. Our preliminary experiments indicated that secreted ExlA, recovered from the medium (LB) used to grow *P. aeruginosa* or from cell culture medium, is unable to induce epithelial cell lysis. Moreover, addition of chloramphenicol to washed bacteria prior to infection abolished the bacterial cytotoxicity, suggesting the requirement for *de novo* ExlA synthesis for efficient pore formation (Fig. S2A). Additionally, recombinant ExlA variants incubated with nucleated cells (epithelial A549 cells and RAW macrophages) and RBCs had no detectable cytolytic activity (Fig. S2A, B, and C). These observations suggest that ExlA is relatively unstable following secretion into the medium and, consequently, its action requires a contact between the toxin-producing bacteria and the eukaryotic cell. To determine whether a contact was indeed important for cytotoxicity, we used a Transwell system in which bacteria and the monolayer of A549 cells are separated by a filter (0.2-μm-diameter pores), permeable by proteins but not the bacteria. Cytotoxicity after "in Transwell" infection was determined by the measurement of lactate dehydrogenase (LDH) release from A549 cells into the supernatant and compared to direct infection conditions (without separation by a filter) performed in parallel (Fig. 5A). When the bacteria are separated from the eukaryotic cells in the Transwell chamber, no LDH release at any time point can be detected and the result is

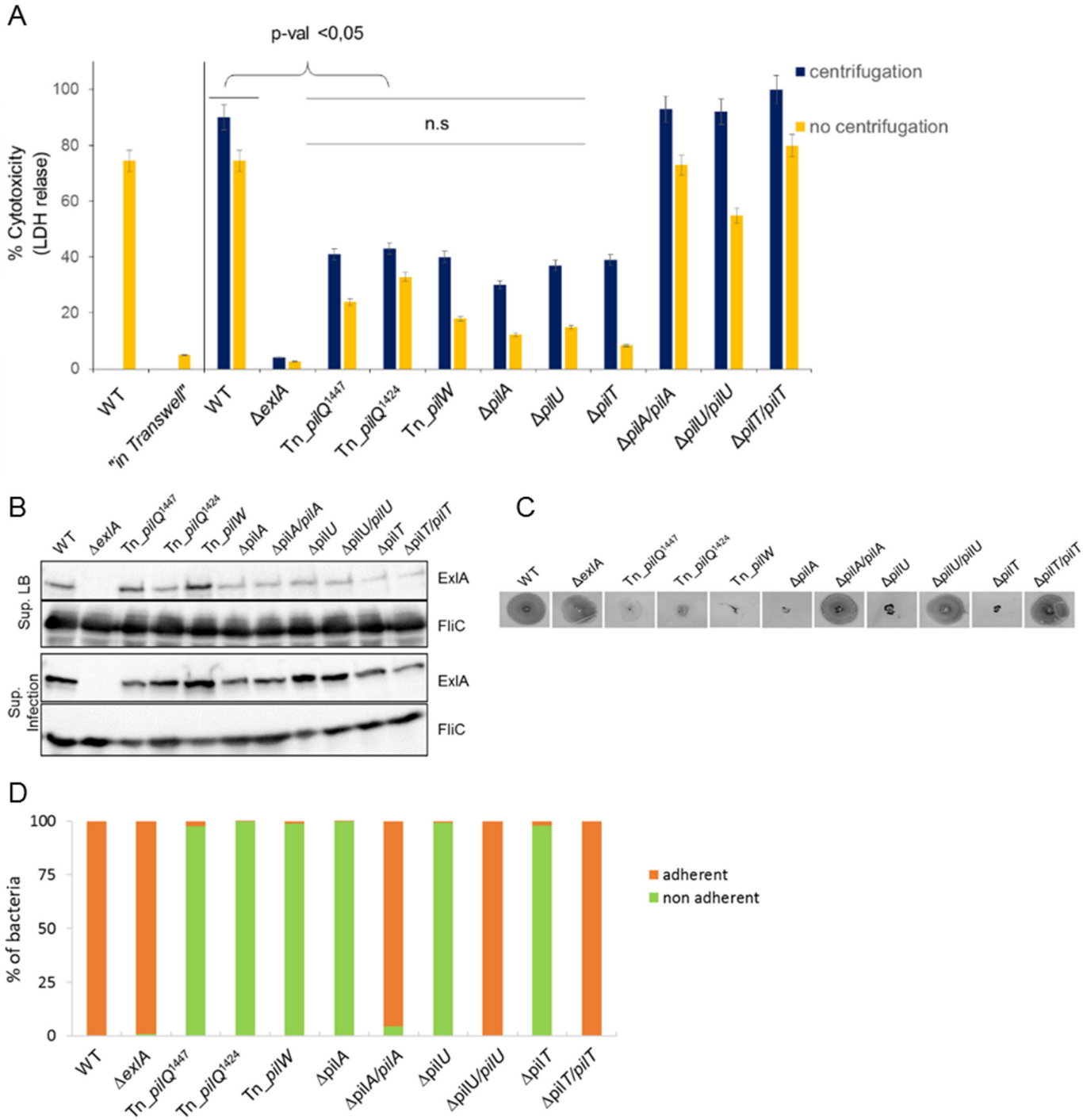

FIG 5 Type IV pili are required for ExlA-dependent cytolysis. (A) Cytotoxicity assays were performed using A549 cells and mutants identified during screening of a transposon (Tn) library, strains with engineered chromosomal deletions (Δ*pilA*, Δ*pilU*, and Δ*pilT*), and the complemented strains. The LDH release was measured as described in the Fig. 1 legend. Where indicated, infections were done in the Transwell system, where bacteria and A549 cells were separated with a membrane. Note the absence of LDH release for "in Transwell" conditions. When indicated, centrifugation was performed immediately after initiation of infection. Analysis of variance was used to compare *pil* mutants to WT ($P \leq 0.05$; n.s., not significant). (B) Secretion of ExlA in *pil* mutants. Immunoblot analysis was performed using anti-ExlA and anti-FliC antibodies on proteins TCA precipitated from the LB growth medium (Sup. LB) or from cell culture medium following infection of A549 cells with the bacteria (Sup. Infection). (C) Twitching motility of IHMA (WT), IHMAΔ*exlA* and *pil* mutants, and complemented strains, assessed by Coomassie blue staining of motility plates after 48 h. (D) Adhesion of *P. aeruginosa* IHMA, IHMAΔ*exlA* and various *pil* mutants, and complemented strains to A549 cells, quantified after 30 min of infection by enumerating the bacteria (as CFU) in cell-associated (adherent) and supernatant (nonadherent) fractions.

comparable to that seen with an *exlA* mutant. In contrast, infection under normal conditions induced the release of >90% of total cell LDH within 90 min postinfection. Therefore, it appears that the ExlA cytotoxic effect depends on the bacteria being in close proximity to or even in contact with the eukaryotic target cell.

We thus hypothesized that other bacterial factors, possibly adhesive organelles, may be required for ExlA-dependent cytolysis. To identify these factors, we developed a miniaturized cellular assay to screen a *mariner* transposon (Tn) library of *P. aeruginosa* for the loss of ExlA-mediated cytolysis. The clinical isolate *P. aeruginosa* IHMA was mutagenized by random insertions of the transposon, and a library of 7,400 mutants was obtained. A cytotoxicity test utilizes A549 cells, in which Draq7 and vital Hoechst staining revealed dead and live cells, respectively. Fluorescence images on both channels detecting Draq7 and Hoechst labeling were acquired with an automated high-throughput microscope. The primary screen was carried out in 384-well plates and yielded >200 low-cytotoxicity or noncytotoxic mutants using 30% cytotoxicity as a cutoff. The secondary screen was done manually in 96-well plates by measuring LDH release from infected A549 cells. Finally, 20 mutants were selected as being noncytotoxic, showing similar kinetics and levels of LDH release as the negative control IHMAΔ*exlA*. The transposon insertion sites were determined by semiarbitrary PCR, sequencing, and a BLAST search against the PA7 genome on the *Pseudomonas* website (http://www.pseudomonas.com). Interestingly, out of the 20 selected mutants (Table S1), three mutants harbor the transposon insertion in genes shown previously to be required for type IV pilus biogenesis, with two different Tn insertions within *pilQ* encoding the outer membrane secretin (36) and one insertion in *pilW* encoding a minor pilus subunit (37). These results strongly suggest that T4P are necessary for ExlA to exert its full cytolytic activity. To support this conclusion, we engineered additional isogenic deletions affecting formation of type IV pili, including a mutant lacking the main T4P subunit PilA, and strains with deletions of *pilU* and *pilT* genes, encoding the two ATPases required for pilus extension and retraction (38, 39) (IHMAΔ*pilA*, IHMAΔ*pilU*, and IHMAΔ*pilT*). We also created the corresponding complemented strains (IHMAΔ*pilA*::*pilA*, IHMAΔ*pilU*::*pilU*, and IHMAΔ*pilT*::*pilT*, respectively). We examined these strains for cytotoxicity, ExlA secretion, twitching, and adhesion to eukaryotic cells. In agreement with the results obtained from the transposon library screen and the levels of cytotoxicity provoked by the original transposon T4P mutants, the *pilA*, *pilU*, and *pilT* deletions significantly affected the cytotoxicity, while complemented strains restored the cytotoxicity to wild-type levels (Fig. 5A). Interestingly, bacteria affected in the biogenesis of the pili were still able to secrete ExlA (Fig. 5B), both into LB medium and during epithelial cell infection, suggesting that pili are not required for toxin expression and/or production but rather for promoting its cytolytic activity. We tested also the twitching motility of the mutants and their capacity to adhere to eukaryotic cells. As expected, mutants deleted for *pilA*, *pilU*, or *pilT* were not able to twitch. The complemented strains restored the twitching motility to the same level as IHMA (Fig. 5C). By comparing the CFU of bacteria attached and not attached to cells, we found that the *exlA*-deleted mutant adhered to cells in the same manner as the wild-type strain. All *pil* mutants, including the *pilU* and *pilT* mutants that were reported previously to produce pili but without the capacity to retract, could not adhere to cells (Fig. 5D). To establish whether the defect in pilus biogenesis affected the bacterial cytotoxic behavior and adhesion on different cell lines, the RAW macrophages were infected with different strains. As shown in Fig. S3 and S4, the absence of pili affected the ExlA-dependent cytotoxicity and bacterial adhesion to RAW macrophages to a similar extent as seen with A549 cells. Finally, to determine whether bringing the bacteria lacking pili artificially to the host cell surface could restore their cytotoxicity, we performed a centrifugation step immediately after infection. In all cases, the centrifugation increased the level of cytotoxic activity of pilus mutants, albeit without reaching the wild-type levels (Fig. 5A and S3).

These experiments demonstrate that adhesion of bacteria to cells is required for ExlA activity. Taken together, these results show that pili are mediating close contact between bacteria and eukaryotic cells, promoting localized action of ExlA, and that this interaction is required for the formation of the pores and subsequent cell death.

DISCUSSION

In this study, we further deciphered the structure-activity relationship and the biological function of exolysin, the recently identified potent toxin expressed by clinical strains of *P. aeruginosa* lacking T3SS (6, 9, 17). We first confirmed that ExlA requires the accessory protein ExlB for cytotoxic activity on epithelial cells. This finding, together with sequence analysis of the *exlBA* locus, shows that in *P. aeruginosa* ExlB and ExlA form a TPS system (TpsBA), in which *exlB* encodes the outer membrane protein TpsB serving as a cognate porin for the secretion of a TpsA protein, *P. aeruginosa* ExlA. All TpsB proteins are characterized by a domain capable of forming a β-barrel channel in the outer membrane and two periplasmic polypeptide transport-associated (POTRA) domains (18). As for other model TpsB proteins (16), secretion analysis and cytotoxicity assays showed that ExlB is required for ExlA secretion and cytolysis of epithelial cells, demonstrating that ExlB-ExlA constitute a new member of the TPS family.

ExlA is a 172-kDa secreted toxin composed of multiple distinct domains. In the majority of polymorphic proteins of the TpsA family, the activity of the protein resides within their C-terminal regions (24). A C-terminal deletion reduced the ExlA cytolytic activity by 85% without affecting its secretion; this is analogous to the effect of C-terminal deletion in FHA, which abolishes its adhesive properties (27). The secondary structure prediction of the C-terminal domain using the PSIPRED Protein Sequence Analysis Workbench (http://bioinf.cs.ucl.ac.uk/psipred/) and the Phyre2 web portal for protein modeling, prediction, and analysis (http://www.sbg.bio.ic.ac.uk/phyre2) (40) indicates a mixture of β-strands and α-helices (see Fig. S5 in the supplemental material). However, attempts to predict its tertiary structure with Phyre2 did not return any statistically reliable result, as the best model exhibited only 17.5% confidence with a coverage of 19% of the sequence. The N-terminal part of the ExlA protein could adopt an elongated form dominated by β-strands, as is the case for several proteins from the hemagglutinin/hemolysin family, represented by FHA and ShlA. In addition to secretion signals (type I secretion signal peptide and TPS) and hemagglutinin domains, ExlA possesses five RGD motifs and the C-terminal domain sharing no homology with any other proteins. The penta-RGD mutant retained full cytolytic activity, implying that ExlA uses other ways to interact with eukaryotic cell surfaces, at least under our *ex vivo* conditions. RGD motifs have been found in other bacterial adhesion molecules, such as in filamentous hemagglutinin of *Bordetella*; however, their role in cell host interaction could not be clearly demonstrated (41).

The efficient cell destruction by *P. aeruginosa* ExlA and the similarity with ShlA of *S. marcescens* prompted us to examine the capacity of exolysin to form pores in biological membranes, characteristics of various secreted bacterial toxins. Using two classical models for studying pore-forming toxins (PFTs), we established that ExlA, upon interaction with cell membranes or artificial lipid vesicles, gives rise to pores of 1.6 nm that ultimately result in leakage of hemoglobin from RBCs and release of fluorescent molecules from liposomes. We further show that the C-terminal domain is required for pore-forming activity. On different types of nucleated cells (epithelial/endothelial cells, macrophages, and lymphocytes), ExlA-expressing *P. aeruginosa* strains cause the release of the cytoplasmic enzyme LDH 3 to 4 h postinfection (17). Using 3D time-lapse microscopy and membrane-impermeant fluorescent dyes, we demonstrate that the membrane rupture is preceded by the formation of membrane pores revealed by the uptake of YoPro-1 within the cell cytoplasm. Therefore, ExlA performs clearly different activity on eukaryotic cells than do any T3S effectors, e.g., ExoS, ExoT, and ExoY, which enzymatically modify intracellular signaling molecules, and ExoU, which destroys membranes by its phospholipase activity (reviewed in reference 11).

The majority of PFTs can be grouped into two families, the α- and β-PFTs; they are secreted as soluble, monomeric molecules that undergo conformational change upon membrane binding followed by formation of membrane-embedded multimers (42). ExlA shares no sequence homology with any other PFTs for which the mechanism of action has been extensively studied, and nothing is known about molecular mecha-

nisms involved in pore formation by the closest ExlA homologue, ShlA. Therefore, the mechanisms of membrane binding, the oligomerization state, and the mechanism of pore formation by this toxin could not be assessed at present.

Recombinant ExlA, at high concentrations, was able to induce *in vitro* liposome leakage, strongly suggesting that the protein adopts the proper pore conformation following lipid binding. Interestingly, the C-terminal part of the protein, essential for ExlA-mediated *P. aeruginosa* cytolytic activity, was also able to induce liposome leakage, albeit only at acidic pH. This suggests that the first part of the protein, composed of several hemagglutinin domains organized in β-sheets, may play a role in lipid binding and/or protein oligomerization, or conformational changes at the C terminus, accounting for the difference in activity between the whole protein and the C-terminal domain alone. ExlA provokes a liposome leakage only in the presence of charged phospholipids (PS), probably involving electrostatic and hydrophobic interactions; a similar effect is seen for T3SS translocon proteins PopB and PopD (35) and several other membrane-binding proteins, such as colicins (43). In general, PFTs often recognize target cells either through binding to specific lipids or by recognition of a cognate receptor which drastically increases their local concentration at the membrane. This high local concentration promotes their oligomerization and membrane incorporation (42). Neither ExlA harvested from *P. aeruginosa* supernatant nor *in vitro*-purified ExlA variants showed lytic activity on nucleated cells, comparably to what was found for the T3SS toxins (35, 44). Moreover, only bacteria in contact with eukaryotic cells were able to exert ExlA-dependent cytolysis. We postulated that *P. aeruginosa* could have adopted a strategy for ExlA-dependent cytolysis conceptually similar to the close-contact requirement for the action of T3SS and toxin translocation (45) with or without a need for translocation machinery. Using a cell-based screen for additional bacterial factors that may promote ExlA pore-forming activity, we identified *P. aeruginosa* pili as being absolutely required for cytolysis. Bacterial T4P are long extracellular appendages with multiple functions, including bacterial motility and adhesion (38). The role of pili in *P. aeruginosa* T3SS-dependent cell intoxication has been clearly documented in an *in vivo* corneal infection model (46) and in *ex vivo* models of epithelial cells (46–49). They are also required for the injection of T3S toxins; however, the T4P could be exchanged for the nonfimbrial adhesin pH 6 antigen of *Yersinia pestis*, indicating that simple adhesion mediated by pili to cells plays a crucial role in T3S intoxication, presumably by positioning the injectisome onto the host cell surface, whereas the other pilus function, twitching, seems to be irrelevant (50). Cooperation between TPS adhesins and surface appendices involved in adhesion/motility has been previously demonstrated. In *Bordetella*, the fimbriae play a role in promoting further the adhesion properties of the TPS hemagglutinin to eukaryotic cells (51) and TPS protein EtpA binds to the flagella and facilitates *Escherichia coli* adhesion to eukaryotic cells (8). In the case of ExlA, T4P are clearly required for ExlA targeting to the eukaryotic cell membranes, as all pilus mutants secrete ExlA. This indicates that T4P play a role in bringing bacteria into close proximity with their target cell and thus possibly promoting a local increase of ExlA concentration (Fig. 6), a role played by specific lipid and/or protein receptors for other PFTs.

In conclusion, some *P. aeruginosa* strains, lacking T3SSs, have evolved a novel strategy of pathogenesis by acquiring the pore-forming TPS toxin exolysin and using pili as extracellular appendages to facilitate their cytolytic action. Whether this cooperation between the TPS pore-forming toxin and adhesive pili is unique for *P. aeruginosa* or is a conserved mechanism in other bacterial species possessing ExlA-like proteins remains to be investigated.

MATERIALS AND METHODS

Bacterial strains, plasmids, and growth conditions. Bacterial strains and plasmids used in this study are listed in Table S2 in the supplemental material. Bacteria were grown in LB medium supplemented with antibiotics when needed. During construction of deletion mutants, introduction of complementing plasmids, and transposon mutagenesis, the selection for *P. aeruginosa* following mating with *E. coli* was done on LB medium supplemented with Irgasan (25 μg/ml) and antibiotics (75 μg/ml gentamicin [Gm], 75 μg/ml tetracycline [Tc], and 500 μg/ml carbenicillin [Cb]).

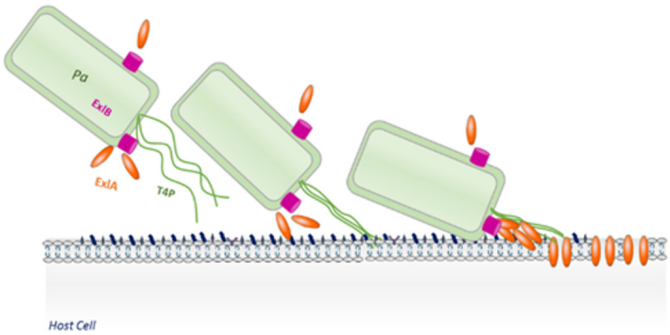

FIG 6 Schematic view of cooperation between T4P and ExlA in cytotoxicity. T4P are required for adhesion of bacteria and promote direct contact between bacterial and mammalian cell surfaces. This brings ExlA-secreting *P. aeruginosa* (*Pa*) to the proximity of the host cell membrane, increasing its local concentration at the site of action. The interaction of ExlA with membranes results in pore formation, followed by LDH release and death of infected eukaryotic cells. ExlB is the cognate outer membrane transporter of ExlA.

Genetic manipulations. All deletion mutants were obtained by gene splice extension overlap (SOE) PCRs. The *exlA*$_{RGA}$ gene was synthesized by GenScript and cloned in BglII-AvrII sites of pUC57. *exlB-exlA*$_{RGA}$ was cloned into pSW196 between the EcoRI and SacI restriction sites, to obtain the plasmid *pSW196exlB-exlA*$_{RGA}$. For complementation of mutants, wild-type genes were amplified by PCR and cloned into the integrative plasmid pSW196 containing the arabinose-inducible promoter pBAD (52). The constructs in the pSW196 plasmid were transferred into *P. aeruginosa* strains by triparental mating. Primers used in PCR are listed in Table S3.

Cell culture and cytotoxicity assays. The epithelial cell line A549 (ATCC CCL-185) was grown in 1× RPMI (Gibco Life Technologies) supplemented with 10% fetal bovine serum (FBS; Sigma) at 37°C and 5% CO_2. Cells were plated in 96-well plates (50,000 cells/well) and incubated for 1 night. Two hours before infection, RPMI medium was replaced by endothelial growth basal medium (EBM-2; Lonza Clonetics). The infection was done at a multiplicity of infection (MOI) of 10 (bacteria per eukaryotic cell). The level of cytotoxicity was determined by measuring the release of lactate dehydrogenase (LDH) using a cytotoxicity detection kit (Roche). Infection supernatants were sampled at 4 h postinfection. Negative controls were noninfected cells; positive controls were cells lysed by the addition of 200 μl of 2% Triton X-100. The optical density (OD) was measured at 492 nm. The extent of cytotoxicity was calculated by determining the percent cytotoxicity.

Time-lapse microscopy. A549 cells were plated in 96-well plates (50,000 cells/well) in RPMI medium (1×) for a night. Before infection, the RPMI medium was replaced with EBM-2 and the cells were labeled with vital Hoechst stain (1 μg/ml) and YoPro-1 (1 μM) followed by infection with the bacteria at an MOI of 10. Cell acquisitions were made using the ArrayScan high-content system (Thermo Fisher) every 5 min. Analyses were performed by measuring the fluorescence intensity of each cell using the HCS studio analysis software. Slopes were calculated between the 5 last time points before a sharp increase of fluorescence. The box plot was made using SigmaPlot software (Systat Software Inc., San Jose, CA), and statistical analysis was done by the Kruskal-Wallis test.

For confocal spinning-disk microscopy, the A549-EGFP cells were grown in RPMI medium supplemented with 10% fetal calf serum (all from Lonza). Cells were seeded at 25,000 cells per well on Lab-Tek II 8-chambered (Dutscher Scientific) coverslips and used 24 h later. Cell membranes were labeled after incubation with WGA-Alexa 647 (Life Technologies) for 10 min at 37°C and then infected with bacteria at an MOI of 10 in EBM-2. Cell infections were observed by confocal spinning-disk microscopy for 4 h, with images recorded every 20 min. Successive planes in 3D stacks were taken every 0.5 μm. The 3D reconstruction was performed using the 3D viewer plug-in of ImageJ software.

Analysis of ExlA secretion. Secretion of ExlA was monitored either in liquid LB cultures or under infection conditions. A 30-ml bacterial culture, in LB at an optical density at 600 nm (OD_{600}) of 1, was centrifuged at 6,000 rpm for 15 min. The supernatants (9 ml) were filtered, followed by addition of 90 μl of 2% sodium deoxycholate (DOC). After a 30-min incubation at 4°C, 900 μl of 100% trichloroacetic acid (TCA) was added and the proteins were allowed to precipitate overnight at 4°C followed by centrifugation at 15,000 × *g* for 15 min at 4°C. Pellets were resuspended in 100 μl of Laemmli loading buffer. For the analysis of proteins during infection of cultured cells, the bacteria were added to 100-mm petri dishes (at an MOI of 10) for 2 h, the supernatants were centrifuged, and the proteins were precipitated with TCA as described above. Samples were separated by SDS-PAGE (12%) and transferred onto polyvinylidene difluoride (PVDF) membranes for Western immunoblotting. Primary rabbit polyclonal antibodies were raised against either synthetic peptides of ExlA (6) or the recombinant C-terminal portion of the ExlA fragment, used at a 1:1,000 dilution. Anti-RpoA (Neoclone) and anti-FliC (39) were used at 1:2,000 and 1:1,000 dilutions, respectively. For the detection of the abundant RpoA protein, the bacterial lysates were further diluted 5-fold. Secondary antibodies were anti-rabbit-horseradish peroxidase (HRP) and anti-mouse-HRP (Sigma). The membranes were developed with Luminata Classico Western HRP (Millipore) substrate.

Hemolysis assay. Human red blood cells (RBCs) were obtained from the Etablissement Français du Sang (EFS), Grenoble, France. RBCs were counted, and 5×10^7 were incubated in 100 μl of EBM-2 with bacteria at the MOI of 10 or with 100 nM α-hemolysin from *S. aureus*, in 96-well plates. After centrifugation at 2,000 rpm and gentle agitation, the plates were incubated at 37°C for 90 min. The plates were centrifuged at 2,000 rpm at 4°C, allowing sampling of 100 μl of the supernatant. The optical density was measured at 560 nm. The negative controls were noninfected RBCs, and the positive control was obtained by inducing complete lysis by adding 100 μl of 1% SDS. For osmoprotection assays, RBCs were incubated with 30 mM osmoprotectants in EBM-2.

Expression and purification of ExlA variants. ExlA genes were cloned in pET15b for $Cter_{ExlA}$ and in pET28a for $ExlA_{noSP}$ and $ExlA_{\Delta Cter}$. *E. coli* BL21(DE3) cells were used for the production of ExlA variants. Precultures were done in 30 ml of LB with ampicillin (Amp; 100 μg/ml) for pET15b and kanamycin (Km; 30 μg/ml) for pET28a at 25°C overnight. Expression of the recombinant proteins was induced in a 1-liter culture grown at 37°C by addition of 0.5 mM isopropyl-β-D-thiogalactopyranoside (IPTG) for 1.5 h. Bacteria were centrifuged, and the pellets were resuspended in 20 ml of IMAC10 buffer (25 mM Tris-HCl, 500 mM NaCl, 10 mM imidazole, pH 8) and lysed using a Microfluidizer M_110P2 (Microfluidics, Westwood, MA) at 15,000 lb/in^2 for 3 min. Soluble fractions were sampled after centrifugation at 30,000 rpm for 30 min at 4°C. Lysates were passed through a Ni^{2+} affinity column (HisTrap HP; GE Healthcare) using the Äkta purifier 10 instrument (GE Healthcare), and the bound proteins were eluted using a 20 mM to 200 mM step gradient of imidazole. Fractions were monitored by gel electrophoresis, pooled, and further purified on cation exchanger (HiTrap SP) and anion exchanger (HiTrap Q) columns (HiTrap; GE Healthcare). Protein concentrations in each fraction were quantified by bicinchoninic acid assay (BCA) using the Optima kit.

Liposome leakage assay. L-R-phosphatidylcholine (PC), L-R-phosphatidylethanolamine (PE), L-R-phosphatidylserine (PS), and cholesterol (Ch) were from Avanti Polar. Lipids and liposomes were stored under nitrogen in chloroform at −20°C. Liposomes containing PS/PC (18%/82%), PC (100%), PC/PE (82%/18%), PC/PS/PE (72%/18%/10%), and PC/Ch (80%/20%) were prepared by evaporation of lipids in a rotatory evaporator, hydrated, and resuspended in 1 ml of 25 mM Tris-HCl, 250 mM NaCl, pH 8, containing 50 mM sulforhodamine B by six cycles of freezing-thawing. To obtain large unilamellar vesicles (LUVs) of 100 nm, liposomes were filtered through a 0.1-μm filter by extrusion and the nonencapsulated dye was removed with size exclusion chromatography on a PD10 column (Amersham) equilibrated with 25 mM Tris-HCl, 250 mM NaCl, pH 8. LUV disruption was monitored by an increase of fluorescence intensity upon dye dilution in the same buffer. Measurements were performed on a Jasco FP6500 fluorimeter with excitation set at 565 nm and emission at 586 nm in 2 ml of 10 μM LUV and recorded during 600 s after the addition of the protein. A 10 μM concentration of LUV was incubated with 10 nM protein in Tris or acetate buffer at different pHs. Fluorescence intensities were normalized considering the initial intensity before protein addition and the maximal intensity generated by the addition of Triton X-100 at the end of each kinetics measurement. The initial rates of dye release were derived from the first 10 s of the kinetics, using linear regression.

Construction of transposon library. A transposon library was constructed in *P. aeruginosa* IHMA by mating with an *E. coli* donor carrying plasmid pBTK24 containing the *mariner* transposon with a Gm resistance cassette (53). *P. aeruginosa* IHMA was grown in LB at 42°C, and *E. coli* SM10λpir harboring pBTK24 was grown at 37°C with agitation for 18 h. Bacteria in 300 separate aliquots (100 μl) from each culture were combined, concentrated by centrifugation to 50 μl, and spotted on LB agar plates which were further incubated for 5 h at 37°C. Spots were scraped off, resuspended in 100 μl LB, and plated on LB agar plates containing Irgasan (25 mg/ml) and Gm (75 μg/ml) to isolate single colonies for testing in the cytotoxicity assay. The locations of the transposon insertions in candidate mutants were determined by semirandom PCR (primers are listed in Table S2) and sequencing.

Cellular screen for noncytotoxic mutants by high-content microscopy. A549 cells were plated in 384-well plates (2,500 cells/well) in 1× RPMI with 10% FBS and incubated overnight. IHMA_tn single colonies from the transposon library were robotically transferred one by one in 96-well plates containing LB with 15 μg/ml Gm. The colonies were then transferred with 96-pin replicators into 384-well plates containing 30 μl of LB and grown statically for 18 h. The day of the screen, A549 cells were washed once with EBM-2, and EBM-2 containing vital Hoechst (1 μg/ml) and Draq7 (3 μM final concentration) stains was added. Infection of cells was initiated with a 384-pin replicator and run for 3 h at 37°C, and then the cells were fixed by adding an equal volume of 2% formaldehyde in phosphate-buffered saline (PBS) to each well. The image acquisition was done using a high-content microscope (ImageXpress Micro; Molecular Devices) at the ICCB Longwood facility, Harvard Medical School, Boston, MA. Analysis was done using MetaXpress software.

Twitching motility assay. A determination of twitching motility by *P. aeruginosa* was carried out by inoculating bacteria at the interface between the plastic petri dish and LB agar (10 g/liter tryptone, 5 g/liter yeast extract, 10 g/liter NaCl, 1% agar). After 48 h of incubation at 37°C, agar was removed and the zone of twitching was revealed following Coomassie blue staining.

Adhesion assay. A549 cells (5×10^5) were cultured in 1× RPMI with 10% FBS. Before the adhesion assay, A549 cells were treated with trypsin (0.05% EDTA) for 2 min at 37°C, suspended in 1× RPMI with 10% FBS, centrifuged at 2,000 rpm for 5 min, and suspended in EBM-2. Bacterial strains (5×10^6 bacteria) were incubated with cells (MOI of 10) at 37°C with agitation. After 30 min, A549 cells and bacteria were centrifuged at 1,200 rpm for 5 min and pellets were resuspended in EBM-2. CFU in the supernatant and pellet fractions were quantified following serial dilutions in 1× PBS and plating on LB agar.

SUPPLEMENTAL MATERIAL

Supplemental material for this article may be found at https://doi.org/10.1128/mBio.02250-16.

MOVIE S1, AVI file, 4.8 MB.
TEXT S1, DOCX file, 0.01 MB.
FIG S1, TIF file, 0.1 MB.
FIG S2, TIF file, 0.1 MB.
FIG S3, TIF file, 0.1 MB.
FIG S4, TIF file, 0.1 MB.
FIG S5, TIF file, 0.1 MB.
TABLE S1, DOCX file, 0.02 MB.
TABLE S2, DOCX file, 0.04 MB.
TABLE S3, DOCX file, 0.02 MB.

ACKNOWLEDGMENTS

We thank Stewart Rudnicki from screening facilities at ICCB-Longwood, Harvard Medical School, Boston, MA; Emmanuelle Soleilhac from the Screening Center for Bioactive Molecules (CMBA), BIG, CEA-Grenoble; and Laëtitia Kurzawa, μLife microscopy facility (BIG, Grenoble), for their help in training, setting up experiments, and data analysis. P.B. thanks Xindan Wang for help in using the colony-transferring robot (Hudson) (Rudner Lab, Department of Microbiology and Immunobiology, Harvard Medical School, Boston, MA). *Pseudomonas aeruginosa* strain IHMA87 was kindly provided by International Health Management Association (IHMA; USA), and *Serratia* strains were obtained from J. Ewbank (CIML, Marseille, France). We thank Thomas Dougherty for critical reading of the manuscript.

This work was supported by grants from Laboratory of Excellence GRAL, ANR-10-LABX-49-01, and Agence national de Recherche ANR-15-CE11-0018-01. P.B. received the Ph.D. fellowship from the French Ministry of Education and Research, and E.R. received the Ph.D. fellowship from Laboratory of Excellence GRAL.

P.B., M.R., S.E., E.R., G.G., S.B., and E.F. performed experiments. P.H., G.G., E.F., and S.L. contributed reagents. P.B., S.E., P.H., S.L., E.F., and I.A. analyzed the data. P.B. and I.A. conceived the study and wrote the manuscript.

The funders had no role in study design, data collection and interpretation, or the decision to submit the work for publication.

REFERENCES

1. Crouch Brewer S, Wunderink RG, Jones CB, Leeper KV, Jr. 1996. Ventilator-associated pneumonia due to Pseudomonas aeruginosa. Chest 109:1019–1029. https://doi.org/10.1378/chest.109.4.1019.
2. Bodey GP, Bolivar R, Fainstein V, Jadeja L. 1983. Infections caused by Pseudomonas aeruginosa. Rev Infect Dis 5:279–313. https://doi.org/10.1093/clinids/5.2.279.
3. Boucher HW, Talbot GH, Bradley JS, Edwards JE, Gilbert D, Rice LB, Scheld M, Spellberg B, Bartlett J. 2009. Bad bugs, no drugs: no ESKAPE! An update from the Infectious Diseases Society of America. Clin Infect Dis 48:1–12. https://doi.org/10.1086/595011.
4. Winsor GL, Griffiths EJ, Lo R, Dhillon BK, Shay JA, Brinkman FS. 2016. Enhanced annotations and features for comparing thousands of Pseudomonas genomes in the Pseudomonas genome database. Nucleic Acids Res 44:D646–D653. https://doi.org/10.1093/nar/gkv1227.
5. Boukerb AM, Marti R, Cournoyer B. 2015. Genome sequences of three strains of the Pseudomonas aeruginosa PA7 clade. Genome Announc 3:e01366-15. https://doi.org/10.1128/genomeA.01366-15.
6. Elsen S, Huber P, Bouillot S, Couté Y, Fournier P, Dubois Y, Timsit JF, Maurin M, Attrée I. 2014. A type III secretion negative clinical strain of Pseudomonas aeruginosa employs a two-partner secreted exolysin to induce hemorrhagic pneumonia. Cell Host Microbe 15:164–176. https://doi.org/10.1016/j.chom.2014.01.003.
7. Kos VN, Déraspe M, McLaughlin RE, Whiteaker JD, Roy PH, Alm RA, Corbeil J, Gardner H. 2015. The resistome of Pseudomonas aeruginosa in relationship to phenotypic susceptibility. Antimicrob Agents Chemother 59:427–436. https://doi.org/10.1128/AAC.03954-14.
8. Roy PH, Tetu SG, Larouche A, Elbourne L, Tremblay S, Ren Q, Dodson R, Harkins D, Shay R, Watkins K, Mahamoud Y, Paulsen IT. 2010. Complete genome sequence of the multiresistant taxonomic outlier Pseudomonas aeruginosa PA7. PLoS One 5:e8842. https://doi.org/10.1371/journal.pone.0008842.
9. Huber P, Basso P, Reboud E, Attrée I. 2016. Pseudomonas aeruginosa renews its virulence factors. Environ Microbiol Rep 8:564–571. https://doi.org/10.1111/1758-2229.12443.
10. Toska J, Sun Y, Carbonell DA, Foster AN, Jacobs MR, Pearlman E, Rietsch A. 2014. Diversity of virulence phenotypes among type III secretion negative Pseudomonas aeruginosa clinical isolates. PLoS One 9:e86829. https://doi.org/10.1371/journal.pone.0086829.
11. Hauser AR. 2009. The type III secretion system of Pseudomonas aeruginosa: infection by injection. Nat Rev Microbiol 7:654–665. https://doi.org/10.1038/nrmicro2199.
12. Engel J, Balachandran P. 2009. Role of Pseudomonas aeruginosa type III effectors in disease. Curr Opin Microbiol 12:61–66. https://doi.org/10.1016/j.mib.2008.12.007.
13. Le Berre R, Nguyen S, Nowak E, Kipnis E, Pierre M, Quenee L, Ader F, Lancel S, Courcol R, Guery BP, Faure K, Pyopneumagen Group. 2011. Relative contribution of three main virulence factors in Pseudomonas aeruginosa pneumonia. Crit Care Med 39:2113–2120. https://doi.org/10.1097/CCM.0b013e31821e899f.
14. Shaver CM, Hauser AR. 2004. Relative contributions of Pseudomonas aeruginosa ExoU, ExoS, and ExoT to virulence in the lung. Infect Immun 72:6969–6977. https://doi.org/10.1128/IAI.72.12.6969-6977.2004.

15. Vance RE, Rietsch A, Mekalanos JJ. 2005. Role of the type III secreted exoenzymes S, T, and Y in systemic spread of Pseudomonas aeruginosa PAO1 in vivo. Infect Immun 73:1706–1713. https://doi.org/10.1128/IAI.73.3.1706-1713.2005.
16. Jacob-Dubuisson F, Guérin J, Baelen S, Clantin B. 2013. Two-partner secretion: as simple as it sounds? Res Microbiol 164:583–595. https://doi.org/10.1016/j.resmic.2013.03.009.
17. Reboud E, Elsen S, Bouillot S, Golovkine G, Basso P, Jeannot K, Attrée I, Huber P. 2016. Phenotype and toxicity of the recently discovered exlA-positive Pseudomonas aeruginosa strains collected worldwide. Environ Microbiol 18:3425–3439. https://doi.org/10.1111/1462-2920.13262.
18. Clantin B, Delattre AS, Rucktooa P, Saint N, Méli AC, Locht C, Jacob-Dubuisson F, Villeret V. 2007. Structure of the membrane protein FhaC: a member of the Omp85-TpsB transporter superfamily. Science 317:957–961. https://doi.org/10.1126/science.1143860.
19. Simmerman RF, Dave AM, Bruce BD. 2014. Structure and function of POTRA domains of Omp85/TPS superfamily. Int Rev Cell Mol Biol 308:1–34. https://doi.org/10.1016/B978-0-12-800097-7.00001-4.
20. Locht C, Berlin P, Menozzi FD, Renauld G. 1993. The filamentous haemagglutinin, a multifaceted adhesin produced by virulent Bordetella spp. Mol Microbiol 9:653–660.
21. Delattre AS, Clantin B, Saint N, Locht C, Villeret V, Jacob-Dubuisson F. 2010. Functional importance of a conserved sequence motif in FhaC, a prototypic member of the TpsB/Omp85 superfamily. FEBS J 277:4755–4765. https://doi.org/10.1111/j.1742-4658.2010.07881.x.
22. Guérin J, Saint N, Baud C, Meli AC, Etienne E, Locht C, Vezin H, Jacob-Dubuisson F. 2015. Dynamic interplay of membrane-proximal POTRA domain and conserved loop L6 in Omp85 transporter FhaC. Mol Microbiol 98:490–501. https://doi.org/10.1111/mmi.13137.
23. Maier T, Clantin B, Gruss F, Dewitte F, Delattre AS, Jacob-Dubuisson F, Hiller S, Villeret V. 2015. Conserved Omp85 lid-lock structure and substrate recognition in FhaC. Nat Commun 6:7452. https://doi.org/10.1038/ncomms8452.
24. Zhang D, de Souza RF, Anantharaman V, Iyer LM, Aravind L. 2012. Polymorphic toxin systems: comprehensive characterization of trafficking modes, processing, mechanisms of action, immunity and ecology using comparative genomics. Biol Direct 7:18. https://doi.org/10.1186/1745-6150-7-18.
25. Jacob-Dubuisson F, Kehoe B, Willery E, Reveneau N, Locht C, Relman DA. 2000. Molecular characterization of Bordetella bronchiseptica filamentous haemagglutinin and its secretion machinery. Microbiology 146:1211–1221. https://doi.org/10.1099/00221287-146-5-1211.
26. Ruoslahti E. 1996. RGD and other recognition sequences for integrins. Annu Rev Cell Dev Biol 12:697–715. https://doi.org/10.1146/annurev.cellbio.12.1.697.
27. Julio SM, Inatsuka CS, Mazar J, Dieterich C, Relman DA, Cotter PA. 2009. Natural-host animal models indicate functional interchangeability between the filamentous haemagglutinins of Bordetella pertussis and Bordetella bronchiseptica and reveal a role for the mature C-terminal domain, but not the RGD motif, during infection. Mol Microbiol 71:1574–1590. https://doi.org/10.1111/j.1365-2958.2009.06623.x.
28. Schiebel E, Braun V. 1989. Integration of the Serratia marcescens haemolysin into human erythrocyte membranes. Mol Microbiol 3:445–453. https://doi.org/10.1111/j.1365-2958.1989.tb00190.x.
29. Lobo AL, Welch RA. 1994. Identification and assay of RTX family of cytolysins. Methods Enzymol 235:667–678. https://doi.org/10.1016/0076-6879(94)35180-5.
30. Menestrina G, Dalla Serra M, Comai M, Coraiola M, Viero G, Werner S, Colin DA, Monteil H, Prévost G. 2003. Ion channels and bacterial infection: the case of beta-barrel pore-forming protein toxins of Staphylococcus aureus. FEBS Lett 552:54–60. https://doi.org/10.1016/S0014-5793(03)00850-0.
31. Hertle R, Hilger M, Weingardt-Kocher S, Walev I. 1999. Cytotoxic action of Serratia marcescens hemolysin on human epithelial cells. Infect Immun 67:817–825.
32. Sato H, Frank DW. 2004. ExoU is a potent intracellular phospholipase. Mol Microbiol 53:1279–1290. https://doi.org/10.1111/j.1365-2958.2004.04194.x.
33. Matteï PJ, Faudry E, Job V, Izoré T, Attree I, Dessen A. 2011. Membrane targeting and pore formation by the type III secretion system translocon. FEBS J 278:414–426. https://doi.org/10.1111/j.1742-4658.2010.07974.x.
34. Hertle R. 2002. Serratia marcescens hemolysin (ShlA) binds artificial membranes and forms pores in a receptor-independent manner. J Membr Biol 189:1–14. https://doi.org/10.1007/s00232-001-0191-1.
35. Faudry E, Vernier G, Neumann E, Forge V, Attree I. 2006. Synergistic pore formation by type III toxin translocators of Pseudomonas aeruginosa. Biochemistry 45:8117–8123. https://doi.org/10.1021/bi060452+.
36. Koo J, Tang T, Harvey H, Tammam S, Sampaleanu L, Burrows LL, Howell PL. 2013. Functional mapping of PilF and PilQ in the *Pseudomonas aeruginosa* type IV pilus system. Biochemistry 52:2914–2923. https://doi.org/10.1021/bi3015345.
37. Giltner CL, Habash M, Burrows LL. 2010. Pseudomonas aeruginosa minor pilins are incorporated into type IV pili. J Mol Biol 398:444–461. https://doi.org/10.1016/j.jmb.2010.03.028.
38. Burrows LL. 2012. Pseudomonas aeruginosa twitching motility: type IV pili in action. Annu Rev Microbiol 66:493–520. https://doi.org/10.1146/annurev-micro-092611-150055.
39. Chiang P, Sampaleanu LM, Ayers M, Pahuta M, Howell PL, Burrows LL. 2008. Functional role of conserved residues in the characteristic secretion NTPase motifs of the Pseudomonas aeruginosa type IV pilus motor proteins PilB, PilT and PilU. Microbiology 154:114–126. https://doi.org/10.1099/mic.0.2007/011320-0.
40. Kelley LA, Mezulis S, Yates CM, Wass MN, Sternberg MJ. 2015. The Phyre2 web portal for protein modeling, prediction and analysis. Nat Protoc 10:845–858. https://doi.org/10.1038/nprot.2015.053.
41. Ishibashi Y, Relman DA, Nishikawa A. 2001. Invasion of human respiratory epithelial cells by Bordetella pertussis: possible role for a filamentous hemagglutinin Arg–Gly–Asp sequence and alpha5beta1 integrin. Microb Pathog 30:279–288. https://doi.org/10.1006/mpat.2001.0432.
42. Dal Peraro M, van der Goot FG. 2016. Pore-forming toxins: ancient, but never really out of fashion. Nat Rev Microbiol 14:77–92. https://doi.org/10.1038/nrmicro.2015.3.
43. Zakharov SD, Kotova EA, Antonenko YN, Cramer WA. 2004. On the role of lipid in colicin pore formation. Biochim Biophys Acta 1666:239–249. https://doi.org/10.1016/j.bbamem.2004.07.001.
44. Schoehn G, Di Guilmi AM, Lemaire D, Attree I, Weissenhorn W, Dessen A. 2003. Oligomerization of type III secretion proteins PopB and PopD precedes pore formation in pseudomonas. EMBO J 22:4957–4967. https://doi.org/10.1093/emboj/cdg499.
45. Hayashi N, Nishizawa H, Kitao S, Deguchi S, Nakamura T, Fujimoto A, Shikata M, Gotoh N. 2015. *Pseudomonas aeruginosa* injects type III effector ExoS into epithelial cells through the function of type IV pili. FEBS Lett 589:890–896. https://doi.org/10.1016/j.febslet.2015.02.031.
46. Zolfaghar I, Evans DJ, Fleiszig SM. 2003. Twitching motility contributes to the role of pili in corneal infection caused by Pseudomonas aeruginosa. Infect Immun 71:5389–5393. https://doi.org/10.1128/IAI.71.9.5389-5393.2003.
47. Comolli JC, Hauser AR, Waite L, Whitchurch CB, Mattick JS, Engel JN. 1999. Pseudomonas aeruginosa gene products PilT and PilU are required for cytotoxicity in vitro and virulence in a mouse model of acute pneumonia. Infect Immun 67:3625–3630.
48. Heiniger RW, Winther-Larsen HC, Pickles RJ, Koomey M, Wolfgang MC. 2010. Infection of human mucosal tissue by Pseudomonas aeruginosa requires sequential and mutually dependent virulence factors and a novel pilus-associated adhesin. Cell Microbiol 12:1158–1173. https://doi.org/10.1111/j.1462-5822.2010.01461.x.
49. Shikata M, Hayashi N, Fujimoto A, Nakamura T, Matsui N, Ishiyama A, Maekawa Y, Gotoh N. 2016. The pilT gene contributes to type III ExoS effector injection into epithelial cells in Pseudomonas aeruginosa. J Infect Chemother 22:216–220. https://doi.org/10.1016/j.jiac.2015.12.012.
50. Sundin C, Wolfgang MC, Lory S, Forsberg A, Frithz-Lindsten E. 2002. Type IV pili are not specifically required for contact dependent translocation of exoenzymes by Pseudomonas aeruginosa. Microb Pathog 33:265–277. https://doi.org/10.1006/mpat.2002.0534.
51. Scheller EV, Cotter PA. 2015. Bordetella filamentous hemagglutinin and fimbriae: critical adhesins with unrealized vaccine potential. Pathog Dis 73:ftv079. https://doi.org/10.1093/femspd/ftv079.
52. Baynham PJ, Ramsey DM, Gvozdyev BV, Cordonnier EM, Wozniak DJ. 2006. The Pseudomonas aeruginosa ribbon-helix-helix DNA-binding protein AlgZ (AmrZ) controls twitching motility and biogenesis of type IV pili. J Bacteriol 188:132–140. https://doi.org/10.1128/JB.188.1.132-140.2006.
53. Kulasekara HD, Ventre I, Kulasekara BR, Lazdunski A, Filloux A, et al. 2005. A novel two-component system controls the expression of Pseudomonas aeruginosa fimbrial cup genes. Molecular Microbiology 55:368–380.

Pseudomonas aeruginosa pore-forming Exolysin and Type IV pili cooperate to induce host-cell lysis

Supplementary informations

Movie S1. The A549-EGFP cells labeled with WGA-Alexa647 were infected with IHMAΔ*exlA* (left) and IHMA (right) at an MOI of 10 and imaged by confocal spinning disc microscopy for 4h. The 3D images were constructed from 150 z-planes. The film was assembled by ImageJ from 19 time points taken every 20 minutes. (https://www.ncbi.nlm.nih.gov/pmc/articles/PMC5263249/)

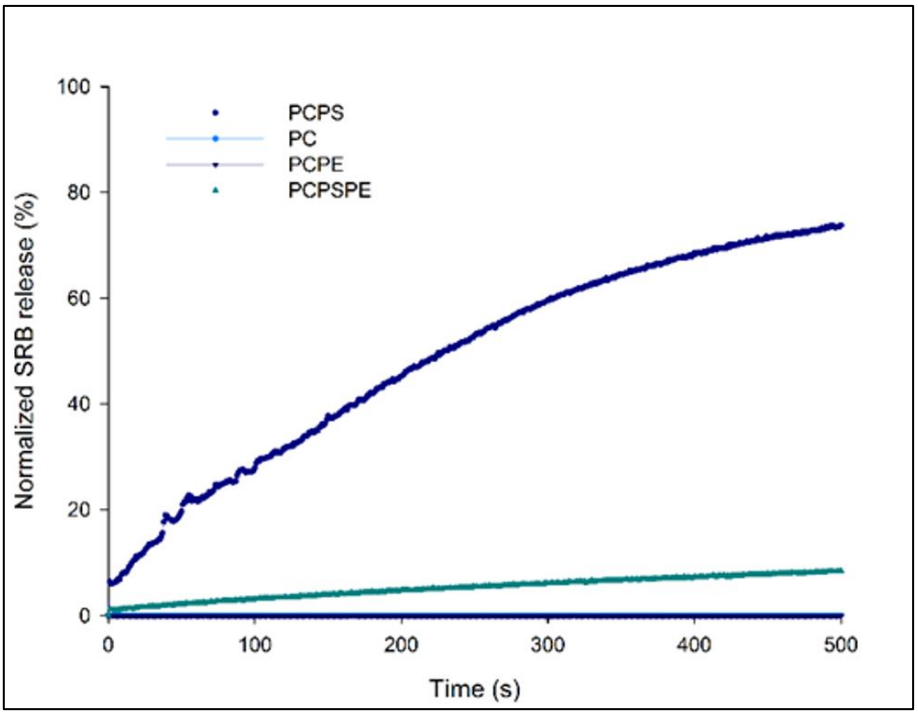

Fig.S1. Kinetic of Sulforhodamine B (SRB) release from liposomes after ExlA incubation at pH7. SRB-containing liposomes composed of PC/PS, PC, PC/PS/PE or PC/PE were incubated with ExlA protein at pH7 and the release of SRB was measured during 500 s.

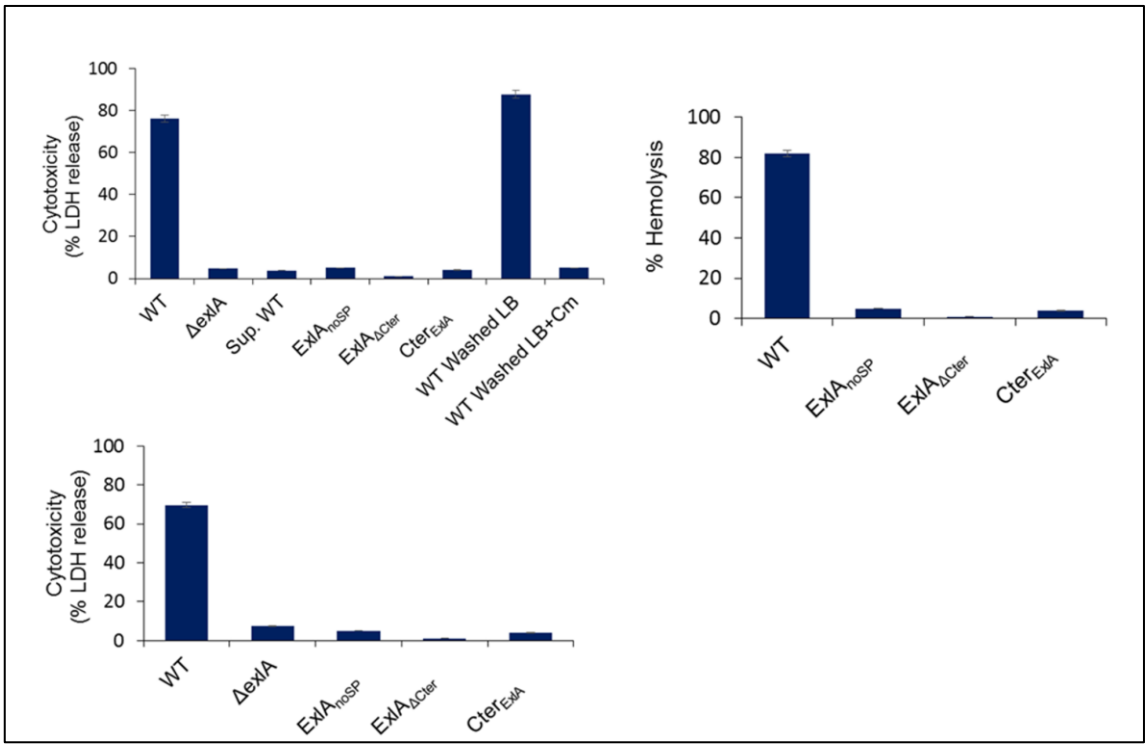

Fig.S2. Cytotoxicity and hemolysis induced by ExlA (A) Cytotoxicity assay of *P. aeruginosa* expressing different ExlA mutant proteins on A549 cells. Histogram shows the viability of epithelial A549 cells infected with *P. aeruginosa* strains IHMA (WT) or Δ*exlA*, incubated with the supernatant of IHMA culture ("Sup. WT"), 0.5 mg/ml of purified recombinant proteins (ExlA, ExlA$_{\Delta Cter}$ or Cter$_{ExlA}$), bacteria washed with LB ("WT Washed LB") or LB + chloramphenicol (25µg/ml) ("WT Washed +Cm"). The cytotoxicity was measured by the release of LDH. (B) Cytotoxicity assay on macrophage cell line RAW 264.7 with 0.5 mg/ml of purified proteins (ExlA, ExlA$_{\Delta Cter}$ or Cter$_{ExlA}$). (C) Hemolysis with 0.5 mg/ml purified proteins (ExlA, ExlA$_{\Delta Cter}$ or Cter$_{ExlA}$). Hemolysis assay was performed as described for Figure 3A. In B and C, infections by the wild-type and Δ*exlA* strains were done as positive and negative controls, respectively.

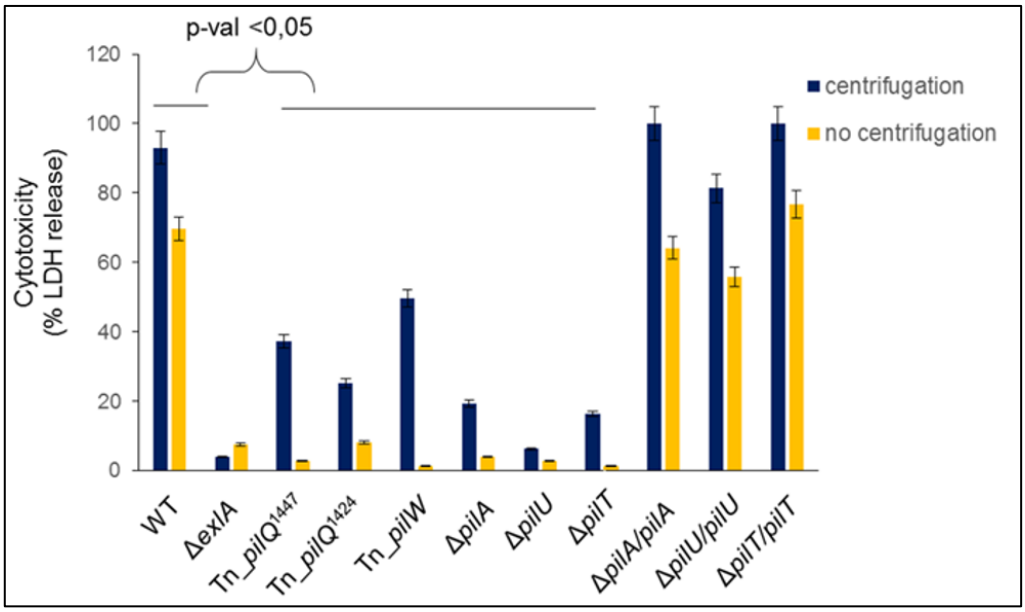

Fig. S3. Cytotoxicity of *P. aeruginosa* mutants on macrophage cell line RAW 264.7. Histogram shows the viability of RAW cells. Cytotoxicity assay of *pil* mutants with or without a centrifugation step. The cytotoxicity was measured by the release of LDH. ANOVA test was used to compare *pil* mutant to WT: *, P ≤0.05.

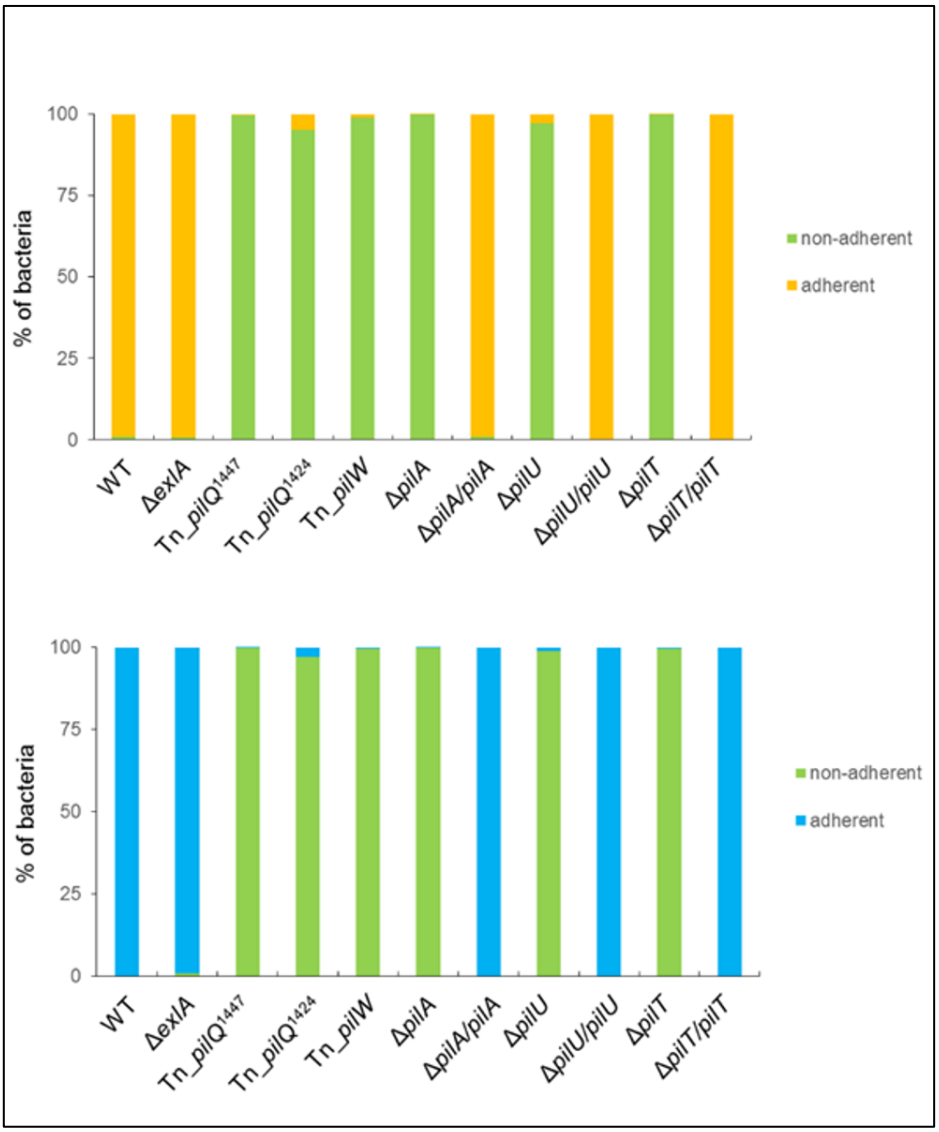

Fig. S4. Adhesion of *P. aeruginosa* to the macrophage cell line RAW 264.7. (A) Adhesion of IHMA, IHMAΔ*exlA* and various *pil* mutants and complemented strains to macrophages and (B) macrophages treated with cytochalasine D.

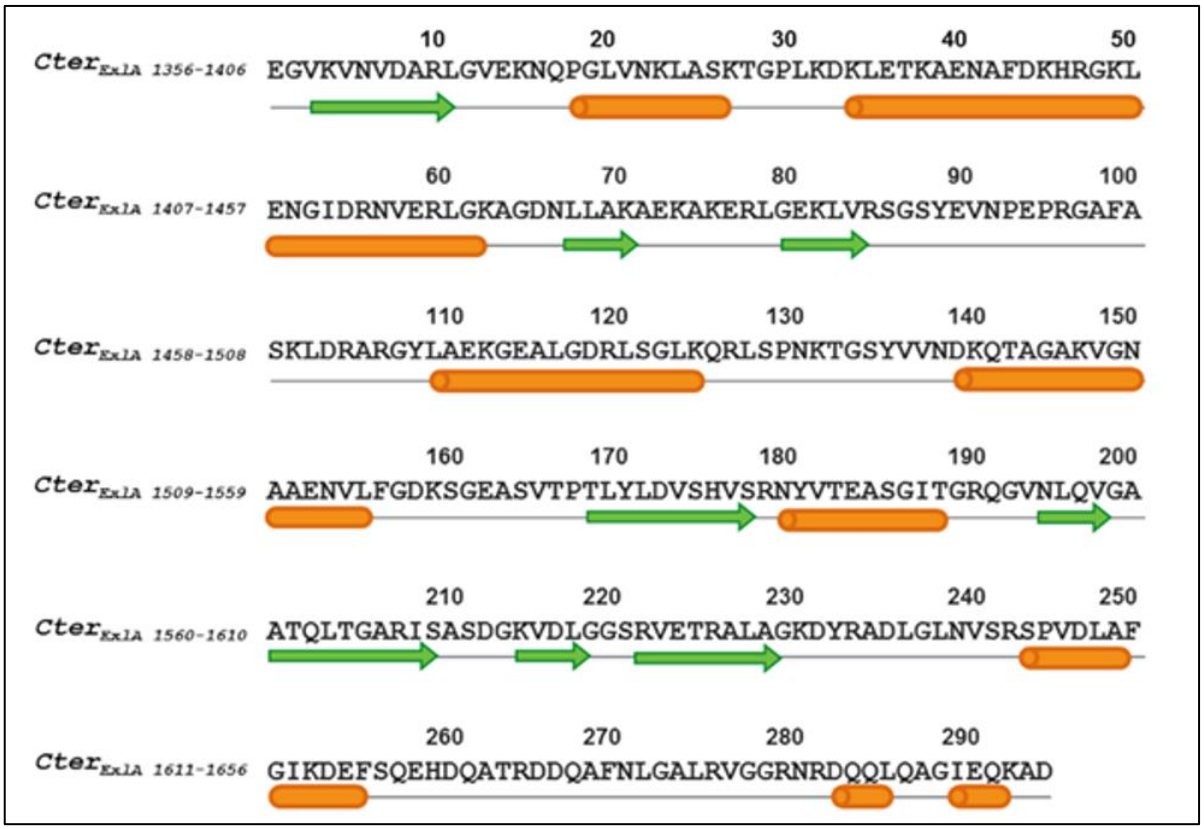

Fig. S5. Schematic representation of secondary structure prediction for the C terminal domain (residues 1356 to 1656) of ExlA. Green arrows and orange cylinders correspond to β-strands and α-helices, respectively. The prediction was done by PsiPred and Phyre2.

Table S1. List of 20 Tn mutants selected after secondary screen as displaying the cytotoxicity of less than 30% compared to the parental strain IHMA.

Gene disrupted or intergenic region[1]	Predicted operon	Protein(s)
pilQ	*PSPA7_5774 /aroB/ aroK / pilQ/ pilP/ pilO/ pilN/ pilM*	OM secretin type IV pili
pilQ		
pilW	*fimU/ pilV/ pilW/ pilX/ pilY1/ pilY2/ pilE*	minor pilin
PSPA7_1554	*PSPA7_1549 /PSPA7_1550 /PSPA7_1551 / PSPA7_1552 /PSPA7_1553 / PSPA7_1554*	putative porin
PSPA7_0652		hydroxypyruvate isomerase
PSPA7_6248	*PSPA7_6247, 49, 50,51*	FAD linked oxidase
pqqE	*PSPA7_3304 / pqqE / pqqD / pqqC / pqqB/ pqqA*	pyrroloquinolonine quinone biosynthetic protein
pqqE		
mfd		
mfd	PSPA7_2156	Transcription repair coupling factor
mfd		
PSPA7_2595	*ftsK/ lolA/ PSPA7_2595*	Recombinaison factor protein RarA
PSPA7_4936 -SOD		Putative transporter and SOD
PSPA7_6278 - PSPA7_6279		Hypothetical protein
PSPA7_5266 – PSPA7_5267		Putative oxidoreductase – hypothetical protein
PSPA7_5735 - PSPA7_5736		Glycosyl transferase family protein
PSPA7_2206- PSPA7_2207		Putative lipoprotein and hypothetical cytoplasmique protein
PSPA7_4573		Hypothetical protein
MO62_20290[2]		hypothetical protein, RHS toxin domain

[1] Tn junctions were PCR amplified and blasted against the PA7 genome on *Pseudomonas* genome data base (http://www.pseudomonas.com/). [2] *MO62_20290* is present in the strain RP73. Predicted operons and proteins names are retrieved from *Pseudomonas* genome database.

Table S2. List of bacterial strains and plasmids used in this work.

Strains or plasmids	Characteristics	References
Strains		
Pseudomonas aeruginosa		
PAO1 Δ*xcpR*Δ*pscC*	PAO1 lacking the Xcp T2SS and T3SS	This work
PAO1Δ*xcpR*Δ*pscC::exlBA*	PAO1 mutant with pSW196::*exlBA*	[1],This work
PAO1Δ*xcpR*Δ*pscC::exlBA*$_{RGA}$	PAO1 mutant with pSW196::*exlBA*$_{RGA}$	This work
PAO1Δ*xcpR*Δ*pscC::exlBA*$_{\Delta Cter}$	PAO1 mutant with pSW196::*exlBA*$_{\Delta Cter}$	This work
PAO1Δ*xcpR*Δ*pscC::exlA*	PAO1 mutant with pSW196::*exlA*	[1],This work
PAO1Δ*xcpR*Δ*pscC::exlB*$_{\Delta P1}$*A*	PAO1 mutant with pSW196::*exlB*$_{\Delta P1}$*A*	This work
PAO1Δ*xcpR*Δ*pscC::exlB*$_{\Delta P2}$*A*	PAO1 mutant with pSW196::*exlB*$_{\Delta P2}$*A*	This work
PP34	*P. aeruginosa* expressing ExoU	[2]
PP34ΔExoU	Isogenic ExoU mutant of PP34	[2]
IHMA879472 (IHMA)*	ExlA+, Urinary strain IHMA	[3],This work
IHMAΔ*exlA*	*exlA* deletion	This work
IHMAΔ*exlA*::*exlBA*	*exlBA* genes cloned into pSW196 and introduced into Δ*exlA*	This work
IHMAΔ*pilA*	*pilA* deletion	This work
IHMAΔ*pilA*::*pilA*	*pilA* cloned into pSW196 and introduced into Δ*pilA*	This work
IHMAΔ*pilT*	*pilT* deletion	This work
IHMAΔ*pilT*::*pilT*	*pilT* cloned into pSW196 and introduced into Δ*pilT*	This work
IHMAΔ*pilU*	*pilU* deletion	This work
IHMAΔ*pilU*::*pilU*	pilU cloned into pSW196 and introduced into Δ*pilU*	This work
IHMA879472*pilQ*^{1447}_tn	Tn insertion in *pilQ* at nucleotide 1447	This work
IHMA879472*pilQ*^{1424}_tn	Tn insertion in *pilQ* at nucleotide 1424	This work
IHMA879472*pilW*^{127}_tn	Tn insertion in *pilW* at nucleotide 127	This work
Escherichia coli		
DH5α	Cloning strain	Lab collection
BL21(DE3)	Protein expression	NEB
SM10 λpir	Strain used in bi-parental mating	Lory lab collection
Plasmids		
pSW196	Tc^R, Integrative plasmid at the *attB* site, derived from miniCTX, p*BAD*	[4]
pSW196*exlBA*	pSW196 with *Eco*RI-*Sac*I insertion of operon *exlBA* under p*BAD*	[1]
pSW196*exlA*	pSW196 with *Eco*RI-*Sac*I insertion of *exlA* gene under p*BAD*	[1]
pSW196*exlBΔP1-exlA*	pSW196*exlBA* with deletion of POTRA domain 1 of *exlB*	This work
pSW196*exlBΔP2-exlA*	pSW196*exlBA* with deletion of POTRA domain 2 of *exlB*	This work

pSW196*exlB-exlA*$_{RGA}$	pSW196*exlBA* with penta RGA mutant in *exlA*	This work
pSW196exlB-*exlA*$_{\Delta C\text{-}Ter}$	pSW19 *exlBA* with deletion of C-terminal domain of *exlA*	This work
pEXG2*pilA*	Gm^R, suicide plasmid used into *pilA* mutagenesis	
pEXG2*pilT*	Gm^R, suicide plasmid used into *pilT* mutagenesis	This work
pEXG2*pilU*	Gm^R, suicide plasmid used into *pilU* mutagenesis	This work
pSW196*pilA*	pSW196 with *EcoRI-SacI* insertion of *pilA* gene	This work
pSW196*pilT*	pSW196 with *Pst*I-*Spe*I insertion of *pilT* gene	This work
pSW196*pilU*	pSW196 with *Pst*I-*Spe*I insertion of *pilT* gene	This work
pBTK24	Gm^R, Plasmid with mariner transposon	[5]
pRK2013	Km^R, helper plasmid	[6]
pET15b*Cter-ExlA*	Amp^R , pET15b with *Nco*I-*Hin*dIII insertion of the Cter domain of ExlA; plasmid used in protein expression	This work
pET28a*ExlAnoSP*	Km^R , pET28a with *Nde*I-*Hin*dIII insertion of the ExlA^{noSP}; plasmid used in protein expression	This work
pET28a*ExlAΔCter*	Km^R , pET28a with *Nde*I-*Hin*dIII insertion of the ExlAΔCter; plasmid used in protein expression	This work

Cb^R: carbenicillin resistance, Tc^R: Tetracycline resistance, Amp^R: Ampicilin resistance, Km^R: Kanamycin resitance

*IHMA: International Health Management Association

Table S3. Primers used in this study.

Primers	Sequences (5'-3')
PA7_4642_2F	GCACCAGCCAGGTGAACG
PA7_4642_2R	CTCCGCCGCCCTGGCGTC
exlB-*Eco*RI	GAATTCGATACATGAAGGATGC
exlB-*Sac*I	GAGCTCTCAGATCTGCAGGCTCAG
SOE-ΔPOTRA1 $_{rev}$	GCCGTCGTGGTCTGCGATGG
SOE-ΔPOTRA1 $_{Forw}$	CCATCGCAGACCACGACGGCTACGTCGAGTCCATC
SOE-ΔPOTRA2 $_{rev}$	GGCGCCTTCGTCGACCAGGATATC
SOE-ΔPOTRA2 $_{Forw}$	GATATCCTGGTCGACGAAGGCGCCGCGCGCTGGAGCC
Round-1 RndomPA-1	GGCCACGCGTCGACTAGTACNNNNNNNNNNCGATG
Round-1a	GGCCACGCGTCGACTAGTAGNNNNNNNNNCAGCAG
Round-1 pBTK	GAAGCTGTGGTATGGCTGTGCAGG
Round-2PA	GGCCACGCGTCGACTAGTAC
Round-2 pBTK	CGCACTCCCGTTCTGGATAATGTT
IHMA-Mut-pilA-F1	GGATCCGCCGTCGAGATCGACATCGT
IHMA-Mut-pilA-R1	AGCGAAGCGCGCAACATCCTGATTT
IHMA-Mut-pilA-F2	TCAGGATGTTGCGCTTTAGCGCTCAAAATAGATTGCA
IHMA-Mut-pilA-R2	GAATTCGGTAGATTCCGCCAGCGGAGT
IHMA-Comp-pilA-F1	GAATTCTTGGGTTTGGCATGGATCCTGCTGAA
IHMA-Comp-pilA-R1	GGATCCTTAGGGCTTGCTTGCAGGCGCGTTCG
IHMA-Mut-pilT-F1	CC GAA TTC CTG CAG GTA GTT CTC GCC GAA
IHMA-Mut-pilT-R1	CTC GGT AAT ATC CAT GGG ACT C
IHMA-Mut-pilT-F2	G AGT CCC ATG GAT ATT ACC GAG TGA CAC CTG GTA TTC GGC ACC CTG
IHMA-Mut-pilT-R2	CC CCC GGG CTA GAC GCA GTT CCG GGA TTC
IHMA-Comp-pilT-F	CC CTG CAG ACG GCG GCT TTG GCG GC
IHMA-Comp-pilT-R	CC ACT AGT CTA GAC GCA GTT CCG GGA TTC
IHMA-Mut-pilU-F1	CC CTG CAG CGA GAA GGC GAA GAT CCC GGA
IHMA-Mut-pilU-R1	TCA CTG CTC GTT CAT CAC GCC GAG
IHMA-Mut-pilU-F2	GGC GTG ATG AAC GAG CAG TGA ATC GAG GTG CTG CTG AAC ACT C
IHMA-Mut-pilU-R2	CC CTC GAG ACT AGT CGC TAC GAG ATC GAA CAC AGC A
IHMA-Comp-pilU-F	CC CTG CAG CCA AAT CCT TGT CGG CGA GCG

Additional results

Characterization of the Tn mutants isolated after the screening.

The goal of this cell-based screening of Transposon library was to identify bacterial factors involved in the ExlA-mediated cytolysis. As described in the main publication, after a secondary screen on A549 cells, we obtained 20 Tn mutants presenting cytotoxicity lower than 30%. The transposon insertion sites were determined by semi-arbitrary PCR, sequencing, and a BLAST search against the PA7 genome on the Pseudomonas database[1]. All genes disrupted by the transposon are presented in the Table S1. Three mutants had a Tn insertion in *pil* genes and we demonstrated that Type IV pili are essential to the pore formation activity of ExlA [320]. The 17 other mutants were further characterized in collaboration with Alice Berry, PhD student working with Dr. Sylvie Elsen on the *exlBA* regulation.

We determined the exact position of the insertion and the orientation of the promoter carried by the mariner transposon. The genes interrupted have been classified by their predicted functions into five classes. Three mutants have transposon insertion in genes involved in the adhesion and the motility of the bacteria (*pil* genes), five interrupted genes play a role in the DNA repair and metabolism (mfd, PSPA7_2595), five transposons are located in intergenic regions (PSPA7_4936-SOD, PSPA7_6278-79, PSPA7_5266-67, PSPA7_5735-36), three transposons are inserted in genes coding for hypothetical proteins (PSPA7_2207, PSPA7_4573, PSPA7_5946) and finally, one transposon is inserted in a gene coding for RHS-like toxin identified in RP73 genome (M062_20290).

To identify the step of the ExlA-dependent cytotoxicity affected by the mutation, namely the transcription or translation of *exlA*, secretion, activity of ExlA or the activity of a ExlA co-factor, we introduced in *trans exlBA* genes under a promoter inducible by arabinose (*pSW196 exlBA*) in each Tn mutant. We measured the cytotoxicity towards epithelial cells, by the incorporation of propidium iodide (PI) in the nuclei. If the transposon is inserted in a gene coding for a protein involved in the activity of ExlA, the cytotoxicity would not be restored. However, if the transposon is inserted in a gene coding for a transcriptional regulator or protein involved in secretion of ExlA, the cytotoxicity would be restored.

By measuring the kinetics of PI incorporation of cells infected with Tn mutants carrying *pSW196 exlBA* genes, we observed that four mutants ($pilQ^{1447}$, $pilQ^{1424}$, *pilW* and *PSPA7_6248*) were not cytotoxic towards epithelial cells. However the cytotoxicity was totally restored with the other mutants (Figure 5.1).

[1] http://www.pseudomonas.com

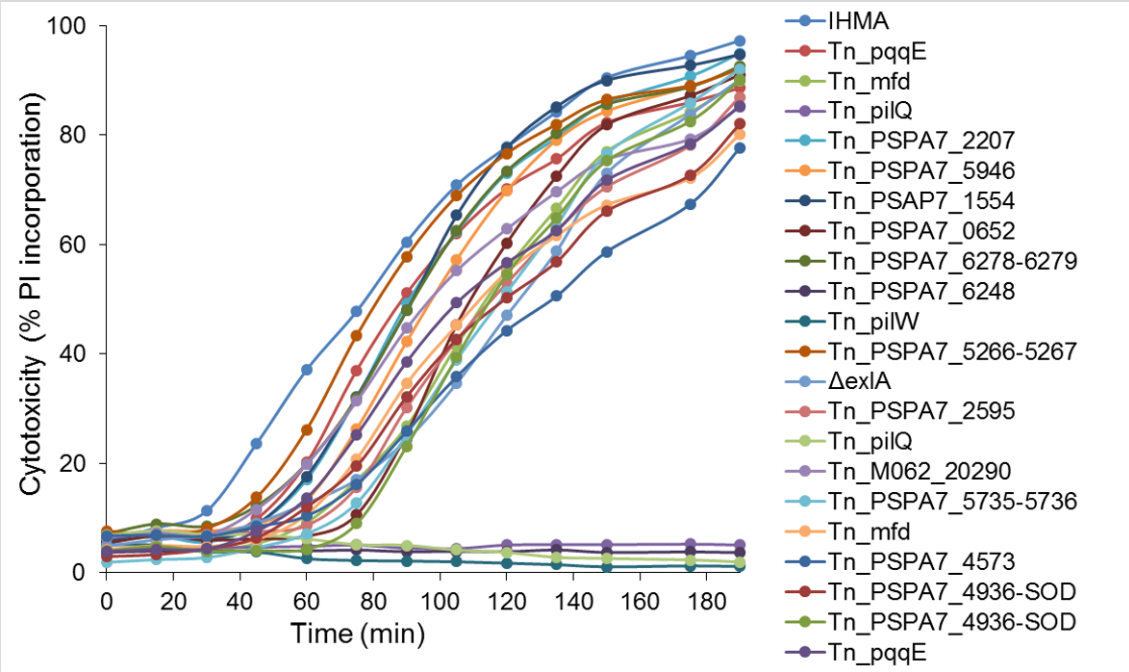

Figure 5.1. **Characterization of Tn mutants.** Kinetic of PI incorporation into A549 cells infected at MOI 10 for 190 min with Tn mutants carrying *pSW196 exlBA*. Percentage of PI positive cells were calculated for each time point.

Characterization of Tn PSPA7_6248 mutant

Among the four mutants in which the cytotoxicity was not restored, three mutants concern *pil* genes, and their characterization was already described in the main publication (Figure 5).

In the fourth mutant the transposon was inserted at 976 pb in PSPA7_6248 gene (Figures 5.2 A and B). This gene is encoded in the operon PSPA7 _6247-6251, and no homologue was found in the classical strains of *P. aeruginosa*, including PAO1 and PA14. Annotated as a FAD-linked oxidase in IHMA87 and PA7 genomes, this gene was renamed *dprE1*, at the beginning of February 2017 by Dr. Lori Burrows. The DprE1 protein is involved in the synthesis of D-arabinofuranose, a sugar that is attached to the type IV pilins of PA7 and its related strains [321]. DrpE1 catalyzes the epimerization of the decaprenyl-P-D-ribose (DPR) to decaprenyl-P-2'-keto-D-ribose, a precursor of the decaprenyl-P-D-arabinofuranose (DPA). Inactivation of *drpE1* gene resulted in a decrease in twitching motility, and in pilin production compared to the WT, suggesting that DrpE1 is involved in the pilus assembly. The secretion of ExlA in Tn *drpE1* mutant was the same as the secretion in the wild-type IHMA, and in the Tn *pil* mutants used as controls. This result confirms that DrpE1 was not involved in production and secretion of ExlA (Figure 5.2 C).

In conclusion, in addition to the three *pil* mutants, we identified another mutant that may have impaired pilus biogenesis, supporting our findings that pili and ExlA cooperate in host cell intoxication.

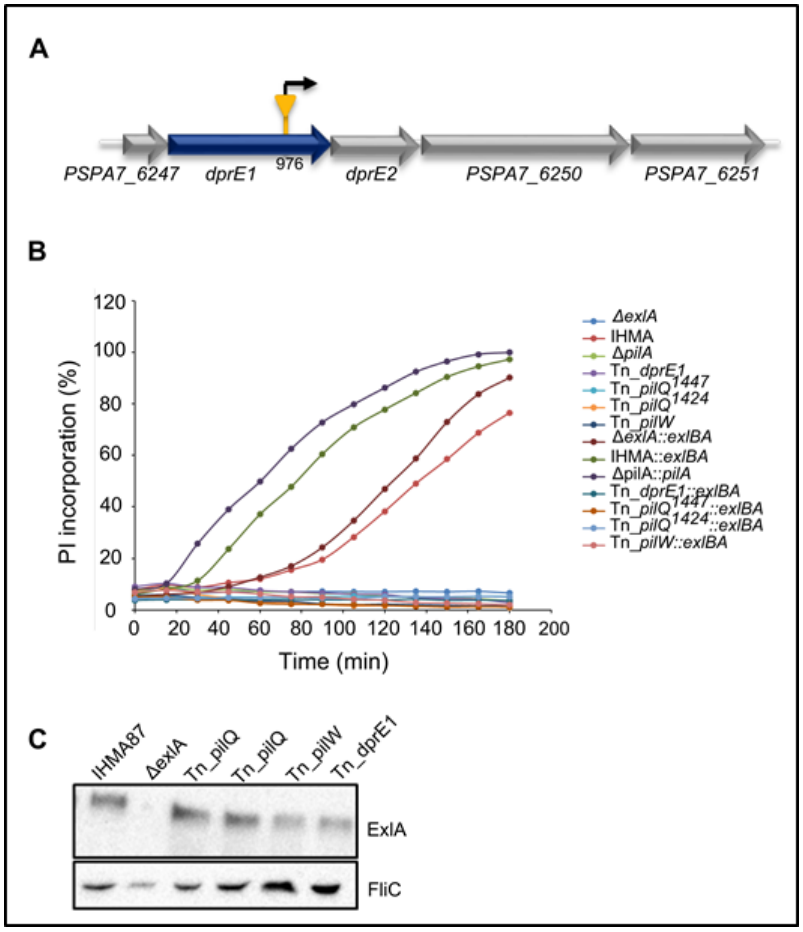

Figure 5.2. **Characterization of *drpE1* mutant**. (A) Genetic organization of the *drpE1* locus with the position of the transposon insertion. (B) Kinetic of PI incorporation into A459 cells infected with Tn mutants, Tn mutants supplemented with *pSW196exlBA*. As control we used Tn *pil* mutants, Δ*exlA* and IHMA WT. (C) Immunoblot analysis of the Tn mutants. Western blot were performed after 3 hours of A549 cells infection at MOI 10. Proteins were revealed by anti-ExlA antibodies. FliC was used as loading controls, probed with the corresponding antibodies.

Examination of ExlA secretion in Tn mutants

To understand the role of genes disrupted by the transposon we examined the ExlA secretion after 3 hours of A459 cell infection, for each Tn mutant. We observed that the cytotoxicity was restored for mutants carrying *pSW196 exlBA*. However, Tn mutants were not able to secrete ExlA in infection conditions (Figure 5.3), suggesting that the gene disrupted by the transposon, might be involved in the production of ExlB or ExlA proteins or in ExlA secretion processes.

Twitching motility of Tn mutants

P. aeruginosa motility is mainly dependent on its T4P and its flagellum. As we showed that T4P are necessary for ExlA-dependent cytotoxicity in IHMA strain, we

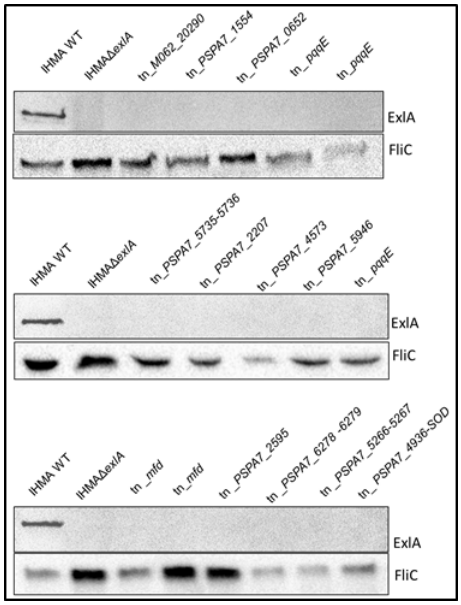

Figure 5.3. **Immunoblot analysis of the Tn mutants.** Western blots were performed after 3 hours of A549 cells infection at MOI 10. Proteins were revealed by anti-ExlA antibodies. FliC was used as loading control, probed with the corresponding antibodies.

evaluated the twitching motility of other mutants to see if the insertion of transposon in gene other than *pil* genes can affect the twitching motility. We assessed the capacity of twitching motility of all the Tn mutants at the surface of semi-solid agar plate. All the mutants were able to twitch in the same manner as IHMA WT (Figure 5.4). These results suggest that the genes disrupted by transposons were not involved in the regulation or the activity of Type IV pili. In all these Tn mutants the Type IV pili were functional and the secretion of ExlA was lost, suggesting that some mutants might be affecting the regulation of the production of ExlA.

Protease activity of Tn mutants

LasB and AprA are the two major proteases secreted by the T2SS and T1SS respectively, of *P. aeruginosa* and have a significant impact on virulence of the bacteria [31, 131]. LasB is involved in the VE-cadherin cleavage of endothelial cells after more than 4 hours of infection [31]. To assess whether the mutations have a pleitropic effect, the proteolytic activity of the 20 Tn mutants was tested for casein, using milk-agar plates. PAO1 was used as the positive control for T1SS and T2SS-dependent proteolytic activities and showed a proteolytic halo on plates (Figure 5.5). PAO1Δ*xcpR* and PAO1Δ*lasB*, which cannot secrete T2SS proteases and LasB, also presented a proteolytic activity, probably due to AprA secretion. IHMA, as previously described by Reboud et al., displayed a strong proteolytic activity (Figure 5.5). All the Tn mutants presented a proteolytic halo of similar size, indicating that the gene disrupted by the transposons does not affect protease activity.

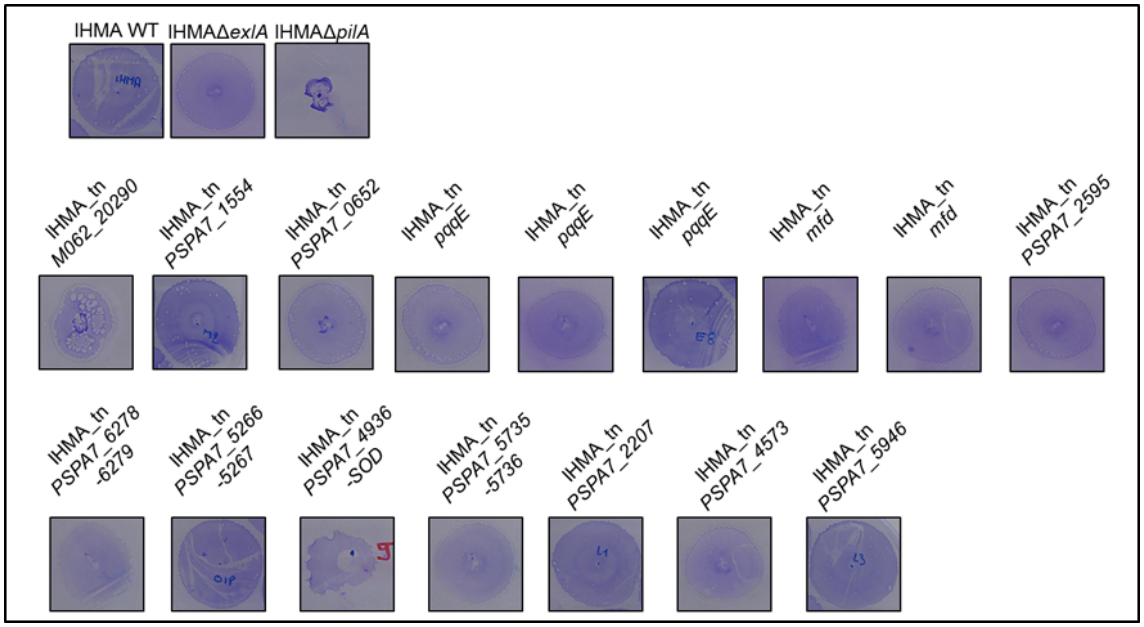

Figure 5.4. **Twitching motility of the Tn mutants.**Twitching motility of IHMA (WT), IHMAΔexlA, Transposon mutants assessed by Coomassie Blue staining of motility plates after 48 hours

Moreover, Emeline Reboud, a PhD student in our team, showed that ExlA induced the E- and VE-cadherin cleavage via the ADAM10 activity (Plos Pathogen, accepted). Interestingly, Emeline Reboud, has demonstrated that the type IV pili were not essential for the E-cadherin cleavage. It would be interesting to see whetherany of the Tn mutants have an effect on the E-cadherin cleavage. Real-time automatized microscopy using epithelial cells expressing GFP-cadherin might be used to follow the kinetic of cadherin cleavage.

Discussion on some potentially interesting mutants

Rhs-like toxin The gene annotated RS20690 (contig 35, AZPAE15042) in IHMA87 codes for "rearrangement hot spot" (rhs)-like protein. *rhsT* is an *rhs* gene found within the genomic island PAGI-9 of *P. aeruginosa*, and was first identified in a screen for genetic elements present in highly virulent PSE9 strain of *P. aeruginosa*. This gene was also found in another PA7-like strain LMG5031 but was absent in PA7, CLJ1, PAO1 and PA14, suggesting that this toxin was probably not essential for the activity of ExlA. Rhs-like toxin is a polymorphic toxin and carried a predicted RNase toxin domain. The toxin possesses an α/β fold with two conserved histidine residues. In bacterial polymorphic toxin systems, the toxin is usually exported by the T2SS or TcdB/TcaC-type secretion system of *Photorhabdus*. It was demonstrated that the expression of *rhsT* was induced upon contact with phagocytic cells. The RhsT protein is exposed to the bacteria and leads to the activation of ACS-dependent inflammasome and the production of proinflammatory cytokines IL-1β and IL-18 [322]. In other bacteria including *D. dadantii 3937* Rhs-toxin is involved in the intercellular

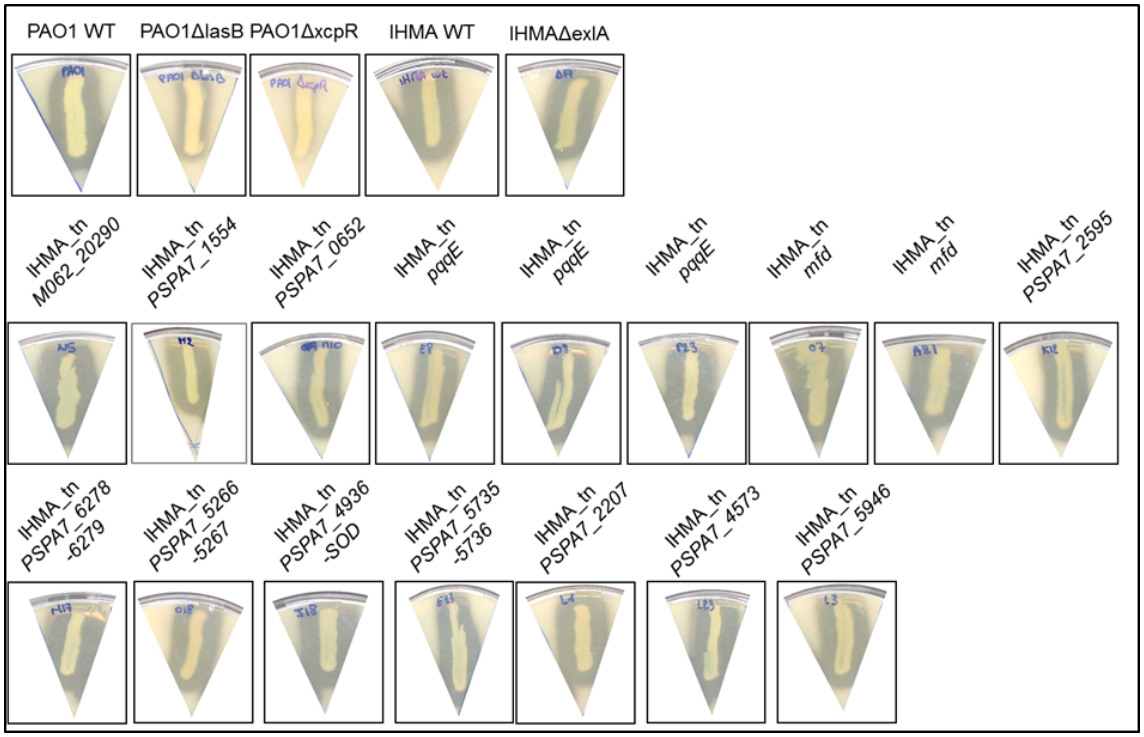

Figure 5.5. **Proteases activities of the Tn mutants.** LasB and AprA activities of Tn mutants determined by growing bacteria onto milk-agar plates for 24 hours at 37°C. As control we used PAO1, PAO1ΔlasB, PAO1ΔxcpR.

competition by the degradation of the DNA [323].

It would be interesting to see how Rhs-Toxin plays a role in the ExlA-dependent toxicity. To that aim, we could examine the production and the secretion of Rhs-toxin in IHMA and IHMAΔ*exlA*, to see the level of the expression of both toxins, and to see if they are co-regulated.

A mutant lacking ExlA is not cytotoxic towards eukaryotic cells, there is no plasma-membrane rupture, PI incorporation or E-cadherin cleavage. However, it has been shown by Emeline Reboud, using confocal microscopy that bacteria lacking ExlA were able to cross between epithelial cells and growth the bottom of the cells, like IHMA WT bacteria, but without provoking E-cadherin cleavage. We hypothesize that Rhs and ExlA cooperate to cleave cellular junctions, allow the bacteria going to the basal pole of the cells to form the pore. To assess the role of Rhs in the passage of the bacteria behind the cells, we could repeat this experiment with a Rhs mutant, and see whether the bacteria are still able to pass under the cells.

PSPA7_5946 The gene PSPA7_5946 encoded a hypothetical protein, in operon with PSPA7 _5945 which encoded a protein with a "toxin expression" (tex) motif. This motif was originally described in *B. pertussis* in an essential protein involved in expression of critical toxin genes. The *tex* gene from *P. aeruginosa* appears to play an important role in pathogenesis, being required for lung infection in a chronic disease model. We hypothesized that the *tex* gene, encoded in the same orientation

as the promoter of the transposon might play a role in the expression of ExlA. We created mutants in which either the *tex* gene was deleted or in which we inserted the pEXG2 plasmid to destabilize the whole operon.

The cytotoxicity of the *tex* mutants were assessed toward A549 cells. We did not observe significant differences compared to the IHMA WT (Figure 5.6A). In addition, no difference in ExlA secretion neither in LB condition nor in condition of infection was observed (Figure 5.6B). These results demonstrated that the Tex proteins were not involved in the ExlA dependent toxicity. However, we did not yet construct a mutant in the PSPA7_5946, in which the transposon was inserted. Moreover, downstream PSPA7_5946, is found the *gshA* gene. GshA is a Glutamate-cysteine ligase and it was shown to be required for full virulence of PA14 in *C. elegans* model [324]. It was demonstrated by a genome-wide screening of a Tn library in PA14, that *C. elegans* infected with *gshA* mutant survives better than that infected with WT bacteria. We hypothesize that GshA plays an indirect role in the ExlA-mediated cytotoxicity. The construction of the *gshA* mutant is underway. For further characterization, we would test the cytotoxicity of this mutant toward epithelial cells, and examine the ExlA secretion.

Additional experimental procedures.

Construction of the mutants. All deletion mutants were obtained by gene Splice Extention Overlap (SOE) PCRs using the primers listed in the Table 5.1. During construction of deletion mutants, the selection for *P. aeruginosa* following mating with *E.coli* was done on LB agar medium supplemented with Irgasan (25 μg/ml) and antibiotics (75 μg/ml gentamicin (Gm)).

Name	**Sequence**
IHMA-Mut-tex-F1	GGGAATTCGCGGGACAGCAGGCGAT
IHMA-Mut-tex-R1	TTGCTGCGGTTGAACGCGGC
IHMA-Mut-tex-F2	GGCCGCGTTCAACCGCAGCAAGA--GTTCCAGGAAGGCGTCGAG
IHMA-Mut-tex-R2	CCAAGCTTTCTTCTTCAGTTGCCTGGCGT
IHMA-Verif-tex-F0	GAGGACCACCAGCTGGAACAG
IHMA-Verif-tex-R0	GCTCATGGACGGCTCCGTCA

Table 5.1. **Primers used for *tex* mutant construction.**

Cell culture and Cytotoxicity assays The epithelial cell line A549 (ATCC CCL-185) was grown in RMPI 1X (Gibco Life Technology) supplemented with 10% Fetal Bovine Serum (FBS, Sigma) at 37°C, 5 % CO_2. Cells were plated in 96-well plates (50,000 cells/well) and incubated for one night. Two hours before

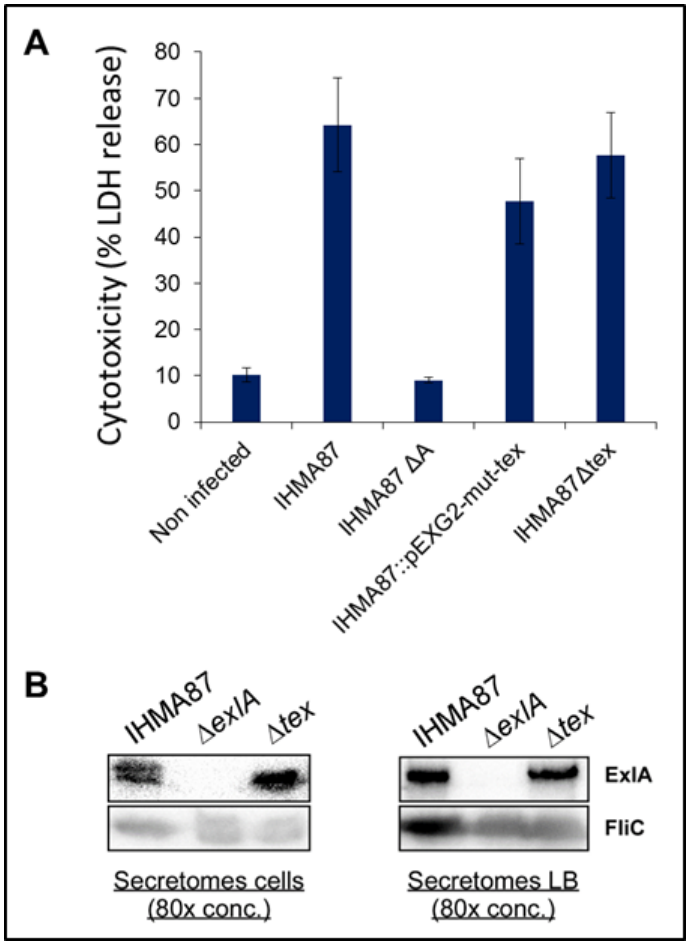

Figure 5.6. **Characterization of the *tex* mutant.** (A) Cytotoxicity of IHMAΔ*tex* mutant towards A459 cells. Cells were infected for 3 hours at MOI 10. (B) Western Blot of ExlA secretion after 3 hours of A459 cells infection or in LB conditions.

infection, RPMI medium was replaced by Endothelial growth Basal Medium (EBM-2) (LONZA Clonetics) medium. The infection was done with a multiplicity of infection (MOI) of 10 (bacteria per eukaryotic cell). The level of cytotoxicity was determined by measuring the release of lactate dehydrogenase (LDH) using the Cytotoxicity Detection Kit (Roche). Infection supernatants were sampled at 3 hours post infection. Negative controls were non-infected cells; positive controls were cells lysed by the addition of 200 μl of 2 % TritonX-100. The optical density (OD) was measured at 492 nm. The extent of cytotoxicity was calculated by determining the % cytotoxicity. For the kinetics of PI incorporation, A549 cells were plated in 96-well plate (50,000 cells/wells) in RPMI (1X) for a night. Before infection, the RPMI medium was replaced with EBM-2 medium and the cells were labeled with vital Hoechst (1 μg/ml) and PI (1 μM) followed by infection with the bacteria at an MOI of 10. Image acquisitions were made using the High Content system Array Scan (Thermo Fisher) every 15 min. Analyses were performed by measuring the fluorescence intensity of each cell using the HCS studio analysis software.

Analysis of ExlA secretion Secretion of ExlA was monitored either in liquid LB cultures or in infection conditions. A 30 ml bacterial culture, in LB at an OD600 of 1 was centrifuged at 6,000 rpm for 15 min. The supernatants (9 mL) were filtered followed by addition of 90 μl of 2 % sodium deoxycholate (DOC). After a 30 min incubation at 4 °C, 900 μl of 100 % TCA was added and the proteins were allowed to precipitate overnight at 4 °C followed by centrifugation at 15,000 g for 15 min at 4°C. Pellets were resuspended in 100 μl of Laemmli loading buffer. For the analysis of proteins during infection of cultured cells, the bacteria were added to 100 mm Petri dishes (at an MOI of 10) for 2 hours, supernatants were centrifuged and the proteins were precipitated with TCA as described above. Samples were separated by SDS-PAGE (8 %) and transferred onto polyvinyl difluoride (PVDF) membranes for Western immunobloting. Primary rabbit polyclonal antibodies were raised against either synthetic peptides of ExlA or the recombinant C-terminal of ExlA fragment were used at a 1:1,000 dilution. Anti-FliC was used at 1:1,000 dilution. Secondary antibodies were anti-rabbit-HRP and anti-mouse-HRP (Sigma). The membranes were developed by Luminata Classico Western HRP (Millipore) substrate.

Twitching motility assay Twitching motility by *P. aeruginosa* was tested out by inoculating bacteria at the interface between plastic petri dish and LB agar (10 g/L tryptone, 5 g/L yeast extract, 10 g/L NaCl, 1 % agar. After 48 hour incubation at 37°C, agar was removed and the zone of twitching was revealed following Coomassie Blue staining.

Proteolytic activity assays Elastase and alkaline protease activities were observed after plating bacteria on 'milk plates' (40 g L21 Tryptic soy agar and 10 % skim-milk from Difco) for 24 hours at 37°C.

6

Multiple *Pseudomonas* species secrete Exolysin-like toxins and provoke Caspase-1-dependent macrophage death.

Pauline Basso, Pierre Wallet, Sylvie Elsen, Emmanuelle Soleilhac, Thomas Henry, Eric Faudry, Ina Attree (Environmental Microbiology (2017))

In this Chapter I present the identification of the pathway leading to the death induced by *Pseudomonas aeruginosa* secreting ExlA using a high-throughput live-imaging method and primary Bone Marrow-Derived Macrophages (BMDMs).

The method developed here allowed to follow the kinetics of infection mediated by several bacteria toward different eukaryotic cell genotypes by the incorporation of propidium iodide (PI) in the nuclei of dead cells. We compared the kinetics of macrophage mortality provoked by two major virulence factors of *P. aeruginosa*, ExlA and T3SS secreting either ExoS or ExoU.

As mentioned previously, ShlA is the closest homolog of ExlA. Recently, it has been shown that ShlA provoked a necroptosis cell death. We demonstrated, using inhibitors (Necrostatin 1, 5) directed against kinases (RIPK1, RIPK3) of the necroptosis pathways, that in RAW macrophages the cytotoxicity mediated by ShlA and ExlA was decreased. Moreover, we showed that the cytotoxicity with both toxins (ExlA and ShlA) was diminished after a treatment with a pan-caspases-inhibitor. These results suggest that caspases are involved in the death pathway. Furthermore, we compared the kinetic of PI incorporation and morphology of cells treated with drugs leading to apoptosis (Gliotoxin) pyroptosis (LPS+Nigericin) to cells infected with IHMA (ExlA). We observed that cells infected with ExlA, undergo rounding with rapid PI incorporation, similar to the cells treated with LPS+Nig, suggesting that ExlA provoked pyroptosis.

Pyroptosis is an inflammatory cell death largely described for the pore-forming

toxins such as Streptolysin O (*S. pyogenes*), Listeriolysin O (*L. monocytogenes*) and α-hemolysin (*E. coli*) [325]. Therefore we studied the response of macrophages deficient for the Caspase-1, NLRP3 sensor and ASC adaptor proteins upon infection with strains secreting ExlA. We demonstrated that the macrophages deleted for those pyroptosis effectors were resistant to ExlA intoxication. In contrast, strain PP34 (ExoU) provoked a rapid cell death independent of the Caspase-1 pathway and PAO1 (ExoS) led to the activation of Caspase-1 through the NLRC4 inflamasomme.

We also demonstrated that the Caspase-1 is activated during infection with ExlA-secreting strains and that pro-inflammatory cytokines interleukin-1β (IL-1β) and TNF were produced and secreted. Finally, we showed that the flagellum plays a role in macrophage activation probably through its interaction with the TLR5.

Mining of microbial genomic databases revealed the presence of *exlA*-like genes in other environmental *Pseudomonas* species *P. putida*, *P. entomophila*, *P. protegens* and *P. fluorescens*. Surprisingly, we showed that these environmental species secrete ExlA-like toxins and provoke a cell lysis through the Caspase-1 pathway.

In summary, we proposed a model in which flagellated bacteria activate macrophages by interaction with TLR5 leading to the transcription of genes encoding inflammatory cytokines (IL-1β). ExlA-like toxins, by forming pores in membranes allowed the efflux of ions, especially potassium, leading to the NLRP3-inflamasomme activation. The active Caspase-1 lead to the maturation of the IL-1β and pro-inflammatory cell death. Therefore, ExlA contributes to virulence of *P. aeruginosa* clonal outliers by provoking pro-inflammatory death of macrophages.

environmental microbiology

Environmental Microbiology (2017) **00**(00), 00–00 doi:10.1111/1462-2920.13841

Multiple *Pseudomonas* species secrete exolysin-like toxins and provoke Caspase-1-dependent macrophage death

Pauline Basso,[1] Pierre Wallet,[2] Sylvie Elsen,[1] Emmanuelle Soleilhac,[3] Thomas Henry,[2] Eric Faudry[1]* and Ina Attrée[1]**

[1]*CNRS-ERL5261, INSERM, U1036, CEA, Bacterial Pathogenesis and Cellular Responses, Biosciences and Biotechnology Institute of Grenoble, University Grenoble Alpes, France.*

[2]*CIRI, Centre International de Recherche en Infectiologie, INSERM, U1111, Université Claude Bernard Lyon 1, CNRS, UMR5308, École Normale Supérieure de Lyon, Univ Lyon, Lyon, F-69007, France.*

[3]*CMBA Platform, Biosciences and Biotechnology Institute of Grenoble, University Grenoble Alpes, CEA, INSERM; Genetics & Chemogenomics, France.*

Summary

Pathogenic bacteria secrete protein toxins that provoke apoptosis or necrosis of eukaryotic cells. Here, we developed a live-imaging method, based on incorporation of a DNA-intercalating dye into membrane-damaged host cells, to study the kinetics of primary bone marrow-derived macrophages (BMDMs) mortality induced by opportunistic pathogen *Pseudomonas aeruginosa* expressing either Type III Secretion System (T3SS) toxins or the pore-forming toxin, Exolysin (ExlA). We found that ExlA promotes the activation of Caspase-1 and maturation of interleukin-1β. BMDMs deficient for Caspase-1 and Caspase-11 were resistant to ExlA-induced death. Furthermore, by using KO BMDMs, we determined that the upstream NLRP3/ASC complex leads to the Caspase-1 activation. We also demonstrated that *Pseudomonas putida* and *Pseudomonas protegens* and the *Drosophila* pathogen *Pseudomonas entomophila*, which naturally express ExlA-like toxins, are cytotoxic toward macrophages and provoke the same type of pro-inflammatory death as does ExlA$^+$ *P. aeruginosa*. These results demonstrate that ExlA-like toxins of two-partner secretion systems from diverse *Pseudomonas* species activate the NLRP3 inflammasome and provoke inflammatory pyroptotic death of macrophages.

Received 25 April, 2017; revised 2 June, 2017; accepted 19 June, 2017. For correspondence. *E-mail eric.faudry@cea.fr; Tel. 334 38 78 35 74; Fax 33 438 78 50 58 or **E-mail ina.attree-delic@cea.fr; Tel. 334 38 78 34 83.

Introduction

Toxicogenic bacterial pathogens employ variable virulence strategies to colonize host tissues and cause infections. *Pseudomonas aeruginosa* is a major Gram-negative human opportunistic pathogen responsible for diverse acute nosocomial infections (urinary tracts, lungs, burned wounds) and chronic infections in cystic fibrosis patients (Lyczak *et al.*, 2000). The virulence of most *P. aeruginosa* clinical strains is multifactorial, but greatly relies on Exotoxins transported through a molecular syringe, called Type III Secretion System (T3SS), into the host eukaryotic cell cytoplasm (Engel and Balachandran, 2009; Hauser, 2009). A direct correlation between T3SS-active strains and patients' morbidity has been pointed out in several studies (Roy-Burman *et al.*, 2001; Hauser *et al.*, 2002; Ledizet *et al.*, 2012). Recently, a new *P. aeruginosa* clade, represented by the fully sequenced PA7 strain, has been identified (www.pseudomonas.com) (Roy *et al.*, 2010; Winsor *et al.*, 2011; 2016; Elsen *et al.*, 2014; Boukerb *et al.*, 2015; Kos *et al.*, 2015; Thrane *et al.*, 2015). Members of this clade have been isolated from different human infections (burns, urinary infection and chronic lung infections) and from noninfectious environments (lakes, plants). Genetically, aside to differences in composition of islands in regions of genomic diversity (RGDs), they lack the entire T3SS due to the internal deletions of the locus and of all T3S toxin-encoded genes (Huber *et al.*, 2016; Reboud *et al.*, 2016). In the absence of T3SS, the virulence strategy of clinical isolates belonging to this group is based on a pore-forming toxin, named Exolysin (ExlA). ExlA is a secreted 172 kDa protein, exported by a two-partner secretion (TPS) system (Elsen *et al.*, 2014; Reboud *et al.*, 2016; Basso *et al.*, 2017). In contrary to classical pore-forming toxins that are secreted as soluble proteins and active (Dal Peraro and van der Goot, 2016), ExlA requires

close bacterium-host cell contact and Type IV pili for its full cytolytic activity on eukaryotic cells (Basso *et al.*, 2017). Mice infected by a clinical isolate, CLJ1, secreting high quantities of ExlA, show dramatic damages of pulmonary tissue with presence of red blood cells within the alveolar space, reminiscent of the CLJ1-infected patient status declared with hemorrhagic pneumonia (Elsen *et al.*, 2014; Bouillot *et al.*, in press).

Pore-forming toxins are important weapons of bacterial pathogens. Depending on their origin, structure and targets, they show diverse mechanisms of action and effects on eukaryotic cells (Dal Peraro and van der Goot, 2016). Some toxins, such as Anthrax Lethal Toxin and VacA, provoke apoptosis (Moayeri and Leppla, 2009; Rassow, 2011), a noninflammatory programmed cell death, whereas an increasing number of pore-forming toxins trigger necroptosis or pyroptosis (Bischofberger *et al.*, 2012). Necroptosis is a Caspase-independent programmed cell death triggering inflammation through the release of Damage-Associated Molecular Patterns (DAMPs) (Jorgensen *et al.*, 2017). On the other hand, pyroptosis (from Greek *pyro*: fire) is a highly pro-inflammatory cell death resulting from Caspase-1 or Caspase-11 (the latter corresponding to Caspase-4 and Caspase-5 in human) activation through the host cell inflammasomes, the multiprotein signalling platforms that directly or indirectly sense microbes (Storek and Monack, 2015).

Sensing components of the inflammasome, the nucleotide-binding domain and leucine-rich repeat containing gene family (NLRs), are composed of (i) a sensor domain, (ii) a NACHT nucleotide-binding domain (NBD) and (iii) a signalling/effector domain: either an acidic transactivation domain, a Pyrin domain, a baculoviral inhibitory repeat (BIR)-like domain or a CARD (Caspase Recruitment Domain) domain [reviewed in (Broz and Dixit, 2016)]. NLRC4 contains a CARD domain that directly interacts with the Pro-Caspase-1 (Miao *et al.*, 2007). In contrast, NLRP3 contains a Pyrin signalling domain that recruits the adaptor protein ASC, allowing an indirect binding to the Pro-Caspase-1 (Schroder and Tschopp, 2010). Finally, the Pro-Caspase-1 is activated by a proteolytic cleavage within the inflammasome (Broz *et al.*, 2010). Caspase-1 is the major pro-inflammatory Caspase responsible for the maturation of Interleukin-1ß (IL-1ß) into its mature cleaved form. Of note, the Toll-Like Receptor (TLR) pathway primes the NLRP3 inflammasome through the recognition of bacterial lipopolysaccharide (LPS) and flagellin inducing the expression of the pro-IL-1ß and regulating NLRP3 expression and post-translational modifications (Hajjar *et al.*, 2002; Feuillet *et al.*, 2006; Franchi *et al.*, 2007; Miao *et al.*, 2007; Bauernfeind *et al.*, 2009; Descamps *et al.*, 2012; Py *et al.*, 2013).

The inflammasome is activated by a broad spectrum of pathogens such as *P. aeruginosa*, *Salmonella enterica*, *Shigella flexneri*, *Bacillus anthracis* and *Listeria monocytogenes* (Bergsbaken *et al.*, 2009). In *P. aeruginosa*, a substantial piece of work has been done to decipher the effects of $T3SS^+$ strains, showing that the T3SS needle subunit PscF and the inner rod PscI activate the NLRC4 pathway (Miao *et al.*, 2010; Yang *et al.*, 2013; Faure *et al.*, 2014; Monlezun *et al.*, 2015) as does the flagellin upon its injection into the host cell by the T3SS (Sutterwala *et al.*, 2007; Ince *et al.*, 2015).

In this work, we examined the cell death pathway induced by a $T3SS^-$ *P. aeruginosa* strain secreting ExlA, and compared it to the effects of strains expressing either ExoU or ExoS, two major, well-described, T3SS effectors, using a high-throughput live-imaging method and primary Bone Marrow-derived Macrophages (BMDMs). We found that BMDMs lacking Caspase-1 and Caspase-11 (*Casp-1*$^{-/-}$*Casp-11*$^{-/-}$) are resistant to the cytotoxicity induced by $ExlA^+$ *P. aeruginosa*. Using *ASC*$^{-/-}$ and *NLRP3*$^{-/-}$ BMDMs, we demonstrated that Caspase-1 is activated through the NLPR3 inflammasome, leading to the release of IL1-β. Interestingly, *Pseudomonas putida*, *Pseudomonas entomophila* and *Pseudomonas protegens* also secrete ExlA-like toxins and provoke the same pyroptotic cell death as $ExlA^+$ *P. aeruginosa*.

Results

Macrophage killing by P. aeruginosa *strains using live high-content imaging*

P. aeruginosa strains are divided in three main groups depending on their host-cell destruction toolbox. Two major groups with active T3SS express either ExoS or ExoU exoenzymes to provoke cytotoxicity toward eukaryotic cell, with ExoS displaying GTPase activating and ADP-ribosyltransferase activities and ExoU being a phospholipase (Vallis *et al.*, 1999; Sato *et al.*, 2003; Hauser, 2009). On the other hand, a minor group of strains lacks T3SS but uses ExlA, a recently identified TPS pore-forming toxin (Allen *et al.*, 2014; Elsen *et al.*, 2014). To further gain knowledge on the characteristics of eukaryotic cell death triggered by ExlA, we developed a robust, reproducible high-throughput method to assess the kinetics of bacteria-induced macrophage death by live cellular imaging using a high-content (HC) microscope system. The timeline of a representative experiment is shown in Fig. 1A. Bacteria and macrophages were co-incubated in multiwell plates in the presence of two nuclear dyes, the membrane-permeable vital-Hoechst and the membrane-impermeable, propidium iodide (PI). In each well, images from four non-contiguous fields were taken in bright field and in fluorescence every 30 min to detect morphological changes and PI entry, respectively (Fig. 1B). PI entry and labelling of the nucleus only occur upon membrane permeabilization, which is the gold criterion of cell death (Galluzzi

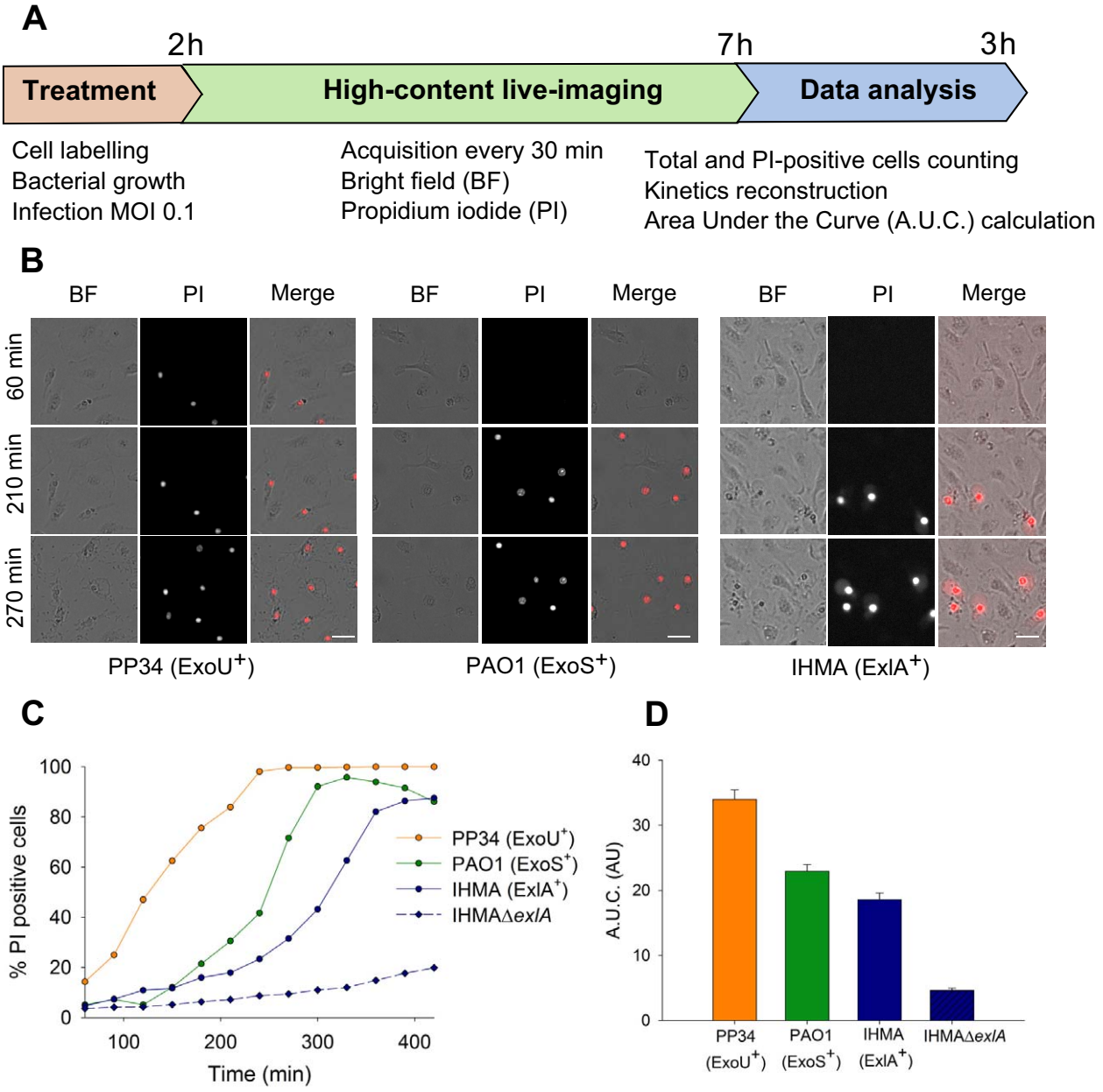

Fig. 1. Quantification of bacteria-induced cell death by high-content live-imaging.
A. Schematic workflow of the quantification of PI-incorporation into eukaryotic cells incubated with cytotoxic bacteria using high-content live imaging. Major steps are indicated, as well as time course of each step.
B. Images of BMDMs incubated at a MOI of 0.1 with *P. aeruginosa* strains: PP34 (ExoU$^+$), PAO1 (ExoS$^+$) and IHMA (ExlA$^+$). Bright field, PI fluorescence and merge images are shown at 60 min, 210 min and 270 min postinfection. Scale bars correspond to 10 μm.
C. Kinetics of PI incorporation into BMDMs incubated at a MOI of 0.1 with PP34 (ExoU$^+$), PAO1 (ExoS$^+$), IHMA (ExlA$^+$) and IHMAΔ*exlA*. Percentages of PI positive cells were calculated for each time point over 400 min period of incubation with the bacteria.
D. Areas under the curves (A.U.C.) were calculated for each curve presented in panel C using SigmaPlot macro as described in the Materials and Methods.

et al., 2015). The percentage of PI positive cells was automatically calculated and reached a plateau commonly after 3 to 7 h of incubation depending on used strains. Three *P. aeruginosa* strains harbouring different types of toxins were tested. PAO1 and PP34 both possess active T3SS and express either ExoS (PAO1) or ExoU (PP34) (Table S1). The IHMA strain secretes the pore-forming toxin ExlA (Elsen *et al.*, 2014; Reboud *et al.*, 2016; Basso *et al.*, 2017). The three strains provoked incorporation of PI into BMDMs (Fig. 1B and C), in accordance to their published cytotoxic activities toward macrophages, where PAO1 strain lysis macrophages through PopB/D translocon

insertion into target plasma membrane (Fauvarque *et al.*, 2002; Berthelot *et al.*, Groupe d'Etudes des Septicémies à *Pseudomonas aeruginosa*, 2003; Reboud *et al.*, 2016; Basso *et al.*, 2017). The area under the curves (A.U.C.) of the percentage of PI positive cells kinetics calculated for each condition allowed relative comparison between strains (Fig. 1D). We also checked that the method reflects the rates of target membrane destruction obtained by the standard colorimetric assay based on the activity of the lactate dehydrogenase (LDH) released from the cytosol of cells with damaged membranes. To that aim, BMDMs were incubated with the three strains and, at different time-points postinfection (p.i), supernatants were collected for LDH assay and images were taken in parallel on the ArrayScan microscope. As presented in Supporting Information Fig. S1, the percentage of PI-positive cells and LDH release were very similar at the different time-points p.i. for all strains. Beyond reducing reagents cost, this HC method is almost an homogenous assay which permits to follow bacteria-induced cytotoxicity in real time without sample pipetting contrary to LDH quantification. Furthermore, it allows an extended recording of cell infection because only few samples can be successively taken from the same well of a 96-well plate in the case of LDH assays.

The live time-lapse imaging of cell death showed that selected strains exhibit different kinetics of cytotoxicity, reaching the plateau at different times p.i. The ExoU-producing strain (PP34) was the most aggressive, with 50% of dead cells detected after 120 min p.i. followed by ExoS-expressing PAO1 strain (50% reached in 240 min p.i.). The ExlA-dependent cytotoxicity was assessed using the IHMA isolate (Reboud *et al.*, 2016; Basso *et al.*, 2017) and its isogenic mutant IHMAΔ*exlA*. This strain provoked a somewhat slower cytotoxic effects on macrophages than the ExoS$^+$ strain: 50% of PI-positive cells being reached at 300 min p.i. The isogenic mutant lacking ExlA (IHMA-*exlA*) exhibited very low cytotoxicity on macrophages, with less than 20% dead cells after 420 min p.i., clearly demonstrating the importance of the toxin in triggering the death of primary macrophages. Overall, HC-live imaging of *P. aeruginosa*-induced cell death allows measurement of bacterial cytotoxicity on macrophages and revealed differences in kinetics between strains.

ExlA and ShlA induce Caspase-dependent death in primary macrophages

We previously showed that ExlA is a pore-forming toxin (PFT) (Basso *et al.*, 2017). It has been established that some PFTs cause pro-inflammatory cell death, either pyroptosis or necroptosis (Bischofberger *et al.*, 2012). ExlA shares 33% identity with the *Serratia marcescens* toxin ShlA which leads to necroptosis in different macrophage cell lines, including RAW 264.7 (González-Juarbe *et al.*, 2015). However, some immortalized macrophages carry defects in the cell death pathways; notably the RAW 264.7 macrophage cell line does not express ASC, a central player in Caspase-1-mediated pyroptosis (Pelegrin *et al.*, 2008). Therefore, we reexamined cell death pathways initiated by ShlA and ExlA in RAW 264.7 and in primary macrophages BMDMs. We compared the macrophage cytotoxicity induced by *P. aeruginosa* strains and the ShlA-positive *S. marcescens* strain Db10 in presence of the necroptosis-inhibitors necrostatin-1 and necrostatin-5, respectively targeting Receptor-Interacting serine/threonine-Protein Kinase 1 (RIPK1) and RIPK3, key components of the necroptosis pathway (Jorgensen *et al.*, 2017). As reported, both inhibitors diminished Db10-induced cytotoxicity toward RAW 264.7 macrophages. Notably, these drugs protected RAW 264.7 macrophages from the ExlA-dependent cytotoxicity (Fig. 2A). Conversely, neither necrostatin-1 nor necrostatin-5 showed a significant inhibitory effect on RAW 264.7 death rate provoked by PP34 and PAO1. Surprisingly, when using BMDMs, necroptosis inhibitors showed no significant effect on Db10 (ShlA$^+$) and IHMA (ExlA$^+$) cytotoxicity (Fig. 2B), suggesting that alternative death pathways are activated and that necroptosis is not the predominant pathway induced in primary macrophages. Furthermore, the kinetics of BMDM death induced by Db10 (ShlA$^+$) and IHMA (ExlA$^+$) were delayed in presence of the pan-Caspase inhibitor Z-VAD-FMK (Fig. 2B), further pointing out to other host pathways involved in macrophage cell death. Taken together, these results indicate that Caspase-dependent death pathways, rather than necroptosis, are the main contributors to primary macrophages death induced by *S. marcescens* and *P. aeruginosa* ExlA$^+$ strains.

ExlA induces a Caspase-1/Caspase-11-dependent pyroptotic cell death

The main cell death pathways involving Caspase proteins are apoptosis and pyroptosis. To gain insights into the type of cell death caused by ExlA, we compared morphological changes and PI entry occurring upon incubation with bacteria and upon stimulation by known inducers of apoptosis and pyroptosis (Fig. 3A). Indeed, BMDM cells displayed 'swelling' and PI entry upon incubation with the IHMA (ExlA$^+$) strain that is reminiscent of the signs of pyroptosis induced by treatment consisting in LPS-priming followed by addition of the microbial toxin Nigericin known to induce Caspase-1 activation (LPS + Nig) (Cheneval *et al.*, 1998). On the contrary, gliotoxin, known to induce apoptosis (Stanzani, 2005; Pardo *et al.*, 2006), provoked a severe cell shrinkage with delayed PI entry. Thus, the IHMA (ExlA$^+$) strain clearly does not induce apoptosis of macrophages. To further ascertain this conclusion, we took advantage of BMDMs isolated from mice with different

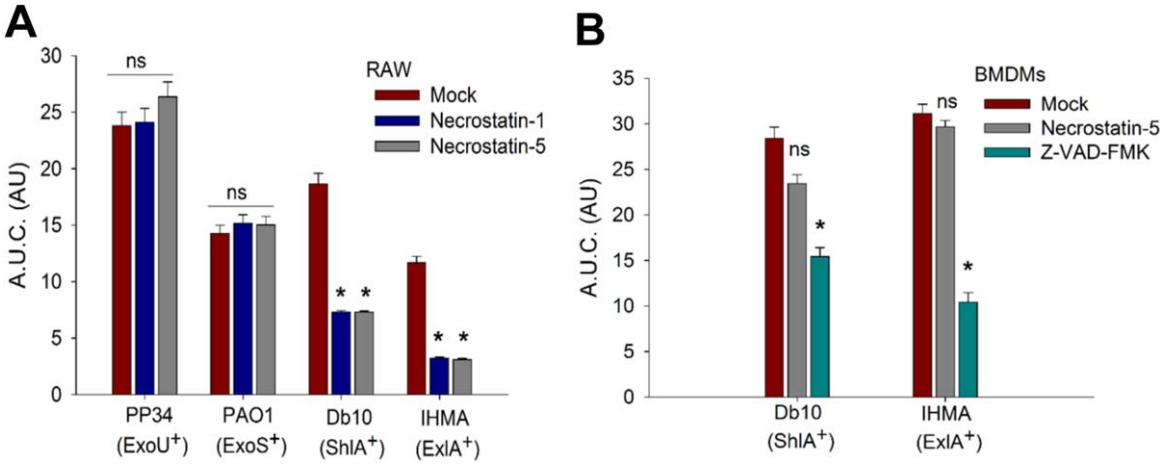

Fig. 2. Pharmacological inhibition of ShlA- and ExlA-induced macrophage cell death.
A. A.U.C. of PI incorporation kinetics in RAW 264.7 macrophages incubated at a MOI of 0.1 with PP34 (ExoU$^+$), PAO1 (ExoS$^+$), IHMA (ExlA$^+$) and *S. marcescens* Db10 (ShlA$^+$) strains, after 1 h-pretreatment with Necrostatin-1 (100 μM) or Necrostatin-5 (50 μM). One-way ANOVA was used to compare Necrostatin treatments to the mock control. Stars indicate statistically significant differences with $p < 0.05$.
B. A.U.C. of PI incorporation kinetics in BMDMs incubated at MOI 0.1 with Db10 (ShlA$^+$) or IHMA (ExlA$^+$) after 1 h of pretreatment with Necrostatin-5 (50 μM) or Z-VAD-FMK (10 μM). One-way ANOVA was used to compare treatments to the mock control. Stars indicate statistically significant differences with $p < 0.05$ and ns = nonsignificant.

genetic knock-outs (KO; $^{-/-}$) in components of known cell death pathways. We incubated wild-type and BMDMs deficient for pyroptotic caspases, that is, Caspase-1 and Caspase-11 (*Casp-1*$^{-/-}$*Casp-11*$^{-/-}$), with the selected strains and evaluated the kinetics of bacteria-induced cytotoxicity by live-imaging (Fig. 3B). As positive control, we used the LPS + Nig treatment to induce pyroptosis (Mariathasan *et al.*, 2006). As reported, *Casp-1*$^{-/-}$*Casp-11*$^{-/-}$BMDMs were largely resistant to LPS + Nig treatment (Sagulenko *et al.*, 2013). The ExoU$^+$ strain provoked rapid BMDMs death independently of macrophages' genetic background, the same PI incorporation kinetics as the wild-type cells, suggesting that the phospholipase activity of ExoU (Sato and Frank, 2004) could kill macrophages in a Caspase-1/Caspase-11 independent manner. On the contrary, *Casp-1*$^{-/-}$*Casp-11*$^{-/-}$ macrophages resisted to both PAO1- and IHMA-dependent cytotoxicity. To quantify the global inhibition of macrophage death, the A.U.C. of PI incorporation kinetics were calculated and compared. Indeed, the cytotoxicity toward *Casp-1*$^{-/-}$*Casp-11*$^{-/-}$ BMDMs was reduced by 80% and 70% comparing to the wild-type macrophages for PAO1 and IHMA strains, respectively, while there was no significant difference for ExoU-positive strain. The Db10 ShlA$^+$ strain displayed only 40% of cytotoxicity reduction when calculated from A.U.C., and the levels of PI-positive cells were equal with both BMDM types 300 min p.i. (Fig. 3B). Furthermore, cell infection was performed in the presence of extracellular glycine, which is described to reduce macrophage death rate in the case of Caspase-dependent pyroptosis through a nonspecific blockage of ions fluxes (Fink and Cookson, 2006; Bergsbaken *et al.*, 2009). Comparison of calculated A.U.C. clearly shows a significant reduction of cytotoxicity in the presence of glycine in the case of LPS + Nig (positive control), PAO1, IHMA and Db10 but not PP34 cell infection (Fig. 3C).

Altogether, the results obtained here indicate that ExlA produced by the IHMA strain induces a Caspase-1/Caspase-11 pyroptotic cell death.

ExlA induces Caspase-1 activation and IL-1ß release

To confirm the induction of pyroptosis by the IHMA ExlA$^+$ strain, Caspase-1 activation was evaluated by immunoblotting using cellular lysates and supernatants recovered following incubation of BMDMs with bacteria. Anti-Caspase-1 antibodies recognize two forms of the protein: the nonactivated pro-Caspase-1 (47 kDa) and the cleaved, mature form of 10 kDa (Caspase-1 p10). As shown in Fig. 4A, a decrease of the intracellular pro-Caspase-1 amount along with the accumulation of the p10 fragment in the supernatants could be readily observed when macrophages were treated by LPS + Nig, as well as in samples from PP34, PAO1 and IHMA incubations. On the contrary, no release of the activated p-10 fragment was observed upon incubation with the Db10 (ShlA$^+$) strain and the level of intracellular pro-Caspase-1 remained similar to the one of the untreated cells. Caspase-1 activation results in the cleavage and release of the pro-inflammatory cytokine Interleukin-1 β, IL-1β. Therefore, IL-1β release from wild-type and *Casp-1*$^{-/-}$*Casp-11*$^{-/-}$ BMDM was quantified by ELISA (Fig. 4B). Comparing to *Casp-1*$^{-/-}$*Casp-11*$^{-/-}$

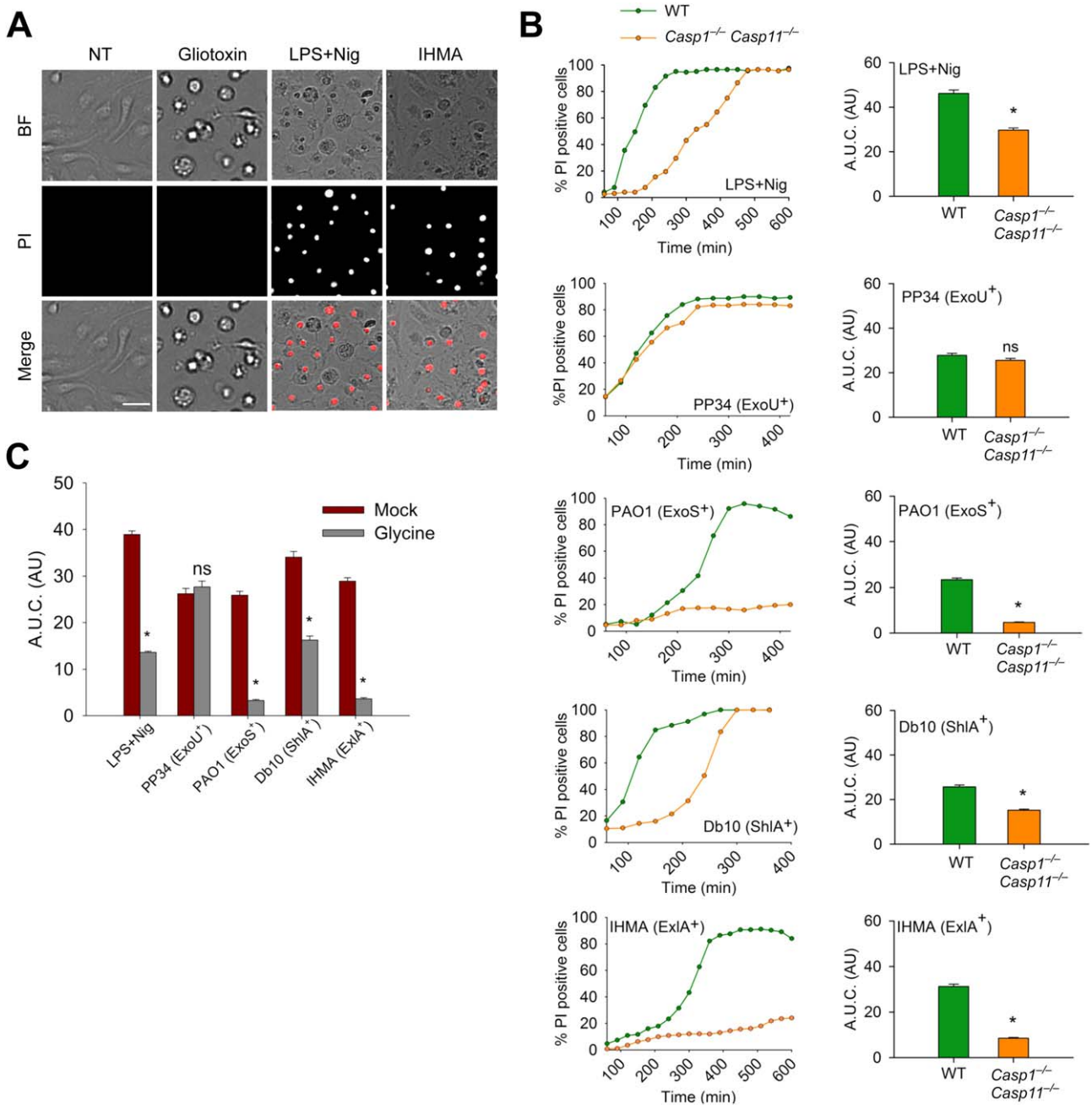

Fig. 3. Pyroptotic Caspase-1/Caspase-11-dependent cell death is induced by ExlA$^+$ *P. aeruginosa*.
A. Images of WT BMDMs non treated (NT) or incubated with LPS + Nig or Gliotoxin, or incubated with IHMA (ExlA$^+$) at a MOI of 0.1 for 210 min. Bright field (BF), PI fluorescence and merge images are shown. Bars correspond to 10 μm.
B. Kinetics of PI incorporation in wild-type (WT) BMDMs compared to Caspase-1/Caspase-11 KO BMDMs (*Casp1*$^{-/-}$*Casp11*$^{-/-}$). Cells were incubated at a MOI of 0.1 with PP34 (ExoU$^+$), PAO1 (ExoS$^+$), IHMA (ExlA$^+$) and Db10 (ShlA$^+$). As positive control of pyroptosis, cells were treated with LPS (10 ng/mL) for 3 h and then Nig (10 μM) for 1 h. For each condition, the A.U.C. was calculated. Statistical analysis were done using Mann–Whitney test. Stars indicate statistically significant differences with $p < 0.05$.
C. Infection of wild-type BMDMs in the presence of extracellular glycine. WT BMDMs were incubated at a MOI of 0.1 with PP34 (ExoU$^+$), PAO1 (ExoS$^+$), IHMA (ExlA$^+$) and Db10 (ShlA$^+$) in the presence or absence of glycine (5 mM) and the A.U.C. of PI incorporation were calculated at the end of each kinetic and compared with one-way ANOVA.

BMDMs, large amounts of IL-1β were detected in the supernatants of wild-type cells upon incubation with LPS + Nig, PP34, PAO1 and IHMA, but not with Db10. The absence of substantial IL-1β release with the IHMA strain devoid of ExlA (IHMA*ΔexlA)* revealed the direct role of ExlA in pro-inflammatory signal activation. To gain

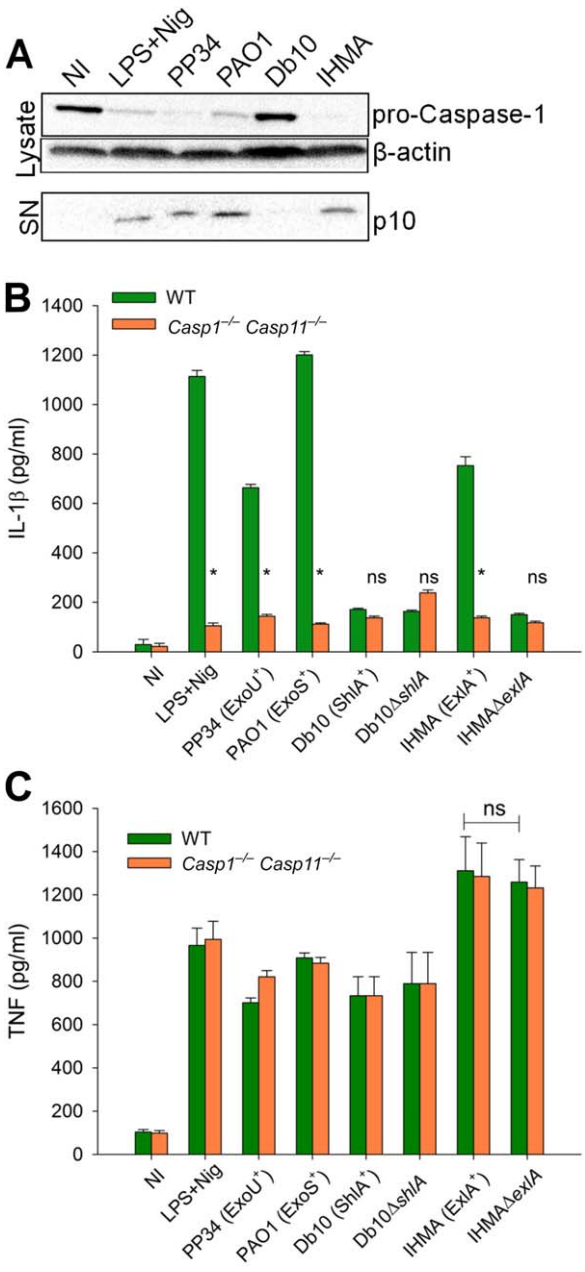

Fig. 4. Caspase-1 is activated in ExlA-induced cell death and provokes IL-1ß release.
A. Western blot analysis of Caspase-1 activation. Total cell lysates and infection supernatants (SN) were prepared from WT BMDMs, noninfected (NI), incubated with LPS + Nig (positive control) or incubated with PP34 (ExoU$^+$), PAO1 (ExoS$^+$), Db10 (ShlA$^+$) and IHMA (ExlA$^+$) at a MOI of 0.1 for 210 min. Caspase-1 p10 corresponds to one subunit of the activated form of Caspase-1.
B. Quantification of IL-1β by ELISA. Levels of IL-1ß were measured in supernatants of WT and *Casp1*$^{-/-}$*Casp11*$^{-/-}$ BMDMs treated for 3 h with LPS+Nig, or incubated for 6 h with PP34 (ExoU$^+$), PAO1 (ExoS$^+$), Db10 (ShlA$^+$), Db10Δ*shlA*, IHMA (ExlA$^+$) and IHMAΔ*exlA*.
C. Quantification of TNF by ELISA. Levels of TNF were measured in supernatants of WT and *Casp1*$^{-/-}$*Casp11*$^{-/-}$ BMDMs treated for 3 h with LPS+Nig, or incubated for 4 h with PP34 (ExoU$^+$), PAO1 (ExoS$^+$), Db10 (ShlA$^+$), Db10Δ*shlA*, IHMA (ExlA$^+$) and IHMAΔ*exlA*.

information on the specificity of pro-inflammatory cytokine release, we measured TNF release in both types of BMDMs by ELISA (Fig. 4C). The production of TNF is known to be induced through the TLR/NFκB pathway (Kawai and Akira, 2007), which is notably induced by LPS and flagellin (Hajjar *et al*., 2002; Feuillet *et al*., 2006; Franchi *et al*., 2007; Miao *et al*., 2007; Descamps *et al*., 2012). Contrary to IL-1β, TNF was detected in similar levels following infection by all tested strains, with slightly higher levels detected upon macrophages incubation with IHMA strains with or without ExlA. Therefore, TNF was induced by the bacteria independently of their cytotoxicity and of the presence/absence of different types of toxins. Furthermore, TNF levels were equal in wild-type and Caspase-1 KO BMDMs. These results show that all tested strains here have similar capacity to 'prime' macrophages through the TLR pathway and that the detection of IL-1 β in the macrophage supernatant was directly linked to Caspase-1 activation by ExlA.

Together, these results demonstrate that *P. aeruginosa* secreting ExlA specifically induces an inflammatory-Caspase-1-dependent macrophage death, along with the release of IL-1β.

NLRP3 sensor is required for ExlA-induced pyroptosis

Several upstream sensors, and their associated inflammasomes, induce Caspase-1 activation (Storek and Monack, 2015). The NLRP3 pathway can be triggered by pore-forming toxins and is fully dependent on ASC for Caspase-1 activation while the NLRC4 pathway, which is activated by T3SS components delivered into the cytosol, is ASC-independent (Broz *et al*., 2010; Case and Roy, 2011; Zhao and Shao, 2015). Indeed, upon incubation with the T3SS$^+$ PAO1 strain known to activate the NLRC4 pathway, no significant delay of cell death kinetics of *ASC*$^{-/-}$ and *NLRP3*$^{-/-}$ BMDMs compared to wild-type BMDMs was observed (Fig. 5A). Strikingly, the macrophages deficient for ASC or NLRP3 were resistant to the infection by the IHMA strain, showing that the NLRP3 pathway was triggered by ExlA (Fig. 5A). The AIM2-inflammasome is dedicated to the detection of microbial DNA and was shown to poorly contribute to inflammasome activation by *P. aeruginosa* T3SS$^+$ strains (Jabir *et al*., 2015; Pang *et al*., 2015). We tested the *AIM2*$^{-/-}$ cells and showed here that they were similarly sensitive to both ExoS$^+$ and ExlA$^+$ strains, indicating that the new ExlA$^+$ strain does not differ, on this point, from the classical strains.

Potassium efflux is a central signalling event activating the NLRP3 response and the reduction of cell death in the presence of extracellular potassium is a hallmark of the NLRP3 pyroptotic pathway (Pétrilli *et al*., 2007; Muñoz-Planillo *et al*., 2013). Therefore, BMDMs incubation with the different bacterial strains was performed in the presence of 130 mM potassium (Fig. 5B). Under these conditions, a decrease of cell death rate was observed for the IHMA strain but not for

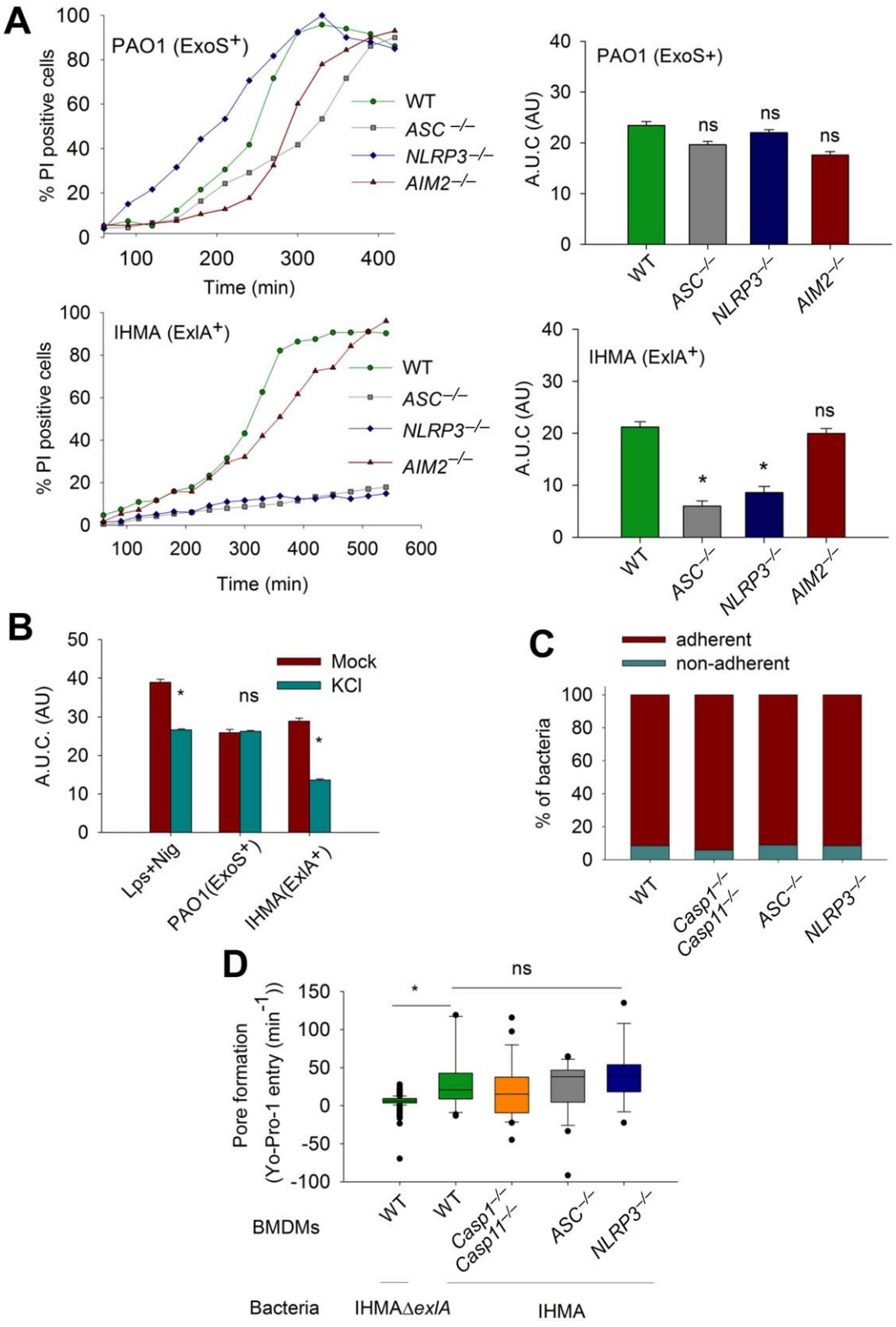
A
PAO1 (ExoS+)
% PI positive cells
Time (min)
WT
ASC −/−
NLRP3−/−
AIM2−/−
PAO1 (ExoS+)
A.U.C (AU)
ns
IHMA (ExlA+)
*
B
A.U.C. (AU)
Mock
KCl
Lps+Nig
PAO1(ExoS+)
IHMA(ExlA+)
C
adherent
non-adherent
% of bacteria
Casp1−/− Casp11−/−
D
Pore formation (Yo-Pro-1 entry (min-1))
BMDMs
Bacteria
IHMAΔexlA
IHMA

Fig. 5. Inflammasome-mediated cell death is NLRP3-dependent during IHMA infection.
A. Kinetics of PI incorporation in WT, ASC$^{-/-}$ and NLRP3$^{-/-}$ BMDMs. BMDMs were incubated with PAO1 (ExoS^{+}) and IHMA (ExlA^{+}). A.U.C. were calculated and used in One-way ANOVA with Dunn's *post hoc* test to compare *ASC*$^{-/-}$ and *NLRP3*$^{-/-}$ to WT BMDMs. Stars indicate statistically significant differences between KO and WT BMDMs with $p < 0.05$.
B. A.U.C. of PI incorporation for WT BMDMs treated with KCl at 130 mM and then incubated at MOI of 0.1 with PAO1 (ExoS^{+}) or IHMA (ExlA^{+}). LPS + Nigericin was used as positive control. Statistical analyses were done using ANOVA test. Stars indicate statistically significant differences between KCl and Mock treatments with $p < 0.05$. ns = nonsignificant.
C. Adhesion assay of IHMA to WT, *Casp1*$^{-/-}$*Casp11*$^{-/-}$, *ASC*$^{-/-}$ and *NLRP3*$^{-/-}$ BMDMs. BMDMs were incubated with IHMA at a MOI of 0.1 for 30 min and CFU were counted in supernatants and cells fractions. No significant difference was found by one-way ANOVA.
D. Pore formation by ExlA in WT, *Casp1*$^{-/-}$*Casp11*$^{-/-}$, *ASC*$^{-/-}$ and *NLRP3*$^{-/-}$ BMDMs. BMDMs were incubated at a MOI of 0.1 for 3 h with IHMA and IHMAΔ*exlA*. YoPro1 entry in cytoplasm was quantified by HC microscopy. Fluorescence slopes were calculated from 100 different cells. Statistical analyses using One-way ANOVA with Dunn's *post hoc* test were performed. The star indicates a statistically significant difference between IHMA and IHMAΔ*exlA* groups. No significant difference was found between the different BMDMs incubated with IHMA.

the PAO1 strain. This lack of inhibition of the PAO1-induced cytotoxicity is expected as this strain harbours an active T3SS, which is known to induce NLRC4 activation. On the other hand, the inhibition observed with the IHMA strain further shows that it triggers the NLRP3 pathway.

In order to exclude that the observed 'resistance' phenotypes of the KO BMDMs were due to an impairment of bacterial adhesion or ExlA activity *per se*, these features were compared in wild-type and KO macrophages. Bacterial adhesion was quantified by enumerating bacteria bound to the BMDMs and in the supernatant, as previously described (Basso *et al*., 2017). As expected, bacterial adhesion to wild-type and KO BMDMs was indistinguishable (Fig. 5C). We previously showed that the formation of ExlA pores in host plasma membranes can be detected by monitoring the early incorporation of YoPro-1 into the cell cytoplasm that occurs before incorporation of PI into cell nuclei (Basso *et al*., 2017). To ascertain that the membranes of macrophages KO for inflammasome components are not resistant to the formation of the ExlA pores *per se*, we measured the incorporation of YoPro-1 in wild-type, *Casp-1*$^{-/-}$*Casp-11*$^{-/-}$, *ASC*$^{-/-}$ and *NLRP3*$^{-/-}$ BMDMs by live-cell imaging of YoPro-1 incorporation during incubation with IHMA (Basso *et al*., 2017). Contrary to PI, the YoPro-1 dye displays a high affinity for cytoplasmic nucleic acids and can therefore be used to detect early perturbation and pore formation in the plasma membrane before its global rupture. As presented in Fig. 5D no significant difference in the kinetics of YoPro-1 incorporation into the cytoplasm could be detected for the different cell types, indicating that ExlA pores are readily formed in the mutants BMDMs. Taken together, these results show that ExlA pores are detected by NLRP3 probably through potassium effluxes, triggering pyroptosis.

Role of bacterial flagella in ExlA-induced pro-inflammatory signalling

In addition to detection of flagellin by TLR5 and subsequent activation of TLR pathways (Feuillet *et al*., 2006; Franchi *et al*., 2007; Miao *et al*., 2007; Descamps *et al*., 2012), flagellar motility by *P. aeruginosa* has been shown to be essential for high levels of IL-1β production (Patankar *et al*., 2013). As ExlA^{+} strains possess variable flagellum-related swimming capacities (Reboud *et al*., 2016), we tested the flagellin-deficient strain IHMAΔ*fliC* for cytotoxicity, IL-1β and TNF release and Caspase-1 maturation (Fig. 6). Although IHMAΔ*fliC* induced the same levels of pyroptosis as the wild-type strain, the levels of IL-1β and TNF production were significantly lower for the strain devoid of flagellin than for the WT strain (Fig. 6A–C). These results show that IL-1β release from BMDMs depends on a priming event that relies at least partially on bacterial flagellin, in addition to inflammasome activation through ExlA pore. The two most studied ExlA^{+} strains, PA7 and CLJ1 (Table 1), were also included in these experiments. PA7 is a fully sequenced *exlA*$^{+}$ T3SS-negative strain that is avirulent in a mouse model of pneumonia, certainly due to low ExlA secretion (Roy *et al*., 2010; Elsen *et al*., 2014; Reboud *et al*., 2016). CLJ1 is a recent hyper-virulent clinical isolate secreting high levels of ExlA, but, in contrary to PA7 and CLJ1, lacking the flagellum (Elsen *et al*., 2014; Reboud *et al*., 2016). As expected, CLJ1 induced high levels of pyroptosis, but lower levels of IL-1 β and TNF, whereas PA7 was less efficient both in promoting pyroptosis and release of IL-1β and TNF, in agreement with the results obtained with IHMA strains. All strains induced different levels of Caspase-1 cleavage. Therefore, the IL-1β release results from the integration of flagellin recognition by TLR5 and ExlA-induced inflammasome activation.

Exolysin-like toxins of different Pseudomonas *species induce BMDM death*

The initial BLAST queries identified Exolysin as a member of the TPS hemagglutinin/hemolysin family, sharing 33% of amino acid identity with ShlA (Elsen *et al*., 2014). To extend this search and possibly find other ExlA orthologues, we explored bacterial genomes using the *exlA* sequence as bait by Reciprocal Best BLAST (Ward and Moreno-Hagelsieb, 2014) from the *Pseudomonas* Genome Database [www.pseudomonas.com (Winsor *et al*., 2011; 2016)]. Interestingly, *exlA*-like sequences were found in different

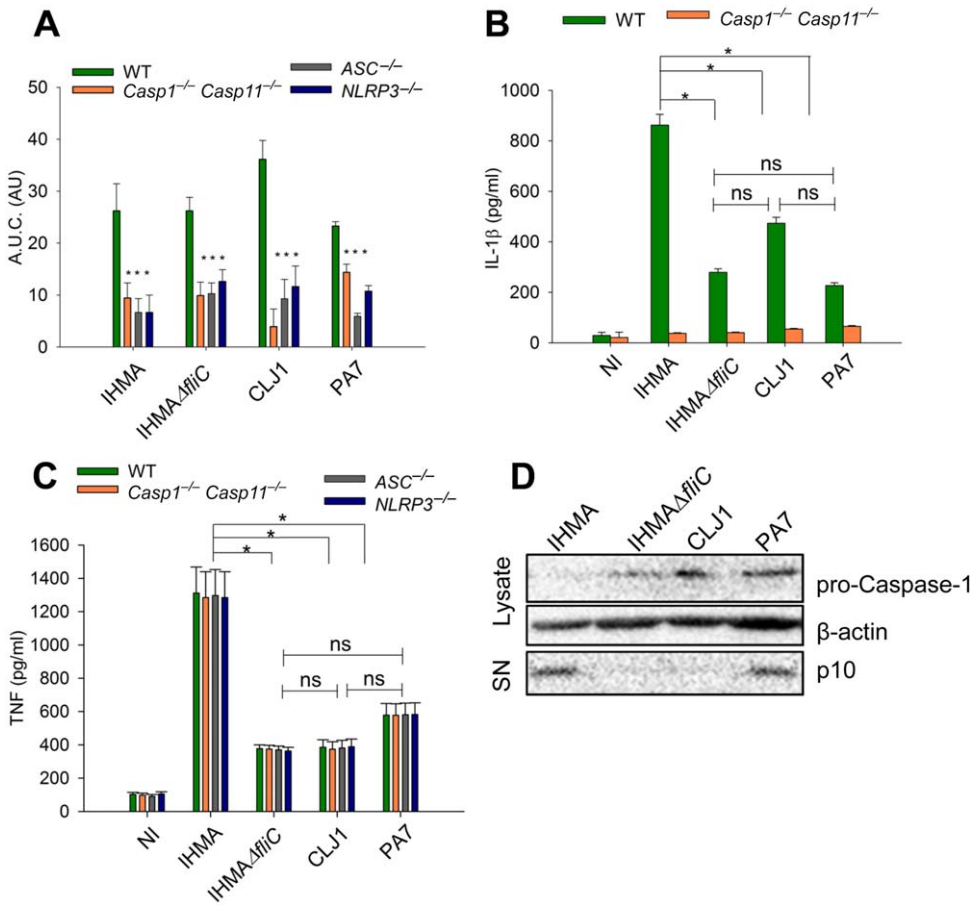

Fig. 6. Role of flagellum in pyroptosis and inflammatory response.
A. WT, *Casp1*$^{-/-}$*Casp11*$^{-/-}$, *ASC*$^{-/-}$ and *NLRP3*$^{-/-}$ BMDMs were incubated with different T3SS-negative, *exlA*+ *P. aeruginosa* strains at a MOI of 0.1. A.U.C. from kinetics of PI incorporation were calculated and used in ANOVA tests to compare KO to WT BMDMs. Stars indicate statistically significant differences with $p < 0.05$.
B. Quantification of IL-1β by ELISA. Levels of IL-1ß were measured in supernatants of WT and *Casp1*$^{-/-}$*Casp11*$^{-/-}$ BMDMs treated for 3 h with LPS+Nig, or incubated with *P. aeruginosa* strains as indicated.
C. Quantification of TNF by ELISA. Levels of TNF were measured in supernatants of WT and *Casp1*$^{-/-}$*Casp11*$^{-/-}$, *ASC*$^{-/-}$ and *NLRP3*$^{-/-}$ BMDMs, noninfected (NI), treated for 3 h with LPS+Nig, or incubated with strains as indicated.
D. Western blot analysis of Caspase-1 activation. Total cell lysates and infection supernatants (SN) were prepared from WT BMDMs incubated with strains as indicated.

Pseudomonas species, notably in *P. putida*, *P. fluorescens, P. protegens* and *P. entomophila* (Fig. 7A). The closest orthologues of *P. aeruginosa* ExlA (59% identity) are found in the plant-associated bacteria *P. fluorescens* A506 (Stockwell *et al.*, 2013) and *P. protegens* CHA0 that represent highly diverse groups in *Pseudomonas* genus, as reported (Silby *et al.*, 2009; Garrido-Sanz *et al.*, 2016). In all cases, *exlB*-like gene encoding the TpsB outer membrane partner of the TPS system, was located adjacent to *exlA*. As previously reported (Reboud *et al.*, 2016), T3SS or ExlA are mutually exclusive in all *P. aeruginosa* strains sequenced to date. In other *Pseudomonas* species in which *exlA* was present T3SS was also absent, except for the plant-protective biological control agent *P. fluorescens* A506 (Wilson and Lindow, 1994; Loper *et al.*, 2012).

To gain insight into their pathogenicity repertoire we wondered whether selected strains of different *Pseudomonas* species harboring *exlA*-like sequences were able to provoke macrophage death. To that aim, BMDMs were incubated with selected strains of *P. entomophila*, *P. fluorescens*, *P. protegens* and *P. putida* and the cytotoxicity was monitored by live-cell imaging of PI incorporation (Fig. 7B). Three strains, *P. entomophila* L48, *P. protegens* CHA0 and *P. putida* KT2440, showed highly toxic phenotype on macrophages reaching 100% PI positive cells at 240, 210 and 270 min p.i., respectively. The engineered mutants in which *exlA*-like genes were disrupted (see Materials and Methods) lost the ability to kill macrophages as assayed by PI incorporation (Fig. 7B). These results strongly suggest that those selected *Pseudomonas* species synthetize and

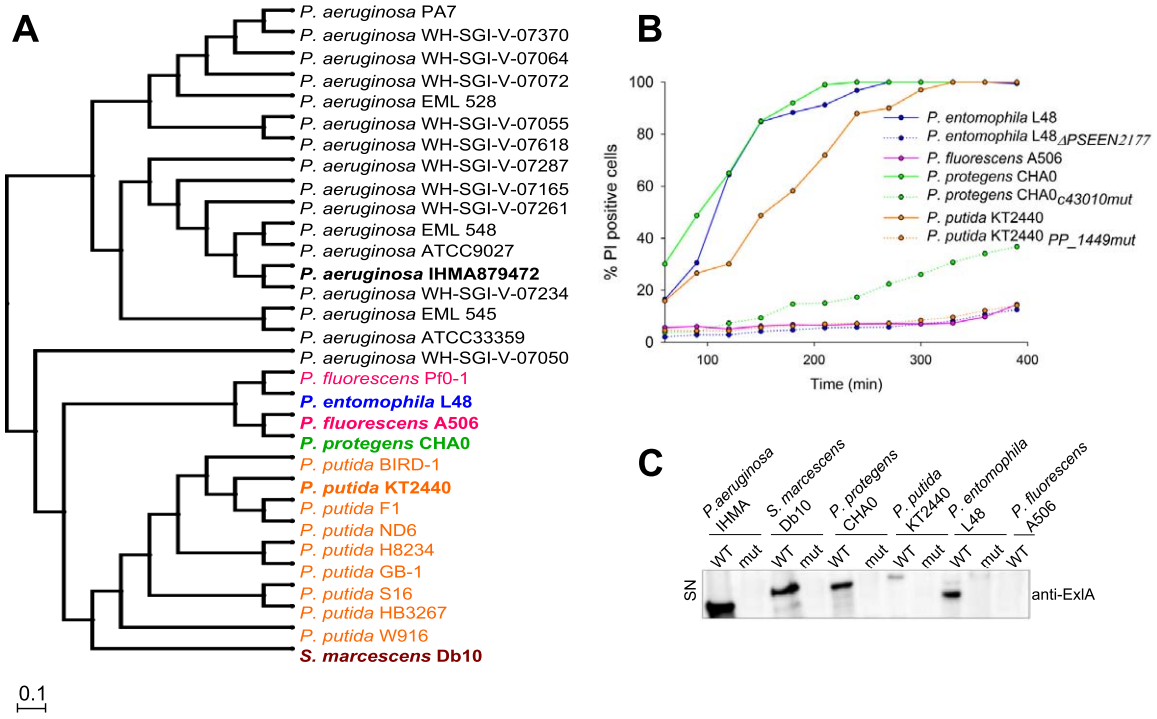

Fig. 7. ExlA-like toxins present through the *Pseudomonas* species are responsible for BMDM death.
A. Phylogram of ExlA-like proteins in several *Pseudomonas* species. ExlA-like sequences were retrieved by BLAST and aligned using ClustalW. The tree was constructed using the neighbor-joining method. The percentages of identity were calculated by pairwise comparison using CLC software (CLC workbench genomic-Qiagen), scale bar 0.1 substitutions per site. Strains indicated in bold were used for the subsequent experiments.
B. Kinetics of PI incorporation in WT BMDMs incubated with *P. entomophila* L48, *P. putida* KT2440, *P. protegens* CHA0 and their isogenic ExlA-like negative strains, and *P. fluorescens* A506 at a MOI of 0.1 for 400 min.
C. Immunodetection of ExlA-like proteins in supernatants obtained from cell infection experiment. Proteins were detected using antibodies directed against the ExlA protein from *P. aeruginosa*. WT indicates the wild-type strains and *mut* their isogenic mutants.

secrete active ExlA-like toxins. The ExlBA-like system from *P. putida* studied in this work was previously described by Molina *et al.* as the HlpBA TPS involved in the seed and root colonization (Molina *et al.*, 2006) and were considered to be putative adhesins (Nelson *et al.*, 2002). Therefore, we attempted to use anti-ExlA polyclonal antibodies raised against *P. aeruginosa* protein (Basso *et al.*, 2017) to detect the ExlA-like proteins. *S. marcescens* wild-type strain Db10 and its isogenic ShlA-negative mutant were included for immunoblot assay. Secreted proteins from cell infection supernatants were prepared and analyzed by immunoblotting (Fig. 7C). Anti-ExlA antibodies were able to detect the ShlA protein, but also ExlA-like proteins in supernatant fractions of *P. protegens*, *P. putida* and *P. entomophila*, in accordance to their cytotoxic activities on macrophages.

Pseudomonas spp. secreting exolysin-like toxins induce NLRP3-dependent pro-inflammatory cell death

Finally, we asked whether the strains of *P. putida*, *P. entomophila* and *P. protegens*, in which ExlA-like toxins are secreted, could provoke Caspase-1 activation and pyroptosis through NLRP3 pathway triggering. We thus incubated *Casp-1*$^{-/-}$ *Casp-11*$^{-/-}$, *ASC*$^{-/-}$ and *NLRP3*$^{-/-}$ macrophages with the different bacteria and compared the cytotoxicity kinetics. As shown in Fig. 8A, in all cases the KO macrophages died with significant delays compared to wild-type cells when incubated with indicated bacteria. As expected, no diminished death rate of the KO macrophages was observed with *P. fluorescens*, which does not secrete any Exolysin-like protein and induces a low basal cytotoxicity toward wild-type macrophages. Furthermore, Caspase-1 was examined by immunoblotting (Fig. 8B). In agreement with the previous results, no Caspase-1 activation could be detected with the noncytotoxic *P. fluorescens* strain. Inversely, *P. protegens*, *P. putida* and *P. entomophila* triggered the apparition of the mature Caspase-1 p10 fragment in the cells supernatants. The amounts of released IL-1ß in the supernatants of wild-type and KO BMDMs incubated with the different bacteria were quantified by ELISA (Fig. 8C). The levels of IL-1ß were low and comparable in the supernatants of all types of KO BMDMs. In contrast, upon incubation of WT BMDMs with *P. protegens*, *P. putida* and *P. entomophila*, but not *P. fluorescens*, the

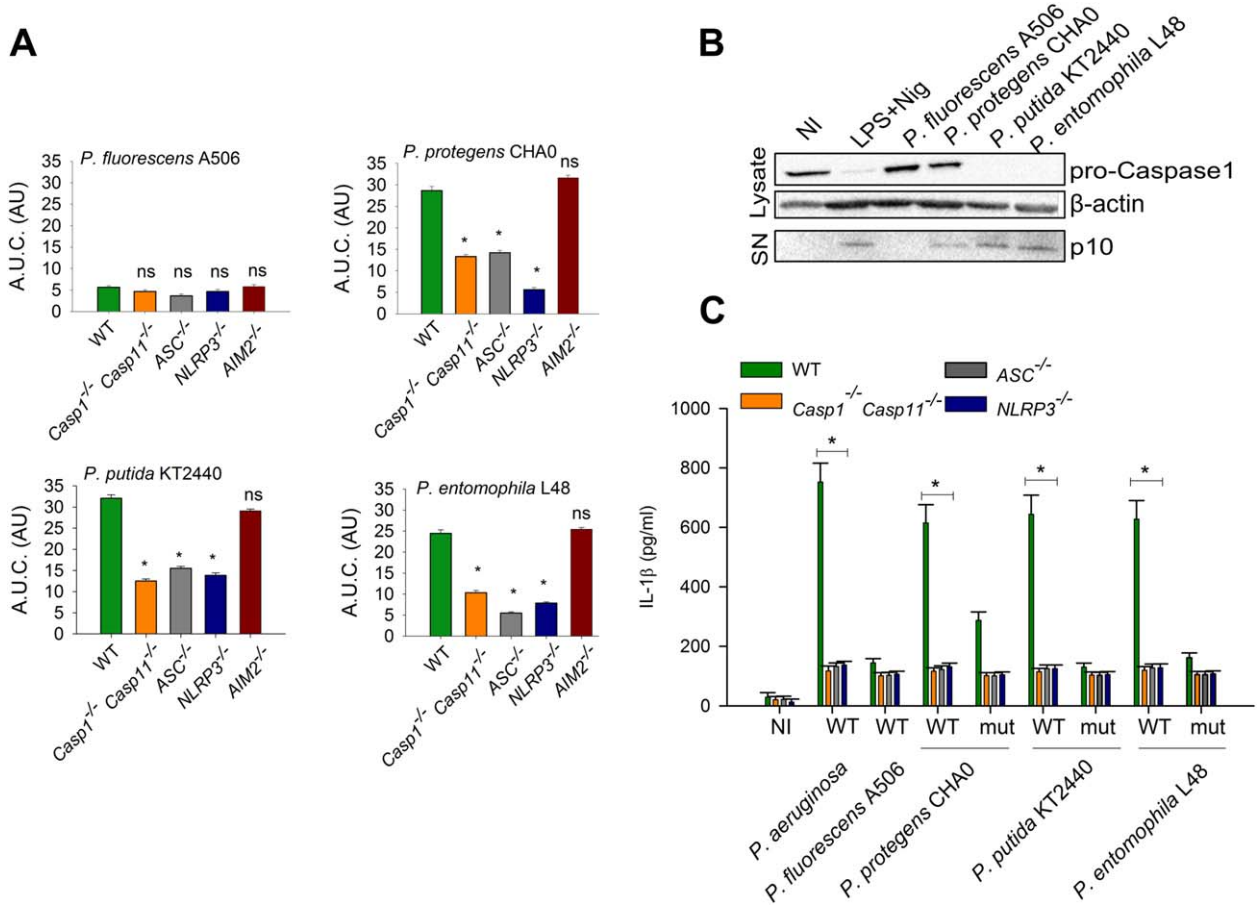

Fig. 8. *Pseudomonas* species secreting ExlA homologues induce NLPR3-dependent pyroptosis.
A. WT, *Casp1*$^{-/-}$*Casp11*$^{-/-}$, *ASC*$^{-/-}$ and *NLRP3*$^{-/-}$ BMDMs were incubated with *Pseudomonas* species at a MOI of 0.1 for 7 h. A.U.C. from kinetics of PI incorporation were calculated and used in ANOVA tests to compare KO to WT BMDMs. Stars indicate statistically significant differences with $P < 0.05$.
B. Caspase-1 activation was assessed by immunoblotting. BMDMs were incubated with the indicated *Pseudomonas* species for 220 min at a MOI of 0.1. Caspase-1 levels were analyzed in supernatants (SN) and in cell lysates. Caspase-1 p10 corresponds to one subunit of the activated form of Caspase-1.
C. WT, *Casp1*$^{-/-}$*Casp11*$^{-/-}$, *ASC*$^{-/-}$ and *NLRP3*$^{-/-}$ BMDMs were incubated with *Pseudomonas* species at a MOI of 0.1 for 6 h, negative control was done with noninfected (NI) BMDMs. IL-1ß levels were quantified by ELISA in supernatants from BMDMs. Stars indicate statistically significant differences with $P < 0.05$.

amount of released IL-1ß was similar to the one obtained with the IHMA strain and was significantly reduced with the isogenic mutants lacking the ExlA-like proteins. Based on these results, we conclude that ExlA toxins present in several different *Pseudomonas* species endow those bacteria with the capacity to induce programmed pro-inflammatory macrophage death through the NLRP3-Caspase-1 complex.

In summary, we proposed an overview of the mechanism of pyroptosis in macrophages induced by *Pseudomonas* species harbouring ExlA-like toxins (Fig. 9). BMDMs priming by the LPS or the flagellin lead to the release of TNF. In parallel, ExlA-like toxins form pores within the macrophage plasma membrane. The potassium efflux through the ExlA pore leads to a decrease of intracellular concentration and triggers the activation of NLRP3 inflammasome. Caspase-1 is activated and induces the maturation of IL-1β. This lead to an inflammatory response and pyroptotic death. We showed that other ExlA-like toxins from diverse *Pseudomonas* species share the same mechanisms.

Discussion

P. aeruginosa is a major nosocomial bacterial pathogen ranked by the World Health Organization among the top three bacterial agents the most difficult to eradicate due to acquisition of drug-resistance (http://www.who.int/fr/).

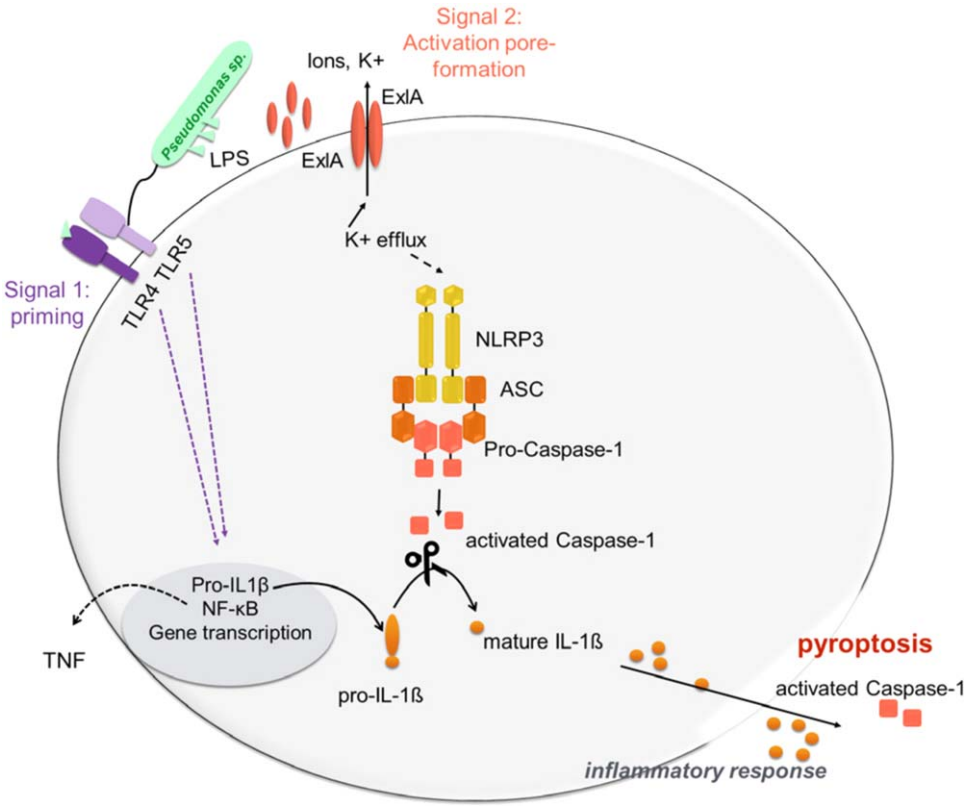

Fig. 9. Schematic view of ExlA-induced pyroptosis in macrophages. *Pseudomonas* bacteria adhere to macrophages and secrete ExlA toxins to form the pore within the plasma membrane. Potassium efflux occurs via the ExlA pore, leading to the activation of NLRP3 inflammasome. Caspase-1 is activated provoking the maturation of pro-IL-1β into mature IL-1β. This leads to an inflammatory response and pyroptotic death. The activation of the TLR pathways by the bacterial LPS and flagellin leads to the priming of the signal inducing a release of TNF and increasing the expression of the pro-IL-1ß.

Extensive work has been done on the *P. aeruginosa* T3SS and its role in the modulation of the innate immune response. In particular, the inner rod PscI and the needle subunit PscF of the toxin-injection machinery T3SS, activate the NLRC4 inflammasome, which is also induced by the flagellin FliC that is injected by the T3SS (Sutterwala *et al.*, 2007; Miao *et al.*, 2008; 2010; Yang *et al.*, 2013; Faure *et al.*, 2014; Ince *et al.*, 2015; Monlezun *et al.*, 2015). In addition, flagellin within the bacterial flagellum and LPS have been demonstrated as critical extracellular PAMPs (pathogen associated molecular patterns) recognized by the host through the toll-like-receptors TLR5 and TLR4, respectively (Hajjar *et al.*, 2002; Feuillet *et al.*, 2006; Franchi *et al.*, 2007; Descamps *et al.*, 2012). On the other hand, the ExoU and ExoS T3SS toxins were shown to partially counteract the pro-inflammatory process through their cytotoxic activity (Sutterwala *et al.*, 2007; Galle *et al.*, 2008). The integration of these signals results in processing and activation of pro-inflammatory cytokine IL-1β which, in the case of T3SS-positive *P. aeruginosa* infections, contributes to increased tissue damage and reduced bacterial clearance (Schultz *et al.*, 2002; Cohen and Prince, 2013; Faure *et al.*, 2014).

The recent discovery of *P. aeruginosa* lacking T3SS but employing the PFT ExlA for tissue destruction and proliferation raised the question of the host-cell responses to those groups of clinical strains (Reboud *et al.*, 2016; Basso *et al.*, 2017). The originality of ExlA compared to other PFTs is that its membrane pore forming activity requires close contact between bacterial and eukaryotic cells and viable bacteria are needed for active ExlA delivery (Basso *et al.*, 2017). In this work, we investigated the kinetics of macrophage death and the role of different inflammasome-related components induced by *P. aeruginosa* secreting ExlA, and compared to those induced by T3SS-positive *P. aeruginosa* strains expressing either ExoU or ExoS. ExoU$^+$ strains' cytotoxicity was Caspase1/Caspase11-independent, in agreement with ExoU being a powerful phospholipase that engenders rapid unregulated necrosis leading to the total plasma membrane disruption (Sato *et al.*, 2003; Sato and Frank, 2004). Infection of mice by ExoU$^+$ *P. aeruginosa* provokes considerable tissue injury and inflammation, with ExoU counteracting the function of neutrophils in bacterial clearance (Diaz *et al.*, 2008; Howell *et al.*, 2013). In contrast, we demonstrated that BMDMs KO for Caspase-1/Caspase-11 were resistant to cytotoxicity of ExoS$^+$ and ExlA$^+$ strains. Furthermore, both strains trigger Caspase-1 and IL-1β processing, demonstrating that, similarly to PAO1, the ExlA$^+$ strain, IHMA, leads to Caspase-1/Caspase-11-pyroptosis accompanied by release of pro-inflammatory cytokine IL-1β.

PFTs are major virulence factors of bacterial human pathogens such as *Streptoccocus pneumonia*, *Staphylococcus aureus* and *Escherichia coli* (Los *et al.*, 2013).

Their activity frequently leads to the activation of NLRP3 inflammasome, Caspase-1 processing and the maturation of IL-1β (Greaney *et al.*, 2015), features of pyroptosis (Lamkanfi and Dixit, 2014). Indeed, the efflux of cellular ions such as the potassium ions through the toxins pores, and the subsequent decrease of cellular potassium concentration, activate the NLRP3 inflammasome (Yaron *et al.*, 2015), leading to pyroptosis (Fink and Cookson, 2006). Here, we showed that both NLRP3$^{-/-}$ and ASC$^{-/-}$ macrophages are resistant to the ExlA cytotoxicity, compared to ExoS^{+} strain which induces a NLRP3-independent cell death. Moreover, the presence of KCl in excess in the extracellular medium inhibits macrophages death following infection with ExlA^{+} but not with ExoS^{+}. These findings further confirmed that Caspase-1 is activated by the NLRP3 inflammasome in the case of ExlA^{+} strains whereas ExoS^{+} strains induce the NLRC4 inflammasome (Miao *et al.*, 2008; Yang *et al.*, 2013; Faure *et al.*, 2014; Monlezun *et al.*, 2015). Therefore, *P. aeruginosa* clinical strains belonging to different clades and using different virulence strategy provoke similar pro-inflammatory response of immune cells, although through different pathways.

Recent study by Gonzalez-Juarbe *et al.*, (González-Juarbe *et al.*, 2015) proposes that ShlA, and others PFTs from *S. pneumoniae*, *L. monocytogenes* and uropathogenic *E. coli*, induce necroptosis death of macrophages. ShlA and ExlA share 33% of identity, raising the question whether the two toxins share the same mechanisms. Indeed, our results show that ExlA-provoked cell death could be inhibited in RAW macrophages by necroptosis inhibitors, as described for ShlA. However, these inhibitors have no effect on the cytotoxicity toward BMDMs neither for ShlA nor for ExlA indicating that necroptosis is not a prominent cell-death pathway in primary macrophages, which harbour all inflammasome components. Furthermore, we observe a significant delay in the PI incorporation in Caspase-1/Caspase-11$^{-/-}$ meaning that caspase(s) are involved, at least, at the beginning of the ShlA cytotoxicity. Still, ShlA did not provoke cleavage of Caspase-1 and maturation of IL-1β. Therefore, our results suggest an implication of the noncanonical inflammasome triggered by cytoplasmic LPS and involving the capase-11 (Shi *et al.*, 2014). This could be related to *S. marcescens* internalization involving ShlA (Hertle and Schwarz, 2004; Di Venanzio *et al.*, 2017) and deserves further investigations.

We recently found that the ExlA-secreting Chronic Obstructive Pulmonary Disease (COPD) isolate CLJ1 induces deleterious effects on pulmonary tissue without an important recruitment of neutrophils at the site of infection. The absence of neutrophils correlated with a low increased of IL-1β and TNF levels in broncho-alveolar lavages of CLJ1-infected mice compared to uninfected mice. However, in addition to ExlA, these features could be attributed to other, yet unidentified, strain-specific characteristics ((Elsen *et al.*, 2014; Bouillot *et al.*, in press). Indeed, different *P. aeruginosa* strains potentially harbour a diversity of surface molecules such as the flagella, Type IV pili, polysaccharides and filamentous hemagglutinins. Flagellar motility, main flagellar subunit protein FliC and pilin expression contribute also to the activation of the inflammasome (Franchi *et al.*, 2007; Sutterwala *et al.*, 2007; Miao *et al.*, 2008; Lindestam Arlehamn and Evans, 2011; Patankar *et al.*, 2013). Furthermore, the flagellin is recognized by TLR5 (Feuillet *et al.*, 2006; Franchi *et al.*, 2007; Descamps *et al.*, 2012), while LPS is sensed by the TLR4 (Hajjar *et al.*, 2002). Because the TLR pathways prime the innate immune response by inducing the synthesis of Pro-IL-1β, both, TLR and inflammasome pathways contribute to the inflammatory response. The CLJ1 strain does not swim nor twitch (Reboud *et al.*, 2016), in agreement with the presence of insertion sequences within flagellum and pili-encoding genes revealed by the analysis of the CLJ1 genome. This particularity could explain the low pro-inflammatory response observed *in vivo*. Indeed, clearly lower levels of IL-1β were produced by BMBMs infected by FliC-negative IHMA mutant or CLJ1, which correlated with lower TNF production and caspase activation, although the level of cell death measured by PI incorporation was similar in all strains. The IHMA strain was shown to be less virulent than CLJ1 in the mouse pneumonia model while PA7 is avirulent (Reboud *et al.*, 2016). This could be explained by, on one hand the high pro-inflammatory signalling induced by IHMA, and on the other hand, the low secretion of ExlA by PA7 (Reboud *et al.*, 2016). Therefore, the comparative study of the three ExlA^{+} strains (CLJ1, IHMA and PA7) uncovers the importance of the balance between inflammatory signalling and toxin secretion, explaining the high virulence of CLJ1 that combines low immune recognition and high toxin secretion.

In addition to *P. aeruginosa* isolates from different niches (Huber *et al.*, 2016; Reboud *et al.*, 2016), bioinformatics searches for *exlA*-like sequences revealed the presence of putative ExlA-encoding gene in *P. entomophila*, a drosophila pathogen, in the soil bacterium *Pseudomonas putida*, and plant-associated *P. fluorescens* and *P. protegens*. The sequence alignment of ExlA-proteins showed a global percentage of identity comprised between 35% and 59%. However, the different domains of the protein do not display equal degree of sequence conservation: the TPS domains are much conserved in all *Pseudomonas* species (over 60% of identity) compared to the filamentous haemagglutinin domains or the C-terminal domain (30% and 21%, respectively). The immunodetection of ExlA-like proteins in three *Pseudomonas* species raised the question whether those bacteria were able to provoke the pyroptosis of macrophages in a similar manner to *P. aeruginosa*.

Surprisingly, *P. entomophila* L48 and plant-associated *P. protegens* CHA0 were able to provoke an ExlA-like-dependent cell death. Moreover, the TPS system HlpB-HlpA playing a role in seed and root colonization by *P. putida* KT2440 (Molina *et al*., 2006), was found here to be responsible for death of primary macrophages. All ExlA-like toxins (including HplA) trigger the same death pathway in macrophages with activation of Caspase-1 by the NLRP3 inflammasome and release of a high amount of IL-1β during the infection. These finding is of importance considering the emergence over the three last decades of nosocomial infections caused by environmental *Pseudomonas* species (Yoshino *et al*., 2011) particularly with multidrug resistant *P. putida* (Kim *et al*., 2012). Until now, the virulence-associated genes in *P. putida* were not clearly defined, and ExlA toxin may be a good candidate. Indeed, among sequenced *P. putida* strains, we found nine strains harboring *exlA*-like genes. Two of these strains, HB3267 and H8234, are clinical isolates for which attempts were made to identify genetic determinants of their virulence (Molina *et al*., 2016). The inactivation of the *exlA*-like gene in these clinical strains, if feasible, could further establish the role of ExlA in this species. Indeed, here, we show that HlpA/ExlA proteins may confer to the bacteria cytotoxic phenotype on mammalian macrophages and thus may present a threat for immunocompromised individuals, even in soil bacteria. *P. fluorescens* A506 that possesses both, the T3SS and the ExlA-like protein, does not induce macrophages cell death and no ExlA protein was detected in the supernatant of infection. As no mutation(s) could be detected in the *exlA*-like gene, we cannot exclude that its expression might be activated in appropriate environment.

In conclusion, our results demonstrate that ExlA-like toxins from a clinical strain of *P. aeruginosa* are capable of inducing a pro-inflammatory pyroptosis in macrophages via the activation of the Caspase-1 triggered by the NLRP3 inflammasome. The level of produced and secreted IL-1β cytokine depends both on levels of ExlA and probably other bacterial surface molecules, such as flagella. Finally, the screen of *Pseudomonas* species for ExlA-like toxins, revealed that environmental bacteria, rarely associated with human infections, have the potential to secrete ExlA and induce pro-inflammatory pyroptosis.

Experimental procedures

Reagents and inhibitors

Necrostatin-1, -5 and Glycine were obtained from Sigma. The Caspase inhibitor Z-VAD-FMK was from Merck Millipore. Anti-Caspase-1 were from Santa-Cruz antibodies. Fluorescent dyes propidium iodide (PI), YoPro-1 and vital-Hoechst 33342, were from Sigma.

Bacterial strains, plasmids and growth conditions

Bacterial strains and plasmids used in this study are listed in the Supporting Information Table 1. Bacteria were grown in LB medium at 37°C for *P. aeruginosa* strains, 28°C for other *Pseudomonas* species and *S. marcescens* strains. Genetic constructions to generate isogenic mutants were obtained by insertion of internal sequences obtained by PCR and cloned in pEXG2 (Rietsch *et al*., 2005). All primers are listed in the Supporting Information Table S2. *P. protegens* Δc43010 was obtained by tri-parental mating with *E. coli* strain containing pRK2013 helper plasmid and *E. coli* (pEXG2::Δc43010-gm). *P. entomophila* ΔPEEN2177 was obtained by mating with *E. coli* SM10λpir (pINTIM2177). The selection of *Pseudomonas* was performed on PIA medium supplemented with gentamicin (200 μg/ml). The *P. putida* strain with deletion in the PP_1449 gene (Δ1449) was obtained by transformation. To that aim, the overnight culture grown in LB (1.5 ml) was centrifuged at room temperature for 2 min at 14 000 g. The pellet was washed twice with 1 ml of room temperature 300 mM sucrose and then resuspended in 100 μl of 300 mM sucrose. For electroporation, 400 ng of DNA was mixed with 100 μl of competent bacteria and transferred into an electroporation cuvette. Pulse was done at 25 μF, 200 Ω, 2.5 kV. Immediately, 1 ml of room temperature LB was added, then cells were shaken for 2 h at 37°C and plated on LB with gentamicin (30 μg/μl).

Cell culture

Bone marrow derived macrophages (BMDMs) were prepared from the tibia and femurs from C57BL/6 mice and differentiated as previously described (Meunier *et al*., 2015). Before incubation with bacteria, BMDMs were grown in $C0_2$ independent medium (Gibco Life Technology) supplemented with 10% Fetal Bovine Serum (FBS, Sigma), 2 mM Glutamine (Sigma) and 10% M-CSF (Macrophage Colony-Stimulating Factor, Sigma) at 37°C, 5% CO_2. RAW 264.7 (ATCC® TIB-71) macrophages were grown in DMEM 1x without pyruvate (Gibco Life Technology) supplemented with 10% Fetal Bovine Serum (FBS, Sigma) at 37°C, 5% CO_2. Before incubation with bacteria, medium was changed to EBM-2 (Lonza).

Cell infection assays

BMDMs were plated in 96-well plates (50 000 cells/wells) in CO_2-independent medium supplemented with 10% FBS, 2 mM Glutamine and 10% M-CSF, the day before. One hour before the incubation with bacteria, cells were labelled with vital Hoechst (1 μg/ml) at 37°C and propidium iodide (PI) (1 μM) at 37°C followed by incubation with the bacteria at a Multiplicity Of Infection (MOI) of 0.1. All *Pseudomonas* species were grown to optical density at 600 nm (OD_{600}) of 1 before infection. MOI was calculated considering that one millilitre of bacteria suspension at $OD_{600} = 1$ contains 6×10^8 bacteria.

When specified, RAW macrophages and BMDMs were treated with Necrostatin-1 (100 μM), Necrostatin-5 (50 μM), Z-VAD-FMK (10 μM), Glycine (5 mM) or KCl (130 mM) 1 h before incubation with bacteria or with LPS (10 ng/ml) for 3 h and the Nigericin (10 μM) for 1 h.

Time lapse microscopy and data analysis

Propidium iodide (PI) incorporation was followed by time lapse microscopy. Kinetic experiments were performed on the high-content ArrayScan automated fluorescent microscope (Thermo Fisher). Acquisitions were done every 30 min on four distinct fields per well using a 20X objective for 7 h.

Images from bright field (BGRFR-brightfield), UV channel (BGRFR-386/23 nm) and red channel (BGRFR-549/15 nm) were collected in all experiments to monitor cell morphology, vital-Hoechst staining and PI staining, respectively. After infection, the plate was placed in the ArraySacan live-cell chamber 1 h before beginning the acquisition in order to equilibrate the temperature and CO_2 chamber. Autofocus was done on the first time point only using UV channel. Images were analyzed using the ArrayScan HCS studiosoftware. Cell counts per well were obtained based on nuclei segmentation and enumeration in the UV channel. The nuclei mask was then applied to the red channel image, allowing enumerating the PI positive cells based on their fluorescence intensities. Data were used to calculate the percentage of PI positive cells at each time point, and curves in function of time were represented using SigmaPlot software (Systat). Area Under the Curves (A.U.C.) were calculated using the SigmaPlot corresponding macro.

Pore-formation by YoPro-1

YoPro-1 incorporation was monitored as previously described (Basso *et al.*, 2017). Briefly, BMDMs were plated in 96-well plate (50 000 cells/wells) in $C0_2$ independent medium supplement with 10% FBS, 2 mM Glutamine and 10% M-CSF the day before. One hour before the incubation with bacteria, cells were labelled with vital Hoechst (1 μg/ml), YoPro-1 (1 μM) and PI (1 μM) followed by incubation with the bacteria at a MOI of 0.1. Images acquisition were done on the ArrayScan every 5 min. YoPro-1 incorporation in the cytoplasm of each cells was analyzed and the slopes of fluorescence intensities in the cytoplasm were calculated considering the 5 last time points before the entry of YoPro-1 into the nuclei. The box plot was represented using SigmaPlot.

Adhesion assay

Adhesion assays were performed as previously described (Basso *et al.*, 2017). Briefly, BMDMs were detached from the culture plates by scraping into cold PBS and incubated with IHMA at MOI of 0.1 for 30 min at 37°C under gentle agitation. After centrifugation at 300 g for 5 min, cell and supernatants were kept and diluted by serial dilution, and spotted on LB agar plates. Colony Forming Units (CFU) were counted after 16 h incubation at 37°C.

Phylogeny analysis

ExlA protein sequences used in this study were obtained from the *Pseudomonas* genome database (http://pseudomonas.com) (Winsor *et al.*, 2011; 2016). Phylogenetic analyses were performed with the neighbor joining method using Phylowidget (http://www.phylowidget.org). The robustness of the tree was evaluated using a bootstrap test. The percentage of identity was determined using a pairwise comparison.

Analysis of ExlA secretion

Detection of ExlA and ExlA-like proteins was performed as previously described (Basso *et al.*, 2017). Briefly, bacterial cultures, in LB at an optical density at 600 nm (OD_{600}) of 1 were used to infect macrophages at MOI 0.1 for 3 h. Ten mL of cell medium were centrifuged and 0.02% (final concentration) of Sodium Deoxycholate (DOC) were added to the supernatant for 30 min at 4°C. Then, 0.2 N (final concentration) of trichloroacetic acid (TCA) were added for 1 h at 4°C. After a centrifugation at 15 000 g for 15 min, at 4°C, the precipitated proteins were dissolved in 100 μl of Laemmli loading buffer. Samples were separated by SDS-PAGE (8%) and transferred onto polyvinylidene difluoride (PVDF) membranes for Western immunoblotting. Primary rabbit polyclonal antibodies raised against both the recombinant C-terminal fragment of ExlA and ExlAΔCter (Basso *et al.*, 2017) were used combined at a 1:1000 dilution. Secondary antibodies were anti-rabbit-HRP (Sigma). The membranes were developed by Luminata Classico Western HRP (Millipore) substrate.

Analysis of Caspase-1 activation by immunoblotting

BMDMs (7.5×10^6 cells/well) were incubated with bacteria at a MOI of 0.1 for 220 min. Supernatants of cell infection were precipitated for $>$ 16 h by addition of 10% TCA Samples were centrifuged at 14 000 rpm for 10 min, and washed twice in acetone. Proteins were dissolved in 30 μl of Laemmli loading buffer. In parallel cells were lysed in 60 μl of RIPA lysis buffer (50 mM Tris_HCl,150 mM NaCl, 1% NP-40, 0,1% SDS, 1% DOC, pH 7.4) supplemented with Complete protease inhibitor cocktail (Roche). Proteins were separated by SDS-PAGE, transferred onto PVDF membrane and revealed using rabbit anti-Caspase-1 p10.The membranes were developed by Luminata Crescendo Western HRP (Millipore) substrate.

IL-1ß and TNF detection

BMDMs ($0.5\ 10^6$ cells/well) were incubated with bacteria at a MOI of 0.1 for 3 h, 4 h and 6 h. At the indicated times supernatant were collected. IL-1ß quantity was evaluated using the ELISA kit (R&D Systems) following the manufacturer instructions. TNF quantity was evaluated using the ELISA kit (BD Biosciences) following the manufacturer instructions.

Statistical analysis

SigmaPlot Software was used for graph representation and statistical analyses. Mann–Whitney tests were used for two-group comparisons and nonparametric ANOVA (Dunn's tests) were used for multiple-group comparisons.

Acknowledgements

The authors thank to Virginia Stockwell, Sarah Coulthurst, Tobias Löser, Isabelle Vallet and John Willison for sharing strains 4506, Db10, CHA0, L48 and KT2440, respectively and

for proving mice to Vishva Dixit (Genentech, South San Francisco), Virginie Pétrilli (CLB, Lyon) and Bénédicte Py (CIRI, Lyon). Preliminary results on ExlA-like proteins were obtained by Julien Trouillon during his Master 1 fellowship. This work was supported by grants from Laboratoire of Excellence « GRAL », ANR-10-LABX-49–01, Agence Nationale de la Recherche ANR-15-CE11–0018-01 and Fondation Recherche Medical (Equipes FRM 2017, DEQ20170336705). P.B. received the PhD fellowship from French Ministry of Education and Research. The work in T.H. lab is financed by an ERC starting grant 311542.

References

Allen, J.P., Ozer, E.A., and Hauser, A.R. (2014) Different paths to pathogenesis. *Trends Microbiol* **22:** 168–169.

Basso, P., Ragno, M., Elsen, S., Reboud, E., Golovkine, G., Bouillot, S., *et al*. (2017) *Pseudomonas aeruginosa* pore-forming exolysin and type IV pili cooperate to induce host cell lysis. *mBio* **8.** pii: e02250–16. doi: 10.1128/mBio.02250-16.

Bauernfeind, F.G., Horvath, G., Stutz, A., Alnemri, E.S., MacDonald, K., Speert, D., *et al*. (2009) Cutting edge: NF-B activating pattern recognition and cytokine receptors license NLRP3 inflammasome activation by regulating NLRP3 expression. *J Immunol* **183:** 787–791.

Bergsbaken, T., Fink, S.L., and Cookson, B.T. (2009) Pyroptosis: host cell death and inflammation. *Nat Rev Microbiol* **7:** 99–109.

Berthelot, P., Attree, I., Plésiat, P., Chabert, J., de Bentzmann, S., Pozzetto, B., and Grattard, F. Groupe d'Etudes des Septicémies à *Pseudomonas aeruginosa* (2003) genotypic and phenotypic analysis of type III secretion system in a cohort of *Pseudomonas aeruginosa* bacteremia isolates: evidence for a possible association between O serotypes and exo genes. *J Infect Dis* **188:** 512–518.

Bischofberger, M., Iacovache, I., and Gisou van der Goot, F. (2012) Pathogenic pore-forming proteins: function and host response. *Cell Host Microbe* **12:** 266–275.

Bouillot, S., Munro, P., Gallet, B., Reboud, E., Cretin, F., Golovkine, G., *et al*. *Pseudomonas aeruginosa* exolysin promotes bacterial growth in lungs, alveolar damage and bacterial dissemination. *Sci Rep* **7:** 2120. doi: 10.1038/s41598-017-02349-0.

Boukerb, A.M., Marti, R., and Cournoyer, B. (2015) Genome sequences of three strains of the *Pseudomonas aeruginosa* PA7 Clade. *Genome Announc* **3:** e01366–e01315.

Broz, P., and Dixit, V.M. (2016) Inflammasomes: mechanism of assembly, regulation and signalling. *Nat Rev Immunol* **16:** 407–420.

Broz, P., von Moltke, J., Jones, J.W., Vance, R.E., and Monack, D.M. (2010) Differential requirement for caspase-1 autoproteolysis in pathogen-induced cell death and cytokine processing. *Cell Host Microbe* **8:** 471–483.

Case, C.L., and Roy, C.R. (2011) Asc modulates the function of NLRC4 in response to infection of macrophages by *Legionella pneumophila*. *mBio* **2:** e00117-11–e00117-11.

Cheneval, D., Ramage, P., Kastelic, T., Szelestenyi, T., Niggli, H., Hemmig, R., *et al*. (1998) Increased mature interleukin-1 (IL-1) secretion from THP-1 cells induced by nigericin is a result of activation of p45 IL-1 -converting enzyme processing. *J Biol Chem* **273:** 17846–17851.

Cohen, T.S., and Prince, A.S. (2013) Activation of inflammasome signaling mediates pathology of acute *P. aeruginosa* pneumonia. *J Clin Invest* **123:** 1630–1637.

Dal Peraro, M., and van der Goot, F.G. (2016) Pore-forming toxins: ancient, but never really out of fashion. *Nat Rev Microbiol* **14:** 77–92.

Descamps, D., Le Gars, M., Balloy, V., Barbier, D., Maschalidi, S., Tohme, M., *et al*. (2012) Toll-like receptor 5 (TLR5), IL-1 secretion, and asparagine endopeptidase are critical factors for alveolar macrophage phagocytosis and bacterial killing. *Proc Natl Acad Sci USA* **109:** 1619–1624.

Di Venanzio, G., Lazzaro, M., Morales, E.S., Krapf, D., and García Véscovi, E. (2017) A pore-forming toxin enables *Serratia* a nonlytic egress from host cells: *Serratia* exits from host cells by a nonlytic strategy. *Cell Microbiol* **19:** e12656.

Diaz, M.H., Shaver, C.M., King, J.D., Musunuri, S., Kazzaz, J.A., and Hauser, A.R. (2008) *Pseudomonas aeruginosa* induces localized immunosuppression during pneumonia. *Infect Immun* **76:** 4414–4421.

Elsen, S., Huber, P., Bouillot, S., Couté, Y., Fournier, P., Dubois, Y., *et al*. (2014) A type III secretion negative clinical strain of *Pseudomonas aeruginosa* employs a two-partner secreted exolysin to induce hemorrhagic pneumonia. *Cell Host Microbe* **15:** 164–176.

Engel, J., and Balachandran, P. (2009) Role of *Pseudomonas aeruginosa* type III effectors in disease. *Curr Opin Microbiol* **12:** 61–66.

Faure, E., Mear, J.-B., Faure, K., Normand, S., Couturier-Maillard, A., Grandjean, T., *et al*. (2014) *Pseudomonas aeruginosa* type-3 secretion system dampens host defense by exploiting the NLRC4-coupled inflammasome. *Am J Respir Crit Care Med* **189:** 799–811.

Fauvarque, M.-O., Bergeret, E., Chabert, J., Dacheux, D., Satre, M., and Attree, I. (2002) Role and activation of type III secretion system genes in *Pseudomonas aeruginosa*-induced Drosophila killing. *Microb Pathog* **32:** 287–295.

Feuillet, V., Medjane, S., Mondor, I., Demaria, O., Pagni, P.P., Galan, J.E., *et al*. (2006) Involvement of toll-like receptor 5 in the recognition of flagellated bacteria. *Proc Natl Acad Sci USA* **103:** 12487–12492.

Fink, S.L., and Cookson, B.T. (2006) Caspase-1-dependent pore formation during pyroptosis leads to osmotic lysis of infected host macrophages. *Cell. Microbiol* **8:** 1812–1825.

Franchi, L., Stoolman, J., Kanneganti, T.-D., Verma, A., Ramphal, R., and Núñez, G. (2007) Critical role for Ipaf in *Pseudomonas aeruginosa*-induced caspase-1 activation. *Eur J Immunol* **37:** 3030–3039.

Galle, M., Schotte, P., Haegman, M., Wullaert, A., Yang, H.J., Jin, S., and Beyaert, R. (2008) The *Pseudomonas aeruginosa Type* III secretion system plays a dual role in the regulation of caspase-1 mediated IL-1β maturation. *J Cell Mol Med* **12:** 1767–1776.

Galluzzi, L., Bravo-San Pedro, J.M., Vitale, I., Aaronson, S.A., Abrams, J.M., Adam, D., *et al*. (2015) Essential versus accessory aspects of cell death: recommendations of the NCCD 2015. *Cell Death Differ* **22:** 58–73.

Garrido-Sanz, D., Meier-Kolthoff, J.P., Göker, M., Martín, M., Rivilla, R., and Redondo-Nieto, M. (2016) Genomic and

genetic diversity within the *Pseudomonas fluorescens* Complex. *PLoS One* **11:** e0150183.
González-Juarbe, N., Gilley, R.P., Hinojosa, C.A., Bradley, K.M., Kamei, A., Gao, G., *et al*. (2015) Pore-forming toxins induce macrophage necroptosis during acute bacterial pneumonia. *PLoS Pathog* **11:** e1005337.
Greaney, A.J., Leppla, S.H., and Moayeri, M. (2015) Bacterial exotoxins and the inflammasome. *Front Immunol* **6:** 570.
Hajjar, A.M., Ernst, R.K., Tsai, J.H., Wilson, C.B., and Miller, S.I. (2002) Human Toll-like receptor 4 recognizes host-specific LPS modifications. *Nat Immunol* **3:** 354–359.
Hauser, A.R. (2009) The type III secretion system of *Pseudomonas aeruginosa*: infection by injection. *Nat Rev Microbiol* **7:** 654–665.
Hauser, A.R., Cobb, E., Bodi, M., Mariscal, D., Vallés, J., Engel, J.N., and Rello, J. (2002) Type III protein secretion is associated with poor clinical outcomes in patients with ventilator-associated pneumonia caused by *Pseudomonas aeruginosa*. *Crit Care Med* **30:** 521–528.
Hertle, R., and Schwarz, H. (2004) Serratia marcescens internalization and replication in human bladder epithelial cells. *BMC Infect Dis* **4:** 6.
Howell, H.A., Logan, L.K., and Hauser, A.R. (2013) Type III secretion of ExoU is critical during early *Pseudomonas aeruginosa* pneumonia. *mBio* **4:** e00032-13–e00032-13.
Huber, P., Basso, P., Reboud, E., and Attrée, I. (2016) *Pseudomonas aeruginosa* renews its virulence factors: *Pseudomonas aeruginosa* renews its virulence factors. *Environ Microbiol Rep* **8:** 564–571.
Ince, D., Sutterwala, F.S., and Yahr, T.L. (2015) Secretion of flagellar proteins by the *Pseudomonas aeruginosa* type III secretion-injectisome system. *J. Bacteriol* **197:** 2003–2011.
Jabir, M.S., Hopkins, L., Ritchie, N.D., Ullah, I., Bayes, H.K., Li, D., *et al*. (2015) Mitochondrial damage contributes to *Pseudomonas aeruginosa* activation of the inflammasome and is downregulated by autophagy. *Autophagy* **11:** 166–182.
Jorgensen, I., Rayamajhi, M., and Miao, E.A. (2017) Programmed cell death as a defence against infection. *Nat Rev Immunol* **17:** 151–164.
Kawai, T., and Akira, S. (2007) TLR signaling. *Semin Immunol* **19:** 24–32.
Kim, S.E., Park, S.-H., Park, H.B., Park, K.-H., Kim, S.-H., Jung, S.-I., *et al*. (2012) Nosocomial *Pseudomonas putida* bacteremia: high rates of carbapenem resistance and mortality. *Chonnam Med J* **48:** 91.
Kos, V.N., Déraspe, M., McLaughlin, R.E., Whiteaker, J.D., Roy, P.H., Alm, R.A., *et al*. (2015) The resistome of *Pseudomonas aeruginosa* in relationship to phenotypic susceptibility. *Antimicrob Agents Chemother* **59:** 427–436.
Lamkanfi, M., and Dixit, V.M. (2014) Mechanisms and functions of inflammasomes. *Cell* **157:** 1013–1022.
Ledizet, M., Murray, T.S., Puttagunta, S., Slade, M.D., Quagliarello, V.J., and Kazmierczak, B.I. (2012) The ability of virulence factor expression by *Pseudomonas aeruginosa* to predict clinical disease in hospitalized patients. *PLoS One* **7:** e49578.
Lindestam Arlehamn, C.S., and Evans, T.J. (2011) *Pseudomonas aeruginosa* pilin activates the inflammasome: pilin activates the inflammasome. *Cell Microbiol* **13:** 388–401.
Loper, J.E., Hassan, K.A., Mavrodi, D.V., Davis, E.W., Lim, C.K., Shaffer, B.T., *et al*. (2012) Comparative genomics of plant-associated *Pseudomonas* spp.: insights into diversity and inheritance of traits involved in multitrophic interactions. *PLoS Genet* **8:** e1002784.
Los, F.C.O., Randis, T.M., Aroian, R.V., and Ratner, A.J. (2013) Role of pore-forming toxins in bacterial infectious diseases. *Microbiol Mol Biol Rev* **77:** 173–207.
Lyczak, J.B., Cannon, C.L., and Pier, G.B. (2000) Establishment of *Pseudomonas aeruginosa* infection: lessons from a versatile opportunist. *Microbes Infect Inst Pasteur* **2:** 1051–1060.
Mariathasan, S., Weiss, D.S., Newton, K., McBride, J., O'Rourke, K., Roose-Girma, M., *et al*. (2006) Cryopyrin activates the inflammasome in response to toxins and ATP. *Nature* **440:** 228–232.
Meunier, E., Wallet, P., Dreier, R.F., Costanzo, S., Anton, L., Rühl, S., *et al*. (2015) Guanylate-binding proteins promote activation of the AIM2 inflammasome during infection with Francisella novicida. *Nat Immunol* **16:** 476–484.
Miao, E.A., Andersen-Nissen, E., Warren, S.E., and Aderem, A. (2007) TLR5 and Ipaf: dual sensors of bacterial flagellin in the innate immune system. *Semin Immunopathol* **29:** 275–288.
Miao, E.A., Ernst, R.K., Dors, M., Mao, D.P., and Aderem, A. (2008) *Pseudomonas aeruginosa* activates caspase 1 through Ipaf. *Proc Natl Acad Sci USA* **105:** 2562–2567.
Miao, E.A., Mao, D.P., Yudkovsky, N., Bonneau, R., Lorang, C.G., Warren, S.E., *et al*. (2010) Innate immune detection of the type III secretion apparatus through the NLRC4 inflammasome. *Proc Natl Acad Sci USA* **107:** 3076–3080.
Moayeri, M., and Leppla, S.H. (2009) Cellular and systemic effects of anthrax lethal toxin and edema toxin. *Mol Aspects Med* **30:** 439–455.
Molina, L., Udaondo, Z., Duque, E., Fernández, M., Bernal, P., Roca, A., *et al*. (2016) Specific gene loci of clinical *Pseudomonas putida* isolates. *PLoS One* **11:** e0147478.
Molina, M.A., Ramos, J.-L., and Espinosa-Urgel, M. (2006) A two-partner secretion system is involved in seed and root colonization and iron uptake by *Pseudomonas putida* KT2440. *Environ Microbiol* **8:** 639–647.
Monlezun, L., Liebl, D., Fenel, D., Grandjean, T., Berry, A., Schoehn, G., *et al*. (2015) PscI is a type III secretion needle anchoring protein with in vitro polymerization capacities. *Mol Microbiol* **96:** 419–436.
Muñoz-Planillo, R., Kuffa, P., Martínez-Colón, G., Smith, B.L., Rajendiran, T.M., and Núñez, G. (2013) K+ efflux is the common trigger of NLRP3 inflammasome activation by bacterial toxins and particulate matter. *Immunity* **38:** 1142–1153.
Nelson, K.E., Weinel, C., Paulsen, I.T., Dodson, R.J., Hilbert, H., Martins dos Santos, V.A.P., *et al*. (2002) Complete genome sequence and comparative analysis of the metabolically versatile *Pseudomonas putida* KT2440. *Environ Microbiol* **4:** 799–808.
Pang, Z., Sun, G., Junkins, R.D., and Lin, T.J. (2015) AIM2 inflammasome is dispensable for the host defense against *Pseudomonas aeruginosa* infection. *Cell Mol Biol Noisy–Gd Fr* **61:** 63–70.
Pardo, J., Urban, C., Galvez, E.M., Ekert, P.G., Müller, U., Kwon-Chung, J., *et al*. (2006) The mitochondrial protein

Bak is pivotal for gliotoxin-induced apoptosis and a critical host factor of *Aspergillus fumigatus* virulence in mice. *J Cell Biol* **174:** 509–519.

Patankar, Y.R., Lovewell, R.R., Poynter, M.E., Jyot, J., Kazmierczak, B.I., and Berwin, B. (2013) Flagellar motility is a key determinant of the magnitude of the inflammasome response to *Pseudomonas aeruginosa*. *Infect Immun* **81:** 2043–2052.

Pelegrin, P., Barroso-Gutierrez, C., and Surprenant, A. (2008) P2X7 receptor differentially couples to distinct release pathways for IL-1beta in mouse macrophage. *J Immunol Baltim Md 1950* **180:** 7147–7157.

Pétrilli, V., Papin, S., Dostert, C., Mayor, A., Martinon, F., and Tschopp, J. (2007) Activation of the NALP3 inflammasome is triggered by low intracellular potassium concentration. *Cell Death Differ* **14:** 1583–1589.

Py, B.F., Kim, M.-S., Vakifahmetoglu-Norberg, H., and Yuan, J. (2013) Deubiquitination of NLRP3 by BRCC3 critically regulates inflammasome activity. *Mol Cell* **49:** 331–338.

Rassow, J. (2011) Helicobacter pylori vacuolating toxin A and apoptosis. *Cell Commun Signal* **9:** 26.

Reboud, E., Elsen, S., Bouillot, S., Golovkine, G., Basso, P., Jeannot, K., *et al*. (2016) Phenotype and toxicity of the recently discovered exlA-positive *Pseudomonas aeruginosa* strains collected worldwide. *Environ Microbiol* **18:** 3425–3439.

Rietsch, A., Vallet-Gely, I., Dove, S.L., and Mekalanos, J.J. (2005) ExsE, a secreted regulator of type III secretion genes in *Pseudomonas aeruginosa*. *Proc Natl Acad Sci USA* **102:** 8006–8011.

Roy, P.H., Tetu, S.G., Larouche, A., Elbourne, L., Tremblay, S., Ren, Q., *et al*. (2010) Complete genome sequence of the multiresistant taxonomic outlier *Pseudomonas aeruginosa* PA7. *PLoS One* **5:** e8842.

Roy-Burman, A., Savel, R.H., Racine, S., Swanson, B.L., Revadigar, N.S., Fujimoto, J., *et al*. (2001) Type III protein secretion is associated with death in lower respiratory and systemic *Pseudomonas aeruginosa* infections. *J Infect Dis* **183:** 1767–1774.

Sagulenko, V., Thygesen, S.J., Sester, D.P., Idris, A., Cridland, J.A., Vajjhala, P.R., *et al*. (2013) AIM2 and NLRP3 inflammasomes activate both apoptotic and pyroptotic death pathways via ASC. *Cell Death Differ* **20:** 1149–1160.

Sato, H., and Frank, D.W. (2004) ExoU is a potent intracellular phospholipase: ExoU phospholipase activity. *Mol Microbiol* **53:** 1279–1290.

Sato, H., Frank, D.W., Hillard, C.J., Feix, J.B., Pankhaniya, R.R., Moriyama, K., *et al*. (2003) The mechanism of action of the *Pseudomonas aeruginosa*-encoded type III cytotoxin, ExoU. *EMBO J* **22:** 2959–2969.

Schroder, K., and Tschopp, J. (2010) The inflammasomes. *Cell* **140:** 821–832.

Schultz, M.J., Rijneveld, A.W., Florquin, S., Edwards, C.K., Dinarello, C.A., and van der Poll, T. (2002) Role of interleukin-1 in the pulmonary immune response during *Pseudomonas aeruginosa* pneumonia. *Am J Physiol Lung Cell Mol Physiol* **282:** L285–L290.

Shi, J., Zhao, Y., Wang, Y., Gao, W., Ding, J., Li, P., *et al*. (2014) Inflammatory caspases are innate immune receptors for intracellular LPS. *Nature* **514:** 187–192.

Silby, M.W., Cerdeño-Tárraga, A.M., Vernikos, G.S., Giddens, S.R., Jackson, R.W., Preston, G.M., *et al*. (2009) Genomic and genetic analyses of diversity and plant interactions of *Pseudomonas fluorescens*. *Genome Biol* **10:** R51.

Stanzani, M. (2005) Aspergillus fumigatus suppresses the human cellular immune response via gliotoxin-mediated apoptosis of monocytes. *Blood* **105:** 2258–2265.

Stockwell, V.O., Davis, E.W., Carey, A., Shaffer, B.T., Mavrodi, D.V., Hassan, K.A., *et al*. (2013) pA506, a conjugative plasmid of the plant epiphyte *Pseudomonas fluorescens* A506. *Appl Environ Microbiol* **79:** 5272–5282.

Storek, K.M., and Monack, D.M. (2015) Bacterial recognition pathways that lead to inflammasome activation. *Immunol Rev* **265:** 112–129.

Sutterwala, F.S., Mijares, L.A., Li, L., Ogura, Y., Kazmierczak, B.I., and Flavell, R.A. (2007) Immune recognition of *Pseudomonas aeruginosa* mediated by the IPAF/NLRC4 inflammasome. *J Exp Med* **204:** 3235–3245.

Thrane, S.W., Taylor, V.L., Freschi, L., Kukavica-Ibrulj, I., Boyle, B., Laroche, J., *et al*. (2015) The widespread multidrug-resistant serotype O12 *Pseudomonas aeruginosa* clone emerged through concomitant horizontal transfer of serotype antigen and antibiotic resistance gene clusters. *mBio* **6:** e01396–e01315.

Vallis, A.J., Finck-Barbançon, V., Yahr, T.L., and Frank, D.W. (1999) Biological effects of *Pseudomonas aeruginosa* type III-secreted proteins on CHO cells. *Infect Immun* **67:** 2040–2044.

Ward, N., and Moreno-Hagelsieb, G. (2014) Quickly finding orthologs as reciprocal best hits with BLAT, LAST, and UBLAST: how much do we miss? *PLoS One* **9:** e101850.

Wilson, M., and Lindow, S.E. (1994) Ecological similarity and coexistence of epiphytic ice-nucleating (ice) *Pseudomonas syringae* strains and a non-ice-nucleating (ice) biological control agent. *Appl Environ Microbiol* **60:** 3128–3137.

Winsor, G.L., Lam, D.K.W., Fleming, L., Lo, R., Whiteside, M.D., Yu, N.Y., *et al*. (2011) *Pseudomonas* Genome Database: improved comparative analysis and population genomics capability for *Pseudomonas* genomes. *Nucleic Acids Res* **39:** D596–D600.

Winsor, G.L., Griffiths, E.J., Lo, R., Dhillon, B.K., Shay, J.A., and Brinkman, F.S.L. (2016) Enhanced annotations and features for comparing thousands of *Pseudomonas* genomes in the *Pseudomonas* genome database. *Nucleic Acids Res* **44:** D646–D653.

Yang, J., Zhao, Y., Shi, J., and Shao, F. (2013) Human NAIP and mouse NAIP1 recognize bacterial type III secretion needle protein for inflammasome activation. *Proc Natl Acad Sci USA* **110:** 14408–14413.

Yaron, J.R., Gangaraju, S., Rao, M.Y., Kong, X., Zhang, L., Su, F., *et al*. (2015) K+ regulates Ca2+ to drive inflammasome signaling: dynamic visualization of ion flux in live cells. *Cell Death Dis* **6:** e1954.

Yoshino, Y., Kitazawa, T., Kamimura, M., Tatsuno, K., Yotsuyanagi, H., and Ota, Y. (2011) *Pseudomonas putida* bacteremia in adult patients: five case reports and a review of the literature. *J Infect Chemother* **17:** 278–282.

Zhao, Y., and Shao, F. (2015) The NAIP-NLRC4 inflammasome in innate immune detection of bacterial flagellin and type III secretion apparatus. *Immunol Rev* **265:** 85–102.

Supporting information

Additional Supporting Information may be found in the online version of this article at the publisher's web-site:

LDH Cytotoxicity assay BMDMs were plated in 96-well plate (50 000 cells/wells) in CO_2 independent medium supplement with 10% FBS, 2 mM Glutamine and 10% M-CSF, the day before. The cytotoxicity was quantified by measuring the lactate dehydrogenase (LDH) in the media, using the LDH Cytotoxicity Detection Kit (Roche). The absorbance was measured at 492 nm. The positive control was obtained using Triton 2% and the negative control was the supernatant from noninfected cells. The percentage of LDH release was calculated after subtraction of the value obtained for the negative control to the values obtained for the positive control and the samples.

Table S1. List of bacterial strains and plasmids used in this work

Table S2. List of primers used in this work.

Fig. S1. Comparison of PI incorporation and LDH release. WT BMDMs were incubated with PP34 ($ExoU^+$), PAO1 ($ExoS^+$) and IHMA ($ExlA^+$) strains at a MOI 0.1 for 3.5 h. PI incorporation was quantified by High Content microscopy and LDH release was measured by an enzymatic assay, at 2, 2.5, 3 and 3.5 h postinfection. The positive control corresponds to the cells lysed with Triton 2%. The PI incorporation was measured at the same times, in the same wells.

Fig. S2. Cytotoxicity of Pseudomonas spp. producing ExlA-like toxins toward RAW macrophages in the presence of Necroptosis inhibitors. Necrostatin-1 at (100 μM) and Necrostatin-5 at 50 μM respectively inhibit RIPK1 and RIPK3. The cytotoxicity was quantified by the measure of LDH release after bacteria incubation at a MOI of 0.1 for 3 h.

Multiple *Pseudomonas* species secrete Exolysin-like toxins and provoke Caspase-1-dependent macrophage death

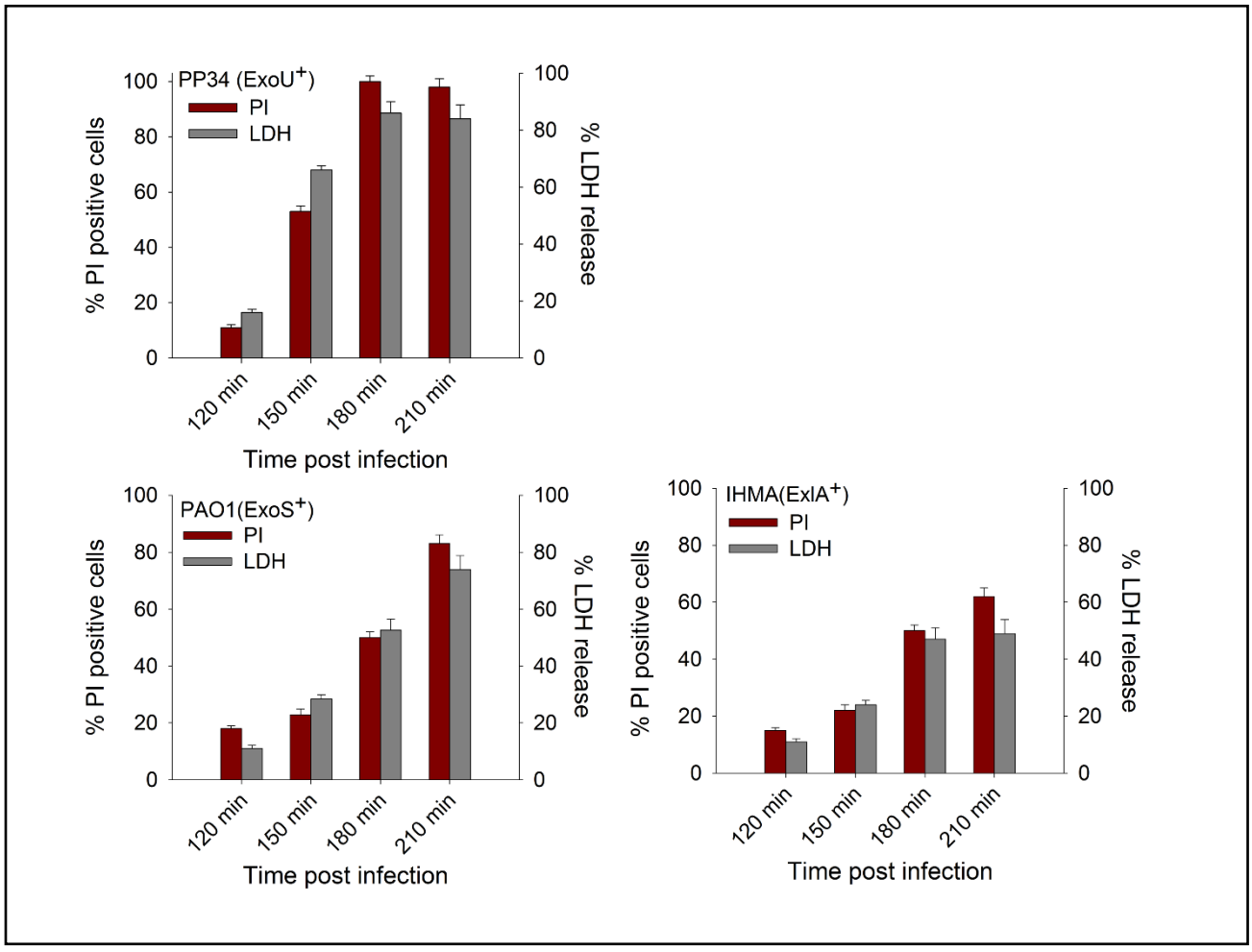

Fig. S1: Comparison of PI incorporation and LDH release.
WT BMDMs were incubated with PP34 (ExoU$^+$), PAO1 (ExoS$^+$) and IHMA (ExlA$^+$) strains at a MOI 0.1 for 3.5 hours. PI incorporation was quantified by High Content microscopy and LDH release was measured by an enzymatic assay, at 2, 2.5, 3 and 3.5 hours post infection. The positive control corresponds to the cells lysed with Triton 2%. The PI incorporation was measured at the same times, in the same wells.

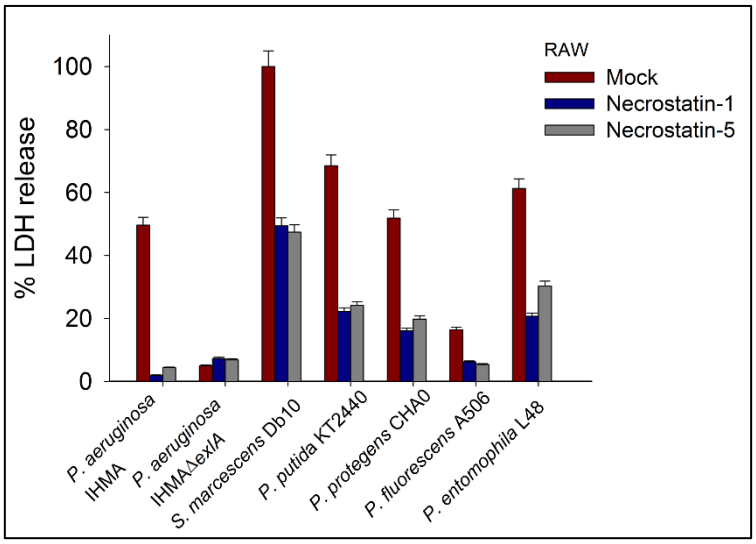

Fig. S2: Cytotoxicity of Pseudomonas spp. producing ExlA-like toxins towards RAW macrophages in the presence of Necroptosis inhibitors.
Necrostatin-1 at (100 µM) and Necrostatin-5 at 50 µM respectively inhibit RIPK1 and RIPK3. The cytotoxicity was quantified by the measure of LDH release after bacteria incubation at a MOI of 0.1 for 3 hours.

Supplementary Table 1. List of bacterial strains and plasmids used in this work.

Strains or plasmids	Characteristics	References
Strains		
Pseudomonas aeruginosa		
PAO1F	*P. aeruginosa* expressing *exoS*	(1)
PP34	*P. aeruginosa* expressing *exoU*	(2)
IHMA879472 (IHMA)	ExlA+, Urinary strain IHMA	(3,4)
IHMAΔ*exlA*	*exlA* deletion	(4)
IHMAΔ*fliC*	*fliC* deletion	This work
CLJ1	*P. aeruginosa* strain lacking the *T3SS* loci, *exlA* positive	(5)
PA7	*P. aeruginosa* strain lacking the *T3SS* loci, *exlA* positive	(6)
Pseudomonas putida		
KT2440	*P. putida* expressing hlpA-hlpB	(7,8)
KT2440$_{PP_1449mut}$	Insertion of pEXG2 plasmid into *PP_1449* locus	This work
Pseudomonas entomophila		
L48		(9)
L48$_{\Delta PSEEN\_2177}$	TGA codon insertion at 442 amino acids using pINT vector	This work
Pseudomonas protegens		
CHA0		(10)
CHA0$_{c43010mut}$	Insertion of pEXG2 plasmid into *PFLCHA0_c43010*	This work
Pseudomonas fluorescens		

A506		(11)
Serratia marcescens		
Db10	*Serratia marscescens strains*	(12)
Db10Δ*shlA*		This work
Escherichia coli		
DH5α	Cloning strain	Lab collection
Plasmids		
pEXG2_PP1149	Gm^R, suicide plasmid used for *PP1449* mutagenesis	This work
pEXG2_c43010	Gm^R, suicide plasmid used for *c43010* mutagenesis	This work
pINTIM2177	Plasmid used for PSEEN2177 mutagenesis	This work

Tc^R: Tetracycline resistance, Gm^R: Gentamicin resistance

Supplementary Table 2. List of primers used in this work.

Name	Sequence (5'-3')
Insert- PFLCHA0_c43010-Ec	CCC GGG AAT TCT GAC AAC ACT CAT AGA TTC AAC C
Insert -PFLCHA0_c43010-Xb	CTA GTC TAG ATC AGA CAT TCA ACT GGT CCC GGG C
Insert- PP_1449-Ec	CCC GGG AAT TCA AAC ACT CTC GCA GTT ACC GC
Insert -PP_1449-Xb	CTA GTC TAG ATC AGA CAG TGA TGT CGA GCG TTT CG

Supplemental method

LDH Cytotoxicity assay

BMDMs were plated in 96-well plate (50,000 cells/wells) in CO_2 independent medium supplement with 10% FBS, 2mM Glutamine and 10% M-CSF, the day before. The cytotoxicity was quantified by measuring the lactate dehydrogenase (LDH) in the media, using the LDH Cytotoxicity Detection Kit (Roche). The absorbance was measured at 492nm. The positive control was obtained using Triton 2% and the negative control was the supernatant from non-infected cells. The percentage of LDH release was calculated after subtraction of the value obtained for the negative control to the values obtained for the positive control and the samples.

REFERENCES

1. Cisz M, Lee P-C, Rietsch A. ExoS controls the cell contact-mediated switch to effector secretion in Pseudomonas aeruginosa. J Bacteriol. 2008 Apr;190(8):2726–38.

2. Berthelot P, Attree I, Plésiat P, Chabert J, de Bentzmann S, Pozzetto B, et al. Genotypic and phenotypic analysis of type III secretion system in a cohort of Pseudomonas aeruginosa bacteremia isolates: evidence for a possible association between O serotypes and exo genes. J Infect Dis. 2003 Aug 15;188(4):512–8.

3. Kos VN, Déraspe M, McLaughlin RE, Whiteaker JD, Roy PH, Alm RA, et al. The Resistome of Pseudomonas aeruginosa in Relationship to Phenotypic Susceptibility. Antimicrob Agents Chemother. 2015 Jan;59(1):427–36.

4. Basso P, Ragno M, Elsen S, Reboud E, Golovkine G, Bouillot S, et al. Pseudomonas aeruginosa Pore-Forming Exolysin and Type IV Pili Cooperate To Induce Host Cell Lysis. mBio. 2017 Jan 24;8(1).

5. Elsen S, Huber P, Bouillot S, Couté Y, Fournier P, Dubois Y, et al. A type III secretion negative clinical strain of Pseudomonas aeruginosa employs a two-partner secreted exolysin to induce hemorrhagic pneumonia. Cell Host Microbe. 2014 Feb 12;15(2):164–76.

6. Roy PH, Tetu SG, Larouche A, Elbourne L, Tremblay S, Ren Q, et al. Complete Genome Sequence of the Multiresistant Taxonomic Outlier Pseudomonas aeruginosa PA7. Ahmed N, editor. PLoS ONE. 2010 Jan 22;5(1):e8842.

7. Nelson KE, Weinel C, Paulsen IT, Dodson RJ, Hilbert H, Martins dos Santos VAP, et al. Complete genome sequence and comparative analysis of the metabolically versatile Pseudomonas putida KT2440. Environ Microbiol. 2002 Dec;4(12):799–808.

8. Molina MA, Ramos J-L, Espinosa-Urgel M. A two-partner secretion system is involved in seed and root colonization and iron uptake by Pseudomonas putida KT2440. Environ Microbiol. 2006 Apr;8(4):639–47.

9. Vodovar N, Vallenet D, Cruveiller S, Rouy Z, Barbe V, Acosta C, et al. Complete genome sequence of the entomopathogenic and metabolically versatile soil bacterium Pseudomonas entomophila. Nat Biotechnol. 2006 Jun;24(6):673–9.

10. Voisard C, Bull CT, Keel C, Laville J, Maurhofer M, Schnider U, et al. Biocontrol of Root Diseases byPseudomonas fluorescens CHA0: Current Concepts and Experimental Approaches. In: O'Gara F, Dowling DN, Boesten B, editors. Molecular Ecology of Rhizosphere Microorganisms [Internet]. Weinheim, Germany: Wiley-VCH Verlag GmbH; 1994 [cited 2017 Apr 14]. p. 67–89. Available from: http://doi.wiley.com/10.1002/9783527615810.ch6

11. Wilson M, Lindow SE. Ecological Similarity and Coexistence of Epiphytic Ice-Nucleating (Ice) Pseudomonas syringae Strains and a Non-Ice-Nucleating (Ice) Biological Control Agent. Appl Environ Microbiol. 1994 Sep;60(9):3128–37.

12. Kurz CL, Chauvet S, Andrès E, Aurouze M, Vallet I, Michel GPF, et al. Virulence factors of the human opportunistic pathogen Serratia marcescens identified by in vivo screening. EMBO J. 2003 Apr 1;22(7):1451–60.

7

Multi-omics approach reveals adaptation strategies of an Exolysin-positive *Pseudomonas aeruginosa* clonal outlier isolated from hemorrhagic pneumonia

Erwin Santausa, Pauline Basso, Alice Berry, Annie Adrait, Yohann Coute, Stephen Lory, Sylvie Elsen and Ina Attree. Manuscript in preparation

Virulent *Pseudomonas aeruginosa* clonal outliers are characterized by the synthesis of a pore-forming toxin, Exolysin (ExlA), which has been first identified by comparative proteomic analysis in CLJ1 strain [126]. CLJ strains were isolated from a patient suffering from hemorrhagic pulmonary infection in Intensive Care Units at Grenoble University Hospital [126]. CLJ1 was susceptible to almost all antibiotics including β-lactam, aminoglycosides and fluoroquinolones. CLJ3, isolated from the patient after 12 days of antibiotherapy, appeared to be resistant to most of commonly used antibiotics [126].

In this chapter I present the first genome-wide analysis of the two clonal CLJ variants. In this work, I participated by preparing the samples for the proteomics analysis, analyzing CLJ genomes, participating in analyzing multi-omics data and preparing figures for publication.

The two strains were analyzed by comparative transcriptomics (RNASeq) and proteomics. Whole-genome comparison of CLJ and PA7 strains revealed, the presence of 15 CLJ-specific regions (SRs), missing from PA7. Fourteen out these 15 SRs are found in other *Pseudomonas aeruginosa* strains. CLJ has also 8 phage-related regions among which five are absent from PA7. 77 genes were found significantly deferentially expressed between CLJ1 and CLJ3, both at the transcriptomic and proteomic levels. Out of these, 35 % are of phage origin, while 42 % are predicted to be localized in bacterial membranes, periplasm or secreted.

CLJ1 was unable to twitch and swim [1, 326]. A genome analysis revealed the presence of transposon insertion belonging to ISL3 family in the *flgL* gene encoding the flagellar hook-filament junction protein. Moreover, the same insertion sequence IS is found in pilM gene, the first gene of the *pilMNOPQ* operon important for Type 4 Pili biogenesis and twitching motility. The major genome modification event in CLJ3 compared to CLJ1 is a deletion of 20 kbs encompassing at least 21 genes. This region includes notably *galU* encoding UDP glucose pyrophosphorylase [327] that add sugar moieties on the inner core lipid core, giving the anchor for the full length LPS. We demonstrated that CLJ3 was non-agglutinable and sensitive to serum compared to CLJ1, both phenotypes being in agreement with the loss of *galU* gene.

The proteomic analysis highlights the expression of six TPS systems annotated hemolysin/hemagglutinin in CLJ1, including Exolysin. These proteins may play an important role during colonization and infection, but their exact roles in adhesion, cytotoxicity and/or interbacterial competition need to be further investigated. In addition, the OprD outer membrane protein involved in the antibiotic fluxes was found absent from CLJ3 proteome [126]. Again, the genome analysis showed that the *oprD* gene was interrupted by the CLJ1-ISL3 insertion sequence. In addition, proteomics, RNAseq and RTq-PCR have shown an over-expression of gene encoding MipA and AmpDH3, respectively involved in peptidoglycan synthesis and recycling, which may play a role in the antibiotic resistance. Proteomics analysis, confirmed by RNASeq, indicated the overexpression of HcnA, HcnB and HcnC, encoded by the same *hcn* operon. Those enzymes produce the metabolic product Hydrogen cyanide [328]. Indeed, *in vitro* CLJ1 was able to produce HCN in higher quantities than CLJ3 and other *P. aeruginosa* strains. Finally, *rsmZ*, was significantly more expressed in CLJ3 which was confirmed by targeted qRT-PCR. *rsmZ* plays a central role in regulatory pathways in classical PAO1 strains by maintaining the balance between virulence determinants involved in acute and chronic infections (e.g. T3SS versus extracellular polysaccharides, Psl and Pel), and its role in shaping the virulence of PA7-like clinical strains stays to be examined.

Running title: Adaptation of ExlA$^+$ *Pa* clonal outliers

Adaptation strategies of an Exolysin-positive *Pseudomonas aeruginosa* during hemorrhagic pneumonia

Antibiotic resistance/Insertion sequences

Erwin Sentausa[1], **Pauline Basso**[1], Alice Berry[1], Annie Adrait[2], Yohann Couté[2], Stephen Lory[3], Sylvie Elsen[1]* and Ina Attrée[1]*

[1]Université Grenoble Alpes, CNRS ERL5261, INSERM U1036, CEA, Bacterial Pathogenesis and Cellular Responses, Biosciences and Biotechnology Institute of Grenoble, France

[2]Université Grenoble Alpes, CNRS, INSERM U1038, CEA, Exploring the Dynamics of Proteomes, Biosciences and Biotechnology Institute of Grenoble, France

[3]Department of Microbiology and Immunobiology, Harvard Medical School, USA

*Corresponding authors

ABSTRACT

Background Virulent *Pseudomonas aeruginosa* clonal outliers are characterized by the synthesis of a pore-forming toxin, Exolysin (ExlA). Here we present the first genome-wide analysis of an ExlA-secreting cytotoxic strain, CLJ, isolated from a patient with chronic obstructive pulmonary disease associated with hemorrhagic pneumonia. Two clonal variants, CLJ1 and CLJ3, differing in cytotoxic and antibiotic resistance profiles were analyzed by comparative genomics, transcriptomics (RNA-Seq) and proteomics.

Results These analyses revealed a number of genome modifications leading to phenotypes distinct to those found in classical laboratory strains, reflecting the bacterial adaptation strategies in patient's lungs. Insertion sequences were found in genes encoding flagellum, pili, OprD and in the OSA locus defining O-specific antigens. Gene deletions and differential gene expressions affected the resistance of strains to several antibiotics, notably those used during hospitalization. Moreover, several virulence factors (CdrBA, Lpt), phages and other yet uncharacterized proteins were found differentially expressed between the two strains.

Conclusions Multi-omics analysis of a hyper-virulent Exolysin-secreting *P. aeruginosa* clinical strain revealed multiple adaptation strategies of the pathogen to host environment and antibiotic treatment.

KEYWORDS: adaptation, antibiotic resistance, virulence, bacterial infection, multiomics

RESULTS AND DISCUSSION

P. aeruginosa CLJ possesses different genomic islands compared to PA7

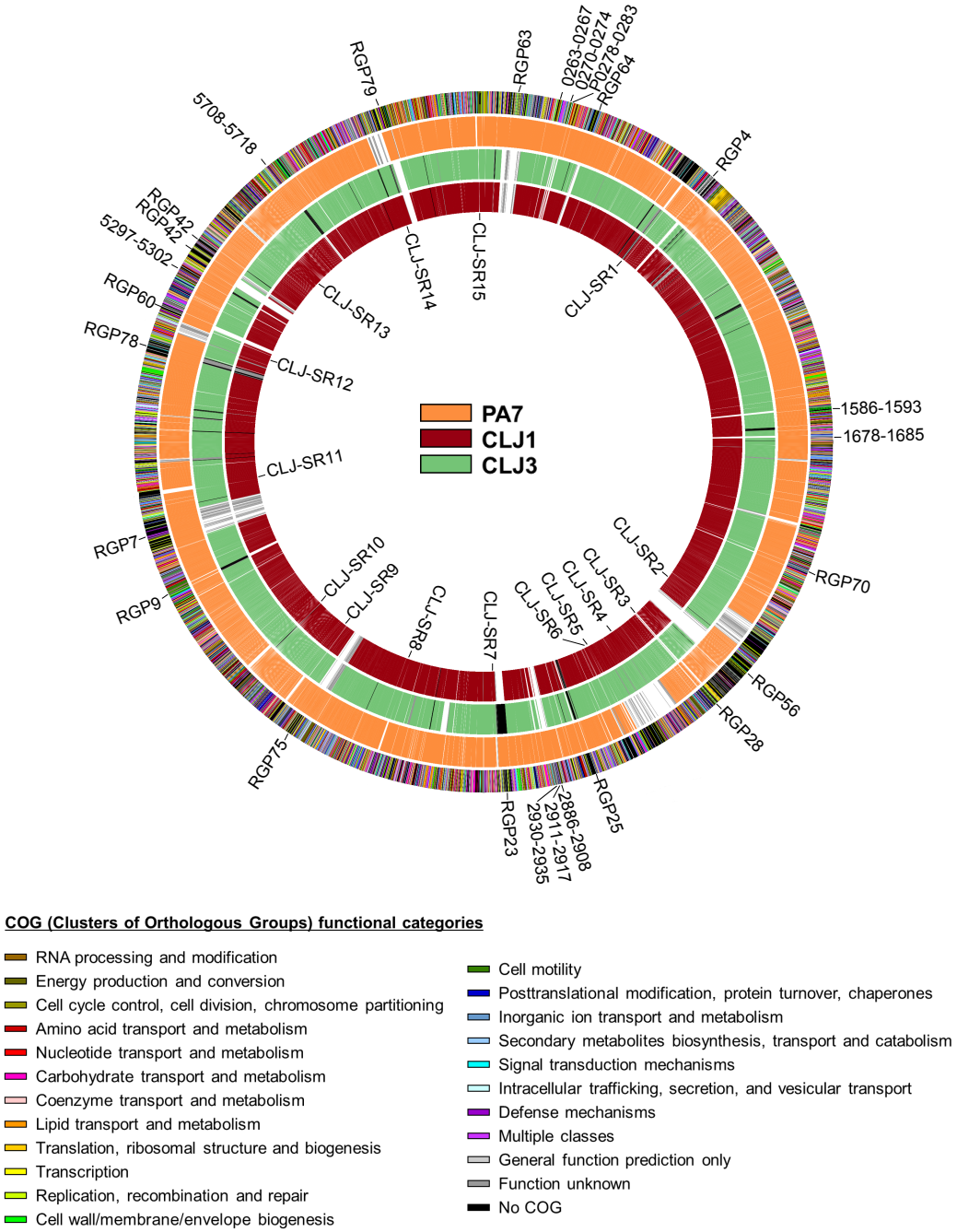

Figure 1. Whole genome comparison between PA7 and CLJ strains. The outer ring shows all the genes in the strains colored according to their COG (Clusters of Orthologous Groups) functional categories as listed on the bottom, and the three other rings represent the PA7 (orange), CLJ3 (green), and CLJ1 (red) genomes, respectively. White color indicates that the gene is absent from the genome, grey color indicates that the gene or its homolog is present in a different position in the genome, while black color in the CLJ rings represents gaps between contigs. The inner labels show the CLJ-specific regions and the outer labels are the PA7-specific regions described in Table 1 and Table 2, respectively.

The proteo-genomics reveals phenotypic adaptation of clonal outliers to the human environment

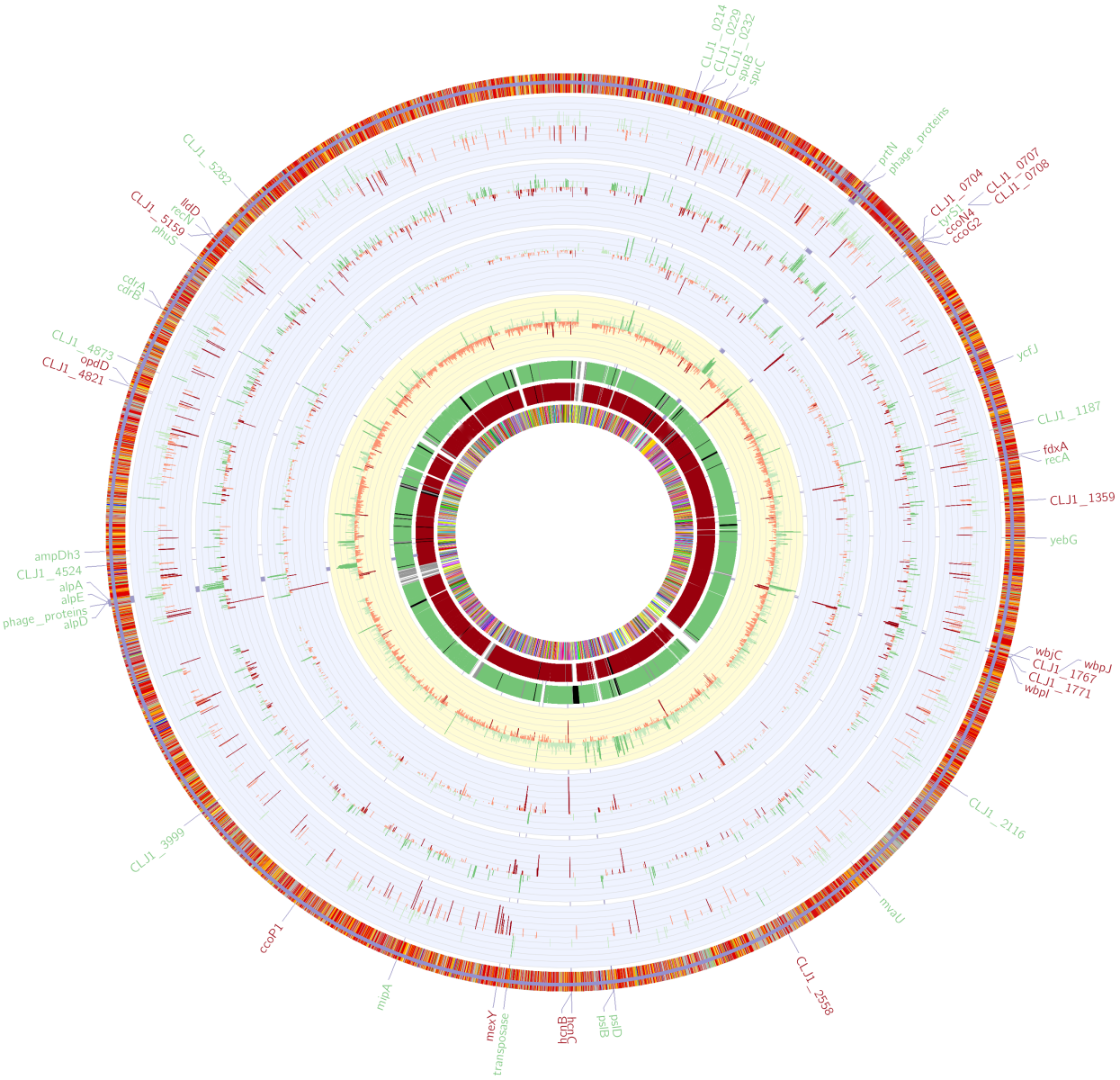

Figure 2. Genome-wide proteomics and transcriptomics comparison between CLJ1 and CLJ3. The three innermost rings are the gene COG categories, CLJ1 (red), and CLJ3 (green) genomes as in Figure 1. The next ring in yellow background is the bar chart of the $\log_2$ fold change of gene expression from RNA-Seq experiment, while the next three rings in blue background are the bar charts of the $\log_2$ fold change of protein expression in total, membrane, and secretome proteome, respectively. The columns in the bar charts are colored red to show that the gene or protein is more expressed in CLJ1, or green in CLJ3; darker tone indicates statistically significant expression difference between the two strains (False Discovery Rate < 0.05). The labels show the genes that are significantly differentially expressed in both RNA-Seq data and at least one of the proteomic data. The outermost ring indicates the protein subcellular localization, colored as in the Pseudomonas Genome Database (Winsor et al 2016, http://pseudomonas.com/).

CLJ strains possess unusual repertoire of surface appendices and putative adhesins

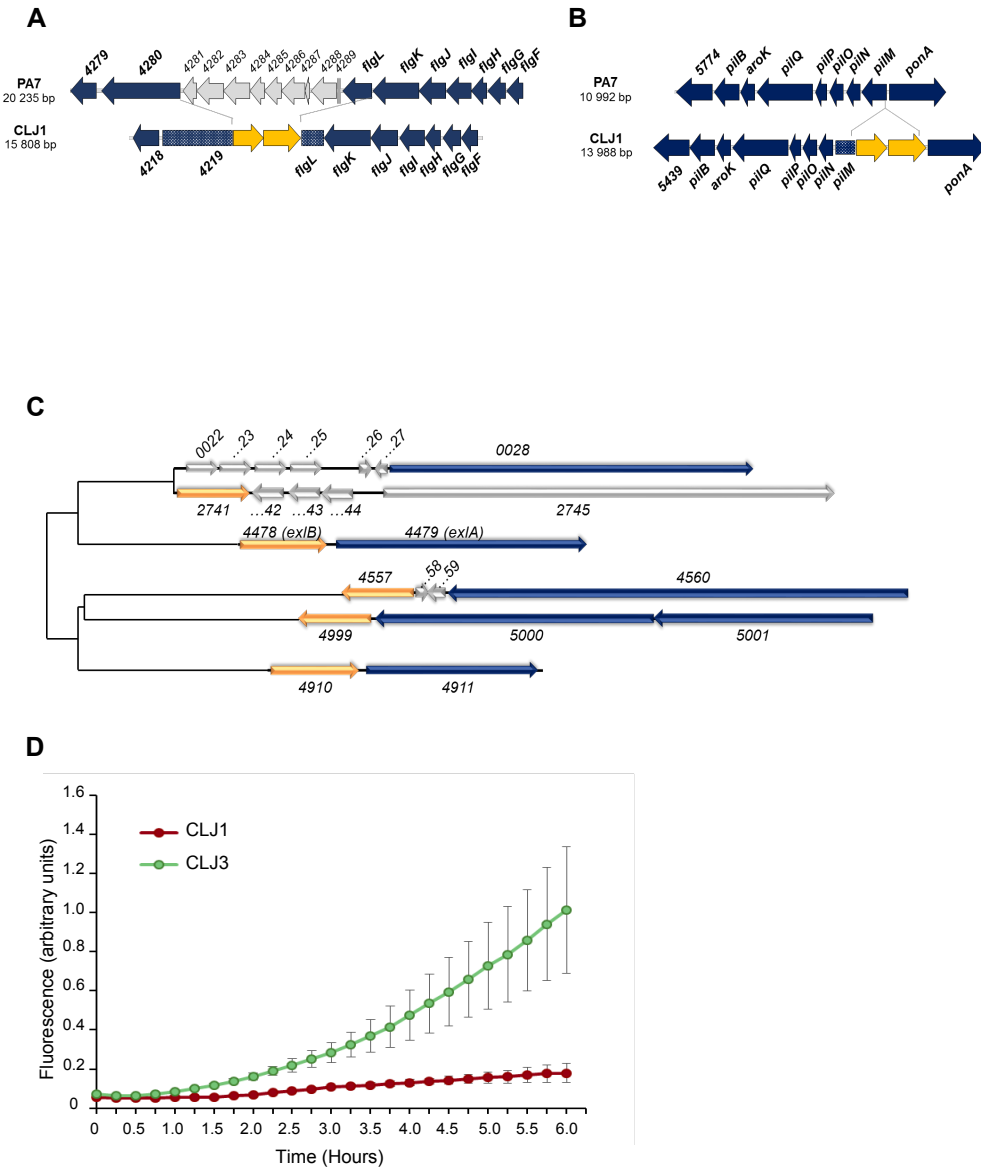

Figure 3. Modifications observed in components associated with surface appendices (A) Gene organization of *flgL* region in PA7 and CLJ1 strains. Genes represented with grey arrows (*PSPA7_4281* to *PSPA7_4289*) in PA7 are deleted in CLJ1 and the genes in orange correspond to the insertion sequences in CLJ1. Note that the genes nomenclature correspond to the nomenclature of PA7 and CLJ1. (B) Representation of the *pilMNOPQ* operon. Orange arrows represent the insertion sequence in *pilM* gene found in CLJ1. (C) *In silico* analysis of heammaglutinins/adhesin proteins. Maximum likelihood tree of TpsB (orange arrow) and TpsA-like (blue arrows) proteins matching with COGxxx. Grey arrows (D) Comparison of c-di-GMP levels in CLJ1 and CLJ3 strains. Fluorescence from CLJ1 or CLJ3 strain carrying p*cdrA-gfp*(ASV)^{c} monitoring plasmid was measured every 15 minutes during 6 hours of growth. The error-bars indicate the standard deviation.

LPS modification due to deletions encompassing galU and OSA loci

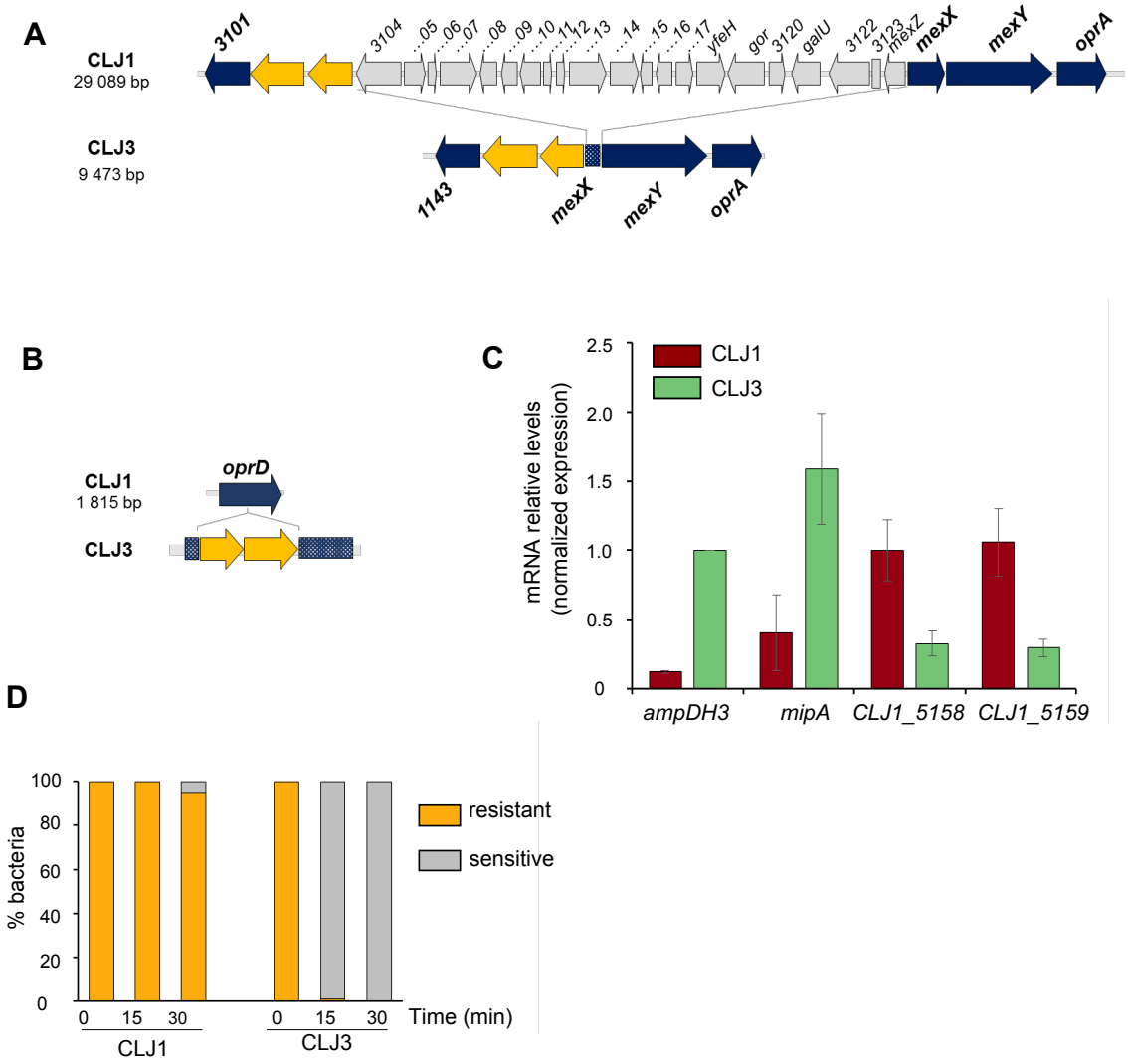

Figure 4. Components involved in antibiotic resistance and LPS modification. (A) Representation of the genes organization in the *gor-galU* region in CLJ1. The grey genes are deleted in the CLJ3 strain (CLJ_3105 to *mexZ*). The *mexX* gene is disrupted by an insertion sequence in CLJ3. Gene names correspond to the according strains CLJ1 or CLJ3. (B) Representation of the *oprD* inactivation in CLJ3. The *oprD* gene is inactivated by an insertion sequence in CLJ3 (orange arrows). (C) Analysis of the relative expression of *mipA* and *ampDH3* in CLJ1 and CLJ3 strains by RT-qPCR. The *rpoD* gene was used as reference. The bars indicate the standard error of the mean. (D) Comparison of serum sensitivity in CLJ1 and CLJ3 strains. CLJ1 and CLJ3 were incubated with human sera and the bacteria were counting on agar plates after 15 and 30 mins

Other putative virulence factors (hcn/lptF) and metabolism

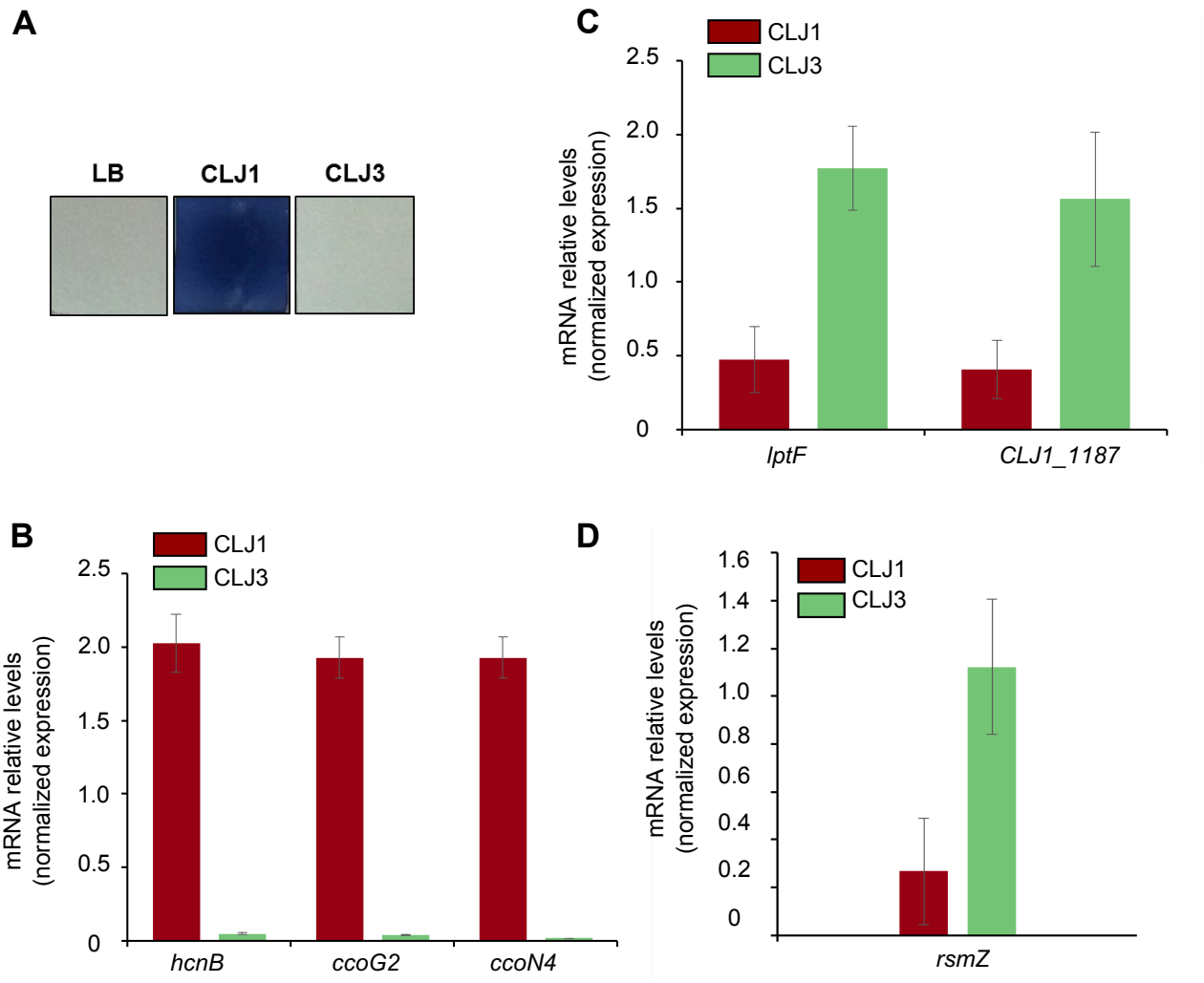

Figure 5. Modification of other virulence factors. (A) Hydrogen cyanide production. (B) Analysis of the relative expression of *hcnB, cccoG2 and cccoN4* in CLJ1 and CLJ3 strains by RT-qPCR. The *rpoD* gene was used as reference. The bars indicate the standard error of the mean. (C) Analysis of the relative expression of *lptF* and CLJ1_1187 in CLJ1 and CLJ3 strains by RT-qPCR. The *rpoD* gene was used as reference. The bars indicate the standard error of the mean. (D) Analysis of the relative expression of *rsmZ* in CLJ1 and CLJ3 strains by RT-qPCR. The *rpoD* gene was used as reference. The bars indicate the standard error of the mean.

CONCLUSIONS

Here we present multi-omics approach on recent isolates belonging to the *P. aeruginosa* clonal outliers. We found that the genome of CLJ is highly dynamic with number of phage sequences and ISs. Global CLJ phenotypes in motility, adhesion and resistance to imipenem are modulated by IS. High expression levels of transposases in the CLJ3 clone suggest their activity in phenotypic adaptation. Although we cannot exclude the co-existence of two isolates at the same time in the patient, the CLJ3 isolate acquired resistance toward antibiotics provided to the patients during the 12 days hospitalization, expresses components that are required for biofilm growth (overproduction of CdrA) and have lost the OSA part of the LPS by *galU* deletion, whereas CLJ1 shows more cytotoxic phenotype by secreting high amounts of pore-forming toxin ExlA.

Table 1. Specific regions of CLJ compared to PA7

Region	RGP	CLJ1 locus	Number of genes	Features
CLJ-SR1	RGP66	0487-0494	8	Phage-related
CLJ-SR2	RGP29*	2128-2214	87	PAGI-2-like island
CLJ-SR3	RGP28	2316-2322	6	Mobile element proteins
CLJ-SR4	RGP27	2415-2573	160	Dit island
CLJ-SR5	RGP72	2579-2583	5	D-galactonate catabolism
CLJ-SR6	RGP26	2615-2621	7	Phage-related; lytic enzymes
CLJ-SR7	RGP23	2917-2924	7	Mobile element proteins; possible DNA helicase
CLJ-SR8		3303-3309	7	ABC transporter ATP-binding protein
CLJ-SR9		3607-3616	9	
CLJ-SR10	RGP15	3774-3784	11	Threonine dehydratase; ABC transporter proteins
CLJ-SR11		4314-4301	14	AlpBCDE-lysis cassette, phage-related
CLJ-SR12		4838-4876	39	Pyrroloquinoline quinone synthesis proteins
CLJ-SR13		5192-5203	10	Phage related; accessory cholera enterotoxin
CLJ-SR14		5811-5871	55	Heavy metal resistance
CLJ-SR15		6156-6161	6	Phage-related

RGP: region of genomic plasticity, *complete RGP

Table 2. Specific regions of PA7 compared to CLJ

PSPA7 numbering	Number of genes	RGP	Features
0069-0139	71	RGP63*	Type I restriction-modification system; mercury resistance cluster
0263-0267	5		Sulfate ester transport system
0270-0274	5		
0278-0283	6		*tonB2-exbB1-exbD1* operon
0355-0369	15	RGP64*	Phage-related
0776-0788	12	RGP4*	Phage-related
1586-1593	8		Polymyxin and cationic antimicrobial peptide resistance cluster
1678-1685	8		Sulfur starvation utilization operon
2109-2112	4	RGP70	Probable transposase
2363-2435	73	RGP56*	Phage-related
2515-2526	10	RGP28	
2790-2795	6	RGP25	Hemagglutinins
2886-2908	23		Hcp secretion island-3 encoded type VI secretion system (H3-T6SS)
2911-2917	7		Methionine ABC transporters; monooxygenases
2930-2935	6		Alkanesulfonate assimilation; nitrate and nitrite ammonification
3034-3071	37	RGP23	Pyocin killing protein; phage-related
3695-3747	53	RGP75*	Conjugal transfer protein cluster; resistance genes; transcriptional regulators
4281-4289	9	RGP9	Rieske family iron-sulfur cluster-binding protein
4427-4530	103	RGP7	Type IV B pilus protein cluster
5053-5075	23	RGP78	Phage-related
5143-5160	17	RGP60*	Phage-related
5297-5302	6		Fimbrial chaperone/usher pathway E operon
5324-5357	34	RGP42	Mobile element proteins; Streptomycin phosphotransferase
5364-5378	15	RGP42	Phage-related
5708-5718	11		Arginine:pyruvate transaminase; 2-ketoarginine decarboxylase
6033-6063	31	RGP79*	Type I restriction-modification system

RGP: region of genomic plasticity, *complete RGP

Table 3. Two-partner secretion (TPS) systems in CLJ1 and their expressions in different proteomic datasets

PA7	CLJ1	Functions	Total	Secretome	Membrane	PAO1
	CLJ1_0022	Putative TpsB	+	+	+	
	CLJ1_0023	Putative TpsA	+	-	+	
	CLJ1_0024	Putative TpsA	-	-	-	
PSPA7_0043	CLJ1_0025	Putative TpsA	-	-	-	-
	CLJ1_0026	Putative TpsA				-
	CLJ1_0027	Putative TpsA				-
PSPA7_0044	CLJ1_0028	TpsA	-	-	+	-
PSPA7_2776	CLJ1_2741	TpsB	+	-	+	-
	CLJ1_2742	Putative TpsA				
	CLJ1_2743	Putative TpsA				
	CLJ1_2744	Putative TpsA				
PSPA7_2777	CLJ1_2745	Putative TpsA	+	+	+	-
PSPA7_4641	CLJ1_4478 (*exlB*)	TpsB	-	-	-	-
PSPA7_4642	CLJ1_4479 (*exlA*)	TpsA	-	+	-	-
PSPA7_4818	CLJ1_4557	TpsB	-	-	-	PA0692 *(pdtB*)
PSPA7_4819	CLJ1_4558		-	-	-	-
PSPA7_4820	CLJ1_4559		-	-	-	PA0691 (*phdA*)
PSPA7_4821	CLJ1_4560	TpsA	-	+	-	PA0690 *(pdtA*)
PSPA7_5270	CLJ1_4999	TpsB	+	-	+	PA4624 (*cdrB*)
PSPA7_5271	CLJ1_5000	TpsA	+	+	+	PA4625 (*cdrA*)
	CLJ1_5001	TpsA	+	+	+	-
PSPA7_5176	CLJ1_4910	TpsB	-	-	-	PA4540 (*lepB*)
PSPA7_5177	CLJ1_4911	TpsA	-	+	-	PA4541 (*lepA*)

+: present, -: absent

8

Genetic screen to identify host factors involved in ExlA-dependent activity

Summary

In parallel to the work presented in the Manuscript 2, I performed a genome-wide loss-of-function screen to identify host factors involved in Exolysin activity in RAW macrophages. This library was provided by Dr. Fikadu TAFESSE (Broad Institute) during my stay in Prof. Stephen LORY laboratory. Out of 130 000 mutated macrophage clones, we selected 200 macrophages that were more resistant to ExlA than the original wild-type cells. We identified *CASP-1*, *IRAK4*, *PRKD2* and microRNA mir-741 as the most enriched hits. We previously validated the Caspase-1 pathway as being activated in ExlA intoxication in mouse primary macrophages. By creating individual KOs, we demonstrated that IRAK4 plays a role in the ExlA-mediated toxicity. Validation of other proteins is underway.

Introduction

Clustered regularly interspaced short palindromic repeats (CRISPR) and Cas genes are the prokaryotic immune systems that are encoded in many bacteria and archaea [329–331]. The CRISPR/Cas9 system from *Streptococcus* is now used for targeted disruption and modification of genes in eukaryotic cells (human, mice, yeast) [332–338], but also in bacterial species [339–341]. Cas9 is a nuclease that can be directed to the sequence of interest by a single guide RNA (sgRNA) sequence to create double strand breaks in the DNA. This induces activation of the host repair mechanisms, often resulting in improper repair of the lesion site and disruption of the target gene. Several CRISPR libraries of sgRNAs targeting more than 20,000 genes were designed for mouse or human cells and created loss-of-function of genes in a variety of cell types. In particular, this technology coupled with the high-throughput sequencing Illumina allowed a better understanding of global host-pathogen interaction (viruses and bacteria). In the case of bacterial toxins (Anthrax, T3SS), screens of CRISPR/Cas libraries led to identification of novel cellular targets, receptors and

regulatory proteins. For example α-HL of *S. aureus* forms pores in cell membranes and requires the A Disintegrin And Metalloproteinase domain-containing protein 10 (ADAM10) for the pore formation [272, 273]. Recently Winter and colleagues [274] used a genome-wide CRISPR screen in U937 cells to identify other host factors that may be involved in the α-HL activity. They demonstrated, in accordance with the previous study that ADAM10 is the protein receptor of the α-HL and also identified three other proteins that participate in ADAM10 regulation (SYS, ARFRP1 and TSPAN14).

Two clades of *P. aeruginosa* employ two distinct mechanism of virulence: the T3SS that injects effectors directly in the cytoplasm of the host cells and the TPS ExlBA, where ExlA is a pore-forming toxin [1, 126, 320]. ExlA, to efficiently form a pore in the host plasma membrane requires close contact between the bacteria and the host cell, mediated by the Type IV pili. This mechanism is not common within the pore-forming toxins, which are usually active in their soluble form. Targeted approaches using individual genetically modified macrophages allowed to show that Caspase-1 and NLRP3 were involved in the ExlA-mediated death [342]. Moreover, the flagellum is able to prime the macrophages to enhance the inflammatory response [80–84, 343, 344]. In this study, we used a genome-wide screening to identify additional host factors interfering with ExlA-mediated cytotoxicity. The CRISPR library that we used contains 130 000 sgRNAs targeting more than 20 000 genes in mouse RAW macrophages. We used the *E. coli* strains expressing *exlA* gene to perform the screen. Approximately 200 macrophage clones survived after 6 hours of infection. High-throughput sequencing revealed several highly enriched genes in the output clones, including those encoding *Casp1*, *IRAK4* and *PRKD2*. Individual gene invalidations of some of them confirmed that these proteins identified in the screen indeed participate in ExlA-mediated cell death.

Experimental procedures

Selection of resistant CRISPR RAW macrophages to ExlA intoxication.

The mouse GecKov2 library[1] contains 130,209 sgRNA sequences in the lentiCRISPR v2 vector [345]. The RAW library was seeded in ten flasks T225 (cm^2) for 16 hours in DMEM 1x without pyruvate (Gibco life technology) in 5 % of CO_2, 37°C.

Optimization steps.

The optimization steps were performed on RAW WT macrophages. We used a strain of *E. coli* expressing *exlBA* under a promoter inducible by arabinose [126] . We optimized arabinose concentration, growth and MOI. For the arabinose concentration, we tested induction from 0.001 % to 0.05 % on the bacterial growth. We also compared two durations (1 hour or 3.5 hours) of induction with 0.05 % of arabinose on the bacterial growth and ExlA secretion.

Escherichia coli strain expressing *exlBA* genes under a promoter inducible with arabinose was cultured overnight and then diluted at OD_{600} of 0.06 into Lysogeny

[1] https://www.addgene.org/pooled-library/zhang-mouse-gecko-v2/

broth (LB) and grown to OD_{600} of 0.6. At this point, the bacterial culture was induced with 0.05% of arabinose for 1.5 hours. CRISPR RAW library was infected at a Multiplicity of Infection (MOI) of 20 and incubated at 37°C with 5 % of CO_2 for 6 hours. After infection, the incubation media were replaced with fresh DMEM medium supplemented with 100 000 U of Penicillin and 100 mg of Streptomycin. The cells that survived were expanded for three weeks until macrophage colonies appeared.

Genomic DNA preparation, sequencing, and analyzes of results.

Genomic DNA (gDNA) was extracted from 8×10^7 cells after the cell expansion. Cells were lysed with 6 ml of Lysis Buffer (50 mM Tris, 50 mM EDTA, 1% SDS, pH 8) in presence of 30 μl of 20 mg/ml Proteinase K at 55°C for 16 hours. The next day, 30 μl of 10 mg/ml RNase A was added to the sample and incubated at 37°C for 30 min. Samples were cooled on ice before addition of 2 ml of pre-chilled 7.5 M ammonium acetate pH 8 to precipitate proteins. Stock solution of 7.5 M ammonium acetate was made in sterile H_2O and kept at 4°C until use. After adding ammonium acetate, the samples were vortexed for 20 s and then centrifuged at 4,000 g for 10 min. After the spin, 6 ml 100% isopropanol was added to the supernatant and centrifuged at 4,000 g for 10 min. The supernatant was discarded, 6 ml of freshly prepared 70 % ethanol was added and centrifuged at 4,000 g for 1 min. The pellet containing the genomic DNA was dried for 10-30 min and then 500 μl of 10 mM Tris-HCl, 1 mM EDTA pH 8 (TE) buffer was added and incubated first at 65°C for 1 hour and then at room temperature overnight. The next day, the gDNA samples were briefly vortexed . PCRs to amplify sgRNA were done with primers PCR1_F: AATGGACTATCATATGCTTACCGTAACTTGAAAGTATTTCG and PCR1_R: CTTTAGTTTGTATGTCTGTTGCTATTATGTCTACTATTCTTTCC. The PCR conditions for 50 μl were 25 μl of Green mix Go-Taq (Promega), 2 μM of each primers, 2 μg of gDNA, 1 μl of Go-Taq enzyme. PCRs were done in two round using the following program, denaturation at 95°C for 3 min, followed by 24 cycles 98 °C for 20 sec, 65°C for 15 sec and 72°C for 7 sec and final elonagtion at 72°C for 5 min. The Illumina libraries were prepared following the method of the NEBNext kit (Biolabs, ref E7645S). Sequencing was performed by MiSeq, Illumina at Harvard Medical School.

Lentiviral vector construction.

The individual gene inactivation by CRISPR/Cas method was performed using the protocol described by Zhang et al. sgRNAs were design using the MIT CRISPR website[2]. For each gene, 3 sgRNAs were designed targeting 3 different exons of the given gene (Table 8.1). LentiCRISPRv2 vector (5 μg) was digested and dephosphorylated for 30 min at 37°C using 3 μl of FastDigest *Bsm*BI enzyme and 3 μg of FastAP (Fermentas). The digested vector was purified on agarose gel. In parallel, each pair of oligos were phosphorylated and annealed. 1 μl of each oligo was mixed with 0.5 μl of T4 Polynucleotide Kinase (PNK) in 10x T4 ligation buffer supplemented with

[2] http://crispr.mit.edu:8079/

1 mM ATP. The reaction was done in a thermocycler using the following parameters: 37°C for 30 min and 95°C for 5 min then ramp down to 25°C at 5 °C/min. Then the annealed oligos were diluted in 1/200 in TE buffer and cloned into the digested lentiCRISPRv2 vector using the ligase (NEB). A negative control was done without oligos (empty vector). Plasmids were selected by transformation into *E. coli* Top10 on LB agar plated supplemented with 100 μg of Ampilicin. The clones were checked by *Bam*HI and *Spe*I restriction enzymes.

Names	Sequence 5'-3'
Oligo sgRNA_ PtprD_ex1_F	CACCGAGCGCTCGCTCGGCGTCGGT
Oligo sgRNA_ PtprD_ex1_R	AAACACCGACGCCGAGCGAGCGCTC
Oligo sgRNA_ PtprD_ex2_F	CACCGCCCCGAAGGGGAGCAGTGAC
Oligo sgRNA_ PtprD_ex2_R	AAACGTCACTGCTCCCCTTCGGGGC
Oligo sgRNA_ PtprD_ex4_F	CACCGTATGCTGGCCCCAATGTTGA
Oligo sgRNA_ PtprD_ex4_R	AAACTCAACATTGGGGCCAGCATAC
Oligo sgRNA_ PTN14_ex1_F	CACCGGCACCGCCGTCCCACGCGAG
Oligo sgRNA_ PTN14_ex1_R	AAACCTCGCGTGGGACGGCGGTGCC
Oligo sgRNA_ PTN14_ex2_F	CACCGTGTTACCCGGATCCGCCTGC
Oligo sgRNA_ PTN14_ex2_R	AAACGCAGGCGGATCCGGGTAACAC
Oligo sgRNA_ PTN14_ex3_F	CACCGGCTCTACCCATCTCGCCTGC
Oligo sgRNA_ PTN14_ex3_R	AAACGCAGGCGAGATGGGTAGAGCC
Oligo sgRNA_ Prkd2_ex1_F	CACCGAAAGTTTAAGTCGGCAGCGG
Oligo sgRNA_ Prkd2_ex1_R	AAACCCGCTGCCGACTTAAACTTTC
Oligo sgRNA_ Prkd2_ex2_F	CACCGATCCGAGAGCTCTCTTGCGG
Oligo sgRNA_ Prkd2_ex2_R	AAACCCGCAAGAGAGCTCTCGGATC
Oligo sgRNA_ Prkd2_ex4_F	CACCGGCGATCAGCTGCAGATATCC
Oligo sgRNA_ Prkd2_ex4_R	AAACGGATATCTGCAGCTGATCGCC
Oligo sgRNA_ Irak4_ex1_F	CACCGATCGGCGTCCCGCCACGGTC
Oligo sgRNA_ Irak4_ex1_R	AAACGACCGTGGCGGGACGCCGATC
Oligo sgRNA_ Irak4_ex2_F	CACCGTTGTATCTGTCGTCGCCGGA
Oligo sgRNA_ Irak4_ex2_R	AAACTCCGGCGACGACAGATACAAC
Oligo sgRNA_ Irak4_ex3_F	CACCGGTCGCCAACTGTGCAGTTCG
Oligo sgRNA_ Irak4_ex3_R	AAACCGAACTGCACAGTTGGCGACC

Table 8.1. **Primers used for sgRNA design.** The sgRNA were designed by using the MIT CRISPR tools[3]. The genes were *PTPRD* for protein tyrosine phosphatase, receptor type, D, *PTN14* for Tyrosine-protein phosphatase non-receptor type 14, *PRKD2* for Serine/threonine-protein kinase D2, and *IRAK4* for Interleukin-1 receptor-associated kinase 4.

Lentivirus production and transduction.

HEK 293T cells were cultivated in DMEM 1x (Gibco Life technology) supplemented with 10 % of SVF. For the lentivirus production, 6×10^5 HEK 293T cells were

plated in 10 cm^2 plates four days before the transfection. The transfection was done using the Calphos mammalian Transfection kit. 8.6 μg of psPAX2 vector expressing *gag*, *pol*, *rev*, and *tat* genes used for vector packaging was mixed with 8.6 μg lentiCRISPRv2sgRNA, 2 μg of pCMV vector carrying *env vsv-g* gene coding for the lentivirus envelope and 250 mM $CaCl_2$. HBS were added drop by drop in the first solution under vortex. The mix was kept 10 min at room temperature and was added to HEK 293T cells overnight at 37°C. The transfection medium was changed with fresh DMEM 1x medium. After 48 hours, the supernatant containing the lentivirus was harvested and centrifuged at 2, 000 rpm at 4°C for a night. 5×10^5 RAW cells were seeded in DMEM 1x without pyruvate, supplemented with 10 % of SVF. Before the transduction, the cell medium was changed with DMEM supplemented with 8 ng/μl of polybrene. Lentiviruses were added and incubated for 6 hours, and then the medium was changed with DMEM for a night. The positive cells were selected by the addition of 7 μg/ml of puromycin for three weeks.

Cytotoxicity assay.

The cytotoxicity assays were performed as previously described [342]. Briefly, 1×10^4 RAW macrophages were seeded per well in 384-well plates for 16 hours and then incubated for 1 hour with Syto24 (0.5 μM, Life Technologies), a dye labelling the nuclei of all the cells. Propidium Iodide (1 μM, Sigma), an impermeant dye was added just before the infection. Cells were infected with different bacterial strains (Table 8.2) for 6 hours at an MOI of 20. The kinetics of PI incorporation was followed using an automatized microscope IncuCyte[4]. Acquisitions were done every hour using a 10X objective for 6 hours. Images from bright field (phase), green channel (acquisition time 200 nm) and red channel (acquisition time 200 nm) were collected. Number of live macrophages was calculated from the formula: Number of total cells (Syto24 positive cells) - number of dead cells (PI positive cells)

Strains	**Characteristics**	**References**
PAO1F	*P. aeruginosa* expressing *exoS, T, Y*	[346]
PP34	*P. aeruginosa* expressing *exoU, T, Y*	[347]
IHMA879472	*P. aeruginosa* expressing *exlA* (IHMA)	[320, 348]
KT2440	*P. putida* expressing *hlpA-hlpB exlA*-like toxin	[349, 350]
L48	*P. entomophila* expressing *exlA*-like toxin	[351]
CHA0	*P. protegens* expressing *exlA*-like toxin	[352]
Db10	*S. marcescens* expressing *shlA*	[353]
E. coli BA	*E. coli* expressing *exlBA*	(This work)

Table 8.2. **Bacterial strains used in this work.**

[4]http://www.essenbioscience.com/en/products/incucyte

Results

Overview of the screening approach.

Prior to the screening of the library, we optimized several parameters such as bacterial growth, concentration of arabinose for ExlA induction and MOI. The goal was to eliminate more than 99 % of the RAW library in a relatively long period (5-6 hours) of infection. To summarize, based on the number of macrophage clones that we recovered in three independent experiments, we determined that the infection at a MOI of 20 for 6 hours was the best condition to perform the screen (Figure 8.1A).

A

Time (h)	Number of macrophages colonies			Mean	Standard deviation
	Exp. #1	Exp. # 2	Exp. # 3		
5	120	130	110	120	10
5.5	110	115	98	107,7	8,7
6	50	60	55	55	5
6.5	0	10	5	5	5

B

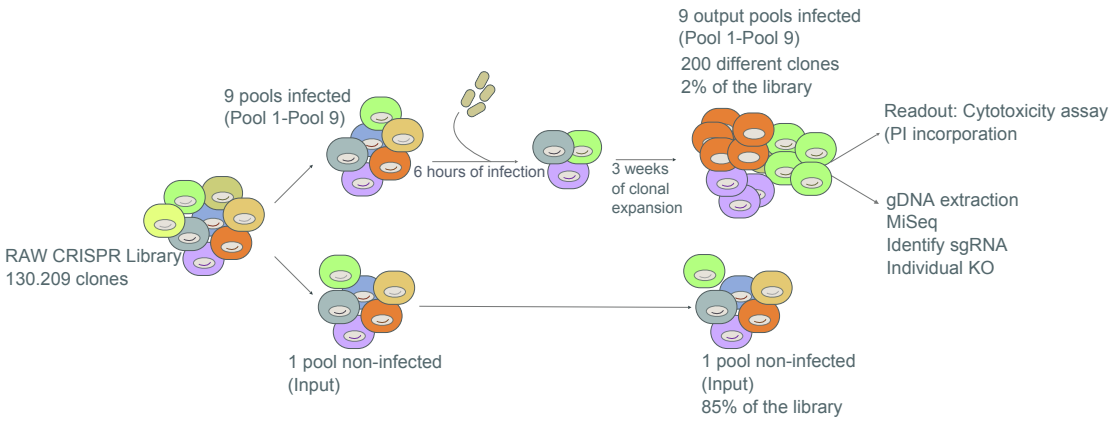

Figure 8.1. **Overview of the screening approach.** Number of macrophage colonies in function of time of infection.

The library was seeded in 10 flasks and infected under optimized conditions (Figure 8.2). At the end of infection remaining cells were expanded for three weeks giving 20-30 clones per flask. Therefore, more than 99% of the library was killed confirming the stringency of the screen.

Screen of the Raw CRISPR/cas library revealed different susceptibility to ExlA in "output pools".

After the screen the output pools were amplified and tested for resistance by high-throughput method based on live-cell imaging of PI incorporation [342].

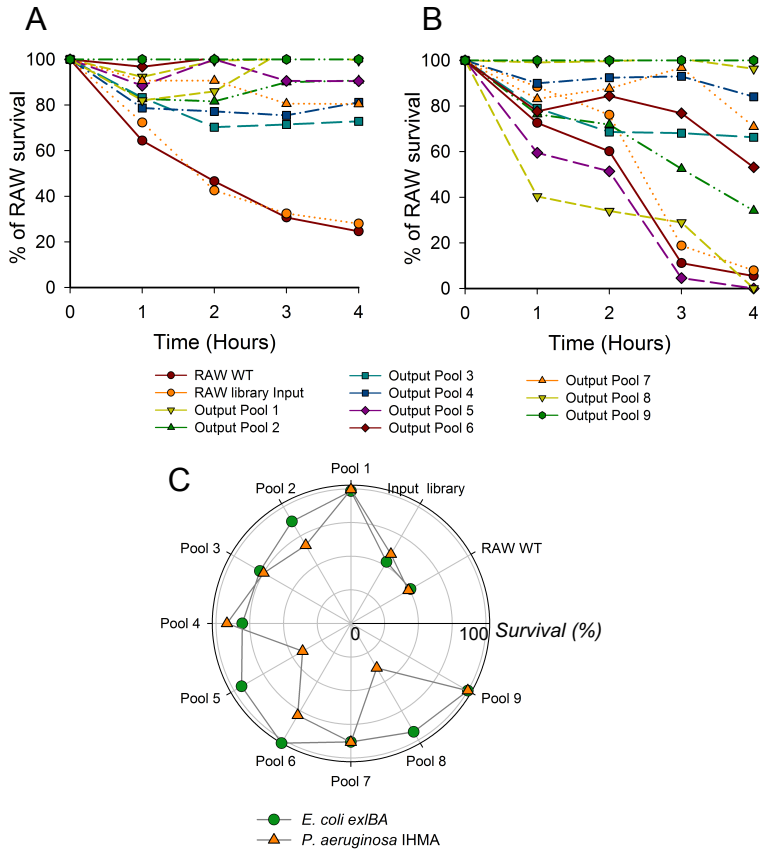

Figure 8.2. **Response of output pools to ExlA-mediated cytotoxicity.** Survival rates of nine output pools after infection at MOI 20 with *E.coli exlBA* (A) and *P. aeruginosa* IHMA (B) for 4 hours. As controls RAW WT macrophages and input library were used. (C) Polar Plot representing the area under the curves (A.U.C) for each kinetic of survival for *E. coli exlBA* and *P. aeruginosa* IHMA. Note that pools 1,4,7 and 9 contain macrophages resistant to ExlA secreted by both *E. coli* and *P. aeruginosa*.

E. coli exlBA provoked rapid cell death of WT RAW macrophages, reaching 70 % of cytotoxicity after four hours. The input library showed a similar kinetics. On the contrary, the selected macrophages from the nine output pools were more resistant to ExlA and presented a survival between 70 % and 99 % (Figure 8.2 A). This result showed that the screen greatly enriched for the resistant macrophages.

Then, we tested the survival of output macrophages following infection with *P. aeruginosa* IHMA secreting ExlA. Compared to the cytotoxicity of wild-type cells and "input" library, we observed a range of survival rates within the nine pools of macrophages. Pools numbered 2, 5 and 8 were found to be more sensitive to infection with *P. aeruginosa* IHMA compared to *E. coli exlBA*, suggesting that *P. aeruginosa* cytotoxicity involved other bacterial factors, in addition to ExlA. Finally, the other pools (1, 3, 4, 6, 7 and 9) were more resistant and presented a survival of 70 % compared to the input (Figure 8.2 B), similarly to the assay with *E. coli exlBA*.

To quantify the global survival of the macrophages from the nine output pools,

the A.U.C of PI incorporation kinetics were calculated, compared and represented by polar plots (Figure 8.2 C). The more the macrophages were resistant to ExlA-mediated toxicity, the higher is the A.U.C. We observed that the survival of output macrophages from pools 1, 3, 4, 6, 7 and 9, infected with *E. coli exlBA* and *P. aeruginosa* IHMA were increased between 2 and 3 fold (Figure 8.2 C), suggesting that in these pools we enriched macrophages containing a disruption of gene(s) involved in the ExlA-mediated toxicity.

Response to infection by different *Pseudomonas* strains.

We previously demonstrated that ExlA-like toxins were secreted by *P. putida* KT2440, *P. entomophila* L48 and *P. protegens* CHA0 and provoked a cell death dependent on the Caspase-1 [342]. We compared the survival of the "output" macrophages after infection with those *Pseudomonas* species. As control, we tested the *S. marcescens* strain Db10, secreting ShlA, the closest homolog of ExlA. For all the species, the kinetics of survival of output macrophages were monitored, the A.U.C were calculated and represented by a polar plot (Figure 8.3 A).

Macrophages present in "output" pools showed different kinetics of mortality when infected with ExlA-secreting *Pseudomonas*. For the majority of pools the survival was increased for 2.5 fold compared to the WT cells, whereas, the pools 7 and 9 were more susceptible. In addition, the macrophages from pool 6 were more susceptible to *S. marcescens* (ShlA) than the other pools. Interestingly, macrophages from the pool 1 are totally resistant to the ExlA-like toxin effect (Figure 8.3 A).

These results suggest that all the ExlA-like toxins from *Pseudomonas* species target the same host factors modified at least in output pool 1.

Classical strains of *P. aeruginosa* with active T3SS, PAO1 (ExoS+) and PP34 (ExoU+) were also tested to challenge the survival of the macrophages. It has been previously shown that the two strains induced different cell responses, with ExoS-positive strain (PAO1) causing a cell death dependent of Caspase-1 in contrast to ExoU-positive strain (PP34). We observed that the survival of the nine output pools was not homogeneous and varied when challenged with the 2 strains. Indeed, pools 1, 2 and 3 were more susceptible to infection with PAO1 (ExoS+), whereas pools 2 and 3 infected with PP34 (ExoU+) were resistant (more than 2.5 fold) (Figure 8.3 B). In addition, pools 5, 6, 7, 8 and 9 were resistant to an infection with ExoS positive strains. The contribution of the effectors (ExoU and ExoS) and the pore formation by the translocon needs to be explored in more detail.

Altogether these results showed different patterns of macrophage survival in function of the bacterial virulence factors (ExlA vs T3SS) (Figure 8.3 C).

Identification of disrupted genes in resistant macrophages.

To identify the genes disrupted by the sgRNAs in the resistant macrophages, we isolated the genomic DNA, amplified the sgRNA by PCRs and analyzed the relative sgRNA abundance by high throughput sequencing. For the analysis, the reads were mapped to the initial library of sgRNAs using CLC workbench software and

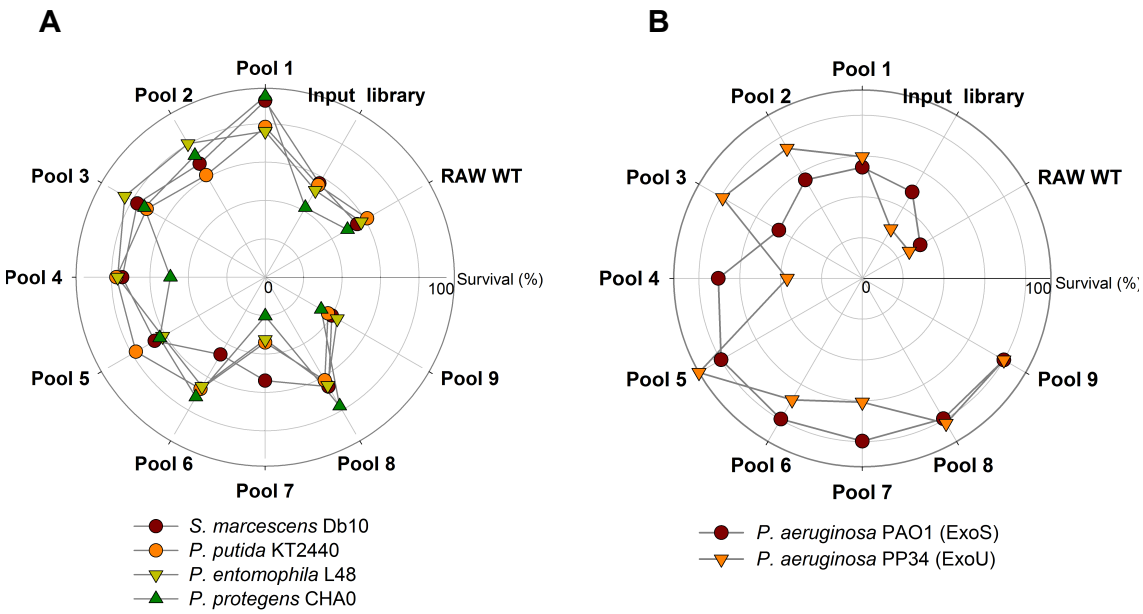

Figure 8.3. Responses of selected pools of macrophages following infection with various *Pseudomonas* strains. (A) Polar plot representing the area under the curves for the survivor macrophages infected with *Pseudomonas* producing ExlA-like toxins at MOI 20 for 4 hours. (B) Polar plot of the A.U.C of survivor macrophages infected with T3SS positive strains at MOI 20 for 4 hours.

CaRpool[5]. Reads from each of nine output pools were treated individually or they were merged and compared to the input. These different analyses allow to distinguish the enrichment of all sgRNAs in each pool. High throughput sequencing revealed that the input pool i.e, CRISPR library macrophages contained 85% (120 000) of all sgRNAs present in the initial Geckov2 library, whereas the output pools contained 2% of sgRNA (2 531). The number of reads per sgRNAs ranged from 1-1,000 (input library) to 1-400,000 (infected) showing that infection with *E.coli exlBA* greatly enriched the portion of sgRNAs (Figure 8.4 A).

We extracted the 30 most enriched genes where at least 3 different sgRNAs were found (Figure 8.4B). Among the 30 genes, we found Sperm Associated Antigen 16 (*SPAG16*), the protein phosphatase 1 regulatory subunit 27 (*PPP1R27*), the interleukin-1 receptor-associated kinase 4 (*IRAK4*), the Caspase-1 (*CASP1*) and the protein Kinase D2 (*PRKD2*) were most enriched. We also found four sgRNAs targeting micro RNAs, mir-6358, mir-741, mir-1969 and mir-192, which are small noncoding RNAs acting as potent regulators of gene expression (Table 8.5).

The correlation matrix between the pools (Figure 8.4C) shows that the input pool was very different from all the output pools. Nevertheless, within the output pools we can define 3 clusters. The first comprised the pools 3 and 4 in which *IRAK4*, canopy FGF signaling regulator 3 (*CNPY3*), transmembrane protein 201 (*TMEM201*), and zinc finger protein 606 *ZFP606* were highly enriched. For these two

[5]R package, www.caRpool.com

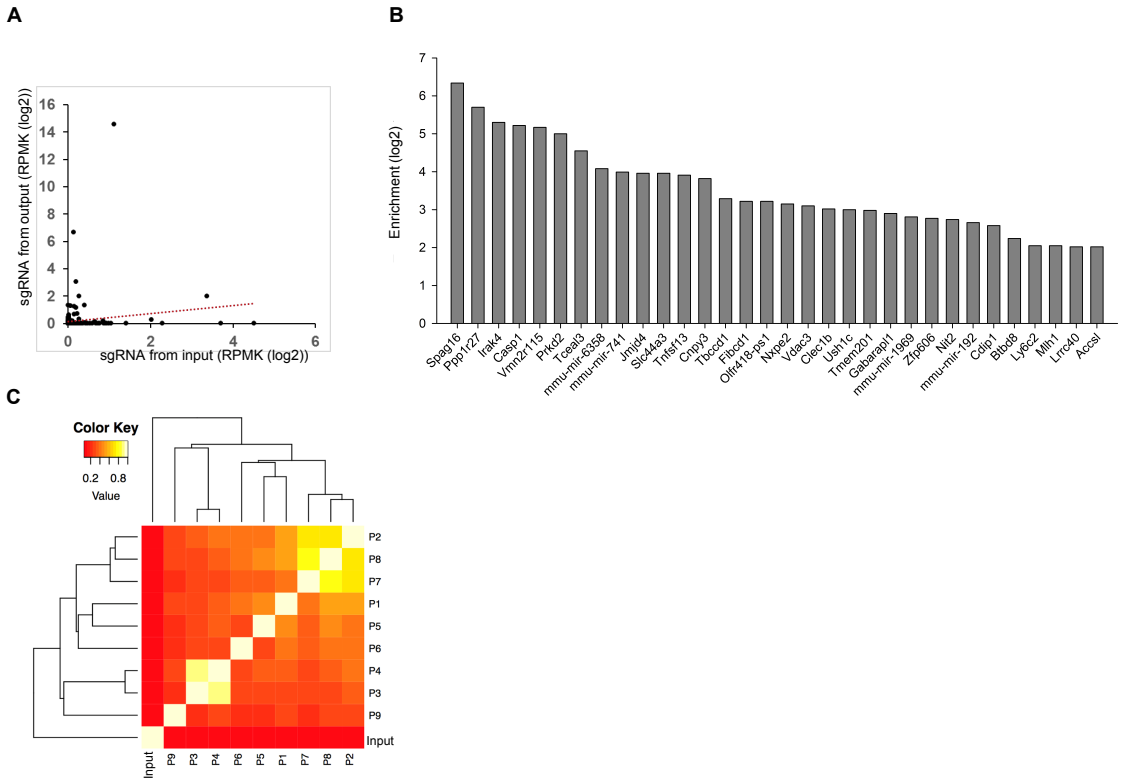

Figure 8.4. Analysis of the enriched sgRNAs and correspond genes after the screen. (A) Scatterplot showing the enrichment of the specific sgRNA after a screen with ExlA. (B) Enrichment of sgRNAs of the 30 most enriched genes after screen. (C) Correlation matrix of the principal component analysis. Figures A and B were obtained by a global analysis by merging reads and figure C with an analysis per pools

pools the survival of the macrophages after intoxication with ExlA was around 80 % as shown in Figure 8.2. The second cluster contains pools 6, 5 and 1. In the pool 6, the *CASP1* gene was highly enriched compared to the other pools. In the pool 1 we found that a micro RNA mir-741 present the most important enrichment (7.5 log(2)). The last cluster comprised pools 7, 8 and 2, in which the *PRKD2*, *Tceal3*, *VMN2R* genes was very enriched. Finally, the pool 9 was found highly different from the other output pools (Figure 8.4C and Figure 8.5). We classified targeted genes by their known or predicted cellular localization, biological processes and molecular functions they might be involved in, by using a mouse genes database (www.informatics.jax.org). Predicted targets for each miRNAs were defined using MirNET database[6](Figure 8.5).

Among 30 hits, 23% of the proteins, such as *PRKD2*, *TNFSF13* (tumor necrosis factor (ligand) superfamily, member 13), *CLEC1B* (C-type lectin domain family 1, member b), *USH1C* (USH1 protein network component harmonin), *GABRAPL1* (gamma-aminobutyric acid (GABA) A receptor-associated protein-like 1), *LY6c2*

[6]http://www.mirnet.ca/

Genes	Pool 1	Pool 2	Pool 3	Pool 4	Pool 5	Pool 6	Pool 7	Pool 8	Pool 9	Merged
Spag16	3,87	2,36	2,35	0,07	1,6	2,62	9,09	9,15		6,34
Ppp1r27	6,6	1,41				9,33				5,7
Irak4	0,9	1,07	2,3	5,25	0,26	0,31	2,3			5,3
Casp1	0,26					3,5				5,22
Vmn2r115	3,3	6					5,66	5,71		5,17
Prkd2	2,6	9,06					5,07	5		5
Tceal3	0,02	6,74					5,7	5,85		4,55
mmu-mir-6358	0,3	5,69					2,86	2,92		4,08
mmu-mir-741	7,5									3,99
Slc44a3	0,19								7,61	3,96
Jmjd4	0,84	5,6				3,57	2,73	2,79		3,96
Tnfsf13	7,4									3,91
Cnpy3	1,2		6	4,51						3,82
Tbccd1	0,8				7,14					3,29
Fibcd1	0,6								6,71	3,22
Olfr418-ps1	6,7									3,22
Nxpe2				0,14					6,63	3,15
Vdac3	0,7				6,96					3,1
Clec1b					6,84					3,02
Ush1c						6,66				3
Tmem201			4,87	5,06						2,98
Gabarapl1									6,4	2,9
mmu-mir-1969	6,3									2,81
Zfp606			4,52	5,2						2,77
Nit2	3,5		2,23	0,78	1,2	5,63	4,08	4,05	0,2	2,74
mmu-mir-192					6,51					2,66
Cdip1			3,6	5,8						2,58
Btbd8_			4	4,47						2,24
Mlh1					5,9					2,05
Ly6c2			3,63	3,62						2,05
Lrrc40			4,09	3,39						2,021
Accsl		5,21					2,95			2,02
Tmod4	1,23	0,13	6,31	8,44					6,3	2,019

Figure 8.5. List of the 30 most enriched genes. Enrichment fold (log2) obtained by individual pool analysis and by global merged analysis is indicated for each gene.

(lymphocyte antigen 6 complex, locus C2) and *LRRC40* (leucine rich repeat containing 40) were located in the plasma membrane (Figure 8.6). Those proteins could play a role as receptors for ExlA. For Example, *PRKD2* that has one transmembrane domain, can bind to diacylglycerol (DAG) in the trans-Golgi network (TGN) and may regulate basolateral membrane protein exit from TGN was chosen for further validation by creating targeted CRISP/cas gene KOs.

Moreover, many cytoplasmic proteins were also enriched and among them were found *CASP-1* and *IRAK4*. Caspase-1 is often associated with the defense against pathogens. It is a key protein of pyroptosis cell death and is responsible for the maturation of the Interleukin-1β to provoke an inflammatory cell death. As described in Chapter 6, we showed that Caspase-1-negative primary macrophages are resistant to ExlA which validates our screen [342].

Interleukin-Receptors-associated Kinase (IRAK4) is a Serine-Threonine kinase and is an essential component of the signal transduction complex downstream of the interleukin and Toll-like receptors playing a crucial role in pro-inflammatory response [191, 354]. Indeed, TLR4 is activated by bacterial LPS, that allows the recruitment of MyD88 and IRAK4 leading to the expression of inflammatory cytokines such as IL-1β, IL-6 and IL-12. The validation of IRAK4 in the ExlA-mediated cytotoxicity will be detailed in the Figure 8.7.

The most interesting target, miRNA mir-741 plays a role in the regulation

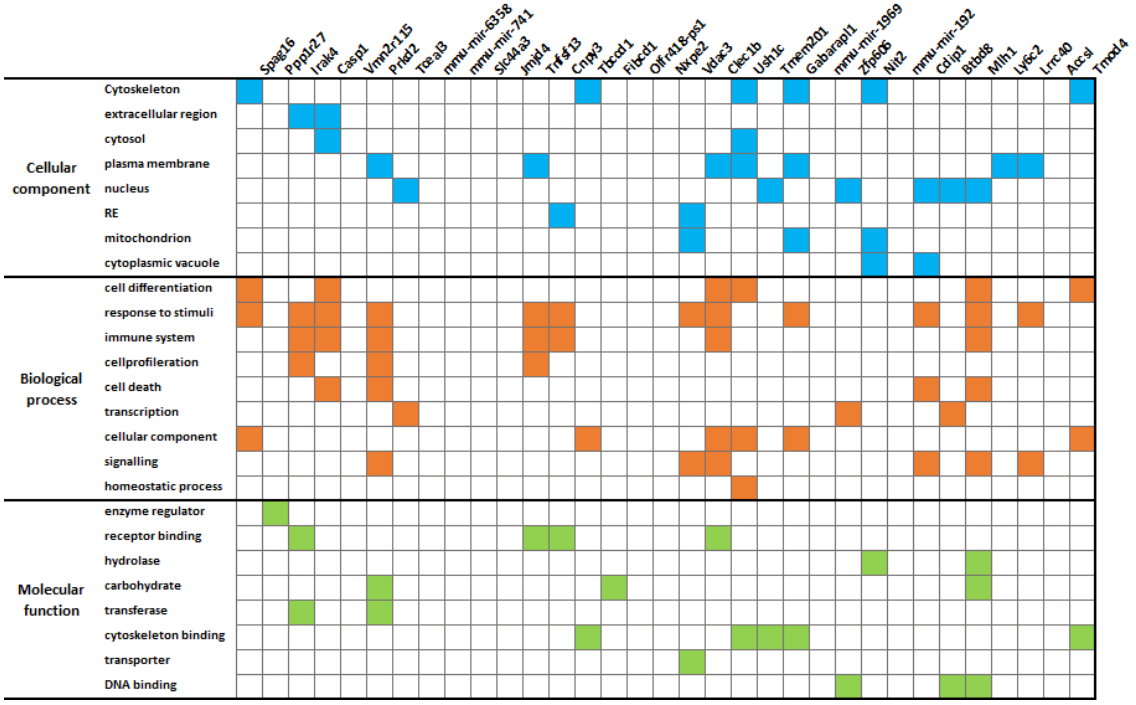

Figure 8.6. **Overview of the cellular components, and the biological function for the specific enriched genes.** (A) Classification of the proteins coded by the enriched gene, in function of the cellular component, biological process and molecular function.(B) MiRNA pathways

of enzymes involved in the biosynthesis and metabolism of the sphingolipid and glycerophospholipid pathways, involving ST8SIA1 and AGPAT5 enzymes. Both classes of lipids are the major components of the plasma membrane of eukaryotic cells [355]. The composition of lipids in the plasma membrane may be important for the ExlA activity during the pore formation, and needs to be investigated in more detail. To that aim, we will target mir-741 by siRNA approach, create individual CRISPR KO for ST8SIA1 and AGPAT5 enzymes and use drugs to inhibits the sphingolipid biosynthesis pathway.

IRAK4 KO macrophages are resistant to ExlA-mediated cytotoxicity

To validate the role of IRAK4 in the ExlA-mediated cytotoxicity, we designed three new sgRNAs that target the three first exons of the gene in RAW macrophages. To increase the chance to inactivate the gene we combined the sgRNA targeting the different exons to obtain seven different combination of sgRNAs. As a control, we used an empty vector for the transfection (Table 5.1). After selection with puromycin, we isolated and amplified macrophages that integrated the sgRNA in the chromosome. Although, the inactivation of the IRAK4 gene needs to be further confirmed by RT-qPCR and Western Blot, we tested the survival of these individual CRISPR

macrophages after infection with *E. coli exlBA* or *P. aeruginosa* IHMA (ExlA+). We followed the kinetics of PI incorporation and calculated the A.U.C for each curve.

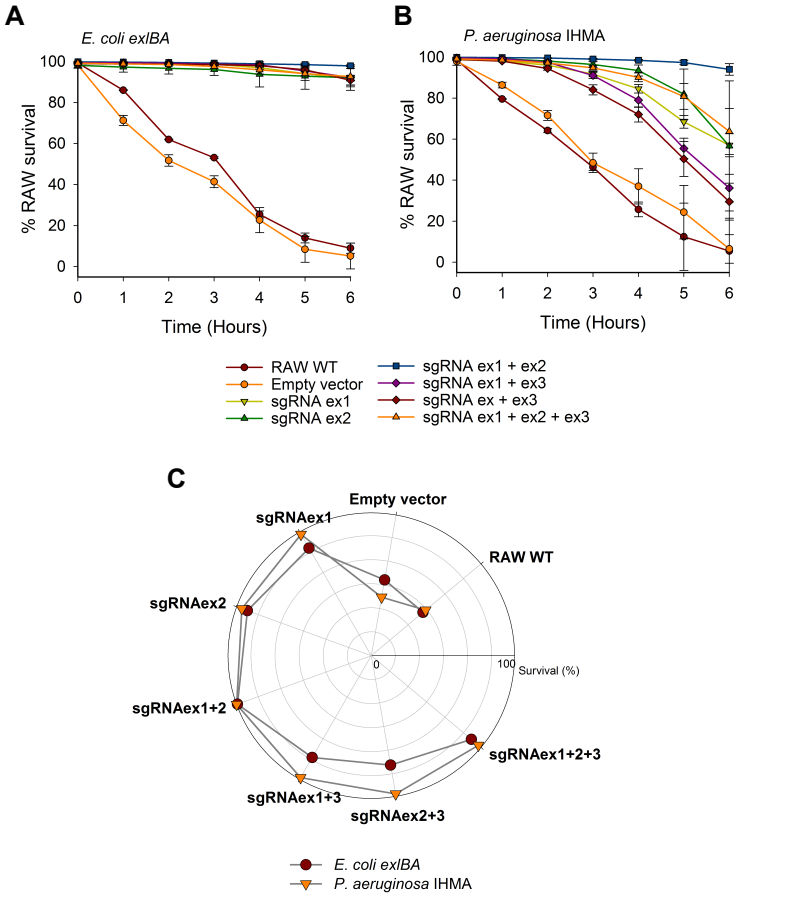

Figure 8.7. Role of *IRAK4* gene in the resistance of ExlA. (A) Survival of IRAK4 RAW mutant infected with *E. coli*exlBA at MOI 20 for six hours. (B) Survival of IRAK4 RAW mutant infected with *P. aeruginosa* IHMA at MOI 20 for six hours. (C) Polar plot representing the A.U.C of the survival kinetics showed in panels A and B.

The results showed that individual CRISPR macrophages were more resistant to *E. coli exlBA* toxicity than the control (empty vector) (Figure 8.7A). We can notice than the sgRNAs targeting the three individual exons or combined presented the same survival rate. However, to rule out that the resistant macrophages resulted from off-target mutation, complementation with the *IRAK4* gene need to be performed. The survival of the individual IRAK knockout macrophages was also tested after *P. aeruginosa* IHMA infection. In this case, we observed that the IRAK KO macrophages were resistant to the ExlA activity at the beginning of the infection, during the first four hours, and then the survival decreased to 25 % at six hours post infection (Figure 8.7B). This result showed that IRAK4 promotes resistance against ExlA-mediated cytotoxicity, although to lower levels for *P. aeruginosa* ExlA+. To further characterize the role of IRAK4 in the ExlA cytotoxicity, we will also quantify

the pro-inflammatory cytokines, and the activation of the Caspase-1.

The output pools 3 and 4, in which *IRAK4* was highly enriched were shown to be resistant to the action of ExlA-like toxins for the diverse species of *Pseudomonas*. Survival of individual KOs for IRAK4 was measured and the A.U.C for each curve was calculated and represented by a polar plot. We observed that the survival of the macrophages was around 40% (Figure 8.8A) and did not vary between the *Pseudomonas* species. This result suggested that IRAK4 plays a role in the ExlA-like toxin-dependent cytotoxicity and its role needs to be characterized in more detail.

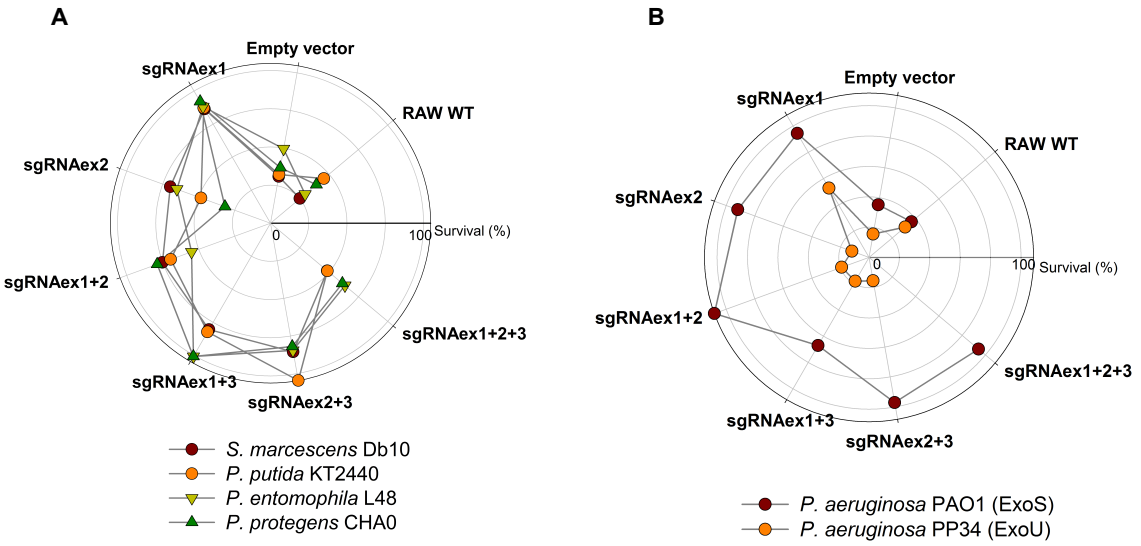

Figure 8.8. Individual CRISPR mutant to target IRAK4 gene. (A) Polar plot of the A.U.C of the survival kinetics obtained with an infection with *Pseudomonas* species secreting ExlA-like toxins at MOI 20 for six hours. (B) Polar plot of the A.U.C of the survival kinetics obtained with an infection with T3SS + strains of *Pseudomonas* at MOI 20 for six hours.

In contrast, when we tested the T3SS positive strains PAO1 and PP34, we observed two different phenomena. IRAK4 KO macrophages infected with PAO1 (ExoS) were highly resistant to the infection (Figure 8.8 B). In contrast, with PP34 (ExoU) the IRAK4 KO macrophages were totally susceptible, confirming the caspase-independent pathway death. These results suggest that the effectors of the T3SS act differently during an infection. It would be interesting to understand the difference between the two mechanisms.

Discussion

Genome editing technologies are powerful tools for studying biology, disease and host pathogen interaction. The advent of CRISPR/Cas technology revolutionized our capacity to inactivate genes in eukaryotes [332–334] or in bacteria [339–341].

In this work we used a genome-wide CRISPR/cas9 mutants library of RAW macrophages library to identify host factors required in ExlA-dependent cytotoxicity. The library used here targeted more than 20 000 genes in RAW macrophages. The screen was performed with *E. coli* expressing *exlA*. At the end of the selection, we obtained around 200 macrophage clones which resist ExlA toxicity. The high-throughput sequencing allowed us to identify genes targeted by sgRNA. 30 genes were highly enriched in the resistant macrophages. Among them two distinct host cell pathways could be defined, one involved in the immune system, response to stimuli and inflammation and the other potentially involved in the lipid bio-synthesis pathway.

We investigated the kinetics of output macrophage survival following an infection with *E. coli* secreting ExlA or IHMA, a clinical isolate or *P. aeruginosa* secreting ExlA. Resistant macrophages from the nine output pools showed different survival rates after an infection with ExlA. This result is in agreement with the different genes enriched in these nine output pools. Pools 3 and 4 were enriched in IRAK4 KO macrophages. IRAK4 is recruited by MyD88 after the activation of the TLR4 by LPS leading to an inflammatory response [354]. The macrophages in pools 3 and 4, were resistant to ExlA-intoxication showing 80 % of survival (Figure 8.3). This global survival is comparable to individual IRAK KO (Figure 8.7), confirming that IRAK4 is involved in the ExlA-mediated toxicity. The inflammatory response induced by IRAK4-dependent pathway needs to be further explored.

We previously demonstrated that ExlA-like toxins from environmental species of *Pseudomonas* provoked a Caspase-1-dependent cell death in macrophages [342]. The survival of macrophages from output pools 3, 4 and from individual IRAK4 KOs were tested towards the bacterial infection and surprisingly we observed the same survival rate as those observed with *E. coli* and IHMA. These results strongly suggest that ExlA-like toxins define a new class of pore-forming toxins and their activity probably induces the same cellular pathways to cytotoxicity with involvement of IRAK4. Classical strains of *P. aeruginosa* secreting either ExoS or ExoU were also tested toward selected macrophages. Two cell responses were observed. ExoU+ strain PP34 was highly cytotoxic, fewer than 10 % of the IRAK KO macrophages survived the infection. ExoU is a phospholipase acting on cell membranes and engenders an unregulated cell death. This result was not surprising and is in agreement with our previous work. However, the macrophages from pools 3 and 4 and individual IRAK4 KO infected with from PAO1 (ExoS) showed a resistance around 70-80 %.

The pool 6 is particularly interesting because the *CASP-1* is one of the genes the most enriched. The survival of macrophages selected in this pool was evaluated with other species and showed that they were not cytotoxic towards these cells. Moreover, macrophages infected with ExoS-positive strain did not present a cell death in comparison with ExoU-positive strain which was highly toxic. These results are in agreement with our previous work. Other genes were highly enriched such as *PRKD2*, *TNFSF13* and *LRRC40*. Their link with the CASP-1 needs to be further explored.

Construction of individual PRKD2 KOs is in progress. PRKD2 is a plasma membrane protein involved in cell death and response to bacterial stimuli.

In the pool 1, the most enriched sgRNAs are targeting mir-741. Micro RNAs are non-coding RNA that regulate the expression of many genes. mir-741 is involved in regulation of the expression of two major enzymes (ST8SIA1 and AGPAT5) involved in the lipid synthesis pathway. ST8SIA1 is an Alpha-N-acetylneuraminide alpha-2,8-sialyltransferase that plays a role in the production of gangliosides GD3 and GT3 from GM3 [356, 357]. Gangliosides are glycosphingolipids (ceramide and oligosaccharide) with one or more sialic acids. This class of lipids is abundant in the plasma membrane.

The second enzyme is AGPAT5, a 1-acyl-sn-glycerol-3-phosphate acyltransferase epsilon that converts lysophosphatidic acid to phosphatidic acid, the second step in *de novo* phospholipid biosynthesis [358]. Indeed, the plasma membrane composition is very important for the pore forming toxin activity [359–361]. The lipids are targeted by the pore-forming toxins and promote their oligomerization. mir-741 might negatively regulate the gene coding for the enzymes involved in the ganglioside and phospholipid synthesis. Hence, targeting mir-741, enhances the expression of these enzymes and activates the ganglioside and sphingolipid production involved in the membrane repair mechanism. This hypothesis could explain that the CRISPR/Cas macrophages, in which the sgRNA targets mir-741, are resistant to ExlA-mediated toxicity. In future work, we will target the mir-741 by siRNA approach, target ST8SIA1 and AGPAT5 by individual CRISPR/cas KOs, or use drugs to inhibit the sphingolipid biosynthesis.

Part III

General conclusion

9

Discussion and future directions

Contents

P. aeruginosa is a major nosocomial bacterial pathogen responsible for severe acute and chronic infections. The WHO has recently named *P. aeruginosa* as a target of the highest priority for the development of new antibiotics. Up to now, the T3SS has been considered as the major virulence factor of *P. aeruginosa*. However, our team recently characterized a new group of 30 strains, majority isolated from clinical samples, that do not possess the T3SS locus and the genes for the effectors, but employ a novel T5SS toxin, Exolysin (ExlA) for their virulence [1, 2, 126].

9.1 Diversity of the PA7-like strains

The genomic characterization of the PA7-like strains has shown that these 30 strains could be divided into three major groups (A, B and C) based on the MLST analysis. This classification into groups is correlated with the type of deletion that occurred at the T3SS locus; namely, strains from groups A and C lack entirely the T3SS genes with only 47 nucleotides left from the intergenic region between *PA1689* and *pscU*, whereas strains of the group B present the "bigger scar" with up to 800 nucleotides of the first and the last gene of the T3SS locus. Those analyses suggested that the acquisition of *exlBA* genes occurred before the deletion of the T3SS genes [1, 2].

Moreover, the phylogenetic analysis done on the SNP of the core genome from 97 *P. aeruginosa* strains (Figure 1.8), revealed that among the *exlA*-positive strains, the group B (first identified by the MLST analysis) is closer to PA14-like strains than the group A, however without any presence of the *exoU* gene. These results also showed that all the *exlA*-positive strains are probably more divergent between them than the group of the PAO1- or PA14-like strains. The whole core genome comparison of all the strains used in the SNP analysis showed the same results as the SNP analysis (data not shown). Other comparative analyses are underway in the team for several strains, including strains LMG, JT87, CPHL, DVL, Can 5 and PA70 that we have sequenced by MiSeq. This whole genome comparison could further allow the characterization of strains from the group B, identify potential specific regions from these strains, or on the contrary some missing genes. Interestingly, it was shown that strains of the groups B were not able to secrete ExlA, and were not virulent in mice [1], suggesting that the regulatory mechanism leading to the activation of *exlBA* is mutated or the secretion of ExlA is not functional. It has been widely documented that some major virulence factors, for example ExoU, are acquired by gene transfer [66]. It would be interesting to determine the origin and the time when *exlBA* had been acquired by some *P. aeruginosa* strains. This may be done using time-dependent phylogenetic reconstructions and calculations of evolutionary rates of these different strains using BEAST software [362].

The molecular mechanisms leading to tight regulation of *exlBA* are starting to be elucidated in our laboratory, with cAMP/Vfr being involved in *exlBA* activation (Berry *et al.*, submitted). *exlBA* is under control of cAMP and its receptor Vfr and the absence of a functional Vfr in PA7 was found responsible for its reduced cytotoxicity. However, Vfr was present in all the strains of the group B. Moreover, a sequence alignment of the Vfr binding site on *exlBA* promoters did not reveal specific mutations, suggesting that Vfr was not responsible for the defect of cytotoxicity of the group B strains.

Finally, we still do not know whether there are some strains that possess both systems or the reason why strains favored one system rather than keeping both.

9.2 ExlA is a TPS pore forming toxin of *P. aeruginosa*

ExlA is a polymorphic toxin composed of a signal peptide required for its export in the periplasm by the Sec-pathway, a TPS domain, assumed to be essential for its secretion through the OM, filamentous haemagglutinin domains and a C-terminal domain which has been shown to be non-homologous to any other proteins in databases [320]. ExlA is encoded by *exlA* gene in operon with *exlB*. ExlB is an outer membrane protein belonging to the Omp85 superfamily of porins and possessing two periplasmic POTRA domains and a β-barrel anchored in the OM. We first demonstrated that ExlB is absolutely required for the secretion of ExlA in the extracellular medium. Moreover, the POTRA domains of ExlB are essential for the secretion of ExlA. These results were in agreement with the results described for FHA, the major adhesin of *B. pertussis*. In this FhaC-FHA system, the deletion of the POTRA domains of FhaC abolished the secretion of FHA without destabilizing the FhaC protein conformation [188]. The TPS systems are widespread among the gram-negative bacteria. The TPS domains of the TpsA proteins are highly conserved, possessing more than 45% of identity. TpsB proteins are highly similar. The interaction of TPS domains from TpsA proteins and the POTRA domains of the TpsB proteins have been widely demonstrated for FhaC-FHA system, using Surface Plasmon Resonance (SPR) [363].

ExlA was identified in the secretome of bacterial culture by comparative proteomic analysis and shared 35% of amino-acids identity with ShlA, the hemolysin of *S. marcescens* [126]. ShlB not only secretes ShlA across the OM, but also converts inactive, periplasmic ShlA to hemolytic, secreted ShlA [197, 364]. Indeed, purified rExlA has no activity toward eukaryotic cells and ExlA obtained from the bacterial supernatants is inactive. However, those proteins are active on liposomes [320], suggesting that they do not require ExlB for activation.

The X-ray structures of the TPS domains have been solved for Fha30 [182], Hpm, Hmw1 [185], and HxuA [186] showing similar β-helical structure with 3 helical motifs displaying a triangular shape. The structure of the TPS domain does not explain the secretion signal, because interactions between the TpsA and the POTRA domains only occur with unfolded TPS domain [188].

ExlA provokes a plasma membrane rupture *in vitro* on eukaryotic cells, characterized by an entry of EtBr in the nuclei [1, 126, 320]. Using red blood cells model, currently employed for studying pore forming toxins, we demonstrated that ExlA, secreted from *P. aeruginosa* is able to lyse RBCs. The addition of sugars and PEGs of different sizes in the medium, deferentially inhibited the lysis of RBCs and allowed the determination of the diameter of the pore to 1.6 nm, demonstrating that ExlA is a pore forming toxin (PFTs). PFTs are classified into two large groups, α and β-PFTs based on the secondary structure of their membrane-spanning elements, composed of α-helices or β-barrels, respectively. Among the β-PFTs, the α-haemolysin of *S. aureus* was described to form pores of 1 nm [365]. In addition, ShlA, the hemolysin of *S. marcescens* forms pore of 2 nm [174] and was predicted to belong to β-PFTs

class, however, there is no data concerning the oligomerization and pore formation. The close relation of pore formation mechanism between ExlA and ShlA suggests that ExlA belongs to the β-PFTs group.

As in many polymorphic toxins, the C-terminal domain is responsible for the pore forming activity of ExlA, similarly to ShlA. The second model used to characterize the pore formation was liposomes composed of different lipids. Recombinant proteins were able to induce *in vitro* liposome leakage strongly suggesting that lipid binding helps ExlA to adopt its proper pore conformation. ExlA provokes a liposomes leakage only in presence of charged phospholipids (PS), probably involving electrostatic and hydrophobic interactions, a similar effect seen for T3SS translocon proteins PopB and PopD. Another well-studied example is the interaction of colicins with lipids. The presence of anionic lipids species, such as cardiolipin in the bacterial IM promotes the "umbrella" conformation and the active pore formation [366]. In the case of ShlA, the liposome leakage was also favored in presence of PS and PE [229]. Interestingly, the C-terminal part of the protein, essential for ExlA-mediated *P. aeruginosa* cytolytic activity was also able to induce liposome leakage, albeit only at acidic pH. This suggests that the first part of the protein, composed of several haemagglutinin domains organized in β-sheets, may play a role in lipid binding and/or protein oligomerization, or conformational changes at the C-terminus, accounting for the difference in the activity between the whole protein and the C-terminal domain alone. The determination of the crystal structure of this domain is a project of a PhD student in the Dr. Andrea DESSEN team at the IBS. The structure of this "toxic" domain of ExlA would help to understand its oligomerization and its insertion in plasma membrane. The 3D-structure would also help to determine the class of the PFTs to which ExlA belongs.

Another consequence of the pore formation in epithelial cells was the entry of calcium in the cytoplasm. Indeed, it has been demonstrated for several PFTs, such as HlA from *S. aureus*, that the pore formed by the toxin lead to the modification of ion concentration [367]. Most of the time an entry of calcium and an efflux of potassium have been observed [367]. Our team demonstrated that after the pore formation by ExlA, there is a massive calcium entry in the cytosol. This change in calcium promotes the maturation of ADAM10 that triggers the cleavage of E- and VE-cadherins, main proteins of the adherens junctions of epithelial and endothelial cells, respectively ([368]). In many PFTs, for example SLO, PLY, and HlA [272, 318], calcium entry leads to the activation of ADAM10 where ADAM10 plays the role of the receptor for these PFTs. However, ADAM10 did not directly interact with ExlA and a deletion of ADAM10 done by CRISPR/Cas9 did not prevent the ExlA pore formation.

9.3 Role of type IV pili in the ExlA pore formation

Neither ExlA harvested from *P. aeruginosa* supernatant nor *in vitro* purified ExlA variants showed lytic activity on eukaryotic cells. Moreover, only bacteria in contact with eukaryotic cells were able to exert ExlA-dependent cytolysis. Using a cell-based screen for bacterial factors that may promote ExlA pore-forming activity, we identified *P. aeruginosa* pili as being required for pore formation.

The bacterial pili are long extracellular appendages that play a vital role in the bacterial adhesion and initial colonization, particularly in mucosal cell surfaces [369]. Several studies based on Tn-seq have shown that type IV pili are involved in the GI tract colonization and the systemic dissemination [87]. Bacteria carrying transposons in *pil* genes were more able to disseminate in secondary organs than WT strain, suggesting that pili play a negative role in the bacterial fitness. This increase of dissemination and fitness can be explained by a lack of immune response from the host. Indeed, flagellum and type IV pili are recognized by the TLR5 [295, 296, 370, 371].

Type IV pili have been also reported to be involved at the beginning of the urinary tract colonization [372]. Type IV pili can further contribute to virulence and bacterial adaptation through the mediation of pili-dependent phage infection [111]. The role of pili in *P. aeruginosa* T3SS-dependent cell intoxication has been clearly demonstrated in an *in vivo* corneal infection model [109] and in *ex vivo* models of epithelial cells. They are required for the injection of T3S toxins; however, the type IV pili could be exchanged for the nonfimbrial adhesin pH 6 antigen of *Yersinia pestis*, indicating that adhesion to cells mediated by pili plays a crucial role in T3S intoxication, probably by positioning the injectisome onto the host cell surface [106]. Moreover, it was suggested that type IV pili act as "mechanical sensors" during the infection, detecting the surfaces and promoting the expression of virulence factors [110]. The type IV pili are important for the adhesion phase of colonization through the binding of asialoGM1 [373]. The Asialo Gangliosides M1 are expressed at the apical surface of the respiratory epithelial cells. At the basal surface of the cells, pili interact with integrins, mediated by the PilY1 that harbors an RGD motif[373]. Therefore, in our ExlBA TPS system, type IV pili may facilitate bringing the bacteria to the proximity of the host cell membrane. This close proximity would enhance a local concentration of ExlA near the membrane and trigger the pore formation.

TPS systems, with auto-transporter (AT) systems belong to T5SSs. It has been demonstrated that many ATs including IcsA of *S. flexeneri* localize at the pole of bacteria [374]. This polar localization was required for the secretion of the protein. The secretion at the pole of the bacteria suggests that the bacteria are oriented during the interaction with the host [374]. It would be interesting to see whether ExlB is located at a specific region in the OM, for example close to the type IV pili in order to cooperate to the pore formation. Immunofluorescence of ExlB and pilin would help in co-localization of these systems *in vivo* in the OM.

ExlA was first identified by comparative proteomics in the CLJ1 strain from a patient suffering from hemorraghic pneumonia [126]. CLJ1 was characterized as a highly virulent strain. CLJ1 strain is unable to twitch or swim, as demonstrated by Reboud *et al.* [1]. The examination of the CLJ1 genomes has revealed the presence of insertion sequence in *flgL* and *pilM* gene coding for proteins of flagellum and type IV pili (Santausa., et al, in preparation). In a mouse model of pneumonia, CLJ1 strain was able to disseminate in secondary organs, including spleen, liver, kidney, and blood, demonstrating that pili are not involved in the dissemination [375]. However, proteomic analyses have revealed the presence of five additional TPS systems annotated as filamentous haemagglutinin/adhesins proteins. The synthesis of all these TPSs in CLJ1 strain indicates that these secreted proteins may play an important role during colonization and infection, but their exact roles in adhesion,

cytotoxicity and/or inter-bacterial competition needs to be further investigated.

The dissemination of CLJ1 in the secondary organs was comparable to the T3SS-positive strains, but ExlA provokes more severe damage in the lungs, such as alveolar lesions [375]. Therefore it would be interesting to repeat these experiments with T4P+, Flagella+, ExlA+ IHMA87 strain, to compare the dissemination of this strain to CLJ1. Dissemination of the bacteria in the lung tissues is facilitated by the capacity of ExlA to cleave cells barriers, in particular E-cadherin and VE-caderin junctions ([368]). However, type IV pili mutants also showed the E-cadherin cleavage ([368]). Chronologically, ExlA forms the pore facilitated by adhesion through type IV pili, the calcium enters in the cytoplasm by the ExlA pore allowing the maturation of ADAM10 that will cleave the E-cadherin. At the same time, in the macrophages, the formation of the pore activates pyroptotic pathway and triggers cell death.

9.4 Role of ExlA in inflammation

Many factors of *P. aeruginosa*, including the T3SS, the type IV pili, the flagellum and the LPS, have been shown to play an important role in the modulation of the innate immune response. In particular, the inner rod PscI and the needle subunit PscF of the toxin-injection T3SS machinery, activate the NLRC4 inflammasome [79]. Flagellin FliC that is injected by the T3SS is able also to activate NLRC4 pathway [79–84, 343]. Flagellin and LPS have been demonstrated as critical extracellular PAMPs (Pathogen Associated Molecular Patterns) recognized by the host through the Toll-Like-Receptors TLR5 and TLR4, respectively [295, 370, 376]. As mentioned previously, unflagellated CLJ1, due to the presence of an insertion sequence in *flgL* gene, was less immunogenic than flagellated strains. No pro-inflammatory cytokines, including IL-1β, TNF and IFNγ and no neutrophil recruitment were detected in the mice broncho alveolar lavages after an infection with CLJ1 [375].

CLJ3 was isolated 12 days after antibiotherapy from the same patient as CLJ1, and was shown to be less virulent but resistant to almost all antibiotics. Whole-genome comparison between CLJ1 and CLJ3 allowed to show the deletion of 20 kbs encompassing at least 21 genes including notably *galU* encoding UDP glucose pyrophosphorylase [327]. GalU adds sugar moieties on the inner lipid core, giving the anchor for the full length LPS. *In vitro* experiments have demonstrated that CLJ3 was non-agglutinable and sensitive to human serum compared to CLJ1. It would be interesting to perform mouse experiments to examine the role of the LPS in the inflammatory response, and in the dissemination.

In addition, *in vitro* experiments done on BMDM macrophages, invalidated for major actors of pyroptosis, have shown that IHMA provokes a caspase-1 dependent cell death by the recruitment of the NLRP3 inflamasomme. The activity of several PFTs of major human bacterial pathogens such as *S. pneumonia*, *S. aureus* and *E. coli* [318] leads to the activation of NLRP3 inflammasome, caspase-1 processing and the maturation of IL-1β [325, 377]. Indeed, the efflux of cellular ions such as the potassium through the toxin pores and the decrease of cellular potassium concentration, activate the NLRP3 inflammasome [378] leading to pyroptosis [379]. Strains lacking flagellum (IHMAΔ*fliC*, CLJ1) showed the same cytotoxicity as the WT, but a 2-fold decrease of the caspase-1 activation and the IL-1β production.

Flagellin is recognized by TLR5 and the TLR pathway primes the innate immune response. IHMA strain was demonstrated to be less virulent than CLJ1 in a mouse pneumonia model [1]. This could be explained by the high pro-inflammatory response induced by IHMA and lower secretion of ExlA. On the other hand, higher amount of toxin explains the hyper virulence of CLJ1 and lower immune recognition due to the absence of pili and flagellum. *exlA* was found in several *Pseudomonas* species including *P. putida*, *P. entomophila*, *P. fluorescens* and *P. protegens*. Sequence alignment of the ExlA proteins showed that the TPS domain was highly conserved (60 % of identity). The phylogenetic tree analysis based on the ExlA comparison suggested that *exlA* has been acquired by horizontal gene transfer from environmental species. The response of the BMDMs infected by different *Pseudomonas* species was the same as for IHMA [342]. The emergence of nosocomial infections with environmental species has been noted over this last decade. Among the nine sequenced *P. putida* strains (NCBI databases) harboring *exlA*, two strains have been isolated from patients; H8234 was isolated from a patient presenting bacteremia, and HB3267, isolated from a patient that passed away, exhibited a broad antibiotic resistance spectrum [380]. The contribution of ExlA in this kind of bacteremia could be investigated by creating *exlA* negative mutants and testing them in a bacteremia mouse model for virulence, survival in blood and for the inflammatory response of the host induced after the infection.

9.5 Search for host factors potentially involved in ExlA action

PFTs often recognize target cells through binding either to specific, sugar, lipid or protein receptors creating a high local concentration that promotes their oligomerization and membrane insertion. Colicins are bacterial toxins that recognize cardiolipin in bacterial membranes as receptors to adopt their "umbrella" conformation and form an active pore [237]. Hla from *S. aureus* recognizes ADAM10 at the surface of the eukaryotic cells. This binding increases the protease activity of ADAM10, which disrupts the epithelial barrier and leads to lung injuries. The interaction of Hla with ADAM10 was first demonstrated using co-immunoprecipitation followed by mass spectrometry. The recent development of the CRISPR/cas9 system allowed to target and to modify eukaryotic genes. CRISPR loss-of function genes libraries of eukaryotic cells have been created for mouse and human genomes. Recently described screens coupled to the next generation sequencing enhanced our understanding of global host-pathogen interaction for viruses and bacteria. In the case of bacterial toxins (Hla, anthrax, T3SS), screens of CRISPR/Cas libraries led to identification of novel cellular targets, receptors and regulatory proteins. In accordance with previous study, Winter and colleagues demonstrated that ADAM10 is the protein receptor of the HlA and also identified three other proteins that participate in the ADAM10 regulation (SYS, ARFRP1 and TSPAN14) [274].

In the case of ExlA, co-immunoprecipitation assays did not allow us to identify a putative protein receptor of ExlA due to the small amount of ExlA inserted in the host membrane. Therefore, we set up a high-throughput screening of a CRISPR/Cas

library made in RAW macrophages to identify potential protein or non-protein receptors of ExlA. The first analysis revealed several potentially interesting host cell molecules that be involved in ExlA-induced cytotoxicity in macrophages. One of those was a small RNA mir-741 that regulates the expression of two enzymes ST8SIA1 and AGPAT5. ST8SIA1 is a sialyltransferase playing a role in the production of gangliosides GD3 and GT3 from GM3 [381]. Gangliosides are glycosphingolipid (ceramide and oligosaccharide) very abundant in the plasma membrane. AGPAT5 is an acyltransferase that converts lysophosphatidic acid to phosphatidic acid, the second step in *de novo* phospholipid biosynthesis [381]. The composition of the host plasma membrane is a very important factor for the pore forming activity of several toxins. The lipids are targeted by the pore-forming toxins and promote their oligomerization, as was shown for SLO from *L. monocytogenes* or PLY from *S. pneumonia*, that both require cholesterol for their pore formation. Taking into account that in the case of ExlA, pili may be employed for creating high local concentration of the toxin at the host membrane proximity, it is possible that it does not require any specific protein receptor. However, the proper lipid environment may be required for its oligomerization and/or insertion. Lipid rafts are postulated to be cholesterol- and glycosphingolipid-enriched microdomains of the cell plasma membrane that differ in their physical properties from the rest of the membrane [382, 383] clearly demonstrated the physiological relevance of raft integrity to toxin effects. Anthrax toxin PA binds to either CMG2 or TEM8 at the cell surface clustered in the lipid rafts. By using β-methyl-cyclodextrin, a reagent that removes cholesterol from the plasma membrane and thus disaggregates rafts, it has been demonstrated that anthrax toxin was less internalized [384, 385]. Thus β-methyl-cyclodextrin will be used on eukaryotic cells to test the role of the lipid rafts and cholesterol in the ExlA pore activity. Also, some inhibitors of lipid biosynthesis pathways may be used to confirm the data obtained by CRISPR/Cas screen.

In conclusion, I propose a general view of the mechanism leading to ExlA secretion and its action toward eukaryotic cells (Figure 9.1). I demonstrated that ExlB is absolutely required for the secretion of ExlA, involving the ExlA POTRA domains. Moreover, I showed that ExlA forms 1.6 nm-pores in the plasma membrane of eukaryotic cells leading to the complete plasma rupture. The pore formation of ExlA is possible thanks to the Type IV pili that promote a close contact between the bacteria and the host cells. ExlA toward primary macrophages induces a pyroptosis cell death with high levels of IL-1β release. Finally, I started the determination of the host factors involved in the ExlA-mediated cytotoxicity.

Figure 9.1. Mechanisms leading to ExlA secretion and its action toward eukaryotic cells.

Part IV

Annexes

10

Exolysin Shapes the Virulence of *Pseudomonas aeruginosa* Clonal Outliers.

Reboud E, Basso P, Maillard A, Huber P and Attree I (Toxins (2017))

In this chapter we review the structural features of the Exolysin, the mechanism of its secretion and the effects of the pore formation on eukaryotic cells ([386]). This part includes results from Chapters 5, 6 and the work done by Emeline Reboud, PhD ([368]).

Bacterial toxins are important weapons of toxicogenic pathogens. Depending on their origin, structure and targets, they show diverse mechanisms of action and effects on eukaryotic cells. Exolysin is a secreted 170 kDa pore-forming toxin employed by clonal outliers of *Pseudomonas aeruginosa* providing to some strains a hyper-virulent behaviour. This group of strains lacks the major virulence factor used by classical strains, the Type III secretion system.

toxins

MDPI

Review

Exolysin Shapes the Virulence of *Pseudomonas aeruginosa* Clonal Outliers

Emeline Reboud †, Pauline Basso †, Antoine P. Maillard †, Philippe Huber * and Ina Attrée *

CNRS-ERL5261, INSERM, U1036, CEA, Bacterial Pathogenesis and Cellular Responses, Biosciences and Biotechnology Institute of Grenoble, University Grenoble Alpes, 17 rue des Martyrs, CEA-Grenoble, 38054 Grenoble, France; emeline.reboud@gmail.com (E.R.); pauline.basso@gmail.com (P.B.); antoine.maillard@cea.fr (A.P.M.)

* Correspondence: philippe.huber@cea.fr (P.H.); ina.attree-delic@cea.fr (I.A.); Tel.: +33-4-3878-5847 (P.H.); +33-4-3878-3483 (I.A.)

† These authors contributed equally to this work.

Academic Editor: Adam J. Ratner

Received: 13 October 2017; Accepted: 2 November 2017; Published: 9 November 2017

Abstract: Bacterial toxins are important weapons of toxicogenic pathogens. Depending on their origin, structure and targets, they show diverse mechanisms of action and effects on eukaryotic cells. Exolysin is a secreted 170 kDa pore-forming toxin employed by clonal outliers of *Pseudomonas aeruginosa* providing to some strains a hyper-virulent behaviour. This group of strains lacks the major virulence factor used by classical strains, the Type III secretion system. Here, we review the structural features of the toxin, the mechanism of its secretion and the effects of the pore formation on eukaryotic cells.

Keywords: two-partner secretion; pore-forming toxin; type IV pili; cell junctions; ADAM10; inflammation; PA7-like strains; ExlA

1. Introduction

Protein toxins are main weapons of bacterial pathogens. Most Gram-negative pathogens, including the major human opportunist *Pseudomonas aeruginosa*, secrete toxins in their surrounding milieu or inject toxic effectors directly into host-cell cytoplasm.

P. aeruginosa is a ubiquitous bacillus that thrives in most moisture environments and colonizes different hosts from plants to insects, and to mammals [1–3]. *P. aeruginosa* is particularly well adapted to human hosts and is capable of provoking infections of different tissues and organs, such as urinary tract, lungs, eyes and damaged skin. It is often associated with nosocomial infections in Intensive Care Units and affects elderly patients with underlying chronic diseases, as well as patients with cystic fibrosis where it is the primary cause of morbidity and mortality [4]. Whole-genome analysis approaches have clustered environmental and clinical isolates of *P. aeruginosa* into three major groups [5,6], represented by reference strains PAO1, PA14 and PA7 [7–10]. While the majority of world-wide collected samples populates the two first groups ("PAO1" and "PA14"), the third group ("PA7") harbours strains qualified as clonal outliers based on their sequence and genome divergence [5,6,11–13].

The main difference between clonal outliers and the rest of the population is the way those bacteria exert their cytotoxicity and virulence toward mammalian hosts. The "classical" strains belonging to "PAO1" and "PA14" groups possess the well-studied virulence determinant Type III Secretion System (T3SS). T3SS is a molecular syringe that allows the export of bacterial proteins and their injection directly into the host cell across three membranes [14,15]. The T3SS machinery is encoded by a four-operon chromosomal locus of ~25 kb containing genes for structural and regulatory proteins (reviewed in [14]). Four toxin-effectors are transported by the T3SS machinery, two of them, ExoS and ExoU, being mutually exclusive in a majority of clinical strains [16,17]. In contrast, clonal outliers of the

"PA7" group are devoid of a T3SS machinery and all T3SS toxins [7,18]. Instead, they employ a secreted toxin of 170 kDa, named Exolysin (ExlA), to establish infection [19]. Exolysin has been first detected by non-targeted proteomics in the secreted medium of a highly cytotoxic strain CLJ1, isolated from a patient with chronic obstructive pulmonary disease (COPD) accompanied by signs of haemorrhage in lungs [19]. The recombinant expression of *exlBA* was found to be sufficient to cause fatal outcome in a mouse model of acute pneumonia and both genes are necessary for cytotoxicity toward eukaryotic cells. The *exlBA* locus encoding the toxin is absent in classical strains of *P. aeruginosa*, and is located between genes corresponding to PA0874 and PA0873 in the reference strain PAO1. This genetic organization is conserved in all clonal outliers sequenced to date. Bioinformatics analysis performed on all genomes available in the *Pseudomonas* database [10] revealed the presence of *exlBA* genes in several *Pseudomonas* species, including *P. putida*, *P. entomophila*, *P. protegens* and *P. fluorescens* [20]. Here we bring insights regarding the structural and functional features of this novel toxin acquired by some multi-resistant *P. aeruginosa* strains.

2. Exolysin Belongs to a Family of Two-Partner-Secretion Pore-Forming Toxins

The *exlA* gene encodes a 1651 residue-long polypeptide that bears successive sequence signatures typical of (i) a signal peptide recognized by the general Sec machinery, (ii) a so-called Two-Partner Secretion (TPS) domain and (iii) several filamentous hemagglutinin (FH) repeats (Figure 1A). The absence of any known sequence signature beyond residue 1364 defines a ~280 residue-long C-terminal domain that was proved necessary for ExlA activity toward eukaryotic cells (see below) [19,21]. Upstream from *exlA* is *exlB* that encodes a 60 kDa outer membrane (OM) protein channel of the Omp85 superfamily [22]. Proteins of this superfamily possess a C-terminal 16-stranded membrane-embedded β-barrel downstream a variable number of POlypeptide TRansport Associated (POTRA) domains, of which ExlB has two. Together, *P. aeruginosa* ExlB and ExlA make a secretion system that belongs to a system that was named TPS systems, such as to account for the minimal set of proteins specifically involved in secretion, i.e., the effector and its cognate transporter [23]. This dominant picture shall not occlude instances where additional dedicated partners may modify, neutralize or proteolyse the substrate [22], although none of this seems to apply to ExlA which was detected as a single ~170 kDa band after SDS-PAGE analysis of bacterial culture supernatants. Some founding members of that group are well characterized homologs of ExlBA, like *S. marcescens* ShlBA and *B. pertussis* FhaCB. With analogy to these well-studied TPS systems [24], ExlA secretion is predicted to occur in two steps: (i) the 34 residue-long, cleavable signal peptide at the N-terminus of ExlA targets the precursor to the general secretion pathway, which delivers ExlA to the periplasm after signal peptide processing and (ii) mature ExlA gets translocated across the outer membrane through ExlB (Figure 1B). Targeting of ExlA to ExlB across the periplasm probably requires the TPS domain of ExlA to interact with ExlB POTRA domains 1 and 2, making them indispensable for ExlA secretion [21].

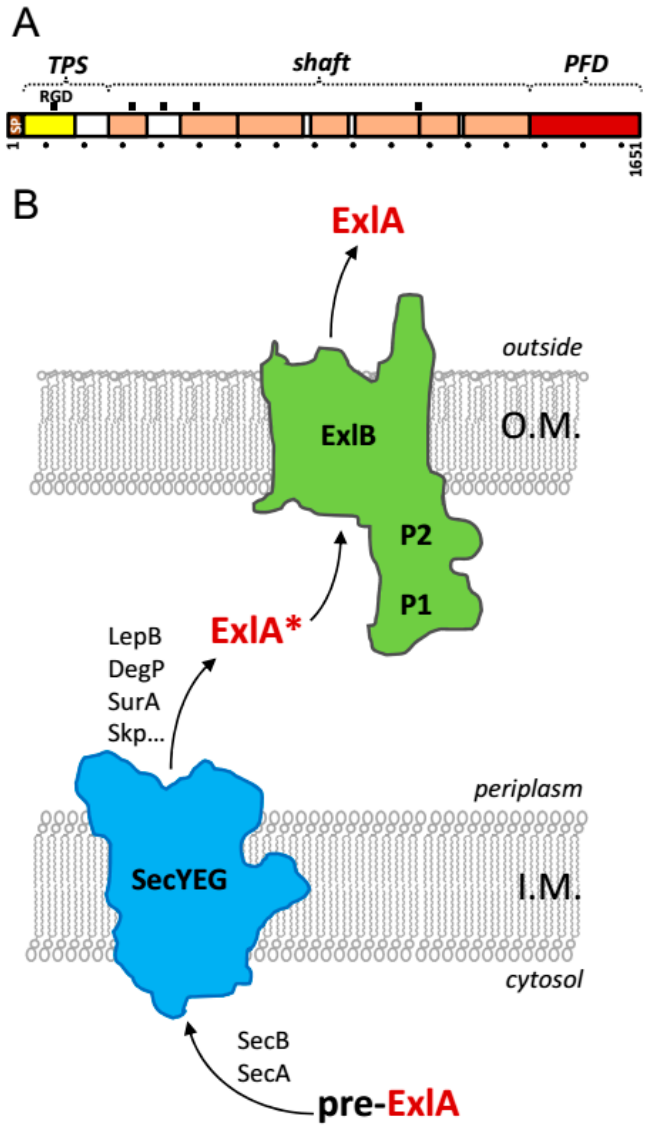

Figure 1. (**A**) Linear representation of ExlA showing the signal peptide (SP) and Pfam annotations [25] corresponding to the TPS domain (yellow) and Fil_Haemagg_2 repeats (salmon). The C-terminal pore-forming domain (PFD, red) made no hit in Pfam. A ruler is displayed below the diagram with a mark of every 100 residues. The five RGD motifs and the putative domains of ExlA are shown on top. (**B**) Schematic representation of the ExlA secretion pathway. ExlB and ExlA precursors are targeted to the periplasm via the general secretion pathway by recognition of their N-terminal signal peptides. With analogy to the ShlBA TPS, ExlB inserts into the outer-membrane where it forms the translocation pore to which the non-functional periplasmic intermediate ExlA* is targeted via the interaction between its TPS domain and ExlB POTRA domains P1 and P2. Some chaperones usually involved in protein secretion are mentioned (SecB, SurA, Skp, DegP).

While ExlA was originally detected in the bacterial culture supernatant, it is not clear whether the secreted form is the active one, i.e., its poor solubility could severely restrain diffusion of the toxin in the milieu, perhaps tethering it to the envelope. Indeed, the fact that ExlA-mediated virulence requires close contact between bacteria and target cell also suggests that the diffusion of secreted ExlA is confined around *P. aeruginosa*. This is in agreement with the limited diffusion reported for *S. marcescens* ShlA [26], with whom ExlA shares 34% overall identity.

ExlA belongs to a family of cytolysins/hemolysins, whose activity has been best characterized for ShlA. ShlA is responsible for the cell-bound hemolytic phenotype of *S. marcescens* [27]. ShlB and ShlA

have been a major model in the early characterization of TPS. With bacterial cells and urea-extracts to palliate the minute-long half-life of the native toxin (hence "cell-bound"), in vitro hemolysis experiments allowed to establish that ShlA was secreted in two steps, the periplasmic form ShlA* being inactive, and hemolytic activity being acquired by ShlA concomitantly with outer-membrane translocation [28]. Strikingly, periplasmic ShlA obtained from *shlB* mutants of *S. marcescens* could be activated by either ShlB or secreted ShlA truncation constructs comprising the TPS domain [26]. A similar mechanism of activation has been documented for HpmA [29] and likely operates for ExlA. Active ShlA inserts in erythrocyte membranes where it adopts a new conformation [30] and makes 1-to-3 nm wide pores [27,31], similarly to what was found for ExlA (Figure 2A).

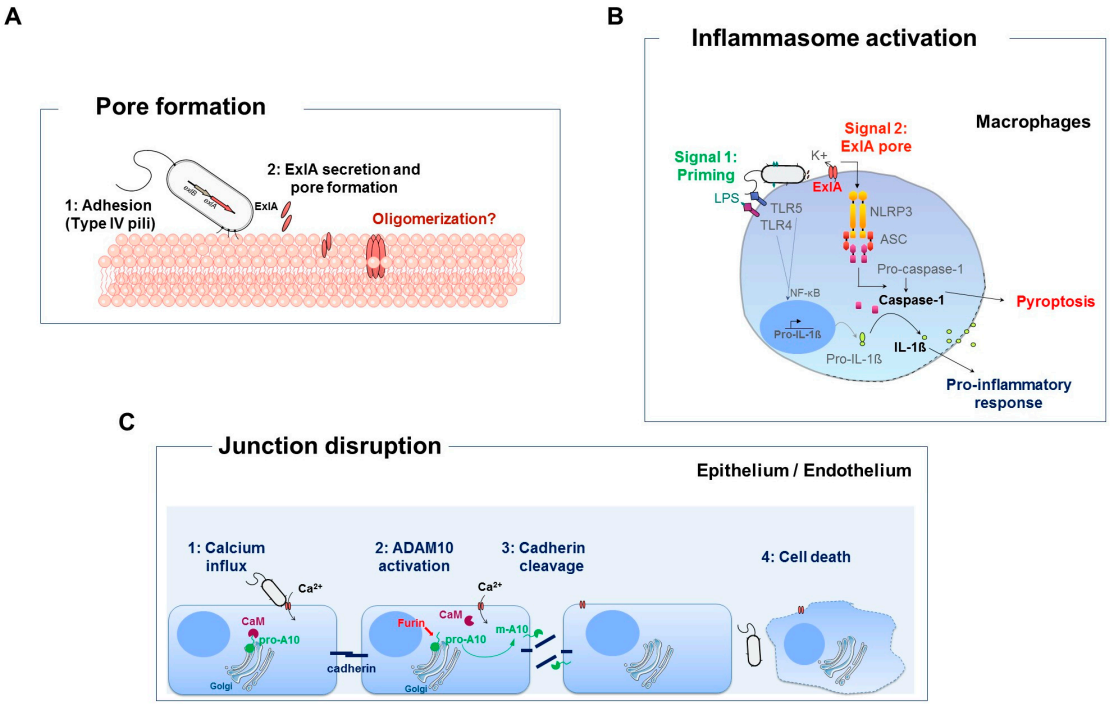

Figure 2. Effects of pore formation on eukaryotic cells. (**A**) When ExlA is secreted close to host cells, it can insert into the plasma membrane. Whether ExlA oligomerizes to form a pore is unknown. The type IV pili facilitate ExlA pore formation by promoting bacterial adhesion to the host cell, and thus its delivery near the membrane. (**B**) ExlA-secreting bacteria induce inflammasome activation and pyroptosis of macrophages (adapted from [20]). The priming signal is provided by LPS-TLR-4 or flagellum-TLR-5 interaction, leading to NF-κB nuclear translocation and synthesis of pro-IL-1β. The second signal is provided by ExlA pore formation inducing K^+ efflux. Alteration in K^+ cytosolic concentration elicits NLRP3/ASC inflammasome activation, which in turn activates caspase-1. Caspase-1 has two major effects, (i) cleavage of pro-IL-1β into mature IL-1β and (ii) the rupture of the macrophage plasma membrane and the massive release if IL-1β, which promotes pro-inflammatory response. (**C**) ExlA induces the cleavage of the intercellular adhesive proteins E- and VE-cadherins in epithelial and endothelial cells, respectively, by diverting a natural mechanism of cadherin shedding of the host (adapted from [32]). In resting conditions, the metalloprotease ADAM10 is maintained inactive (pro-A10) within a complex with calmodulin (CaM), a protein with high affinity for Ca^{2+}. ExlA pore formation induces a massive entry of Ca^{2+} in the cytosol. The CaM-Ca^{2+} association liberates pro-A10, which is available for cleavage by furin and for export to the plasma membrane. In turn, ADAM10 (A10) cleaves the cadherins, inducing junction disruption. Later on, Ca^{2+} entry also induces necrotic cell death by unknown mechanisms.

3. Affinity of Exolysin to Membranes

Pore forming toxins (PFT) classically dock to a receptor as they reach a target membrane, be it a protein, a sugar moiety or a lipid head group. After binding, the PFTs oligomerize then form a pore into the plasma membrane [33]. The measure of haemoglobin release from red blood cells in presence of osmoprotectants of different sizes allowed to suggest that once inserted, ExlA assembles into ~1.6 nm-wide pores [21]. The requirement for lipids in ExlA-mediated pore formation was investigated in vitro using liposomes. It was found that ExlA requires phosphatidylserine (PS) to provoke liposome leakage, probably involving electrostatic and hydrophobic interactions with this anionic phospholipid [21]. Likewise, a dependence on lipid head group ionic charge was shown for the membrane insertion of T3SS translocon proteins PopB and PopD [34]. In the case of ShlA, liposome leakage was observed in presence of PS and enhanced in presence of phosphatidylethanolamine (PE) [35].

Neither ExlA harvested from *P. aeruginosa* supernatant nor purified non-native ExlA showed lytic activity on eukaryotic cells. Moreover, only bacteria in contact with eukaryotic cells were able to exert ExlA-dependent cytolysis. Using a cellular based screen for bacterial factors that may promote ExlA pore-forming activity, type IV pili were identified to facilitate ExlA-mediated cytotoxicity. Therefore, pili may support ExlBA function by bringing the bacteria close to the host cell membrane. This proximity would enhance a local concentration of ExlA near the membrane and trigger pore formation [21] (Figure 2A) highlighting the originality of this TPS pore-forming toxin. The question whether or not ExlA/ShlA family of pore forming toxins use a specific cellular receptor for docking to the host membranes, and if yes, the identity of this receptor, remains open.

4. Virulence of *P. aeruginosa* Strains Secreting Exolysin

The current cohort of ExlA-positive strains (ExlA+) includes isolates from various pathological conditions (ear and urinary tract infections, burns, abscesses, bacteremia, cystic fibrosis, pneumonia, COPD) or from the environment (plant and pond water) [18]. Laboratory assays for some general virulence features showed that only a small number of these strains exert LasB-type proteolytic activity or production of HCN, two virulence factors produced by most classical strains ("PAO1" and "PA14"). Similar to other *P. aeruginosa* strains, ExlA+ strains display a great diversity in their capacity to swim, swarm or twitch. All eukaryotic cell types tested (epithelial, endothelial, fibroblastic, myeloid) were found permissive to ExlA-cytotoxicity, suggesting that ExlA+ bacteria may affect various organs and tissues in vivo. The role of ExlA in the virulence of PA7-like strains was provided by two experiments: (i) strain toxicity levels on cells were correlated with the amount of secreted ExlA, and (ii) *exlA* mutation abrogated cytoxicity. Moreover, survival curves in mice showed gradient in in vivo toxicity, which was not directly predictable from in vitro cytotoxicity assays on cell lines, suggesting that the interaction with the immune components is variable between strains and plays a pivotal role in global pathogenesis [18]. In a pulmonary infection model in mice, the most virulent strain, CLJ1, induces a mortality significantly higher than that of the PAO1 strain expressing the T3SS and ExoS, ExoT and ExoY effectors [19]. The histological examination of CLJ1-infected lungs indicated the presence of erythrocytes in the alveoli space, in addition to infiltration of neutrophils, thus reproducing the hemorrhagic symptoms of the patient. Transmission electron microscopy showed that CLJ1 provoked striking lesions in the alveolar wall. In particular, the tissues were disorganized and some pneumocytes and endothelial cells were necrotic with their cytoplasmic contents spilled in alveoli and capillaries [36]. These types of lesions were not observed in lungs infected with the T3SS-positive strain PAO1. ExlA clearly endows the bacteria with the ability to proliferate in lungs and to disseminate from lungs to other organs: liver, spleen, kidney and brain. Therefore, the rupture of the alveolo-capillary barrier induced by ExlA opens the passage to the blood compartment allowing bacterial dissemination. However, when the blood was directly infected in a mouse bacteremia model, all *P. aeruginosa* strains were promptly eliminated, independently of the secretion of ExlA or T3SS-toxins, and even more rapidly for the ExlA+ strain CLJ1. These results show that the bacterial survival in blood and their

ability to resist to the immune system depends mostly on bacterial genetic background rather than on the particular secreted toxin(s) [36].

The ShlA toxin from *S. marcescens* induces similar damage on lungs, i.e., hemorrhagic pneumonia, recruitment of neutrophils and rapid lung dysfunction followed by mouse death [37]. Some other PFTs induce dramatic damage on lungs, either by direct tissue damage or by inflammatory side effects; the two mechanisms being often dependent on each other. For example, *Streptococcus pneumoniae*, PLY toxin causes the destruction of lung tissue, mediated by the induction of apoptosis and the massive recruitment of neutrophils at the site of infection. The purified protein induces the permeability of pulmonary alveoli in mice, as well as severe pulmonary hypertension and dysfunction of the pulmonary barrier [38]. The leucocidin PVL of *S. aureus* indirectly induces deleterious effects on the lungs by increasing secretion of pro-inflammatory chemokines IL-8 and MCP-1 (monocyte chemotactic protein 1) by immune cells, which induces massive infiltration of monocytes at the site of infection. This infiltration is responsible for necrosis of lung tissue, alveolar hemorrhage, leading to rupture of the pulmonary barrier [39]. Thus, similar to ExlA, these PFTs, once delivered in the lung produce comparable deleterious effects, although using different mechanisms.

5. Caspase-1 Dependent Death of Macrophages

Pore formation by some PFTs induces additional effects on eukaryotic cells such as the activation of the inflammasome, ultimately leading to cell death [40]. ExlA-secreting bacteria induce inflammasome activation of primary macrophages by a two-step mechanism. The first, so called "priming" signal is mediated by the recognition of the LPS and the flagellum by TLR4 and TLR5, respectively, leading to transcription of genes encoding pro-inflammatory cytokines such as pro-Interleukin-1β (IL-1β). The second signal is initiated by the ExlA pore itself which leads to massive efflux of ions, among them potassium (K^+). The decrease in K^+ concentration triggers NLRP3-inflamasomme activation, which in turn activates caspase-1. Active caspase-1 induces the maturation of the pro-IL-1β into IL-1β. Caspase-1 also provokes the rupture of macrophage plasma membrane by a process called pyroptosis, releasing massive quantities of pro-inflammatory IL-1β in the surrounding environment [20] (Figure 2B). Therefore, similarly to T3SS-positive strains, ExlA-secreting bacteria are capable of triggering inflammasome activation and pro-inflammatory cell death of macrophages in vitro. How those effects contribute to overall pathogenicity of ExlA strains in vivo stays to be examined.

6. Exolysin Targets Host Cell Junctions

ExlA induces the degradation of E- and VE-cadherins, two adhesive proteins required for tissue integrity [32]. The cleavage is triggered by the ExlA pores formed in the plasma membrane and occurs earlier than plasma membrane breach. Following pore formation, a massive, rapid entry of calcium ions into the cytosol results in the maturation and activation of ADAM10, a eukaryotic protease inducing cadherin shedding (Figure 2C). In normal conditions, the ADAM10 precursor is maintained inactive within a complex with calmodulin, a protein having a high affinity for calcium. When intracellular calcium increases, calmodulin binds to calcium and dissociates from ADAM10, which in turn is proteolytically activated by furin, a proprotein convertase [41–44]. ADAM10 is then exported to the membrane, where it can exert its proteolytic activity against E- and VE-cadherins. Hence, bacterial strains secreting ExlA divert an endogenous cellular mechanism to compromise tissue integrity [32]. The disruption of adherens junctions by pore-forming toxins via ADAM10 activation was previously described for Hla from *S. aureus*, PLY from *Streptococcus pneumoniae* [45] and ShlA from *S. marcescens* [32]. While ADAM10 is the cellular receptor of Hla, two other toxins (PLY and ShlA) activate ADAM10 through pore-formation and calcium influx without using ADAM10 as the receptor [45,46], similar to ExlA. The dissociation of the junctions and the rupture of the plasma membrane induced by ExlA give an explanation for the striking effects observed in mouse alveoli

during infection. This explains the facility of the bacteria to transmigrate across the lung mucosa and to colonize other organs.

7. Structural Features of Exolysin

Nothing is known about the molecular basis of the pore-forming activity of ShlA/ExlA toxins. In the case of ShlA, it has been reported that the hemolytic activity was virtually lost upon C-terminal truncation [47]. The C-terminal location of the activity is common in TPS substrates [48] and consistently, ExlA-mediated-hemolysis and cytotoxicity have been impaired when the last 295 residues of the protein were deleted [21]. PFTs belong to six classes clustered in two groups, α-helical and β-stranded, based on the secondary structure of the peptide lining the pore [33], with each family displaying characteristic stoichiometry and pore size. Due to the lack of homology to any other toxin and considering the lack of experimental data on pore formation or pore-forming (C-terminal) domain structure in the ShlA/ExlA family, how ExlA pores assemble in the host membranes is still unknown.

The C-terminal domain set aside, the structure of ShlA/ExlA proteins can be pictured by homology. TPS domains are very well conserved in sequence and in structure; sequence alignments allow to discriminate between at least two groups of TPS domains, depending on whether their closest homolog is *B. pertussis* FhaB, which is the case of ExlA, or *H. influenzae* HMW1A [48]. Several TPS domains have been crystallised to high resolution, including that of *P. mirabilis* HpmA which shares 44% identity with ExlA's [29]. All TPS domains are built on a right-handed β-helix, i.e., a helical arrangement of β-strands where each rung of the helix is made of three β-strands and each strand contributes to one of the three parallel β-sheets that together make the helix (Figure 3A). Based on the structure of a complete TPS substrate [49], it is possible to envision how the helix primed in the TPS domain extends into the filamentous repeats-rich domain of ExlA to yield a fiber-like structure of 1000–1200 residues called the shaft domain (Figure 3B). A remarkable feature of ExlA is to display five or six Arg-Gly-Asp (RGD) motifs depending on the strain; these motifs are usually involved in cell-to-cell interactions through integrin binding [50]. All but one of the RGD motifs belong to the shaft domain (Figure 1A) and none displays a clear conservation pattern beyond *P. aeruginosa*. When all five RGD motifs were mutated to RGA in ExlA, the cytotoxicity of ExlA was preserved, implying that ExlA uses other ways to interact with eukaryotic cells [21]. Similarly, the filamentous hemagglutinin FhaB harbours an RGD motif whose mutation had no phenotype in vivo [51,52]. Thus, until now no clear function is specifically associated to the shaft domain. When pore formation was tested in vitro, full-length ExlA induced liposome leakage and C-terminal truncation was found to inactivate ExlA thus suggesting that the shaft domain is inactive [21]. Accordingly, the isolated C-terminal domain was also active but to a lower extent than the full-length ExlA. Therefore, the shaft may contribute indirectly to the function of the C-terminal domain, e.g., by supporting target cell binding, ExlA oligomerization and/or conformational changes of the C-terminus [21]. Altogether, the secretion of mature ExlA by *P. aeruginosa* would release the ~30 kDa cytotoxicity domain at the tip of a-more-than-230 Å-long fiber (Figure 3B).

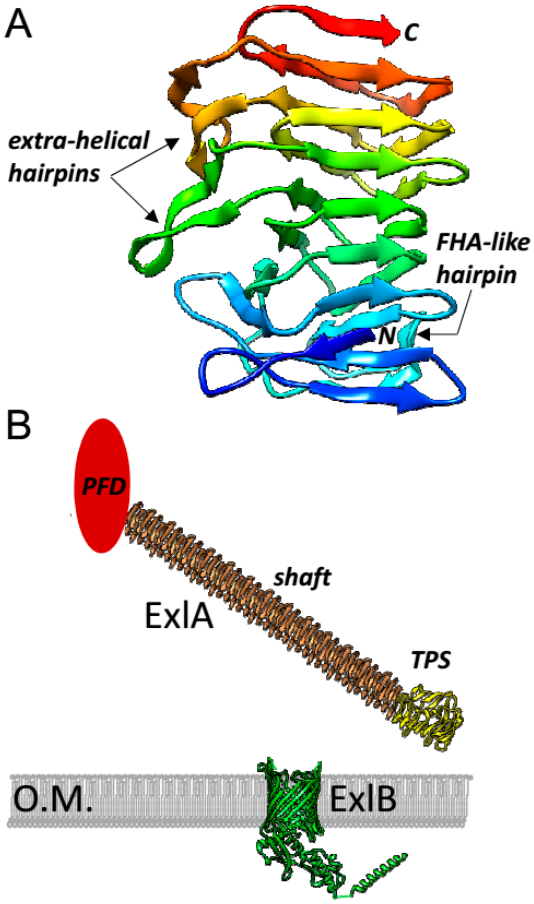

Figure 3. (**A**) Ribbon representation of the TPS domain of ExlA, as modeled by homology with HpmA as template by the Phyre2 webserver [53]. The polypeptidic chain is rainbow colored from the N- (blue) to the C-terminus (red). At its N-terminus, the helix is capped, possibly primed by three β-strands whose particular arrangement is conserved (a β-arc ending in a hairpin, here in blue). In FHA-like TPS domains, a loop is inserted in rung number 2 of the helix and is predicted to fold as a hairpin back onto the core, next to the cap [54]. In all TPS domains, two extra-helical elements stem from rungs number 4 and 6: in FHA and HpmA, hence probably in ExlA as well, these are hairpin structures folded next to each other onto the core [54,55]. (**B**) Model representation of ExlA and ExlB as they could be pictured from the X-ray structures of HpmA (Protein Data Bank code: 4W8Q) and FhaC (4QKY), respectively [54,55]. The filamentous domain of ExlA was modeled by replicating the three last rungs present in the structure of the HpmA TPS domain, after extra-helical hairpin trimming. To estimate the number of rungs in the shaft domain, the number of residues actually spanned by the Fil_Haemagg_2 repeats annotated in Pfam [25] (Figure 1A, same color code applies here) was divided by the average 20-residue length of a β-helical rung [56]. This allows to suggest that the shaft domain of ExlA contains approximately 41 rungs. As an average pitch of 4.8 Å was measured in β-helices of known structure, the shaft domain could be 200 Å-long, in addition to the 30 Å-length of TPS domains. The C-terminal domain of ExlA is displayed as an oval shape where a 30-kDa globular protein could fit, as no other structural information is available. The ribbon representation of the models was prepared with UCSF Chimera [57].

8. Conclusions and Future Directions

ExlA is a toxin secreted by a growing family of *P. aeruginosa* strains, provoking devastating injuries in infected lungs. As such, ExlA-related histological lesions are highly different from those produced by classical *P. aeruginosa* strains, and patients infected with *exlA*+ strains should probably be treated differently than those infected with classical *P. aeruginosa* strains. Hospitals are not prepared

to identify these types of strains. Relevant tests should be developed to specifically identify strains secreting Exolysin in patients, which would also help to estimate the incidence of these strains in hospital-acquired infections.

ExlA is a member of a distinct family of PFTs for which little structural information is available. One of the main hindrance to study its 3-dimensional structure and the formation of the pore within membranes is the instability of the toxin in solution, complicating its manipulation. The related toxin ShlA was previously purified [58], which brings hope for a possible purification of active ExlA in the future.

The expression of ExlA is variable in different strains, with some strains harboring the genes without any detectable protein secretion. These observations suggest that *exlBA* expression and/or ExlBA secretion are regulated by yet unknown mechanisms. As most virulence factors of *P. aeruginosa*, *exlBA* expression may be susceptible to complex regulatory circuits.

Two main cellular effects have been reported for ExlA: cadherin degradation via ADAM10 activation and induction of cell death in various cell types. The mechanisms of ExlA-dependent cell death in macrophages were clarified, yet they are unknown and likely different in other cell types, including epithelial and endothelial cells. It will also be of particular importance to understand why membrane repair mechanisms, induced by several other PFTs [59–62], are ineffective for ExlA.

Finally, the identity and the nature of the cellular receptor for ExlA are unknown. The receptor is probably quite ubiquitous as many cell types are susceptible to ExlA toxicity. Large screening approaches or biochemical copurification studies should be undertaken to identify the host receptor(s) of ExlA.

The history of the ExlA toxin started in 2014 [19] and is still at its very beginning. The next few years should bring more information about the properties of the protein and more details on its mode of action, information that is needed to eventually prevent its action.

Acknowledgments: The work of the team is supported by grants from Laboratoire of Excellence "GRAL" (ANR-10-LABX-49-01), Agence Nationale de la Recherche (ANR-15-CE11-0018-01) and Fondation pour la Recherche Médicale "Equipe FRM 2017" (DEQ20170336705). We further acknowledge support from CNRS, INSERM, CEA and University Grenoble-Alpes.

Author Contributions: All authors wrote the review.

Conflicts of Interest: The authors declare no conflict of interest.

References

1. Lyczak, J.B.; Cannon, C.L.; Pier, G.B. Establishment of *Pseudomonas aeruginosa* infection: Lessons from a versatile opportunist. *Microbes Infect.* **2000**, *2*, 1051–1060. [CrossRef]
2. Cao, H.; Baldini, R.L.; Rahme, L.G. Common mechanisms for pathogens of plants and animals. *Annu. Rev. Phytopathol.* **2001**, *39*, 259–284. [CrossRef] [PubMed]
3. Rahme, L.G.; Ausubel, F.M.; Cao, H.; Drenkard, E.; Goumnerov, B.C.; Lau, G.W.; Mahajan-Miklos, S.; Plotnikova, J.; Tan, M.W.; Tsongalis, J.; et al. Plants and animals share functionally common bacterial virulence factors. *Proc. Natl. Acad. Sci. USA* **2000**, *97*, 8815–8821. [CrossRef] [PubMed]
4. Brewer, C.; Wunderink, R.G.; Jones, C.B.; Leeper, K.V. Ventilator-associated pneumonia due to *Pseudomonas aeruginosa*. *Chest* **1996**, *109*, 1019–1029. [CrossRef]
5. Kos, V.N.; Deraspe, M.; McLaughlin, R.E.; Whiteaker, J.D.; Roy, P.H.; Alm, R.A.; Corbeil, J.; Gardner, H. The resistome of *Pseudomonas aeruginosa* in relationship to phenotypic susceptibility. *Antimicrob. Agents Chemother.* **2015**, *59*, 427–436. [CrossRef] [PubMed]
6. Huber, P.; Basso, P.; Reboud, E.; Attree, I. *Pseudomonas aeruginosa* renews its virulence factors. *Environ. Microbiol. Rep.* **2016**. [CrossRef] [PubMed]
7. Roy, P.H.; Tetu, S.G.; Larouche, A.; Elbourne, L.; Tremblay, S.; Ren, Q.; Dodson, R.; Harkins, D.; Shay, R.; Watkins, K.; et al. Complete genome sequence of the multiresistant taxonomic outlier *Pseudomonas aeruginosa* PA7. *PLoS ONE* **2010**, *5*, e8842. [CrossRef] [PubMed]

8. Stover, C.K.; Pham, X.Q.; Erwin, A.L.; Mizoguchi, S.D.; Warrener, P.; Hickey, M.J.; Brinkman, F.S.; Hufnagle, W.O.; Kowalik, D.J.; Lagrou, M.; et al. Complete genome sequence of *Pseudomonas aeruginosa* PAO1, an opportunistic pathogen. *Nature* **2000**, *406*, 959–964. [PubMed]
9. Lee, D.G.; Urbach, J.M.; Wu, G.; Liberati, N.T.; Feinbaum, R.L.; Miyata, S.; Diggins, L.T.; He, J.X.; Saucier, M.; Deziel, E.; et al. Genomic analysis reveals that *Pseudomonas aeruginosa* virulence is combinatorial. *Genome Biol.* **2006**, *7*. [CrossRef] [PubMed]
10. *Pseudomonas* Database. Available online: www.pseudomonas.com (accessed on 9 November 2017).
11. Wiehlmann, L.; Cramer, N.; Tummler, B. Habitat-associated skew of clone abundance in the *Pseudomonas aeruginosa* population. *Environ. Microbiol. Rep.* **2015**, *7*, 955–960. [CrossRef] [PubMed]
12. Thrane, S.W.; Taylor, V.L.; Freschi, L.; Kukavica-Ibrulj, I.; Boyle, B.; Laroche, J.; Pirnay, J.P.; Levesque, R.C.; Lam, J.S.; Jelsbak, L. The Widespread Multidrug-Resistant Serotype O12 *Pseudomonas aeruginosa* Clone Emerged through Concomitant Horizontal Transfer of Serotype Antigen and Antibiotic Resistance Gene Clusters. *mBio* **2015**, *6*, e01396-15. [CrossRef] [PubMed]
13. Hilker, R.; Munder, A.; Klockgether, J.; Losada, P.M.; Chouvarine, P.; Cramer, N.; Davenport, C.F.; Dethlefsen, S.; Fischer, S.; Peng, H.; et al. Interclonal gradient of virulence in the *Pseudomonas aeruginosa* pangenome from disease and environment. *Environ. Microbiol.* **2015**, *17*, 29–46. [CrossRef] [PubMed]
14. Hauser, A.R. The type III secretion system of *Pseudomonas aeruginosa*: Infection by injection. *Nat. Rev. Microbiol.* **2009**, *7*, 654–665. [CrossRef] [PubMed]
15. Filloux, A. Protein Secretion Systems in *Pseudomonas aeruginosa*: An Essay on Diversity, Evolution, and Function. *Front. Microbiol.* **2011**, *2*, 155. [CrossRef] [PubMed]
16. Berthelot, P.; Attree, I.; Plesiat, P.; Chabert, J.; de Bentzmann, S.; Pozzetto, B.; Grattard, F.; Groupe d'Etudes des Septicémies à Pseudomonas aeruginosa. Genotypic and phenotypic analysis of type III secretion system in a cohort of *Pseudomonas aeruginosa* bacteremia isolates: Evidence for a possible association between O serotypes and *exo* genes. *J. Infect. Dis.* **2003**, *188*, 512–518. [CrossRef] [PubMed]
17. Shaver, C.M.; Hauser, A.R. Relative contributions of *Pseudomonas aeruginosa* ExoU, ExoS, and ExoT to virulence in the lung. *Infect. Immun.* **2004**, *72*, 6969–6977. [CrossRef] [PubMed]
18. Reboud, E.; Elsen, S.; Bouillot, S.; Golovkine, G.; Basso, P.; Jeannot, K.; Attree, I.; Huber, P. Phenotype and toxicity of the recently discovered exlA-positive *Pseudomonas aeruginosa* strains collected worldwide. *Environ. Microbiol.* **2016**, *18*, 3425–3439. [CrossRef] [PubMed]
19. Elsen, S.; Huber, P.; Bouillot, S.; Coute, Y.; Fournier, P.; Dubois, Y.; Timsit, J.F.; Maurin, M.; Attree, I. A type III secretion negative clinical strain of *Pseudomonas aeruginosa* employs a two-partner secreted exolysin to induce hemorrhagic pneumonia. *Cell Host Microbe* **2014**, *15*, 164–176. [CrossRef] [PubMed]
20. Basso, P.; Wallet, P.; Elsen, S.; Soleilhac, E.; Henry, T.; Faudry, F.; Attrée, I. Multiple *Pseudomonas* species secrete Exolysin-like toxins and provoke Caspase-1-dependent macrophage death. *Environ. Microbiol.* **2017**. [CrossRef] [PubMed]
21. Basso, P.; Ragno, M.; Elsen, S.; Reboud, E.; Golovkine, G.; Bouillot, S.; Huber, P.; Lory, S.; Faudry, E.; Attree, I. *Pseudomonas aeruginosa* Pore-Forming Exolysin and Type IV Pili Cooperate To Induce Host Cell Lysis. *mBio* **2017**, *8*. [CrossRef] [PubMed]
22. Jacob-Dubuisson, F.; Guerin, J.; Baelen, S.; Clantin, B. Two-partner secretion: as simple as it sounds? *Res. Microbiol.* **2013**, *164*, 583–595. [CrossRef] [PubMed]
23. Jacob-Dubuisson, F.; Locht, C.; Antoine, R. Two-partner secretion in Gram-negative bacteria: A thrifty, specific pathway for large virulence proteins. *Mol. Microbiol.* **2001**, *40*, 306–313. [CrossRef] [PubMed]
24. Jacob-Dubuisson, F.; Villeret, V.; Clantin, B.; Delattre, A.S.; Saint, N. First structural insights into the TpsB/Omp85 superfamily. *Biol. Chem.* **2009**, *390*, 675–684. [CrossRef] [PubMed]
25. Finn, R.D.; Coggill, P.; Eberhardt, R.Y.; Eddy, S.R.; Mistry, J.; Mitchell, A.L.; Potter, S.C.; Punta, M.; Qureshi, M.; Sangrador-Vegas, A.; et al. The Pfam protein families database: towards a more sustainable future. *Nucleic Acids Res.* **2016**, *44*, D279–D285. [CrossRef] [PubMed]
26. Ondraczek, R.; Hobbie, S.; Braun, V. In vitro activation of the *Serratia marcescens* hemolysin through modification and complementation. *J. Bacteriol.* **1992**, *174*, 5086–5094. [CrossRef] [PubMed]
27. Braun, V.; Neuss, B.; Ruan, Y.; Schiebel, E.; Schoffler, H.; Jander, G. Identification of the *Serratia marcescens* hemolysin determinant by cloning into *Escherichia coli*. *J. Bacteriol.* **1987**, *169*, 2113–2120. [CrossRef] [PubMed]
28. Schiebel, E.; Schwarz, H.; Braun, V. Subcellular location and unique secretion of the hemolysin of *Serratia marcescens*. *J. Biol. Chem.* **1989**, *264*, 16311–16320. [PubMed]

29. Weaver, T.M.; Smith, J.A.; Hocking, J.M.; Bailey, L.J.; Wawrzyn, G.T.; Howard, D.R.; Sikkink, L.A.; Ramirez-Alvarado, M.; Thompson, J.R. Structural and functional studies of truncated hemolysin A from *Proteus mirabilis*. *J. Biol. Chem.* **2009**, *284*, 22297–22309. [CrossRef] [PubMed]
30. Schiebel, E.; Braun, V. Integration of the *Serratia marcescens* haemolysin into human erythrocyte membranes. *Mol. Microbiol.* **1989**, *3*, 445–453. [CrossRef] [PubMed]
31. Schonherr, R.; Hilger, M.; Broer, S.; Benz, R.; Braun, V. Interaction of *Serratia marcescens* hemolysin (ShlA) with artificial and erythrocyte membranes. Demonstration of the formation of aqueous multistate channels. *Eur. J. Biochem.* **1994**, *223*, 655–663. [CrossRef] [PubMed]
32. Reboud, E.; Bouillot, S.; Patot, S.; Beganton, B.; Attree, I.; Huber, P. *Pseudomonas aeruginosa* ExIA and *Serratia marcescens* ShIA trigger cadherin cleavage by promoting calcium influx and ADAM10 activation. *PLoS Pathog.* **2017**, *13*. [CrossRef] [PubMed]
33. Dal Peraro, M.; van der Goot, F.G. Pore-forming toxins: ancient, but never really out of fashion. *Nat. Rev. Microbiol.* **2016**, *14*, 77–92. [CrossRef] [PubMed]
34. Faudry, E.; Vernier, G.; Neumann, E.; Forge, V.; Attree, I. Synergistic pore formation by type III toxin translocators of *Pseudomonas aeruginosa*. *Biochemistry* **2006**, *45*, 8117–8123. [CrossRef] [PubMed]
35. Hertle, R. *Serratia marcescens* hemolysin (ShIA) binds artificial membranes and forms pores in a receptor-independent manner. *J. Membr. Biol.* **2002**, *189*, 1–14. [CrossRef] [PubMed]
36. Bouillot, S.; Munro, P.; Gallet, B.; Reboud, E.; Cretin, F.; Golovkine, G.; Schoehn, G.; Attree, I.; Lemichez, E.; Huber, P. *Pseudomonas aeruginosa* Exolysin promotes bacterial growth in lungs, alveolar damage and bacterial dissemination. *Sci. Rep.* **2017**, *7*, 2120. [CrossRef] [PubMed]
37. Gonzalez-Juarbe, N.; Mares, C.A.; Hinojosa, C.A.; Medina, J.L.; Cantwell, A.; Dube, P.H.; Orihuela, C.J.; Bergman, M.A. Requirement for *Serratia marcescens* cytolysin in a murine model of hemorrhagic pneumonia. *Infect. Immun.* **2015**, *83*, 614–624. [CrossRef] [PubMed]
38. Garcia-Suarez Mdel, M.; Florez, N.; Astudillo, A.; Vazquez, F.; Villaverde, R.; Fabrizio, K.; Pirofski, L.A.; Mendez, F.J. The role of pneumolysin in mediating lung damage in a lethal pneumococcal pneumonia murine model. *Respir. Res.* **2007**, *8*, 3. [CrossRef] [PubMed]
39. Diep, B.A.; Chan, L.; Tattevin, P.; Kajikawa, O.; Martin, T.R.; Basuino, L.; Mai, T.T.; Marbach, H.; Braughton, K.R.; Whitney, A.R.; et al. Polymorphonuclear leukocytes mediate *Staphylococcus aureus* Panton-Valentine leukocidin-induced lung inflammation and injury. *Proc. Natl. Acad. Sci. USA* **2010**, *107*, 5587–5592. [CrossRef] [PubMed]
40. Greaney, A.J.; Leppla, S.H.; Moayeri, M. Bacterial exotoxins and the inflammasome. *Front. Immunol.* **2015**, *6*, 570. [CrossRef] [PubMed]
41. Ebsen, H.; Lettau, M.; Kabelitz, D.; Janssen, O. Identification of SH3 Domain Proteins Interacting with the Cytoplasmic Tail of the A Disintegrin and Metalloprotease 10 (ADAM10). *PLoS ONE* **2014**, *9*, e102899. [CrossRef] [PubMed]
42. Seals, D.F.; Courtneidge, S.A. The ADAMs family of metalloproteases: multidomain proteins with multiple functions. *Genes Dev.* **2003**, *17*, 7–30. [CrossRef] [PubMed]
43. Horiuchi, K.; Le Gall, S.; Schulte, M.; Yamaguchi, T.; Reiss, K.; Murphy, G.; Toyama, Y.; Hartmann, D.; Saftig, P.; Blobel, C.P. Substrate selectivity of epidermal growth factor-receptor ligand sheddases and their regulation by phorbol esters and calcium influx. *Mol. Biol. Cell* **2007**, *18*, 176–188. [CrossRef] [PubMed]
44. Nagano, O.; Murakami, D.; Hartmann, D.; de Strooper, B.; Saftig, P.; Iwatsubo, T.; Nakajima, M.; Shinohara, M.; Saya, H. Cell-matrix interaction via CD44 is independently regulated by different metal loproteinases activated in response to extracellular Ca2+ influx and PKC activation. *J. Cell Biol.* **2004**, *165*, 893–902. [CrossRef] [PubMed]
45. Inoshima, I.; Inoshima, N.; Wilke, G.A.; Powers, M.E.; Frank, K.M.; Wang, Y.; Wardenburg, J.B. A *Staphylococcus aureus* pore-forming toxin subverts the activity of ADAM10 to cause lethal infection in mice. *Nat. Med.* **2011**, *17*, U1310–U1314. [CrossRef] [PubMed]
46. Powers, M.E.; Kim, H.K.; Wang, Y.; Wardenburg, J.B. ADAM10 Mediates Vascular Injury Induced by *Staphylococcus aureus* alpha-Hemolysin. *J. Infect. Dis.* **2012**, *206*, 352–356. [CrossRef] [PubMed]
47. Poole, K.; Schiebel, E.; Braun, V. Molecular characterization of the hemolysin determinant of *Serratia marcescens*. *J. Bacteriol.* **1988**, *170*, 3177–3188. [CrossRef] [PubMed]

48. Guérin, J.; Bigot, S.; Schneider, R.; Buchanan, S.K.; Jacob-Dubuisson, F. Two-Partner Secretion: Combining Efficiency and Simplicity in the Secretion of Large Proteins for Bacteria-Host and Bacteria-Bacteria Interactions. *Front. Cell. Infect. Microbiol.* **2017**, *7*, 148. [CrossRef] [PubMed]
49. Zambolin, S.; Clantin, B.; Chami, M.; Hoos, S.; Haouz, A.; Villeret, V.; Delepelaire, P. Structural basis for haem piracy from host haemopexin by *Haemophilus influenzae*. *Nat. Commun.* **2016**, *7*, 11590. [CrossRef] [PubMed]
50. Ruoslahti, E. RGD and other recognition sequences for integrins. *Annu. Rev. Cell Dev. Biol.* **1996**, *12*, 697–715. [CrossRef] [PubMed]
51. Ishibashi, Y.; Relman, D.A.; Nishikawa, A. Invasion of human respiratory epithelial cells by *Bordetella pertussis*: Possible role for a filamentous hemagglutinin Arg-Gly-Asp sequence and alpha 5 beta 1 integrin. *Microb. Pathog.* **2001**, *30*, 279–288. [CrossRef] [PubMed]
52. Julio, S.M.; Inatsuka, C.S.; Mazar, J.; Dieterich, C.; Relman, D.A.; Cotter, P.A. Natural-host animal models indicate functional interchangeability between the filamentous haemagglutinins of *Bordetella pertussis* and *Bordetella bronchiseptica* and reveal a role for the mature C-terminal domain, but not the RGD motif, during infection. *Mol. Microbiol.* **2009**, *71*, 1574–1590. [CrossRef] [PubMed]
53. Kelley, L.A.; Mezulis, S.; Yates, C.M.; Wass, M.N.; Sternberg, M.J. The Phyre2 web portal for protein modeling, prediction and analysis. *Nat. Protoc.* **2015**, *10*, 845–858. [CrossRef] [PubMed]
54. Clantin, B.; Hodak, H.; Willery, E.; Locht, C.; Jacob-Dubuisson, F.; Villeret, V. The crystal structure of filamentous hemagglutinin secretion domain and its implications for the two-partner secretion pathway. *Proc. Natl. Acad. Sci. USA* **2004**, *101*, 6194–6199. [CrossRef] [PubMed]
55. Yeo, H.J.; Yokoyama, T.; Walkiewicz, K.; Kim, Y.; Grass, S.; Geme, J.W., 3rd. The structure of the *Haemophilus influenzae* HMW1 pro-piece reveals a structural domain essential for bacterial two-partner secretion. *J. Biol. Chem.* **2007**, *282*, 31076–31084. [CrossRef] [PubMed]
56. Kajava, A.V.; Steven, A.C. The turn of the screw: variations of the abundant beta-solenoid motif in passenger domains of Type V secretory proteins. *J. Struct. Biol.* **2006**, *155*, 306–315. [CrossRef] [PubMed]
57. Pettersen, E.F.; Goddard, T.D.; Huang, C.C.; Couch, G.S.; Greenblatt, D.M.; Meng, E.C.; Ferrin, T.E. UCSF Chimera–a visualization system for exploratory research and analysis. *J. Comput. Chem.* **2004**, *25*, 1605–1612. [CrossRef] [PubMed]
58. Walker, G.; Hertle, R.; Braun, V. Activation of *Serratia marcescens* hemolysin through a conformational change. *Infect. Immun.* **2004**, *72*, 611–614. [CrossRef] [PubMed]
59. Los, F.C.O.; Randis, T.M.; Aroian, R.V.; Ratner, A.J. Role of Pore-Forming Toxins in Bacterial Infectious Diseases. *Microbiol. Mol. Biol. Rev.* **2013**, *77*, 173–207. [CrossRef] [PubMed]
60. Cassidy, S.K.B.; O'Riordan, M.X.D. More Than a Pore: The Cellular Response to Cholesterol-Dependent Cytolysins. *Toxins* **2013**, *5*, 618–636. [CrossRef] [PubMed]
61. Romero, M.; Keyel, M.; Shi, G.L.; Bhattacharjee, P.; Roth, R.; Heuser, J.E.; Keyel, P.A. Intrinsic repair protects cells from pore-forming toxins by microvesicle shedding. *Cell Death Differ.* **2017**, *24*, 798–808. [CrossRef] [PubMed]
62. Von Hoven, G.; Rivas, A.J.; Neukirch, C.; Meyenburg, M.; Qin, Q.; Parekh, S.; Hellmann, N.; Husmann, M. Repair of a Bacterial Small beta-Barrel Toxin Pore Depends on Channel Width. *mBio* **2017**, *8*. [CrossRef] [PubMed]

11

Structural basis of lipid targeting and destruction by the type V secretion system of *P. aeruginosa*

da Mata Madeira PV, Zouhir S, Basso P, Neves D, Laubier A, Salacha R, Bleves S, Faudry E, Contreras-Martel C, Dessen A (Journal of molecular biology (2016))

The type V secretion system is a macromolecular machine employed by a number of bacteria to secrete virulence factors into the environment. The human pathogen Pseudomonas aeruginosa employs the newly described type Vd secretion system to secrete a soluble variant of PlpD, a lipase of the patatin-like family synthesized as a single macromolecule that also carries a polypeptide transport-associated domain and a 16-stranded β-barrel. Here we report the crystal structure of the secreted form of PlpD in its biologically active state. PlpD displays a classical lipase α/β hydrolase fold with a catalytic site located within a highly hydrophobic channel that entraps a lipidic molecule. The active site is covered by a flexible lid, as in other lipases, indicating that this region in PlpD must modify its conformation in order for catalysis at the water-lipid interface to occur. PlpD displays phospholipase A1 activity and is able to recognize a number of phosphatidylinositols and other phosphatidyl analogs. PlpD is the first example of an active phospholipase secreted through the type V secretion system, for which there are more than 200 homologs, revealing details of the lipid destruction arsenal expressed by *P. aeruginosa* in order to establish infection.

Structural Basis of Lipid Targeting and Destruction by the Type V Secretion System of *Pseudomonas aeruginosa*

Paulo Vinicius da Mata Madeira [1], Samira Zouhir [1], Pauline Basso [2,3,4,5], David Neves [1], Aurélie Laubier [6], Richard Salacha [6], Sophie Bleves [6], Eric Faudry [2,3,4,5], Carlos Contreras-Martel [3,4,7] and Andréa Dessen [1,3,4,7]

*1 - **Brazilian National Laboratory for Biosciences (LNBio),** CNPEM, Campinas, São Paulo, Brazil*
*2 - **Univ. Grenoble Alpes,** Bacterial Pathogenesis and Cellular Responses Group, Institut de Biosciences et Biotechnologies de Grenoble (BIG), Grenoble, France*
*3 - **CNRS,** IBS and BIG, Grenoble, France*
*4 - **CEA,** IBS and BIG, Grenoble, France*
*5 - **INSERM,** UMR-S 1036 Biology of Cancer and Infection Laboratory, Grenoble, France*
*6 - **CNRS & Aix-Marseille Université,** Laboratoire d'Ingénierie des Systèmes Macromoléculaires (UMR7255), Institut de Microbiologie de la Méditerranée, Marseille, France*
*7 - **Univ. Grenoble Alpes,** Institut de Biologie Structurale (IBS), Grenoble, France*

***Correspondence to Carlos Contreras-Martel and Andréa Dessen:** carlos.contreras@ibs.fr; andrea.dessen@ibs.fr*
http://dx.doi.org/10.1016/j.jmb.2016.03.012
Edited by M. Guss

Abstract

The type V secretion system is a macromolecular machine employed by a number of bacteria to secrete virulence factors into the environment. The human pathogen *Pseudomonas aeruginosa* employs the newly described type Vd secretion system to secrete a soluble variant of PlpD, a lipase of the patatin-like family synthesized as a single macromolecule that also carries a polypeptide transport-associated domain and a 16-stranded β-barrel. Here we report the crystal structure of the secreted form of PlpD in its biologically active state. PlpD displays a classical lipase α/β hydrolase fold with a catalytic site located within a highly hydrophobic channel that entraps a lipidic molecule. The active site is covered by a flexible lid, as in other lipases, indicating that this region in PlpD must modify its conformation in order for catalysis at the water–lipid interface to occur. PlpD displays phospholipase A_1 activity and is able to recognize a number of phosphatidylinositols and other phosphatidyl analogs. PlpD is the first example of an active phospholipase secreted through the type V secretion system, for which there are more than 200 homologs, revealing details of the lipid destruction arsenal expressed by *P. aeruginosa* in order to establish infection.

Introduction

Microbial pathogens have developed multiple means to subvert target cell functions in order to facilitate infection or outgrow competing bacteria in polymicrobial environments. Gram-negative bacteria possess a number of translocation nanomachines that allow passage of proteins, small molecules or DNA across the cell envelope to the external surroundings, or directly into the cytoplasm of target cells. To date, seven different secretion systems (types I–VI and IX) have been described in Gram-negative organisms, many of which play key roles in establishment of infection in eukaryotic hosts or in bacterial warfare [1,2]. Effectors that are translocated through the type I, III, IV and VI secretion systems (T1SS, T3SS, T4SS and T6SS), bypass periplasmic steps and are released into the surrounding environment (T1SS) or are injected directly into the eukaryotic cytoplasm (T3SS, T4SS and T6SS) or target bacteria (T6SS). This is distinct from the two-step mechanisms of the type II, V and IX secretion systems (T2SS, T5SS and T9SS) that involve the synthesis of a precursor and a periplasmic intermediate of the effector [1,3–5]. The T5SS is the simplest secretion system, in which all substrates depend on the Sec machinery for transit

Please cite this article as: P. V. da Mata Madeira, et al., Structural Basis of Lipid Targeting and Destruction by the Type V Secretion System of *Pseudomonas aeruginosa*..., J. Mol. Biol. (2016), http://dx.doi.org/10.1016/j.jmb.2016.03.012

through the inner membrane, and subsequently employ their common β-barrel domain to become inserted into the outer lipid bilayer, where they remain attached and exposed, or are secreted into the surrounding medium [1,6]. The T5SS secretes mainly virulence factors that target eukaryotic cells, but also plays roles in biofilm formation and cellular adherence [7]. The T5SS can also target other bacteria through a CDI (contact-dependent growth inhibition) mechanism [8] exerting both anti-eukaryotic and antibacterial functions.

The T5SS includes autotransporters (ATs) and two-partner secretion (TPS) systems [9]. Classical ATs (T5aSS) are synthesized as large precursors consisting of a signal sequence, followed by a passenger domain and a C-terminal, 12-stranded β-barrel transporter domain (Fig. 1a). Interestingly, the presence of the β-barrel domain is common to all T5SS molecules; the most notable distinction between ATs and TPS is that, in the latter, this domain is located on a different polypeptide, while in ATs, it is localized at the C-terminus of a unique protein [6]. It is commonly accepted that upon transport of the protein to the bacterial periplasm through the Sec system, the BamA complex plays an important role in the insertion of the transporter domain into the outer membrane [6,7]. This facilitates exposure of the "passenger" domain at the surface of the cell, where it may remain attached or be cleaved into the extracellular medium [6,10]. While the passenger domains of ATs differ widely in size and function, most of them display a similar overall structure feature a β-helical system.

TPS (T5bSS) systems are mostly dedicated to the secretion of elongated proteins that fold as extended β-helices; the transporter domain (also called TpsB) is nonetheless essential for secretion of the functional region, the TpsA (Fig. 1b) [11]. Interestingly, in addition to the aforementioned β-barrel made up of 16 β-strands, TpsB proteins may also carry successive polypeptide transport-associated (POTRA) domains, whose function is to recognize the TPS domain of the TpsA in an unfolded conformation and aid in its threading through the C-terminal β-barrel. The growing complexity of details arising for T5SS has led to their classification into types Va–Ve [6,7,9].

Pseudomonas aeruginosa is a Gram-negative pathogen that harbors numerous secretion systems that translocate damaging enzymes and toxins to the outside environment, whose function is to initiate infection in eukaryotic hosts and/or compete with other bacteria for nutrients [12]. Recently, *P. aeruginosa* was shown to secrete a patatin-like protein, PlpD, through the type T5dSS [13]. PlpD is a 728-residue protein that harbors an N-terminal signal peptide, a central functional domain and a C-terminal region that is predicted to fold into a predicted 16-stranded β-barrel (Fig. 1c). Despite the fact that this arrangement is reminiscent of an AT system, the β-domain of PlpD displays characteristics of TpsB proteins of TPS systems, in that a POTRA motif precedes the sequence corresponding to the β-barrel [13]. Interestingly, sequence comparisons between PlpD and other bacterial lipolytic enzymes revealed that the N-terminal, functional domain of PlpD harbors 4 motifs that are found in bacterial patatin-like proteins (PLPs) which display lipolytic activities that are dependent on a Ser-Asp catalytic dyad [14]. The fact that recombinant PlpD present in whole cell extracts of *Escherichia coli* displays activity toward a lipidic substrate is evidence of its capacity to recognize and degrade/hydrolyze lipids [13]. TpsA proteins have been reported to exert functions ranging from contact-dependent growth inhibition to pore formation and adherence [10]. However, the only other lipolytic T5SS are ATs with GDSL passenger domains, notably *P. aeruginosa* EstA, an esterase required for rhamnolipid production [15].

In this work, we have solved the crystal structure of the passenger domain of PlpD ($PlpD_{20–333}$) to 2.14 Å. $PlpD_{20–333}$ displays a compact fold that is highly reminiscent of the catalytic domains of PLPs such as ExoU, $cPLA_2$ and patatin. Interestingly, all catalytic motifs of $PlpD_{20–333}$ are clearly traceable in the electron density map, indicating that the crystallized form is in its active state. The active site resides at the bottom of a tight "channel" region that is rich in hydrophobic residues and is towered by an elongated α-helix not present in the structures of other lipases that have been characterized to date. Notably, a region of elongated electron density is snugly nestled within a channel in the vicinity of the active site, suggesting that our crystal structure of $PlpD_{20–333}$ harbors a "trapped" lipidic substrate or metabolized product. Purified, wild-type $PlpD_{20–333}$ displays phospholipase A_1 activity and recognizes phosphatidylinositols, indicating that it could play a role in the targeting of eukaryotic membranes. PlpD is thus the first example of an active lipase that is secreted through the T5SS and whose fold and structural arrangement are totally distinct from other passenger proteins secreted by the system.

Results

PlpD structure determination

Full-length PlpD is composed of a signal peptide, followed by the passenger domain, a TpsB region consisting of a POTRA domain, and the β domain at the C-terminus (Fig. 1c). In order to characterize the passenger region (TpsA) of PlpD from *P. aeruginosa* PAO1 (and due to the fact that the exact cleavage site between the passenger and the TpsB domains of PlpD was unknown), we initially constructed a short form containing all four "conserved lipase activity blocks" ($PlpD_{27–220}$) as well as a longer

Please cite this article as: P. V. da Mata Madeira, et al., Structural Basis of Lipid Targeting and Destruction by the Type V Secretion System of *Pseudomonas aeruginosa*..., J. Mol. Biol. (2016), http://dx.doi.org/10.1016/j.jmb.2016.03.012

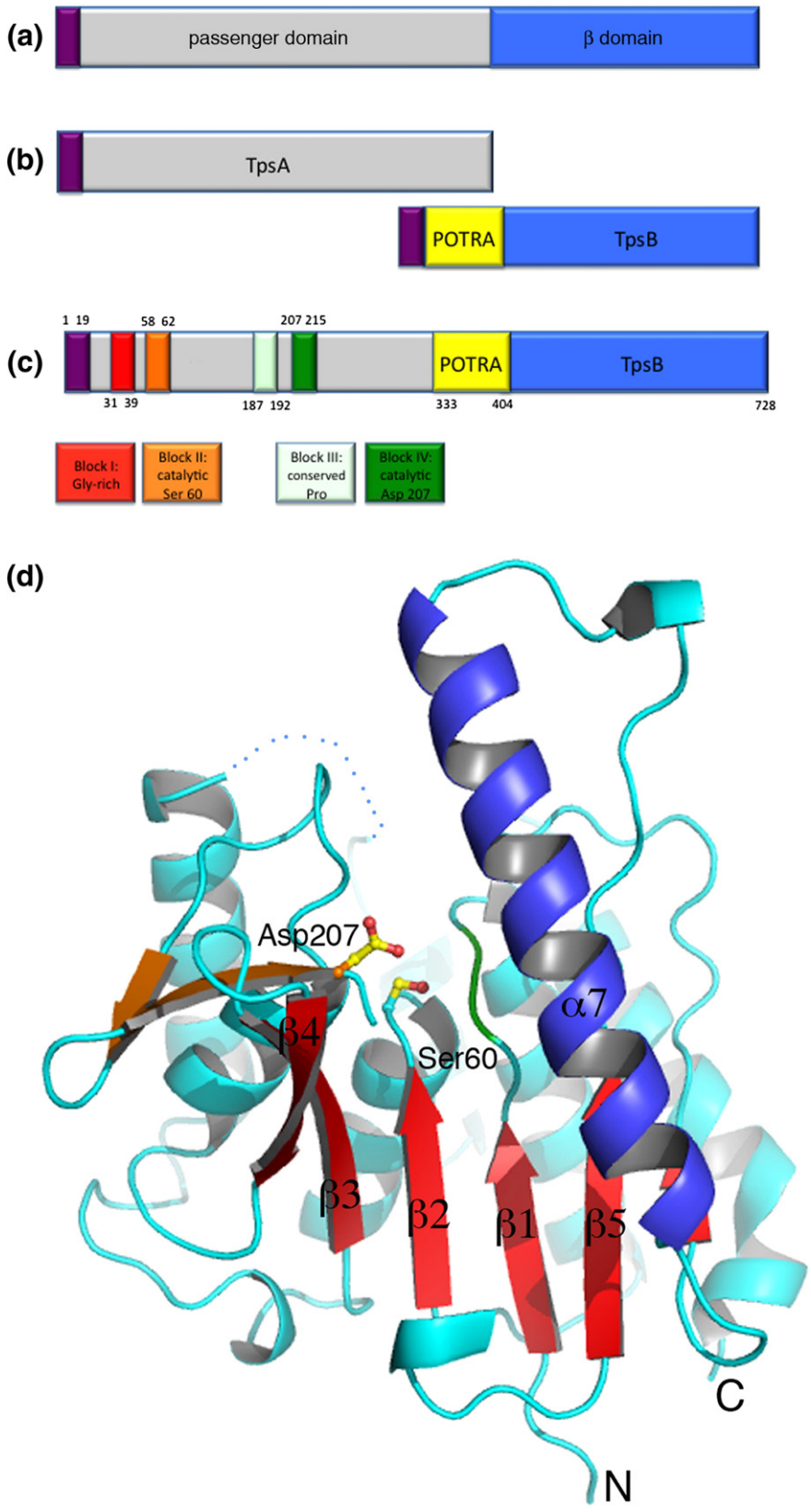

Fig. 1. PlpD represents a new type of T5SS substrate. Schematic diagrams of autotransporters (a), TPS proteins (b) and PlpD (c) from *Pseudomonas aeruginosa*. (d) Tertiary fold of $PlpD_{20–333}$. $PlpD_{20–333}$ presents a compact α/β hydrolase fold and an unusual 23-residue helix (α7) towering over the active site.

Please cite this article as: P. V. da Mata Madeira, et al., Structural Basis of Lipid Targeting and Destruction by the Type V Secretion System of *Pseudomonas aeruginosa*..., J. Mol. Biol. (2016), http://dx.doi.org/10.1016/j.jmb.2016.03.012

form ($PlpD_{20–333}$), whose C-terminal boundary was located before the beginning of the sequence corresponding to the predicted POTRA domain. The two recombinant forms were N-terminally His-tagged. Only $PlpD_{20–333}$ could be produced in stable form in *E. coli*. This recombinant form was thus expressed, purified and crystallized. Native $PlpD_{20–333}$ crystals diffracted to 2.14 Å; crystals were in space group $P2_13$ with two molecules in the asymmetric unit. In order to phase reflections, a selenomethionine derivative form of $PlpD_{20–333}$ was purified and crystallized in space group $P2_12_12_1$. Anomalous data to 2.91 Å were collected on the f″ edge of selenium, and the structure of $PlpD_{20–333}$ was solved using single wavelength anomalous dispersion; the model constructed using the selenomethionine data was used to solve the higher-resolution diffraction data by molecular replacement using phase extension protocols. Data collection, phasing and refinement statistics are included in Table 1.

Table 1. PlpD data collection, phasing, molecular replacement and structure refinement statistics

Data set	Se derivative	Native
Data collection		
X-ray source	ID29-ESRF	ID29-ESRF
Wavelength (Å)	0.97939	0.97625
Oscillation (°)	0.25	0.1
Space group	$P2_12_12_1$	$P2_13$
a (Å)	47.74	145.91
b (Å)	113.39	145.91
c (Å)	130.42	145.91
Mosaicity (°)	0.093	0.068
Overall resolution (Å)	85.58–2.74	48.64–2.14
No. observed/unique reflections	157830/ 35016	319438/ 54378
High resolution shell (Å)	2.90–2.74	2.27–2.14
Completeness (%) (last shell)	99.5 (93.3)	95.3 (85.4)
R_{sym} (last shell)	10.2 (52.7)	1.8 (57.3)
$I/\lceil(I)$ (last shell)	10.4 (2.9)	61.6 (3.0)
Wilson plot *B*-factor (Å^2)	47.04	64.20
Phasing		
Mol/ASU	2	
Residues/Mol	314	
Solvent fraction	0.518	
Se atoms/Mol	9	
SHELXC/D resolution limits	43.22–3.56	
Heavy atoms found	13	
Correlation heavy atoms sites	0.391	
SHARP FOM (acentric/centric)	0.24033/ 0.10125	
Phasing power (anomalous differences)	0.666	
Hand contrast	0.6296/ 0.5263	
Parrot best phases score	3.1198	
Buccaneer automatic model building (Residues/chains/sequenced)	524/18/402	
R_{work}/R_{free}	0.223/0.297	
Molecular replacement		
Phaser LLG		490
Phenix Autobuild (Residues/chains/waters)		488/4/374
R_{work}/R_{free}		0.238/ 0.282
Refinement		
R_{work}/R_{free}	0.209/0.242	0.205/ 0.231
No. of protein atoms	3716	3766
No. of solvent atoms	40	134
RMS deviation, bond lengths (Å)	0.010	0.009
RMS deviation, bond angles (°)	1.430	1.080
Mean B factor (Å^2)	69.29	76.07
Residues in most favored/allowed region of Ramachandran plot (%)	100	100

PlpD displays a compact phospholipase fold

$PlpD_{20–333}$ displays an α/β hydrolase fold with a twisted six-stranded central β-sheet surrounded by eight major helices, which is common to a number of esterases and hydrolytic enzymes, including human $cPLA_2$, or VipD and ExoU, PLPs from *Legionella pneumophila* and *P. aeruginosa*, respectively [16–18]. The only regions that could not be traced in the electron density map were the C-terminus beyond residue 307 and amino acids 89–126, which lie in the proximity of the active site. The structure of $PlpD_{20–333}$ seems to represent a "minimalistic" α/β hydrolase fold required for catalysis, in that it displays secondary structure elements necessary to support the formation of the catalytic site, but none of the other major helical regions observed in the abovementioned enzymes, which in those proteins participate in target lipid recognition (see below). One notable feature, however, is a major hydrophobic helix (α7; Fig. 1b), whose direct interaction with its counterpart in a neighboring molecule (Fig. 2a) stabilizes the dimer that is present in the asymmetric unit.

In order to further characterize $PlpD_{20–333}$, we performed dynamic light scattering, size exclusion chromatography (SEC) and analytical ultracentrifugation experiments. SEC analyses revealed that $PlpD_{20–333}$ eluted as a single peak with a hydrodynamic radius of 4.1 nm (not shown); this was confirmed by DLS, which also pointed to a homogeneous sample with a hydrodynamic radius of 4.0 nm (Fig. 2b). To confirm these states, $PlpD_{20–333}$ was studied by analytical ultracentrifugation. The protein was submitted to sedimentation velocity measurements at different concentrations (0.5, 1.0 and 3.0 mg/ml), and the absorbance signal was monitored at 280 nm. The *c*(*s*) analysis of the data revealed that $PlpD_{20–333}$ sedimented as a unique species with an *S* value of 3.25 (Fig. 2d $s_{20,w} = 3.8S$ for more than 95% of each preparation; Fig. 2c and d). The constant value of the sedimentation coefficient at different protein concentrations demonstrates that all samples presented the same stable oligomeric state. Solutions of the Lamm equation were obtained considering a frictional ration of 1.55, which is in agreement with a Stoke's radius of 4 nm. Consequently, the experimental *s* value observed corresponds to a protein with a molecular mass of 70 kDa, thus confirming the dimeric nature of

Please cite this article as: P. V. da Mata Madeira, et al., Structural Basis of Lipid Targeting and Destruction by the Type V Secretion System of *Pseudomonas aeruginosa*..., J. Mol. Biol. (2016), http://dx.doi.org/10.1016/j.jmb.2016.03.012

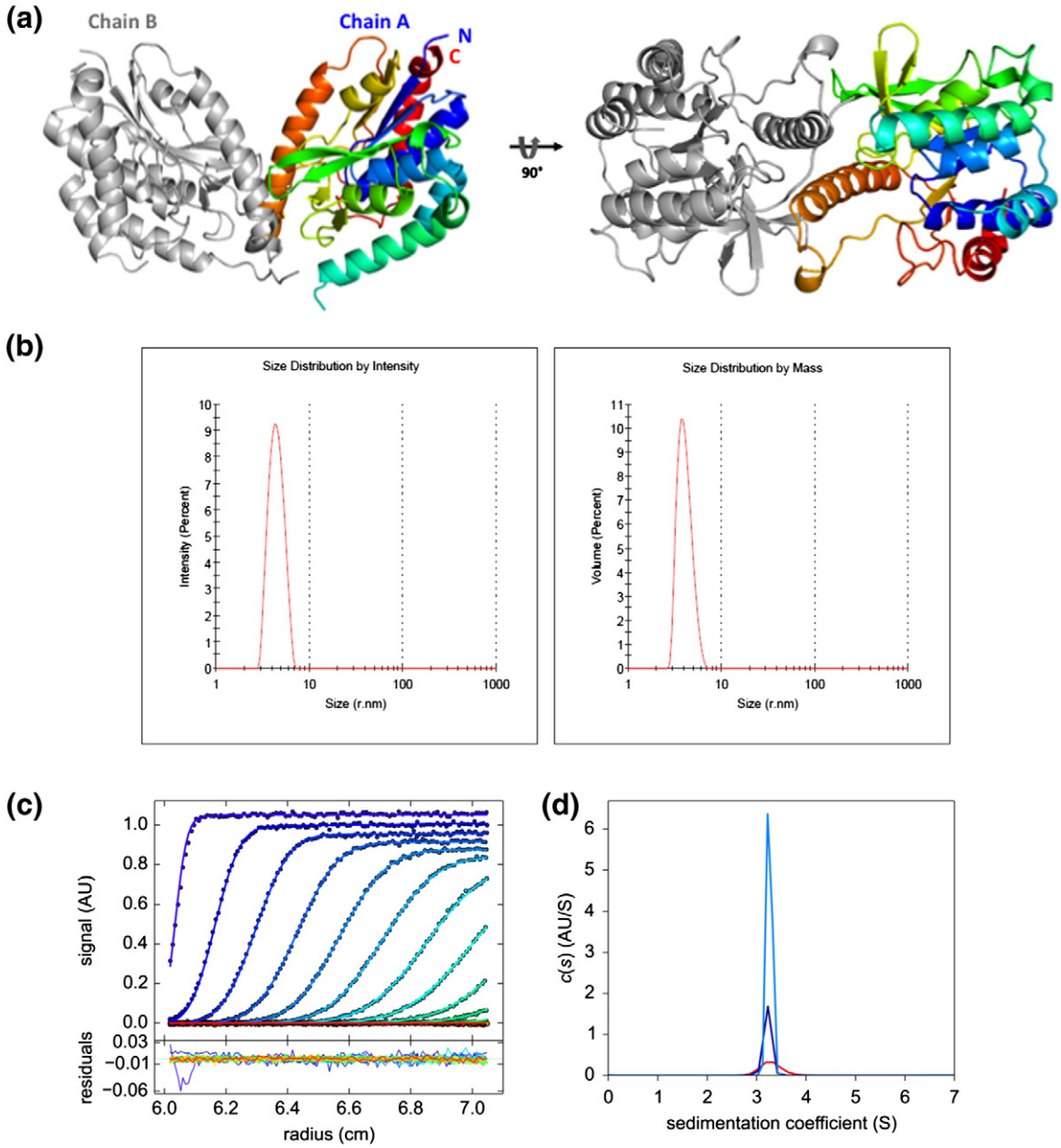

Fig. 2. PlpD is stable as a biological dimer. (a) The asymmetric unit of the PlpD$_{20–333}$ crystal contains a dimer whose central feature is the association of helix 7. The area of the interface between the two monomers is equal to 1259 Å^2. (b) Dynamic light scattering analyses of PlpD$_{20–333}$ indicate a monodisperse species with a hydrodynamic radius of 4.0 nm. (c) Experimental sedimentation profiles of PlpD$_{20–333}$ fit using Sedfit (top) and corresponding residuals (bottom). (d) *c*(*s*) analysis of PlpD$_{20–333}$ at 0.5, 1.0 and 3.0 mg/ml (red, blue and light blue lines, respectively). Samples were studied at 15 °C with a rotor velocity of 40,000 rpm with absorbance being monitored at 280 nm. The Lamm equation was solved considering the buffer viscosity and density values of η = 1.139 cp and ρ = 1.0088 g/ml. For PlpD$_{20–333}$, the partial specific volume v = 0.738 ml/g and the frictional ratio f/f^o = 1.5 were considered.

PlpD$_{20–333}$. This organization could play a key role in the function of the secreted form of the molecule (see below).

An active catalytic site

Bacterial PLPs and their eukaryotic counterparts share conserved motifs including a Ser-Asp active site dyad instead of the classical Ser-His-Asp(Glu) triad of lipolytic enzymes [19]. The catalytic serine (Ser60) of PlpD$_{20–333}$ is located at an elbow between β2 and the following helix (α2), and lies at the bottom of a highly hydrophobic channel-like region. Two consecutive Gly residues (Gly31, Gly32), located in the loop between β1 and α1 and in close proximity to Ser60 (green in Fig. 3a), point their backbone residues

Please cite this article as: P. V. da Mata Madeira, et al., Structural Basis of Lipid Targeting and Destruction by the Type V Secretion System of *Pseudomonas aeruginosa*..., J. Mol. Biol. (2016), http://dx.doi.org/10.1016/j.jmb.2016.03.012

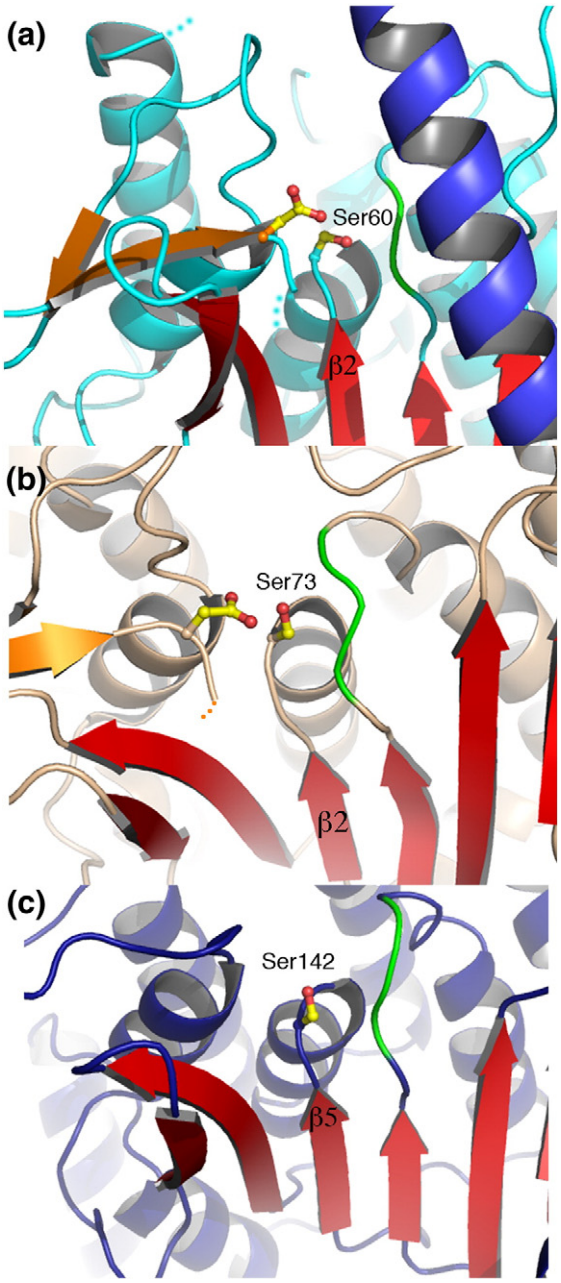

Fig. 3. Details of active sites of bacterial lipases. $PlpD_{20–333}$ (a), VipD (b) and ExoU (c) all carry a nucleophilic Ser at the center of the α/β fold. The catalytic Asp of $PlpD_{20–333}$ is traceable and the dyad is complete, indicating that the molecule was crystallized in an active conformation.

toward Ser60 and could thus correspond to the oxyanion hole required to stabilize the charge that is developed during catalysis. Asp207, whose side chain (atom Oδ2) is 4.1 Å away from the OH moiety of Ser60, is in optimal position to complete the typical lipase active site. Notably, Asp207 is located at the tip of a β-hairpin (orange in Figs. 1d and 3a) suggested as being part of a flexible "cap" region in the eukaryotic phospholipase $cPLA_2$ [17]; this region is also flexible in the structure of the catalytic domain of ExoU, the main PLP secreted by the T3SS of *P. aeruginosa*. Notably, in ExoU, the catalytic Asp could not be traced in the electron density map (Fig. 3c), indicating that this region was not apt for substrate recognition and that the crystallized structure was in the inactive form [16]. The visualization of Asp207 in the structure of $PlpD_{20–333}$ (Fig. 3a) suggests that it was crystallized in the active form. However, despite the fact that many lipases carry a classical Ser-Asp-His catalytic triad [20], the active site of $PlpD_{20–333}$ does not present any His residue in the vicinity of Ser60 and Asp207 that could play the role of the third member of such a triad, and thus, it carries only a Ser-Asp catalytic dyad, as seen in other PLPs such as ExoU, $cPLA_2$ and secreted phospholipases (Fig. 3b; [16,18,20–23]). This arrangement is thus typical of patatin-like proteins [14,20].

Despite the fact that all catalytic elements of $PlpD_{20–333}$ were visible, residues 89–126, indicated as a dotted line in Fig. 1d, were not. Due to the proximity to the active site, this region could represent a "cap" or "lid" that becomes stabilized during the catalytic reaction in order to increase substrate stability within the active site. Interestingly, such a "lid" was also observed in $cPLA_2$ [17], monoacylglycerol lipases [24,25]and a number of other lipid-metabolizing enzymes [26,27] and is thought to play an important role in allowing such enzymes to carry out catalysis at the lipid–water interface [20].

A hydrophobic channel traps lipidic substrates

A remarkable feature of $PlpD_{20–333}$ is the presence of a hydrophobic channel in the vicinity of the active site, which places the catalytic cleft one-third of the way into the core of the protein. Notably, the 23-residue helix α7, which towers over the region, blocks direct access to the active site from any other side of the molecule that is not the channel itself. A comparison of the structure of $PlpD_{20–333}$ and those other bacterial lipases reveals that this "protective helix" feature is unique to PlpD (visible in the close-up images in Fig. 3). This suggests that, in addition to the "lid" described above, helix α7 could play a role in regulating substrate access or determining substrate specificity upon *P. aeruginosa* host cell targeting, by, for example, regulating lipolytic activity until PlpD is in the presence of its target substrate (outside of the bacterial cell; see below).

The elongated shape and hydrophobic characteristics of the channel that harbors the active site, as well as its approximate length of 20 Å, suggest that it has the potential to accommodate a C_{18}–C_{20} acyl chain from a lipidic molecule (Fig. 4a; hydrophobic residues in green). Notably, while we were refining the structure of $PlpD_{20–333}$, we noticed a tube-like electron density feature that did not correspond to any protein regions and that was located within the channel itself (Fig. 4b).

Please cite this article as: P. V. da Mata Madeira, et al., Structural Basis of Lipid Targeting and Destruction by the Type V Secretion System of *Pseudomonas aeruginosa*..., J. Mol. Biol. (2016), http://dx.doi.org/10.1016/j.jmb.2016.03.012

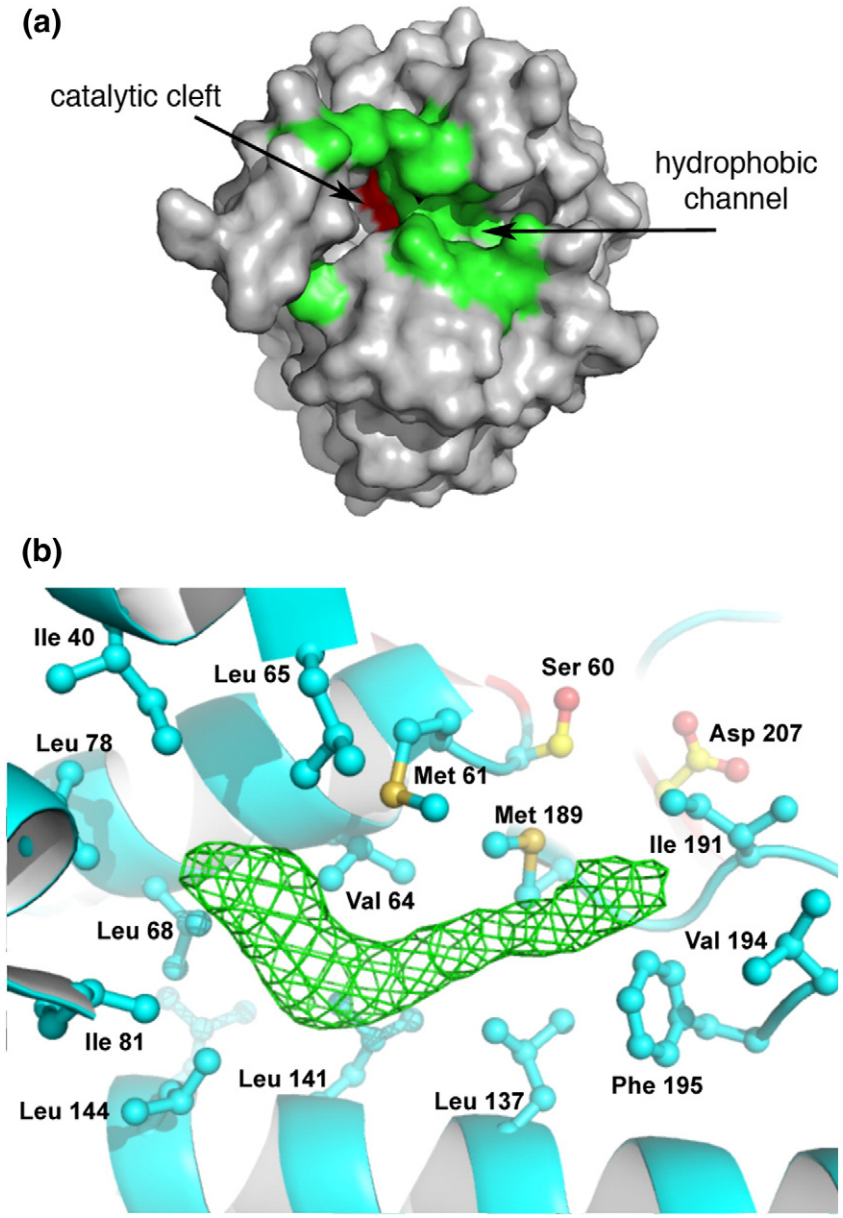

Fig. 4. PlpD$_{20–333}$ recognizes lipids in a specific binding site. (a) Surface diagram of PlpD$_{20–333}$ indicating an elongated channel that leads to the active site cavity. Hydrophobic residues in that region are shown in green, and the active site in red. Helix α7 blocks active site access from any other side of the molecule, limiting access of substrates uniquely through the channel. (b) Tube-like electron density within the hydrophobic channel of PlpD$_{20–333}$. The figure displays the same color code as Fig. 1d. The green mesh indicates a Fo–Fc electron density map contoured at 3.5 α. Apolar residues which surround the electron density are displayed in sticks and colored in cyan, while the Cα atoms of the catalytic dyad are highlighted in yellow.

It is conceivable that this density corresponds to a lipidic substrate (acquired during the purification procedure, potentially from the *E. coli* cytoplasm), or metabolized product, that remained trapped within the hydrophobic channel of PlpD$_{20–333}$. This observation comforts our theory that hydrophobic channel is in fact the binding site for substrates/products; the close proximity of α7 could play a role binding, stabilization or release.

PlpD displays phospholipase A$_1$ activity with broad phosphatidylinositol binding capacity

The lipase function of PlpD$_{20–333}$ had previously been studied in the context of whole cellular extracts [13]. In order to characterize this activity with the purified enzyme, we performed enzymatic tests by incubating PlpD$_{20–333}$ with *p*-nitrophenyl palmitate, a generic fluorogenic lipase substrate, and subsequently measuring the release of *p*-nitrophenol by following the spectrophotometric signal at 410 nm (Fig. 5a). PlpD$_{20–333}$ demonstrated clear lipolytic activity toward the substrate, while the active site mutant PlpD$_{20–333}$Ser60Ala did not. This confirms that PlpD$_{20–333}$ catalyzes the release of *p*-nitrophenol in a manner that is dependent on the catalytic Ser60.

P. aeruginosa ExoU is a well-studied virulence factor that displays a patatin-like domain and shows clear phospholipase A activity [28–31]. In order to determine if PlpD$_{20–333}$ also possessed phospholipase

Please cite this article as: P. V. da Mata Madeira, et al., Structural Basis of Lipid Targeting and Destruction by the Type V Secretion System of *Pseudomonas aeruginosa*..., J. Mol. Biol. (2016), http://dx.doi.org/10.1016/j.jmb.2016.03.012

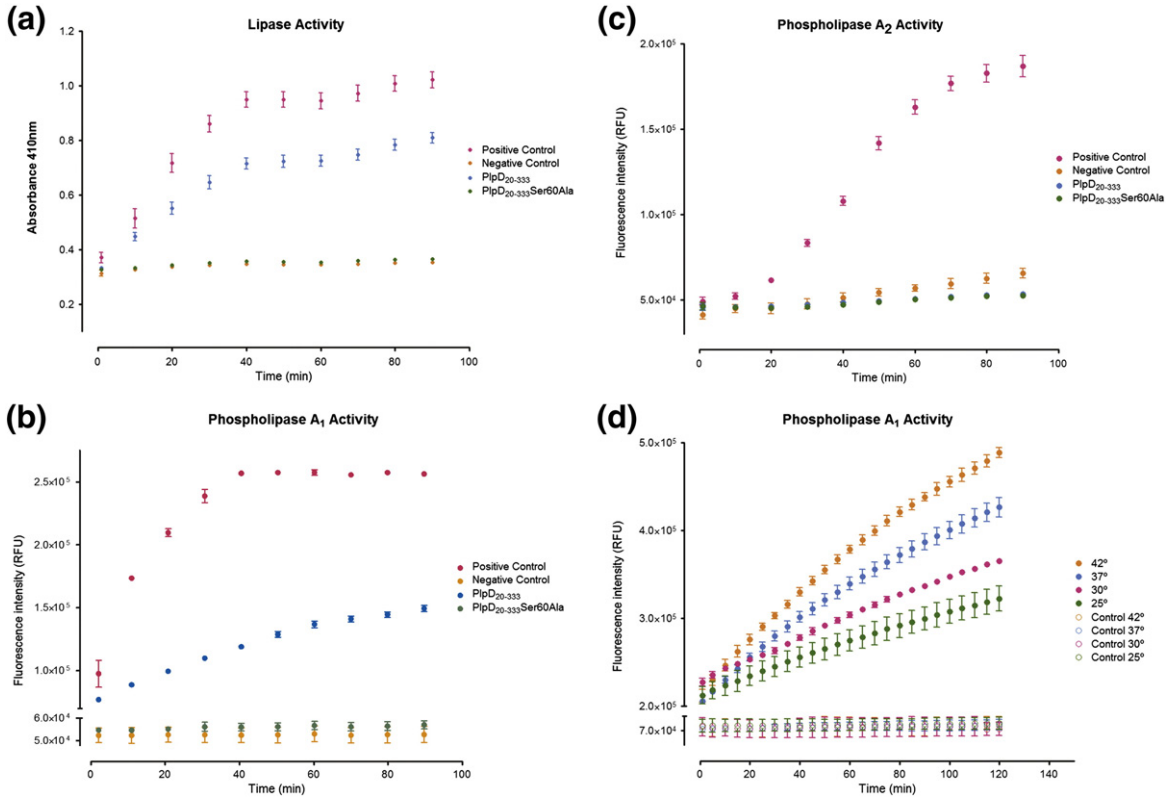

Fig. 5. $PlpD_{20–333}$ shows lipoytic activity. Experiments were performed using phospholipid derivatives with fluorescent moieties: (a) para-nitrophenyl palmitate; (b) PED-A1 [(*N*-((6-(2,4-dinitrophenyl)amino)hexanoyl)-1-(4,4-difluoro-5,7-dimethyl-4-bora-3*a*,4*a*-diaza-*s*-indacene-3-pentanoyl)-2-hexyl-*sn*-glycero-3-phosphoethanolamine)]; (c) BODIPY PC-A2 (1-O-(6-BODIPY® 558/568-aminohexyl)-2-BODIPY® FL C5-*sn*-glycero-3-phosphocholine). A.U., arbitrary units. (d) PLA_1 activity values measured at 25, 30, 37 and 42 °C indicate that $PlpD_{20–333}$ not only retains activity but also is more active at temperatures that are relevant for the infection of eukaryotic targets.

activity, we used fluorescent phospholipid derivatives PED-A1 and BODIPY PC-A2 to test for phospholipase A_1 and A_2 activities, respectively. These results (Fig. 5b and c) clearly showed that $PlpD_{20–333}$ is a phospholipase A_1 but does not carry A_2 activity in these conditions, thus validating $PlpD_{20–333}$'s specificity for the *sn*-1 position of phospholipids and its capacity to generate fatty acids and lysophospholipids from target membranes. It is of note that the phospholipase A_1 activity of $PlpD_{20–333}$ is accentuated at 37 °C and even 42 °C when compared to tests performed at room temperature (25 °C) (Fig. 5d), indicating a robust activity that could be required for participation in infection of eukaryotic cells. To further explore this possibility, we performed protein–lipid overlay assays and demonstrated that the enzyme strongly interacts with phosphatidyl inositols (PI), as well as phosphatidic acid, phosphatidyl serine and phosphatidyl glycerol (Fig. 6a). Due to the participation of many of these lipids in eukaryotic cell signaling processes, this suggests a role for $PlpD_{20–333}$ in virulence toward eukaryotic targets. Furthermore, $PlpD_{20–333}$ displayed a concentration-dependent activity toward lipid bilayers (Fig. 6b). Dye encapsulated within lipid vesicles was readily released upon incubation with $PlpD_{20–333}$, pointing the capacity of this phospholipase to disrupt membrane integrity. Interestingly, the active site variant $PlpD_{20–333}$Ser60Ala also displayed liposome-disruption capacity, albeit with less efficiency than the wild-type enzyme. This points to the possibility that PlpD could employ both its catalytic activity and its membrane-interacting C-terminal region to bind to and disrupt bilayers, possibly in a cooperative fashion.

Discussion

Bacteria have devised a number of secretion systems with the goal of releasing enzymes and toxins toward the surrounding environment. Translocated molecules participate in overcoming host immune systems, penetrating eukaryotic targets or competing with different bacteria in a polymicrobial environment. The T5SS is a simple secretion system that depends on the insertion of a β-barrel protein or domain in the outer membrane, interaction with the

Please cite this article as: P. V. da Mata Madeira, et al., Structural Basis of Lipid Targeting and Destruction by the Type V Secretion System of *Pseudomonas aeruginosa*..., J. Mol. Biol. (2016), http://dx.doi.org/10.1016/j.jmb.2016.03.012

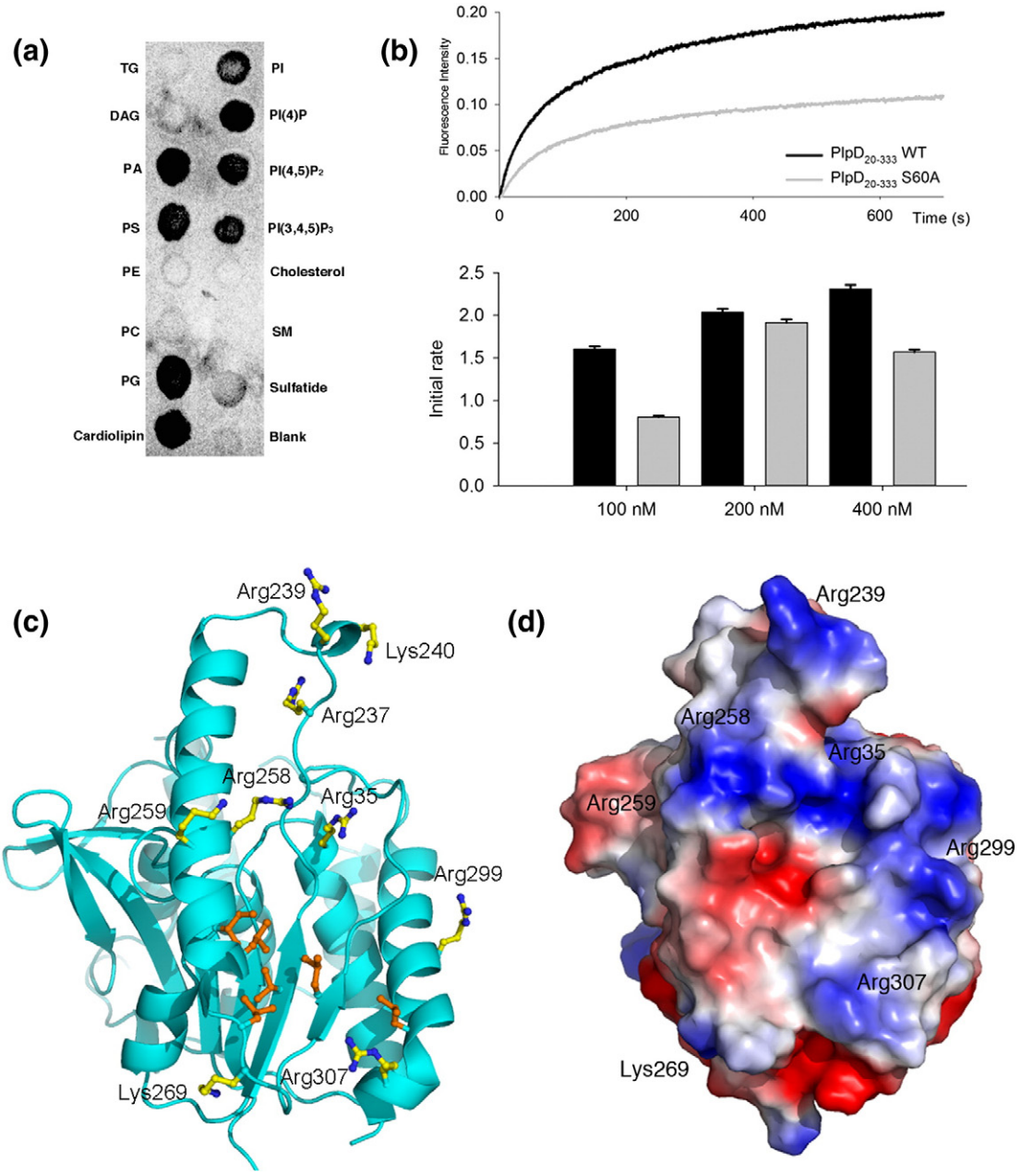

Fig. 6. $PlpD_{20–333}$ displays basic/hydrophobic regions that could bind phospholipids. (a) Protein–lipid overlay of $PlpD_{20–333}$ reveals affinity for lipids involved in eukaryotic cell signaling. TG, triglyceride; DAG, diacylglycerol; PA, phosphatidic acid; PS, phosphatidylserine; PE, phosphatidylethanolamine; PC, phosphatidylcholine; PG, phosphatidylglycerol; CL, cardiolipin; PI, phosphatidyl-inositol; PI (4)P, phosphatidylinositol 4 phosphate; PI (4,5)P2, phosphatidylinositol (4,5) di-phosphate; PI (3,4,5)P3, phosphatidylinositol (3,4,5) triphosphate; chol, cholesterol; SM, sphingomyelin; SGC, 3-sulfogalactosylceramide. Blank = no lipid spotted. (b) Liposome disruption assay showing that $PlpD_{20–333}$ is active against lipid bilayers. Large unilamellar vesicles containing the encapsulated sulforhodamine B dye were incubated with 100 nM $PlpD_{20–333}$ (black) or $PlpD_{20–333}$Ser60Ala (gray) and fluorescence increase was monitored, reflecting dye release upon vesicle disruption (top). Note that the $PlpD_{20–333}$Ser60Ala variant also disrupts liposomes, albeit less efficiently than the wild-type molecule. (Bottom) Initial rates were calculated during the first 50 s of liposome disruption at three protein concentrations. (c) A constellation of basic residues on the C-terminal surface of PlpD forms a positively charged patch that could recognize negatively charged lipids. A hydrophobic central patch could also participate in stabilization of apolar regions. (D) Electrostatic surface potential of $PlpD_{20–333}$. Acidic regions are shown in red, and basic regions in blue.

Please cite this article as: P. V. da Mata Madeira, et al., Structural Basis of Lipid Targeting and Destruction by the Type V Secretion System of *Pseudomonas aeruginosa*..., J. Mol. Biol. (2016), http://dx.doi.org/10.1016/j.jmb.2016.03.012

BamA complex and finally translocation of the effector or domain. Despite the fact that a number of effector domains of T5SS molecules have been characterized, these are mostly elongated, multi-β-strand proteins, and represent systems T5aSS, T5cSS and T5eSS. Here we have structurally and functionally characterized the first effector of the T5dSS, PlpD, and shown that it is a compact, active phospholipase, in clear contrast to previously reported structures of T5SS passengers. It is of note that the only exception for the aforementioned structural rule for T5SS secretion is EstA, a mostly α-helical esterase [32].

$PlpD_{20–333}$ displays an extremely compact fold and clear PLA_1 activity. The overall size of the molecule (30 × 36 × 38 Å) would preclude it from being translocated in its fully folded state, but its compactness could be a particular advantage for partial refolding upon translocation to the exterior of the cell. It is of interest, however, that the full-length sequence of PlpD (Fig. 1a) carries a POTRA domain between the PLP domain and the β-domain. Since POTRA domains are commonly found in TPS (T5bSS) and their function is to aid in targeting the TpsA to the TpsB, the function of PlpD's POTRA domain remains unclear. Moreover, the POTRA in PlpD is strikingly different from a TpsB POTRA, being more comparable to the Omp85/BamA family, suggesting a different function [33]. It is conceivable that prior to translocation, the passenger domain of PlpD could be docked onto the POTRA in order to prevent its premature folding. This could make sense given the fact that $PlpD_{20–333}$ is active even in the absence of any cofactors, indicating that if folded within the bacterial cytoplasm, it could be highly deleterious for the cell. Subsequent to translocation, the exposed (or secreted) form of the passenger domain of PlpD could act on target membranes either as a monomer or as a multimeric species, as shown here, the latter potentially displaying a higher capacity to metabolize target lipids. It is of note that the PlpD residues located at the dimer interface (Leu242, Val248, Leu255, Met256) are highly non-polar and are mostly located within helix α7 (which is unique to $PlpD_{20–333}$ when compared to other phospholipases, as mentioned above), which could point to a potential unique role for this helix.

$PlpD_{20–333}$ carries a Ser-Asp catalytic dyad seen in other patatin-like molecules [14] and displays a flexible "lid" region in the proximity of the active site. It is of interest that VipD, a well-studied lipase from *L. pneumophila*, also displays a lid region in the vicinity of its catalytic cleft. The binding of VipD to its partner molecule Rab5 causes a conformational modification of the lid, opening the active site, providing evidence of an allosteric mechanism that activates the lipase [18]. The presence of a lid region in PlpD, as in other structurally characterized lipases, underlines the possibility that substrate access to the active site or activity itself must be regulated, either viewing lipid target binding or macromolecular partner recognition.

$PlpD_{20–333}$ displays PLA_1 activity toward model substrates, is able to disrupt lipid bilayers and recognizes lipids involved in eukaryotic signaling or apoptosis, such as PIs and phosphatidyl serine, and phosphatidylgycerol, a lipid that is normally found in pulmonary surfactant (Fig. 6a). Another phospholipase of note that is secreted by *P. aeruginosa* is ExoU, whose basic C-terminal membrane-recognition helix-turn-helix region has been shown to play a key role in the enzyme's affinity for PI (4,5)P2 [16,34]. $PlpD_{20–333}$ also displays a highly basic region on its surface, which also involves its C-terminal helix and is in proximity to a hydrophobic patch located in the region of β6 (Fig. 6c and d). It is thus conceivable that this face of the molecule is responsible for recognition of PI analogs, with Lys and Arg residues participating in binding to the negative charges of the phosphate moieties of the lipids, while the hydrophobic patch could play a role in stabilization of the apolar regions.

Interestingly, $PlpD_{20–333}$ does not bind to phosphatidylethanolamine, the principal phospholipid in bacterial membranes. This observation, as well as the increased PLA_1 activity of $PlpD_{20–333}$ at physiological temperatures, argues toward the action of $PlpD_{20–333}$ as an eukaryotic-targeted virulence factor, rather than an enzyme involved in bacterial warfare. Indeed, we were not able to measure any difference in *E. coli* killing capacity between wild type and Δ*plpD P. aeruginosa* strains (not shown). Notably, bacterial pathogens secrete a number of phospholipase-like virulence factors in order to initiate infection. Despite the fact that phospholipases C are the best-studied bacterial phospholipases involved in virulence [14], a number of bacterial outer-membrane or secreted phospholipases are involved in tissue damage in infectious processes [35]. *Helicobacter pylori*, for example, employs PLA_1, PLA_2 and phospholipase C activities to degrade phospholipid components of the mucosal barrier, which is crucial for colonization and bacterial persistence [35,36]. In addition, the lung pathogen *L. pneumophila* expresses at least 15 different phospholipases, one of which was shown to play a role in bacterial replication in the lung and dissemination to the spleen in a guinea pig infection model [37]. ExoU itself, mentioned above, is addressed to the plasma membrane by translocation through the T3SS, where it destroys the bilayer upon recognition of PI $(4,5)P_2$ [16,28–31,34,38]. However, PlpD is the first phospholipase reported to be secreted through the T5SS, reflecting the flexibility that bacteria have developed in order to secrete virulence factors and establish infection. Since genomic searches have identified more than 200 PlpD-like molecules in bacterial genomes [13], it is clear that target membrane destruction is a mechanism of choice in the virulence factor arsenal of bacterial pathogens.

Please cite this article as: P. V. da Mata Madeira, et al., Structural Basis of Lipid Targeting and Destruction by the Type V Secretion System of *Pseudomonas aeruginosa*..., J. Mol. Biol. (2016), http://dx.doi.org/10.1016/j.jmb.2016.03.012

Materialsand Methods

Protein production, purification and crystallization

The *plpD* gene was amplified from *P. aeruginosa* strain PAO1, and the region corresponding to residues 27–220 (primers ALO9: 5′-CATATGCTGGTCCTCTCCGGCGG TGCC-3′ and ALO10: 5′-CTCGAGTTATTAGCGCGC-CACGTCCACCGGGAT-3′) and 20–333 (ALO7: 5′-CATA TGGAGGCCCGGCCGAAGATC-3′ and ALO8: 5′-CTCGAG TTATTACGGCTTGCGCTGGTTCGG-3′) were cloned into pET15b (Novagen) leading to pAL17 and pAL18, respectively. For the Ser60Ala mutant, the mutation was inserted by overlapping PCR using ALO1 (5′-CTATAATAGCCGCCTT TTCA-3′)/RSO37 (5′-CCGCGCCCATGGCGGTGCCGGC-GAT-3′), RSO41 (5′-ATCGGCCGGCACCGCCATGGGC GCGGT-3′)/ALO2 (5′-TTAATGGTGATGGTGATGATG-GAAGTTCTGCCCGAGGTT-3′), the former introducing a 6His-tag at the C-terminus of PlpD. The PCR product was cloned into pCR2.1 (TA-cloning KIT, Invitrogen) under the P_{lac} promote r (pAL5). For the Ser60Ala mutant, the mutation was inserted by overlapping PCR using ALO1 (5′-CTATAA-TAGCCGCCTTTTCA-3′)/RSO37 (5′-CCGCGCCCATG GCGGTGCCGGCGAT-3′), RSO41 (5′-ATCGGCCGG-CACCGCCATGGGCGCGGT-3′)/ALO2 (5′-TTAATGGT-GATGGTGATGATGGAAGTTCTGCCCGAGGTT-3′), the former introducing a 6His-tag at the C-terminus of PlpD. The PCR product was cloned into pCR2.1 (TA-cloning KIT, Invitrogen) under the P_{lac} promote r (pAL5). The PlpD variants were produced in *E. coli* strain C41 (DE3). Bacteria were grown in LB medium containing 100 μg/ml of ampicillin at 37 °C. At mid-exponential growth phase (OD_{600nm} = 0.6–0.8 A.U.), 0.1 mM of IPTG was added to induce expression of the recombinant gene during 16 h at 18 °C. Cells were harvested by centrifugation at 6000*g* for 15 min at 4 °C, and the cell pellet was subsequently resuspended in lysis buffer [50 mM Tris–HCl (pH 7.5), 200 mM NaCl]. A commercial mixture of protease inhibitors (Sigma) was added to the suspension, which was then sonicated, and the cell lysate was centrifuged at 20,000*g* for 40 min at 4 °C. The supernatant was loaded onto a Ni^{2+}-NTA column equilibrated in lysis buffer. After extensive washing with lysis buffer with 75 mM imidazole, $PlpD_{20–333}$ was eluted in lysis buffer containing 200 mM imidazole. The eluate was further purified on a SEC column (Superdex S200 16/60) equilibrated in 50 mM Tris–HCl (pH 7.5), 200 mM NaCl. The $PlpD_{20–333}$Ser60Ala mutant was purified using the same protocol.

Selenomethionine-labeled protein was produced from *E. coli* strain C41 (DE3) transformed with the $PlpD_{20–333}$-expressing plasmid. An isolated colony was grown in 50 ml of LB medium containing 100 μg/ml of ampicillin at 37 °C during 16 h. Cells were then harvested twice by centrifugation at 5000*g* for 15 min. The cell pellet was resuspended in 10 ml of M9 minimal medium supplemented with 200 mg/L thiamine and 100 μg/ml ampicillin. Bacteria were grown in M9 minimal medium at 37 °C until the culture reached OD_{600nm} = 0.4 A.U., at which point 100 mg/L of lysine, phenylalanine, threonine and 50 mg/L of isoleucine, leucine, valine and 60 mg/L of selenomethionine were added. Protein was expressed by addition of 0.1 mM of IPTG and growth continued during 16 h at 18 °C. The purification protocol employed was the same as described for the wild-type protein.

Samples for crystallization were gel filtered in HiLoad 16/600 Superdex 200 column (GE Healthcare). Crystals were obtained by vapor diffusion using the hanging drop method. Native crystals of $PlpD_{20–333}$ were obtained in 1.4 M magnesium sulfate and 0.1 M Bis–Tris propane (pH 7.0), while the selenomethionine protein crystallized in 20% (wt/vol) PEG 3350, 200 mM sodium nitrate and 0.6% *N*-dodecyl-β-D-maltoside.

Data collection, structure determination and refinement

Crystals were flash cooled in the crystallization solution supplemented with 20% glycerol prior to collection of diffraction data collection at 100K on beamline ID29 at the European Synchrotron Radiation Facility (ESRF, Grenoble). Diffraction data from selenomethionine labeled crystals were collected at a single energy (12.663 eV) corresponding to the maximum value of f″, while the native data set was collected at a wavelength of 0.980 Å. Both data sets were processed using the XDS package [39], and the single wavelength anomalous dispersion data set was further improved excluding the high mosaicity images identified with XDSAPP [40]. The sub-structure determination was performed with SHARP/autoSHARP [41,42]. All 16 selenium sites were used for initial phase calculation using PHASER [43] and density modification for map improvement was carried out with PARROT [44]. The partial model was built using Autobuild and then used as input for phase improvement and completion of the sub-structure using PHASER, followed by a new run of PARROT. Subsequent model building was done manually with COOT [45] alternating with cycles of refinement using BUSTER [46] and PHENIX [43]. Non-crystallographic symmetry was applied in the first steps of refinement using the local structure similarity restraints method. The resulting model was used for refinement against the 2.14 Å resolution data set of the native $PlpD_{20–333}$. During the last rounds of refinement, water molecules were added manually. The quality of the final model was evaluated using MolProbity [47]. Data collection, structure solution and refinement statistics are summarized in Table 1.

Dynamic light scattering

Prior to analysis, the sample was centrifuged at 20,000*g* for 10 min. Purified $PlpD_{20–333}$ (20 μl) at 1 mg/ml was used for the measurement of the Z-average particle size and the polydispersity index (%Pd). Experiments were performed at 20 °C with a Zetasizer Nano ZS90 (Malvern, UK) system using a 633 nm He-Ne laser.

Analytical ultracentrifugation

Sedimentation velocity experiments were performed in a Beckman Coulter OptimaTM XL-A (Beckman) ultracentrifuge at 15 °C for 22 h. Samples were rotated at 40,000 rpm (rotor ANTI60), with the absorbance being monitored at 280 nm. Protein concentrations ranged from 0.5 to 3.0 mg/ml, and samples were tested in storage buffer [50 mM Tris–HCl (pH 7.5), 200 mM NaCl]. Consecutive scans were automatically recorded at regular intervals and analyzed with Sedfit [48] using the continuous size

Please cite this article as: P. V. da Mata Madeira, et al., Structural Basis of Lipid Targeting and Destruction by the Type V Secretion System of *Pseudomonas aeruginosa*..., J. Mol. Biol. (2016), http://dx.doi.org/10.1016/j.jmb.2016.03.012

distribution *c*(*s*) analysis method to determine *s20,w* values. Buffer density (1.0088 g/ml) and viscosity (1.139 cp) at 15 °C were calculated by SEDNTERP (http://www.rasmb.bbri.org/). The partial specific volume *v* was computed as 0.73821 ml/g.

Activity assays

The lipase activity of the purified $PlpD_{20–333}$ was tested according to the previously described protocol of Salacha and co-workers [13] by employing para-nitrophenyl-palmitate as a substrate. The substrate solution was prepared by mixing 5 ml of para-nitrophenyl palmitate stock solution (8 mM in propan-2-ol) with 50 ml of a solution containing 50 mM Na_2HPO_4, 50 mM KH_2PO_4, 5 mM sodium deoxycholate, 0.1% (wt/vol) gum arabic and 1 ml Triton X-100. A volume of 200 µl of substrate was added to a 10 µl aliquot of purified $PlpD_{20–333}$ for a final concentration of 7 µM in a 96-well plate. As the positive control, 10 units of commercial phospholipase A_1 from *Thermomyces lanuginosus* was employed (Sigma). As negative controls, both gel filtration buffer and the active site mutant $PlpD_{20–333}$Ser60Ala were tested. The absorbance of para-nitrophenol was recorded in 1-min intervals for 1 h at 30 °C. Each sample was measured in triplicate.

The phospholipase A_1 activity of the purified $PlpD_{20–333}$ was tested employing PED-A1 [(*N*-((6-(2,4-dinitrophenyl)amino)hexanoyl)-1-(4,4-difluoro-5,7-dimethyl-4-bora-3*a*,4*a*-diaza-*s*-indacene-3-pentanoyl)-2-hexyl-*sn*-glycero-3-phosphoethanolamine)] purchased from Life Technologies as a substrate. All reagents were dissolved in buffer consisting of 50 mM Tris (pH 8.0) and 200 mM NaCl. The substrate solution was used at a final concentration of 5 µM. $PlpD_{20–333}$ was added to a final concentration of 7 µM and fluorescence intensity was measured using 485 nm and 530 nm as excitation and emission wavelengths, respectively. Fluorescence points were recorded after an incubation period of 30 min in 1-min intervals during 1 h at 30 °C. As the positive control, 10 units of commercial phospholipase A_1 from *T. lanuginosus* was employed (Sigma). As negative controls, both gel filtration buffer and the active site mutant $PlpD_{20–333}$Ser60Ala were tested. Each sample was measured in triplicate.

$PlpD_{20–333}$ was tested for phospholipase A_2 activity employing Red/Green BODIPY PC-A2 (1-O-(6-BODIPY® 558/568-Aminohexyl)-2-BODIPY® FL C5-Sn-Glycero-3-Phosphocholine) purchased from Life Technologies as a substrate. All reagents were dissolved in buffer containing 50 mM Tris pH 8.0, 200 mM NaCl and 1 mM $CaCl_2$. The substrate solution was used at a final concentration of 7 µM. The experiment was conducted as above. As the positive control, 5 units of commercial phospholipase A_2 from bovine pancreas were employed (Sigma). As negative controls, both gel filtration buffer and the active site mutant $PlpD_{20–333}$Ser60Ala were tested. Each sample was measured in triplicate.

Detection of protein–lipid interactions

Membrane lipid strips (Echelon Biosciences) were blocked in Tris-buffered saline + 3% bovine serum albumin, and incubated overnight with $PlpD_{20–333}$ at 0.5 µg/ml. Detection of bound proteins was performed according to the manufacturer's recommendations.

Liposome disruption assays

Liposome disruption assay was performed as previously described [49] with some modifications. Phosphatidylserine and phosphatidylcholine (Avantipolar) were dissolved in chloroform and mixed to a 18:82 molar ratio. After solvent evaporation, lipids were hydrated and resuspended in 25 mM Tris and 250 mM NaCl (pH 8) containing 50 mM sulforhodamine B (Sigma) prior to extrusion through 0.1-µm filters and removal of the non-encapsulated dye by gel filtration. This led to the production of large unilamellar vesicles of 100 nm (verified by DLS) containing sulforhodamine B at a concentration that precludes fluorescence emission due to self-quenching. Membrane disruption and the subsequent dye dilution in the buffer could thus be monitored as an increase in fluorescence intensity. This was performed on a Jasco FP6500 fluorimeter with excitation set at 565 nm and emission at 586 nm and recorded for 700 s after the addition of the protein. The reaction took place in a 2-ml cuvette containing the liposomes (100 µM) diluted in a pH 7 solution containing 50 mM Na_2HPO_4 and 50 mM KH_2PO_4. Fluorescence intensities were normalized considering the initial intensity before protein addition and the maximal intensity generated by the addition of Triton X100 at the end of each kinetic measurement.

Accession numbers

Coordinates and structure factors of $PlpD_{20–333}$ were deposited in the Protein Data Bank with accession numbers 5FQU (selenomethionine) and 5FYA (native).

Acknowledgments

We wish to thank the European Synchrotron Radiation Facility (ESRF) for access to beamlines. This work was supported by the Laboratoire International Associé BACWALL, by grants 11/52067-6, 2014/11980-9 and 2013/01962-0 from FAPESP (Fundação de Amparo à Pesquisa do Estado de São Paulo), and by the French Cystic Fibrosis Foundation (Vaincre la Mucoviscidose) by way of grants RF20120600685, RF20130500911, and a PhD fellowship to A.L. This work used the platforms of the Grenoble Instruct Centre (ISBG; UMS 3518 CNRS-CEA-UJF-EMBL) with support from FRISBI (ANR-10-INSB-05-02) and GRAL (ANR-10-LABX-49-01) within the Grenoble Partnership for Structural Biology. The authors would like to thank Juliana Fattori for technical assistance with and access to the Analytical Ultracentrifugation platform (LEC) of the LNBio in Campinas, Brazil, and Michel Ragno (iRTSV Grenoble) for assistance with protein purification.

Received 15 December 2015;
Received in revised form 5 March 2016;
Accepted 14 March 2016
Available online xxxx

Keywords:
bacterial secretion;
phospholipase;
crystallography;
lipid affinity;
infection

Abbreviations used:
ATs, autotransporters; TPS, two-partner secretion; PLPs, patatin-like proteins; SEC, size exclusion chromatography; PIs, phosphatidyl inositols.

References

[1] T.R.D. Costa, C. Felisberto-Rodrigues, A. Meir, M.S. Prevost, A. Redzej, M. Trokter, G. Waksman, Secretion systems in gram-negative bacteria: structural and mechanistic insights, Nat. Rev. Microbiol. 13 (2015) 343–359.
[2] K. Sato, M. Naito, H. Yukitake, H. Hirakawa, M. Shoji, M.J. McBride, R.G. Rhodes, K. Nakayama, A protein secretion system linked to bacteroidete gliding motility and pathogenesis, Proc. Natl. Acad. Sci. U. S. A. 107 (2010) 276–281.
[3] T. Izoré, V. Job, A. Dessen, Biogenesis, regulation, and targeting of the type III secretion system, Structures 19 (2011) 603–612.
[4] C.S. Hayes, S.K. Aoki, D.A. Low, Bacterial contact-dependent delivery systems, Annu. Rev. Genet. 44 (2010) 567–573.
[5] L.J. Worrall, E. Lameignere, N.C. Strynadka, Structural overview of the bacterial injectisome, Curr. Opin. Microbiol. 14 (2011) 3–8.
[6] J. Grijpstra, J. Arenas, L. Rutten, J. Tommassen, Autotransporter secretion: varying on a theme, Res. Microbiol. 164 (2013) 562–582.
[7] J.C. Leo, I. Grin, D. Linke, Type V secretion: mechanism(s) of autotransport through the bacterial outer membrane, Philos. Trans. R. Soc. Lond. B 367 (2012) 1088–1101.
[8] S.K. Aoki, R. Pamma, A.D. Hernday, J.E. Bickham, B.A. Braaten, D.A. Low, Contact-dependent inhibition of growth in *Escherichia coli*, Science 309 (2005) 1245–1248.
[9] I.R. Henderson, F. Navarro-Garcia, M. Desvaux, R.C. Fernandez, D. Ala'Aldeen, Type V protein secretion pathway: the autotransporter story, Mol. Biol. Rev. 68 (2004) 692–744.
[10] P. van Ulsen, S. Rahman, W.S.P. Jong, M.H. Daleke-Schermerhorn, J. Luirink, Type V secretion: from biogenesis to biotechnology, Biochim. Biophys. Acta 1843 (2014) 1592–1611.
[11] F. Jacob-Dubuisson, J. Guerin, S. Baelen, B. Clantin, Two-partner secretion: as simple as it sounds? Res. Microbiol. 164 (2013) 583–595.
[12] S. Bleves, V. Viarre, R. Salacha, G.P. Michel, A. Filloux, R. Voulhoux, Protein secretion systems in *Pseudomonas aeruginosa*: a wealth of pathogenic weapons, Int. J. Med. Microbiol. 300 (2010) 534–543.
[13] R. Salacha, F. Kovacic, C. Brochier-Armanet, S. Wilhelm, J. Tommassen, A. Filloux, R. Voulhoux, S. Bleves, The *Pseudomonas aeruginosa* patatin-like protein PlpD is the archetype of a novel type V secretion system, Environ. Microbiol. 12 (2010) 1498–1512.
[14] S. Banerji, A. Flieger, Patatin-like proteins: a new family of lipolytic enzymes present in bacteria? Microbiology 150 (2004) 522–525.
[15] S. Wilhelm, F. Rosneau, H. Kolmar, K.E. Jaeger, Autotransporters with GDSL passenger domains: molecular physiology and biotechnological applications, Chembiochem 12 (2011) 1476–1485.
[16] C. Gendrin, C. Contreras-Martel, S. Bouillot, S. Elsen, D. Lemaire, D.A. Skoufias, P. Huber, I. Attree, A. Dessen, Structural basis of cytotoxicity mediated by the type III secretion toxin ExoU from *Pseudomonas aeruginosa*, PLoS Pathog. 8 (2012), e1002637.
[17] A. Dessen, J. Tang, H. Schmidt, M. Stahl, J.D. Clark, J. Seehra, W.S. Somers, Crystal structure of human cytosolic phospholipase A_2 reveals a novel topology and catalytic mechanism, Cell 97 (1999) 349–360.
[18] M. Lucas, A.H. Gaspar, C. Pallara, A.L. Rojas, J. Fernandez-Recio, M.P. Machner, A. Hierro, Structural basis for the recruitment and activation of the *Legionella* phospholipase VipD by the host GTPase Rab5, Proc. Natl. Acad. Sci. U. S. A. 111 (2014) E3514–E3523.
[19] H.J. Hirschberg, J.W. Simons, N. Dekker, M.R. Egmond, Cloning, expression, purification and characterization of patatin, a novel phospholipase A, Eur. J. Biochem. 268 (2001) 5037–5044.
[20] E.A. Dennis, J. Cao, Y.H. Hsu, V. Magrioti, G. Kokotos, Phospholipase A2 enzymes: physical structure, biological function, disease implication, chemical inhibition, and therapeutic intervention, Chem. Rev. 111 (2011) 6130–6185.
[21] A.S. Halavaty, D. Borek, G.H. Tyson, J.L. Veesenmeyer, L. Shuvalova, G. Minasov, Z. Otwinowski, A.R. Hauser, W.F. Anderson, Structure of the type III secretion effector protein ExoU in complex with its chaperone SpcU, PLoS One 7 (2012), e49388.
[22] R.H. Schaloske, E.A. Dennis, The phospholipase A2 superfamily and its group numbering system, Biochim. Biophys. Acta 1761 (2006) 1246–1259.
[23] B. Ku, K.H. Lee, W.S. Park, C.S. Yang, J. Ge, S.G. Lee, S.S. Cha, F. Shao, W.D. Heo, J. Jung, B.H. Oh, VipD of *Legionella pneumophila* targets activated Rab5 and Rab22 to interfere with endosomal trafficking in macrophages, PLoS Pathog. 8 (2012), e1003082.
[24] S. Rengachari, P. Aschauer, M. Schittmayer, N. Mayer, K. Gruber, R. Breinbauer, R. Birner-Gruenberger, I. Dreveny, M. Oberer, Conformational plasticity and ligand binding of bacterial monoacylglycerol lipase, J. Biol. Chem. 288 (2013) 31093–31104.
[25] C. Schalk-Hihi, C. Schubert, R. Alexander, S. Bayoumy, J.C. Clemente, I. Deckman, R.L. DesJarlais, K.C. Dzordzorme, C.M. Flores, B. Grasberger, J.K. Kranz, F. Lewandowski, L. Liu, H. Ma, D. Maguire, M.J. Macielag, M.E. McDonnell, T. Mezzasalma Haarlander, R. Miller, C. Milligan, C. Reynolds, L.C. Kuo, Crystal structure of a soluble form of human monoglyceride lipase in complex with an inhibitor at 1.35 Å resolution, Protein Sci. 20 (2011) 670–683.
[26] L. Liu, C. Gao, D. Lan, Y. Yang, Molecular basis for substrate selectivity of a mono- and diacylglycerol lipase from *Malassezia globosa*, Biochem. Biophys. Res. Commun. 424 (2012) 285–289.
[27] T. Xu, L. Liu, S. Hou, J. Xu, B. Yang, Y. Wang, J. Liu, Crystal structure of a mono- and diacylglycerol lipase from *Malassezia globosa* reveals a novel lid conformation and insights into the substrate specificity, J. Struct. Biol. 178 (2012) 363–369.
[28] H. Sato, D.W. Frank, ExoU is a potent intracellular phospholipase, Mol. Microbiol. 53 (2004) 1279–1290.
[29] H. Sato, D.W. Frank, Intoxication of host cells by the T3SS phospholipase ExoU: PI(4,5)P2-associated, cytoskeletal

Please cite this article as: P. V. da Mata Madeira, et al., Structural Basis of Lipid Targeting and Destruction by the Type V Secretion System of *Pseudomonas aeruginosa*..., J. Mol. Biol. (2016), http://dx.doi.org/10.1016/j.jmb.2016.03.012

collapse and late phase membrane blebbing, PLoS One 9 (2014), e103127.
[30] H. Sato, D.W. Frank, C.J. Hillard, J.B. Feix, R.R. Pankhaniya, K. Moriyama, V. Finck-Barbançon, A. Buchaklian, M. Lei, R.M. Long, J. Wiener-Kronish, T. Sawa, The mechanism of action of the *Pseudomonas aeruginosa*-encoded type III cytotoxin, ExoU, EMBO J. 22 (2003) 2959–2969.
[31] R.M. Phillips, D.A. Six, E.A. Dennis, P. Ghosh, In vivo phospholipase activity of the *Pseudomonas aeruginosa* cytotoxin ExoU and protection of mammalian cells with phospholipase A2 inhibitors, J. Biol. Chem. 278 (2003) 41326–41332.
[32] B. van den Berg, Crystal structure of a full-length autotransporter, 2010 396 (2010) 627–633.
[33] E. Heinz, T. Lithgow, A comprehensive analysis of the Omp85/TpsB protein superfamily structural diversity, taxonomic occurrence, and evolution, Front. Microbiol. 5 (2014) 370.
[34] G.H. Tyson, A.S. Halavaty, H. Kim, B. Geissler, M. Agard, K.J. Satchell, W. Cho, W.F. Anderson, A.R. Hauser, A novel phosphatidylinositol 4,5-bisphosphate binding domain mediates plasma membrane localization of ExoU and other patatin-like phospholipases, J. Biol. Chem. 290 (2015) 2919–2937.
[35] T.S. Istivan, P.J. Coloe, Phospholipase A in Gram-negative bacteria and its role in pathogenesis, Microbiology 152 (2006) 1263–1274.
[36] J. Xerry, R.J. Owen, Conservation and microdiversity of phospholipase A (pldA) gene of *Helicobacter pylori* infecting dyspeptics from different countries, FEMS Immunol. Med. Microbiol. 32 (2001) 17–25.
[37] E. Schunder, P. Adam, F. Higa, K.A. Remer, U. Lorenz, J. Bender, T. Schulz, A. Flieger, M. Steinert, K. Heuner, Phospholipase PlaB is a new virulence factor of *Legionella pneumophila*, Int. J. Med. Microbiol. 300 (2010) 313–323.
[38] J.L. Veesenmeyer, H. Howell, A.S. Halavaty, S. Ahrens, W.F. Anderson, A.R. Hauser, Role of the membrane localization domain of the *Pseudomonas aeruginosa* effector protein ExoU in cytotoxicity, Infect. Immun. 78 (2010) 3346–3357.
[39] W. Kabsch, XDS, Acta Crystallogr. Sect. D 66 (2010) 125–132.
[40] M. Krug, M.S. Weiss, U. Mueller, U. Heinemann, XDSAPP: a graphical user interface for the convenient processing of diffraction data using XDS, J. Appl. Crystallogr. 45 (2012) 568–572.
[41] E. de la Fortelle, G. Bricogne, Maximum-likelihood heavy-atom parameter refinement for multiple isomorphous replacement and multiwavelength anomalous diffraction methods, Methods Enzymol. 276 (1997) 472–494.
[42] C. Vonrhein, E. Blanc, P. Roversi, G. Bricogne, Automated structure solution with autoSHARP, Methods Mol. Biol. 364 (2007) 215–230.
[43] P.D. Adams, P.V. Afonine, G. Bunkóczi, V.B. Chen, I.W. Davis, N. Echols, J.J. Headd, L.W. Hung, G.J. Kapral, R.W. Grosse-Kunstleve, A.J. McCoy, N.W. Moriarty, R.D. Oeffner, R.J. Read, D.C. Richardson, J.S. Richardson, T.C. Terwilliger, P.H. Zwart, PHENIX: a comprehensive python-based system for macromolecular structure solution, Acta Crystallogr. Sect. D 66 (2010) 213–221.
[44] K. Cowtan, Recent developments in classical density modification, Acta Crystallogr. Sect. D 66 (2010) 470–478.
[45] P. Emsley, K. Cowtan, Coot: model-building tools for molecular graphics, Acta Crystallogr. Sect. D 60 (2004) 2126–2132.
[46] E. Blanc, P. Roversi, C. Vonrhein, C. Flensburg, S.M. Lea, G. Bricogne, Refinement of severely incomplete structures with maximum likelihood in BUSTER-TNT, Acta Crystallogr. Sect. D 60 (2004) 2210–2221.
[47] I.W. Davis, A. Leaver-Fay, V.B. Chen, J.N. Block, G.J. Kapral, X. Wang, L.W. Murray, W.B. Arendall, J. Snoeyink, J.S. Richardson, D.C. Richardson, Molprobity: all-atom contacts and structure validation for proteins and nucleic acids, Nucleic Acids Res. 35 (2007) W375–W383.
[48] P. Schuck, Size-distribution analysis of macromolecules by sedimentation velocity ultracentrifugation and lamm equation modeling, Biophys. J. 78 (2000) 1609–1616.
[49] E. Faudry, G. Vernier, E. Neumann, V. Forge, I. Attree, Synergistic pore formation by type III toxin translocators of *Pseudomonas aeruginosa*, Biochemistry 45 (2006) 8117–8123.

Please cite this article as: P. V. da Mata Madeira, et al., Structural Basis of Lipid Targeting and Destruction by the Type V Secretion System of *Pseudomonas aeruginosa*..., J. Mol. Biol. (2016), http://dx.doi.org/10.1016/j.jmb.2016.03.012

12

IFNγ extends the immune functions of Guanylate Binding Proteins to inflammasome-independent antibacterial activities during *Francisella novocida* infection

Wallet P, Benaoudia S, Mosnier A, Lagrange B, Martin A, Lindgren H, Golovliov I, Michal F, Basso P, Djebali S, Provost A, Allatif O, Meunier E, Broz P, Yamamoto M, Py B.F, Faudry E, Sjostedt A, Henry T (Plos Pathogens (2017))

Guanylate binding proteins (GBPs) are interferon-inducible proteins involved in the cell-intrinsic immunity against numerous intracellular pathogens. The molecular mechanisms underlying the potent antibacterial activity of GBPs are still unclear. GBPs have been functionally linked to the NLRP3, the AIM2 and the caspase-11 inflammasomes. Two opposing models are currently proposed to explain the GBPs-inflammasome link: i) GBPs would target intracellular bacteria or bacteria-containing vacuoles to increase cytosolic PAMPs release ii) GBPs would directly facilitate inflammasome complex assembly. Using *Francisella novicida* infection, we investigated the functional interactions between GBPs and the inflammasome. GBPs, induced in a type I IFN-dependent manner, are required for the *F. novicida*-mediated AIM2-inflammasome pathway. Here, we demonstrate that GBPs action is not restricted to the AIM2 inflammasome, but controls in a hierarchical manner the activation of different inflammasomes complexes and apoptotic caspases. IFN-γ induces a quantitative switch in GBPs levels and redirects pyroptotic and apoptotic pathways under the control of GBPs. Furthermore, upon IFN-γ priming, *F. novicida*-infected macrophages restrict cytosolic bacterial replication in a GBP-dependent and inflammasome-independent manner. Finally, in a mouse model of tularemia, we demonstrate that the inflammasome and the GBPs are two key immune pathways functioning largely independently to control F. novicida infection. Altogether, our results indicate that GBPs are the master effectors of IFN-γ-mediated responses

against *F. novicida* to control antibacterial immune responses in inflammasome-dependent and independent manners.

In this work, I set experiment of time-lapse microscopy to demonstrates the BMDMs cell death triggered by *F. novicida* (Figure S3 and Movies S1-S2)[1].

[1] https://doi.org/10.1371/journal.ppat.1006630

PLOS | PATHOGENS

RESEARCH ARTICLE

IFN-γ extends the immune functions of Guanylate Binding Proteins to inflammasome-independent antibacterial activities during *Francisella novicida* infection

Pierre Wallet[1‡], Sacha Benaoudia[1‡], Amandine Mosnier[1], Brice Lagrange[1], Amandine Martin[1], Helena Lindgren[2], Igor Golovliov[2], Fanny Michal[1], Pauline Basso[3], Sophia Djebali[1], Angelina Provost[1], Omran Allatif[1], Etienne Meunier[4], Petr Broz[5], Masahiro Yamamoto[6], Bénédicte F. Py[1], Eric Faudry[3], Anders Sjöstedt[2], Thomas Henry[1]*

1 CIRI, Centre International de Recherche en Infectiologie, Inserm, U1111, Université Claude Bernard Lyon 1, CNRS, UMR5308, École Normale Supérieure de Lyon, Univ Lyon, Lyon, France, **2** Laboratory for Molecular Infection Medicine Sweden and Department of Clinical Microbiology, Umeå University, Umeå, Sweden, **3** University of Grenoble Alpes, CNRS, ERL5261, CEA, BIG-BCI, Inserm, U1036, Grenoble, France, **4** Institut de Pharmacologie et de Biologie Structurale (IPBS), CNRS, Université Paul Sabatier (UPS), Toulouse, France, **5** Focal Area Infection Biology, Biozentrum, University of Basel, Basel, Switzerland, **6** Department of Immunoparasitology, Research Institute for Microbial Diseases, Osaka University, Osaka, Japan

‡ PW and SB share first authorship on this work.
* thomas.henry@inserm.fr

Citation: Wallet P, Benaoudia S, Mosnier A, Lagrange B, Martin A, Lindgren H, et al. (2017) IFN-γ extends the immune functions of Guanylate Binding Proteins to inflammasome-independent antibacterial activities during *Francisella novicida* infection. PLoS Pathog 13(10): e1006630. https://doi.org/10.1371/journal.ppat.1006630

Editor: Denise M. Monack, Stanford University School of Medicine, UNITED STATES

Received: March 24, 2017

Accepted: September 6, 2017

Published: October 2, 2017

Data Availability Statement: All relevant data are within the paper and its Supporting Information files.

Funding: This work was supported by an European Research Council (ERC: https://erc.europa.eu/) starting grant 311542 to TH and the Swedish Medical Research Council (http://www.vr.se/inenglish.4.12fff4451215cbd83e4800015152.html) (K2013-8621 and 2013-4581) to AS. The funders had no role in study design, data collection and

Abstract

Guanylate binding proteins (GBPs) are interferon-inducible proteins involved in the cell-intrinsic immunity against numerous intracellular pathogens. The molecular mechanisms underlying the potent antibacterial activity of GBPs are still unclear. GBPs have been functionally linked to the NLRP3, the AIM2 and the caspase-11 inflammasomes. Two opposing models are currently proposed to explain the GBPs-inflammasome link: i) GBPs would target intracellular bacteria or bacteria-containing vacuoles to increase cytosolic PAMPs release ii) GBPs would directly facilitate inflammasome complex assembly. Using *Francisella novicida* infection, we investigated the functional interactions between GBPs and the inflammasome. GBPs, induced in a type I IFN-dependent manner, are required for the *F. novicida*-mediated AIM2-inflammasome pathway. Here, we demonstrate that GBPs action is not restricted to the AIM2 inflammasome, but controls in a hierarchical manner the activation of different inflammasomes complexes and apoptotic caspases. IFN-γ induces a quantitative switch in GBPs levels and redirects pyroptotic and apoptotic pathways under the control of GBPs. Furthermore, upon IFN-γ priming, *F. novicida*-infected macrophages restrict cytosolic bacterial replication in a GBP-dependent and inflammasome-independent manner. Finally, in a mouse model of tularemia, we demonstrate that the inflammasome and the GBPs are two key immune pathways functioning largely independently to control *F. novicida* infection. Altogether, our results indicate that GBPs are the master effectors of IFN-γ-mediated responses against *F. novicida* to control antibacterial immune responses in inflammasome-dependent and independent manners.

analysis, decision to publish, or preparation of the manuscript.

Competing interests: The authors have declared that no competing interests exist.

Author summary

The cell-intrinsic immunity is defined as the mechanisms allowing a host cell infected by an intracellular pathogen to mount effective immune mechanisms to detect and eliminate pathogens without any help from other immune cells. In infected macrophages, the Guanylate Binding Proteins (GBPs) are immune proteins, induced at low levels in a cell autonomous manner by endogenous type I IFN or at high levels following IFN-γ production by innate and adaptive lymphocytes. The antibacterial activity of GBPs has been recently tightly linked to the inflammasomes. Inflammasomes are innate immune complexes leading to inflammatory caspases activation and death of the infected cell. *Francisella novicida*, a bacterium replicating in the macrophage cytosol, is closely related to *F. tularensis*, the agent of tularemia and is used as a model to study cytosolic immunity. GBPs contribute to *F. novicida* lysis within the host cytosol leading to DNA release and AIM2 inflammasome activation. In addition to their regulation of the AIM2 inflammasome, we identified that GBPs also control several other pyroptotic and apoptotic pathways activated in a hierarchical manner. Furthermore, we demonstrate that IFN-γ priming extends GBPs antimicrobial responses from the inflammasome-dependent control of cell death to an inflammasome-independent control of cytosolic bacterial replication. Our results, validated in a mouse model of tularemia, thus segregate the antimicrobial activities of inflammasomes and GBPs as well as highlight GBPs as the master effectors of IFN-γ-mediated cytosolic immunity.

Introduction

Intracellular pathogens have evolved sophisticated mechanisms to invade and replicate within host cells. In parallel, multi-cellular organisms have evolved multiple mechanisms allowing a host cell to detect microbial infection and to mount an effective antimicrobial response. Key actors of the host cell intrinsic immunity include the Guanylate Binding Proteins (GBPs)[1–3]. GBPs constitute a family of interferon-inducible dynamin-like GTPases [4,5]. 11 GBPs are encoded by the murine genome in two clusters on chromosomes 3 and 5 [6,7]. The antimicrobial functions of GBPs are still poorly understood. One key mechanism of GBPs' potent antimicrobial activity resides in their ability to target and disrupt pathogen-containing vacuoles. Indeed, chromosome 3-encoded GBPs (Gbp^{chr3}) are required to disrupt *Toxoplasma gondii* parasitophorous membrane and to control the parasite replication in mice [8,9]. Similarly, Gbp^{chr3} are required to lyse the *Salmonella*-containing vacuole leading to the release of this bacterium into the host cytosol and to the subsequent activation of the caspase-11 non-canonical inflammasome [10].

Cooperation between GBPs and the NLRP3, the AIM2 and the non-canonical caspase-11 inflammasome complexes have emerged recently as central to the innate immune responses against intracellular bacteria [10–14]. However, the functional molecular links between GBPs and the inflammasomes remain unclear. GBP5 was described to bind NLRP3 and directly promote NLRP3-dependent inflammasome assembly [14]. This finding was later challenged by several groups [10,15]. Chromosome 3-encoded GBPs are key host factors to trigger the non-canonical caspase-11 inflammasome in macrophages infected with various Gram-negative bacteria [16] including *Salmonella typhimurium* [10], *Legionella pneumophila* [12] and *Chlamydia trachomatis* [11]. Three different models have been proposed to explain the role of GBPs in promoting non-canonical inflammasome activation. Similarly to what have been

demonstrated for IFN-γ-inducible Immunity-Related GTPases (IRG) in their antimicrobial role against *Toxoplasma gondii* [17], GBPs might disrupt the *Salmonella*-containing vacuole leading to the release of this bacterium and its associated LPS into the host cytosol [10]. Alternatively, GBPs might orchestrate the recruitment of IRGB10 onto cytosolic bacteria to liberate LPS for sensing by caspase-11 [16]. Finally, as GBPs can promote caspase-11 activation without any detectable recruitment around *Chlamydia muridarum* inclusions and upon *Legionella* LPS transfection into the host cytosol, Coers and colleagues suggested that GBPs might directly facilitate caspase-11 activation [11,12].

The link between GBPs and the AIM2 inflammasome is less controversial and has been mostly studied by our group and others in macrophages infected with *Francisella novicida* [13,15,18]. *F. novicida* is a close relative of *F. tularensis*, the agent of tularemia. The virulence of *Francisella* strains is linked to their ability to rapidly lyse the phagosome, escape into the host cytosol [19,20] and replicate within this compartment. This process is dependent on a cluster of genes in the *Francisella*-pathogenicity island [21,22], which encodes an atypical type VI secretion system [23]. GBP2 and GBP5 are recruited onto cytosolic *F. novicida* and are required to lyse bacteria and release the bacterial genomic DNA into the host cytosol. DNA in the host cytosol is then recognized by AIM2 [13,15,24–26]. Recently, GBPs were demonstrated to be required for IRGB10 recruitment onto cytosolic *F. novicida* to mediate cytosolic bacterial killing, DNA release and AIM2 inflammasome activation [16].

Chromosome 3-encoded GBPs and the AIM2 inflammasome are both equally required to resist *F. novicida* infection *in vivo* [13,15]. Yet, whether GBPs might have anti-*F. novicida* functions dependent on other inflammasomes or inflammasome-independent antibacterial responses remain unclear [10,16]. In this work, we demonstrate that GBPs control *F. novicida*-mediated host cell death in a hierarchical manner implicating at least 3 different canonical and non-canonical inflammasome complexes as well as apoptotic caspases 8, 9 and 3. Furthermore, we demonstrate that upon IFN-γ treatment, GBPs control *F. novicida* replication independently of the canonical and non-canonical inflammasome pathways and independently of macrophage cell death. IFN-γ-, GBPs-mediated inhibition of intracellular bacterial growth was also effective during *F. tularensis* spp. *holarctica* Live Vaccine Strain infection, while IFN-γ was inefficient to block the replication of the highly virulent *F. tularensis* SCHU S4 strain. Finally, we demonstrate *in vivo* that IFN-γ-mediated host protection against *F. novicida* is largely GBPs-dependent and inflammasome-independent. Our work thus positions the GBPs as the master effectors of the IFN-γ-mediated anti-*F. novicida* responses.

Results

Gbp^{chr3} and the inflammasome control in vivo host resistance to *F. novicida* in a non-redundant manner

We and others have previously reported that *Gbp*^{chr3}-deficient and inflammasome-deficient mice (*Aim2*$^{-/-}$, *Asc*$^{-/-}$ and *Casp1/Casp11*$^{-/-}$ mice) were highly susceptible to *F. novicida* infection [13,15,24,25,27,28]. *In vitro* studies have demonstrated that GBPs act upstream of the AIM2 inflammasome [13,15,16] suggesting that the *Gbp*^{chr3} deficiency should phenocopy deficiencies in the AIM2 inflammasome. In a survival experiment, *Gbp*^{chr3}-KO and *Asc*$^{-/-}$ were almost as susceptible to *F. novicida* infection (Fig 1A) although we consistently noticed that *Gbp*^{chr3}KO mice died slightly faster than *Asc*$^{-/-}$ mice. Similarly, *Gbp*^{chr3}-KO and *Asc*$^{-/-}$ mice displayed very high bacterial burden both in the spleen and in the liver at day 2 post-infection (PI) with an average of 40-fold more bacteria than WT mice (Fig 1B). Surprisingly, at 48 h PI, IFN-γ level in the serum of *Gbp*^{chr3}-deficient mice reached WT levels while in agreement with previous work [28], IFN-γ level in the serum of *Asc*$^{-/-}$ mice was strongly decreased (Fig 1C).

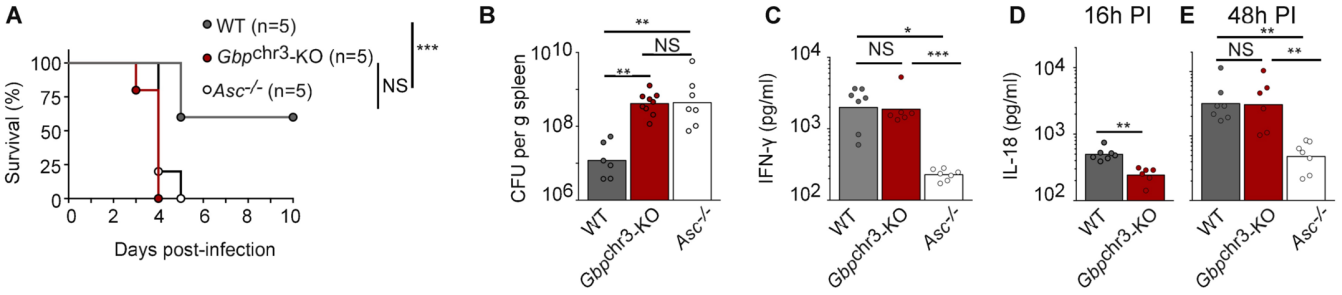

Fig 1. *Gbp*^{chr3} and the inflammasome control the *in vivo* host resistance to *F. novicida* in a divergent manner. Mice of the indicated genotypes were subcutaneously (sc) injected with 5×10^3 (A-B) or 4×10^5 (C-E) *F. novicida*. (A) Survival was monitored twice a day for 10 days. (B) Bacterial burden in the spleen, (C) IFN-γ or (D, E) IL-18 levels in the serum were quantified at 16 h (D) and 48 h post-inoculation (C, E). IFN-γ concentration at 16 h post-inoculation was under the limit of detection. Each symbol represents the value of an individual mouse; the bars indicate the geometric mean. (A-E) one experiment representative of one (D), to at least three (A-C, E) independent experiments is shown. Mantel Cox log-rank test (A), Kruskal-Wallis analysis with Dunn's correction for multiple comparisons (B, C, E) and Mann-Whitney test (D) were performed.

https://doi.org/10.1371/journal.ppat.1006630.g001

We and others have previously reported that early (16 h PI [13], 24 h PI [16]) IL-18 production *in vivo* is GBPs-dependent, a finding which we reproduced here (Fig 1D). However, at later time points (48 h PI), IL-18 levels were similar in *Gbp*^{chr3}-KO and in WT mice (Fig 1E). As expected, IL-18 levels in infected *Asc*$^{-/-}$ mice were not statistically different from the levels observed in uninfected mice. These results indicated that inflammasome activation was only delayed *in vivo* in *Gbp*^{chr3}-deficient mice. The increase in IL-18 levels observed over 48h in infected *Gbp*^{chr3}-KO mice likely explained the high IFN-γ serum level observed in these mice. The high susceptibility of *Gbp*^{chr3}-KO mice to *F. novicida* infection despite high levels of circulating IFN-γ is remarkable since IFN-γ is considered to be one of the most important cytokine to fight *Francisella* infection [29–31]. This conundrum led us to hypothesize that GBPs might be the main IFN-γ effector in *F. novicida*-infected mice. Furthermore, this result indicates that while the overall susceptibility of *Gbp*^{chr3}-deficient mice and *Asc*$^{-/-}$ mice to *F. novicida* infection are similar, the *in vivo* antibacterial mechanisms of GBPs are, at least partially, independent of the inflammasome.

IFN-γ priming induces a quantitative shift in GBPs levels

The action of GBPs against *F. novicida* has been mostly studied in unprimed macrophages [13,15,16]. Under these conditions, GBPs induction relies on the endogenous recognition of nucleic acids by the cGAS pathway, secretion of type I IFN, signaling through the type I IFN receptor (IFNAR1) and activation of the IRF-1 pathway [15,24,32]. Importantly, there was a drastic quantitative shift in GBP2 and GBP5 transcripts levels upon priming with IFN-γ compared with *F. novicida*-mediated endogenous induction or to induction following IFN-β priming (S1A Fig). Indeed while GBP2 transcript levels increased by a factor of 15 upon *F. novicida* infection, IFN-γ priming of infected macrophages, led to a 325-fold increase in GBP2 transcript levels relative to its level in uninfected macrophages. As previously reported, this very strong induction likely results from synergistic NF-κB and IFN signaling [14,33,34]. Indeed, we obtained comparable levels of GBP2 induction when BMDMs were primed with both IFN-γ and Pam_3CSK_4, a TLR2 agonist (S1A Fig). ProIL-1β transcript levels were not impacted by IFN-γ priming (S1C Fig) indicating that this synergy was specific for GBPs induction. Similar results were obtained while investigating GBP5 transcript levels (S1B Fig) or while monitoring GBP2 and GBP5 protein levels (S1D Fig). This quantitative shift in GBPs levels upon IFN-γ treatment led us to investigate the impact of IFN-γ on the *F. novicida*-mediated cell death.

GBPs control *F. novicida*-mediated cell death in an AIM2 inflammasome-dependent and -independent manner

In *F. novicida*-infected bone marrow-derived macrophages (BMDMs), the only reported cell death pathways are dependent on the AIM2/ASC complex [24,25,27,35]. By monitoring, in real time, propidium iodide influx and fluorescence over 24 h in unprimed macrophages deficient for various inflammasome components, we observed substantial differences in the kinetics of propidium iodide between various knock-out macrophages suggesting that several cell death pathways were engaged following *F. novicida* infection (Fig 2A). These differences in the kinetics of propidium iodide incorporation/ fluorescence were demonstrated to be statistically significant by calculating the area under the curve corresponding to each kinetics (Fig 2B). As previously described [13,15,24,25], in the absence of IFN-γ priming, *F. novicida*-infected BMDMs died in an AIM2-dependent manner. Indeed, at MOI 10, propidium iodide incorporation/fluorescence sharply increased around 6 h post-infection in WT macrophages while *Aim2*$^{-/-}$ BMDMs presented cell death kinetics delayed by more than 7 h compared with that of WT macrophages. Interestingly, incorporation/fluorescence increase of propidium iodide was significantly further delayed in *Gbp*^{chr3}-KO BMDMs compared to *Aim2*$^{-/-}$ BMDMs suggesting that GBPs control both AIM2-dependent and -independent cell death pathways. Accordingly, by monitoring macrophage cell death in real time and in single cells using time-lapse microscopy (Fig 2E and 2F; S3 Fig), we clearly observed that the number of propidium iodide-positive cells increased significantly later in *Gbp*^{chr3}-KO BMDMs compared to *Aim2*$^{-/-}$ BMDMs. This difference in cell death kinetics was exacerbated in the presence of IFN-γ priming (Fig 2C, 2D and 2F). Finally, to exclude any bias associated with propidium iodide incorporation, we used a luminescent cell viability assay based on the quantitation of ATP, a signature of metabolically active cells (CellTiter-Glo; Fig 2G). This assay confirmed that *Gbp*^{chr3}-KO BMDMs survived longer than *Aim2*$^{-/-}$ BMDMs upon *F. novicida* infection. Altogether, our data strongly suggest that GBPs control both AIM2-dependent and -independent cell death/survival pathways.

F. novicida infection triggers GBPs-dependent AIM2-, NLRP3-dependent canonical and non-canonical caspase-11 inflammasomes

In *F. novicida*-infected murine macrophages, the only inflammasomes described so far are dependent on AIM2, while our results (Fig 2A–2G) clearly demonstrate that *F. novicida*-mediated cell death can proceed independently of AIM2. We thus used *Aim2*$^{-/-}$ macrophages to unravel other cell death pathways controlled by GBPs. Using siRNA, we first knock-downed various inflammasome NLRs (S4A Fig) and observed a contribution of NLRP3 in *F. novicida*-mediated cell death (S4B Fig). To confirm this result, we generated *Aim2*$^{-/-}$/*Nlrp3*$^{-/-}$ mice and compared their BMDMs response with that of BMDMs single knock-out for *Aim2* (Fig 3A and 3B). *Aim2*$^{-/-}$/*Nlrp3*$^{-/-}$ BMDMs displayed a kinetics of propidium iodide incorporation/fluorescence slower than that of *Aim2*$^{-/-}$ BMDMs, indicating that in the absence of AIM2, NLRP3 controls *F. novicida*-mediated cell death. *Aim2*$^{-/-}$/*Nlrp3*$^{-/-}$ BMDMs phenocopied *Asc*$^{-/-}$ BMDMs indicating that activation of the canonical inflammasome pathways in *F. novicida*-infected BMDMs is exclusively dependent on AIM2 and NLRP3.

To assess whether the non-canonical caspase-11 inflammasome could be involved in the AIM2-independent detection of *F. novicida*, we used siRNA against caspase-11. We observed a consistent and significant delay in *Aim2*$^{-/-}$ macrophage death upon treatment with a caspase-11 siRNA (Fig 3C and 3D and S4B Fig) indicating that while *F. novicida* is largely able to escape caspase-11 detection ([36], Fig 3E, S4C and S4D Fig), caspase-11 may contribute to macrophage cell death at late time points of the infection in the absence of AIM2. The contribution

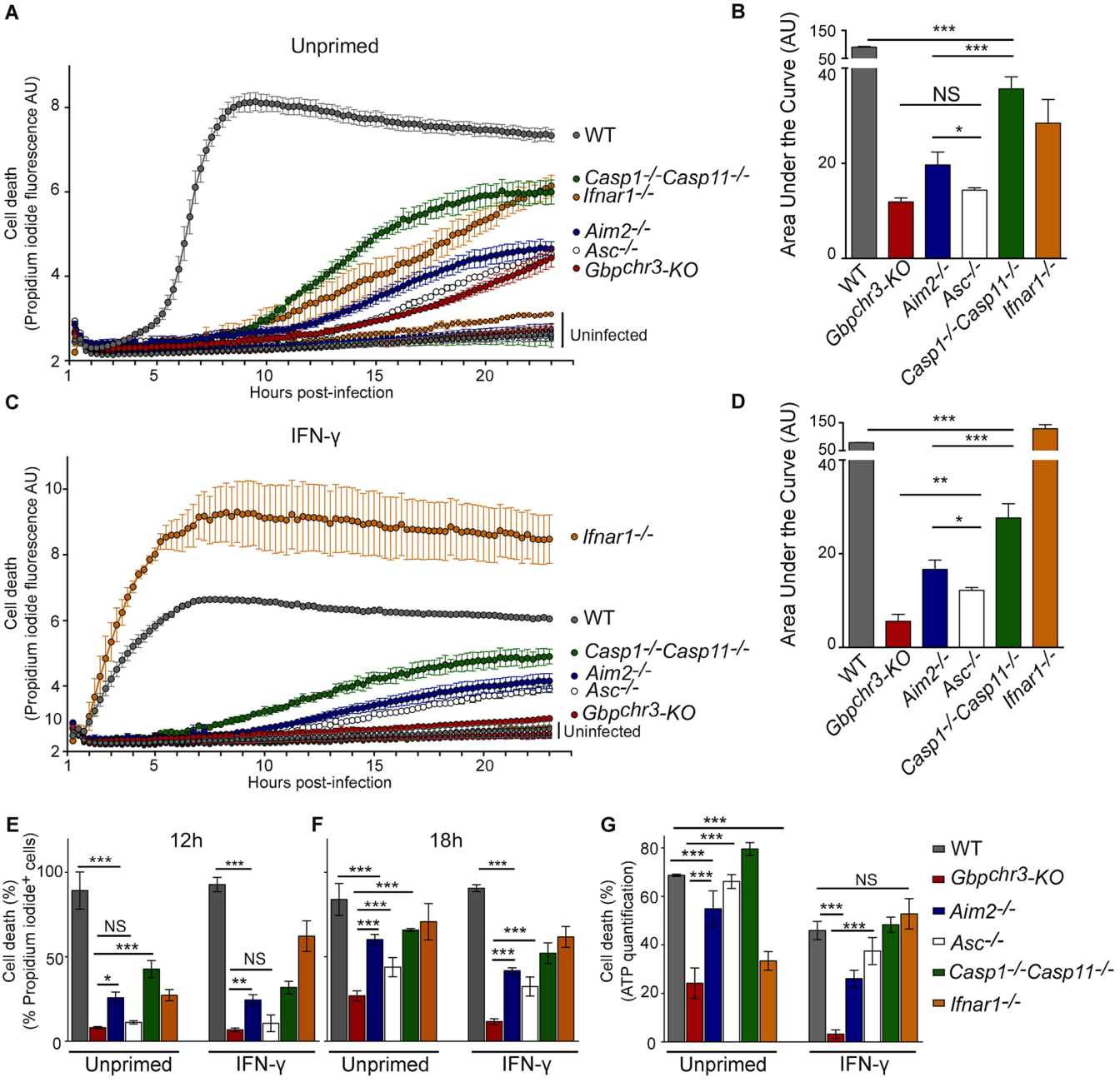

Fig 2. IFN-γ-induced GBPs control *F. novicida*-mediated cell death in an inflammasome-dependent and -independent manner. Cell death was measured in real-time by assessing propidium iodide fluorescence in (A, B) unprimed or (C, D) IFN-γ-primed (100 U/ml for 16 h) BMDMs from the indicated genotypes infected or not with *F. novicida* at a MOI of 10. (B, D) Kinetics were quantified by calculating the corresponding area under the curve. (E-F) The number of propidium iodide positive cells was quantified from time-lapse video-microscopy images (see S3 Fig and S1 and S2 Movies) at 12 h (E) and 18 h (F) post-infection. (G) ATP-based cell viability was monitored at 24 h post-infection. Cell death is shown. (A-G) Mean and s.d. are shown. One experiment representative of two (E, F) to at least three independent experiments is shown. (B, D, E-G) One-way ANOVA analysis was performed with Tukey's correction for multiple comparisons.

https://doi.org/10.1371/journal.ppat.1006630.g002

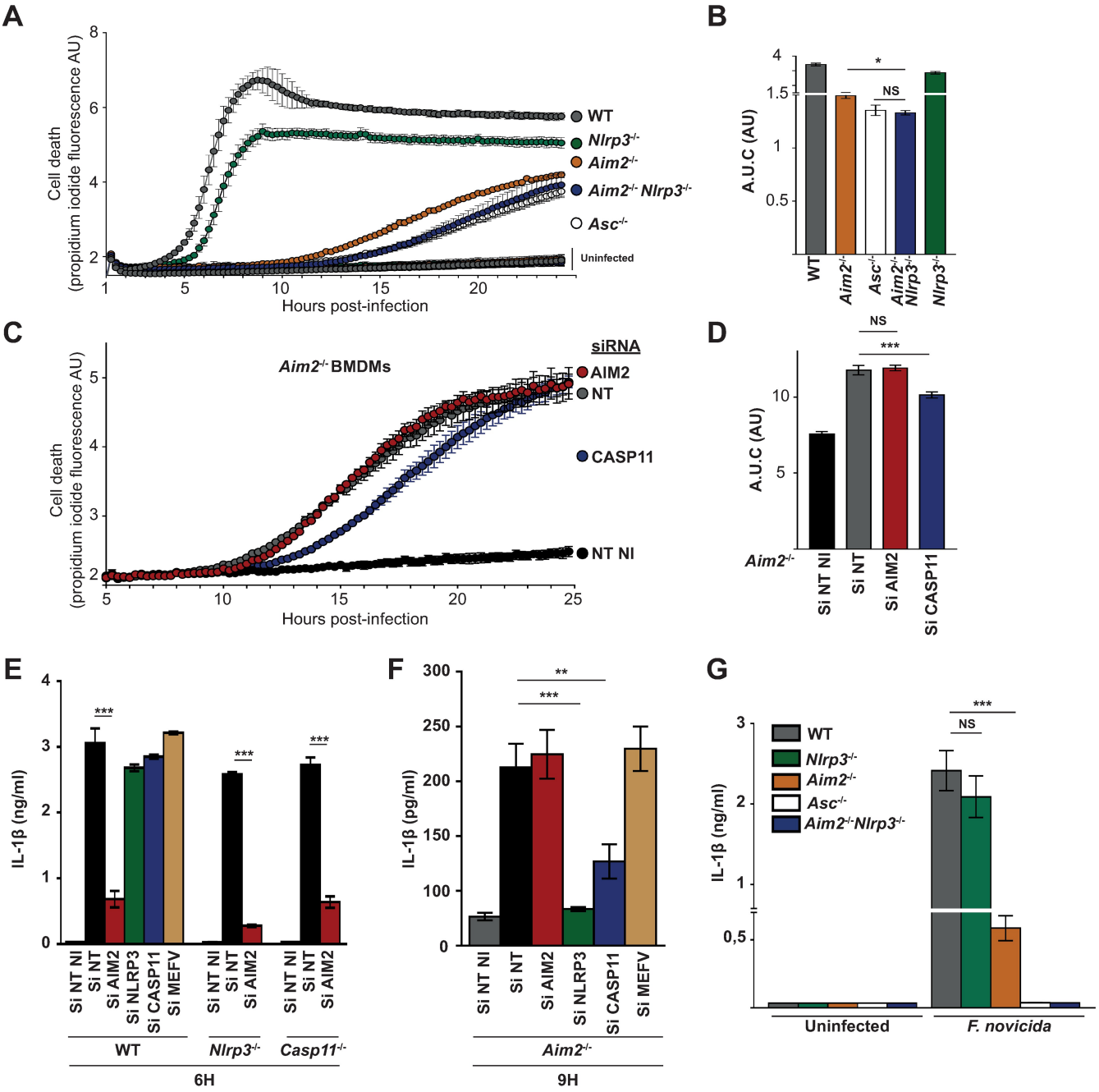

Fig 3. *F. novicida* infection triggers AIM2-, NLRP3-dependent canonical and caspase-11 non-canonical inflammasomes activation in a hierarchical manner. (A-D) Cell death was measured in real-time by assessing propidium iodide fluorescence in BMDMs of the indicated genotype infected with *F. novicida* at an MOI of 10. (B, D) Kinetics were quantified by calculating the corresponding area under the curve. (C) *Aim2*$^{-/-}$ BMDMs were treated with Non-Targeting (NT) or indicated gene-specific siRNA. (E-G) IL-1β levels in the supernatant of BMDMs of the indicated genotype treated (E, F) or not (G) with the indicated siRNA and infected with *F. novicida* at an MOI of 10 were quantified at 6 or 9 h post-infection as indicated. Graphs show mean and s.d. of triplicate assays. Data are representative of three independent experiments. (B, D, E-G) One-way ANOVA analysis was performed with Tukey's correction for multiple comparisons. (NI: Not infected).

https://doi.org/10.1371/journal.ppat.1006630.g003

of caspase-11 in the immune response of *Aim2*$^{-/-}$ macrophages was further strengthened by investigating IL-1β release. Indeed, *caspase-11* expression knock-down strongly decreased the late secretion of IL-1β observed in *Aim2*$^{-/-}$ macrophages (Fig 3F). *Nlrp3* expression knock-down or knock-out also consistently decreased IL-1β release in *Aim2*$^{-/-}$ macrophages (Fig 3F and 3G). This decrease may be partly due to its involvement downstream of caspase-11 [37].

Altogether, our data demonstrate the involvement of at least two sequential cell death pathways (mediated by the sensors AIM2, NLRP3 and caspase-11) elicited in response to *F. novicida* infection. The extensive survival of *Gbp*^{chr3}-KO BMDMs strongly suggests that GBPs contribute to activation of these three inflammasome complexes during *F. novicida* infection. Of note, at 24 h post-infection in absence of IFN-γ, propidium iodide incorporation/ fluorescence was similar in *Asc*$^{-/-}$ and *Gbp*^{chr3}-KO BMDMs. The late cell death occurring in *Gbp*^{chr3}-KO BMDMs was associated with IL-1β release while as expected no IL-1β was observed in the supernatant of *Asc*$^{-/-}$ BMDMs (S5 Fig). This result suggests that while chromosome 3-encoded GBPs are instrumental in promoting fast inflammasome activation upon *F. novicida* infection, they are not strictly required to trigger inflammasome activation likely explaining the bi-phasic dependence of IL-18 serum level on GBPs (Fig 1D and 1E). Interestingly, analysis of macrophages deficient for both *Asc* and *Gbp*^{chr3} demonstrated a strong delay in propidium iodide incorporation/fluorescence increase compared to that of *Asc*$^{-/-}$ and *Gbp*^{chr3}-KO BMDMs (S6A and S6C Fig) providing genetic evidence that GBPs can act independently of the canonical inflammasomes.

GBPs control *F. novicida*-mediated apoptotic pathways

In addition to uncovering AIM2-independent cell death pathways, real time cell death analysis of *F. novicida*-infected BMDMs (Figs 2A–2F and 3A–3D and S3 and S4 Figs) revealed both known and unsuspected cell death pathways. In agreement with previously reported LDH-release quantifications [13], IFN-γ could complement *Ifnar1*$^{-/-}$ BMDMs inability to rapidly undergo cell death upon *F. novicida* infection (Fig 2). Furthermore, as previously described [35,38], *Casp1/Casp11*$^{-/-}$ BMDMs died significantly faster than *Aim2*$^{-/-}$ BMDMs (Fig 2A–2G, S3 Fig). Apoptosis is associated with cell retraction while pyroptosis is associated with cell swelling [39]. We took advantage of wheat germ agglutinin (which binds cell membrane glycoproteins) staining intensity to quantify cell retraction and of well-characterized stimuli triggering pyroptosis (LPS + nigericin [40]) and apoptosis (gliotoxin [41]) to validate this cell retraction quantification (Fig 4A). *F. novicida*-infected *Casp1/Casp11*$^{-/-}$ BMDMs cell death proceeded via a major cell retraction (S1 Movie, Fig 4B and 4C), a morphological feature of apoptosis. The ability of AIM2/ASC complex to recruit caspase-8 and trigger apoptosis in *Casp1/Casp11*$^{-/-}$ BMDMs [35,38] may explain the kinetics of cell death observed in *Casp1/Casp11*$^{-/-}$ BMDMs. Indeed, at 10 h post-infection, we observed processing of the apoptotic caspases-8, 9 and 3 in infected *Casp1/Casp11*$^{-/-}$ BMDMs. As expected and as previously reported [35], we did not observe such apoptotic caspases processing in WT pyroptotic macrophages (Fig 4D). Furthermore, a strong DEVDase activity suggestive of active caspase-3 (or caspase-7) was observed in *Casp1/Casp11*$^{-/-}$ BMDMs but not in WT macrophages (Fig 4E and 4F). Interestingly, the kinetics of propidium iodide incorporation/fluorescence in infected *Gbp*^{chr3}-KO BMDMs were even slower than the corresponding kinetics of *Casp1/Casp11*$^{-/-}$ BMDMs (Fig 2A–2D). This difference strongly suggests that GBPs not only control pyroptosis, but also has the ability to control apoptotic pathways.

This conclusion was further strengthened by comparing cell death kinetics, morphological and molecular features of IFN-γ-primed *Asc*$^{-/-}$ and *Gbp*^{chr3}-KO BMDMs. Priming with IFN-γ accelerated the cell death kinetics in the different macrophages with one notable exception

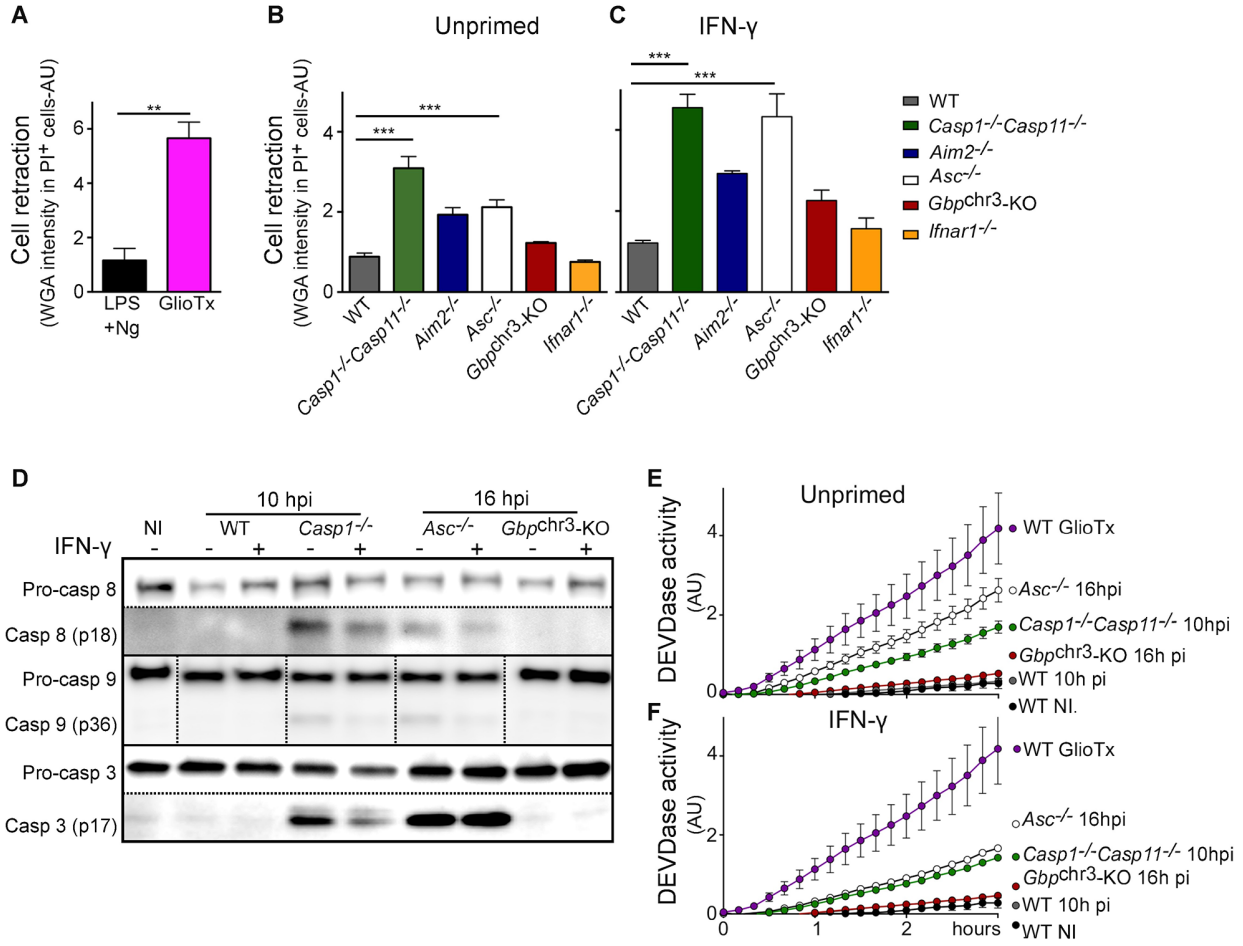

Fig 4. GBPs control apoptosis in inflammasome-deficient BMDMs. (A-C) Cell retraction in propidium iodide positive cells was assessed by quantifying wheat germ agglutinin staining intensity at (A) 90 minutes post Nigericin (Ng, a pyroptotis stimulus) or post-Gliotoxin (GlioTx, an apoptotic stimulus) or at (B, C) 21 h post-infection in (A, B) unprimed or (C) IFN-γ-primed (100 U/ml for 16 h) BMDMs from the indicated genotypes infected (B, C) or not with *F. novicida* at a MOI of 10. (D) Lysates from BMDMs from the indicated genotypes infected or not with *F. novicida* at a MOI of 10 were analyzed by Western blotting analysis. IFN-γ-priming (100 U/ml for 16 h) is indicated. The dotted vertical lines in Casp9 Western blot illustrate that the samples from a single original Western blot gel/ image were reorganized to fit the indicated order without any other image manipulation. The dotted horizontal lines in Casp8 and Casp3 Western blot indicate images from two different exposure times or from the use of two different primary antibodies (pro- and cleaved Casp3), respectively. (E, F) DEVDase activity was analyzed using a fluorogenic caspase3/7 substrate at 4 h post-GlioTx addition or at the indicated time post-infection in BMDMs from the indicated genotypes infected or not with *F. novicida* at a MOI of 10 and primed (F) or not (E) with IFN-γ (100 U/ml for 16 h). (A-C, E) Mean and s.d. are shown. (A-F) One experiment representative of two independent experiments is shown. Unpaired t-test (A) and one-way ANOVA analysis with Tukey's correction for multiple comparisons (B-C) were performed. (NI: non-infected).

https://doi.org/10.1371/journal.ppat.1006630.g004

(Fig 2C–2F). Indeed, we did not detect any substantial propidium iodide incorporation/fluorescence increase in IFN-γ-primed *Gbp*^{chr3}-KO macrophages while IFN-γ-primed *Asc*$^{-/-}$ BMDMs died although with delayed kinetics compared with that of WT macrophages (Fig 2C–2F, S3B Fig). The death of *Asc*$^{-/-}$ BMDMs was confirmed by addition of triton (TX100) at the end of the 24 h kinetics. Indeed, TX100 treatment did not further increase propidium iodide incorporation/fluorescence in *Asc*$^{-/-}$ BMDMs (S2B Fig). In contrast, TX100 addition in *Gbp*^{chr3}-KO BMDMs led to a strong increase in propidium iodide fluorescence indicating that the plasma membrane of most *Gbp*^{chr3}-KO BMDMs was still intact (and not permeable to

propidium iodide) at 24 h PI. The relatively lower intensity of propidium iodide fluorescence in *Asc*$^{-/-}$ BMDMs compared to WT BMDMs might be related to intrinsic differences in propidium iodide incorporation/fluorescence upon incorporation in apoptotic vs. pyroptotic nuclei. Cell death of IFN-γ-primed *Asc*$^{-/-}$ BMDMs was associated with cell retraction (S2 Movie and Fig 4C) and was reminiscent of the morphological cell death observed in *Casp1/Casp11*$^{-/-}$ BMDMs although it progressed with a ≈6 h delay compared to the latter BMDMs. Accordingly, apoptotic caspase-8/9/3 processing and DEVDase activity were clearly detectable in *Asc*$^{-/-}$ BMDMs infected for 16 h corroborating the morphological features and demonstrating that at late time points of infection, *Asc*$^{-/-}$ BMDMs die by apoptosis.

The extensive survival of *Gbp*^{chr3}-KO BMDMs upon IFN-γ priming was confirmed using CellTiter-Glo assay (Fig 2G). Furthermore, we observed a limited number of cell death events in infected *Gbp*^{chr3}-KO BMDMs using time-lapse microscopy (Fig 2F, S3 Fig and S2 Movie) suggesting that a limited GBPs-independent cell death pathway occurs at late time points of infection. The cell survival effect of IFN-γ on *Gbp*^{chr3}-KO BMDMs (compare Figs 2A and 2B with 2C and 2D; S3A with S3B and S6A with S6B, 2F and 2G, S3C and S6C) correlates with a decrease in IL-1β release (S5 Fig). This result suggests that in infected *Gbp*^{chr3}-KO BMDMs, IFN-γ might inhibit inflammasome activation possibly via nitrosylation, an IFN-inducible mechanism previously reported to inhibit inflammasome activation [42,43]. While the three different cell death/survival assays showed subtle differences [44], these assays converge to indicate that upon IFN-γ priming, *Gbp*^{chr3}-KO BMDMs survive better than *Casp1/Casp11*$^{-/-}$ and *Asc*$^{-/-}$ BMDMs suggesting that GBPs control both pyroptotic and apoptotic pathways. Importantly, the GBPs-mediated control of apoptosis was confirmed by generating mice doubly deficient for *Asc* and *Gbp*^{chr3}. Macrophages deficient for both *Asc* and *Gbp*^{chr3} failed to demonstrate caspase-8/9 and 3 maturation and DEVDase activity in contrast to *Asc*$^{-/-}$ macrophages (S6D and S6E Fig). Altogether, our results demonstrate that GBPs act as major cell death regulators by controlling numerous pyroptotic and apoptotic cell death pathways.

IFN-γ-induced GBPs control bacterial killing independently of inflammasomes

The high IFN-γ levels observed in *Gbp*^{chr3}-KO mice in the mouse model of tularemia coupled to the inability of *Gbp*^{chr3}-KO mice to control *F. novicida* burden (Fig 1) led us to investigate if GBPs contribute to the IFN-γ-mediated growth restriction observed *in vitro* [45]. As previously described [13,15,24,35], we observed a robust *F. novicida* replication in unprimed macrophages (Fig 5A corresponding to the Raw data presented in S7 Fig), which was partially controlled in a GBP-dependent manner by the inflammasome. IFN-γ priming led to *F. novicida* killing as visualized by a net decrease in the recovered intracellular colony forming units (Fig 5A) as soon as 6 h PI. Bacterial killing was highly dependent on GBPs. Indeed, *F. novicida* was not killed in IFN-γ-primed *Gbp*^{chr3}-KO macrophages, but robustly replicated by a 40-fold over 12 h of infection. We did not observe any substantial effect of IFN-γ on phagosomal rupture (S8 Fig) suggesting that IFN-γ does not act by restricting *F. novicida* access to its cytosolic niche. This finding is consistent with a previous study demonstrating a direct activity of IFN-γ on cytosolic *F. tularensis* [45]. Furthermore, the IFN-γ-mediated bacterial growth inhibition was independent of the NADPH oxidase and of the IFN-γ-inducible NO synthase (iNOS also known as NOS2), two immune effectors described to act downstream of GBPs [46] (S9C–S9E Fig). In WT macrophages, the GBPs-mediated bacterial killing was difficult to segregate from the antibacterial effects of host cell death due to the very rapid inflammasome activation (see Fig 2B). Yet, bacterial killing was also observed in IFN-γ-primed *Asc*$^{-/-}$ macrophages infected for 6 h at a MOI of 1 in the absence of substantial pyroptotic and apoptotic cell death.

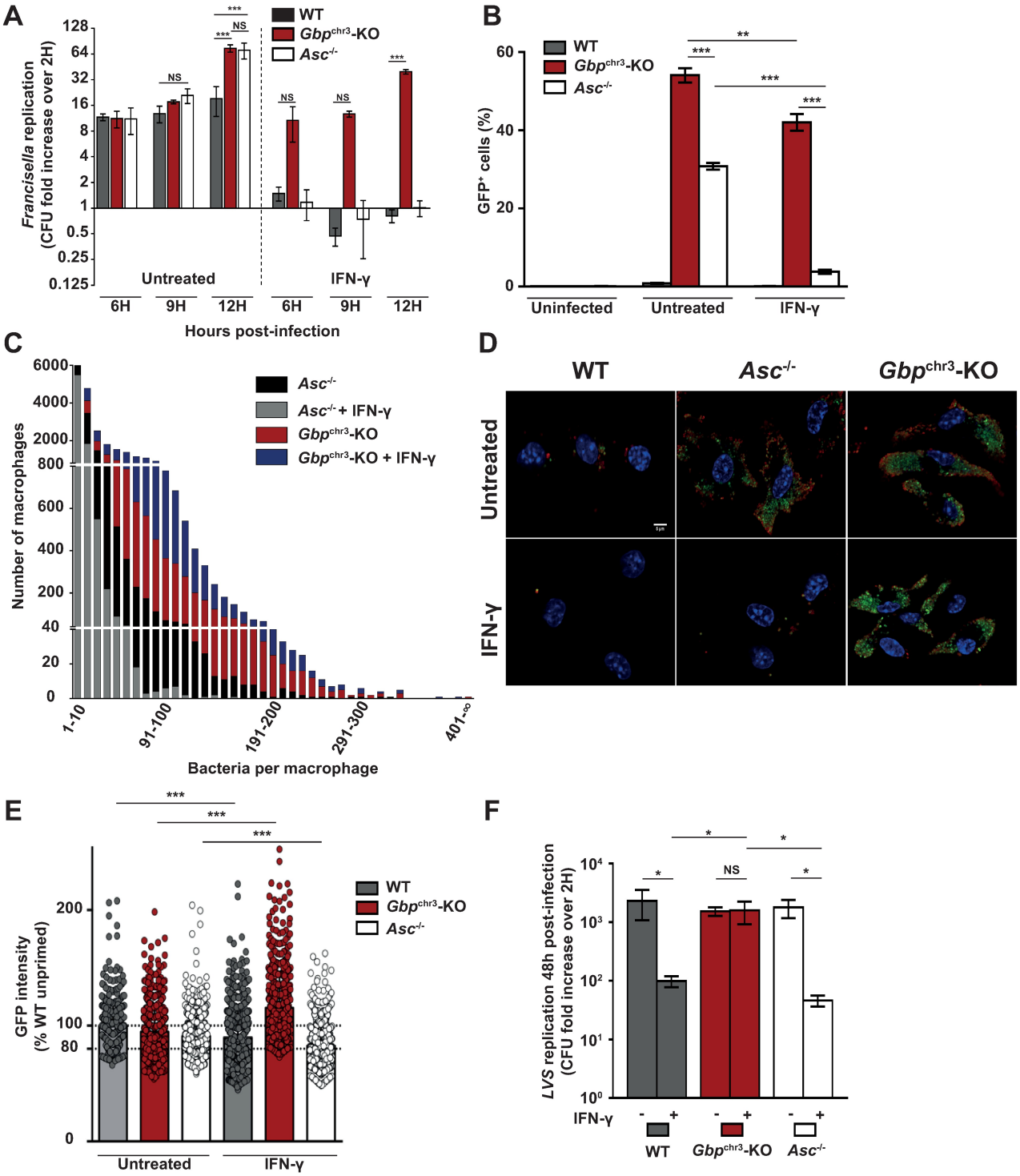

Fig 5. IFN-γ-induced GBPs control intracellular bacterial replication independently of inflammasomes. (A-F) BMDMs from the indicated genotypes were primed or not overnight with 100 U/ml of IFN-γ. BMDMs were infected with (A-E) *F. novicida* or (F) *F. tularensis* LVS at a multiplicity of infection (MOI) of 1 and 0.4, respectively. Intracellular bacterial burden was assessed by determination of viable counts at the indicated times post-infection. Results were normalized with viable counts detected at 2h post-infection. The corresponding raw data are presented in S7 Fig. (B) Flow cytometry-based quantification of infected cells (GFP^+) among live (propidium $iodide^-$) BMDMs after 10h of infection with GFP-expressing *F. novicida* at a MOI of 10. (C) Quantification of bacterial loads in single cells after 10h of infection with GFP-

expressing *F. novicida* at a MOI of 10, assessed by high-resolution microscopy in flow and presented as a comparison of both genotypes, with bacteria-per-cell values grouped by increments of 10. (D) Immunofluorescence of BMDMs infected for 10h with GFP-expressing *F. novicida* at a MOI of 1 (stained with DAPI (blue) and with an antibody to *F. novicida* (red); scale bars: 5 μm. (E) GFP intensity was quantified in single GFP-expressing *F. novicida* in BMDMs from the indicated genotypes primed or not overnight with 100 U/ml of IFN-γ and infected for 10 h. Cumulative data from two independent experiments are shown. The GFP intensity of single bacteria was normalized in each experiment to the average intensity of single bacteria in unprimed WT BMDMs. Dots represent the normalized GFP intensity of a single bacteria, the bar represents the mean. Fluorescence of ≈300 bacteria per sample and per experiment was analyzed. The dotted lines indicate the average intensity in unprimed WT BMDMs (100%) and the threshold set to quantify GFP^{low} bacteria (80%). Data are representative of two (C, D, F) or at least three (A, B) independent experiments. (A, B, F) Mean and s.d. of triplicate wells are shown. One-way ANOVA analysis with Tukey's correction for multiple comparisons (A-B, F) were performed. The distribution of GFP intensity in the different sample was analyzed using Komogorov-Smirnov test with Bonferroni correction.

https://doi.org/10.1371/journal.ppat.1006630.g005

Similarly, IFN-γ-mediated blockage in bacterial replication was observed in *Casp1/Casp11*$^{-/-}$ and *Aim2*$^{-/-}$ macrophages (S9A Fig) suggesting that intracellular bacterial killing is independent of canonical and non-canonical inflammasomes. To assess whether IFN-γ-mediated inhibition of bacterial growth was dependent or independent of cell death we took advantage of flow cytometry using GFP-expressing *F. novicida* and propidium iodide to exclude dead cells. In the absence of IFN-γ priming, replication was observed in ≈30% of live *Asc*$^{-/-}$ and ≈50% *Gbp*^{chr3}-KO macrophages (as determined by the number of propidium iodide^{-} GFP^{+} cells). In the presence of IFN-γ, this number dropped to less than 4% in *Asc*$^{-/-}$ macrophages indicating a robust bacterial growth restriction in these cells. In contrast, a large number of *Gbp*^{chr3}-KO macrophages (>40%) sustained *F. novicida* replication despite IFN-γ priming (Fig 5B). These results suggest that this anti-bacterial GBP-dependent mechanism proceeds independently of cell death at least in *Asc*$^{-/-}$ BMDMs.

To quantify *F. novicida* replication in a large number of macrophages, we analyzed infected macrophages using high-resolution microscopy in Flow (ImagestreamX). This single cell quantification technique further demonstrated that in the absence of *Gbp*^{chr3}, IFN-γ was almost ineffective to control bacterial replication. Indeed, in the presence of IFN-γ, there was a 100-fold increase in the number of *Gbp*^{chr3}-KO macrophages permissive for bacterial replication (containing more than 100 bacteria) compared with that of *Asc*$^{-/-}$ macrophages (Fig 5C, S9F Fig). Representative immunofluorescence images of this striking phenotype are presented in Fig 5D. While this difference was exacerbated in the presence of IFN-γ and as previously noticed using *Aim2*$^{-/-}$ macrophages [13], we observed that in unprimed macrophages, GBPs also controlled in an ASC-independent manner the bacterial burden.

GBP5-associated *F. novicida* loose their GFP expression, which has been associated with a loss of bacterial viability [15]. We thus quantified GFP intensity in single bacteria in propidium iodide-negative BMDMs as a surrogate marker of bacterial viability/metabolic activity (Fig 5E). In WT macrophages, IFN-γ treatment led to a significant reduction in the average GFP intensity (-10.2%) of intracellular *F. novicida* with a large increase (30%, n = 640) in the number of bacteria expressing low GFP levels (as defined by a GFP intensity <80% of the average intensity of bacteria in unprimed WT macrophages). Similarly, IFN-γ priming significantly reduced the average GFP intensity of bacteria in *Asc*$^{-/-}$ BMDMs (-8.4%) with a large increase (+19%, n = 843) in the number of low GFP-expressing bacteria. Surprisingly, IFN-γ priming had a paradoxical effect on bacterial GFP expression in *Gbp*^{chr3}-KO BMDMs with an increase in the average GFP intensity (+20.6%) and a strong decrease in the number of low GFP-expressing bacteria (-30%, n = 658). While this paradoxical increase (also visible in Fig 5D) remains to be understood, this experiment demonstrates that IFN-γ-induced GBPs in live macrophages affect the metabolic activity of bacteria. The decrease GFP expression observed in the presence of IFN-γ and GBPs is likely due to GBP-mediated antibacterial activity

although we were unable to directly quantify bacteriolysis in single cells. Importantly, the antibacterial activity of IFN-γ against *F. tularensis* live vaccine strain (LVS) was also fully dependent on *Gbp*^{chr3} extending our results to an attenuated strain of the *F. tularensis* species (Fig 5F). While an IFN-γ-dependent GBPs antibacterial activity was clearly observed upon LVS infection (Fig 5F; 23x fold reduction in WT BMDMs upon IFN-γ treatment), LVS sustained a substantial replication (≈100x) in IFN-γ-primed BMDMs. More strikingly, we were unable to observe a robust IFN-γ-mediated growth restriction of *F. tularensis* SCHU S4 in BMDMs (S10 Fig). These results suggest that *F. tularensis* strains have evolved mechanisms to avoid, at least partially, IFN-γ-mediated GBPs-dependent antibacterial activity.

The synergistic roles of GBP2 and 5 in promoting the antibacterial effect of IFN-γ could be demonstrated in J774.1 macrophage-like cells using CRISPR/cas9 (S11 Fig). This result rules out that the extensive replication observed in *Gbp*^{chr3}-KO BMDMs despite the priming with IFN-γ could be due to a non-specific defect of *Gbp*^{chr3}-KO BMDMs associated with their large genomic deletion. This is well in line with control experiments previously performed on *Gbp*^{chr3}-KO mice demonstrating normal induction of IFN-inducible genes and normal susceptibility/resistance to certain pathogens including *L. monocytogenes* [8,16]. Altogether, these findings demonstrate that, *in vitro*, in infected macrophages, the anti-bacterial function of IFN-γ, a cytokine known to induce a large number of antibacterial effectors relies almost exclusively on *Gbp*^{chr3}.

rIFN-γ administration partly rescues the in vivo antimicrobial function of *Asc*$^{-/-}$ mice but fails to complement *Gbp*^{chr3} deficiency

GBPs have been tightly linked to inflammasome complexes [10–16]. Yet our *in vitro* data clearly demonstrate that GBPs have potent inflammasome-independent antimicrobial functions. Particularly, *in vitro*, GBPs are the main IFN-γ antimicrobial effectors. In contrast, in the presence of IFN-γ, the inflammasome complex seems largely facultative to control *F. novicida* replication. ASC is required *in vivo* to induce IFN-γ via IL-18 release [27,28,47]. To further explore these potential differences *in vivo*, we administered rIFN-γ to *F. novicida*-infected mice. Early rIFN-γ administration allowed WT mice to survive *F. novicida* infection (Fig 6A). rIFN-γ administration clearly extended *ASC*$^{-/-}$ mice survival (Fig 6B) and strongly delayed *Asc*$^{-/-}$ mice weight loss (S12 Fig), while it had a very moderate (although statistically significant) effect on *Gbp*^{chr3}-KO mice survival and weight loss (Fig 6C and 6D, S12 Fig). To assess the functional links *in vivo* between IFN-γ, GBPs or the inflammasomes and their impact on bacterial replication, we analyzed the bacterial burden in the spleen and the liver at 48h PI following rIFN-γ injection at day 0 and day 1 PI. rIFN-γ was highly efficient to control the bacterial burden in both WT (Fig 6E) and *Asc*$^{-/-}$ mice (Fig 6F). In contrast, upon IFN-γ injection in *Gbp*^{chr3}-deficient mice, there was no statistical reduction in the bacterial burden in the liver and the spleen (4-fold reduction in the average splenic burden in *Gbp*^{chr3}-KO mice versus a 40-fold reduction in *Asc*$^{-/-}$ mice) (Fig 6F). These results demonstrate that, as observed in infected macrophages, the antibacterial action of IFN-γ is mostly mediated by GBPs *in vivo* and is largely independent of the canonical inflammasomes.

Discussion

With the recent discoveries of the tight links between the inflammasome complexes and the GBPs, it became unclear whether most antimicrobial functions of GBPs in infected macrophages were mediated by various inflammasome complexes or were independent of the inflammasomes [48]. Indeed, *Gbp*^{chr3}- and inflammasome-deficient mice are similarly highly susceptible to *F. novicida* infection. One of the current models to explain the link between

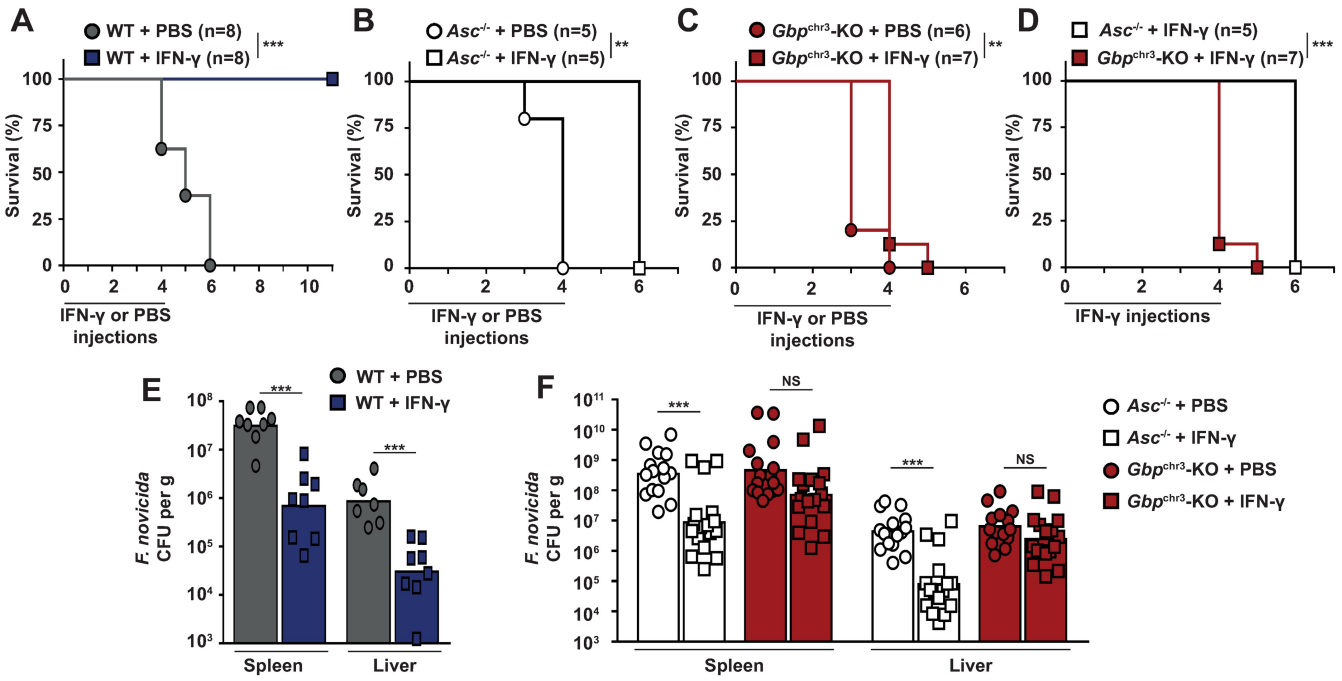

Fig 6. rIFN-γ administration largely rescues the *in vivo* antimicrobial function of *Asc*$^{-/-}$ mice but fails to complement *Gbp*^{chr3} deficiency. (A-D) Survival of mice treated by daily intraperitoneal injection of PBS or 10^5 U of rIFN-γ during 5 days after sc inoculation with 5×10^4 *F. novicida* (A) or 5×10^3 *F. novicida* (B-D). (A-C) effect of IFN-γ treatment in each genotype, (D) comparison of IFN-γ -treated *Asc*$^{-/-}$ and *Gbp*^{chr3}-KO mice. (E-F) Bacterial burden in the liver and spleen 2 days after sc inoculation with 5×10^4 *F. novicida* (E) or or 5×10^3 *F. novicida* (F). Each symbol represents the value of an individual mouse, geometric mean is shown. Data are representative of two independent experiments. Log-rank Cox-Mantel test (A-D), Mann-Whitney (E) and Kruskal-Wallis analysis with Dunn's correction (F) were performed.

https://doi.org/10.1371/journal.ppat.1006630.g006

GBPs and the inflammasomes positions GBPs as the molecular platform promoting the inflammasome supramolecular complex [2,3,48,49]. This model is strongly supported by evolution since GBPs from jawed fish display inflammasome-related CARD domains [14]. During *F. novicida* infection, we and other have previously demonstrated that GBPs are required to trigger AIM2 inflammasome activation while they are dispensable upon direct delivery of DNA into the host cytosol [13,15]. GBPs, in cooperation with IRGB10, were demonstrated to participate in *F. novicida* lysis into the host cytosol [13,15,16] suggesting that GBPs mostly act to release bacterial DNA into the host cytosol. The polymeric nature of DNA might alleviate the requirement for host factors to promote AIM2 inflammasome activation. Indeed, cytosolic dsDNA could provide the scaffold for AIM2 oligomerization and subsequent inflammasome activation [50,51].

In this work, we demonstrate that GBPs are required not only for the AIM2 canonical inflammasome activation but for most of the programmed cell death pathways that can take place in *F. novicida*-infected macrophages. *In vitro*, in *F. novicida*-infected WT murine BMDMs, so far the only described cell death pathway was the AIM2 inflammasome. Yet, using various knock-out macrophages, we have demonstrated here that several canonical and non-canonical inflammasome complexes can be active during *F. novicida* infection. These alternative pathways were revealed thanks to the use of *Aim2*$^{-/-}$ BMDMs and are masked in WT macrophages. Interestingly, Harton and colleagues recently demonstrated that *F. tularensis* strains, in contrast to *F. novicida*, elicit NLRP3 inflammasome activation in BMDMs [52]. This result

suggests that *F. tularensis* has evolved to escape AIM2 inflammasome activation while the delayed NLRP3-dependent sensing is conserved in response to various *Francisella* species. The identification of a caspase-11-dependent role in mediating *Aim2*$^{-/-}$ BMDMs death and IL-1β release in the absence of AIM2 was unexpected. Indeed, the direct delivery of *Francisella* LPS into BMDMs cytosol does not activate caspase-11 due to its underacylated structure ([36]). It is still unclear whether the delayed caspase-11-dependent activation observed in *Aim2*$^{-/-}$ BMDMs is due to sensing of *F. novicida* LPS or of another endogenous or bacterial ligand. The large number of inflammasome complexes activated upon *F. novicida* infection is reminiscent of what have been observed during infection with other intracellular bacteria [11,53,54], although *F. novicida* infection of murine macrophages is somewhat unique due to its high dependence on AIM2 [18]. Remarkably, IFN-γ-induced GBPs are required to trigger all these pathways suggesting that they either act upstream of the inflammasomes or that they have conserved mechanisms to facilitate activation of several (AIM2, NLRP3, caspase-11) inflammasome sensors. Such facilitation of the activation of multiple inflammasomes by GBPs has been previously observed upon *Chlamydia* infection [11]. Yet, GBPs-mediated control of *Chlamydia*-mediated cell death was only partial in contrast to what we observed upon *F. novicida* infection. Importantly, *Asc*$^{-/-}$ (and *Casp1/Casp11*$^{-/-}$) BMDMs died by apoptosis as demonstrated by morphological and molecular analyses (Fig 4, S1 and S2 Movies)[35] indicating that GBPs control both pyroptotic and apoptotic pathways. Indeed, processing of caspase-8, 9 and 3 and DEVDase activity were clearly visible in *Asc*$^{-/-}$ BMDMs but absent in *Asc*$^{-/-}$*Gbp*^{chr3}-KO BMDMs (S6D and S6E Fig). The GBP-dependent pathway leading to apoptotic caspase activation in *Asc*$^{-/-}$ BMDMs is still unclear. Antibiotic-mediated bacteriolysis of another cytosolic pathogen (*Shigella flexneri*) triggers massive caspase-9-dependent apoptosis of epithelial cells [55]. Based on the antibacterial role of GBPs ([13,15,16], this work), we speculate that GBPs-mediated action releases a PAMPs that directly or indirectly triggers apoptosis in the absence of the inflammasome adaptor ASC. The concurrent maturation of both caspase-8 and caspase-9 suggests activation of both extrinsic and intrinsic (e.g. mitochondrial) apoptotic pathways. This dual activation may be due to the cross-activation of the mitochondrial intrinsic apoptosis pathway following cleavage of Bid by caspase-8 [56]. Yet, we cannot exclude a direct GBPs-dependent induction of mitochondrial dysfunction such as the one occurring in *S. flexneri*-infected cells of non-myeloid lineages [57]. IRGs can lyse *T. gondii* vacuole leading to parasite permeabilisation and a caspase-1-independent necrotic death in mouse embryonic fibroblats [58]. Due to the diversity of cell death pathways controlled by GBPs and IRGs, we favor the hypothesis that these IFN-induced GTPases act as PAMPs-shedders to release/uncover various microbial cell death-activating ligands. Future studies are needed to establish the pathways linking GBPs to the different cell death pathways.

IFN-γ is the most potent cytokine against intracellular bacteria due to its ability to induce hundreds of genes promoting host defense [1]. Remarkably, our data indicate that the antimicrobial action of IFN-γ against *F. novicida* and *F. tularensis* Live Vaccine Strain is almost exclusively dependent on GBPs. While it was previously known that IFN-γ could restrict cytosolic *Francisella* growth independently of cell death, reactive oxygen or nitrogen species, autophagy and IDO-mediated tryptophan degradation [45], the mechanisms responsible for this growth restriction were unknown. The IFN-γ-mediated *F. novicida* growth restriction is independent of caspase-1 and caspase-11 (S3 Fig). It thus differs from the recently described mechanisms responsible for growth inhibition of cytosolic *Salmonella* [59]. Interestingly, the highly virulent *F. tularensis* SCHU S4 largely escaped IFN-γ-mediated antibacterial activity in BMDMs (S10 Fig). It remains unclear whether this escape is the result of an active process or due to the failure of innate immune sensors to detect/recognize cytosolic *F. tularensis* SCHU S4.

In a concurrent work, Kanneganti and colleagues identified IRGB10 as an IFN-inducible GTPase recruited onto cytosolic *F. novicida* and required to lyse the bacterium and trigger AIM2 inflammasome activation [16]. IRGB10 recruitment is abolished in Gbp^{chr3}-KO macrophages indicating that GBPs and IRGB10 may act together and that the latter protein is likely involved in IFN-γ-mediated growth restriction in murine macrophages. In contrast to GBPs [6], IRGs (with the exception of the constitutively expressed IRGM) are absent in humans [60]. Yet, IFN-γ priming efficiently restricts cytosolic *Francisella* growth in human macrophages ([45], S13 Fig) indicating that IRGs are facultative for the IFN-γ-mediated antimicrobial role. While our results identify that GBPs are required for IFN-γ-mediated killing of cytosolic bacteria, other host factors are likely involved upstream of GBPs to facilitate GBPs targeting onto cytosolic bacteria. The molecular mechanisms sustaining IFN-γ-dependent GBPs-mediated antibacterial activity remains to be understood.

Materials and methods

Ethics statement

All animal experiments were reviewed and approved by the animal ethics committee (CECCAPP, Lyon) of the University of Lyon, France under the protocol number #ENS_2012_061, #ENS_2014_017 and #ENS_2017_002 and in strict accordance with the European regulations (#2010/63/UE from 2010/09/22) and the French laws ("Décret n 2013–118 du 1er février 2013 relatif à la protection des animaux utilisés à des fins scientifiques" and "Arrêté ministériel du 1er février 2013 relatif à l'évaluation éthique et à l'autorisation des projets impliquant l'utilisation d'animaux dans des procédures expérimentales").

Mice

Gbp^{chr3}-KO, $Nos2^{-/-}$, $Cybb^{-/-}$, $Casp1^{-/-}/Casp11^{-/-}$(a.k.a caspase-1 knockout), $Asc^{-/-}$, $Aim2^{-/-}$, $Nlrp3^{-/-}$mice, all in the C57BL/6, have been previously described [8,24]. Double knock-out mice ($Nlrp3^{-/-}Aim2^{-/-}$ and $Asc^{-/-}$ Gbp^{chr3}-KO) were generated in the framework of this project. The presence of the functional C57BL/6 caspase-11 was verified by PCR amplification of exon 7 boundaries followed by sequencing [37]. Mice were bred at the PBES (Lyon, France).

Mouse infections

Age- and sex-matched animals (6–10 weeks old) were infected subcutaneously with $5x10^3$ or $5x10^4$ or $4x10^5$ CFU of *F. novicida* in 100 μl PBS (as indicated in the figure legends). When applicable, 10^6 U/ml of rIFN-γ was injected intraperitonealy in 100 μl PBS. Blood was collected by retro-orbital bleeding at 16 h post-infection or intra-cardiac puncture at 48 h post-infection. Animals were sacrificed at the indicated time point post-infection. Mice were examined twice daily for signs of severe infection and euthanized as soon as they displayed signs of irreversible morbidity or as soon as weight loss exceeded 20%.

Bacterial strains and plasmids

F. novicida strain U112, its isogenic ΔFPI mutant [61] and *F. tularensis* subspecies *holarctica* Live Vaccine Strain (LVS) were used. When applicable, strains were transformed with pKK219-GFP [62].

Cell culture and infections

Preparation and culture of BMDMs were performed as previously described [63]. BMDMs were differentiated in DMEM medium (Invitrogen) with 10% v/v FCS (Thermo Fisher

Scientific), 10% MCSF (L929 cell supernatant), 10 mM HEPES (Invitrogen), 5% Sodium pyruvate. 1 day before infection, macrophages were seeded into 6-, 24-, or 96-well plates at a density of $1.25x10^6$, $2.5x10^5$, or $5x10^4$ per well. When applicable macrophages were pre-stimulated with 100ng/ml Pam_3CSK_4, LPS O111:B4 (InvivoGen) or 100u/ml mIFN-β or mIFN-γ (immunotools). For infections with *F. novicida*, bacteria were grown overnight in TSB supplemented with 0.1% (w/v) cysteine at 37˚C with aeration. The bacteria were added to the macrophages at the indicated MOI. The plates were centrifuged for 15 min at 1500 g and placed at 37˚C for 60 min. Cells were washed and fresh medium containing 10 $\mu g.ml^{-1}$ gentamycin (Invitrogen) was added. For LVS, cells were infected for 2 h at an MOI of 0.4, washed and incubated in the presence of gentamicin at 5 $\mu g.ml^{-1}$.

Replication assay

For *F. novicida* intracellular replication assay, macrophages were lysed with 1% (w/v) saponin (Sigma) in water for 5 min. Dilution, plating on TSA supplemented with 0.1% (w/v) cysteine and counting was performed using the easySpirale Dilute (Interscience). For LVS replication assay, cells were lysed in PBS with 0.1% deoxycholate, serially diluted in PBS and plated on modified GC-agar base plates.

siRNA knockdown

Gene expression knockdown was done using GenMute (SignaGen laboratories) and siRNA pools (siGenome, Dharmacon). Briefly, wild-type BMDMs were seeded into 24-, or 96-well plates at a density of $1.5x10^5$ or $3x10^4$ per well. siRNA complexes were prepared at 25 nM in GenMute Buffer according to the manufacturer's instructions for forward knockdowns. siRNA complexes were mixed with BMDMs medium and added onto the cells. BMDMs were infected with *F. novicida* at an MOI of 10:1 after 48 h of knockdown and analyzed for inflammasome activation as outlined below. siRNA pools included: Aim2 (M-044968-01), Caspase-11 (that is, Casp4) (M-042432-01), Mefv (M-048693-00), Nlrp3 (M-053455-01), Caspase-1 (M-048913-01) and NT (non-targeting) pool 2 (D-001206-14).

Cytokine measurement and cell death assays

IL-1β and IL-18 were measured by ELISA (R&D systems and platinum ebioscience, respectively). Cell viability was determined by the CellTiter-Glo Luminescent Cell Viability Assay (Promega). Global cell death kinetics was monitored in BMDMs by assessing in real time incorporation of propidium iodide (used at 5 μg/ml) through measurement of fluorescence emission at 635 nm every 15 min on a microplate reader (Tecan, see. S2A Fig for the sensitivity of the technique). When indicated triton X100 (Sigma) at 1% (v/v) was added at the end of the kinetics to further control cell death/viability. Area under the curve were computed using Prism software (GraphPad) to obtain a single quantitative readout of the full kinetics as recently described [64]. Gliotoxin (Enzo Pharma) and Nigericin (Sigma) were used at 5 μM, the latter after a 3 h priming with LPS at 100 ng/ml. Single cell death kinetics was determined using an automated time-lapse video microscope (Arrayscan high-content system, Thermo Fisher Scientific). Image analyses of four sparse fields per well were performed using the HCS studio analysis software. Wheat-germ agglutinin (WGA)-labelled BMDMs were used. Individual dead cells were detected and numerated based on the propidium iodide fluorescence staining and normalized to the total number of cells numerated through the vital Hoechst staining at time 0. WGA intensity in propidium iodide positive cells was calculated to quantify cell retraction using HCS studio software. CO2-independent medium (ThermoFisher Scientific) was used for all cytokines dosage and cell death kinetics.

Protein lysates and caspase activity assay

Following BMDMs infection, protein extracts were obtained by lysing cells in the following buffer (10 mM Hepes/KOH, 2mM EDTA, 0.1% CHAPS, 250 mM sucrose, 5mM dithiothreitol). Samples were clarified by centrifugation at 4˚C, 13 000g for 15 minutes. Protein concentration was determined using Bradford method (Bio-Rad). Fluorimetric analysis of caspase-3/7 activity was performed as previously described [35] by incubating protein extracts (4 μg/sample) with Ac-DEVD-AFC (Enzo pharma, ALX-260-037) at 40 μM final concentration. Fluorescent reading over 3 h was performed on a fluorimeter (Tecan).

Immunoblotting

Blotting was done as described before using 15 to 20 μg of protein sample per lane depending on the antibodies [13]. Antibodies used were rabbit anti-GBP2 and rabbit anti-GBP5 (1:1,000; 11854-1-AP/13220-1-AP; Proteintech), anti-caspase-8 (1:2,000; Enzo pharma; ALX-804-447), anti-caspase-9 (1:2,000; MBL; M054), anti-caspase-3 and anti-cleaved caspase-3 (1:1,000; Cell signaling Technologies; #9662 and #9661, respectively). Cell lysates were probed with anti-β-actin antibody (Sigma) at 1:2,000.

Immunofluorescence and GFP quantification in single bacteria

Macrophages were seeded on glass coverslips and infected as described above. At the desired time, cells were washed 3 times with PBS and fixed with 4% paraformaldehyde for 15 min at 37˚C. Following fixation, coverslips were washed and the fixative was quenched with 0.1 M glycine for 10 min at room temperature. Coverslips were stained with primary antibodies at 4˚C for 16 h, washed with PBS, incubated for 1 h with appropriate secondary antibodies at room temperature (1:500, AlexaFluor, Invitrogen), washed with PBS and mounted on glass slides with Vectashield containing 6-diamidino-2-phenylindole (DAPI) (Vector Labs). Antibodies used were chicken anti-*Francisella* (1:1000, a gift from D. Monack). Coverslips were imaged on a Zeiss LSM710.

Quantification of GFP in GFP-expressing *F. novicida* was performed using an automated process in ImageJ (NIH, USA). The threshold was adjusted using the moments-preserving thresholding method with the dark background option. Binary watershed process was used to separate individual bacteria. Fluorescence intensity quantification was restricted to individual particle of 0.2 to 2 μm^2 with a circularity comprised between 0.5 and 1.

Flow cytometry and microscopy in flow

For assessment of bacterial replication by flow cytometry, macrophages seeded onto non-tissue culture-treated plates were infected as described above with GFP-expressing *F. novicida* strains. At desired time, cells were lifted with trypsin and immediately analyzed by Flow cytometry on a Canto 2 cytometer (BD biosciences). Dead cells were excluded based on staining with propidium iodide.

For the microscopy in flow experiments, macrophages infected with GFP-expressing bacteria were fixed in PFA 4% and analyzed on ImageStream X mark II (Amnis, EMD-Millipore) using the Inspire software with the Extended depth of field (EDF) function activated to increase the spot counts accuracy. Images of single cells were analyzed with the Ideas Software (Amnis, EMD-Millipore) as previously described [13] to quantify the number of bacteria per cell.

Statistical analysis

Statistical data analysis was done using Prism 5.0a (GraphPad Software, Inc.). To evaluate the differences between three selected groups or more (cell death, cytokine release, FACS, CFU and immunofluorescence-based counts) one-way ANOVA analysis was performed with Tukey's correction for multiple analysis. Komogorov-Smirnov test was used to compare the cell distribution as determined by Imagestream and the distribution of GFP intensity in single bacteria. P values were adjusted for multiple comparisons with the Bonferroni correction approach. Animal experiments were evaluated using Kruskal-Wallis analysis with Dunn's correction except when only two groups were present in the analysis, Mann-Whitney analysis was performed. Survival experiment was analyzed thanks to log-rank Cox-Mantel test. In figures NS indicates 'not significant', P values are given according to the following nomenclature: $^{*}P<0.05$; $^{**}P<0.01$; $^{***}P<0.001$.

Supporting information

S1 Material and Methods. Supplemental methods including CCF4 measurements, SCHU S4 infection, real-time PCR, CRISPR/Cas9-mediated knock-out procedures.
(DOCX)

S1 Fig. IFN-γ priming induces a quantitative shift in GBPs levels. (A) GBP2, (B) GBP5 (C) ProIL-1β mRNA levels, (D) GBP2, GBP5 and β-actin protein levels were analyzed by qRT-PCR (A-C) or western blotting analysis (D) in BMDMs from the indicated genotypes infected with *F. novicida* at a MOI of 10 for 4 h or treated for 16 h with 100 U/ml of IFN-β, IFN-γ or 100 ng/ml of Pam_3CSK_4 (NT: not treated). (A-B) One-way ANOVA analysis was performed with Tukey's correction to compare GBP induction following IFN-β and IFN-γ priming. (A-D) One experiment representative of two independent experiments, (A-C) mean and standard deviations are shown.
(TIF)

S2 Fig. Controls related to the real time measurement of propidium iodide incorporation/fluorescence. (A) WT BMDMs were seeded at different cell density as indicated and treated with Triton X100 (1% v/v final) in the presence of propidium iodide. Cell death was analyzed in real time by quantifying propidium iodide fluorescence every 5 minutes. (B) IFN-γ-primed BMDMs from the indicated genotypes were infected with *F. novicida* at a MOI of 10. Cell death was analyzed by quantifying propidium iodide fluorescence every 15 minutes. At 26 h post-infection, TX-100 (1% v/v final) was added leading to a strong increase in fluorescence in Gbp^{chr3}-KO BMDMs but not in WT nor $Asc^{-/-}$ BMDMs confirming that most Gbp^{chr3}-KO BMDMs had an intact (propidium iodide-impermeant) plasma membrane before TX-100 addition in contrast to most WT and $Asc^{-/-}$ BMDMs. One experiment representative of two (A) to at least three (B) independent experiments is shown.
(TIF)

S3 Fig. Time-lapse microscopy demonstrates that *F. novicida*-infected BMDMs trigger, in a hierarchical manner, various GBPs-dependent cell death pathways. (A,B) Cell death was monitored at single cell level and in real time using automated microscopy and propidium iodide. BMDMs of the indicated genotypes were primed (B) or not (A) with rIFN-γ (100 U/ml) for 16h before infection with *F. novicida* at an MOI of 10. Automated image analysis was used to quantify the percentage of dead cells at each time points of the kinetics. (C) The area under the curve (corresponding to the above kinetics from 1.5 to 20 h post-infection) was

computed. One-way ANOVA analysis was performed with Tukey's correction. (A-C) One experiment representative of two independent experiments is shown.
(TIF)

S4 Fig. Knock-down of the expression of inflammasome components demonstrated hierarchical activation of several cell death pathways. (A) Knock-down efficiency and specificity was determined by qRT-PCR at 48 h post-transfection in BMDMs. The specific transcript levels were normalized to β-actin transcript level and rationalized with the corresponding transcript level in BMDMs treated with a non-targeting (NT) siRNA. (B) *Aim2*$^{-/-}$ BMDMs transfected with the indicated siRNA were infected with *F. novicida* at a MOI of 10 and cell death was monitored by measuring propidium iodide fluorescence at 17 h PI. (C) WT BMDMs transfected with the indicated siRNA were infected with *F. novicida* at a MOI of 10 and cell death was monitored in real time by measuring propidium iodide fluorescence. (D) The area under the curve corresponding to the (C) kinetics from 1 to 20h is shown. NI: Non-infected. (B-D) One-way ANOVA analysis was performed with Tukey's correction. (A-D) One experiment representative of three independent experiments is shown.
(TIF)

S5 Fig. IFN-γ modulates the kinetics of IL-1ß release in *Gbp*^{chr3}-KO BMDMs. BMDMs from the indicated genotypes were infected or not with *F. novicida* at a MOI of 10 after priming or not with IFN-γ (100u / ml 16 h). At 10 h post-infection (A) or 24 h post-infection (B) IL-1ß concentrations were determined by ELISA. One experiment representative of three independent experiments with mean and standard deviations is shown. One-way ANOVA analysis was performed with Tukey's correction.
(TIF)

S6 Fig. Comparison of the responses of macrophages doubly deficient in *Asc* and *Gbp*^{chr3} with that of macrophages with single deficiencies demonstrates that GBP and ASC control different pathways. BMDMs from the indicated genotypes (DKO corresponds to *Asc*$^{-/-}$ *Gbp*^{Chr3}-KO doubly-deficient macrophages) were infected or not with *F. novicida* at a MOI of 10 after priming (B) or not (A) with IFN-γ (100 U/ml, 16 h). (A, B) Real time propidium incorporation/ fluorescence, (C) area under the curve corresponding to the kinetics in A and B, (D) apoptotic caspases processing analysis by Western blotting, (E) DEVDase activity as determined using a fluorogenic caspase-3 substrate and (F) bacterial replication assay by CFU are shown. (C) The dotted vertical lines in Casp9 Western blot illustrate that the samples from a single original Western blot gel/ image were reorganized to fit the indicated order without any other image manipulation. The plain vertical line in Casp-3 Western blot illustrates that the samples from two Western blot gels run and analyzed side by side with the same exposure time are presented. The dotted horizontal lines in Casp8 and Casp3 Western blot indicate images from two different exposure times or from the use of two different primary antibodies (pro- and cleaved Casp3), respectively. The Western blots presented correspond to the ones presented in Fig 4D of the main manuscript. (A, B, C) one experiment representative of two independent experiments is shown. (C) One way ANOVA analysis with Tukey's correction for multiple tests was performed. (D-F) One experiment is shown. Mean and standard deviations are shown.
(TIF)

S7 Fig. IFN-γ-induced GBPs control intracellular bacterial replication. (A-B) BMDMs from the indicated genotypes were primed or not overnight with 100 U/ml of IFN-γ. BMDMs were infected with (A) *F. novicida* or (B) *F. tularensis* LVS at a multiplicity of infection (MOI) of 1 and 0.4, respectively. Intracellular bacterial burden was assessed by determination of viable

counts at the indicated times post-infection. The corresponding data expressed as Fold increase are presented in Fig 5.
(TIF)

S8 Fig. IFN-γ does not modify substantially phagosomal rupture. BMDMs from the indicated genotypes were primed or not with 100 U/ml of IFN-γ for 16 h. BMDMs were infected with the indicated *F. novicida* strains at a multiplicity of infection (MOI) of 10. At 2 h post-infection, cells were incubated with the FRET substrate CCF4. Cytosolic ß-lactamase-mediated CCF4 hydrolysis (a marker of phagosomal permeabilization) was analysed by flow cytometry after gating on live (propidium iodide negative) cells. One experiment representative of two independent experiments is shown. One-way ANOVA analysis was performed with Tukey's correction.
(TIFF)

S9 Fig. IFN-γ-induced GBPs control bacterial killing independently of inflammasomes, the NADPH oxidase and iNOS. (A-E) BMDMs from the indicated genotypes were primed or not overnight with IFN-γ (100 U/ml) and infected at a MOI of 1 with *F. novicida* (A-D) or at a MOI of 10 with GFP-expressing *F. novicida* (E). (A, D) Intracellular bacterial burden was assessed by determination of viable counts at 12 h. (A, C) Results were normalized with the viable counts detected at 2 h post-infection. The corresponding Raw data are presented in (B, D). (E) Flow cytometry-based quantification of infected (GFP^+) cells among live BMDMs at 10 h post-infection. (F) Sample ImageStreamX images of BMDMs from the indicated genotypes, treated or not for 16 h with IFN-γ (100 U/ml) and infected at a MOI of 10 with GFP-expressing *F. novicida*.
(TIF)

S10 Fig. Highly virulent *F. tularensis* SCHU S4 strain largely escapes IFN-γ-mediated growth restriction in BMDMs. WT BMDMs primed or not overnight with IFN-γ (100 U/ml) were infected at a MOI of 0.4 with *F. tularensis* SCHU S4 or *F. novicida* U112. Intracellular bacterial burden was assessed by determination of viable counts at 48 h. (A) Results were normalized with the viable counts detected at 2 h post-infection. (B) The corresponding Raw data are presented.
(TIF)

S11 Fig. IFN-γ-induced GBP2 and 5 control bacterial killing in the J774.1 macrophage cell line as determined using CRISPR/Cas9 technology. Cas9-expressing J774.1 cells were transduced with non-targeting (NT) gRNA or gRNAs targeting the indicated gene(s). Following puromycin selection, the obtained cell lines primed or not with IFN-γ (100 U/ml for 16 h) were infected with GFP-expressing *F. novicida*. Live (propidium iodide-negative) cells were analyzed by flow cytometry at 14 h post-infection. One experiment representative of three independent experiments, mean and standard deviations are shown. One-way ANOVA analysis was performed with Tukey's correction.
(TIFF)

S12 Fig. rIFN-γ administration protects WT and *$ASC^{-/-}$* and to a much lower extent *Gbp^{chr3}-KO* mice from *F. novicida*-mediated weight loss. Weight loss of mice of the indicated genotypes (see associated Fig 6) treated by daily i.p injection of PBS or 10^5 U of rIFN-γ during 5 days after s.c. inoculation with 5×10^4 (A) or $5x10^3$ (B) *F. novicida*.
(TIF)

S13 Fig. IFN-γ priming efficiently restricts cytosolic *F. novicida* growth in primary human macrophages. Flow cytometry-based quantification of live infected (PI^-, GFP^+) primary

human macrophages from one healthy donor primed or not with hrIFN-γ (100 U/ml) of and infected for 16 h with GFP-expressing *F. novicida* strain U112 or the isogenic ΔFPI mutant at a MOI of 1. Mean and s.d. of triplicate wells are shown. Data are representative of two independent experiments.
(TIFF)

S1 Movie. Cell death kinetics of unprimed BMDMs as assessed by time-lapse videomicroscopy. WGA-labeled WT, *Gbp*^{chr3}-KO, *Casp1*$^{-/-}$*Casp11*$^{-/-}$ and *Asc*$^{-/-}$ BMDMs were infected with *F. novicida* at a MOI of 1 in the presence of propidium iodide. Images were recorded every 30 minutes from 3 h PI to 23 h PI. Bright-field (top panels) and WGA (bottom panels) are shown. Note the increase in WGA intensity associated with cell retraction in *Casp1*$^{-/-}$*Casp11*$^{-/-}$ BMDMs previously demonstrated to die by apoptosis.
(AVI)

S2 Movie. Cell death kinetics of IFN-γ-primed BMDMs as assessed by time-lapse videomicroscopy. IFN-γ-primed (100 U/ml for 16h) WGA-labeled WT, *Gbp*^{chr3}-KO, *Casp1*$^{-/-}$*Casp11*$^{-/-}$ and *Asc*$^{-/-}$ BMDMs were infected with *F. novicida* at a MOI of 1 in the presence of propidium iodide. Images were recorded every 30 minutes from 3 h PI to 23 h PI. Bright-field (top panels) and WGA (bottom panels) are shown.
(AVI)

Acknowledgments

We thank D. Monack (Stanford University), V. Dixit (Genentech), J. Yuan (Harvard Medical School, Boston) and V. Petrilli (Centre de Recherche en Cancérologie de Lyon, Lyon) for reagents. We acknowledge the contribution of the PBES, flow cytometry and imaging platforms of SFR Biosciences Gerland—Lyon Sud; the Labex GRAL and IBiSA for support to the CMBA platform (Screening center for bioactive molecules—BIG-BGE-Gen&Chem-CMBA, U1038 INSERM/CEA/UGA, CEA-Grenoble, France). This work was performed within the framework of the LABEX ECOFECT of Université de Lyon, within the program "Investissements d'Avenir".

Author Contributions

Conceptualization: Pierre Wallet, Sacha Benaoudia, Anders Sjöstedt, Thomas Henry.

Formal analysis: Pauline Basso, Omran Allatif, Eric Faudry, Thomas Henry.

Funding acquisition: Anders Sjöstedt, Thomas Henry.

Investigation: Pierre Wallet, Sacha Benaoudia, Amandine Mosnier, Brice Lagrange, Amandine Martin, Helena Lindgren, Igor Golovliov, Fanny Michal, Pauline Basso, Sophia Djebali, Angelina Provost, Etienne Meunier.

Methodology: Pauline Basso, Eric Faudry.

Project administration: Anders Sjöstedt, Thomas Henry.

Resources: Petr Broz, Masahiro Yamamoto, Bénédicte F. Py.

Supervision: Petr Broz, Eric Faudry, Anders Sjöstedt, Thomas Henry.

Writing – original draft: Thomas Henry.

Writing – review & editing: Pierre Wallet, Sacha Benaoudia, Thomas Henry.

References

1. MacMicking JD. Interferon-inducible effector mechanisms in cell-autonomous immunity. Nat Rev Immunol. 2012; 12: 367–382. https://doi.org/10.1038/nri3210 PMID: 22531325
2. Pilla-Moffett D, Barber MF, Taylor GA, Coers J. Interferon-Inducible GTPases in Host Resistance, Inflammation and Disease. J Mol Biol. 2016; 428: 3495–3513. https://doi.org/10.1016/j.jmb.2016.04.032 PMID: 27181197
3. Meunier E, Broz P. Interferon-inducible GTPases in cell autonomous and innate immunity. Cell Microbiol. 2016; 18: 168–180. https://doi.org/10.1111/cmi.12546 PMID: 26572694
4. Prakash B, Praefcke GJ, Renault L, Wittinghofer A, Herrmann C. Structure of human guanylate-binding protein 1 representing a unique class of. Nature. 2000; 403: 567–571. https://doi.org/10.1038/35000617 PMID: 10676968
5. Praefcke GJK, McMahon HT. The dynamin superfamily: universal membrane tubulation and fission molecules? Nat Rev Mol Cell Biol. 2004; 5: 133–147. https://doi.org/10.1038/nrm1313 PMID: 15040446
6. Olszewski MA, Gray J, Vestal DJ. In silico genomic analysis of the human and murine guanylate-binding protein (GBP) gene clusters. J Interferon Cytokine Res Off J Int Soc Interferon Cytokine Res. 2006; 26: 328–352. https://doi.org/10.1089/jir.2006.26.328 PMID: 16689661
7. Kresse A, Konermann C, Degrandi D, Beuter-Gunia C, Wuerthner J, Pfeffer K, et al. Analyses of murine GBP homology clusters based on in silico, in vitro and in vivo studies. BMC Genomics. 2008; 9: 158. https://doi.org/10.1186/1471-2164-9-158 PMID: 18402675
8. Yamamoto M, Okuyama M, Ma JS, Kimura T, Kamiyama N, Saiga H, et al. A cluster of interferon-gamma-inducible p65 GTPases plays a critical role in host defense against Toxoplasma gondii. Immunity. 2012; 37: 302–13. https://doi.org/10.1016/j.immuni.2012.06.009 PMID: 22795875
9. Degrandi D, Kravets E, Konermann C, Beuter-Gunia C, Klumpers V, Lahme S, et al. Murine guanylate binding protein 2 (mGBP2) controls Toxoplasma gondii replication. Proc Natl Acad Sci U S A. 2013; 110: 294–299. https://doi.org/10.1073/pnas.1205635110 PMID: 23248289
10. Meunier E, Dick MS, Dreier RF, Schurmann N, Kenzelmann Broz D, Warming S, et al. Caspase-11 activation requires lysis of pathogen-containing vacuoles by IFN-induced GTPases. Nature. 2014; 509: 366–70. https://doi.org/10.1038/nature13157 PMID: 24739961
11. Finethy R, Jorgensen I, Haldar AK, de Zoete MR, Strowig T, Flavell RA, et al. Guanylate Binding Proteins Enable Rapid Activation of Canonical and Noncanonical Inflammasomes in Chlamydia-Infected Macrophages. Infect Immun. 2015; 83: 4740–4749. https://doi.org/10.1128/IAI.00856-15 PMID: 26416908
12. Pilla DM, Hagar JA, Haldar AK, Mason AK, Degrandi D, Pfeffer K, et al. Guanylate binding proteins promote caspase-11-dependent pyroptosis in response to cytoplasmic LPS. Proc Natl Acad Sci U S A. 2014; 111: 6046–51. https://doi.org/10.1073/pnas.1321700111 PMID: 24715728
13. Meunier E, Wallet P, Dreier RF, Costanzo S, Anton L, Ruhl S, et al. Guanylate-binding proteins promote activation of the AIM2 inflammasome during infection with Francisella novicida. Nat Immunol. 2015; 16: 476–484. https://doi.org/10.1038/ni.3119 PMID: 25774716
14. Shenoy AR, Wellington DA, Kumar P, Kassa H, Booth CJ, Cresswell P, et al. GBP5 promotes NLRP3 inflammasome assembly and immunity in mammals. Science. 2012; 336: 481–5. https://doi.org/10.1126/science.1217141 PMID: 22461501
15. Man SM, Karki R, Malireddi RKS, Neale G, Vogel P, Yamamoto M, et al. The transcription factor IRF1 and guanylate-binding proteins target activation of the AIM2 inflammasome by Francisella infection. Nat Immunol. 2015; 16: 467–475. https://doi.org/10.1038/ni.3118 PMID: 25774715
16. Man SM, Karki R, Sasai M, Place DE, Kesavardhana S, Temirov J, et al. IRGB10 Liberates Bacterial Ligands for Sensing by the AIM2 and Caspase-11-NLRP3 Inflammasomes. Cell. 2016; 167: 382–396. e17. https://doi.org/10.1016/j.cell.2016.09.012 PMID: 27693356
17. Martens S, Parvanova I, Zerrahn J, Griffiths G, Schell G, Reichmann G, et al. Disruption of Toxoplasma gondii parasitophorous vacuoles by the mouse p47-resistance GTPases. PLoS Pathog. 2005; 1: e24. https://doi.org/10.1371/journal.ppat.0010024 PMID: 16304607
18. Wallet P, Lagrange B, Henry T. Francisella Inflammasomes: Integrated Responses to a Cytosolic Stealth Bacterium. Curr Top Microbiol Immunol. 2016; 397: 229–256. https://doi.org/10.1007/978-3-319-41171-2_12 PMID: 27460813
19. Golovliov I, Baranov V, Krocova Z, Kovarova H, Sjostedt A. An attenuated strain of the facultative intracellular bacterium Francisella tularensis can escape the phagosome of monocytic cells. Infect Immun. 2003; 71: 5940–50. https://doi.org/10.1128/IAI.71.10.5940-5950.2003 PMID: 14500514
20. Clemens DL, Lee BY, Horwitz MA. Virulent and avirulent strains of Francisella tularensis prevent acidification and maturation of their phagosomes and escape into the cytoplasm in human macrophages. Infect Immun. 2004; 72: 3204–17. https://doi.org/10.1128/IAI.72.6.3204-3217.2004 PMID: 15155622

21. Nano FE, Zhang N, Cowley SC, Klose KE, Cheung KK, Roberts MJ, et al. A Francisella tularensis pathogenicity island required for intramacrophage growth. J Bacteriol. 2004; 186: 6430–6. https://doi.org/10.1128/JB.186.19.6430-6436.2004 PMID: 15375123

22. Lindgren H, Golovliov I, Baranov V, Ernst RK, Telepnev M, Sjostedt A. Factors affecting the escape of Francisella tularensis from the phagolysosome. J Med Microbiol. 2004; 53: 953–8. https://doi.org/10.1099/jmm.0.45685-0 PMID: 15358816

23. Broms JE, Sjostedt A, Lavander M. The Role of the Francisella Tularensis Pathogenicity Island in Type VI Secretion, Intracellular Survival, and Modulation of Host Cell Signaling. Front Microbiol. 2010; 1. https://doi.org/10.3389/fmicb.2010.00136 PMID: 21687753

24. Jones JW, Kayagaki N, Broz P, Henry T, Newton K, O'Rourke K, et al. Absent in melanoma 2 is required for innate immune recognition of Francisella tularensis. Proc Natl Acad Sci U S A. 2010; 107: 9771–6. https://doi.org/10.1073/pnas.1003738107 PMID: 20457908

25. Fernandes-Alnemri T, Yu JW, Juliana C, Solorzano L, Kang S, Wu J, et al. The AIM2 inflammasome is critical for innate immunity to Francisella tularensis. Nat Immunol. 2010; 11: 385–93. https://doi.org/10.1038/ni.1859 PMID: 20351693

26. Rathinam VA, Jiang Z, Waggoner SN, Sharma S, Cole LE, Waggoner L, et al. The AIM2 inflammasome is essential for host defense against cytosolic bacteria and DNA viruses. Nat Immunol. 2010; 11: 395–402. https://doi.org/10.1038/ni.1864 PMID: 20351692

27. Mariathasan S, Weiss DS, Dixit VM, Monack DM. Innate immunity against Francisella tularensis is dependent on the ASC/caspase-1 axis. J Exp Med. 2005; 202: 1043–9. https://doi.org/10.1084/jem.20050977 PMID: 16230474

28. Pierini R, Perret M, Djebali S, Juruj C, Michallet MC, Forster I, et al. ASC Controls IFN-gamma Levels in an IL-18-Dependent Manner in Caspase-1-Deficient Mice Infected with Francisella novicida. J Immunol. 2013; 191: 3847–57. https://doi.org/10.4049/jimmunol.1203326 PMID: 23975862

29. Elkins KL, Rhinehart-Jones TR, Culkin SJ, Yee D, Winegar RK. Minimal requirements for murine resistance to infection with Francisella tularensis LVS. Infect Immun. 1996; 64: 3288–93. PMID: 8757866

30. Elkins KL, Colombini SM, Meierovics AI, Chu MC, Chou AY, Cowley SC. Survival of secondary lethal systemic Francisella LVS challenge depends largely on interferon gamma. Microbes Infect. 2010; 12: 28–36. https://doi.org/10.1016/j.micinf.2009.09.012 PMID: 19781659

31. Sjostedt A, North RJ, Conlan JW. The requirement of tumour necrosis factor-alpha and interferon-gamma for the expression of protective immunity to secondary murine tularaemia depends on the size of the challenge inoculum. Microbiol Read Engl. 1996; 142 (Pt 6): 1369–1374. https://doi.org/10.1099/13500872-142-6-1369 PMID: 8704976

32. Storek KM, Gertsvolf NA, Ohlson MB, Monack DM. cGAS and Ifi204 Cooperate To Produce Type I IFNs in Response to Francisella Infection. J Immunol Baltim Md 1950. 2015; 194: 3236–3245. https://doi.org/10.4049/jimmunol.1402764 PMID: 25710914

33. Wei L, Fan M, Xu L, Heinrich K, Berry MW, Homayouni R, et al. Bioinformatic analysis reveals cRel as a regulator of a subset of interferon-stimulated genes. J Interferon Cytokine Res Off J Int Soc Interferon Cytokine Res. 2008; 28: 541–551. https://doi.org/10.1089/jir.2007.0136 PMID: 18715197

34. Degrandi D, Konermann C, Beuter-Gunia C, Kresse A, Wurthner J, Kurig S, et al. Extensive characterization of IFN-induced GTPases mGBP1 to mGBP10 involved in host defense. J Immunol Baltim Md 1950. 2007; 179: 7729–7740.

35. Pierini R, Juruj C, Perret M, Jones CL, Mangeot P, Weiss DS, et al. AIM2/ASC triggers caspase-8-dependent apoptosis in Francisella-infected caspase-1-deficient macrophages. Cell Death Differ. 2012; 19: 1709–21. https://doi.org/10.1038/cdd.2012.51 PMID: 22555457

36. Hagar JA, Powell DA, Aachoui Y, Ernst RK, Miao EA. Cytoplasmic LPS activates caspase-11: implications in TLR4-independent endotoxic shock. Science. 2013; 341: 1250–3. https://doi.org/10.1126/science.1240988 PMID: 24031018

37. Kayagaki N, Warming S, Lamkanfi M, Vande Walle L, Louie S, Dong J, et al. Non-canonical inflammasome activation targets caspase-11. Nature. 2011; 479: 117–21. https://doi.org/10.1038/nature10558 PMID: 22002608

38. Sagulenko V, Thygesen SJ, Sester DP, Idris A, Cridland JA, Vajjhala PR, et al. AIM2 and NLRP3 inflammasomes activate both apoptotic and pyroptotic death pathways via ASC. Cell Death Differ. 2013;Epub 2013 May 3: 1–12.

39. Fink SL, Cookson BT. Caspase-1-dependent pore formation during pyroptosis leads to osmotic lysis of infected host macrophages. Cell Microbiol. 2006; 8: 1812–25. https://doi.org/10.1111/j.1462-5822.2006.00751.x PMID: 16824040

40. Mariathasan S, Weiss DS, Newton K, McBride J, O'Rourke K, Roose-Girma M, et al. Cryopyrin activates the inflammasome in response to toxins and ATP. Nature. 2006; 440: 228–32. https://doi.org/10.1038/nature04515 PMID: 16407890

41. Pardo J, Urban C, Galvez EM, Ekert PG, Muller U, Kwon-Chung J, et al. The mitochondrial protein Bak is pivotal for gliotoxin-induced apoptosis and a critical host factor of Aspergillus fumigatus virulence in mice. J Cell Biol. 2006; 174: 509–19. https://doi.org/10.1083/jcb.200604044 PMID: 16893972

42. Mishra BB, Rathinam VAK, Martens GW, Martinot AJ, Kornfeld H, Fitzgerald KA, et al. Nitric oxide controls the immunopathology of tuberculosis by inhibiting NLRP3 inflammasome-dependent processing of IL-1beta. Nat Immunol. 2013; 14: 52–60. https://doi.org/10.1038/ni.2474 PMID: 23160153

43. Hernandez-Cuellar E, Tsuchiya K, Hara H, Fang R, Sakai S, Kawamura I, et al. Cutting edge: nitric oxide inhibits the NLRP3 inflammasome. J Immunol Baltim Md 1950. 2012; 189: 5113–5117. https://doi.org/10.4049/jimmunol.1202479 PMID: 23100513

44. Galluzzi L, Aaronson SA, Abrams J, Alnemri ES, Andrews DW, Baehrecke EH, et al. Guidelines for the use and interpretation of assays for monitoring cell death in higher eukaryotes. Cell Death Differ. 2009; 16: 1093–107. https://doi.org/10.1038/cdd.2009.44 PMID: 19373242

45. Edwards JA, Rockx-Brouwer D, Nair V, Celli J. Restricted cytosolic growth of Francisella tularensis subsp. tularensis by IFN-{gamma} activation of macrophages. Microbiology. 2009; Available: http://www.ncbi.nlm.nih.gov/entrez/query.fcgi?cmd=Retrieve&db=PubMed&dopt=Citation&list_uids=19926654

46. Kim BH, Shenoy AR, Kumar P, Das R, Tiwari S, MacMicking JD. A family of IFN-gamma-inducible 65-kD GTPases protects against bacterial infection. Science. 2011; 332: 717–21. https://doi.org/10.1126/science.1201711 PMID: 21551061

47. del Barrio L, Sahoo M, Lantier L, Reynolds JM, Ceballos-Olvera I, Re F. Production of anti-LPS IgM by B1a B cells depends on IL-1beta and is protective against lung infection with Francisella tularensis LVS. PLoS Pathog. 2015; 11: e1004706. https://doi.org/10.1371/journal.ppat.1004706 PMID: 25768794

48. Kim B-H, Chee JD, Bradfield CJ, Park E-S, Kumar P, MacMicking JD. Interferon-induced guanylate-binding proteins in inflammasome activation and host defense. Nat Immunol. 2016; 17: 481–489. https://doi.org/10.1038/ni.3440 PMID: 27092805

49. Tyrkalska SD, Candel S, Angosto D, Gomez-Abellan V, Martin-Sanchez F, Garcia-Moreno D, et al. Neutrophils mediate Salmonella Typhimurium clearance through the GBP4 inflammasome-dependent production of prostaglandins. Nat Commun. 2016; 7: 12077. https://doi.org/10.1038/ncomms12077 PMID: 27363812

50. Morrone SR, Matyszewski M, Yu X, Delannoy M, Egelman EH, Sohn J. Assembly-driven activation of the AIM2 foreign-dsDNA sensor provides a polymerization template for downstream ASC. Nat Commun. 2015; 6: 7827. https://doi.org/10.1038/ncomms8827 PMID: 26197926

51. Jin T, Perry A, Jiang J, Smith P, Curry JA, Unterholzner L, et al. Structures of the HIN domain:DNA complexes reveal ligand binding and activation mechanisms of the AIM2 inflammasome and IFI16 receptor. Immunity. 2012; 36: 561–71. https://doi.org/10.1016/j.immuni.2012.02.014 PMID: 22483801

52. Periasamy S, Le HT, Duffy EB, Chin H, Harton JA. Inflammasome-Independent NLRP3 Restriction of a Protective Early Neutrophil Response to Pulmonary Tularemia. PLoS Pathog. 2016; 12: e1006059. https://doi.org/10.1371/journal.ppat.1006059 PMID: 27926940

53. Theisen E, Sauer J-D. Listeria monocytogenes and the Inflammasome: From Cytosolic Bacteriolysis to Tumor Immunotherapy. Curr Top Microbiol Immunol. 2016; 397: 133–160. https://doi.org/10.1007/978-3-319-41171-2_7 PMID: 27460808

54. Crowley SM, Knodler LA, Vallance BA. Salmonella and the Inflammasome: Battle for Intracellular Dominance. Curr Top Microbiol Immunol. 2016; 397: 43–67. https://doi.org/10.1007/978-3-319-41171-2_3 PMID: 27460804

55. Tattoli I, Lembo-Fazio L, Nigro G, Carneiro LAM, Ferraro E, Rossi G, et al. Intracellular bacteriolysis triggers a massive apoptotic cell death in Shigella-infected epithelial cells. Microbes Infect. 2008; 10: 1114–1123. https://doi.org/10.1016/j.micinf.2008.06.004 PMID: 18606244

56. Kantari C, Walczak H. Caspase-8 and bid: caught in the act between death receptors and mitochondria. Biochim Biophys Acta. 2011; 1813: 558–63. https://doi.org/10.1016/j.bbamcr.2011.01.026 PMID: 21295084

57. Carneiro LAM, Travassos LH, Soares F, Tattoli I, Magalhaes JG, Bozza MT, et al. Shigella induces mitochondrial dysfunction and cell death in nonmyeloid cells. Cell Host Microbe. 2009; 5: 123–136. https://doi.org/10.1016/j.chom.2008.12.011 PMID: 19218084

58. Zhao YO, Khaminets A, Hunn JP, Howard JC. Disruption of the Toxoplasma gondii parasitophorous vacuole by IFNgamma-inducible immunity-related GTPases (IRG proteins) triggers necrotic cell death. PLoS Pathog. 2009; 5: e1000288. https://doi.org/10.1371/journal.ppat.1000288 PMID: 19197351

59. Thurston TLM, Matthews SA, Jennings E, Alix E, Shao F, Shenoy AR, et al. Growth inhibition of cytosolic Salmonella by caspase-1 and caspase-11 precedes host cell death. Nat Commun. 2016; 7: 13292. https://doi.org/10.1038/ncomms13292 PMID: 27808091

60. Bekpen C, Hunn JP, Rohde C, Parvanova I, Guethlein L, Dunn DM, et al. The interferon-inducible p47 (IRG) GTPases in vertebrates: loss of the cell autonomous resistance mechanism in the human lineage. Genome Biol. 2005; 6: R92. https://doi.org/10.1186/gb-2005-6-11-r92 PMID: 16277747

61. Weiss DS, Brotcke A, Henry T, Margolis JJ, Chan K, Monack DM. In vivo negative selection screen identifies genes required for Francisella virulence. Proc Natl Acad Sci U A. 2007; 104: 6037–42.

62. Kuoppa K, Forsberg A, Norqvist A. Construction of a reporter plasmid for screening in vivo promoter activity in Francisella tularensis. FEMS Microbiol Lett. 2001; 205: 77–81. PMID: 11728719

63. Henry T, Brotcke A, Weiss DS, Thompson LJ, Monack DM. Type I interferon signaling is required for activation of the inflammasome during Francisella infection. J Exp Med. 2007; 204: 987–94. https://doi.org/10.1084/jem.20062665 PMID: 17452523

64. Basso P, Wallet P, Elsen S, Soleilhac E, Henry T, Faudry E, et al. Multiple Pseudomonas species secrete exolysin-like toxins and provoke Caspase-1-dependent macrophage death. Environ Microbiol. 2017; https://doi.org/10.1111/1462-2920.13841 PMID: 28654176

S1 Materials and Methods

CCF4 measurements. Quantification of escape from vacuoles with the β-lactamase–CCF4 assay was performed following manufacturer's instructions (Life Technologies) as previously described [1]. The β-lactamase (Δ*bla*) mutant deleted in the FTN_1072 gene was previously described [2]. Macrophages seeded onto non-treated plates were infected for 1 h then were washed and then incubated for 1 h at room temperature in CCF4 in the presence of 2.5 mM probenicid (Sigma). The quantification of cells containing cytosolic *F. novicida* was performed on propidium iodide-negative (live) cells with excitation at 405 nm and detection at 450 nm (cleaved CCF4) or 510 nm (intact CCF4) by Flow cytometry.

SCHU S4 infection. Infection with *F. tularensis* SCHU S4 strain was performed in BSL3 laboratory as previously described [3] with the following modifications: BMDMs were used instead of Peritoneal exudate cells and a MOI of 0.4 was used.

Real-time PCR. The following primers were used for mRNA quantification: mAIM2 Forward (F): 5'AGTACCGGGAAATGCTGTTG3', mAIM2 Reverse (R): 5'GCACCTGCACTTTGAATCAG3', mNLRP3 F: 5'CCCTTGGAGACACAGGACTC3', mNLRP3 R: 5'GAGGCTGCAGTTGTCTAATTCC3', mMEFV F: 5'GGAGATGAGGGGATATGTGG3', mMEFV R: 5'TGGATTTCTGTTTGTTTCAGGA3', mCaspase-11 F: 5'TCCAGACATTCTTCAGTGTGGA3', mCaspase-11R: 5'TCTGGTTCCTCCATTTCCAG3', mβ-Actin F: 5'GTGGATCAGCAAGCAGGAGT3', mβ-Actin R: 5'AGGGTGTAAAACGCAGCTCA3'. Experiments were performed with an iCycler (Bio-Rad) using SYBR green (Applied Biosystems) and standard protocols.

CRISPR/Cas9-mediated Knock-out. J774.1 murine macrophage-like cells were transduced using lentiviral particles produced in 293T cells using the plasmid LentiCas9-Blast (Gift from Feng Zhang, Addgene plasmid # 52962). Blasticidin selection was applied and clones were isolated by limit dilution method. A high Cas9-expressing clone was selected and transduced with lentiviral particles packaged with the pKLV-U6gRNA(BbsI)-PGKpuro2ABFP plasmid (Gift from Kosuke Yusa, Addgene plasmid # 50946). Two pairs of gRNAs (as indicated in the table below) were used for each knock-out. gRNA-expressing J774.1 cells were selected for 10 days in puromycin. Control experiments targeting GFP routinely give >90% of the cells demonstrating efficient knock-out. Production of lentiviral particle was performed in 293T cells by co-transfection of the following plasmids: pMD2.G

(Gift from Didier Trono, Addgene plasmid #12259), psPAX2 (Gift from Didier Trono, Addgene plasmid #12260), and LentiCas9-Blast or pKLV-U6gRNA(BbsI)-PGKpuro2ABFP.

		Sens	Antisens
GBP2	gRNA 1	AAAGTTCCAGACAGAATTAG	CTAATTCTGTCTGGAACTTT
	gRNA 2	TCTTCTGTCAAGACTCTGTG	CACAGAGTCTTGACAGAAGA
GBP5	gRNA 1	ACACAGTAGTAACCTTGGCC	GGCCAAGGTTACTACTGTGT
	gRNA 2	CTCAAACATTCAATCTACCG	CGGTAGATTGAATGTTTGAG
GBP1/2b	gRNA 1	CAAACTAGAGTGGATACAG G	CCTGTATCCACTCTAGTTTG
	gRNA 2	TGCTATCCAAAATCCTGTGG	CCACAGGATTTTGGATAGCA
Asc	gRNA 1	CAGCTGCAAACGACTAAAG A	TCTTTAGTCGTTTGCAGCTG
	gRNA 2	CGCTCTTGAAAACTTGTCAG	CTGACAAGTTTTCAAGAGCG
gNT (non targeting)	gRNA 1	GTTCGCGGGGGCTTCTATCA	TGATAGAAGCCCCCGCGAAC
	gRNA 2	TAACACGCACTCACGTCCGG	CCGGACGTGAGTGCGTGTTA

Supplemental references:

1. Juruj C, V L, Pierini R, Perret M, Py BF, jamilloux Y, et al. caspase-1 activity affects AIM2 speck formation/ stability through a negative feedback loop. Front Cell Infect Microbiol. 2013; 1–11.

2. Rigard M, Broms JE, Mosnier A, Hologne M, Martin A, Lindgren L, et al. Francisella tularensis IglG Belongs to a Novel Family of PAAR-Like T6SS Proteins and Harbors a Unique N-terminal Extension Required for Virulence. PLoS Pathog. 2016;12: e1005821. doi:10.1371/journal.ppat.1005821

3. Lindgren H, Stenman L, Tarnvik A, Sjostedt A. The contribution of reactive nitrogen and oxygen species to the killing of Francisella tularensis LVS by murine macrophages. Microbes Infect Inst Pasteur. 2005;7: 467–75. doi:10.1016/j.micinf.2004.11.020

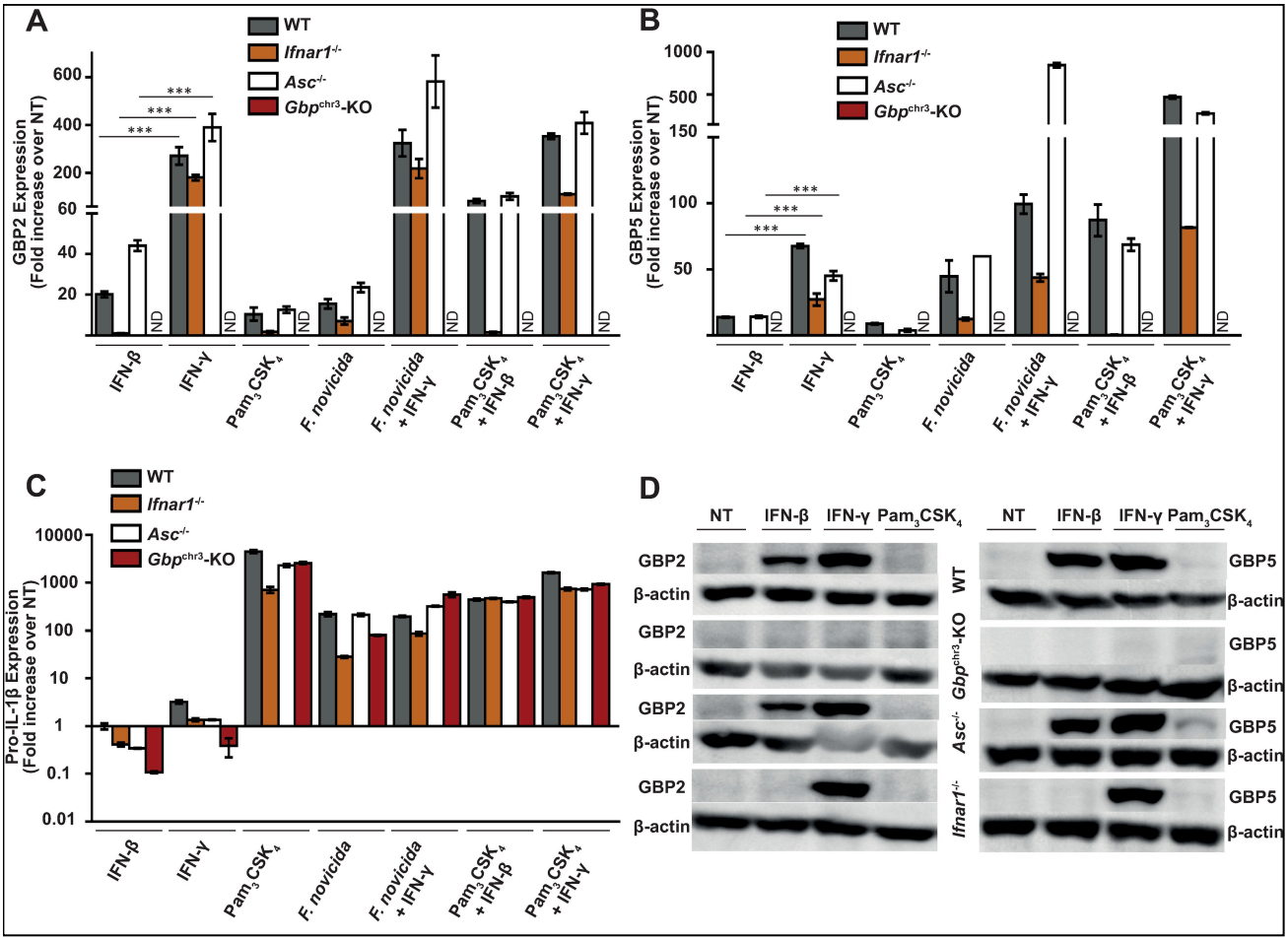

S1 Fig. IFN-γ priming induces a quantitative shift in GBPs levels.
(A) GBP2, (B) GBP5 (C) ProIL-1β mRNA levels, (D) GBP2, GBP5 and β-actin protein levels were analyzed by qRT-PCR (A-C) or western blotting analysis (D) in BMDMs from the indicated genotypes infected with *F. novicida* at a MOI of 10 for 4 h or treated for 16 h with 100 U/ml of IFN-β, IFN-γ or 100 ng/ml of Pam3CSK4 (NT: not treated). (A-B) One-way ANOVA analysis was performed with Tukey's correction to compare GBP induction following IFN-β and IFN-γ priming. (A-D) One experiment representative of two independent experiments, (A-C) mean and standard deviations are shown.

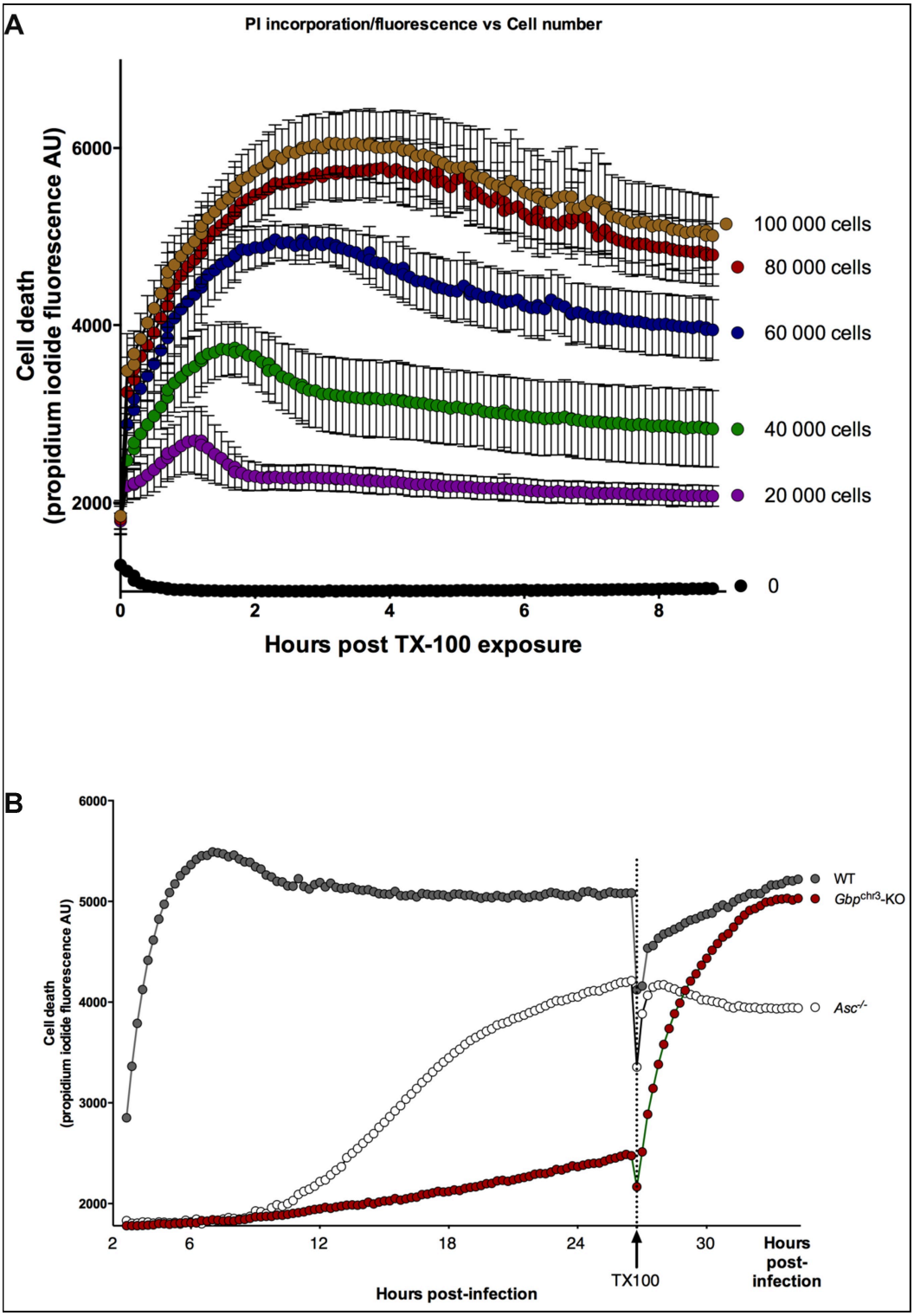

S2 Fig. Controls related to the real time measurement of propidium iodide incorporation/ fluorescence.
(A) WT BMDMs were seeded at different cell density as indicated and treated with Triton X100 (1% v/v final) in the presence of propidium iodide. Cell death was analyzed in real time by quantifying propidium iodide fluorescence every 5 minutes. (B) IFN-γ-primed BMDMs from the indicated genotypes were infected with *F. novicida* at a MOI of 10. Cell death was analyzed by quantifying propidium iodide fluorescence every 15 minutes. At 26 h post-infection, TX-100 (1% v/v final) was added leading to a strong increase in fluorescence in Gbpchr3-KO BMDMs but not in WT nor Asc-/- BMDMs confirming that most Gbpchr3-KO BMDMs had an intact (propidium iodide-impermeant) plasma membrane before TX-100 addition in contrast to most WT and Asc-/- BMDMs. One experiment representative of two (A) to at least three (B) independent experiments is shown

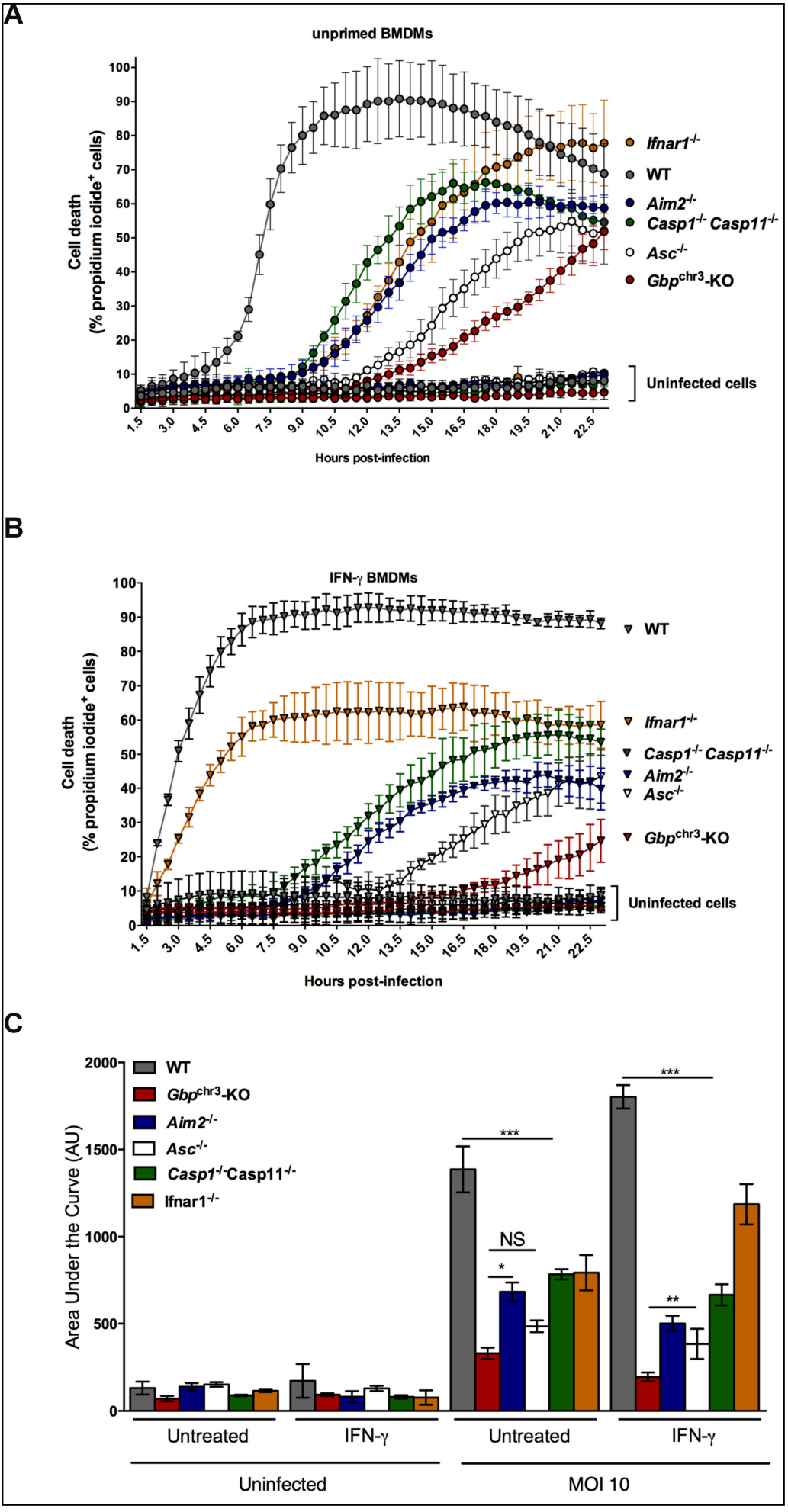
A
unprimed BMDMs
Cell death
(% propidium iodide+ cells)
Hours post-infection
Ifnar1-/-
WT
Aim2-/-
Casp1-/- Casp11-/-
Asc-/-
Gbpchr3-KO
Uninfected cells
B
IFN-γ BMDMs
Cell death
(% propidium iodide+ cells)
Hours post-infection
WT
Ifnar1-/-
Casp1-/- Casp11-/-
Aim2-/-
Asc-/-
Gbpchr3-KO
Uninfected cells
C
Area Under the Curve (AU)
WT
Gbpchr3-KO
Aim2-/-
Asc-/-
Casp1-/-Casp11-/-
Ifnar1-/-
***
NS
*
***
**
Untreated
IFN-γ
Untreated
IFN-γ
Uninfected
MOI 10

S3 Fig. Time-lapse microscopy demonstrates that *F. novicida*-infected BMDMs trigger, in a hierarchical manner, various GBPs-dependent cell death pathways.
(A,B) Cell death was monitored at single cell level and in real time using automated microscopy and propidium iodide. BMDMs of the indicated genotypes were primed (B) or not (A) with rIFN-γ (100 U/ml) for 16h before infection with *F. novicida* at an MOI of 10. Automated image analysis was used to quantify the percentage of dead cells at each time points of the kinetics. (C) The area under the curve (corresponding to the above kinetics from 1.5 to 20 h post-infection) was computed. One-way ANOVA analysis was performed with Tukey's correction. (A-C) One experiment representative of two independent experiments is shown.

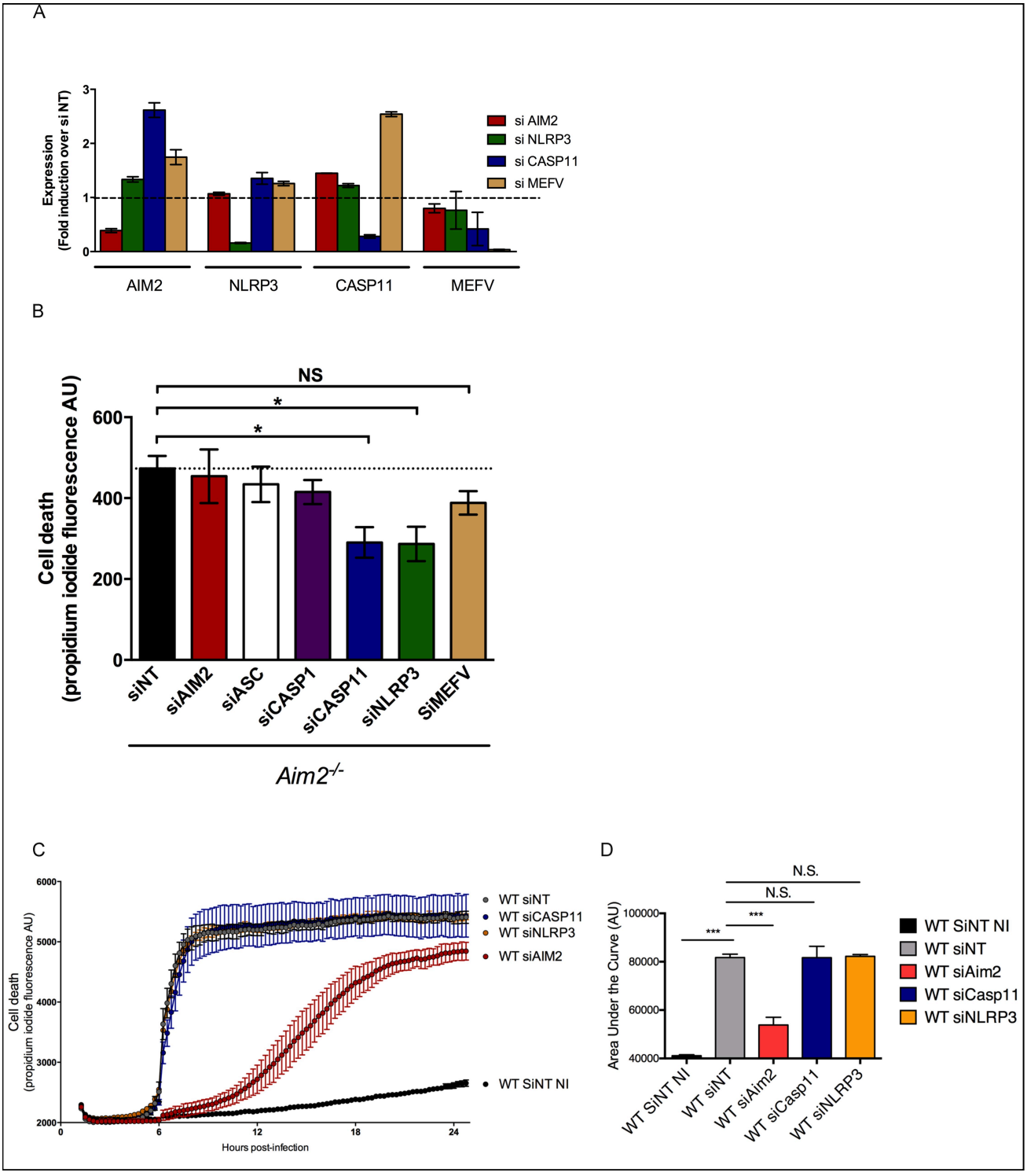

S4 Fig. Knock-down of the expression of inflammasome components demonstrated hierarchical activation of several cell death pathways.
(A) Knock-down efficiency and specificity was determined by qRT-PCR at 48 h post-transfection in BMDMs. The specific transcript levels were normalized to β-actin transcript level and rationalized with the corresponding transcript level in BMDMs treated with a non-targeting (NT) siRNA. (B) Aim2-/- BMDMs transfected with the indicated siRNA were infected with *F. novicida* at a MOI of 10 and cell death was monitored by measuring propidium iodide fluorescence at 17 h PI. (C) WT BMDMs transfected with the indicated siRNA were infected with *F. novicida* at a MOI of 10 and cell death was monitored in real time by measuring propidium iodide fluorescence. (D) The area under the curve corresponding to the (C) kinetics from 1 to 20h is shown. NI: Non-infected. (B-D) One-way ANOVA analysis was performed with Tukey's correction. (A-D) One experiment representative of three independent experiments is shown.

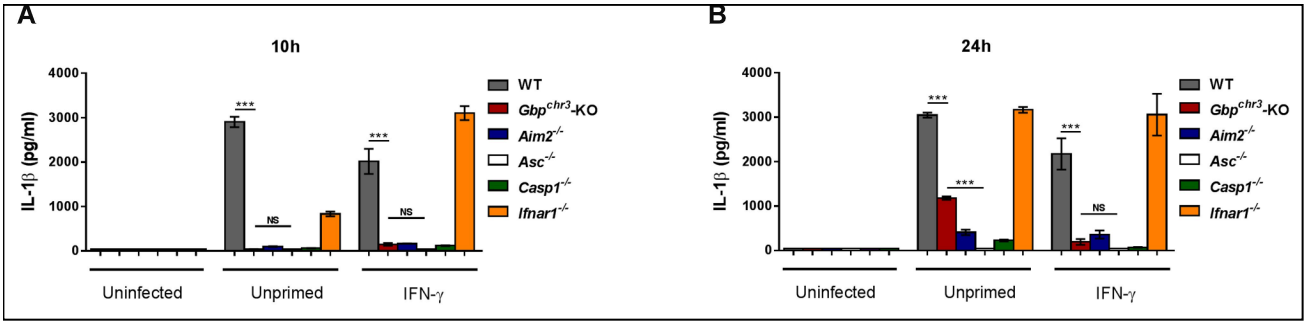

S5 Fig. IFN-γ modulates the kinetics of IL-1ß release in Gbpchr3-KO BMDMs.
BMDMs from the indicated genotypes were infected or not with *F. novicida* at a MOI of 10 after priming or not with IFN-γ (100u / ml 16 h). At 10 h post-infection (A) or 24 h post-infection (B) IL-1ß concentrations were determined by ELISA. One experiment representative of three independent experiments with mean and standard deviations is shown. One-way ANOVA analysis was performed with Tukey's correction.

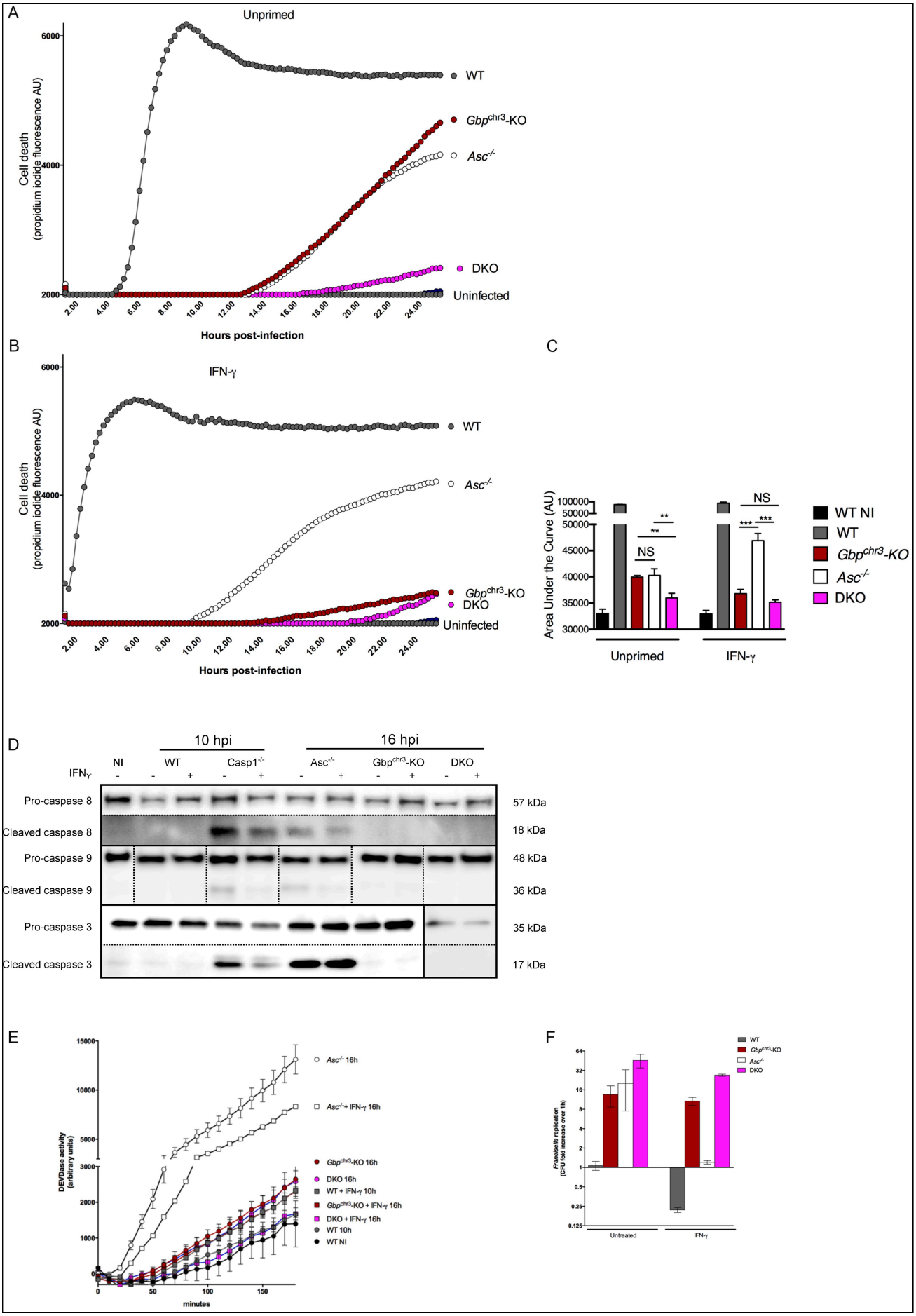
A
Unprimed
Cell death
(propidium iodide fluorescence AU)
6000
4000
2000
WT
Gbpchr3-KO
Asc-/-
DKO
Uninfected
2.00
4.00
6.00
8.00
10.00
12.00
14.00
16.00
18.00
20.00
22.00
24.00
Hours post-infection
B
IFN-γ
Cell death
(propidium iodide fluorescence AU)
6000
4000
2000
WT
Asc-/-
Gbpchr3-KO
DKO
Uninfected
Hours post-infection
C
Area Under the Curve (AU)
100000
50000
50000
45000
40000
35000
30000
**
**
NS
NS
***
***
Unprimed
IFN-γ
WT NI
WT
Gbpchr3-KO
Asc-/-
DKO
D
10 hpi
16 hpi
NI
WT
Casp1-/-
Asc-/-
Gbpchr3-KO
DKO
IFNγ
Pro-caspase 8
Cleaved caspase 8
Pro-caspase 9
Cleaved caspase 9
Pro-caspase 3
Cleaved caspase 3
57 kDa
18 kDa
48 kDa
36 kDa
35 kDa
17 kDa
E
DEVDase activity
(arbitrary units)
15000
10000
5000
3000
2000
1000
0
0
50
100
150
minutes
Asc-/- 16h
Asc-/- + IFN-γ 16h
Gbpchr3-KO 16h
DKO 16h
WT + IFN-γ 10h
Gbpchr3-KO + IFN-γ 16h
DKO + IFN-γ 16h
WT 10h
WT NI
F
Francisella replication
(CFU fold increase over 1h)
64
32
16
8
4
2
1
0.5
0.25
0.125
Untreated
IFN-γ
WT
Gbpchr3-KO
Asc-/-
DKO

S6 Fig. Comparison of the responses of macrophages doubly deficient in Asc and Gbpchr3 with that of macrophages with single deficiencies demonstrates that GBP and ASC control different pathways.
BMDMs from the indicated genotypes (DKO corresponds to Asc-/- GbpChr3-KO doubly-deficient macrophages) were infected or not with *F. novicida* at a MOI of 10 after priming (B) or not (A) with IFN-γ (100 U/ml, 16 h). (A, B) Real time propidium incorporation/ fluorescence, (C) area under the curve corresponding to the kinetics in A and B, (D) apoptotic caspases processing analysis by Western blotting, (E) DEVDase activity as determined using a fluorogenic caspase-3 substrate and (F) bacterial replication assay by CFU are shown. (C) The dotted vertical lines in Casp9 Western blot illustrate that the samples from a single original Western blot gel/ image were reorganized to fit the indicated order without any other image manipulation. The plain vertical line in Casp-3 Western blot illustrates that the samples from two Western blot gels run and analyzed side by side with the same exposure time are presented. The dotted horizontal lines in Casp8 and Casp3 Western blot indicate images from two different exposure times or from the use of two different primary antibodies (pro- and cleaved Casp3), respectively. The Western blots presented correspond to the ones presented in Fig 4D of the main manuscript. (A, B, C) one experiment representative of two independent experiments is shown. (C) One way ANOVA analysis with Tukey's correction for multiple tests was performed. (D-F) One experiment is shown. Mean and standard deviations are shown.

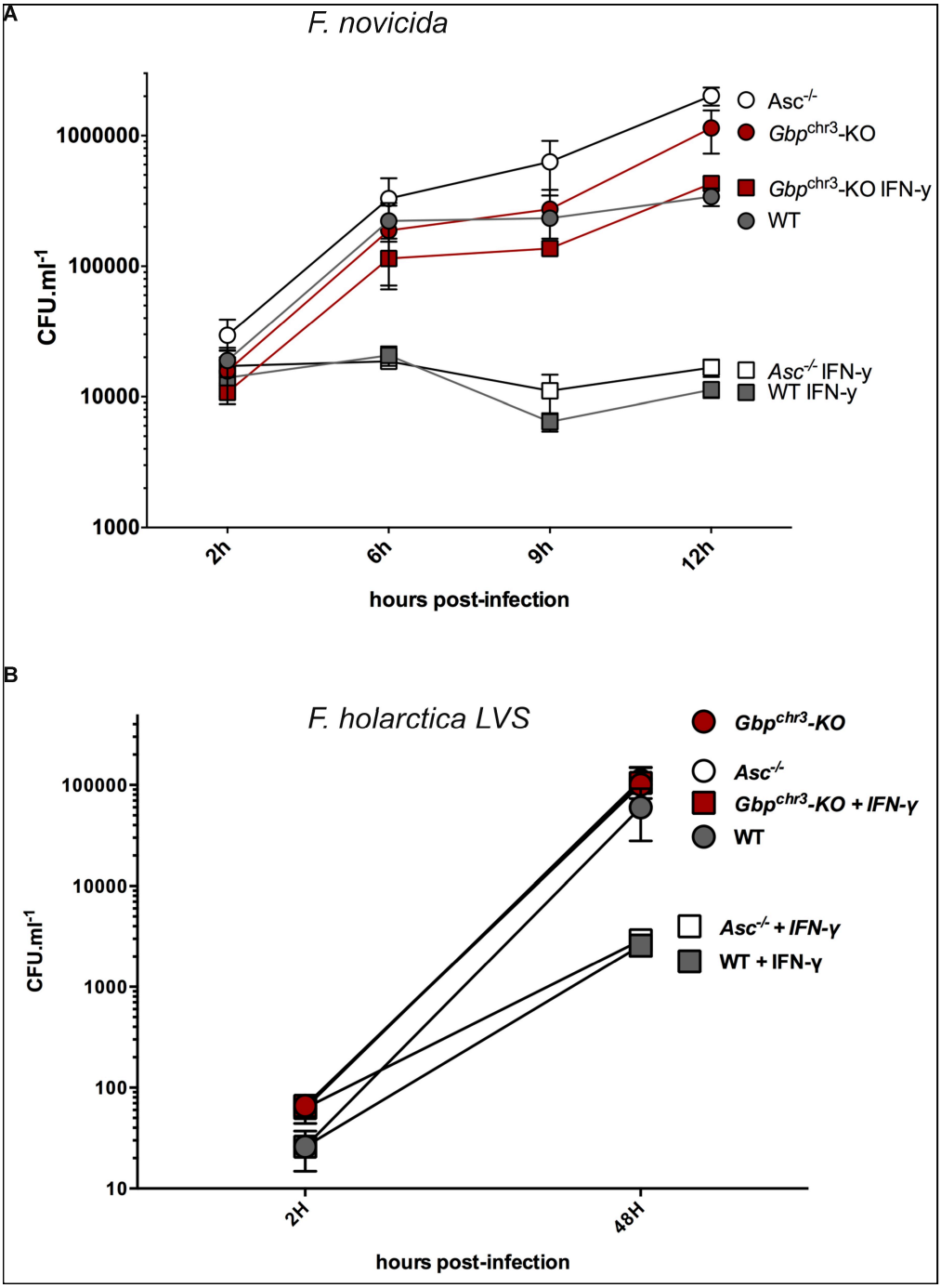

S7 Fig. IFN-γ-induced GBPs control intracellular bacterial replication.
(A-B) BMDMs from the indicated genotypes were primed or not overnight with 100 U/ml of IFN-γ. BMDMs were infected with (A) *F. novicida* or (B) F. tularensis LVS at a multiplicity of infection (MOI) of 1 and 0.4, respectively. Intracellular bacterial burden was assessed by determination of viable counts at the indicated times post-infection. The corresponding data expressed as Fold increase are presented in Fig 5.

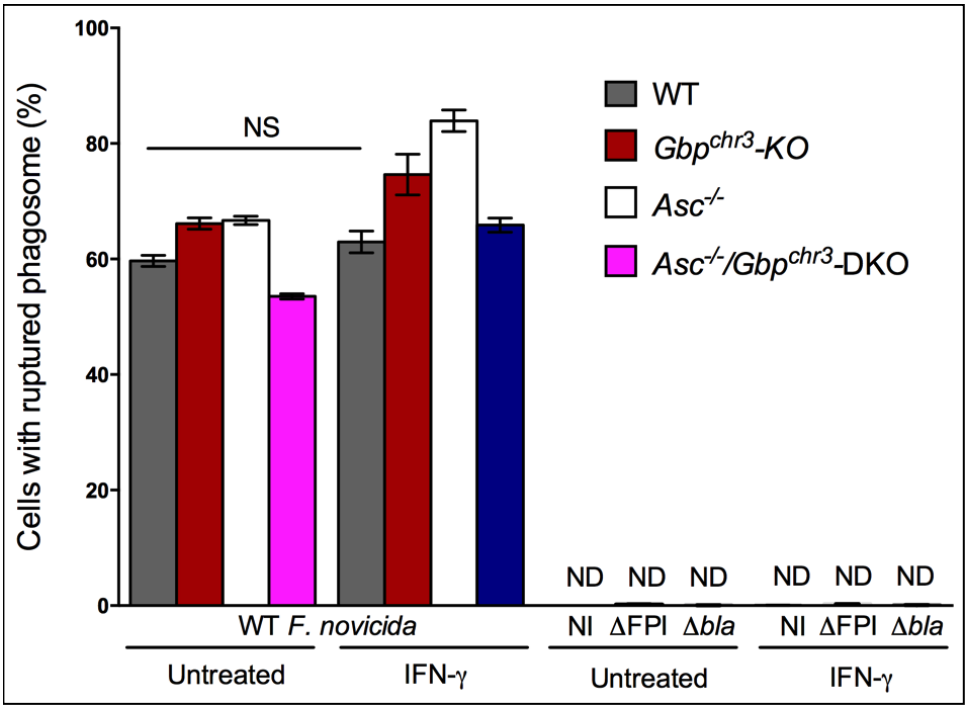

S8 Fig. IFN-γ does not modify substantially phagosomal rupture.
BMDMs from the indicated genotypes were primed or not with 100 U/ml of IFN-γ for 16 h. BMDMs were infected with the indicated *F. novicida* strains at a multiplicity of infection (MOI) of 10. At 2 h post-infection, cells were incubated with the FRET substrate CCF4. Cytosolic ß-lactamase-mediated CCF4 hydrolysis (a marker of phagosomal permeabilization) was analysed by flow cytometry after gating on live (propidium iodide negative) cells. One experiment representative of two independent experiments is shown. One-way ANOVA analysis was performed with Tukey's correction.

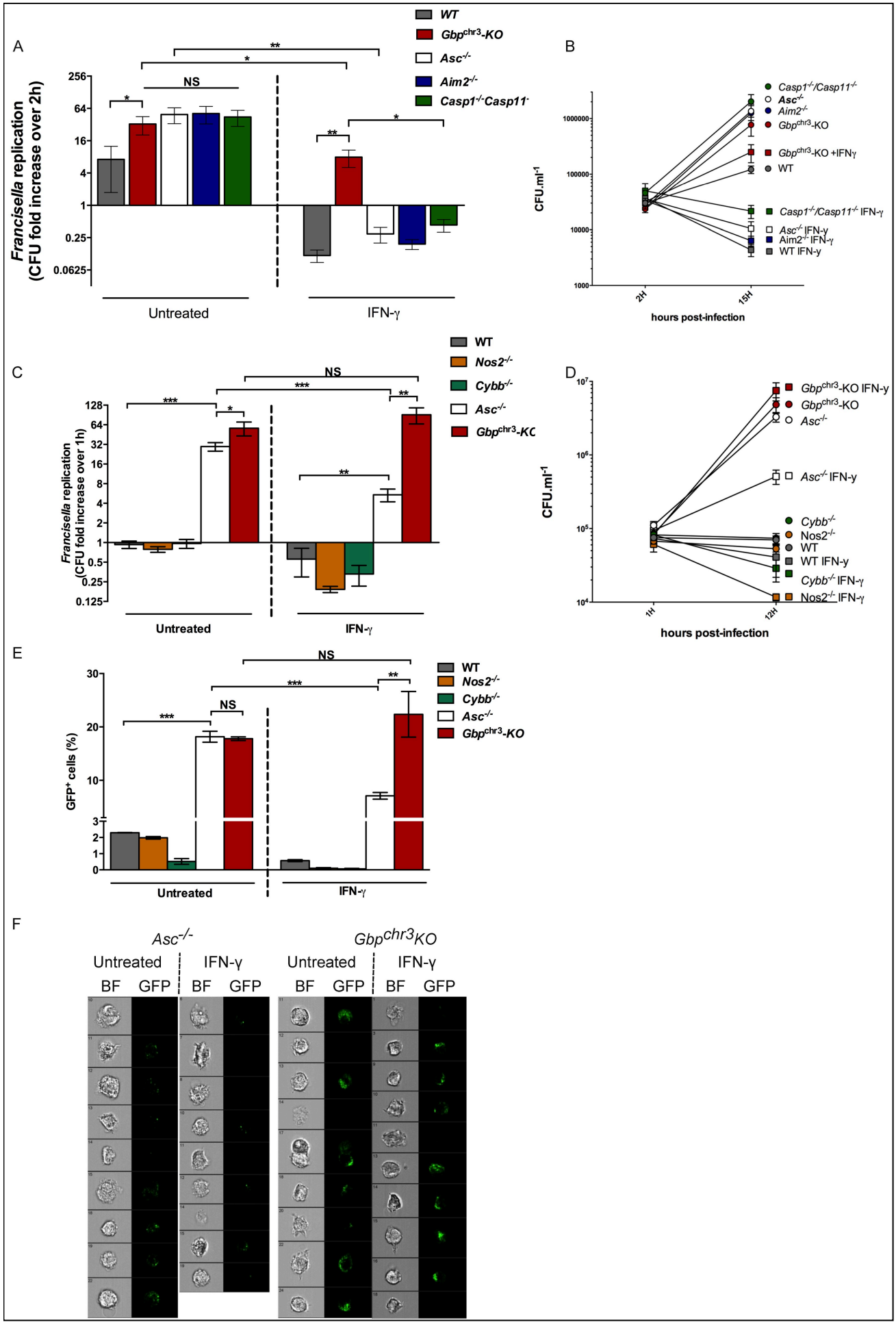
A
WT
Gbpchr3-KO
Asc-/-
Aim2-/-
Casp1-/-Casp11-
Francisella replication (CFU fold increase over 2h)
256
64
16
4
1
0.25
0.0625
NS
*
**
Untreated
IFN-γ
B
Casp1-/-/Casp11-/-
Asc-/-
Aim2-/-
Gbpchr3-KO
Gbpchr3-KO +IFNγ
WT
Casp1-/-/Casp11-/- IFN-γ
Asc-/- IFN-γ
Aim2-/- IFN-γ
WT IFN-γ
CFU.ml-1
1000000
100000
10000
1000
2H
15H
hours post-infection
C
WT
Nos2-/-
Cybb-/-
Asc-/-
Gbpchr3-KC
Francisella replication (CFU fold increase over 1h)
128
64
32
16
8
4
2
1
0.5
0.25
0.125
NS
***
**
*
Untreated
IFN-γ
D
Gbpchr3-KO IFN-γ
Gbpchr3-KO
Asc-/-
Asc-/- IFN-γ
Cybb-/-
Nos2-/-
WT
WT IFN-γ
Cybb-/- IFN-γ
Nos2-/- IFN-γ
CFU.ml-1
1H
12H
hours post-infection
E
WT
Nos2-/-
Cybb-/-
Asc-/-
Gbpchr3-KO
GFP+ cells (%)
30
20
10
3
2
1
0
NS
***
**
Untreated
IFN-γ
F
Asc-/-
Gbpchr3KO
Untreated
IFN-γ
BF
GFP

S9 Fig. IFN-γ-induced GBPs control bacterial killing independently of inflammasomes, the NADPH oxidase and iNOS.
(A-E) BMDMs from the indicated genotypes were primed or not overnight with IFN-γ (100 U/ml) and infected at a MOI of 1 with *F. novicida* (A-D) or at a MOI of 10 with GFP-expressing *F. novicida* (E). (A, D) Intracellular bacterial burden was assessed by determination of viable counts at 12 h. (A, C) Results were normalized with the viable counts detected at 2 h post-infection. The corresponding Raw data are presented in (B, D). (E) Flow cytometry-based quantification of infected (GFP+) cells among live BMDMs at 10 h post-infection. (F) Sample ImageStreamX images of BMDMs from the indicated genotypes, treated or not for 16 h with IFN-γ (100 U/ml) and infected at a MOI of 10 with GFP-expressing *F. novicida*.

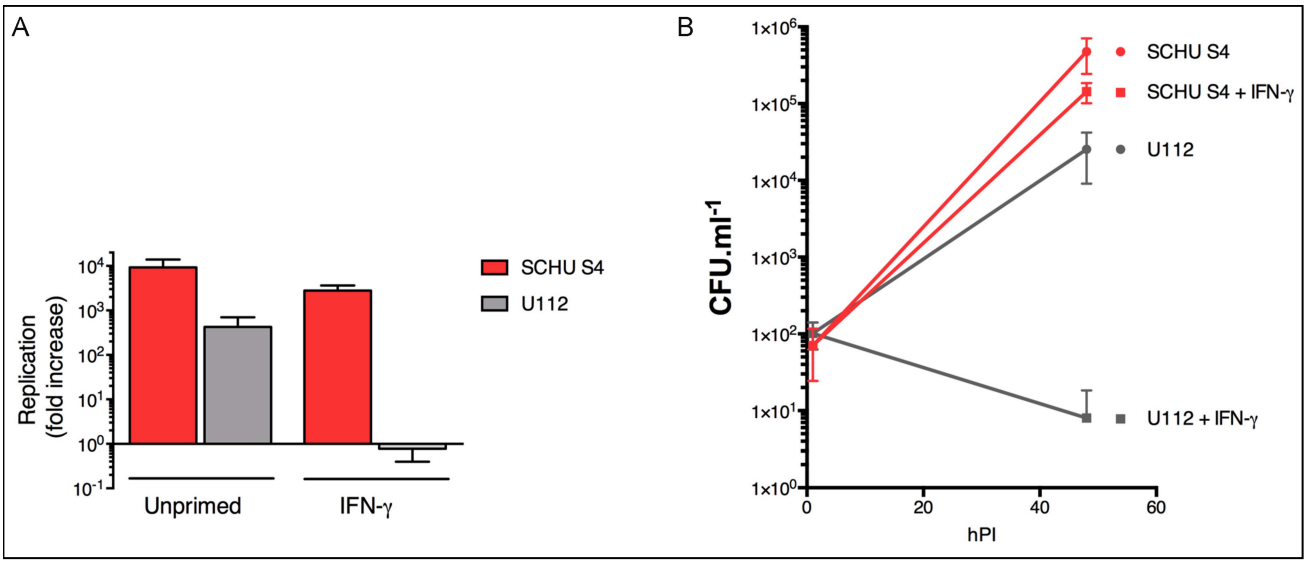

S10 Fig. Highly virulent F. tularensis SCHU S4 strain largely escapes IFN-γ-mediated growth restriction in BMDMs.
WT BMDMs primed or not overnight with IFN-γ (100 U/ml) were infected at a MOI of 0.4 with F. tularensis SCHU S4 or *F. novicida* U112. Intracellular bacterial burden was assessed by determination of viable counts at 48 h. (A) Results were normalized with the viable counts detected at 2 h post-infection. (B) The corresponding Raw data are presented.

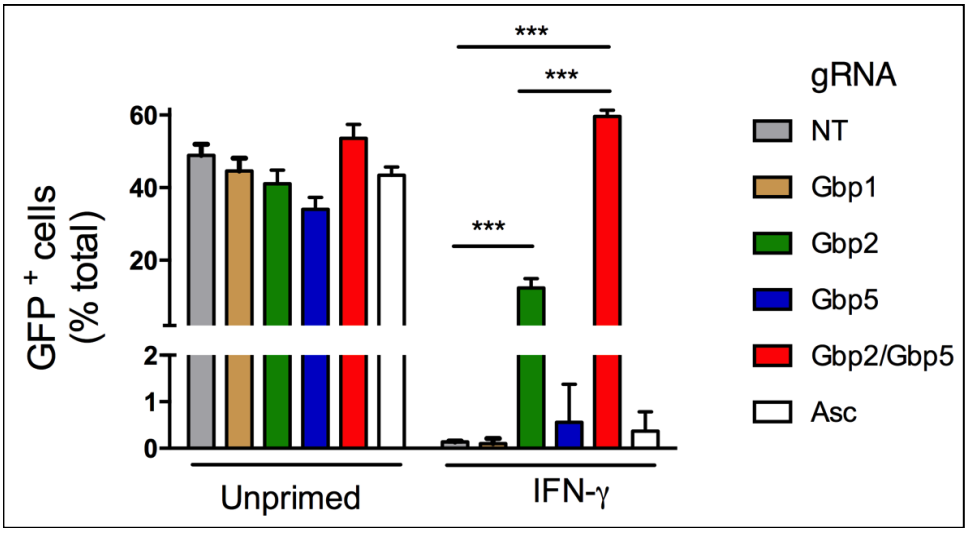

S11 Fig. IFN-γ-induced GBP2 and 5 control bacterial killing in the J774.1 macrophage cell line as determined using CRISPR/Cas9 technology.
Cas9-expressing J774.1 cells were transduced with non-targeting (NT) gRNA or gRNAs targeting the indicated gene(s). Following puromycin selection, the obtained cell lines primed or not with IFN-γ (100 U/ml for 16 h) were infected with GFP-expressing *F. novicida*. Live (propidium iodide-negative) cells were analyzed by flow cytometry at 14 h post-infection. One experiment representative of three independent experiments, mean and standard deviations are shown. One-way ANOVA analysis was performed with Tukey's correction.

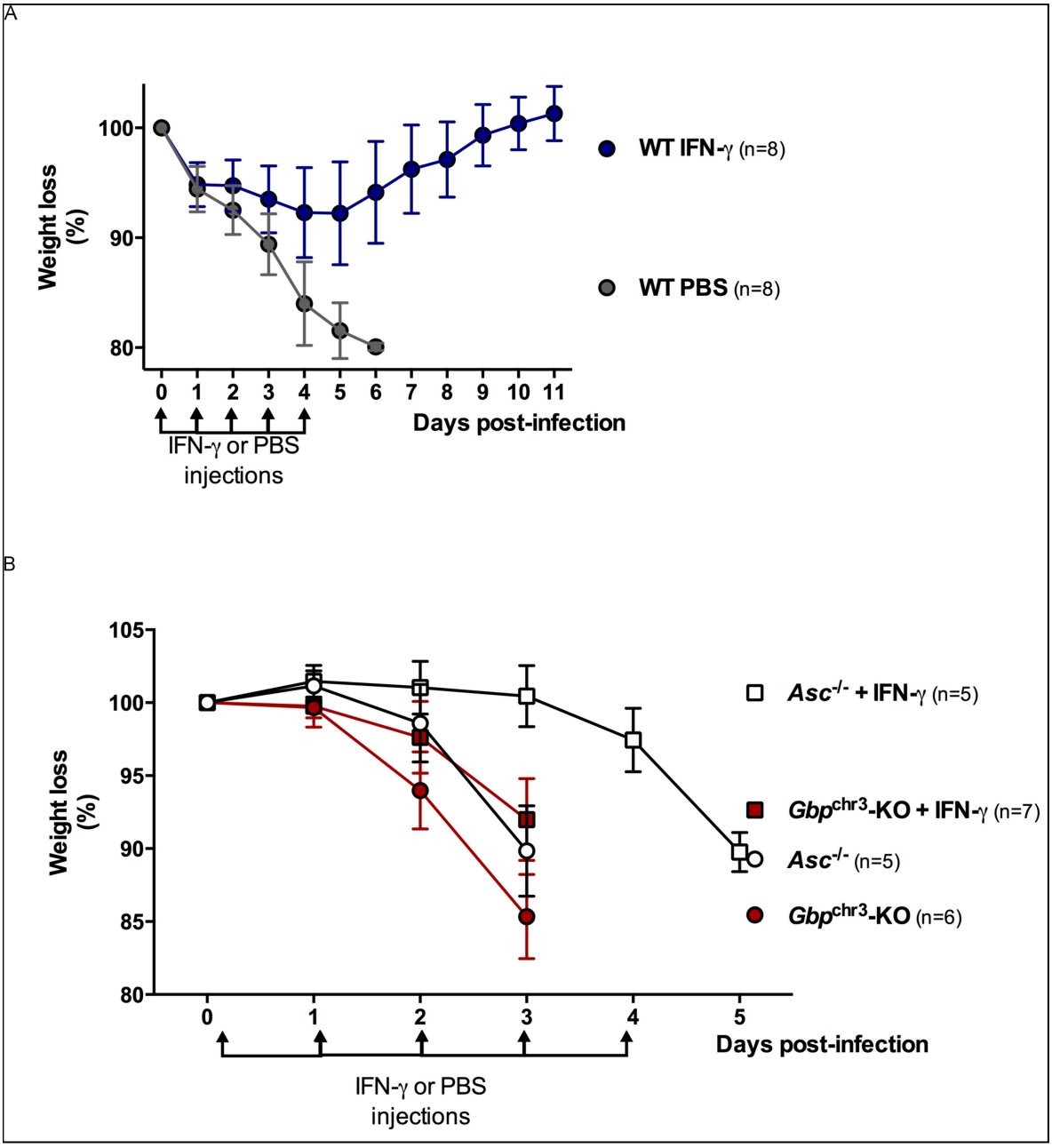

S12 Fig. rIFN-γ administration protects WT and ASC-/- and to a much lower extent Gbpchr3-KO mice from *F. novicida*-mediated weight loss.
Weight loss of mice of the indicated genotypes (see associated Fig 6) treated by daily i.p injection of PBS or 105 U of rIFN-γ during 5 days after s.c. inoculation with 5×104 (A) or 5x103 (B) *F. novicida*.

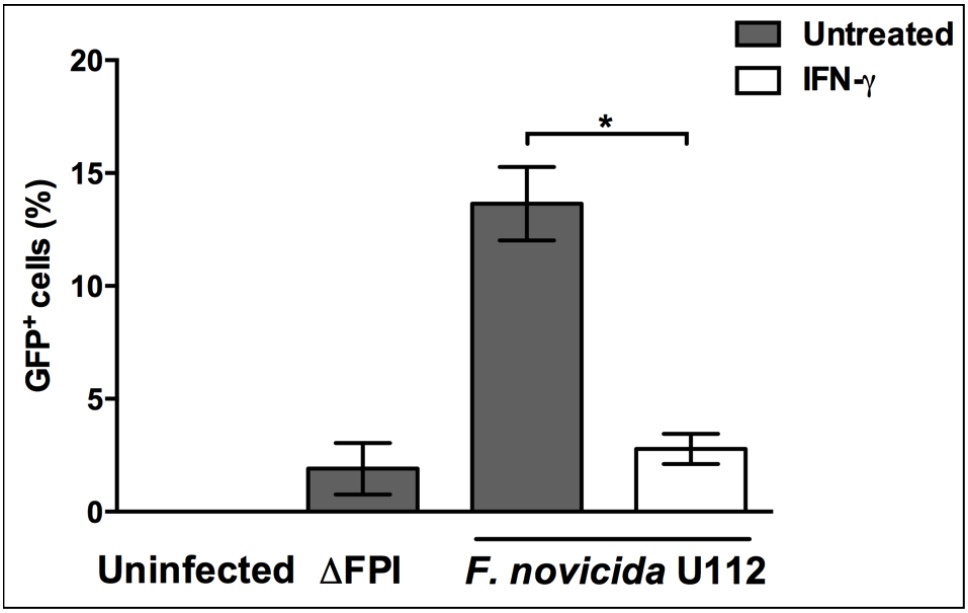

S13 Fig. IFN-γ priming efficiently restricts cytosolic *F. novicida* growth in primary human macrophages.
Flow cytometry-based quantification of live infected (PI-, GFP+) primary human macrophages from one healthy donor primed or not with hrIFN-γ (100 U/ml) of and infected for 16 h with GFP-expressing *F. novicida* strain U112 or the isogenic ΔFPI mutant at a MOI of 1. Mean and s.d. of triplicate wells are shown. Data are representative of two independent experiments.

S1 Movie. Cell death kinetics of unprimed BMDMs as assessed by time-lapse videomicroscopy.
WGA-labeled WT, Gbpchr3-KO, Casp1-/-Casp11-/- and Asc-/- BMDMs were infected with *F. novicida* at a MOI of 1 in the presence of propidium iodide. Images were recorded every 30 minutes from 3 h PI to 23 h PI. Bright-field (top panels) and WGA (bottom panels) are shown. Note the increase in WGA intensity associated with cell retraction in Casp1-/-Casp11-/- BMDMs previously demonstrated to die by apoptosis.

S2 Movie. Cell death kinetics of IFN-γ-primed BMDMs as assessed by time-lapse videomicroscopy.
IFN-γ-primed (100 U/ml for 16h) WGA-labeled WT, Gbpchr3-KO, Casp1-/-Casp11-/- and Asc-/- BMDMs were infected with *F. novicida* at a MOI of 1 in the presence of propidium iodide. Images were recorded every 30 minutes from 3 h PI to 23 h PI. Bright-field (top panels) and WGA (bottom panels) are shown.

13
Scientific Contributions

The scientific newsletter of our institute an electronic publication that aim to diffuse the new discoveries along all the institute. The article presented thought this letter was published in mBio in February 2017, and presented a cooperation between to virulence factor of *P. aeruginosa* to induce a cell lysis.

Pas de virulence sans coopération

Pseudomonas aeruginosa est le pathogène opportuniste majeur pour l'homme. Cette bactérie multi-résistante aux antibiotiques est notamment responsable d'infections graves dans les hôpitaux. La virulence majeure de *P. aeruginosa* est généralement attribuée au système de sécrétion de type 3 (SST3) qui est une machinerie moléculaire complexe mimant une aiguille injectant des toxines directement dans le cytoplasme des cellules hôtes. Ce système est-il universel chez *Pseudomonas aeruginosa* ou bien ce pathogène a-t-il développé d'autres stratégies de virulence ?

Contacts : Pauline Basso et Ina Attrée
BCI
Laboratoire Biologie du Cancer et de l'Infection
UMR_S 1036 - CEA - Inserm - UGA

Récemment, l'équipe *Pathogenèse Bactérienne et Réponses Cellulaires* du Laboratoire Biologie du Cancer et de l'Infection a mis en évidence un nouveau mécanisme de virulence chez des souches cliniques dépourvues de SST3 et provoquant des pneumonies hémorragiques [1, 2]. Ces travaux ont mis en évidence une toxine, nommée l'Exolysine (ExlA), qui forme des pores dans les membranes des cellules eucaryotes ce qui provoque le relargage du contenu cytoplasmique. ExlA est caractérisée par la présence de plusieurs domaines permettant son export à travers la membrane bactérienne, son adhésion aux cellules et la formation de pores *per se* dans la membrane de la cellule eucaryote cible. Les études de la cytotoxicité induite par ExlA ont suggéré que d'autres facteurs bactériens sont nécessaires à l'action d'ExlA.

C'est à la recherche de tels facteurs que Pauline Basso, doctorante dans l'équipe *Pathogenèse Bactérienne et Réponses Cellulaires*, en collaboration avec le laboratoire du Pr S. Lory au Harvard Medical School de Boston, a construit une banque de 7 000 mutants par transposition dans un isolat clinique exprimant ExlA. Elle a ensuite criblé cette banque par imagerie à haut débit à la recherche de mutants qui ne sont pas capables d'induire la cytotoxicité [3]. Par cette approche, les chercheurs ont mis en évidence que les appendices extracellulaires appelés pili de type 4 (PT4) sont nécessaires à la cytotoxicité et la mobilité des bactéries et à leur adhésion aux cellules eucaryotes. PT4 permettent un contact rapproché entre la bactérie et la cellule hôte, provoquant ainsi la création de fortes concentrations locales en ExlA ce qui favorise la formation du pore (*Figure*).

Ainsi, cette étude a permis de proposer un modèle de coopération entre deux systèmes de virulence chez *P. aeruginosa*.

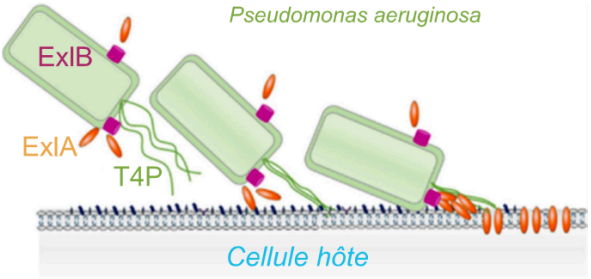

Coopération entre ExlA et pili de type 4 (T4P). ExlB : protéine dans la membrane externe permettant l'export d'ExlA.

Références

[1] **Elsen *et al.*** A Type III Secretion negative clinical strain of *Pseudomonas aeruginosa* employs a two-partner secreted Exolysin to induce hemorrhagic pneumonia. *Cell Host & Microbe*, 2014

[2] **Huber *et al.*** *Pseudomonas aeruginosa* renews its virulence factors. *Environmental Microbiology Reports*, 2016

[3] **Basso P, Ragno M, Elsen S, Reboud E, Golovkine G, Bouillot S, Huber P, Lory S, Faudry E and Attrée I.** *Pseudomonas aeruginosa* pore-forming Exolysin and Type IV Pili cooperate to induce host cell lysis. *mBio*, 2017

Structure-function relationship of the *Pseudomonas aeruginosa* two-partner secreted toxin Exolysin

Basso P, Faudry E, Ragno M, Elsen S, Attree I.

INSERM-UMR-S1036; Bacterial Pathogenesis and Cellular Responses, ERL5261 CNRS, iRTSV, CEA/Grenoble, France

The *Pseudomonas aeruginosa* CLJ1 strain isolated from hemorrhagic pneumonia exerts its virulence through a two partner secreted toxin, that we named Exolysin ExlA (Elsen *et al*., 2014). ExlA belongs to a large family of polymorphic toxins (Zhang *et al.*, 2012) characterized by the presence of a secretion domain in the N-terminus, multiple repeats proposed to participate in host-cell adhesion, and a toxic domain usually present in C-terminal part. In addition, ExlA possesses five Arginine-Glycine-Aspartic Acid (RGD) motifs that may be involved in integrin binding.
ExlA secretion provokes damages of the eukaryotic membrane and cell lysis, which can be attenuated by addition of PEG 3350 during the infection. We further characterized the activity of ExlA by cellular and *in vitro* assays. We showed that the C-Terminal domain was absolutely required for cell lysis, and that RGD motifs were not essential for the action of ExlA on eukaryotic cells. In addition, the recombinant C-terminal domain of ExlA exhibited permeabilization activity on liposomes.

Elsen S*, Huber P*, Bouillot S, Couté Y, Fournier P, Dubois Y, Timsit JF, Maurin M, Attrée I. 2014. A type III secretion negative clinical strain of Pseudomonas aeruginosa employs a two-partner secreted exolysin to induce hemorrhagic pneumonia. Cell Host Microbe. 15(2):164-76

Zhang D, de Souza RF, Anantharaman V, Iyer LM, Aravind L : Po
lymorphic toxin systems : comprehensive characterization of trafficking modes, processing mechanisms of action, immunity and ecology using comparative genomics. Biol Direct 2012, 7:18.

Pseudomonas aeruginosa Exolysin (ExlA) requires its C-terminus and Type IV pilus for cytolysis

P. Basso[1], E. Faudry[1], M. Ragno[1], S. Elsen[1], S. Lory[2], and I. Attrée[1,2]

[1]UMR-S1036 INSERM/CEA/UJF, Bacterial Pathogenesis and Cellular Responses, ERL5261 CNRS, BCI iRTSV, CEA/Grenoble, France;
[2]Dept. of Microbiology and Immunology, Harvard Medical School, Boston, Massachusetts, USA.

Introduction

ExlA is a polymorphic toxin secreted by PA7-like strains

Pseudomonas aeruginosa strains belonging to the PA7-like group of taxonomic outliers do not possess Type 3 Secretion System, a major virulence determinant. Instead, they produce a Two Partner Secreted toxin, named Exolysin (ExlA). Expression and secretion of Exolysin provide to the strains a hyper virulent phenotype, as documented for the CLJ1 strain, isolated from a patient with hemorrhagic pneumonia in Intensive Care Unit at Grenoble (France) (Elsen *et al.*, 2014). Exolysin induces cell membrane permeabilization *in vitro* and is sufficient for mouse mortality *in vivo*. Exolysin is homologous to ShlA hemolysin from *Serratia marecesens* and is conserved in different bacterial species (Figure 1).

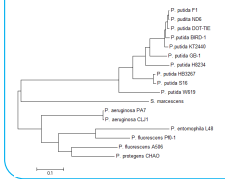

Figure 1: Phylogenetic tree of *exlA* gene sequences throughout *Pseudomonas* species.
Gene alignment was done with CLC software, and tree was constructed with MEGA 6 software

ExlA is a 172 kDa secreted protein, belonging to the family of polymorphic toxins (Zhang *et al.*, 2012). It carries a Two Partner Secretion domain (TPS), filamentous haemaglutinin-like domains and a C-terminal domain of unknown function. In addition, ExlA possesses five RGD motifs that may be involved in integrin recognition (Figure 2). ExlA is secreted via a TPS system through ExlB, an outer membrane protein belonging to the Omp85 family. ExlB is composed of a beta barrel, anchored in the outer membrane and two Polypeptides Associated Transport (POTRA) domains (Figure 3). The ExlA secretion is mediated by its TPS domain and the ExlB POTRA domains are required

Figure 2: Characteristic domains of ExlA, a polymorphic toxin.

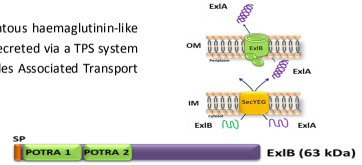

Figure 3: Two Partner Secretion system. ExlB with its characteristic POTRA domains.

Results

Structure-function relationship of ExlA

To decipher the ExlA structure-function relationship, we created a mutant protein in which the five RGD motifs were changed into RGA, and a mutant deleted for the 300 amino acids in the C-terminal part.

$ExlA_{\Delta Cter}$ and $ExlA_{RGA}$ are expressed and secreted, as verified by Western blot (Figure 4). While RGD motifs do not play any role in cytotoxicity, the deletion of the Cter completely abolishes ExlA cytolytic activity.

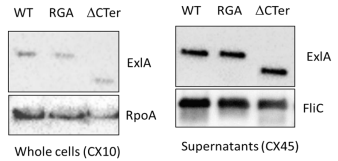

Figure 4: We used PAO1Δ*xcpRΔpscC* recombinant strain to express *exlA* $_{WT}$ genes, $exlA_{RGA}$ gene or $exlA_{\Delta Cter}$ gene to assess the production and secretion of ExlA. The expression of *exlBA* is under the control of a promotor inducible by arabinose. Supernatants were precipitated using TCA-DOC. The samples were analyzed by immunoblotting using anti-ExlA antibodies.

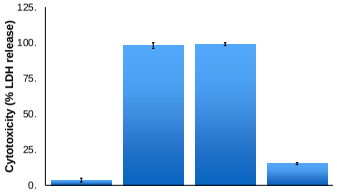

Figure 5: A549 epithelial cells were infected at MOI 5 with PAO1 recombinant strains induced with 0.025% of arabinose in EBM2 medium. 4 hours after infection LDH release from cells was measured using a colorimetric assay.

Characteristics of ExlA-cytolysis

To demonstrate the contact-dependence between bacteria and host cells in ExlA-dependent cytotoxicity we used a Transwell migration assay.

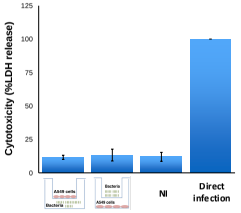

Figure 6: A549 epithelial cells were infected for 4 hours in EBM2 medium at MOI 5 with the CLJ1 strain in direct contact with the cells or separated by a transwell.

Transposon mutagenesis strategy was used to determine the bacterial factors involved in ExlA-dependent cytotoxicity

We created a library of 7400 mutants from the *exlA*-positive IHMA 87 strain by *mariner* transposon mutagenesis. Mutants were screened for a loss of ExlA-dependent cytotoxicity towards A549 epithelial cells. Screen was based on live/dead system using appropriate dyes (Hoechst and Draq7). The permeabilization of plasma membrane allowed the incorporation of Draq7 in the nucleus (Figure7).

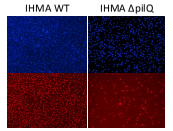

Figure 7: A549 epithelial cells were infected at MOI 5 with IHMA87 library mutants in EBM2 medium for 3 hours.

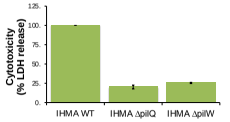

Figure 8: A549 epithelial cells were infected at MOI 5 with IHMA WT strain and pili mutants in EBM2 medium. 4h after infection LDH release from cells was measured using a colorimetric assay.

Among 20 selected mutants that lost ExlA-dependent cytotoxicity, we identified three independent Tn-insertions in genes required for type IV pilus biogenesis. Therefore, these pili seem to be involved in the ExlA-dependent cytotoxicity (Figure 8).

Activity of $ExlA^{cter}$ toward lipid vesicles

To understand the role of the C-terminal domain of ExlA in cytolysis, we compared the sequences from several bacterial species and highlighted the most conserved residues (Figure 9) . To decipher the role of the ExlA C-terminal part in cytotoxicity, we produced and purified the recombinant C-terminal part, and evaluated its activity toward lipid vesicles.

We cloned the C-terminal part of *exlA* in pET15b vector, expressed and purified the recombinant protein on a His-trap column (Figure 10). We tested the ability to the recombinant protein to disrupt liposome with different lipids composition. We demonstrated that the recombinant protein is able to disrupt liposomes composed of PS-PC (80%-20%) (Figure 11). We also tested the rate of of liposome disruption at different pH and we showed that the membrane disrupting activity of the Cter part was dependent on pH, with an optimum activity at pH4 (Figure12) .

Figure 9: Conserved residues of the C-terminal part of Exolysin-like toxin

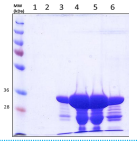

Figure 10: SDS-PAGE analysis of the C-terminal recombinant domain purification. The C-terminal part of Exla is a 33kDa protein.

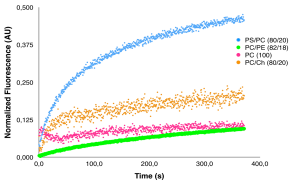

Figure 11: Time course data of liposomes disruption. The release of the SRB dye encapsulated into the vesicles was measured at excitation and emission wavelenghts of 565 and 586 nm, respectively, for 400s. 10uM of liposomes was mixed with 10nM of Cter protein in Tris acetate buffer with 250mM NaCl.

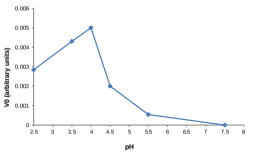

Figure 12: Initial rates (V0) of SRB release from PS-PC liposome at different pH.

Conclusion

The C-terminal domain of ExlA is required, unlike RGD motifs for the cytotoxicity of ExlA toward epithelial cells. We demonstrated that the ExlA related cytotoxicity is contact dependent and that the Type IV pilus is involved in the ExlA-dependent cytotoxicity. By *in vitro* approaches, we showed that the C-terminal part of ExlA is highly conserved in Exolysin-like toxins through the bacterial species, and that it is able to disrupt liposomes made of PS and PC.

References:
Elsen *et al.*, A type III secretion negative clinical strain of *Pseudomonas aeruginosa* employs a two-partner secreted exolysin to induce hemorrhagic pneumonia, Cell Host Microbes, 2014.
Zhang *et al.*, Polymorphic toxin systems: Comprehensive characterization of trafficking modes, processing, mechanisms of action, immunity and ecology using comparative genomics, Biology Direct, 2012.

Pseudomonas aeruginosa **Exolysin requires Type IV Pili for cytolysis**

Pauline Basso[1], M. Ragno, S. Elsen, E. Reboud, G. Golovkine, S. Bouillot, P. Huber, S. Lory, E. Faudry and I. Attrée

[1]UMR-S1036 INSERM/CEA/UGA, Bacterial Pathogenesis and Cellular Responses, ERL5261 CNRS, BCI BIG, CEA/Grenoble, France

Pseudomonas aeruginosa clinical strains lacking Type III secretion system genes employ a novel toxin, Exolysin (ExlA), for host cell destruction. Here, we demonstrated that ExlA uses a predicted outer membrane protein ExlB for its export through two POTRA domains showing that ExlA-ExlB represent new members of a Two-Partner Secretion (TPS) systems. In addition of TPS secretion signals, ExlA harbors several distinct domains, which comprise notably hemagglutinin FHA domains, five integrin binding motifs Arginine-Glycine-Aspartic acid (RGD) and a non-conserved C-terminal region. Cytotoxic assays showed that the deletion of the C-terminal region abolishes host-cell cytolysis. Using red blood cells and lipid vesicles, we demonstrate that ExlA has a pore-forming activity that precedes cell membrane disruption in nucleated cells. Finally, by setting up a miniaturized cellular live-death assay, we screened a transposon mutant library of an ExlA-producing *P. aeruginosa* clinical strain for bacterial factors required for ExlA-dependent toxicity. The screen allowed the identification of proteins of Type IV pili as being absolutely required for ExlA-dependent cell destruction. This is the first example of cooperation between a TPS pore-forming toxin and surface appendages in host cell intoxication.

Pseudomonas aeruginosa Exolysin requires Type IV Pili for cytolysis

Pauline Basso[1], M. Ragno, S. Elsen, E. Reboud, G. Golovkine, S. Bouillot, P. Huber, S. Lory, E. Faudry and I. Attrée

[1]UMR-S1036 INSERM/CEA/UGA, Bacterial Pathogenesis and Cellular Responses, ERL5261 CNRS, BCI BIG, CEA/Grenoble, France

pauline.basso@cea.fr

Pseudomonas aeruginosa strains belonging to the PA7-like group of taxonomic outliers do not possess Type 3 Secretion System, a major virulence determinant. Instead, they produce a Two Partner Secreted toxin, named Exolysin (ExlA). Expression and secretion of Exolysin provide to the strains a hyper virulent phenotype

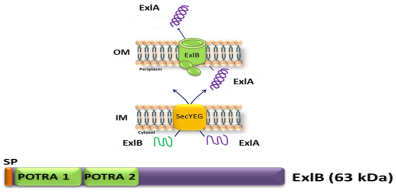

Two Partner Secretion system. ExlB with its characteristic POTRA domains.

ExlA is secreted via a TPS system through ExlB, an outer membrane protein belonging to the Omp85 family. ExlB is composed of a beta barrel, anchored in the outer membrane and two Polypeptides Associated Transport (POTRA) domains. The ExlA secretion is mediated by its TPS domain and the ExlB POTRA domains are required

ExlA is a polymorphic toxin

ExlA is a 172 kDa secreted protein, belonging to the family of polymorphic toxins (Zhang *et al.*, 2012). It carries a Two Partner Secretion domain (TPS), filamentous haemaglutinin-like domains and a C-terminal domain of unknown function. In addition, ExlA possesses five RGD motifs that may be involved in integrin recognition.

To decipher the role of ExlA domains, we created different mutant in ExlA.

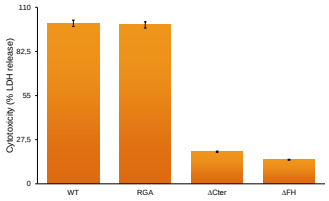

While RGD motifs do not play any role in cytotoxicity, the deletion of the C-ter and Filamentous Heammaglutinin domains completely abolishes ExlA cytolytic activity.

ExlA is a pore forming toxin

To decipher how ExlA induce plasma membrane rupture in eukaryotic cells, we looked at the pore formation with an *in vitro* approaches.

RBC were incubated in 30 mM of osmoprotectants with PAO1Δ*xcpR*Δ*pscC* recombinant strain expressing *exlA* $_{WT}$ genes or *exlA* $_{\Delta Cter.}$ We used as controls the a-hemolysin from *Staphylococcus aureus*, *Serratia marcescens* secreting ShlA, and PP34 a clinical strain secreting the phospholipase ExoU .

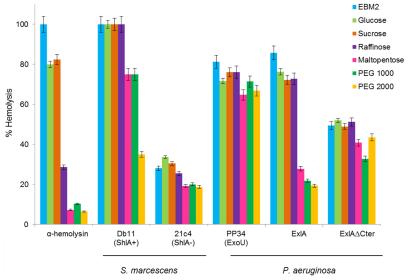

ExlA lyse red blood cells (RBC) in EBM2 medium, Maltopentoase (1.66 nm) protects RBC from hemolysis

ExlA induced plasma membrane rupture

To describe the cell death induced by ExlA we used time time lapse fluorescent confocal microscopy.

We used IHMA87 strain expressing ExlA (WT). A549-EGFP cells were infected at MOI 10 for 6 hours. As negative control, we used IHMA87Δ*exlA*. Membranes were labelled with WGA.

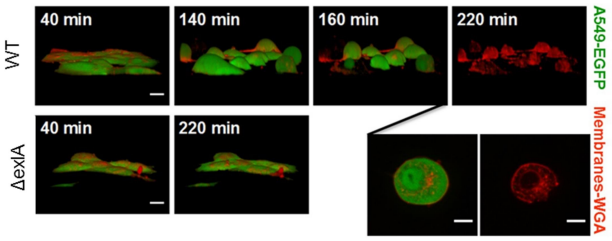

We observed a rounding of epithelial cells at 160 min post infection and a total rupture of plasma membrane at 220 min.

Type IV pili are required for ExlA dependent cytotoxicity

Transposon mutagenesis strategy was used to determine the bacterial factors involved in ExlA-dependent cytotoxicity

We created a library of 7400 mutants from the *exlA*-positive IHMA 87 strain by *mariner* transposon mutagenesis. Mutants were screened for a loss of ExlA-dependent cytotoxicity towards A549 epithelial cells. Screen was based on live/dead system using appropriate dyes (Hoechst and Draq7). The permeabilization of plasma membrane allowed the incorporation of Draq7 in the nucleus

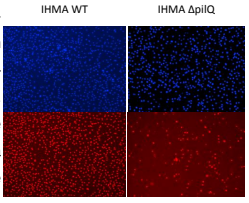

Among 20 selected mutants that lost ExlA-dependent cytotoxicity, we identified three independent Tn-insertions in genes required for type IV pilus biogenesis. We created also three other mutants in *pilA*, *pilU* and *pilT* genes to confirm this phenotype. Therefore, these pili seem to be involved in the ExlA-dependent cytotoxicity.

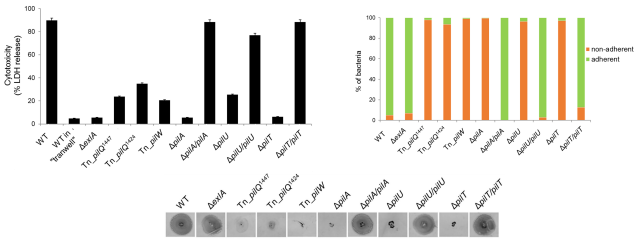

We demonstrated that Type IV pili are implicated in adhesion of bacteria to cells and in motility of bacteria.

The C-terminal domain and Filamentous Heamagglutin domains of ExlA are required, unlike RGD motifs for the cytotoxicity of ExlA toward epithelial cells. We also demonstrated that Type IV pili are play an important role in ExlA-dependent cytotoxicity.

We wish to search for eukaryotic partners to ExlA by a cellular screening of RAW macrophages library mutated by CRISPR-Cas9 technology.

Part V

Bibliography

Bibliography

[1] E. Reboud *et al.*, Phenotype and toxicity of the recently discovered exlA -positive Pseudomonas aeruginosa strains collected worldwide, Environmental Microbiology **18** (2016) 3425.

[2] P. Huber *et al.*, Pseudomonas aeruginosa renews its virulence factors, Environmental Microbiology Reports **8** (2016) 564.

[3] P.V. da Mata Madeira *et al.*, Structural Basis of Lipid Targeting and Destruction by the Type V Secretion System of Pseudomonas aeruginosa, Journal of Molecular Biology **428** (2016) 1790.

[4] P. Wallet *et al.*, IFN-γ extends the immune functions of Guanylate Binding Proteins to inflammasome-independent antibacterial activities during Francisella novicida infection, PLoS Pathogens **13** (2017) e1006630.

[5] B. Bonnemain, Pharmaciens militaires français lors de l'expédition de Tunisie (1881-1887) : Paul-Louis Roeser et Carie Gessard, et les autres, Revue d'histoire de la pharmacie **95** (2008) 163.

[6] J.B. Lyczak, C.L. Cannon and G.B. Pier, Establishment of Pseudomonas aeruginosa infection: lessons from a versatile opportunist, Microbes and infection / Institut Pasteur **2** (2000) 1051.

[7] T.R. Oberhofer, Growth of nonfermentative bacteria at 42??c, Journal of Clinical Microbiology **10** (1979) 800.

[8] K. Kerr and A. Snelling, Pseudomonas aeruginosa: a formidable and ever-present adversary, Journal of Hospital Infection **73** (2009) 338.

[9] M.F. Moradali, S. Ghods and B.H.A. Rehm, Pseudomonas aeruginosa Lifestyle: A Paradigm for Adaptation, Survival, and Persistence, Frontiers in Cellular and Infection Microbiology **7** (2017).

[10] M.D. Obritsch *et al.*, Nosocomial Infections Due to Multidrug-Resistant Pseudomonas aeruginosa : Epidemiology and Treatment Options, Pharmacotherapy **25** (2005) 1353.

[11] V.D. Rosenthal *et al.*, International Nosocomial Infection Control Consortium report, data summary of 50 countries for 2010-2015: Device-associated module, American Journal of Infection Control **44** (2016) 1495.

[12] M.S. Thomas and S. Wigneshweraraj, Regulation of virulence gene expression, Virulence **5** (2014) 832.

[13] S.L. Vogt *et al.*, The stringent response is essential for pseudomonas aeruginosa virulence in the rat lung agar bead and drosophila melanogaster feeding models of infection, Infection and Immunity **79** (2011) 4094.

[14] F. Aujoulat *et al.*, From environment to man: Genome evolution and adaptation of human opportunistic bacterial pathogens, Genes **3** (2012) 191.

[15] C.K. Stover *et al.*, Complete genome sequence of Pseudomonas aeruginosa PAO1, an opportunistic pathogen., Nature **406** (2000) 959.

[16] K. Mathee *et al.*, Dynamics of Pseudomonas aeruginosa genome evolution, Proceedings of the National Academy of Sciences **105** (2008) 3100.

[17] B. Valot *et al.*, What It Takes to Be a Pseudomonas aeruginosa? The Core Genome of the Opportunistic Pathogen Updated, PLOS ONE **10** (2015) e0126468.

[18] J. Klockgether *et al.*, Pseudomonas aeruginosa Genomic Structure and Diversity, Frontiers in Microbiology **2** (2011).

[19] V.L. Kung, E.A. Ozer and A.R. Hauser, The Accessory Genome of Pseudomonas aeruginosa, Microbiology and Molecular Biology Reviews **74** (2010) 621.

[20] P.H. Roy *et al.*, Complete genome sequence of the multiresistant taxonomic outlier Pseudomonas aeruginosa PA7., PloS one **5** (2010) e8842.

[21] J.J. Varga *et al.*, Genotypic and phenotypic analyses of a Pseudomonas aeruginosa chronic bronchiectasis isolate reveal differences from cystic fibrosis and laboratory strains, BMC Genomics **16** (2015) 883.

[22] L. Cullen and S. McClean, Bacterial Adaptation during Chronic Respiratory Infections, Pathogens **4** (2015) 66.

[23] E.B. Breidenstein, C. de la Fuente-Núñez and R.E. Hancock, Pseudomonas aeruginosa: all roads lead to resistance, Trends in Microbiology **19** (2011) 419.

[24] E.E. Smith *et al.*, Genetic adaptation by Pseudomonas aeruginosa to the airways of cystic fibrosis patients, Proceedings of the National Academy of Sciences **103** (2006) 8487.

[25] R. Adamo *et al.*, Pseudomonas aeruginosa Flagella Activate Airway Epithelial Cells through asialoGM1 and Toll-Like Receptor 2 as well as Toll-Like Receptor 5, American Journal of Respiratory Cell and Molecular Biology **30** (2004) 627.

[26] E. Mahenthiralingam, M.E. Campbell and D.P. Speert, Nonmotility and phagocytic resistance of Pseudomonas aeruginosa isolates from chronically colonized patients with cystic fibrosis., Infection and immunity **62** (1994) 596.

[27] C. Winstanley, S. O'Brien and M.A. Brockhurst, Pseudomonas aeruginosa Evolutionary Adaptation and Diversification in Cystic Fibrosis Chronic Lung Infections, Trends in Microbiology **24** (2016) 327.

[28] A.R. Hauser, The type III secretion system of Pseudomonas aeruginosa: infection by injection, Nature Reviews Microbiology **7** (2009) 654.

[29] D.L. McEwan, N.V. Kirienko and F.M. Ausubel, Host Translational Inhibition by Pseudomonas aeruginosa Exotoxin A Triggers an Immune Response in Caenorhabditis elegans, Cell Host & Microbe **11** (2012) 364.

[30] A.J. Laarman *et al.*, Pseudomonas aeruginosa Alkaline Protease Blocks Complement Activation via the Classical and Lectin Pathways, The Journal of Immunology **188** (2012) 386.

[31] G. Golovkine *et al.*, VE-Cadherin Cleavage by LasB Protease from Pseudomonas aeruginosa Facilitates Type III Secretion System Toxicity in Endothelial Cells, PLoS Pathogens **10** (2014) e1003939.

[32] A. Ghafoor, I.D. Hay and B.H.A. Rehm, Role of Exopolysaccharides in Pseudomonas aeruginosa Biofilm Formation and Architecture, Applied and Environmental Microbiology **77** (2011) 5238.

[33] E. Kipnis, T. Sawa and J. Wiener-Kronish, Targeting mechanisms of Pseudomonas aeruginosa pathogenesis, Médecine et Maladies Infectieuses **36** (2006) 78.

[34] N. Høiby, O. Ciofu and T. Bjarnsholt, Pseudomonas aeruginosa biofilms in cystic fibrosis, Future Microbiology **5** (2010) 1663.

[35] M. Hentzer *et al.*, Alginate Overproduction Affects Pseudomonas aeruginosa Biofilm Structure and Function, Journal of Bacteriology **183** (2001) 5395.

[36] T.I. Nicas and R.E. Hancock, Pseudomonas aeruginosa outer membrane permeability: isolation of a porin protein F-deficient mutant., Journal of bacteriology **153** (1983) 281.

[37] W. Wu *et al.*, MucA-Mediated Coordination of Type III Secretion and Alginate Synthesis in Pseudomonas aeruginosa, Journal of Bacteriology **186** (2004) 7575.

[38] L.F. Wood and D.E. Ohman, Identification of Genes in the 22 Regulon of Pseudomonas aeruginosa Required for Cell Envelope Homeostasis in Either the Planktonic or the Sessile Mode of Growth, mBio **3** (2012) e00094.

[39] E.S. Garrett, D. Perlegas and D.J. Wozniak, Negative control of flagellum synthesis in Pseudomonas aeruginosa is modulated by the alternative sigma factor AlgT (AlgU)., Journal of bacteriology **181** (1999) 7401.

[40] A.L. Goodman *et al.*, A Signaling Network Reciprocally Regulates Genes Associated with Acute Infection and Chronic Persistence in Pseudomonas aeruginosa, Developmental Cell **7** (2004) 745.

[41] A. Brencic *et al.*, The GacS/GacA signal transduction system of Pseudomonas aeruginosa acts exclusively through its control over the transcription of the RsmY and RsmZ regulatory small RNAs, Molecular Microbiology **73** (2009) 434.

[42] P. Jorth *et al.*, Regional Isolation Drives Bacterial Diversification within Cystic Fibrosis Lungs, Cell Host & Microbe **18** (2015) 307.

[43] C. Winstanley, S. O'Brien and M.A. Brockhurst, Pseudomonas aeruginosa Evolutionary Adaptation and Diversification in Cystic Fibrosis Chronic Lung Infections, Trends in Microbiology **24** (2016) 327.

[44] R. Le Berre *et al.*, Relative contribution of three main virulence factors in Pseudomonas aeruginosa pneumonia*, Critical Care Medicine **39** (2011) 2113.

[45] A. Roy-Burman *et al.*, Type III protein secretion is associated with death in lower respiratory and systemic Pseudomonas aeruginosa infections, The Journal of Infectious Diseases **183** (2001) 1767.

[46] A.R. Hauser, The type III secretion system of Pseudomonas aeruginosa: infection by injection, Nature Reviews Microbiology **7** (2009) 654.

[47] T.R.D. Costa *et al.*, Secretion systems in Gram-negative bacteria: structural and mechanistic insights, Nature Reviews Microbiology **13** (2015) 343.

[48] G.R. Cornelis, The type III secretion injectisome, Nature Reviews Microbiology **4** (2006) 811.

[49] T. Morita-Ishihara *et al.*, Shigella Spa33 Is an Essential C-ring Component of Type III Secretion Machinery, Journal of Biological Chemistry **281** (2006) 599.

[50] A. Pastor *et al.*, PscF is a major component of the Pseudomonas aeruginosa type III secretion needle, FEMS Microbiology Letters **253** (2005) 95.

[51] P.J. Matteï *et al.*, Membrane targeting and pore formation by the type III secretion system translocon, FEBS Journal **278** (2011) 414.

[52] V. Job *et al.*, Structural Basis of Chaperone Recognition of Type III Secretion System Minor Translocator Proteins, Journal of Biological Chemistry **285** (2010) 23224.

[53] A. Filloux, Protein Secretion Systems in Pseudomonas aeruginosa: An Essay on Diversity, Evolution, and Function, Frontiers in Microbiology **2** (2011).

[54] D. Dacheux *et al.*, Pore-forming activity of type III system-secreted proteins leads to oncosis of Pseudomonas aeruginosa-infected macrophages, Molecular Microbiology **40** (2001) 76.

[55] T.L. Yahr, J. Goranson and D.W. Frank, Exoenzyme S of Pseudomonas aeruginosa is secreted by a type III pathway., Molecular microbiology **22** (1996) 991.

[56] M.L. McCaw *et al.*, ExsD is a negative regulator of the Pseudomonas aeruginosa type III secretion regulon., Molecular microbiology **46** (2002) 1123.

[57] N. Dasgupta *et al.*, A novel anti-anti-activator mechanism regulates expression of the Pseudomonas aeruginosa type III secretion system, Molecular Microbiology **53** (2004) 297.

[58] M.L. Urbanowski, E.D. Brutinel and T.L. Yahr, Translocation of ExsE into Chinese Hamster Ovary Cells Is Required for Transcriptional Induction of the Pseudomonas aeruginosa Type III Secretion System, Infection and Immunity **75** (2007) 4432.

[59] T. Sawa *et al.*, Association between Pseudomonas aeruginosa type III secretion, antibiotic resistance, and clinical outcome: a review, Critical Care **18** (2014) 668.

[60] C. Vareechon *et al.*, Pseudomonas aeruginosa Effector ExoS Inhibits ROS Production in Human Neutrophils, Cell Host & Microbe **21** (2017) 611.

[61] S.M. Rangel *et al.*, The Role of ExoS in Dissemination of Pseudomonas aeruginosa during Pneumonia, PLOS Pathogens **11** (2015) e1004945.

[62] S. Wood, J. Goldufsky and S.H. Shafikhani, Pseudomonas aeruginosa ExoT Induces Atypical Anoikis Apoptosis in Target Host Cells by Transforming Crk Adaptor Protein into a Cytotoxin, PLOS Pathogens **11** (2015) e1004934.

[63] P. Huber *et al.*, Sequential inactivation of Rho GTPases and Lim kinase by Pseudomonas aeruginosa toxins ExoS and ExoT leads to endothelial monolayer breakdown, Cellular and Molecular Life Sciences **71** (2014) 1927.

[64] Y. Sun *et al.*, ExoS and ExoT ADP Ribosyltransferase Activities Mediate Pseudomonas aeruginosa Keratitis by Promoting Neutrophil Apoptosis and Bacterial Survival, The Journal of Immunology **188** (2012) 1884.

[65] E.M. Harrison *et al.*, Pathogenicity Islands PAPI-1 and PAPI-2 Contribute Individually and Synergistically to the Virulence of Pseudomonas aeruginosa Strain PA14, Infection and Immunity **78** (2010) 1437.

[66] B.R. Kulasekara *et al.*, Acquisition and Evolution of the exoU Locus in Pseudomonas aeruginosa, Journal of Bacteriology **188** (2006) 4037.

[67] C. Gendrin *et al.*, Structural Basis of Cytotoxicity Mediated by the Type III Secretion Toxin ExoU from Pseudomonas aeruginosa, PLoS Pathogens **8** (2012) e1002637.

[68] S. Bouillot, I. Attrée and P. Huber, Pharmacological Activation of Rap1 Antagonizes the Endothelial Barrier Disruption Induced by Exotoxins ExoS and ExoT of Pseudomonas aeruginosa, Infection and Immunity **83** (2015) 1820.

[69] M.C. Plotkowski *et al.*, ExoU-induced procoagulant activity in Pseudomonas aeruginosa-infected airway cells, European Respiratory Journal **32** (2008) 1591.

[70] M.H. Diaz and A.R. Hauser, Pseudomonas aeruginosa Cytotoxin ExoU Is Injected into Phagocytic Cells during Acute Pneumonia, Infection and Immunity **78** (2010) 1447.

[71] U. Beckert *et al.*, ExoY from Pseudomonas aeruginosa is a nucleotidyl cyclase with preference for cGMP and cUMP formation, Biochemical and Biophysical Research Communications **450** (2014) 870.

[72] C.D. Ochoa *et al.*, Pseudomonas aeruginosa Exotoxin Y Is a Promiscuous Cyclase That Increases Endothelial Tau Phosphorylation and Permeability, Journal of Biological Chemistry **287** (2012) 25407.

[73] M.T. Ganter *et al.*, Role of Small GTPases and $\alpha v\beta 5$ Integrin in Pseudomonas aeruginosa -Induced Increase in Lung Endothelial Permeability, American Journal of Respiratory Cell and Molecular Biology **40** (2009) 108.

[74] C.D. Ochoa *et al.*, Pseudomonas aeruginosa Exotoxin Y Is a Promiscuous Cyclase That Increases Endothelial Tau Phosphorylation and Permeability, Journal of Biological Chemistry **287** (2012) 25407.

[75] A. Belyy *et al.*, Actin activates Pseudomonas aeruginosa ExoY nucleotidyl cyclase toxin and ExoY-like effector domains from MARTX toxins, Nature Communications **7** (2016) 13582.

[76] H. Bähre *et al.*, cCMP and cUMP occur in vivo, Biochemical and Biophysical Research Communications **460** (2015) 909.

[77] K. Garey *et al.*, Prevalence of Type III Secretion Protein Exoenzymes and Antimicrobial Susceptibility Patterns from Bloodstream Isolates of Patients with Pseudomonas aeruginosa Bacteremia, Journal of Chemotherapy **20** (2008) 714.

[78] E. Latz, T.S. Xiao and A. Stutz, Activation and regulation of the inflammasomes, Nature Reviews Immunology **13** (2013) 397.

[79] L.M. Faure *et al.*, Characterization of a novel two-partner secretion system implicated in the virulence of Pseudomonas aeruginosa, Microbiology **160** (2014) 1940.

[80] F.S. Sutterwala *et al.*, Immune recognition of Pseudomonas aeruginosa mediated by the IPAF/NLRC4 inflammasome, The Journal of Experimental Medicine **204** (2007) 3235.

[81] E.A. Miao *et al.*, Pseudomonas aeruginosa activates caspase 1 through Ipaf, Proceedings of the National Academy of Sciences **105** (2008) 2562.

[82] J. Yang *et al.*, Human NAIP and mouse NAIP1 recognize bacterial type III secretion needle protein for inflammasome activation, Proceedings of the National Academy of Sciences **110** (2013) 14408.

[83] D. Ince, F.S. Sutterwala and T.L. Yahr, Secretion of Flagellar Proteins by the Pseudomonas aeruginosa Type III Secretion-Injectisome System, Journal of Bacteriology **197** (2015) 2003.

[84] L. Monlezun *et al.*, PscI is a type III secretion needle anchoring protein with in vitro polymerization capacities, Molecular Microbiology **96** (2015) 419.

[85] I. Bianconi *et al.*, Positive Signature-Tagged Mutagenesis in Pseudomonas aeruginosa: Tracking Patho-Adaptive Mutations Promoting Airways Chronic Infection, PLoS Pathogens **7** (2011) e1001270.

[86] N.T. Liberati *et al.*, An ordered, nonredundant library of Pseudomonas aeruginosa strain PA14 transposon insertion mutants, Proceedings of the National Academy of Sciences **103** (2006) 2833.

[87] D. Skurnik *et al.*, A Comprehensive Analysis of In Vitro and In Vivo Genetic Fitness of Pseudomonas aeruginosa Using High-Throughput Sequencing of Transposon Libraries, PLoS Pathogens **9** (2013) e1003582.

[88] A. Beaussart *et al.*, Nanoscale Adhesion Forces of Pseudomonas aeruginosa Type IV Pili, ACS Nano **8** (2014) 10723.

[89] T.L. Leighton *et al.*, Biogenesis of P seudomonas aeruginosa type IV pili and regulation of their function, Environmental Microbiology **17** (2015) 4148.

[90] J. Koo, L.L. Burrows and P. Lynne Howell, Decoding the roles of pilotins and accessory proteins in secretin escort services, FEMS Microbiology Letters **328** (2012) 1.

[91] Y.W. Chang *et al.*, Architecture of the type IVa pilus machine, Science **351** (2016).

[92] K.V. Korotkov, T. Gonen and W.G.J. Hol, Secretins: Dynamic channels for protein transport across membranes, Trends in Biochemical Sciences **36** (2011) 433.

[93] S. Graupner *et al.*, Requirement of novel competence genes pilT and pilU of Pseudomonas stutzeri for natural transformation and suppression of pilT deficiency by a hexahistidine tag on the type IV pilus protein PilAI, Journal of Bacteriology **183** (2001) 4694.

[94] H.K. Takhar *et al.*, The platform protein is essential for type IV pilus biogenesis, Journal of Biological Chemistry **288** (2013) 9721.

[95] C. Li *et al.*, Type IV Pilus Proteins Form an Integrated Structure Extending from the Cytoplasm to the Outer Membrane, PLoS ONE **8** (2013).

[96] M.S. Strom and S. Lory, Structure-Function and Biogenesis of the Type Iv Pili, Annual Review of Microbiology **47** (1993) 565.

[97] L.L. Burrows, Pseudomonas aeruginosa Twitching Motility: Type IV Pili in Action, Annual Review of Microbiology **66** (2012) 493.

[98] C.L. Giltner, Y. Nguyen and L.L. Burrows, Type IV Pilin Proteins: Versatile Molecular Modules, Microbiology and Molecular Biology Reviews **76** (2012) 740.

[99] J.V. Kus, Significant differences in type IV pilin allele distribution among Pseudomonas aeruginosa isolates from cystic fibrosis (CF) versus non-CF patients, Microbiology **150** (2004) 1315.

[100] J.M. Boyd, T. Koga and S. Lory, Identification and characterization of PilS, an essential regulator of pilin expression in Pseudomonas aeruginosa, Molecular and General Genetics **243** (1994) 565.

[101] H. Mikkelsen, M. Sivaneson and A. Filloux, Key two-component regulatory systems that control biofilm formation in Pseudomonas aeruginosa, Environmental Microbiology **13** (2011) 1666.

[102] N.B. Fulcher *et al.*, The Pseudomonas aeruginosa Chp chemosensory system regulates intracellular cAMP levels by modulating adenylate cyclase activity, Molecular Microbiology **76** (2010) 889.

[103] S.E. West, A.K. Sample and L.J. Runyen-Janecky, The vfr gene product, required for Pseudomonas aeruginosa exotoxin A and protease production, belongs to the cyclic AMP receptor protein family., Journal of bacteriology **176** (1994) 7532.

[104] K.K. Lee *et al.*, The binding of Pseudomonas aeruginosa pili to glycosphingolipids is a tip-associated event involving the C-terminal region of the structural pilin subunit., Mol Microbiol **11** (1994) 705.

[105] M.D. Johnson *et al.*, Pseudomonas aeruginosa PilY1 binds integrin in an RGD- and calcium-dependent manner, PLoS ONE **6** (2011) 1.

[106] C. Sundin *et al.*, Type IV pili are not specifically required for contact dependent translocation of exoenzymes by Pseudomonas aeruginosa, Microbial Pathogenesis **33** (2002) 265.

[107] H.B. Sheth *et al.*, The pili of Pseudomonas aeruginosa strains PAK and PAO bind specifically to the carbohydrate sequence ?GalNAc(1?4)?Gal found in glycosphingolipids asialo-GM 1 and asialo-GM 2, Molecular Microbiology **11** (1994) 715.

[108] J.C. Comolli *et al.*, Pili binding to asialo-GM1 on epithelial cells can mediate cytotoxicity or bacterial internalization by Pseudomonas aeruginosa., Infection and immunity **67** (1999) 3207.

[109] I. Zolfaghar, D.J. Evans and S.M.J. Fleiszig, Twitching Motility Contributes to the Role of Pili in Corneal Infection Caused by Pseudomonas aeruginosa, Infection and Immunity **71** (2003) 5389.

[110] A. Persat *et al.*, Type IV pili mechanochemically regulate virulence factors in Pseudomonas aeruginosa, Proceedings of the National Academy of Sciences **112** (2015) 7563.

[111] E.V. Davies *et al.*, Temperate phages both mediate and drive adaptive evolution in pathogen biofilms, Proceedings of the National Academy of Sciences **113** (2016) 8266.

[112] D. Roux *et al.*, Fitness cost of antibiotic susceptibility during bacterial infection, Science Translational Medicine **7** (2015) 297ra114.

[113] S. Wang *et al.*, Coordination of Swarming Motility, Biosurfactant Synthesis, and Biofilm Matrix Exopolysaccharide Production in Pseudomonas aeruginosa, Applied and Environmental Microbiology **80** (2014) 6724.

[114] J.C. Conrad *et al.*, Flagella and Pili-Mediated Near-Surface Single-Cell Motility Mechanisms in P. aeruginosa, Biophysical Journal **100** (2011) 1608.

[115] G. Golovkine *et al.*, Pseudomonas aeruginosa Transmigrates at Epithelial Cell-Cell Junctions, Exploiting Sites of Cell Division and Senescent Cell Extrusion, PLOS Pathogens **12** (2016) e1005377.

[116] M. Floyd *et al.*, Swimming Motility Mediates the Formation of Neutrophil Extracellular Traps Induced by Flagellated Pseudomonas aeruginosa, PLOS Pathogens **12** (2016) e1005987.

[117] D. Parker and A. Prince, Innate Immunity in the Respiratory Epithelium, American Journal of Respiratory Cell and Molecular Biology **45** (2011) 189.

[118] Z. Zhang *et al.*, Human Airway Epithelial Cells Sense Pseudomonas aeruginosa Infection via Recognition of Flagellin by Toll-Like Receptor 5, Infection and Immunity **73** (2005) 7151.

[119] C.J. Blohmke *et al.*, TLR5 as an Anti-Inflammatory Target and Modifier Gene in Cystic Fibrosis, The Journal of Immunology **185** (2010) 7731.

[120] R. Ramphal, C. Guay and G.B. Pier, Pseudomonas aeruginosa adhesins for tracheobronchial mucin, Infection and Immunity **55** (1987) 600.

[121] J. Bruzaud *et al.*, Flagella but not type IV pili are involved in the initial adhesion of Pseudomonas aeruginosa PAO1 to hydrophobic or superhydrophobic surfaces, Colloids and Surfaces B: Biointerfaces **131** (2015) 59.

[122] I. Bucior, J.F. Pielage and J.N. Engel, Pseudomonas aeruginosa Pili and Flagella Mediate Distinct Binding and Signaling Events at the Apical and Basolateral Surface of Airway Epithelium, PLoS Pathogens **8** (2012) e1002616.

[123] C.P. Tanase, I. Ogrezeanu and C. Badiu, Signal Transduction, Molecular Pathology of Pituitary Adenomas (2012) 53.

[124] A.Y. Bhagirath *et al.*, Cystic fibrosis lung environment and Pseudomonas aeruginosa infection, BMC Pulmonary Medicine **16** (2016) 1.

[125] M. Sahoo *et al.*, Role of the Inflammasome, IL-1 β, and IL-18 in Bacterial Infections, The Scientific World JOURNAL **11** (2011) 2037.

[126] S. Elsen *et al.*, A Type III Secretion Negative Clinical Strain of Pseudomonas aeruginosa Employs a Two-Partner Secreted Exolysin to Induce Hemorrhagic Pneumonia, Cell Host & Microbe **15** (2014) 164.

[127] T. Horng, G.M. Barton and R. Medzhitov, No Title, Nature Immunology **2** (2001) 835.

[128] P.R. Imbert *et al.*, A Pseudomonas aeruginosa TIR effector mediates immune evasion by targeting UBAP1 and TLR adaptors, The EMBO Journal (2017) e201695343.

[129] F. Cadoret *et al.*, Txc, a New Type II Secretion System of Pseudomonas aeruginosa Strain PA7, Is Regulated by the TtsS/TtsR Two-Component System and Directs Specific Secretion of the CbpE Chitin-Binding Protein, Journal of Bacteriology **196** (2014) 2376.

[130] P. Braun *et al.*, Secretion of elastinolytic enzymes and their propeptides by Pseudomonas aeruginosa, Journal of Bacteriology **180** (1998) 3467.

[131] S. Bleves *et al.*, Protein secretion systems in Pseudomonas aeruginosa: A wealth of pathogenic weapons., International journal of medical microbiology : IJMM **300** (2010) 534.

[132] H.M. Lu and S. Lory, A specific targeting domain in mature exotoxin A is required for its extracellular secretion from Pseudomonas aeruginosa., The EMBO journal **15** (1996) 429.

[133] L.S. Engel *et al.*, Protease IV, a unique extracellular protease and virulence factor from Pseudomonas aeruginosa., The Journal of biological chemistry **273** (1998) 16792.

[134] J.L. Malloy, Pseudomonas aeruginosa protease IV degrades surfactant proteins and inhibits surfactant host defense and biophysical functions, AJP: Lung Cellular and Molecular Physiology **288** (2004) L409.

[135] A.O. Azghani, E.J. Miller and B.T. Peterson, Virulence factors from Pseudomonas aeruginosa increase lung epithelial permeability., Lung **178** (2000) 261.

[136] F. Casilag *et al.*, The LasB Elastase of Pseudomonas aeruginosa Acts in Concert with Alkaline Protease AprA To Prevent Flagellin-Mediated Immune Recognition, Infection and Immunity **84** (2016) 162.

[137] G. Ball *et al.*, A novel type II secretion system in Pseudomonas aeruginosa, Molecular Microbiology **43** (2002) 475.

[138] J.C. Leo, I. Grin and D. Linke, Type V secretion: mechanism(s) of autotransport through the bacterial outer membrane., Philosophical transactions of the Royal Society of London. Series B, Biological sciences **367** (2012) 1088.

[139] F. Jacob-Dubuisson, R. Fernandez and L. Coutte, Protein Secretion through Autotransporter and Two-Partner Pathways, Biochimica et Biophysica Acta (BBA) - Molecular Cell Research **1694** (2004) 235.

[140] F. Jacob-Dubuisson, C. Locht and R. Antoine, Two-partner secretion in Gram-negative bacteria: a thrifty, specific pathway for large virulence proteins., Molecular microbiology **40** (2001) 306.

[141] J. Guérin *et al.*, Two-Partner Secretion: Combining Efficiency and Simplicity in the Secretion of Large Proteins for Bacteria-Host and Bacteria-Bacteria Interactions, Frontiers in Cellular and Infection Microbiology **7** (2017).

[142] I.R. Henderson, F. Navarro-Garcia and J.P. Nataro, The Great Escape: Structure and Function of the Autotransporter Proteins, Trends in Microbiology **6** (1998) 370.

[143] P. Natale, T. Brüser and A.J. Driessen, Sec- and Tat-mediated protein secretion across the bacterial cytoplasmic membrane-Distinct translocases and mechanisms, Biochimica et Biophysica Acta (BBA) - Biomembranes **1778** (2008) 1735.

[144] T. Palmer and B.C. Berks, The twin-arginine translocation (Tat) protein export pathway, Nature Reviews Microbiology (2012).

[145] I.R. Henderson *et al.*, Type V Protein Secretion Pathway: the Autotransporter Story, Microbiology and Molecular Biology Reviews **68** (2004) 692.

[146] P. Emsley *et al.*, Structure of Bordetella pertussis virulence factor P.69 pertactin, Nature **381** (1996) 90.

[147] B.R. Otto *et al.*, Crystal Structure of Hemoglobin Protease, a Heme Binding Autotransporter Protein from Pathogenic Escherichia coli, Journal of Biological Chemistry **280** (2005) 17339.

[148] B. van den Berg, Crystal Structure of a Full-Length Autotransporter, Journal of Molecular Biology **396** (2010) 627.

[149] D.C. Oliver *et al.*, A conserved region within the Bordetella pertussis autotransporter BrkA is necessary for folding of its passenger domain., Molecular microbiology **47** (2003) 1367.

[150] J.J. Velarde and J.P. Nataro, Hydrophobic Residues of the Autotransporter EspP Linker Domain Are Important for Outer Membrane Translocation of Its Passenger, Journal of Biological Chemistry **279** (2004) 31495.

[151] F. Berthiaume, N. Rutherford and M. Mourez, Mutations affecting the biogenesis of the AIDA-I autotransporter, Research in Microbiology **158** (2007) 348.

[152] C.J. Oomen *et al.*, Structure of the Translocator Domain of a Bacterial Autotransporter, The EMBO Journal **23** (2004) 1257.

[153] T.J. Barnard *et al.*, Autotransporter structure reveals intra-barrel cleavage followed by conformational changes, Nature Structural & Molecular Biology **14** (2007) 1214.

[154] M. Remmert *et al.*, Evolution of Outer Membrane β-Barrels from an Ancestral $\beta\beta$ Hairpin, Molecular Biology and Evolution **27** (2010) 1348.

[155] J. Pohlner *et al.*, Gene structure and extracellular secretion of Neisseria gonorrhoeae IgA protease, Nature **325** (1987) 458.

[156] Q. Ma *et al.*, Protein secretion systems of Pseudomonas aeruginosa and P. fluorescens, Biochimica et Biophysica Acta (BBA) - Biomembranes **1611** (2003) 223.

[157] A. Filloux, The underlying mechanisms of type II protein secretion, Biochimica et Biophysica Acta (BBA) - Molecular Cell Research **1694** (2004) 163.

[158] S. Wilhelm, J. Tommassen and K.E. Jaeger, A novel lipolytic enzyme located in the outer membrane of Pseudomonas aeruginosa., Journal of bacteriology **181** (1999) 6977.

[159] S. Wilhelm *et al.*, The Autotransporter Esterase EstA of Pseudomonas aeruginosa Is Required for Rhamnolipid Production, Cell Motility, and Biofilm Formation, Journal of Bacteriology **189** (2007) 6695.

[160] S. Becker *et al.*, A generic system for the Escherichia coli cell-surface display of lipolytic enzymes, FEBS Letters **579** (2005) 1177.

[161] C.C. Akoh *et al.*, GDSL family of serine esterases/lipases, Progress in Lipid Research **43** (2004) 534.

[162] E. Potvin *et al.*, In vivo functional genomics of Pseudomonas aeruginosa for high-throughput screening of new virulence factors and antibacterial targets, Environmental Microbiology **5** (2003) 1294.

[163] D. Linke *et al.*, Trimeric autotransporter adhesins: variable structure, common function, Trends in Microbiology **14** (2006) 264.

[164] A. Roggenkamp *et al.*, Molecular Analysis of Transport and Oligomerization of the Yersinia enterocolitica Adhesin YadA, Journal of Bacteriology **185** (2003) 3735.

[165] E. Hoiczyk, Structure and sequence analysis of Yersinia YadA and Moraxella UspAs reveal a novel class of adhesins, The EMBO Journal **19** (2000) 5989.

[166] N.K. Surana *et al.*, The Haemophilus influenzae Hia Autotransporter Contains an Unusually Short Trimeric Translocator Domain, Journal of Biological Chemistry **279** (2004) 14679.

[167] P. Szczesny *et al.*, Structure of the Head of the Bartonella Adhesin BadA, PLoS Pathogens **4** (2008) e1000119.

[168] V. Finck-Barbançon *et al.*, ExoU expression by Pseudomonas aeruginosa correlates with acute cytotoxicity and epithelial injury., Molecular microbiology **25** (1997) 547.

[169] A.R. Hauser, P.J. Kang and J.N. Engel, PepA, a secreted protein of Pseudomonas aeruginosa, is necessary for cytotoxicity and virulence., Molecular microbiology **27** (1998) 807.

[170] R. Salacha *et al.*, The Pseudomonas aeruginosa patatin-like protein PlpD is the archetype of a novel Type V secretion system, Environmental Microbiology (2010).

[171] P. Oberhettinger *et al.*, Intimin and Invasin Export Their C-Terminus to the Bacterial Cell Surface Using an Inverse Mechanism Compared to Classical Autotransport, PLoS ONE **7** (2012) e47069.

[172] J.M. Leong, R.S. Fournier and R.R. Isberg, Identification of the integrin binding domain of the Yersinia pseudotuberculosis invasin protein., The EMBO Journal **9** (1990) 1979.

[173] S. Jain *et al.*, Polar Localization of the Autotransporter Family of Large Bacterial Virulence Proteins, Journal of Bacteriology **188** (2006) 4841.

[174] R. Hertle *et al.*, Cytotoxic action of Serratia marcescens hemolysin on human epithelial cells., Infection and immunity **67** (1999) 817.

[175] A.V. Kajava *et al.*, Beta-helix model for the filamentous haemagglutinin adhesin of Bordetella pertussis and related bacterial secretory proteins., Molecular microbiology **42** (2001) 279.

[176] R.J. Willems *et al.*, Mutational analysis of the Bordetella pertussis fim/fha gene cluster: identification of a gene with sequence similarities to haemolysin accessory genes involved in export of FHA., Molecular microbiology **11** (1994) 337.

[177] C.M. Rojas *et al.*, HecA, a member of a class of adhesins produced by diverse pathogenic bacteria, contributes to the attachment, aggregation, epidermal cell killing, and virulence phenotypes of Erwinia chrysanthemi EC16 on Nicotiana clevelandii seedlings, Proceedings of the National Academy of Sciences **99** (2002) 13142.

[178] F. Jacob-Dubuisson *et al.*, Lack of functional complementation between Bordetella pertussis filamentous hemagglutinin and Proteus mirabilis HpmA hemolysin secretion machineries., Journal of bacteriology **179** (1997) 775.

[179] S. Grass and J.W. St Geme, Maturation and secretion of the non-typable Haemophilus influenzae HMW1 adhesin: roles of the N-terminal and C-terminal domains., Molecular microbiology **36** (2000) 55.

[180] R. Schönherr *et al.*, Amino acid replacements in the Serratia marcescens haemolysin ShIA define sites involved in activation and secretion., Molecular microbiology **9** (1993) 1229.

[181] G. Renauld-Mongénie *et al.*, Distinct roles of the N-terminal and C-terminal precursor domains in the biogenesis of the Bordetella pertussis filamentous hemagglutinin., Journal of bacteriology **178** (1996) 1053.

[182] B. Clantin *et al.*, The crystal structure of filamentous hemagglutinin secretion domain and its implications for the two-partner secretion pathway, Proceedings of the National Academy of Sciences **101** (2004) 6194.

[183] H. Hodak *et al.*, Secretion signal of the filamentous haemagglutinin, a model two-partner secretion substrate., Molecular microbiology **61** (2006) 368.

[184] T.M. Weaver *et al.*, Structural and functional studies of truncated hemolysin A from Proteus mirabilis., The Journal of biological chemistry **284** (2009) 22297.

[185] H.J. Yeo *et al.*, The Structure of the Haemophilus influenzae HMW1 Pro-piece Reveals a Structural Domain Essential for Bacterial Two-partner Secretion, Journal of Biological Chemistry **282** (2007) 31076.

[186] S. Baelen *et al.*, Structure of the secretion domain of HxuA from Haemophilus influenzae, Acta Crystallographica Section F Structural Biology and Crystallization Communications **69** (2013) 1322.

[187] S. Zambolin *et al.*, Structural basis for haem piracy from host haemopexin by Haemophilus influenzae, Nature Communications **7** (2016) 11590.

[188] B. Clantin *et al.*, Structure of the Membrane Protein FhaC: A Member of the Omp85-TpsB Transporter Superfamily, Science **317** (2007) 957.

[189] T. Maier *et al.*, Conserved Omp85 lid-lock structure and substrate recognition in FhaC, Nature Communications **6** (2015) 7452.

[190] N. Noinaj *et al.*, Structural insight into the biogenesis of β-barrel membrane proteins, Nature **501** (2013) 385.

[191] T.W. Kim *et al.*, A critical role for IRAK4 kinase activity in Toll-like receptor-mediated innate immunity, The Journal of Experimental Medicine **204** (2007) 1025.

[192] S. Guédin *et al.*, Novel Topological Features of FhaC, the Outer Membrane Transporter Involved in the Secretion of the Bordetella pertussis Filamentous Hemagglutinin, Journal of Biological Chemistry **275** (2000) 30202.

[193] C. Baud *et al.*, Translocation path of a substrate protein through its Omp85 transporter, Nature Communications **5** (2014) 5271.

[194] A.S. Delattre *et al.*, Functional importance of a conserved sequence motif in FhaC, a prototypic member of the TpsB/Omp85 superfamily, FEBS Journal **277** (2010) 4755.

[195] M. Leonard-Rivera and R. Misra, Conserved Residues of the Putative L6 Loop of Escherichia coli BamA Play a Critical Role in the Assembly of -Barrel Outer Membrane Proteins, Including That of BamA Itself, Journal of Bacteriology **194** (2012) 4662.

[196] N.W. Rigel, D.P. Ricci and T.J. Silhavy, Conformation-specific labeling of BamA and suppressor analysis suggest a cyclic mechanism for -barrel assembly in Escherichia coli, Proceedings of the National Academy of Sciences **110** (2013) 5151.

[197] E. Schiebel, H. Schwarz and V. Braun, Subcellular location and unique secretion of the hemolysin of Serratia marcescens., The Journal of biological chemistry **264** (1989) 16311.

[198] P. van Ulsen *et al.*, Two-Partner Secretion Systems of Neisseria meningitidis Associated with Invasive Clonal Complexes, Infection and Immunity **76** (2008) 4649.

[199] P.S. Choi and H.D. Bernstein, Sequential translocation of an Escherchia coli two-partner secretion pathway exoprotein across the inner and outer membranes, Molecular Microbiology **75** (2010) 440.

[200] C. Baud *et al.*, Role of DegP for two-partner secretion in Bordetella, Molecular Microbiology **74** (2009) 315.

[201] C. Baud *et al.*, Membrane-associated DegP in Bordetella chaperones a repeat-rich secretory protein, Molecular Microbiology **80** (2011) 1625.

[202] J.E. Mogensen and D.E. Otzen, Interactions between folding factors and bacterial outer membrane proteins, Molecular Microbiology **57** (2005) 326.

[203] U. Grosskinsky *et al.*, A Conserved Glycine Residue of Trimeric Autotransporter Domains Plays a Key Role in Yersinia Adhesin A Autotransport, Journal of Bacteriology **189** (2007) 9011.

[204] H. Hodak and F. Jacob-Dubuisson, Current Challenges in Autotransport and Two-Partner Protein Secretion Pathways, Research in Microbiology **158** (2007) 631.

[205] J. Mazar and P.A. Cotter, Topology and maturation of filamentous haemagglutinin suggest a new model for two-partner secretion, Molecular Microbiology **62** (2006) 641.

[206] H. Hodak and F. Jacob-Dubuisson, Current challenges in autotransport and two-partner protein secretion pathways, Research in Microbiology **158** (2007) 631.

[207] J. Guérin *et al.*, Conformational dynamics of protein transporter FhaC: large-scale motions of plug helix, Molecular Microbiology **92** (2014) 1164.

[208] G. Walker, R. Hertle and V. Braun, Activation of Serratia marcescens hemolysin through a conformational change., Infection and immunity **72** (2004) 611.

[209] T.M. Weaver *et al.*, Structural and Functional Studies of Truncated Hemolysin A from Proteus mirabilis, Journal of Biological Chemistry **284** (2009) 22297.

[210] M. Junker, R.N. Besingi and P.L. Clark, Vectorial transport and folding of an autotransporter virulence protein during outer membrane secretion, Molecular Microbiology **71** (2009) 1323.

[211] J.H. Peterson *et al.*, Secretion of a bacterial virulence factor is driven by the folding of a C-terminal segment, Proceedings of the National Academy of Sciences **107** (2010) 17739.

[212] R.N. Besingi, J.L. Chaney and P.L. Clark, An alternative outer membrane secretion mechanism for an autotransporter protein lacking a C-terminal stable core, Molecular Microbiology **90** (2013) 1028.

[213] J. Guérin *et al.*, Dynamic interplay of membrane-proximal POTRA domain and conserved loop L6 in Omp85 transporter FhaC, Molecular Microbiology **98** (2015) 490.

[214] M. van Schilfgaarde *et al.*, Characterization of Adherence of Nontypeable Haemophilus Influenzae to Human Epithelial Cells, Infection and Immunity **68** (2000) 4658.

[215] A.Z. Buscher *et al.*, Surface Anchoring of a Bacterial Adhesin Secreted by the Two-Partner Secretion Pathway, Molecular Microbiology **61** (2006) 470.

[216] L. Coutte *et al.*, Subtilisin-like autotransporter serves as maturation protease in a bacterial secretion pathway, The EMBO Journal **20** (2001) 5040.

[217] J. Mazar and P.a. Cotter, New insight into the molecular mechanisms of two-partner secretion., Trends in microbiology **15** (2007) 508.

[218] R. Antoine *et al.*, New virulence-activated and virulence-repressed genes identified by systematic gene inactivation and generation of transcriptional fusions in Bordetella pertussis., Journal of bacteriology **182** (2000) 5902.

[219] D.O. Serra *et al.*, FHA-Mediated Cell-Substrate and Cell-Cell Adhesions Are Critical for Bordetella pertussis Biofilm Formation on Abiotic Surfaces and in the Mouse Nose and the Trachea, PLoS ONE **6** (2011) e28811.

[220] S.E. Cotter, N.K. Surana and J.W. St. Geme, Trimeric autotransporters: a distinct subfamily of autotransporter proteins, Trends in Microbiology **13** (2005) 199.

[221] B.R. Borlee *et al.*, Pseudomonas aeruginosa uses a cyclic-di-GMP-regulated adhesin to reinforce the biofilm extracellular matrix, Molecular Microbiology **75** (2010) 827.

[222] C. Baraquet and C.S. Harwood, FleQ DNA Binding Consensus Sequence Revealed by Studies of FleQ-Dependent Regulation of Biofilm Gene Expression in Pseudomonas aeruginosa, Journal of Bacteriology **198** (2016) 178.

[223] R.B. Cooley *et al.*, Cyclic Di-GMP-Regulated Periplasmic Proteolysis of a Pseudomonas aeruginosa Type Vb Secretion System Substrate, Journal of Bacteriology **198** (2016) 66.

[224] M. Rybtke *et al.*, The LapG protein plays a role in Pseudomonas aeruginosa biofilm formation by controlling the presence of the CdrA adhesin on the cell surface, MicrobiologyOpen **4** (2015) 917.

[225] M. Vakevainen, S. Greenberg and E.J. Hansen, Inhibition of phagocytosis by Haemophilus ducreyi requires expression of the LspA1 and LspA2 proteins., Infection and immunity **71** (2003) 5994.

[226] D.A. Dodd *et al.*, The Haemophilus ducreyi LspA1 Protein Inhibits Phagocytosis By Using a New Mechanism Involving Activation of C-Terminal Src Kinase, mBio **5** (2014) e01178.

[227] K. Roy *et al.*, Enterotoxigenic Escherichia coli EtpA mediates adhesion between flagella and host cells, Nature **457** (2009) 594.

[228] S.K. Aoki, Contact-Dependent Inhibition of Growth in Escherichia coli, Science **309** (2005) 1245.

[229] R. Hertle, Serratia marcescens Hemolysin (ShlA) Binds Artificial Membranes and Forms Pores in a Receptor-independent Manner, Journal of Membrane Biology **189** (2002) 1.

[230] R. Hertle and H. Schwarz, Serratia marcescens internalization and replication in human bladder epithelial cells, BMC Infectious Diseases **4** (2004).

[231] N. González-Juarbe *et al.*, Pore-Forming Toxins Induce Macrophage Necroptosis during Acute Bacterial Pneumonia, PLOS Pathogens **11** (2015) e1005337.

[232] G. Di Venanzio, T.M. Stepanenko and E. García Véscovi, Serratia marcescens ShlA Pore-Forming Toxin Is Responsible for Early Induction of Autophagy in Host Cells and Is Transcriptionally Regulated by RcsB, Infection and Immunity **82** (2014) 3542.

[233] J.E. Alouf, Molecular features of the cytolytic pore-forming bacterial protein toxins., Folia microbiologica **48** (2003) 5.

[234] M.W. Parker *et al.*, Structure of the membrane-pore-forming fragment of colicin A, Nature **337** (1989) 93.

[235] G.G. Alves *et al.*, Clostridium perfringens epsilon toxin: The third most potent bacterial toxin known, Anaerobe **30** (2014) 102.

[236] S.D. Zakharov *et al.*, On the role of lipid in colicin pore formation, Biochimica et Biophysica Acta (BBA) - Biomembranes **1666** (2004) 239.

[237] E. Cascales *et al.*, Colicin Biology, Microbiology and Molecular Biology Reviews **71** (2007) 158.

[238] M.W. Parker *et al.*, Refined structure of the pore-forming domain of colicin A at 2.4 A resolution., Journal of molecular biology **224** (1992) 639.

[239] S.J. Tilley and H.R. Saibil, The mechanism of pore formation by bacterial toxins, Current Opinion in Structural Biology **16** (2006) 230.

[240] M.D. Peraro and F.G. van der Goot, Pore-forming toxins: ancient, but never really out of fashion, Nature Reviews Microbiology **14** (2015) 77.

[241] M. Madegowda *et al.*, X-ray crystal structure of the B component of Hemolysin BL fromBacillus cereus, Proteins: Structure, Function, and Bioinformatics **71** (2008) 534.

[242] S. Hunt, J. Green and P.J. Artymiuk, Hemolysin E (HlyE, ClyA, SheA) and related toxins., Advances in experimental medicine and biology **677** (2010) 116.

[243] A.J. Wallace *et al.*, E. coli hemolysin E (HlyE, ClyA, SheA): X-ray crystal structure of the toxin and observation of membrane pores by electron microscopy., Cell **100** (2000) 265.

[244] M. Mueller *et al.*, The structure of a cytolytic α-helical toxin pore reveals its assembly mechanism, Nature **459** (2009) 726.

[245] M.S. Vaidyanathan *et al.*, Lysis dynamics and membrane oligomerization pathways for Cytolysin A (ClyA) pore-forming toxin, RSC Advances **4** (2014) 4930.

[246] D. Roderer *et al.*, Soluble Oligomers of the Pore-forming Toxin Cytolysin A from Escherichia coli Are Off-pathway Products of Pore Assembly, Journal of Biological Chemistry **291** (2016) 5652.

[247] M. Fahie *et al.*, A Non-classical Assembly Pathway of Escherichia coli Pore-forming Toxin Cytolysin A, Journal of Biological Chemistry **288** (2013) 31042.

[248] A. Soloaga *et al.*, Insertion of Escherichia coli alpha-haemolysin in lipid bilayers as a non-transmembrane integral protein: prediction and experiment., Molecular microbiology **31** (1999) 1013.

[249] L. Sánchez-Magraner *et al.*, The Calcium-binding C-terminal Domain of Escherichia coli α-Hemolysin Is a Major Determinant in the Surface-active Properties of the Protein, Journal of Biological Chemistry **282** (2007) 11827.

[250] A.L. DuMont and V.J. Torres, Cell targeting by the Staphylococcus aureus pore-forming toxins: it's not just about lipids, Trends in Microbiology **22** (2014) 21.

[251] G. Menestrina, M.D. Serra and G. Prévost, Mode of action of beta-barrel pore-forming toxins of the staphylococcal alpha-hemolysin family., Toxicon : official journal of the International Society on Toxinology **39** (2001) 1661.

[252] L. Jayasinghe and H. Bayley, The leukocidin pore: evidence for an octamer with four LukF subunits and four LukS subunits alternating around a central axis., Protein science : a publication of the Protein Society **14** (2005) 2550.

[253] M.J. Aman *et al.*, Structural model of the pre-pore ring-like structure of Panton-Valentine leukocidin: providing dimensionality to biophysical and mutational data., Journal of biomolecular structure & dynamics **28** (2010) 1.

[254] L. Song *et al.*, Structure of staphylococcal alpha-hemolysin, a heptameric transmembrane pore., Science (New York, N.Y.) **274** (1996) 1859.

[255] K. Yamashita *et al.*, Crystal structure of the octameric pore of staphylococcal γ-hemolysin reveals the β-barrel pore formation mechanism by two components., Proceedings of the National Academy of Sciences of the United States of America **108** (2011) 17314.

[256] O. Opota *et al.*, Monalysin, a Novel ß-Pore-Forming Toxin from the Drosophila Pathogen Pseudomonas entomophila, Contributes to Host Intestinal Damage and Lethality, PLoS Pathogens **7** (2011) e1002259.

[257] I. Iacovache *et al.*, Cryo-EM structure of aerolysin variants reveals a novel protein fold and the pore-formation process, Nature Communications **7** (2016) 12062.

[258] C.L. Johnson *et al.*, The antibacterial toxin colicin N binds to the inner core of lipopolysaccharide and close to its translocator protein, Molecular Microbiology **92** (2014) 440.

[259] E.M. Hotze *et al.*, Identification and Characterization of the First Cholesterol-Dependent Cytolysins from Gram-Negative Bacteria, Infection and Immunity **81** (2013) 216.

[260] E.M. Hotze and R.K. Tweten, Membrane assembly of the cholesterol-dependent cytolysin pore complex, Biochimica et Biophysica Acta (BBA) - Biomembranes **1818** (2012) 1028.

[261] S.J. Tilley *et al.*, Structural Basis of Pore Formation by the Bacterial Toxin Pneumolysin, Cell **121** (2005) 247.

[262] D.M. Czajkowsky *et al.*, Vertical collapse of a cytolysin prepore moves its transmembrane β-hairpins to the membrane, The EMBO Journal **23** (2004) 3206.

[263] T.K. Sato, R.K. Tweten and A.E. Johnson, Disulfide-bond scanning reveals assembly state and β-strand tilt angle of the PFO β-barrel, Nature Chemical Biology **9** (2013) 383.

[264] L. Abrami, M. Fivaz and F.G. van der Goot, Adventures of a pore-forming toxin at the target cell surface., Trends in microbiology **8** (2000) 168.

[265] Y. Hong *et al.*, Requirement of N-glycan on GPI-anchored proteins for efficient binding of aerolysin but not Clostridium septicum α-toxin, The EMBO Journal **21** (2002) 5047.

[266] D.B. Diep *et al.*, Glycosylphosphatidylinositol anchors of membrane glycoproteins are binding determinants for the channel-forming toxin aerolysin., The Journal of biological chemistry **273** (1998) 2355.

[267] G. van Meer, D.R. Voelker and G.W. Feigenson, Membrane lipids: where they are and how they behave, Nature Reviews Molecular Cell Biology **9** (2008) 112.

[268] R.K. Tweten, Cholesterol-Dependent Cytolysins, a Family of Versatile Pore-Forming Toxins, Infection and Immunity **73** (2005) 6199.

[269] K.J. Dowd and R.K. Tweten, The Cholesterol-Dependent Cytolysin Signature Motif: A Critical Element in the Allosteric Pathway that Couples Membrane Binding to Pore Assembly, PLoS Pathogens **8** (2012) e1002787.

[270] J.G. Bann, L. Cegelski and S.J. Hultgren, LRP6 Holds the Key to the Entry of Anthrax Toxin, Cell **124** (2006) 1119.

[271] L.P. Pulagam and H.J. Steinhoff, Acidic pH-Induced Membrane Insertion of Colicin A into E. coli Natural Lipids Probed by Site-Directed Spin Labeling, Journal of Molecular Biology **425** (2013) 1782.

[272] G.A. Wilke and J.B. Wardenburg, Role of a disintegrin and metalloprotease 10 in Staphylococcus aureus -hemolysin-mediated cellular injury, Proceedings of the National Academy of Sciences **107** (2010) 13473.

[273] B.J. Berube and J. Bubeck Wardenburg, Staphylococcus aureus α-toxin: nearly a century of intrigue., Toxins **5** (2013) 1140.

[274] S. Virreira Winter, A. Zychlinsky and B.W. Bardoel, Genome-wide CRISPR screen reveals novel host factors required for Staphylococcus aureus α-hemolysin-mediated toxicity, Scientific Reports **6** (2016) 24242.

[275] M.A. Hamon *et al.*, Listeriolysin O: the Swiss army knife of Listeria, Trends in Microbiology **20** (2012) 360.

[276] A.L. Radtke *et al.*, Listeria monocytogenes exploits cystic fibrosis transmembrane conductance regulator (CFTR) to escape the phagosome, Proceedings of the National Academy of Sciences **108** (2011) 1633.

[277] I. Linhartová *et al.*, RTX proteins: a highly diverse family secreted by a common mechanism, FEMS Microbiology Reviews **34** (2010) 1076.

[278] R. Fiser *et al.*, Calcium Influx Rescues Adenylate Cyclase-Hemolysin from Rapid Cell Membrane Removal and Enables Phagocyte Permeabilization by Toxin Pores, PLoS Pathogens **8** (2012) e1002580.

[279] A. Osickova *et al.*, Adenylate cyclase toxin translocates across target cell membrane without forming a pore, Molecular Microbiology **75** (2010) 1550.

[280] A. Richter-Dahlfors *et al.*, No Title, Nature **405** (2000) 694.

[281] R. Jiang *et al.*, Intermediate closed channel state(s) precede(s) activation in the ATP-gated P2X2 receptor, Channels **6** (2012) 398.

[282] M. Skals *et al.*, -Hemolysin from Escherichia coli uses endogenous amplification through P2X receptor activation to induce hemolysis, Proceedings of the National Academy of Sciences **106** (2009) 4030.

[283] M. Skals, J. Leipziger and H.A. Praetorius, Haemolysis induced by α-toxin from Staphylococcus aureus requires P2X receptor activation, Pflügers Archiv - European Journal of Physiology **462** (2011) 669.

[284] C.L. Kennedy *et al.*, Programmed Cellular Necrosis Mediated by the Pore-Forming α-Toxin from Clostridium septicum, PLoS Pathogens **5** (2009) e1000516.

[285] C.F. Lin *et al.*, Different Types of Cell Death Induced by Enterotoxins, Toxins **2** (2010) 2158.

[286] R.R. Craven *et al.*, Staphylococcus aureus α-Hemolysin Activates the NLRP3-Inflammasome in Human and Mouse Monocytic Cells, PLoS ONE **4** (2009) e7446.

[287] J.N. Radin *et al.*, Helicobacter pylori VacA Induces Programmed Necrosis in Gastric Epithelial Cells, Infection and Immunity **79** (2011) 2535.

[288] J. Rassow, Helicobacter pylori vacuolating toxin A and apoptosis, Cell Communication and Signaling **9** (2011) 26.

[289] J.A. Smyth and T.G. Martin, Disease producing capability of netB positive isolates of C. perfringens recovered from normal chickens and a cow, and netB positive and negative isolates from chickens with necrotic enteritis, Veterinary Microbiology **146** (2010) 76.

[290] K.K. Cooper and J.G. Songer, Virulence of Clostridium perfringens in an experimental model of poultry necrotic enteritis, Veterinary Microbiology **142** (2010) 323.

[291] A.L. Keyburn *et al.*, NetB, a New Toxin That Is Associated with Avian Necrotic Enteritis Caused by Clostridium perfringens, PLoS Pathogens **4** (2008) e26.

[292] N. Sugimoto *et al.*, Botulinolysin, a thiol-activated hemolysin produced by Clostridium botulinum, inhibits endothelium-dependent relaxation of rat aortic ring., Toxicon : official journal of the International Society on Toxinology **35** (1997) 1011.

[293] N. Sugimoto *et al.*, Coronary vasoconstriction is the most probable cause of death of rats intoxicated with botulinolysin, a hemolysin produced by Clostridium botulinum., Toxicon : official journal of the International Society on Toxinology **33** (1995) 1215.

[294] P. Broz and V.M. Dixit, Inflammasomes: mechanism of assembly, regulation and signalling, Nature Reviews Immunology **16** (2016) 407.

[295] V. Feuillet *et al.*, Involvement of Toll-like receptor 5 in the recognition of flagellated bacteria, Proceedings of the National Academy of Sciences **103** (2006) 12487.

[296] E.A. Miao *et al.*, TLR5 and Ipaf: dual sensors of bacterial flagellin in the innate immune system, Seminars in Immunopathology **29** (2007) 275.

[297] S.K. Vanaja, V.A. Rathinam and K.A. Fitzgerald, Mechanisms of inflammasome activation: recent advances and novel insights, Trends in Cell Biology **25** (2015) 308.

[298] L.A. Mijares *et al.*, Airway Epithelial MyD88 Restores Control of Pseudomonas aeruginosa Murine Infection via an IL-1-Dependent Pathway, The Journal of Immunology **186** (2011) 7080.

[299] A.J. McCoy *et al.*, Cytotoxins of the human pathogen Aeromonas hydrophila trigger, via the NLRP3 inflammasome, caspase-1 activation in macrophages., European journal of immunology **40** (2010) 2797.

[300] H. Nishiwaki *et al.*, Cloning, Functional Characterization, and Mode of Action of a Novel Insecticidal Pore-Forming Toxin, Sphaericolysin, Produced by Bacillus sphaericus, Applied and Environmental Microbiology **73** (2007) 3404.

[301] K. Srisucharitpanit *et al.*, Expression and purification of the active soluble form of Bacillus sphaericus binary toxin for structural analysis, Protein Expression and Purification **82** (2012) 368.

[302] J.F. Brunet *et al.*, Pore-forming properties of the Bacillus thuringiensis toxin Cry9Ca in Manduca sexta brush border membrane vesicles, Biochimica et Biophysica Acta (BBA) - Biomembranes **1798** (2010) 1111.

[303] E. Gazit *et al.*, The structure and organization within the membrane of the helices composing the pore-forming domain of Bacillus thuringiensis delta-endotoxin are consistent with an "umbrella-like" structure of the pore., Proceedings of the National Academy of Sciences of the United States of America **95** (1998) 12289.

[304] T. Lund, M.L. De Buyser and P.E. Granum, A new cytotoxin from Bacillus cereus that may cause necrotic enteritis., Molecular microbiology **38** (2000) 254.

[305] P. Grochulski *et al.*, Bacillus thuringiensis CryIA(a) insecticidal toxin: crystal structure and channel formation., Journal of molecular biology **254** (1995) 447.

[306] L. Masson *et al.*, A Novel Bacillus thuringiensis (PS149B1) Containing a Cry34Ab1/Cry35Ab1 Binary Toxin Specific for the Western Corn Rootworm Diabrotica virgifera virgifera LeConte Forms Ion Channels in Lipid Membranes, Biochemistry **43** (2004) 12349.

[307] J.L. Schwartz *et al.*, Early response of cultured lepidopteran cells to exposure to delta-endotoxin from Bacillus thuringiensis: involvement of calcium and anionic channels., Biochimica et biophysica acta **1065** (1991) 250.

[308] V. Steinthorsdottir, H. Halldórsson and O.S. Andrésson, Clostridium perfringens beta-toxin forms multimeric transmembrane pores in human endothelial cells, Microbial Pathogenesis **28** (2000) 45.

[309] S. Springer and H.J. Selbitz, The control of necrotic enteritis in sucking piglets by means of a Clostridium perfringens toxoid vaccine., FEMS immunology and medical microbiology **24** (1999) 333.

[310] L. Petit *et al.*, Clostridium perfringens Epsilon Toxin Induces a Rapid Change of Cell Membrane Permeability to Ions and Forms Channels in Artificial Lipid Bilayers, Journal of Biological Chemistry **276** (2001) 15736.

[311] A.J. Brosnahan *et al.*, Cytolysins Augment Superantigen Penetration of Stratified Mucosa, The Journal of Immunology **182** (2009) 2364.

[312] L. Debellis *et al.*, The Vibrio cholerae Cytolysin Promotes Chloride Secretion from Intact Human Intestinal Mucosa, PLoS ONE **4** (2009) e5074.

[313] H.A. Saka *et al.*, Vibrio cholerae cytolysin is essential for high enterotoxicity and apoptosis induction produced by a cholera toxin gene-negative V. cholerae non-O1, non-O139 strain, Microbial Pathogenesis **44** (2008) 118.

[314] M.d.M. García-Suárez *et al.*, The role of pneumolysin in mediating lung damage in a lethal pneumococcal pneumonia murine model, Respiratory Research **8** (2007) 3.

[315] I. Inoshima *et al.*, A Staphylococcus aureus pore-forming toxin subverts the activity of ADAM10 to cause lethal infection in mice, Nature Medicine **17** (2011) 1310.

[316] B.A. Diep *et al.*, Polymorphonuclear leukocytes mediate Staphylococcus aureus Panton-Valentine leukocidin-induced lung inflammation and injury, Proceedings of the National Academy of Sciences **107** (2010) 5587.

[317] S.T. Cooper and P.L. McNeil, Membrane Repair: Mechanisms and Pathophysiology, Physiological Reviews **95** (2015) 1205.

[318] F.C.O. Los *et al.*, Role of Pore-Forming Toxins in Bacterial Infectious Diseases, Microbiology and Molecular Biology Reviews **77** (2013) 173.

[319] G. von Hoven *et al.*, Repair of a Bacterial Small β-Barrel Toxin Pore Depends on Channel Width, mBio **8** (2017) e02083.

[320] P. Basso *et al.*, Pseudomonas aeruginosa Pore-Forming Exolysin and Type IV Pili Cooperate To Induce Host Cell Lysis, mBio **8** (2017) e02250.

[321] H. Harvey *et al.*, Pseudomonas aeruginosa d-Arabinofuranose Biosynthetic Pathway and Its Role in Type IV Pilus Assembly, Journal of Biological Chemistry **286** (2011) 28128.

[322] V.L. Kung *et al.*, An rhs gene of Pseudomonas aeruginosa encodes a virulence protein that activates the inflammasome, Proceedings of the National Academy of Sciences **109** (2012) 1275.

[323] S. Koskiniemi *et al.*, Rhs proteins from diverse bacteria mediate intercellular competition, Proceedings of the National Academy of Sciences **110** (2013) 7032.

[324] R.L. Feinbaum *et al.*, Genome-Wide Identification of Pseudomonas aeruginosa Virulence-Related Genes Using a Caenorhabditis elegans Infection Model, PLoS Pathogens **8** (2012) e1002813.

[325] A.J. Greaney, S.H. Leppla and M. Moayeri, Bacterial Exotoxins and the Inflammasome, Frontiers in Immunology **6** (2015).

[326] P. Huber *et al.*, Pseudomonas aeruginosa renews its virulence factors, Environmental Microbiology Reports **8** (2016) 564.

[327] H.Y. Chang *et al.*, Characterization of a putative Pseudomonas UDPglucose pyrophosphorylase., Proceedings of the National Science Council, Republic of China. Part B, Life sciences **23** (1999) 74.

[328] P.A. Castric, Hydrogen cyanide production by Pseudomonas aeruginosa at reduced oxygen levels., Canadian journal of microbiology **29** (1983) 1344.

[329] R. Barrangou and L.A. Marraffini, CRISPR-Cas Systems: Prokaryotes Upgrade to Adaptive Immunity, Molecular Cell **54** (2014) 234.

[330] L.A. Marraffini and E.J. Sontheimer, CRISPR interference: RNA-directed adaptive immunity in bacteria and archaea, Nature Reviews Genetics **11** (2010) 181.

[331] R. Barrangou *et al.*, CRISPR Provides Acquired Resistance Against Viruses in Prokaryotes, Science **315** (2007) 1709.

[332] C. Yu *et al.*, Small Molecules Enhance CRISPR Genome Editing in Pluripotent Stem Cells, Cell Stem Cell **16** (2015) 142.

[333] F. Wang and L.S. Qi, Applications of CRISPR Genome Engineering in Cell Biology, Trends in Cell Biology **26** (2016) 875.

[334] P.D. Hsu, E.S. Lander and F. Zhang, Development and Applications of CRISPR-Cas9 for Genome Engineering, Cell **157** (2014) 1262.

[335] T. Wang *et al.*, Genetic Screens in Human Cells Using the CRISPR-Cas9 System, Science **343** (2014) 80.

[336] P. Mali *et al.*, RNA-Guided Human Genome Engineering via Cas9, Science **339** (2013) 823.

[337] O. Shalem *et al.*, Genome-Scale CRISPR-Cas9 Knockout Screening in Human Cells, Science **343** (2014) 84.

[338] F.A. Ran *et al.*, Genome engineering using the CRISPR-Cas9 system, Nature Protocols **8** (2013) 2281.

[339] Y. Jiang *et al.*, Multigene Editing in the Escherichia coli Genome via the CRISPR-Cas9 System, Applied and Environmental Microbiology **81** (2015) 2506.

[340] J. Altenbuchner, Editing of the Bacillus subtilis Genome by the CRISPR-Cas9 System, Applied and Environmental Microbiology **82** (2016) 5421.

[341] P. Burby and L. Simmons, CRISPR/Cas9 Editing of the Bacillus subtilis Genome, BIO-PROTOCOL **7** (2017).

[342] P. Basso *et al.*, Multiple Pseudomonas species secrete exolysin-like toxins and provoke Caspase-1-dependent macrophage death, Environmental Microbiology **19** (2017) 4045.

[343] E.A. Miao *et al.*, Innate immune detection of the type III secretion apparatus through the NLRC4 inflammasome, Proceedings of the National Academy of Sciences **107** (2010) 3076.

[344] E. Faure *et al.*, Pseudomonas aeruginosa Type-3 Secretion System Dampens Host Defense by Exploiting the NLRC4-coupled Inflammasome, American Journal of Respiratory and Critical Care Medicine **189** (2014) 799.

[345] N.E. Sanjana, O. Shalem and F. Zhang, Improved vectors and genome-wide libraries for CRISPR screening, Nature Methods **11** (2014) 783.

[346] M. Cisz, P.C. Lee and A. Rietsch, ExoS Controls the Cell Contact-Mediated Switch to Effector Secretion in Pseudomonas aeruginosa, Journal of Bacteriology **190** (2008) 2726.

[347] P. Berthelot *et al.*, Genotypic and Phenotypic Analysis of Type III Secretion System in a Cohort of Pseudomonas aeruginosa Bacteremia Isolates: Evidence for a Possible Association between O Serotypes and exo Genes, The Journal of Infectious Diseases **188** (2003) 512.

[348] V.N. Kos *et al.*, The Resistome of Pseudomonas aeruginosa in Relationship to Phenotypic Susceptibility, Antimicrobial Agents and Chemotherapy **59** (2015) 427.

[349] K.E. Nelson *et al.*, Complete genome sequence and comparative analysis of the metabolically versatile Pseudomonas putida KT2440, Environmental Microbiology **4** (2002) 799.

[350] M.A. Molina, J.L. Ramos and M. Espinosa-Urgel, A two-partner secretion system is involved in seed and root colonization and iron uptake by Pseudomonas putida KT2440, Environmental Microbiology **8** (2006) 639.

[351] N. Vodovar *et al.*, Complete genome sequence of the entomopathogenic and metabolically versatile soil bacterium Pseudomonas entomophila, Nature Biotechnology **24** (2006) 673.

[352] C. Voisard *et al.*, Biocontrol of Root Diseases byPseudomonas fluorescens CHA0: Current Concepts and Experimental Approaches, Molecular Ecology of Rhizosphere Microorganisms, edited by F. O'Gara, D.N. Dowling and B. Boesten, Wiley-VCH Verlag GmbH, Weinheim, Germany.

[353] C. Kurz, Virulence factors of the human opportunistic pathogen Serratia marcescens identified by in vivo screening, The EMBO Journal **22** (2003) 1451.

[354] T. Kawagoe *et al.*, Essential role of IRAK-4 protein and its kinase activity in Toll-like receptor-mediated immune responses but not in TCR signaling, The Journal of Experimental Medicine **204** (2007) 1013.

[355] G. van Meer, D.R. Voelker and G.W. Feigenson, Membrane lipids: where they are and how they behave, Nature Reviews Molecular Cell Biology **9** (2008) 112.

[356] D.P. Lee *et al.*, A novel pathway for lipid biosynthesis: the direct acylation of glycerol., Journal of lipid research **42** (2001) 1979.

[357] R.K. Yu *et al.*, Structures, biosynthesis, and functions of gangliosides–an overview., Journal of oleo science **60** (2011) 537, arXiv:NIHMS150003.

[358] S.S. Prasad, A. Garg and A.K. Agarwal, Enzymatic activities of the human AGPAT isoform 3 and isoform 5: localization of AGPAT5 to mitochondria, Journal of Lipid Research **52** (2011) 451.

[359] G. Fuertes *et al.*, Role of membrane lipids for the activity of pore forming peptides and proteins., Advances in experimental medicine and biology **677** (2010) 31.

[360] M. Marchioretto *et al.*, What planar lipid membranes tell us about the pore-forming activity of cholesterol-dependent cytolysins, Biophysical Chemistry **182** (2013) 64.

[361] N. Rojko and G. Anderluh, How Lipid Membranes Affect Pore Forming Toxin Activity, Accounts of Chemical Research **48** (2015) 3073.

[362] A.J. Drummond *et al.*, Bayesian Phylogenetics with BEAUti and the BEAST 1.7, Molecular Biology and Evolution **29** (2012) 1969.

[363] A.S. Delattre *et al.*, Substrate recognition by the POTRA domains of TpsB transporter FhaC., Molecular microbiology **81** (2011) 99.

[364] K. Poole, E. Schiebel and V. Braun, Molecular characterization of the hemolysin determinant of Serratia marcescens., Journal of bacteriology **170** (1988) 3177.

[365] G. Menestrina *et al.*, Ion channels and bacterial infection: the case of β-barrel pore-forming protein toxins of Staphylococcus aureus, FEBS Letters **552** (2003) 54.

[366] S.D. Zakharov *et al.*, On the role of lipid in colicin pore formation, Biochimica et Biophysica Acta (BBA) - Biomembranes **1666** (2004) 239.

[367] B. Berube and J. Wardenburg, Staphylococcus aureus α-Toxin: Nearly a Century of Intrigue, Toxins **5** (2013) 1140.

[368] E. Reboud *et al.*, Pseudomonas aeruginosa ExlA and Serratia marcescens ShlA trigger cadherin cleavage by promoting calcium influx and ADAM10 activation, PLoS Pathogens **13** (2017) 1.

[369] H.P. Hahn, The type-4 pilus is the major virulence-associated adhesin of Pseudomonas aeruginosa - A review, Gene **192** (1997) 99.

[370] L. Franchi *et al.*, Critical role for Ipaf inPseudomonas aeruginosa-induced caspase-1 activation, European Journal of Immunology **37** (2007) 3030.

[371] D. Descamps *et al.*, Toll-like receptor 5 (TLR5), IL-1 secretion, and asparagine endopeptidase are critical factors for alveolar macrophage phagocytosis and bacterial killing, Proceedings of the National Academy of Sciences **109** (2012) 1619.

[372] J.W. Newman, R.V. Floyd and J.L. Fothergill, The contribution of Pseudomonas aeruginosa virulence factors and host factors in the establishment of urinary tract infections., FEMS microbiology letters (2017).

[373] J.C. Comolli *et al.*, Pili binding to asialo-GM1 on epithelial cells can mediate cytotoxicity or bacterial internalization by Pseudomonas aeruginosa, Infection and Immunity **67** (1999) 3207.

[374] J. Steinhauer *et al.*, The unipolar Shigella surface protein IcsA is targeted directly to the bacterial old pole: IcsP cleavage of IcsA occurs over the entire bacterial surface., Molecular microbiology **32** (1999) 367.

[375] S. Bouillot *et al.*, Pseudomonas aeruginosa Exolysin promotes bacterial growth in lungs, alveolar damage and bacterial dissemination, Scientific Reports **7** (2017) 2120.

[376] A.M. Hajjar *et al.*, Human Toll-like receptor 4 recognizes host-specific LPS modifications, Nature Immunology **3** (2002) 354.

[377] M. Lamkanfi and V.M. Dixit, Mechanisms and Functions of Inflammasomes, Cell **157** (2014) 1013.

[378] J.R. Yaron *et al.*, K+ regulates Ca2+ to drive inflammasome signaling: dynamic visualization of ion flux in live cells, Cell Death and Disease **6** (2015) e1954.

[379] S.L. Fink and B.T. Cookson, Caspase-1-dependent pore formation during pyroptosis leads to osmotic lysis of infected host macrophages, Cellular Microbiology **8** (2006) 1812.

[380] L. Molina *et al.*, Antibiotic Resistance Determinants in a Pseudomonas putida Strain Isolated from a Hospital, PLoS ONE **9** (2014) e81604.

[381] T. Kolter, Ganglioside Biochemistry, ISRN Biochemistry **2012** (2012) 1.

[382] K. Simons and E. Ikonen, Functional rafts in cell membranes, Nature **387** (1997) 569.

[383] L. Abrami *et al.*, Membrane insertion of anthrax protective antigen and cytoplasmic delivery of lethal factor occur at different stages of the endocytic pathway, The Journal of Cell Biology **166** (2004) 645.

[384] S.A. Sanchez *et al.*, Methyl-β-Cyclodextrins Preferentially Remove Cholesterol from the Liquid Disordered Phase in Giant Unilamellar Vesicles, The Journal of Membrane Biology **241** (2011) 1.

[385] S. Mahammad and I. Parmryd, Cholesterol Depletion Using Methyl-β-cyclodextrin.

[386] E. Reboud *et al.*, Exolysin Shapes the Virulence of Pseudomonas aeruginosa Clonal Outliers, Toxins **9** (2017) 364.

Exolysin, a novel virulence factor of *Pseudomonas aeruginosa* clonal outliers

Pseudomonas aeruginosa is a human opportunistic pathogen responsible for nosocomial infections associated with high mortality. The type III secretion system (T3SS) and T3SS-exported toxins have been considered as key infectivity virulence factors. Our team recently characterized a group of strains lacking T3SS, but employing a new toxin: Exolysin (ExlA) that provokes cell membrane disruption. In this work we demonstrated that ExlA secretion requires ExlB, a predicted outer membrane protein encoded in the same operon, showing that ExlA-ExlB define a new active TPS system. In addition to the TPS secretion signals, ExlA harbors several distinct domains, which comprise hemagglutinin domains, five Arginine-Glycine-Aspartic acid (RGD) motifs and a non-conserved C-terminal region lacking any identifiable sequence motifs. Cytotoxic assays showed that the deletion of the C-terminal region abolishes host-cell cytolysis. Using liposomes and eukaryotic cells, we demonstrated that ExlA forms membrane pores of 1.6 nm. Based on a transposon mutagenesis strategy and a high throughput cellular live-dead screen, we identified additional bacterial factors required for ExlA-mediated cell lysis. We identified three transposons inserted in genes encoding components of the Type IV pili, which are adhesive extracellular appendices. Type IV pili probably mediate close contact between bacteria and host cells and facilitate ExlA cytotoxic activity. These findings represent the first example of cooperation between a pore-forming toxin of the TPS family and surface appendages to achieve host cell intoxication. Using mice primary bone marrow macrophages we showed that ExlA pores provoke activation of Caspase-1 via the NLRP3-inflamasomme followed by the maturation of the pro-interleukin-1β. Mining of microbial genomic databases revealed the presence of *exlA*-like genes in other *Pseudomonas* species rarely associated with human infections. Interestingly, we showed that these environmental bacteria are also able to provoke Caspase-1 cleavage and pro-inflammatory cell death of macrophages. Finally, genome-wide loss-of-function CRISPR/cas9 RAW library screen revealed that several components of the immune system response, indirectly linked to Caspase-1 are involved in the ExlA-mediated cell lysis. Moreover, we found that at least three sgRNAs targeting miRNA, mir-741 were highly enriched in resistant macrophages challenged by ExlA. This miRNA regulates enzymes (St8sIa1 and Agpat5) in the sphingolipids and glycerophololipids biosynthesis pathways, suggesting that ExlA activity may require proper lipid environment.

Pore-forming toxin; Type IV pili; Pyroptosis; High-throughput screening; CRISPR/cas9

Exolysine, un facteur de virulence majeur de *Pseudomonas aeruginosa*

Pseudomonas aeruginosa est un pathogène opportuniste responsable d'infections nosocomiales sévères associées à un taux élevé de mortalité. Le système de sécrétion de Type III (SST3) et les effecteurs qu'il injecte sont considérés comme des facteurs de virulence prépondérants de *P. aeruginosa*. Récemment nous avons caractérisé, un groupe de souches ne possédant pas les gènes du SST3, mais dont la virulence repose sur la sécrétion d'une nouvelle toxine: Exolysine (ExlA) qui provoque la perméabilisation de la membrane des cellules hôtes. ExlA est sécrétée dans le milieu par une porine de la membrane externe, nommée ExlB, formant ainsi un nouveau système TPS, ExlBA. ExlA possède différents domaines : des répétitions hémagglutinines, cinq motifs Arginine-Glycine-Acide Aspartique (RGD) et un domaine C-Terminal faiblement conservé. Des tests de cytotoxicité sur des cellules eucaryotes ont montrés que la délétion du domaine C-terminal abolissait l'activité toxique d'ExlA. En utilisant un modèle de liposomes et différents types de cellules eucaryotes, nous avons démontré qu'ExlA forme des pores membranaires de 1.6 nm. De plus, par un criblage cellulaire à haut-débit d'une banque de mutants, nous avons montré qu'un facteur bactérien additionnel était requis dans la toxicité d'ExlA. Nous avons identifiés 3 transposons insérés dans des gènes codant pour le pili de type IV, démontrant ainsi que cet appendice impliqué dans l'adhésion des bactéries participe à la toxicité d'ExlA, en permettant un contact rapproché entre la bactérie et les cellules hôtes. Un criblage de macrophages primaires de souris KO pour différentes protéines impliquées dans la voie de l'activation de l'inflammasome, nous a permis de démontrer que le pore formé par ExlA est responsable de l'activation de la Caspase-1 par l'inflammasome NLRP3 conduisant à la maturation de l'interleukine-1β. Une étude bio-informatique a révélé la présence de gènes homologues à *exlA* chez d'autres espèces de *Pseudomonas* non pathogènes. Nous avons montré que ces bactéries environnementales sont aussi capables de provoquer une mort cellulaire dépendante de la Caspase-1. Finalement, un criblage d'une banque de macrophages dont les gènes ont été invalidés par la technologie CRISPR/cas9 a révélé que plusieurs protéines du système immunitaire, indirectement liées à l'activation de la Caspase-1 sont impliquées dans la mort cellulaire médiée par ExlA. De plus, nous avons montré que plusieurs sgRNAs ciblant un microARN, mir-741, était grandement enrichi dans les macrophages ayant résisté à une infection avec ExlA. Mir-741 est impliqué dans la régulation d'enzymes (St8sIa1 et Agpat5) de la voie de biosynthèse des sphingolipides et des glycérophospholipides.

Toxine formatrice de pore; Pili de type IV; Pyroptose; Criblage à haut débit; CRISPR/cas9